Faculty of Science, Engineering and Technology
Swinburne University of Technology

Multi Scale Investigation of Post-Erosion Mechanical Behaviour of Granular Material

Amirhassan Mehdizadeh

A thesis submitted in total fulfilment of the requirements for the degree of Doctor of Philosophy

March 2018

Faculty of Science, Engineering and Technology
Swinburne University of Technology, Melbourne Australia

ABSTRACT

Internal erosion is believed to be the main reason of approximately 50 per cent of embankment dam failures, equal to failures due to overtopping in floods. According to the literature, internal erosion is divided into four main mechanisms: concentrated leaks, backward erosion, contact erosion and suffusion. The focus of this research is suffusion, which is the migration of fine particles through pre-existing pores between coarse particles caused by seepage flow. This migration changes the content of fine particles along the seepage path and can potentially affect the mechanical properties of cohesionless soils. It is a common phenomenon in earth structures such as embankment dams, levees and dikes.

Several studies have already been conducted on different aspects of internal erosion. However, only a few attempts, with considerable discrepancies in results, have been carried out to investigate the post-erosion behaviour. In fact, variation of soil strength and stiffness due to progressive internal erosion is not well understood. Internal erosion is a non-uniform and time-dependent phenomenon. This means that soil characteristics in terms of particle gradation, residual fine content, hydraulic conductivity and strength parameters may be different along the seepage path. Even computational research falls short in fully explaining the effects of internal erosion on soil behaviour and strength parameters, as they only consider the effect of particle removal. Taking into account the significant impact of erosion on the failure of dams, this research tries to bridge the current gap in the literature through a multi scale experimental study. This research includes investigation of mechanical behaviour of an internally unstable cohesionless soil during internal erosion and post-erosion response under monotonic and cyclic loadings using a newly developed erosion-triaxial apparatus and 3-dimensional X-ray tomography.

First, previous analytical and experimental studies of internal erosion available in the literature is critically reviewed to find limitations of each research study. Next, an erosion-triaxial testing system is developed to perform the erosion phase and post-erosion shearing under monotonic and cyclic loadings successively. This apparatus minimises sample disturbance and loss of saturation, which can affect test results

significantly. A gap-graded cohesionless soil mixture vulnerable to internal erosion is then used to construct triaxial specimens. After an investigation of soil behaviour and variation of soil strength parameters with erosion progress and during shearing under different loading types, a new technique is employed to prepare eroded soil samples for 3-dimensional X-ray tomography. Computational Tomography scans (CT scans) are taken across the height of specimens. These images are stitched together to make 3D images of soil specimens pre- and post-erosion. Particle rearrangement, local accumulation of fine particles and variation of fine, coarse and pore fractions due to internal erosion are investigated across the height of specimens qualitatively and mathematically.

Test results indicated that the undrained behaviour of the original specimen changed from a strain hardening behaviour to a flow type behaviour with limited deformation after internal erosion. The initial peak strength improved and the flow potential decreased during the initial stage of erosion. This observed increase in initial peak strength is believed to be the result of a better interlocking between the coarse particles post-erosion. In contrast, the slip-down movement of the particles, due to an increase in the post-erosion void ratio, postponed the dilation tendency. Test results also suggested that even erosion of a small percentage of fine particles improved the mechanical frictional behaviour of the soil. However, there was a threshold value for the loss of fine particles where this positive effect deteriorated. This might have been due to formation of local metastable structures and/or overcoming contractive behaviour after loss of the semi-active fines and a considerable increase in the global void ratio. Shear strength results, rate of erosion and local vertical strains together suggest that the intergranular void ratio is a powerful index in evaluating the post-erosion mechanical behaviour of internally unstable soils. It was also understood that under the same seepage flow properties, the erosion of fine particles decreased with an increase in length of specimen. During cyclic loading, the eroded specimens behaved in a similar manner to a soil specimen constructed only of coarse particles. Furthermore, the contraction tendency increased during post-cyclic undrained shearing, which led to a reduction in post-cyclic undrained shear strength. In addition, the undrained secant stiffness of the eroded specimens improved after cyclic loading at small strains. Regardless of the seepage velocity and duration, erosion of even a

small amount of fine particles resulted in a significant increase in cyclic resistance. The outcome of this research delivers a better understanding of internal erosion impacts on the soil microstructure and macro behaviour. This not only provides valuable information for the design of hydraulic structures; results can also be used in computational and numerical modellings for future studies.

ACKNOWLEDGMENT

I would like to express my great appreciation to Dr. Mahdi Miri Disfani for his expert advice and encouragement throughout this research, as well as Dr. Robert Evans, Professor Arul Arulrajah and Dr. D.E.L Ong for their valuable and constructive suggestions.

I wish to give my best thanks to Mr. Alec Papanicolaou (the workshop technician at Swinburne University of Technology) for his technical help and guidance to manufacture the complementary laboratory tests devices successfully. My thanks are extended to my colleague Mr. F. Maghoolpilehrood for his valuable assistance during my research.

I am particularly grateful for the support I received from the love of my life, Leila, and my parents Amirhekmat and Ferdus during my studies.

I acknowledge the support provided through "Melbourne-Sarawak Research Collaboration Scheme", funded by Swinburne University of Technology, Australia.

I would also like to acknowledge the support of Australian Synchrotron and the Trace Analysis for Chemical, Earth and Environmental Sciences (TrACEES) platform from the Melbourne Collaborative Infrastructure Research Program at the University of Melbourne and thank Dr Jay Black (School of Earth Sciences) for operating the micro-CT scanner and assistance in processing data.

Finally, I am using this opportunity to express my gratitude to everyone who supported me throughout this chapter of my life.

DECLARATION

This thesis contains no material which has been accepted for the award of any other degree or diploma in any university. To the best of my knowledge and belief this thesis contains no material previously published by any other person except where due acknowledgment has been made.

The following publications have resulted from the work carried out for this degree. Copies of selected published or in print refereed journal and conference papers are presented in Appendix C.

Signature: ……… Mehdizadeh ….
Date: 07/10/2017

REFEREED JOURNAL TECHNICAL PAPERS:

1. **Mehdizadeh, A.,** Disfani, M. M., Evans, R. P., Arulrajah, A. and Ong, D. E. L. (2017). "Mechanical Consequences of Suffusion on Undrained Behaviour of a Gap-graded Cohesionless Soil - An Experimental Approach." *ASTM, Geotechnical Testing Journal*, 40(6), 20160145, DOI: 10.1520/GTJ20160145.
2. **Mehdizadeh, A.**, Disfani, M. M., Arulrajah, A., and Evans, R. P. (2017). "Progressive Internal Erosion in a gap-graded internally unstable soil-Mechanical and Geometrical Effects." *International Journal of Geomechanics, ASCE*, **Accepted for Publication on Aug 2017.**
3. **Mehdizadeh, A.**, Disfani, M. M., Arulrajah, A., and Evans, R. P. (2017). "Influence of Suffusion on Cyclic Resistance and Post Cyclic Behaviour of a Gap-graded cohesionless Soil." *Journal of Soil Dynamic and Earthquake Engineering*, **Submitted and under peer Review.**
4. **Mehdizadeh, A.**, Disfani, M. M., Arulrajah, A., and Evans, R. P. (2017). "Influence of internal erosion on fabric and undrained behaviour of an internally unstable gap-graded soil." Canadian Geotechnical Journal, **Submitted and under peer Review.**

REFEREED JOURNAL DISCUSSION PAPERS:

1. **Mehdizadeh**, **A.**, Disfani, M. M., Evans, R. P., Arulrajah, A., and Ong, D. E. L. (2015). "Discussion of 'Development of an Internal Camera-Based Volume Determination System for triaxial Testing' by S. E. Salazar, A. Barnes and R. A. Coffman." *ASTM*, *Geotechnical Testing Journal*, 39(1), 165-168, DOI: 10.1520/GTJ20150153.
2. **Mehdizadeh**, **A.**, Disfani, M. M., Arulrajah, A., and Evans, R. P. (2015). "Discussion of 'On the distinct phenomena of suffusion and suffosion' by R. J. Fannin and P. Slangen." *Geotechnique Letters*, 5(3), 129-130, DOI: 10.1680/jgele.15.00017.
3. **Mehdizadeh**, **A.**, Disfani and Evans, R. P. (2017). "Discussion of 'Stress-Strain Behaviour of Granular Soils Subjected to Internal Erosion' by Chen et al." *Journal of Geotechnical and Geoenvironmental Engineering*, *ASCE*, 143(9), 07017019-1, DOI: 10.1061/(ASCE)GT.1943-5606.0001561.

REFEREED CONFERENCE PAPERS:

1. **Mehdizadeh**, **A.**, Disfani, M. M., Evans, R. P., Arulrajah, A. and Ong, D. E. L. (2017). "Application of image processing in internal erosion investigation." *Proc. of the 19th Int. Conf. on Soil Mech. and Geotech. Eng.*, 17 to 22 September 2017, Seoul, South Korea, 2925-2928.

TABLE OF CONTENTS

LIST OF FIGURES

LIST OF TABLES

NOTATIONS AND ABBREVIATIONS

i_{crit}: Critical hydraulic gradient

k: Hydraulic conductivity

k_{eq}: Equivalent hydraulic conductivity

k_i: Local hydraulic conductivity

H: Total length of erosion path

H_i: Length of erosion path related to the local hydraulic conductivity k_i

ΔV_f: Change of void ratio caused by the fines loss

ΔV_i: Change of void ratio caused by possible intergranular re-arrangement

e_c: void ratio induced by erosion of fines without soil deformation

ε_v: Volumetric deformation

e_g: Intergranular void ratio

e: Global void ratio

FC: Fine content

$e_{c_{eq}}$: Equivalent intergranular contact index

b: Portion of the fine particles that participate in the soil stress matrix

C_{u_c}: Uniformity coefficients of the coarse fraction

C_{u_f}: Uniformity coefficients of the fine fraction

R_d: Grain size disparity ratio

d'_{50}: Particle diameter for which 50% of fine particles by mass are smaller

$d_{10,Host\ sand}$: Particle diameter for which 10% of host sand particles by mass are smaller

$d_{50,Silt}$: Particle diameter for which 50% of silt particles by mass are smaller

FC_{Thr}: Threshold fine content

FC_l: Limit fines content

D_r: Relative density

D'_{15} or D_{15f} : Grain diameter for which 15% of the grains by weight of the coarse soil are smaller

d'_{85} or d^f_{85} or d_{85b}: Grain diameter for which 85% of the grains by weight of the fine soil are smaller

D_{up}: Largest particle size of the flat zone (gap zone) on a gap-graded gradation curve

D_{bt}: Smallest particle size of the flat zone (gap zone) on a gap-graded gradation curve

S: Secant slope of soil gradation curve at each particle size

D_5: Particle diameter for which 5% of soil particles are smaller

D_{10}: Particle diameter for which 10% of soil particles are smaller

D_{15}: Particle diameter for which 15% of soil particles are smaller

D_{20}: Particle diameter for which 20% of soil particles are smaller

D_{60}: Particle diameter for which 60% of soil particles are smaller

D_{90}: Particle diameter for which 90% of soil particles are smaller

D_c: Constriction size

D_{c35}: Controlling constriction size when 35% of constrictions are smaller

$D_{c35(densest)}$: Constriction sizes in the densest condition when 35% of constrictions are smaller

$D_{c35(loosest)}$: Constriction sizes in the loosest condition when 35% of constrictions are smaller

D'_5: Particle diameter for which 5% of coarse particles by mass are smaller

D'_{10}: Particle diameter for which 10% of coarse particles by mass are smaller

D'_{15}: Particle diameter for which 15% of coarse particles by mass are smaller

D'_{30}: Particle diameter for which 30% of coarse particles by mass are smaller

D'_{50}: Particle diameter for which 50% of coarse particles by mass are smaller

D'_{60}: Particle diameter for which 60% of coarse particles by mass are smaller

D'_{75}: Particle diameter for which 75% of coarse particles by mass are smaller

D'_{95}: Particle diameter for which 95% of coarse particles by mass are smaller

G_r: Gap ratio

S_{min}: Minimum slope of soil gradation

D_{c35}^{c}: Controlling constriction sizes of the coarser fraction

$d_{85,SA}^{f}$: Representative particle sizes of the finer fraction by surface area

α: Stress-reduction factor

σ'_f: Effective stresses on fine particles

σ'_c: Effective stresses on coarse particles

σ'_{vm0}: Initial mean vertical effective stress.

γ_w: Water density

Δz: Specimen height

G^*: Geometric-based stress reduction factor

$\Delta\sigma'_v$: Variation of effective stress

$\emptyset_\mu$: True friction angle between particles of coarser and finer fraction

n^f: Fine fraction volume ratio

S_f: Finer fraction by mass

ρ^f: Unit density of fine fraction

g: Standard Gravity

D_c^*: Controlling constriction size

D_{100}: Maximum particle size

O'_{50}: Actual opening size

d_0: Smallest particle size

$Nl^3/_V$: Normalized contact number per unit volume

$2R$: mean particle size

k_{n0}, k_{t0} and n: Inter-particle elastic constants

$\emptyset_\mu$: Inter-particle friction angle

k_{p0} and $\emptyset_0$: Inter-particle hardening rule

λ and Γor e_{ref} and P_{ref}: Critical state for packing

f_e: Eroded fraction

W_f: Weight of the eroded particles per unit volume

W_s: Initial total solid weight per unit volume

e_c: Critical void ratio

R_d: Particle size ratio

d_{max}: Maximum particle size

v: Specific volume-

η: Shear stress ratio

LL: Liquid Limit

I_P: Plasticity Index

σ_3: Confining Pressure

P_{BP}: Back-pressure

$\varepsilon^{\cdot}$: Strain rate during shearing

t_{50}: Required time for 50 % primary consolidation

C_u: Uniformity coefficient

e_{max}: Maximum void ratio

e_{min}: Minimum void ratio

I_e: Void ratio difference

$e_{max, HS}$: Maximum void ratio of the host sand

IA: Angularity index

FC_i: Initial Fine Content

FC_f: Final Fine Content

S_p: Initial peak shear strength

P'_c: Initial mean effective stress

q_{Peak}: Initial peak deviator stress

S_{us}: Residual strength

q_s: Deviator stress

φ_s: Angle of phase transformation at QSS

u_f: Flow potential

P'_{PT}: Mean effective principal stress

n: Porosity

γ_{max}: Maximum index density

γ_{min}: Minimum index density

e_i: Initial global void ratio

e_f: Final global void ratio

e_{gi}: Initial intergranular void ratio

e_{gf}: Final intergranular void ratio

Chapter 1 Introduction

Internal erosion is believed to be one of the main reasons for embankment dams failure. According to the literature, it is divided into four mechanisms of concentrated leaks, backward erosion, contact erosion and suffusion. The focus of this research is suffusion, which is known as migration of non-plastic fine particles through pre-existing pores between coarse particles caused by seepage flow. This chapter first explains the problem technically and statistically, and then describes the objective and scope of this research.

1.1. Problem Statement

The earliest dams were constructed around 2900 BC. A significant number of dam failures have been reported in the literature due to unpredicted seepage or incorrect filtration. However, the historic record of dam failures shows that there are other effective factors. It was believed that a large fraction of piping failure was due to internal erosion, inappropriate filter design and indecent maintenance. Based on the investigation conducted by Lane (1934) and Jones (1981), Richards and Reddy (2007) reported that almost one-third of all piping failures could be related to suffusion or backwards erosion. Von Thun (1985) reported that up to 26 per cent of piping failures occurred due to poor filter design. Richards and Reddy (2007) summarized the previous reports and showed that approximately half of dam failures was because of soil erosion. Fry et al (2012) reported 23 internal erosion failures from February 2010 to April 2012 (within 26 months). Tables 1-1 and 1-2 show statistics of embankment dam failures were obtained by Foster et al. (1998 and 2000) for large dams constructed between 1800 to 1986, except dams constructed in Japan and China pre-1930. They found that if internal erosion occurred in the foundation, the reservoir level was not important. However, the internal erosion failure occurred in the embankment when the reservoir level was at the highest level or within one meter of that level. Two failures per 10,000 dams per year were reported due to internal erosion. It is evident that internal erosion is the main cause of approximately 50 per cent of embankment dam failures which is equal to failures due to overtopping in floods. The importance of internal erosion is more obvious when compared with percentage of sliding failures due to static and seismic instabilities. Table 1-2 indicates that almost 146 out of 11,192 (1 in 80) embankment dams have failed or experienced an accident due to internal erosion. In addition, it was found that two-thirds of all failures and half of accidents have occurred on first filling or in the first five years of operation (ICOLD, 2015). According to ICOLD (2015), *accident* is defined as an incident that has been prevented from becoming a failure.

Table 1-1. Statistics of embankment dam failures (Foster et al., 1998 and 2000)

Failure Mechanism	Erosion		Embankment Sliding	
Mode of Failure	External Erosion (Overtopping)	Internal Erosion	Static Instability	Seismic Instability
Total Over the World (%)	48%	46%	4%	2%
Total Over the World (%)	94%		6%	

Table 1-2. Failures and accidents in embankments of large dams constructed between 1800 to 1986 (Foster et al., 1998 and 2000)

Case	Total	In Dam	Around Conduits or Walls
Internal Erosion Failures	36	19	17
Internal Erosion Accidents	75	52	23
Seepage accidents with no detected erosion	36	30	6
Population of Dams	11,192	11,192	5,596
Historical Frequency for Failures and Accidents	0.013	0.009	0.0082
Proportion of Failures and Accidents on First Fill	36%	-	-
Proportion of Failures and Accidents after First Fill	64%	-	-
Historical Frequency for First Fill	-	0.0032	0.003
Historical Frequency after First Fill	-	0.0058	0.0052

In another statistical database collected by Brown and Gosden (2004), for 2,500 dams registered in the United Kingdom, 60 per cent of accidents were related to internal erosion with two serious erosion accidents per year. A detailed analysis of internal erosion incidents was carried out by Engemoen and Redlinger (2009) and Engemoen (2011) for 220 embankment dams. It was found that 45 per cent of dams (99 dams) had experienced accidents. Out of the 99 accidents, one accident led to failure, 53 were due to particle transport, and excessive seepage or sand boil were observed for the remainder. Nine accidents occurred in the embankment, 70 in the foundation and others around the conduits. This investigation indicated that dams with successful performance were also vulnerable to an internal erosion accident; it can occur at any time in a dam's service life. Although design and construction methods have been improved over time, ICOLD data presented in Table 1-3 indicates that the problem of internal erosion is on-going, which highlights the importance of further research and investigation.

Table 1-3. Failure statistics for embankment dams excluding China from 1970 to 1989 (ICOLD, 2015)

Modes of failure	Ratio of Failures to the Number of Dams 1970-1979	Ratio of Failures to the Number of Dams 1980-1989
Internal Erosion	0.002	0.0016
Overtopping and Appurtenant Structure Failure Resulting in Overtopping	0.0026	0.0019
Sliding	0.0004	0.0001

Suffusion as one of the main mechanisms of internal erosion normally occurs in internally unstable soils where fine particles are not fully involved in stress transferring and the soil structure is mainly made by coarse particles. Depending on the level of contribution of the fine particles in the soil structure, migration of fine particles can affect both micro and macro soil structural behaviours. Formation of metastable structure, settlement, or, in an extreme case, collapse of the soil structure can be a result of erosion of the fine particles. Literature review indicates that many research has been conducted on different aspects of internal erosion such as susceptibility of soil material, filter design criteria and influential parameters on initiation and progression of internal erosion. While previous studies provided better insight into how internal erosion can initiate and change the soil structure, explanation of soil response after internal erosion is still challenging. There have been a few attempts to discover post-erosion behaviour, with considerable discrepancies in results. In fact, variation of soil strength and stiffness due to progressive internal erosion is not well understood. Internal erosion is a non-uniform and time-dependent phenomenon, which means that soil characteristics in terms of particles gradation, residual fine content, hydraulic conductivity and strength parameters may be different along the seepage path, making it complex and challenging to understand.

Considering the significant impact of erosion on failure of dams, this research attempts to fulfil the current gap in the literature through a multi scale experimental study. This research includes investigation of mechanical behaviour of an internally unstable cohesionless soil during internal erosion (suffusion) under monotonic and cyclic loadings using a newly developed erosion-triaxial apparatus and X-ray tomography.

First, previous analytical and experimental studies of internal erosion available in the literature are critically reviewed to find advantages and disadvantages of each research method. Next, an erosion-triaxial testing system is developed to perform erosion phase and post-erosion shearing under monotonic and cyclic loadings successively. This apparatus helps to avoid sample disturbance and loss of saturation, which can affect test results significantly. A gap-graded cohesionless soil vulnerable to internal erosion is then prepared to make triaxial specimens. After investigation of soil behaviour and variation of soil strength parameters during erosion progress and under different loading types, a new technique is employed to prepare eroded soil samples for 3-dimensional (3D) X-ray tomography. Computational Tomography scans (CT-scans) are taken across the height of specimens and stitched together to make 3D images of soil specimens pre- and post-erosion. Particle rearrangement, local accumulation of fine particles, breakage of force chains and variation of fine, coarse and pore fractions due to internal erosion are investigated across the height of specimens. The outcome of this research delivers a better understanding of internal erosion impacts on the soil microstructure and macro behaviour. This not only provides valuable information for design of hydraulic structures; the result can be used in computational and numerical modellings for future studies.

1.2. Objective and Scope

This research contributes to Geotechnical Engineering, Hydraulic Engineering and Sustainability in Geotechnical Engineering, with particular regards to embankment dams, levees, and dikes, as well as bridges neighbouring rivers. The research presents detailed facts in micro and macro scales regarding response of granular materials during and after internal erosion. The developed erosion-triaxial apparatus provides a platform to determine deformations, local strains and erosion percentage of fine particles during internal erosion. It can also be used to investigate variation of shear strength and development of deformations and excess pore water pressure under undrained/drained monotonic and cyclic loadings after internal erosion. The objectives of this research study are outlined below:

- Development of an erosion-triaxial apparatus to perform saturation, consolidation, erosion and shearing continuously with minimum soil disturbance and loss of saturation to investigate post-erosion mechanical behaviour of soil specimens
- Employment of Particle Image Velocimetry PIV technique to measure local vertical/horizontal strains during erosion to avoid drawbacks of ordinary measuring tools, such as local strain gauges
- Employment of a new technique to prepare non-eroded and eroded specimens for 3D X-ray tomography to investigate the effects of internal erosion on soil structure in a micro scale
- Studying impact of internal erosion on undrained mechanical behaviour of granular soils under monotonic and cyclic loadings
- Investigation of impact of residual fine content, global and intergranular void ratios and seepage properties (i.e. seepage velocity, duration and length) on post-erosion behaviour

1.3. Significance

It has been understood that internal erosion is one of the main causes of approximately 50 per cent of embankment dams' failure. Although internal erosion has been investigated and discussed for a century, and many studies have been carried out on its various aspects, it is still an ongoing problem in geotechnical engineering. This is because the focus of previous studies has been mainly on the identification, characterisation and influential parameters; however there are still many uncertainties about the effect of internal erosion on mechanical behaviour of soils in macro scale, such as soil strength and stiffness. This experimental investigation attempts to study post-erosion mechanical consequences in terms of stress-strain relationship, variation of shear strength and cyclic resistance. The results will assist geotechnical engineers in determining the soil strength deterioration due to internal erosion and designing hydraulic structures safely wherever the potential of internal erosion (suffusion) is believed to be significant.

1.4. Research Method

To achieve aims and objectives, this research is divided into several main sections. The first section is literature review. This includes previous experimental, computational and mathematical studies with focus on laboratory investigation of internal erosion and effect of fine particles on granular soils behaviour.

Unfortunately, the impact of internal erosion on soil strength parameters and soil behaviour are not yet fully understood. Therefore, the development of a new experimental apparatus is necessary to perform erosion and shearing tests successively. Since the main part of this project is investigation of post-erosion behaviour of granular soils, development of an appropriate apparatus is the second phase. Evaluating the previous attempts recorded in the literature, clarifying their drawbacks and problems, and providing a solution to improve the system to achieve reliable and consistent data are some parts of this phase. This phase also includes providing the design drawings for manufacturing and modification of a triaxial test apparatus. The erosion-triaxial apparatus consists of a water supply system, a modified triaxial chamber and a collection tank. The water supply system provides the required seepage flow for initiation and progression of internal erosion. An ordinary triaxial chamber is modified to perform erosion and shearing phases continuously and successively without removing soil specimens (soil disturbance) and loss of saturation.

This chamber holds the soil matrix, but allows fine particles to move freely and leave the sample under hydraulic forces. Eroded particles and discharged water from the triaxial chamber are collected and measured by the collection tank while the back-pressure is kept constant at the same level at the bottom of soil specimens.

The key element of performing reliable experimental investigation is preparing uniform test specimens. Otherwise, the results will not be reliable and repeatable, even if the apparatus works properly. Therefore, the next step is finding the best way to reconstitute granular soil samples that behave completely similarly under the same hydraulic and stress conditions.

Experiments must be carried out on a soil mixture that is geometrically susceptible to internal erosion and can reasonably be a representative of real field materials. It is evident that physical and mechanical properties of soil affect the soil behaviour during and after internal erosion. Therefore, it is essential to assess the influential geotechnical characteristics of the research material before starting erosion tests. These properties are listed below:

- Maximum and minimum void ratios of the soil mixture (relative density)
- Specific gravity of particles
- Particle shape properties: sphericity or ellipticity, roundness or angularity and smoothness or roughness
- Direct shear test at the loosest relative density
- Susceptibility to internal erosion

To achieve valid results, full instrumentation and monitoring is conducted. However, before starting the experimental stage, calibration of all measuring instruments such as load cells, Linear Variable Differential Transducers (LVDTs) and piezometers, accuracy of PIV technique, and repeatability and reliability of tests results need to be evaluated to ensure that the results are trustworthy. The program of experiments includes three stages to examine the impact of the seepage flow velocity, erosion duration and sample dimensions (erosion path) on the soil response during erosion and post-erosion undrained behaviour under monotonic and cyclic loadings.

This provides valuable information about time dependency of internal erosion (erosion progress) and the effect of the seepage force and length on erosion of particles. In addition, variation of shear strength due to various erosion scenarios is investigated, which can be used in the safety and risk assessment of embankment dams.

Three dimensional X-ray tomography of non-eroded and eroded specimens is the next part of this research. This microanalysis helps to understand what happens to the soil structure and force chains after experiencing a seepage flow and relocation of fine particles. In fact, the particle interlocking and global and intergranular void ratios control the soil behaviour and taking 3D CT-scans along the specimens' height facilitates better understanding of macro behaviour of soils. Image analysis is carried out using Avizo software package.

Finally, conclusion is the last part of this research which summarise the achievements of experimental investigation and 3D images processing. Figure 1-1 shows the flow chart of this research.

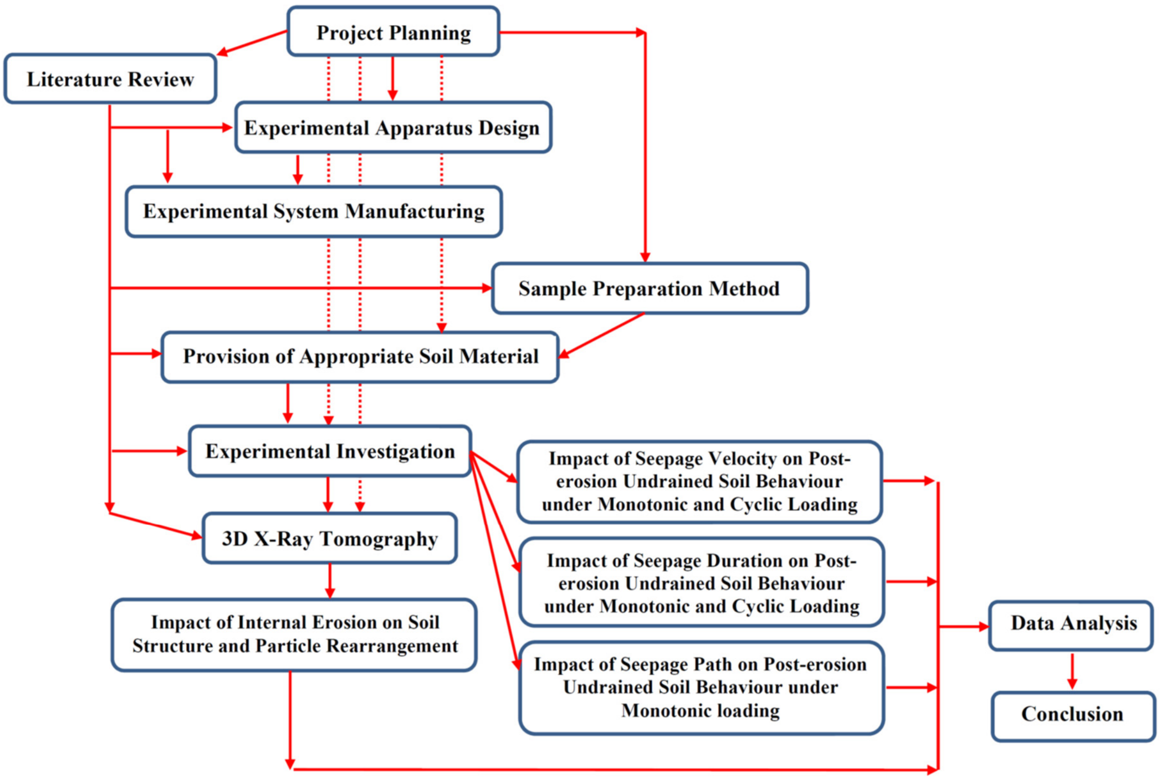

Figure 1-1. Flow chart of the research

1.5. Thesis Outline

The body of this thesis is divided into ten chapters. A brief description of each chapter is provided below:

Chapter 1: Introduction

Chapter 1 consists of an introduction into the present research study. It begins with the definition of internal erosion a brief history of the related problems and their consequences. The chapter continues with a discussion of the shortcomings of current engineering knowledge, the scope and objectives of this study, the research framework and methodology, and finally, outlines of the study.

Chapter 2: Literature Review

A critical literature review in terms of experimental and computational investigations on internal erosion is provided. This includes different mechanisms of internal erosion, internal stability criteria, influential parameters on initiation and progression of internal erosion and impact of fine particles on the soil mechanical behaviour.

There are more than 15 geometric methods that have been developed to investigate internal stability of soil gradations. These techniques are normally used for assessing granular filters criteria. A brief description of practical methods is provided in this chapter.

Before reviewing experimental and computational studies on internal erosion, it is necessary to study the influence of fine particles on mechanical behaviour of granular soils and their contribution to the soil structure, as suffusion is believed to be associated with erosion of non-plastic fine particles. Susceptibility of shear strength, internal friction, dilation tendency and cyclic resistance to the fine content is the main theme of this section.

The focus of laboratory studies in last 30 years has been evaluating influential parameters (e.g. fine content, soil gradation, seepage direction, hydraulic gradient and confining pressure) on initiation and progression of internal erosion. Testing procedure and the result of each experiment, in addition to their challenges, are described. Furthermore, a few available experimental and computational studies related to the post-erosion response are also discussed in this chapter.

Chapter 3: Methodology of Laboratory Study

Extensive erosion-triaxial tests were carried out on a cohesionless gap-graded material in a Geomechanic Laboratory at Swinburne University of Technology, Melbourne, Australia. Three series of tests are carried out in this research. The first series is associated with characterisation of the soil mixture. Erosion-triaxial tests are performed in the second series, and X-ray tomography of eroded and non-eroded samples are conducted in the last series. In this chapter, a brief introduction of each test including sample preparation method, testing procedure, test equipment, number of tests and related standards is presented.

Chapter 4: Geotechnical Characteristics of the Soil Mixture

A gap-graded granular material with 25 per cent non-plastic fine particles susceptible to internal erosion is selected for this study. Erodibility of fine particles in the soil mixture is examined using the presented geometric methods in Chapter 2. It was understood that internal erosion and post-erosion behaviour are affected by some geotechnical characteristics of the soil material, such as relative density, specific gravity, particle shapes and particle interlocking. A testing program is defined to measure the required parameters before initiating the erosion experiments.

Chapter 5: Development of Triaxial-Erosion Apparatus

To investigate the effect of internal erosion on the mechanical behaviour of the soil mixture, a new testing apparatus capable of performing erosion and triaxial phases successively needs to be developed to minimise the soil disturbance and loss of saturation. This chapter describes the details of apparatus design in terms of materials properties, accessories and parts dimensions, fabrication and assembling.

Chapter 6: Influential Parameters on Internal Instability

A back-analysis on available experimental studies in the literature is conducted in this chapter to investigate influential parameters on moveability of fine particles in granular mixtures. A new framework is also presented at the end of the chapter suggesting the most appropriate void ratio equation for non-cohesive soils with fine content between 10 to 30 per cent.

Chapter 7: Mechanical Consequences of Internal Erosion under Monotonic Loading

The results of erosion-triaxial tests under monotonic loading are presented in Chapter 7. This chapter includes investigation of seepage properties on the soil response during erosion and undrained shearing. Downward seepage flows with various velocities and durations are applied to soil specimens with different dimensions. Impact of internal erosion on vertical strains during erosion, hydraulic conductivity, particle size distribution and void ratio and soil strength parameters, such as shear strength and stiffness, are determined and compared to the initial conditions. This comprehensive study sheds some light on one of the most controversial topics in erosion of soils, which can be considered in the embankment dams designing.

Chapter 8: Influence of Internal Erosion on Cyclic Resistance and Post-Cyclic Behaviour

Chapter 8 investigates the impact of internal erosion on cyclic resistance and post cyclic behaviour of the tested mixture. Similar to experiments in Chapter 7, downward seepage flows with different properties are applied to the soil specimens, and the soil response during erosion and post-erosion behaviour under cyclic loading, followed by monotonic undrained shearing are studied and compared with non-eroded specimens. Findings of this chapter can be used in assessment of embankment dams' safety during earthquakes if risk of internal erosion is expected to be high.

Chapter 9: Micro Evaluation of Internal Erosion using 3D X-Ray Tomography

The erosion-triaxial test determines the impact of internal erosion on mechanical behaviour of granular soil in macro scale. However, this impact cannot be understood without microanalysis of the soil structure. This can be done by 3D X-ray tomography of eroded and non-eroded specimens. Chapter 9 describes details of the sample preparation for erosion and X-ray imaging. The effect of removal of fine particles on the pore structure, particle rearrangement, constriction size and the soil stress matrix is also discussed in this chapter.

Chapter 10: Conclusion and Recommendation

Chapter 10 is the summary of this research study. Achievements and findings are simplified in this chapter to be applicable for engineering practices, and suggestions are made for future research works.

Chapter 2 Literature Review

Migration of soil particles to downstream due to a seepage flow within an embankment dam or its foundation and other water management structures is generally known as internal erosion. Hydraulic forces exerted by a seepage flow need to overcome particle contact forces (which are dependent on effective stresses on soil particles) to initiate internal erosion. Initiation and continuation of internal erosion are governed by the mechanics of the equilibrium of the particles and grain transport (ICOLD, 2015). Detachment of particles may occur between the embankment and foundation or other vulnerable zones around conduits, culverts or spillway walls where there is an interface between the embankment fill and structural elements. This phenomenon normally initiates along local flaws such as cracks, holes or small cavities, and is developed over time. It does not always lead to quick failures, but can change soil structure and change the soil mechanical behaviour, such as its shear strength or compressibility. However, the consequences can be catastrophic if it is not identified and controlled quickly. It is believed that internal erosion is one of the major causes of hydraulic structures failure (ICOLD, 2015).

2.1. Internal Erosion Mechanism-Overview and Description

Erosion of soil particles has been an area of interest for decades. However, it has been common for engineers to use the generic term of "piping" for all different types of particles erosion, such as internal erosion or jugging (Richards and Reddy, 2007). It is necessary to classify different types of soil erosion in separate groups or sub-groups to determine the main causes of initiation, progression and, eventually, related failures. Darcy (1856) presented a relationship between length of flow path, fluid velocity and head in granular soils for the first time. Later on, Darcy's theory (1856) was developed to evaluate piping potential from the length of flow path under dams (e.g. Bligh, 1910; 1911a; 1911b; 1913; Lane, 1934). Terzaghi (1925 and 1943) evaluated the piping phenomenon and the associated heave in upward seepage flows in sands. Terzaghi (1925) found that at a critical hydraulic gradient (i_{crit}), effective stresses on particles decreases to zero, which leads to erosion of sand particles. Lane (1934), Terzaghi (1939) and Sherard et al. (1963) defined backward erosion as progressive dislodgement of particles from a soil matrix by intergranular seepage water at exit points. Erosion of particles along pre-existing openings, such as cracks in cohesive material or voids due to erosive forces of water, was defined as internal erosion by Lane (1934). Chemical dispersion of clay particles due to rainfall through open cracks was referred to as jugging or tunnelling by Jones (1981), and "suffusion" was defined as the gradual migration of fine particles through a coarse matrix (e.g. Pavlov 1898; Kral 1975; Galarowski 1976; Jones, 1981; Burenkova, 1993).

Garner and Fannin (2010) stated that a coincidence between material susceptibility, critical stress condition and critical hydraulic load needs to be satisfied to initiate internal erosion (Figure 2-1). These three conditions were defined as below:

- *Material Susceptibility*: erodibility of fine particles with respect to the constriction size
- *Critical Stress Condition*: contribution of fine particles in force chains in terms of providing primary or secondary support for coarse particles
- *Critical hydraulic Load*: the required seepage flow to overcome effective stresses on fine particles

The focus of this research is the investigation of the influence of internal erosion, particularly suffusion, on post-erosion mechanical behaviour of vulnerable soils. Due to the variability of definitions in the literature, the internal erosion classification proposed by ICOLD (2015) is used in this study. According to this classification, internal erosion is divided into four main mechanisms as below:

- *Concentrated leaks*
- *Backward erosion*
- *Contact erosion*
- *Suffusion*

In the next sections, each mechanism is explained briefly in terms of definition and causes.

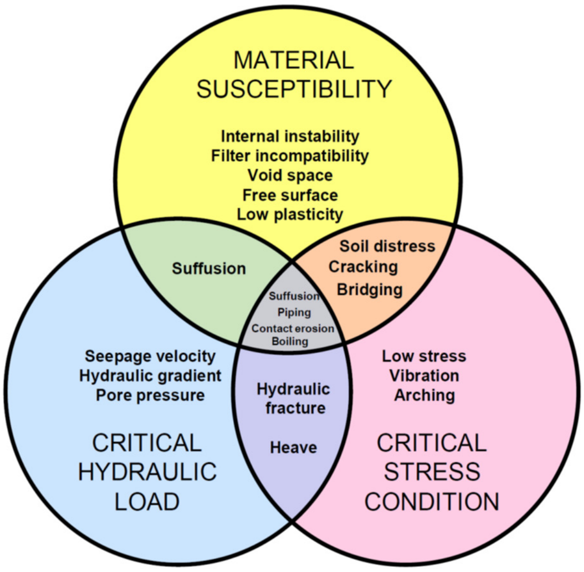

Figure 2-1. Venn diagram illustrating interaction of geometric, hydraulic and mechanical condition for initiation of internal erosion (Garner and Fannin, 2010)

2.1.1. Concentrated Leaks

Openings or cracks may be created in plastic soils, unsaturated silt, silty sand and silty sandy gravel due to differential settlement during construction (poorly compaction) of the dam or in operation, desiccation at high levels in the fill, frost action, and/or hydraulic fracture due to low stresses around conduits. The sides of the opening or gap may be eroded by leaking water. This type of erosion is known as concentrated leaks (ICOLD, 2015). Progression of concentrated leak leads to development of a pipe.

2.1.2. Backward Erosion

Detachment of soil particles at the exit of the erosion path in non-plastic soils is defined as backward erosion. It may occur through or under embankments. Two types of backward erosion are identified as below:

- *Backward erosion piping*: formation of shallow pipes in the opposite direction of the flow beneath an embankment is known as backward erosion piping, which leads to sand boils. It normally occurs during floods where sand layers are covered by a cohesive material. Although several dikes' failure due to backward erosion piping in the USA, China and the Netherlands have been reported, it is not considered as a common failure mode (Beek, 2015). Progression of backward erosion piping forms a network of small channels, and if these small channels reach the reservoir or river, a pipe forms (ICOLD, 2015).
- *Global backward erosion*: failure or collapse of soil above or around a backward erosion piping is defined as global backward erosion. Sinkholes or near vertical cavities are formed if this collapse is upward. This may result in sub-vertical sinkholes or sloughing and unravelling on the downstream face (ICOLD, 2015).

2.1.3. Contact Erosion

Removal of fine particles at the interface of coarse and fine layers when there is a water flow parallel to the soil layers is defined as contact erosion (Cyril et al., 2009). Continuation of contact erosion leads to the development of sinkholes and pipes in the embankment core (ICOLD, 2015).

2.1.4. Suffusion

Transportation of fine particles through pores between coarse particles due to a seepage flow is classified as suffusion. This particle migration occurs only for fine particles, as the coarse particles form the primary soil structure and carry the effective stresses. It may occur within an embankment core or the foundation of hydraulic structures. Internally unstable widely and gap-graded soils are vulnerable to suffusion. However, segregation of broadly graded non-plastic soils during placement (poor construction) increases the risk of suffusion. It is worth mentioning that the term 'fine' is associated with the particles that are relatively smaller than coarse particles and can pass through the pore spaces made by coarse particles. Fine particles here does not mean particles smaller than 0.075 mm (US, Sieve No. 200) (ICOLD, 2015). Variation of local or global hydraulic conductivity (*k*) and gradient, local clogging and settlement have been mentioned as results of suffusion. Progression of suffusion may result in a new stable state between fine particles and seepage stresses or lead to global collapses and hydraulic fractures, which is known as suffosion. However, suffusion may recommence again after a period of stable state due to an increase in river or reservoir water level.

Fannin and Slangen (2014) identified suffusion as a phenomenon accompanied by an increase in hydraulic conductivity. Although this raises no doubts at first glance, interestingly there are studies claiming that k decreases or even remains constant during suffusion. For example, Bendahmane et al. (2008) mentioned that permeability decreased by a factor of 10 when erosion was initiated. Xiao and Shwiyhat (2012) reported a reduction in permeability with progression of suffusion in gap-graded soils. No permeability change was reported as a result of suffusion in poorly graded soils. It appears that the change of k in the suffusion process is heavily dependent on the clogging phenomena. After washing the particles, the local hydraulic conductivity increases; if those washed particles settle or clog somewhere else in the soil, the local hydraulic conductivity of that region decreases. The result of such changes in local hydraulic conductivities provides an equivalent hydraulic conductivity (k_{eq}) that can be higher or lower than the initial magnitude or remain constant after the suffusion process.

This variation can be postulated by an equivalent permeability formula presented in Eq. 2.1:

$$\mathrm{k_{eq}} = \frac{\sum \mathrm{H}}{\sum \frac{\mathrm{H_i}}{\mathrm{k_i}}} \tag{2.1}$$

Fannin and Slangen (2014) attributed volumetric contraction or reduction in volume to one of distinctive features of the suffosion phenomenon. Ke and Takahashi (2014a) stated "Change of void ratio is caused by the fines loss (ΔV_f) and possible intergranular re-arrangement (ΔV_i)." They showed that changes in void ratio are equal to $\varepsilon_v(1+e_c)$ in which ε_v is considered positive if the specimen shows contractive behaviour or negative if it shows dilative behaviour during suffusion. Therefore, the post-suffosion void ratio is obtained by Eq. (2.2).

$$e = e_c - \varepsilon_v(1 + e_c) \tag{2.2}$$

Fannin and Slangen (2014) accurately explained the fluidisation phenomenon for upward seepage flow. Nevertheless, heave and loss of fine particles can happen simultaneously in upward flow. Dilation during internal erosion was later observed by Scholtès et al. (2010) when a shear stress ratio higher than the value related to the critical state was applied to a soil specimen before particle extraction. In addition, Ke and Takahashi (2014a) demonstrated that dilative behaviour can also occur after suffusion. It seems that more clarification is needed in relation to the suffosion phenomenon, especially regarding the type of volumetric deformation. To summarise, a few modifications are suggested by Mehdizadeh et al. (2015a) to make suffusion and suffosion definitions clearer:

- *Suffusion* should be characterised as seepage-induced mass loss without a change in volume and with or without any change in general hydraulic conductivity, but with a change in local hydraulic conductivity
- *Suffosion* should be characterised as seepage-induced mass loss accompanied by a change in volume and a change in hydraulic conductivity

It is understood that gap-graded cohesionless soils are vulnerable to suffusion. Suffusive soils may be observed in alluvium of rivers, embankment cores constructed of glacial soils, and filters where there is a mixture of coarse and fine particles without a certain amount of intermediate sizes. Fine particles in such structures can be transported by a seepage flow along pore spaces. For suffusion to occur, three criteria need to be met (ICOLD, 2015):

1) Coarse fraction must be dominant and make the primary soil structure. This means that the fine fraction must be less than a

threshold value above which coarse particles are floating in the matrix of fine particles (role of fine particles in soil structure)

2) Hydraulic stresses exerted by the seepage flow must be larger than effective stress on fine particles (critical hydraulic gradient)

3) Fine particles must be smaller than the constriction sizes between coarse particles (susceptibility of soil gradation)

Critical hydraulic gradient and susceptibility of soil gradation are discussed in sections 2.2 and 2.3, respectively.

2.2. Critical Hydraulic Gradient

Terzaghi (1925) found that there is a critical hydraulic gradient for sand material in an upward flow that reduces effective stresses to zero and initiates the erosion of soil particles. This critical hydraulic gradient was found to be about one, depending on soil density. However, the laboratory tests conducted by Skempton and Brogan (1994), Wan and Fell (2004 and 2007) and Ke and Takahashi (2012a) indicated that if a soil is internally unstable, onset of internal erosion occurs at a hydraulic gradient much lower than one. This was found to be attributed to the contribution of erodible particles to the primary soil skeleton. Skempton and Brogan (1994) defined the stress-reduction factor (α) to express the influence of fine particles in the soil stress matrix and the fraction of applied effective stresses that was supported by the fine particles (Eq. 2.3).

$$\alpha = \frac{\sigma'_f}{\sigma'_c} \tag{2.3}$$

where σ'_f and σ'_c are effective stresses acting on fine and coarse particles, respectively.

This factor varies in the range of almost zero to one based on the contribution of fine particles to the force chains. If fine particles are fully active in force chains and carry effective stresses at the same level of coarse particles, α is assumed to be one (non-erodible particles). If fine particles sit loose in the pore spaces with no contribution to load transferring, α is almost zero. For semi-active fine particles that provide lateral (secondary) support for the force chains, $0 < \alpha < 1$. When α is less than one, fine particles are vulnerable to erosion under hydraulic forces. Skempton and Brogan (1994) stated that α could be as small as 0.04 considering the required threshold gradient to move fine particles, regardless of gravity and flow direction. Kovacs (1981) and Li (2008) believed that α was related to d'_{85} (grain diameter for which 85% of the grains by weight of the fine soil are smaller) and O_{50} (actual opening size) as below (Eq. 2.4) (ICOLD, 2015):

$$\alpha = 3.85\left(\frac{d'_{85}}{O_{50}}\right) - 0.616 \tag{2.4}$$

For $\frac{d'_{85}}{O_{50}} \geq 0.42$, $\alpha = 1$ and coarse and fine particles carry stresses equally.

For $0.16 < \frac{d'_{85}}{O_{50}} < 0.42$, $0 < \alpha < 1$ and soil becomes increasingly unstable and more vulnerable to internal erosion.

For $\frac{d'_{85}}{O_{50}} = 0.16$ or less, $\alpha = 0$ and fine particles are easily transported out of the soil matrix.

Moffat and Fannin (2011) reported a hydromechanical relation governing the internal stability of cohesionless soils. They showed that the critical hydraulic gradient increased due to an increase in mean effective stress by performing erosion tests on specimens at different consolidation stresses. This relation was found to be linear, and initiation of internal instability can be triggered either by an increase in hydraulic gradient or by a decrease in effective stress. In other words, there is a combined impact of hydraulic and effective stresses that trigger internal erosion. Li and Fannin (2011) developed a theoretical envelope to assess the internal instability of cohesionless soils under upward flow (Eq. 2.5).

$$i = \frac{\alpha}{1-0.5\alpha}\left(\overline{\sigma}'_{vm} + \frac{0.5\gamma'}{\gamma_w}\right) \tag{2.5}$$

Where: $\overline{\sigma}'_{vm} = \overline{\sigma}'_{vm0} - 0.5i$ and $\overline{\sigma}'_{vm0} = \frac{\sigma'_{vm0}}{\gamma_w \Delta z}$ and σ'_{vm0} is initial mean vertical effective stress, γ_w is water density and Δz is the specimen height.

Moffat and Herrera (2014) presented a model that considers the equilibrium of a three-component system (water, soil skeleton and fine fraction) to calculate the critical hydraulic gradient for both upward and downward flow. This model took into account effective stress, porosity of the soil, friction angle between the coarse and fine particles and the portion of the effective stress transmitted by the fine fraction (Eqs. 2.6 and 2.7).

$$i_{cr} = \frac{G^*}{\gamma_w \Delta z}\left(\sigma'_v \,.\tan\left(\emptyset_\mu\right) + \Delta\sigma'_v\right) - \frac{n^f \rho^f g}{\gamma_w}, \text{ for downward flow} \qquad (2.6)$$

$$i_{cr} = \frac{G^*}{\gamma_w \Delta z}\left(\sigma'_v \,.\tan\left(\emptyset_\mu\right) + \Delta\sigma'_v\right) + \frac{n^f \rho^f g}{\gamma_w}, \text{ for upward flow} \qquad (2.7)$$

where G*= geometric-based stress reduction factor, $\Delta\sigma'_v$= variation of effective stress, $\emptyset_\mu$= true friction angle between particles of coarser and finer fraction, n^f= fine fraction volume ratio equal to $\frac{e}{S_f} \times 100$ (e= soil void ratio and S_f= finer fraction by mass (%)) and ρ^f= unit density of fine fraction.

The second part of Eqs. 2.6 and 2.7 considers the effect of the flow direction. Based on available data in their research, it appears that the effect of flow direction on critical hydraulic gradient is less than 5 per cent. This is in agreement with Moffat and Fannin's (2011) hypothesis that the hydromechanical envelope is independent of the direction of seepage flow. In addition, Ahlinhan and Achmus (2010) stated that an increase in instability of soils decreases the effects of flow direction. Therefore, neglecting the second part of these equations will not have a significant impact on the critical hydraulic gradient, especially for soils with higher internal instability potential.

Shire et al. (2014) investigated the stress-reduction factor in gap-graded soils using Discrete Element Modelling (DEM). It was shown that in internally stable soils with a low $(\frac{D'_{15}}{d'_{85}})_{max}$ value (i.e. ≤ 5), the fine particles are part of the main soil fabric and support the effective stress equally (i.e. α=1). For higher $(\frac{D'_{15}}{d'_{85}})_{max}$ values, the size of fine particles becomes smaller in comparison to the pore sizes. In these cases, the level of internal stability depends on the fine fraction. In other words, when the fine fraction is less than 25 per cent, the soil is underfilled and the fine particles can move through the pore network if they are small enough with respect to the pore sizes. Thus, the soil could be internally unstable. When the fine fraction is larger than 35 per cent, the soil is overfilled (internally stable) because the coarse particles are no longer in full contact with each other and both fine and coarse fractions together make the soil stress matrix. For the transitional zone, where the fine fraction is between 25 and 35 per cent, the contribution of fine particles in the force chain depends on D_r. In this case, the higher the D_r, the higher the stress-reduction factor. In the transitional zone, it appears that an increase in density increases the contact and interlocking of the fine and coarse particles, which leads to different pore sizes and stress distribution for the same gradation.

It is evident that apart from geometric susceptibility, contribution of fine particles in the soil skeleton is another substantial factor affecting initiation of suffusion. Therefore, the procedure suggested by Garner and Fannin (2010) needs to be followed for designing a granular filter. In addition, it was understood that there is no generalised or fully-approved method for accurately predicting the critical hydraulic gradient and the stress-reduction factor, which shows the importance of laboratory simulation and experimental investigation.

2.3. Geometric Susceptibility of Soil Gradation to Internal Stability

Geometric susceptibility of a soil to suffusion is related to internal stability of its Particle Size Distribution (PSD). It is a key factor in the design of granular filters in earth dams. A soil is classified as internally stable if all particles (fine and coarse) are involved in the soil structure and stress transferring. Kenney and Lau (1985) showed that all soils have a primary skeleton of particles that support load and transfer stress. However, in an internally unstable soil, a portion of particles are free to migrate into pre-existing pores by a hydraulic flow. The existing pores may vary in terms of dimension, concentration and number, depending on the PSD of soil and relative density (D_r). Therefore, the internal stability of a granular soil mainly depends on PSD and D_r. Overall, broadly graded glacial tills, alluviums with very broad gap-grading, broadly graded colluviums, broadly graded weathered granite and broadly graded drains in dams with excessive fine content are susceptible to suffusion (ICOLD, 2015). In general, a soil gradation curve with a steep slope in the coarse fraction zone and a flat slope in the fine fraction zone is vulnerable to internal instability (Wan and Fell, 2008). On the contrary, for practical gradient experienced in dams and their foundation, soils with plasticity index greater than seven can be considered as non-suffusive soils. However, if the experienced hydraulic gradient raises to four or higher, the critical plasticity index equal to 12 should be considered as the borderline between suffusive and non-suffusive soils (Fell et al, 2008). Segregation during stockpiling or construction is another concern than increases the potential of suffusion.

Internal stability of granular soils can be evaluated by different geometric methods. The literature review shows that widespread research has been carried out in this area, including semi-empirical, experimental and computational methods (e.g. U.S. Army (1953), Mao (2005) or Rönnqvist and Viklander (2014 and 2016)). Table 2-1 shows the most commonly used methods.

Table 2-1. Available methods to identify internal stability of soil gradation

Researchers	Year	Researchers	Year
Istomina	1957	Mao	2005
Kezdi	1969	Wan and Fell	2008
Sherard	1979	Indraratna et al.	2011
Kenney and Lau	1985, 1986	Salehi and Witt	2012
Kwang	1990	Dallo et al.	2013
Chapuis	1992	Chang and Zhang	2013
Burenkova	1993	Moraci et al.	2014

2.3.1. U.S. Army (1953) and Istomina (1957) Criteria

These two criteria are based on uniformity coefficient ($C_u = \frac{D_{60}}{D_{10}}$). A soil is classified as internally stable if:

- $C_u < 20$, U.S. Army (1953)
- $C_u \leq 20$, Istomina (1957)

2.3.2. Kezdi's (1969) and Sherard's (1979) Methods

Kezdi's (1969) and Sherard's (1979) methods were the simplest method to investigate internal stability of granular soils, and were based on the classical retention criteria for granular filters suggested by Terzaghi (1939). The soil gradation is divided into its fine and coarse fractions, and a soil gradation is internally stable if:

- Kezdi's Method: $D'_{15}/d'_{85} < 4$
- Sherard's Method: $D'_{15}/d'_{85} < 5$

D'_{15} and d'_{85} are shown in Figure 2-2. d'_{85} and D'_{15} can be read off from the gradation curve at ($0.85S_f$) and ($0.85S_f$+15) and S_f is a division point at fine content.

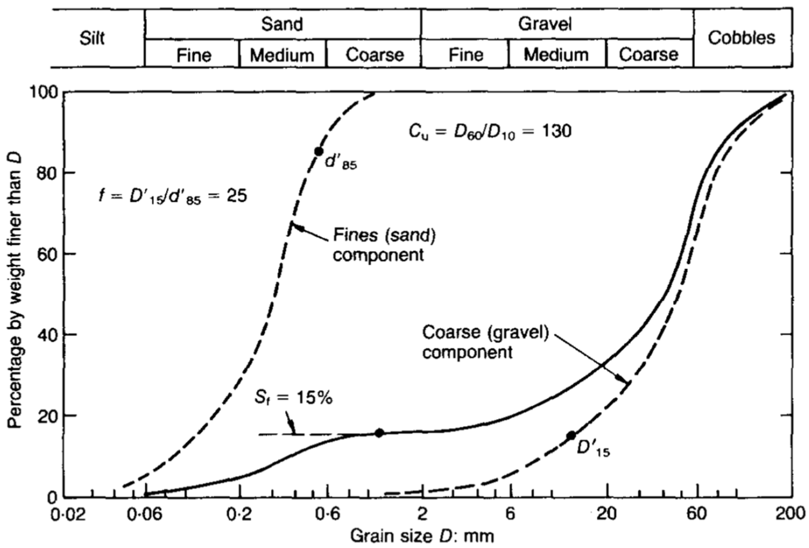

Figure 2-2. D'_{15} and d'_{85} definitions based on Kezdi's (1969) and Sherard (1979) methods (Skempton and Brogan, 1994)

2.3.3. Kenney and Lau's Method (1985 and 1986)

The method proposed by Kenney and Lau (1985 and 1986) is less direct than Kezdi's (1969) and Sherard's (1979). Their method is based on experimental results and theoretical analysis. At any point on the soil particle size distribution, the mass of fraction (*H*) is measured between particle diameters (*D*) and (*4D*) and plotted with the corresponding value of (*F*) (mass fraction smaller than *D*) (Figure 2-3). A soil is classified as internally unstable if:

- $H < 1.3F$ or $H < F$

Kezdi's (1969) and Kenney and Lau's (1985) methods were compared by Li and Fannin (2008) and Semar et al. (2011) based on the available laboratory results in the literature. It was found that Kezdi's method was more successful in distinguishing between internally stable and unstable gap-graded soils, while Kenney and Lau's method is stronger in predicting the potential of internal instability for widely graded soils. In addition, they showed that Kezdi's method was conservative for soils with fine content less than 15 per cent, while Kenney and Lau's method provided a more conservative result for soils with fine content greater than 15 per cent.

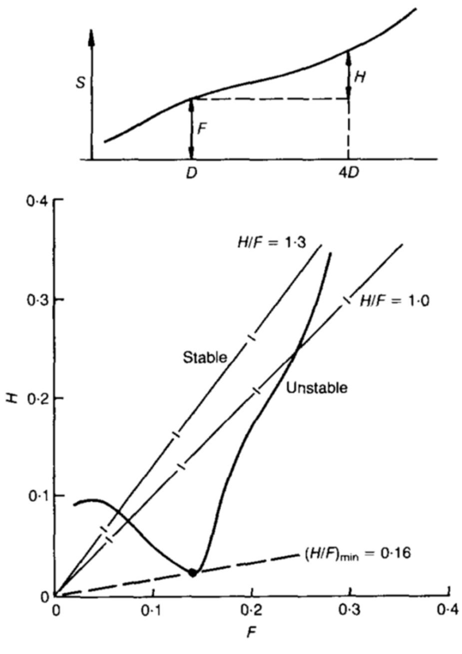

Figure 2-3. F and H parameters based on Kenney and Lau's method (1985 & 1986) (Skempton and Brogan, 1994)

2.3.4. Kwang's Method (1990)

This method is only applicable for gap-graded soil gradations and was developed based on the experimental investigation performed by Kwang (1990). Kwang (1990) found that for a gap-graded soil, internal instability occurs when Eq. 2.8 is satisfied:

$$\frac{D_{up}}{D_{bt}} > 4 \qquad (2.8)$$

where D_{up} and D_{bt} are the largest and smallest particles sizes of the flat zone (gap zone) on a gap-graded gradation curve, respectively (Figure 2-4).

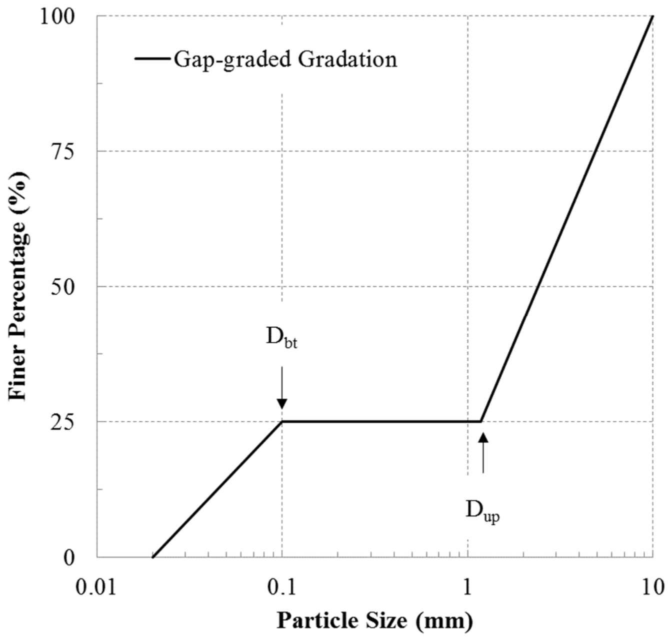

Figure 2-4. D_{up} and D_{bt} on a soil gradation curve

2.3.5. Chapuis's Method (1992)

Chapuis's method was a mathematical expression of previous methods presented by Kezdi (1969), Sherard (1979) and Kenney and Lau (1985). He found that potential of internal instability can be examined based on the secant slope (S) of the soil gradation curve (Figure 2-5).

- Kezdi’s (1969) criterion: soil is considered as internally unstable if there is a slope (S) lower than 24.9% per cycle (0.15/log 4) on the gradation curve.
- Sherard’s (1979) criterion: soil is considered as internally unstable when there is a slope (S) lower than 21.5% per cycle (0.15/log 4) on the gradation curve
- Kenney and Lau’s (1985) criterion: soil is considered as internally unstable if $S < 1.66F$ for each particle size less than or equal to D_{FC} ($FC \leq 30\%$)

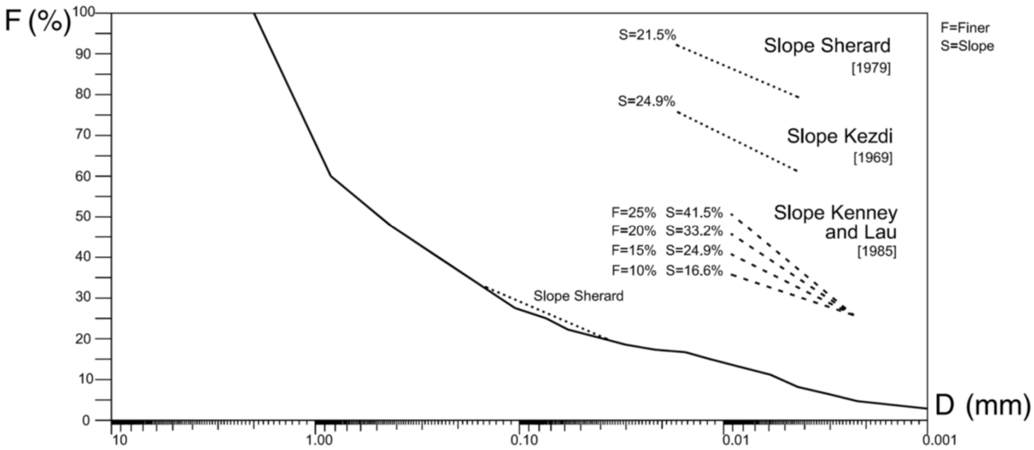

Figure 2-5. Internal instability potential according to Chapuis’s method (1992) (Moraci et al., 2014))

2.3.6. Burenkova’s Method (1993)

Burenkova’s method (1993) was based on the laboratory test results of 22 granular soil mixtures. Two criteria were defined to identify internally unstable soils based on D_{15}, D_{60} and D_{90} (Figure 2-6). Zones I and III represent suffusive soils, internally stable soils (non-suffusive) are located in Zone II, and Zone IV represents artificial soils with $\frac{D_{90}}{D_{60}} \geq \frac{D_{90}}{D_{15}}$. Boundaries of Zone II can be expressed by Eq. 2.9:

$$1 + 0.76\log(h'') \leq h' \leq 1 + 1.86\log(h'') \tag{2.9}$$

where $h' = \frac{D_{90}}{D_{60}}$ and $h'' = \frac{D_{90}}{D_{15}}$.

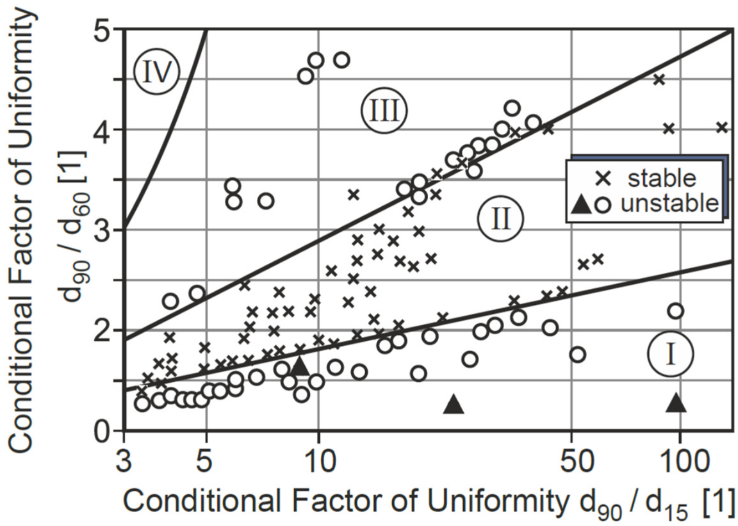

Figure 2-6. Internal instability potential according to Burenkova's Method (1993)

2.3.7. Mao's (2005) Criteria

According to Mao's (2005) Criteria, a soil is internally stable if:

- $4FC(1-n) \geq 1$ (2.10)

where FC in Eq. 2.10 is fine content in decimal and n is porosity.

2.3.8. Wan and Fell's Method (2008)

Wan and Fell (2007) stated that geometric methods suggested by Istomina (1957), Sherard (1979), Kenney and Lau (1985 and 1986) and Sun (1989) were conservative in assessing internal stability of silty sandy gravel soils. They developed a new geometric method based on the laboratory tests' results to assess the potential of internal instability for silt-sand-gravel or clay-silt-sand-gravel soils (Figure 2-7). They found that minor differences in the shape of PSD affects the internal stability of soil gradation and that for important projects, laboratory tests need to be conducted.

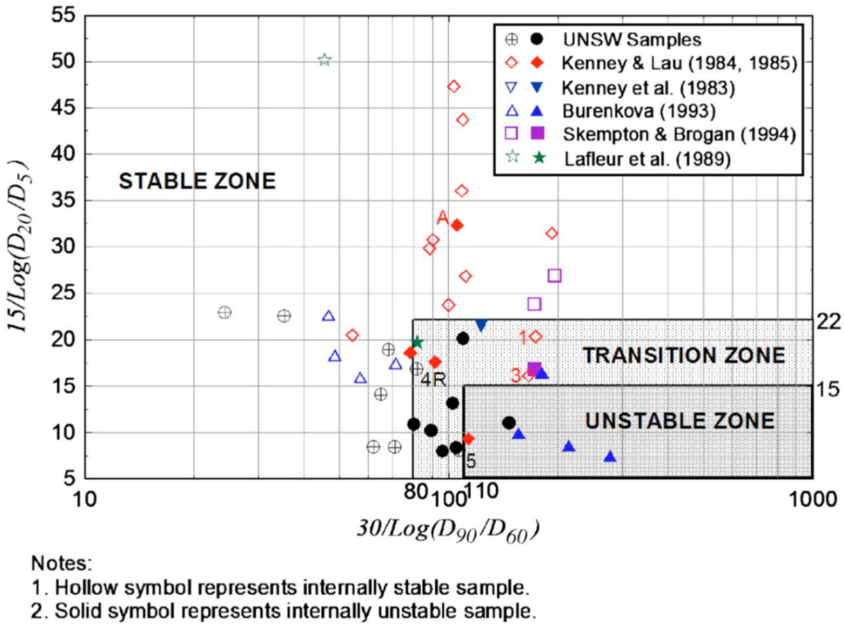

Figure 2-7. Assessing internal stability of broadly graded silt-sand-gravel soils (Wan and Fell's method, 2008)

2.3.9. Indraratna's et al. Method (2011)

Indraratna et al. (2011) stated that it is the controlling constriction size (D_c), rather than the particle size, that affects filtration and internal stability. Therefore, they proposed a mathematical method to determine the controlling constriction size, and subsequently a constriction-based retention criterion for granular filters. Controlling constriction size is defined as a void network size equal to the diameter of the largest particle that can be transported through the pore spaces by a seepage flow (Kenney et al., 1985 and Indraratna et al., 2007). To investigate internal stability of soils, two boundaries were proposed (Figure 2-8):

- Soil is internally unstable if $\frac{D_{c35}}{d_{85}^{f}} > 0.82$
- Soil is internally stable if $\frac{D_{c35}}{d_{85}^{f}} < 0.73$
- Further experimental investigation is required if a given soil falls in the transitional zone ($0.73 \leq \frac{D_{c35}}{d_{85}^{f}} \leq 0.82$)

Indraratna et al. (2007) found that for all practical purposes, a granular filter is unable to retain base soil particles smaller than D_{c35}. Therefore, D_{c35} was chosen as the controlling constriction size. D_{c35} is the constriction size when 35% of constrictions are smaller, and can be calculated using Eq. 2.11 proposed by Locke et al. (2001). Indraratna et al. (2007) developed a computer program to calculate $D_{c35(loosest)}$ and $D_{c35(densest)}$ which are D_{c35} at the loosest and densest states, respectively. However, they can be calculated by validated equations (2.12 and 2.13) suggested by Dallo et al. (2013).

$$D_{c35} = D_{c35(densest)} + 0.35\ (1 - D_r)\ (D_{c35(loosest)} - D_{c35(densest)}) \qquad (2.11)$$

Suggested equations for $D_{c35(densest)}$ and $D_{c35(loosest)}$ (Dallo et al., 2013):

$$D_{c35(densest)} = 0.177D'_{10} + 0.007D'_{15} + 0.003D'_{30} - 0.008D'_{60} - 0.003D'_{95} + 0.003 \qquad (2.12)$$

$$D_{c35(loosest)} = 0.437D'_{10} + 0.114D'_{15} + 0.008D'_{30} - 0.007D'_{60} - 0.015D'_{75} + 0.007D'_{95} - 0.012 \qquad (2.13)$$

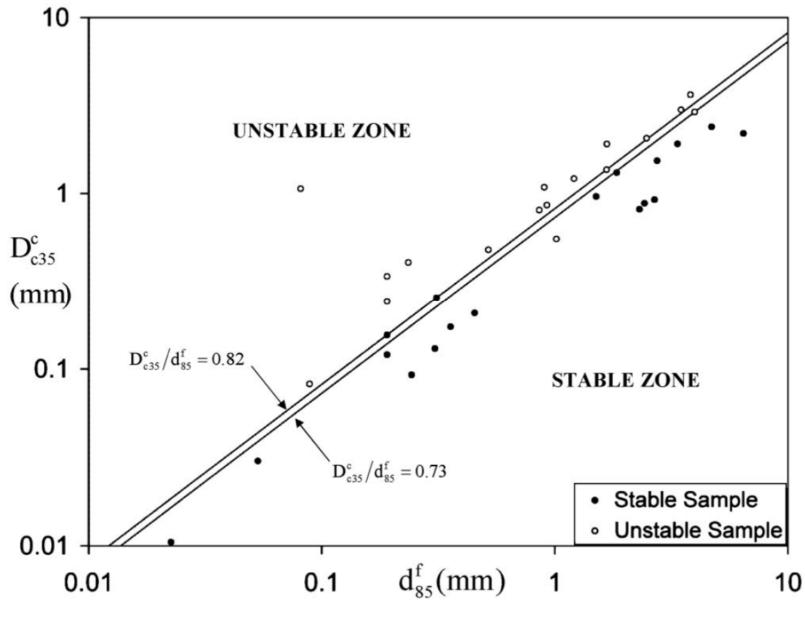

Figure 2-8. Determination of internal stability according to Indraratna’s et al. method (2011)

2.3.10. Salehi Sadaghiani and Witt's Method (2012)

Salehi Sadaghiani and Witt proposed a simple method for assessing internal stability of widely graded soils based on identification of mobile particles. They found that the soil is internally unstable if the slope of the soil gradation curve is less than 15.7 per cent in the semi-logarithmic particle size distribution plot (Figure 2-9).

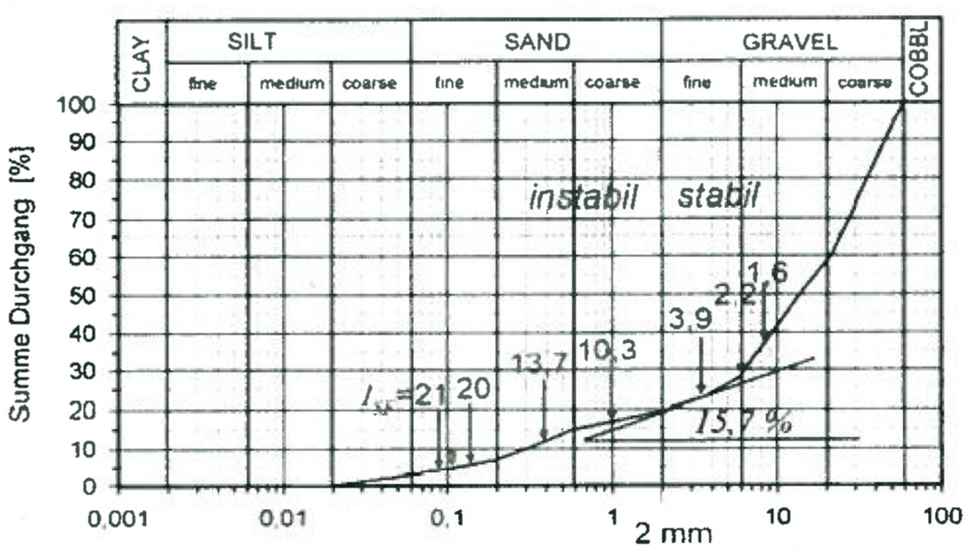

Figure 2-9. Assessing internal stability according to Salehi Sadaghiani and Witt (2012) (ICOLD, 2015)

2.3.11. Dallo's et al. Method (2013)

This method was based on Indraratna's et al method (2011). According to D_{c35} and d_{85}^{f}, three internal stability zones were defined as below (Figure 2-10):

- Soil is internally stable if $\frac{D_{c35}}{d_{85}^{f}} < 1$
- Soil is internally unstable if $\frac{D_{c35}}{d_{85}^{f}} > 1.05$
- Soils with $1 < \frac{D_{c35}}{d_{85}^{f}} < 1.05$ fall in the transitional zone and laboratory test needs to be conducted.

They believed that internal stability of granular filters can be examined more accurately using these criteria in comparison with previous methods. However, it was found that this method was not applicable for soils with $d_{85}^{f} > 1.18$ mm.

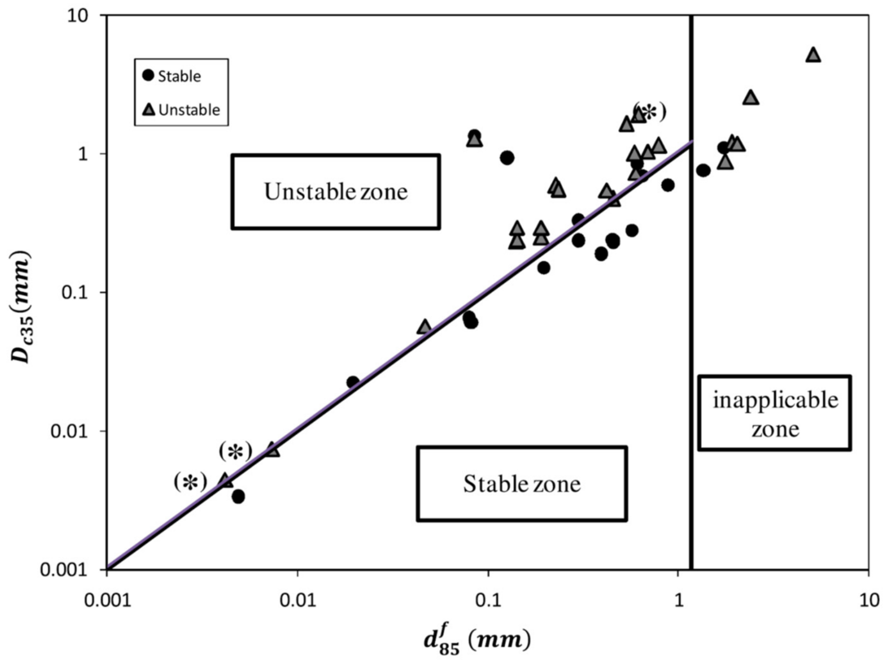

(*) tests of Moffat (2005) were under loading and very high hydraulic gradient

Figure 2-10. Design chart presented by Dallo et al. (2013)

2.3.12. Chang and Zhang's Method (2013)

Information of 131 soils, including gap-graded and well-graded soils, was investigated by Chang and Zhang (2013) to determine internal stability and controlling parameters. They found that the influential parameters that control internal stability were $(H/F)_{min}$ proposed by Kenney and Lau (1985) and fine content (FC) for well-graded soils and gap ratio (G_r) and fine content for gap-graded soils, as shown in Figures 2-11 and 2-12. Gap ratio is defined as ratio of the maximum particle size to the minimum particle size of soil gradation at the gap zone (flat zone) of a gap-graded soil gradation curve.

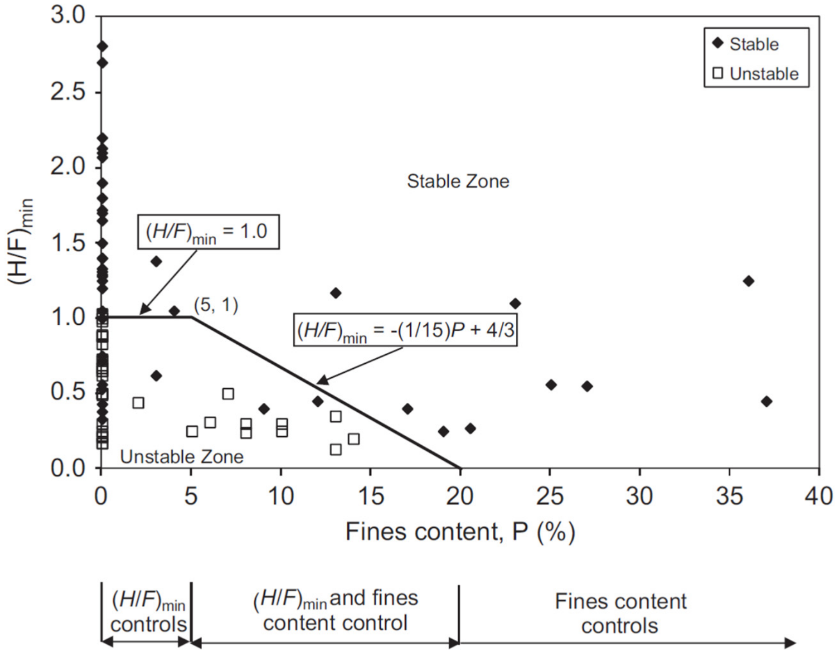

Figure 2-11. Geometric criteria for well-graded soils (Chang and Zhang, 2013)

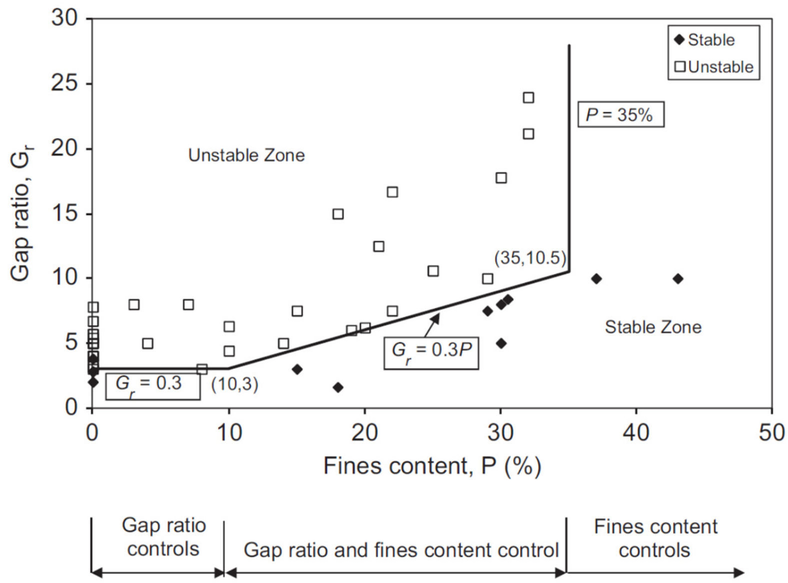

Figure 2-12. Geometric criteria for gap-graded soils (Chang and Zhang, 2013)

2.3.13. Moraci's et al. Method (2014)

Moraci et al. (2014) suggested a new chart for evaluating internal stability of granular soils (Figure 2-13). This chart was in fact a novel presentation of four previous semi-empirical approaches (Kezdi, 1969; Sherard, 1979; Kenney and Lau, 1985 and Chapuis, 1992). This new chart was based on percentage of finer for any particle size and the minimum slope of soil gradation (S_{min}). S_{min} can be calculated according to Figure 2-14. As demonstrated in Figure 2-13, all investigated approaches described a soil as internally unstable if it falls in the striped dotted zone and internally stable if it falls in the square dotted zone. Laboratory tests are required to assess internal stability of soil gradation for zones A and B. Zone A is the stable zone for Kenney and Lau's method (1985) and unstable for Sherard's (1969) and Kezdi's methods (1979) and vice versa for zone B.

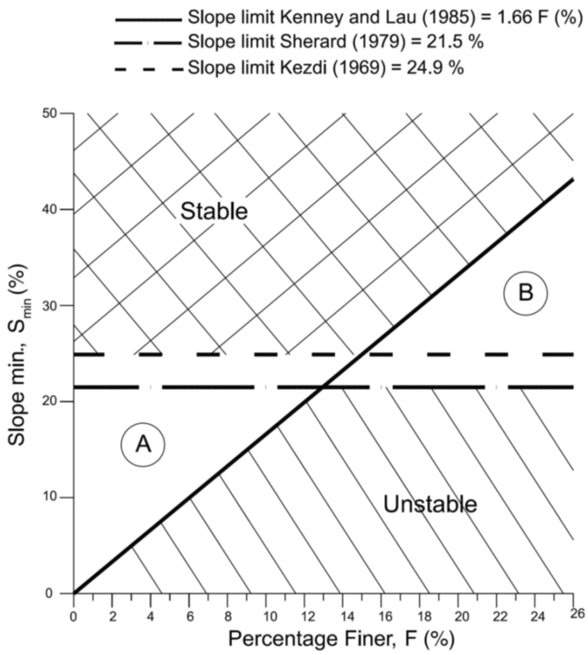

Figure 2-13. Butterfly wings chart proposed by Moraci et al. (2014) for assessing internal stability of granular soils

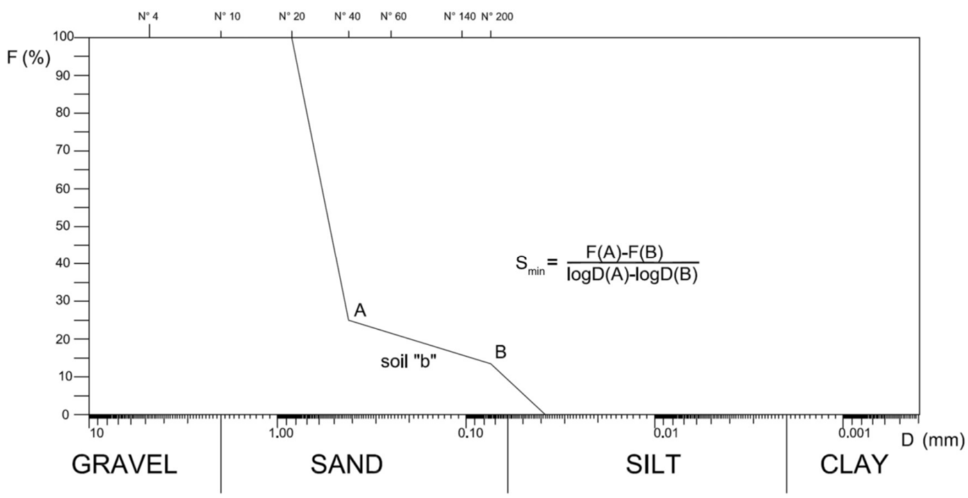

Figure 2-14. Example of evaluation of the minimum slope (Moraci et al., 2014)

All geometric methods evaluate susceptibility of soil gradation to internal stability. Table 2-2 briefly shows internal stability criteria of soil material based on some of the described methods.

Table 2-2. Internal stability criteria based on different methods

Method	Year	Criteria of Stability	Method	Year	Criteria of Stability
U.S. Army	1953	$C_u < 20$	Kwang	1990	$\frac{D_{up}}{D_{bt}} < 4$
Istomina	1957	$C_u \leq 20$	Mao	2005	$4FC(1-n) \geq 1$
Kezdi	1969	$D'_{15}/d'_{85} < 4$	Indraratna et al	2011	$\frac{D_{c35}}{d^f_{85}} < 0.73$
Sherard	1979	$D'_{15}/d'_{85} < 5$	Dallo	2013	$\frac{D_{c35}}{d^f_{85}} < 1$
Kenny and Lau	1985 and 1986	$H > 1.3F$ or $H > F$			

It is worth noting that none of these methods can draw any conclusion about the impact of fine particles erosion on soil behaviour. Many attempts have been made to improve the understanding of influential parameters on initiation and progression of fine particles removal. However, before discussing previous studies, it is necessary to understand the effect of non-plastic fine particles itself on soil behaviour regardless of the erosion phenomenon.

2.4. Effect of Non-plastic Fine Particles on Soil Behaviour

It is generally accepted that the shear strength of the silty sand or clayey sand can decrease or increase in comparison to the clean sand depending on the fine content, particle shape and the plasticity of the fine particles. Mitchell (1993) stated that in coarse skeleton soils, the fine particles are inactive in the soil matrix and can be considered as void in the coarse clusters depending their size, position and nature. As a result, they introduced a new index known as the granular void ratio index (Eq. 2.14).

$$e_g = \frac{e+FC}{1-FC} \tag{2.14}$$

where e_g is the granular void ratio, e is the global void ratio and FC is fine content in decimal.

Based on this concept, Thevanayagam (1998), Thevanayagam and Mohan (2000) and Thevanayagam et al. (2002) proposed a new framework for the microstructure and behaviour of a soil mixture with varying fine content. They showed that if the fine content was less than a threshold value, three subsets of the microstructure can be defined as following:

- Case-i: the coarse grain structure is stable and the fines are inactive and sit loose in the voids with minor participation in the force chain (filler)
- Case-ii: the coarse grain structure is unstable and the fines provide lateral support (secondary support) for the coarse grains
- Case-iii: the fine grains partially separate the coarse grains and contribute directly in transferring stresses. The coarse grain skeleton is unstable without the fine particles.

The recommended index to describe the microstructural characteristics for case-i is the granular void ratio (Eq. 2.3). However, due to contribution of the fine particles in force chains (laterally or directly as a separator), the influence of the fine particles need to be considered in case-ii and iii. Thevanayagam (2000) redefined the intergranular void ratio as the equivalent intergranular contact index ($e_{c_{eq}}$) (Eq. 2.15).

$$e_{c_{eq}} = \frac{e+(1-b)FC}{1-(1-b)FC}; \; 0<b<1 \tag{2.15}$$

where *b* is the portion of the fine particles that participate in the soil stress matrix. Case-i occurs when $b = 0$. When $b = 1$, all of the fine particles are involved in the soil skeleton (Case iii).

Thevanayagam (2001) showed that *b* depends on $C_{u_c}.{C_{u_f}}^2/R_d$, where C_{u_c} and C_{u_f} are uniformity coefficients of the coarse and fine components respectively, and R_d is the grain size disparity ratio equal to ${D'_{50}}/{d'_{50}}$. He calculated *b* equal to 0.35 for an

Ottawa sand-silt mix. Ni et al. (2004) showed that b is related to $\chi = \frac{d_{10,Host\,sand}}{d_{50,Silt}}$ and b will decrease with an increase in χ. They found b to be between 0.7-0.75 and 0.25 for old alluvium and Toyoura sand, respectively. However, Yang et al. (2006) and Rahman and Lo (2007) showed that b is not a constant parameter and is dependent on the fine fraction.

Rahman et al. (2011) proposed a semi-empirical equation to calculate b based on the available data (Eq. 2.16):

$$b = [1 - \exp(-0.3\frac{\left(\frac{FC}{FC_{Thr}}\right)}{k})](r\frac{FC}{FC_{Thr}})^{r} \tag{2.16}$$

where $r = \frac{d'_{50}}{D'_{10}}$, $k = 1 - r^{0.25}$ and FC_{Thr} can be determined by Eq. 2.17.

$$FC_{Thr} = 0.4(\frac{1}{1+e^{\alpha-\beta\chi}} + \frac{1}{\chi}); \text{ for } 2 \leq \chi \leq 42 \tag{2.17}$$

where $\chi = {}^{1}/_{r}$, $\alpha = 0.5$ and $\beta = 0.13$.

Contribution of fine particles in soil structure was investigated again by Thevanayagam (2007). He stated that stress-strain relationship, shear strength, cyclic resistance, modulus of elasticity and shear wave velocity are dependent on intergrain contact density of the soil containing coarse and fine particles, and the global void ratio is unable to describe the contact density. Thevanayagam (2007) proposed a new framework based on the level of intergrain contacts (Figure 2-15). Four different microstructures were defined based on the type of the primary grain contact.

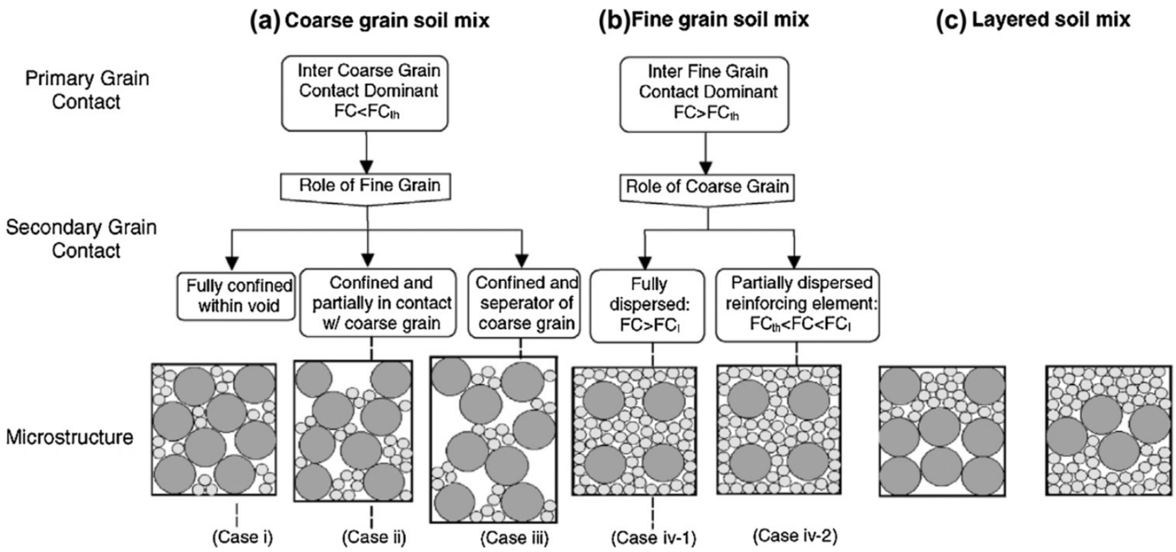

Figure 2-15. Intergranular soil mix classification (Thevanayagam, 2007)

The fine content is less than the threshold value (FC_{Thr}) in cases-i, ii and iii (Figure 2-15 (a)) and the primary soil skeleton is made by the coarse particles. In case-i, fine particles are fully confined in the pore spaces without any contribution in supporting the soil structure and play as filler. In case-ii, fine particles provide lateral (secondary) support for coarse grains. In the third case, some of the fine particles are sandwiched between coarse particles and transfer effective stresses equal to coarse particles. In case-iv (Figure 2-15 (b)), the fine content is greater than FC_{Thr} but less than the second critical fine content value (FC_l). In this case, the soil structure is made by fine particles and coarse particles are floating within fine grains matrix and carry a small percentage of effective stresses. For fine contents greater than FC_l, coarse particles are separated entirely, with no effect on soil behaviour. There is also a final category in which coarse and fine grains form a fully layered system, as shown in Figure 2-15 (c). This case is not common and is beyond the scope of this research.

The presence of silt size particles has been found to slightly improve the liquefaction resistance and increase the dilation tendency of sandy soils (Kuerbis et al., 1988 and Pitman et al., 1994). However, Evans and Zhou (1995) reported that gravely soils become more susceptible to liquefaction with an increase in sand content. Lade and Yamamuro (1997) showed that soil specimens with higher fine content liquefied at lower values of axial strain, even under higher relative density. In other laboratory experiments (e.g. Chang, 1990; Georgiannou et al., 1990; 1991a; 1991b; Chameau and

Sutterer, 1994; Vaid, 1994; Koester, 1994; Finn et al., 1994; Zlatovic and Ishihara, 1995), it was shown that an increase in the fine content decreases the steady state strength and cyclic resistance of silty sand. Thevanayagam (2000) suggested a new framework for silty soils to reflect the effect of fine particles on soil behaviour. He also stated that at the same global void ratio, an increase in fine content up to a threshold value increases the collapse potential; beyond that, the soil strength increases. This threshold value depends on the size disparity ratio (D'_{50}/d'_{50}, where D'_{50} is particle diameter for which 50% of coarse particles by mass are smaller and d'_{50} is particle diameter for which 50% of fine particles by mass are smaller), the global void ratio, and the void ratio of coarse (host) particles. A statistical analysis was conducted by Andrianopoulos et al. (2001) on a large dataset of triaxial tests. It was found that the presence of fine content improved liquefaction resistance when the mean effective consolidation stress was less than 86 kPa. For higher consolidation stress levels, liquefaction potential increased when the fine content increased.

Lade and Yamamuro (1997), Zlatovic and Ishihara (1995), Thevanayagam et al. (1997), Amini and Qi (2000) and Naeini and Baziar (2004) reported that the nature of silty sand is very different in comparison to clean sand; therefore, the global void ratio is unable to represent particle contact and interaction correctly. Therefore, it was decided to later consider the intergranular void ratio as a new index to describe the behaviour of silty sands (Thevanayagam, 1998; Chu and Leong, 2002; and Belkhatir et al., 2010). For example, a series of stress-controlled cyclic triaxial tests were conducted by Belkhatir et al. (2010) on silty sand with varying silt content. The intergranular void ratio was found to increase with silt content in the range of 0 to 50 per cent fine content, and the risk of liquefaction increased due to an increase in intergranular void ratio. Other researchers such as Baki et al. (2014), Qadimi and Mohammadi (2014) and Hsiao and Phan (2016) recommended the use of the state parameter (ψ) or equivalent granular state parameter (ψ*) to describe cyclic instability and strength of sand with varying fine content.

Cyclic triaxial tests conducted by Xenaki and Athanasopoulos (2003) indicated that in soil specimens with the same global void ratio, an increase in fine content from 0 to 44 per cent decreased the liquefaction resistance of mixtures compared to that of clean sand. This trend was found to be the opposite for fine content greater than 44 per cent. Based on laboratory test results, accompanied by data from field liquefaction failure case histories, Sadrekarimi (2013) reported that depending on effective stress, global void ratio, shape and mineralogy of fine particle, the undrained critical strength may decrease, increase or remain constant as the amount of fine content increases. The effect of non-plastic silt content on the liquefaction behaviour of a sand-silt mixture was examined by Karim and Alam (2014). It was found that the cyclic resistance decreased, with an increase in silt content, until a limiting silt content was reached. After this, the cyclic resistance remained relatively constant. The influence of non-plastic fine content on small-strain shear modulus and constrained elastic modulus, shear modulus degradation, damping ratio and threshold shear strain amplitudes was more recently studied by Wichtmann et al. (2015) using resonant column tests with additional P-wave measurements. Test results suggested that increasing the fine content decreased the small-strain shear modulus and constrained and the elastic modulus significantly. However, the shear modulus degradation curves were found to be rather independent of fine content. Moreover, a pressure-dependent reduction in the damping ratio and a slight increase in the threshold shear strain amplitudes with fine content was observed. Table 2-3 summarises previous studies in this area. The table shows that depending on sample preparation method, particle shape and percentage of fine particles, shear strength may decrease or increase with an increase in non-plastic fine content.

Table 2-3. Effect of percentage of fine particles on soil behaviour

Researchers	Year	Research Topic	Conclusion
Ishihara	1993	Liquefaction	Undrained peak shear strength decreases with an increase in non-plastic fine content.
Pitman et al.	1994	Influence of fines on the collapse of loose sands	By increase in fine content, undrained brittleness decreased. Structural instability decreases with an increase in fines content.
Thevanayagam et al.	1997	Effects of fines on monotonic undrained shear strength of sandy soils	Fine particles control the shear strength and by an increase in fine content, undrained shear strength decreases.
Lade and Yamamuro	1997	Effects of non-plastic fines on static liquefaction of sands	Liquefaction potential increases by an increase in fine content.
Thevanayagam et al.	2000	Effect of non-plastic fines on undrained cyclic strength of silty sands	At same global void ratio, an increase in fine content decreases the cyclic strength.
Salgado et al.	2000	Shear strength and stiffness of silty sand	Silty sands with silt content 5-20% show more dilatancy than clean sands. Small-strain stiffness drops but shear strength increases with increasing the fines content.
Andrianopoulos et al.	2001	Effect of fines content on cyclic liquefaction resistance	Liquefaction resistance improves due to the presence of fines for mean effective consolidation stress less than 86 kPa and decreases thereafter.
Carraro et al.	2003	Liquefaction resistance of clean and non-plastic silty sands based on cone penetration resistance	The cyclic resistance of sand with less than 15% silt content is higher than clean sand. After that, fine particles control the soil response and reduce the particle interlocking.
Naeini and Baziar	2004	Effect of fines content on steady-state strength of mixed and layered samples of a sand	Peak and residual strength decrease by an increase in silt content up to 35%.
Ni et al.	2004	Contribution of fines to the undrained compressive strength of a mixed soil	The hardness of non-plastic fines and host sand is nearly the same and they contribute to the strength of the mixture to some extent. Addition of non-plastic crushed silica increased the critical friction angle.
Murthy et al.	2007	Undrained monotonic response of clean and silty sand	Critical friction angle of sand increases with an increase in non-plastic fine content. Contribution of fine particles increases at the critical state by increasing the angularity of fine particles and sphericity of the coarse particles.

Table 2-3. Effect of percentage of fine particles on soil behaviour (continued)

Researchers	Year	Research Topic	Conclusion
Carraro et al.	2009	Effect of non-plastic fines on shear strength and stiffness of sands	Peak and critical state friction angles of the soil increase by an increase in non-plastic silt content due to angularity of fine particles.
Belkhatir et al.	2010	Influence of intergranular void ratio on monotonic and cyclic undrained shear response of sandy soils	Increase in fine content decreases undrained shear strength and cyclic resistance of sand-silt mixture.
Dash and Sitharam	2011	Effect of non-plastic fine on undrained monotonic response	For fine content up to 5%, the peak strength increases. It then decreases rapidly until the threshold silt content.
Yin and Hicher	2013	Modelling of the effect of internal erosion on the behaviour of silty sand	The undrained strength of silty sand decreased due to a decrease in the silt content.
Ke and Takahashi	2014b	Post-erosion behaviour of gap-graded soils	Presence of fine particles decreases the soil strength.
Karim and Alam	2014	Effect of non-plastic silt content on the liquefaction behaviour of sand-silt mixture	Increasing the silt content up to a limiting content decreases the cyclic resistance and thereafter remains nearly constant.
Andrianatrehina et al.	2016	Influence of sand content on gap-graded cohesionless soils behaviour	Reduction in fine content reduces the monotonic undrained peak strength.

2.5. Investigation of Internal Erosion - Experimental Approach

Experimental investigation of internal erosion and influential parameters is presented chronologically in this section from 1984. Each study discussed in this section is described in terms of methodology and achievement, in order to gain insight into which areas are currently overlooked in current literature.

Sherard et al. (1984) were one of the first research groups to investigate sand and gravel filters' properties using a laboratory apparatus. A downward seepage flow was exerted on the top of the base material, and the discharged water and base sand particles were collected. Experiments showed that the accepted criterion of $D'_{15}/d'_{85} \leq 5$ for assessing internal stability was conservative.

Controlling constriction size (D_c^*) was investigated by Kenney et al. (1985). Hydraulic and dry-vibration tests were carried out using two sizes of permeameter cells. To avoid large void channels along the cell wall and the filter material, D_{100} of the filter material was kept less than ${}^{1}/_{10}$ of the cell diameter. A large downward seepage flow was maintained across the filter to wash the erodible particles. Results indicated that D_c^* was only dependent on the size of fine particles.

Kenney and Lau (1985) examined the internal stability of a variety of compacted cohesionless materials using two seepage cells. A new geometric method for assessing internal stability of cohesionless soils was developed based on the test results, as presented in section 2.3.3.

Filtration of broadly graded cohesionless soils was investigated by Lafleur et al (1989). Two series of tests, screen and compatibility, were conducted using a modified permeameter cell. The tests were conducted under downward hydraulic gradients ranging 2.5-6.5. They found that self-filtration of broadly graded soils was related to ratio of $\frac{O'_{50}}{d_0}$ and the profile of the gradation curve.

A seepage-failure test apparatus was developed by Tanaka and Toyokuni (1991) to investigate hydraulic failure of multi-layered sands. It consisted of a seepage cylinder, a constant-head device and an open piezometer. Three different sands of Naka-Umi sand, Lake-Biwa sand and River sand were used in this study. The seepage cylinder was subjected to an upward hydraulic flow with a constant head. It was understood that a one-layered sand with a low relative density failed at a hydraulic gradient smaller than the theoretical critical gradient.

Experimental investigation conducted by Skempton and Brogan (1994) indicated that apart from susceptibility of the soil gradation, contribution of fine particles in stress transferring had an impact on erodibility of fine particles. Several soil gradations were subjected to upward seepage flows using a modified rigid wall permeameter to explore initiation of fine particles erosion. They found that the fine particles that were not fully involved in the soil skeleton were eroded under a critical hydraulic gradient much lower than the theoretical gradient suggested by Terzaghi (1925).

Internal stability of gap-graded cores and filters was studied by Garner and Sobkowicz (2002). A large-scale permeameter was used, and the effect of upward gassy water flows was examined. At the end of the experiment, frozen carbon dioxide was injected into the bottom of the soil specimens, which were then transferred to Santa Susanna rocket test field site in order to conduct computed tomography (CT) scans. It was found that suffusion led to a significant drop in permeability.

Moffat and Fannin (2006) modified a permeable cell to assess internal stability. This apparatus was capable of applying axial load during the erosion phase. A gap-graded soil specimen was prepared using a slurry deposition technique. This apparatus was also used by Moffat and Fannin (2011) and Moffat et al. (2011). Moffat and Fannin (2011) suggested that there was a relationship between effective stress and critical hydraulic gradient. Internal erosion initiated by a decrease in effective stress or an increase in hydraulic gradient. Regardless of which trigger initiated the erosion, the same soil response was observed. Moffat et al. (2011) found that suffusion was a time-dependent phenomenon and changed local hydraulic conductivity. However, soil specimens that experienced suffusion for an extended period of time or higher hydraulic gradients eventually settled and collapsed which is known as suffosion.

A wide range of soil gradations, including silt-sand gravel and clay-silt-sand-gravel soils, were investigated by Wan and Fell (2008). A downward seepage flow with constant head was applied to the top of the specimens and maintained until no fine particle was washed out from the test sample. A new geometric approach was suggested based on the experimental results for assessing internal stability of broadly graded silt-sand-gravel soils.

Richards and Reddy (2008, 2009 and 2012) used a new true-triaxial load chamber. This system was capable of applying different loading paths along three orthogonal axes using pressurised water. They concluded that there was a relationship between confining pressure and critical hydraulic gradient, and that the maximum principal stress was more effective than the intermediate or minor stresses on potential of erosion. The critical seepage velocity was affected by the seepage angle; hence, exit velocity was a better index than the hydraulic gradient for assessing piping potential. In addition, it was revealed that suffusion was the primary mode of piping failure for soil mixtures containing low plastic fine such as kaolin, while a soil with high plastic fines required significantly higher seepage velocity to induce piping.

A new experimental device was developed by Bendahmane et al. (2008) based on an ordinary triaxial apparatus for evaluating initiation of internal erosion in sandy clay samples (Figure 2-16). Applying various vertical and horizontal confining stresses and minimising side wall leakage were the main advantages of this system. In fact, one of the main concerns of previous internal erosion studies in the rigid wall permeameter was the formation of a preferential seepage path at the interface of soil and the permeameter cell wall, which can affect the initiation of erosion significantly. Washed Loire sand with kaolinite contents was used to prepare triaxial samples that were 50 mm in diameter and height. Test results indicated that erosion of clay particles began first; this was classified as suffusion. However, there was a second threshold in the hydraulic gradient above which erosion of sand particles initiated. This led to backward erosion, and eventually the collapse of the entire sample. It was understood that suffusion and backward erosion both were affected by initial clay content. When clay content changed from 20 to 10 percent, the maximum erosion rate of clay particles doubled. In addition, no sand grain erosion was observed for specimens with clay content more than 10 per cent. Confining pressure was another influential parameter on erosion. Erosion rate decreased with an increase in the confining pressure.

Variation of hydraulic conductivity, water flow rate and angularity of coarse particles was investigated by Marot et al. (2009 and 2012a) and Nguyen et al. (2012) using a modified erosion-triaxial apparatus. Test results suggested that erosion of clay particles was accompanied by a clogging in the specimen and a decrease in hydraulic conductivity. Moreover, angularity of coarse particles improved erosion resistance. This apparatus later was used to develop a new interpretative method by Sibille et al. (2015) and Marot et al. (2016) to determine suffusion susceptibility of the cohesionless soils and clayey sand. These methods linked the cumulative dry mass of eroded particles to dissipated energy by the fluid flow.

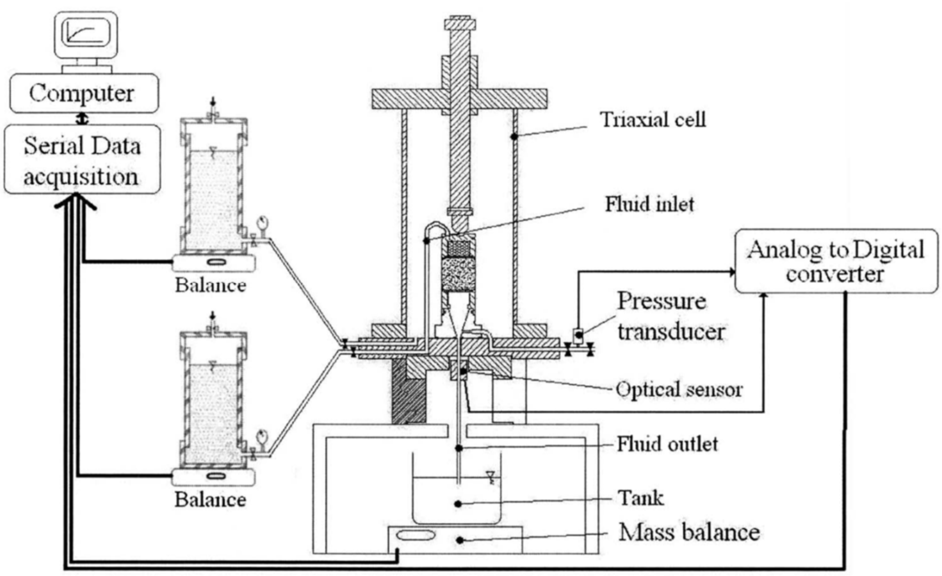

Figure 2-16. Schematic representation of the modified triaxial apparatus for erosion test (Bendahmane et al., 2008)

Erosion of fine particles due to deep pumping wells in urban areas can lead to settlement of shallow foundations (Cividini et al., 2009). A seepage test program was defined by Cividini et al. (2009) to estimate the quantity of eroded material in the vicinity of pumping wells. An experimental setup was adapted based on the experiment conducted by Sterpi (2003). A constant head was applied to the bottom of the specimen to provide an upward flow across the soil specimen height for a maximum duration of 1600 hours. They found that the rate of erosion decreased with time for a constant hydraulic gradient, and that variation of permeability was marginal.

Another triaxial-erosion apparatus was developed by Shwiyhat and Xiao (2010) (Figure 2-17) to study the variation of permeability and volumetric strains during erosion. Clay-silt-sand mixture with approximately 5.5 per cent fine content was prepared under the optimum moisture content and subjected to a constant downward hydraulic gradient. Test results showed that permeability and erosion rate decreased during erosion, which were believed to be due to clogging. Erosion of fine particles led to the specimen settlement and a reduction in the sample volume with a declining rate.

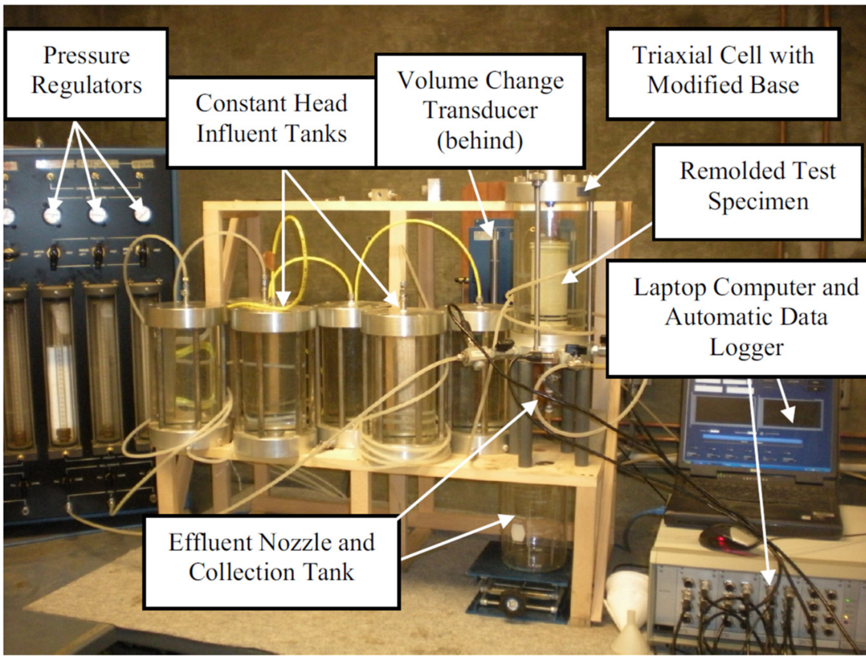

Figure 2-17. Triaxial-erosion test setup (Shwiyhat and Xiao, 2010)

Undrained compressive strength of eroded specimens was later measured using this apparatus (Xia and Shwiyhat, 2012). An increase in the post-erosion undrained compressive strength was observed without a clear conclusion for the reason. However, Xia and Shwiyhat, 2012 thought that this might have been due to loss of saturation during the erosion phase as the bottom of the specimen was subjected to the atmospheric pressure. They recommended that increasing the soil specimen dimensions prevents the effect of boundary condition and provides a better simulation of practical conditions. In addition, they believed that the bottom screen mesh that held the soil specimen while allowing erodible particles be washed out was not selected properly, impacting the test results.

An experimental study was carried out to investigate the dependency of critical hydraulic gradient on the flow direction and soil relative density by Ahlinhan and Achmus (2010) and Ahlinhan et al. (2012). Cylindrical soils samples were prepared for upward vertical seepage tests using the pluviation technique under de-aired water. The required relative density was achieved by vibrating compaction. For the horizontal seepage flow, another test setup was developed. Research results indicated that regardless of flow direction, the critical hydraulic gradient was about 0.2 for internally unstable soils with a minor dependency to relative density. However, for soils on the border of internally stable and unstable, the effect of relative density was substantial. In addition, it was found that the difference between the vertical and horizontal critical hydraulic gradients increases for stable soils.

A stress-controlled erosion apparatus was developed by Chang and Zhang (2011). This system was capable of applying different stress paths during the erosion phase and post-erosion shearing (Figure 2-18). A gap-graded soil with 35 per cent non-plastic fine content was used in this research. Triaxial specimens 100 mm in height and diameter were prepared according to Ladd's (1978) procedure. Saturation, consolidation and erosion were conducted continuously, and mechanical consequences of erosion of non-plastic fine particles were investigated during monotonic drained shearing (Chang and Zhang, 2012; Chang et al., 2012; Chang et al., 2014). Similar to Shwiyhat and Xiao's (2010) apparatus, the bottom of the sample was subjected to atmosphere. The B-value measured 0.85 for most of the tests, which showed that full saturation was not reached. Two critical hydraulic gradients were detected for initiation of internal erosion and deformation of the soil skeleton during the erosion stage. During the initiation phase, only a slight increase in permeability occurred. However, when the hydraulic gradient reached the second threshold, a sudden increase in the eroded particles' mass, permeability and deformation was observed. Loss of a significant amount of fine particles increased the global void ratio, changed the original dilative stress-strain behaviour to contractive behaviour, and decreased the drained peak shear strength. It was found that the peak friction angle reduced by 1.1-5.9 degrees due to loss of 2.5-6.8 per cent fine particles. They suggested that the skeleton-deformation critical gradient can be used for geotechnical design, as a massive change occurs in the soil structure after experiencing this critical hydraulic gradient. Post-erosion particle size distribution (PEPSD) showed that more fine particles were eroded in the top regions of specimens than the bottom parts.

In a separate study, Chen et al. (2016) investigated post-erosion drained behaviour of the tested soil using a dissolution technique, replacing a certain amount of fine particles with salt. The result confirmed the previous study conducted by Chang and Zhang, (2011) that erosion of fine particles increased the global void ratio and decreased the shear strength. The effect of stress path on initiation and progression of erosion was also investigated. Under the same confining stress, the maximum erosion rate and the total weight of the eroded particles increased due to an increase in the deviator stress. Initiation of erosion occurred at a higher hydraulic gradient under triaxial extension stress condition in comparison to the compression condition.

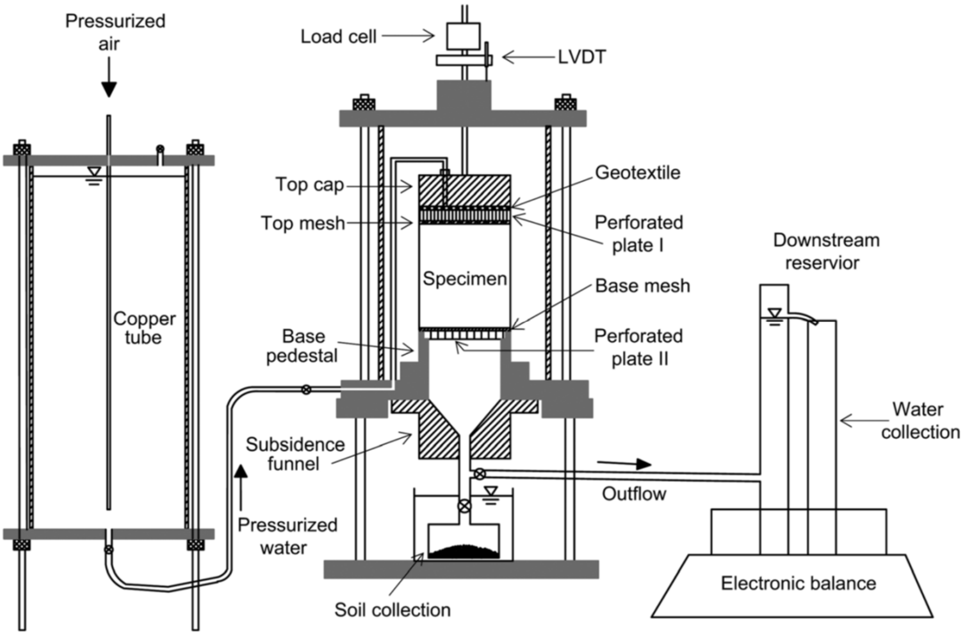

Figure 2-18. Schematic testing apparatus developed by Chang and Zhang (2011)

The effect of applied hydraulic gradient and the specimen length on internal erosion initiation was investigated by Le et al. (2010) and Marot et al (2012b) using centrifuge modelling. A downward seepage flow with a constant head was applied to the top of the specimen to wash the fine particles out of the bottom of the specimen. The soil specimen was a mixture of 90 per cent Fontainebleau sand and 10 per cent clay. This centrifuge modelling indicated that removal of fine particles were dependent on the seepage length. Test results showed that erosion rate increased by a factor of two, and the critical hydraulic gradient decreased by a factor of 0.6 when the specimen length doubled. They believed that the length of the seepage path affected the potential of clogging and filtration.

A new permeameter rigid wall with the ability to measure soil density was developed by Marot et al. (2011a). The gamma-densitometric system was presented first by Alexis et al. (2004). It consisted of a radioactive gamma-ray source and a scintillation counter on the opposite cell side. This system was adapted to a modified permeameter cell to measure soil density along the specimen height pre- and post-suffusion test. Artificial soil specimens were subjected to downward hydraulic gradients. Glass bead mixtures with different fine contents were prepared using the slurry deposition technique suggested by Moffat and Fannin (2006). Test results indicated that the erosion process started first by suffusion, with minor effect on hydraulic conductivity and density. However, a blowout occurred due to further erosion of fine particles, which led to settlement and a considerable increase in hydraulic conductivity. In addition, it was found that soil density decreased at the lower regions of the specimen, and localised interstitial overpressures were detected due to clogging.

Ke and Takahashi (2011, 2012a and 2012b) used a permeameter cell to investigate the impact of internal erosion on bearing capacity of a cohesionless soil using a miniature cone penetrometer. A series of gap-graded soil specimens with different fine contents and relative densities were prepared using a moist tamping method, and were subjected to an upward seepage flow (Figure 2-19). Their experiments confirmed Skempton and Brogan's theory (1994) that in the internally unstable materials, erosion initiates at a hydraulic gradient much lower than Terzaghi's theoretical value. In addition, it was observed that with an increase in the fine content, internal erosion occurred at a lower hydraulic gradient, and the critical hydraulic gradient rose due to an increase in the relative density. They found that internal erosion caused by an upward flow decreased the cone tip resistance. In other words, loss of fine particles resulted in a reduction in the internal friction angle of soil specimens. However, this reduction was less than two per cent in most of their tests with no specific reason provided for this strength reduction (Ke and Takahashi, 2011, 2012a and 2012b).

More recently, Ke and Takahashi (2014b) modified a triaxial chamber to conduct all test phases, including saturation, consolidation, erosion and shearing in a triaxial cell to prevent the specimen disturbance. They developed a new system to collect the discharged water and the eroded particles without loss of saturation (Figure 2-20). Their research focused on the drained and undrained behaviour of a gap-graded soil with various fine contents and confining pressures under monotonic and cyclic loadings pre- and post-erosion. It was found that the post-erosion drained shear strength decreased, while the eroded specimen reached a higher undrained peak shear strength at small strains. In addition, one cyclic triaxial test was performed indicating a higher cyclic resistance for the eroded specimen.

The effect of initial fine content and confining pressure on drained and undrained monotonic shearing of eroded specimens was studied by Ke and Takahashi (2014a), Ke and Takahashi (2015), Ouyang and Takahashi (2015a) and Ke et al. (2016). Drained shear strength of specimens with 15 and 25 per cent initial fine contents did not change after erosion in contrast to the specimen with initial fine content of 35 per cent which showed a drop in shear strength. Surprisingly, the residual post-erosion fine content was approximately similar (10 to 13 per cent) for all specimens under the same confining pressures and hydraulic conditions. In other words, the specimens with higher fine contents lost their fine particles more during the erosion phase. However, apart from the specimen with 35 per cent fine content, erosion of the fines did not affect the mechanical behaviour of the two other specimens. It was also understood that an increase in initial effective confining pressure reduced erosion of fine particles and the drop in the soil strength after suffusion. Moreover, eroded specimens showed larger undrained secant stiffness compared to the non-eroded specimens at a relatively small axial strain level (Ke and Takahashi, 2015 and Ouyang and Takahashi, 2015a).

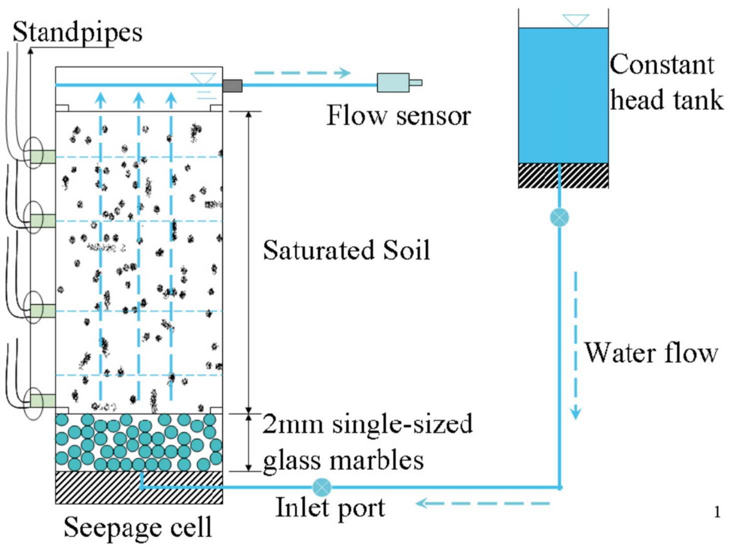

Figure 2-19. Schematic diagram of seepage test (Ke and Takahashi, 2011)

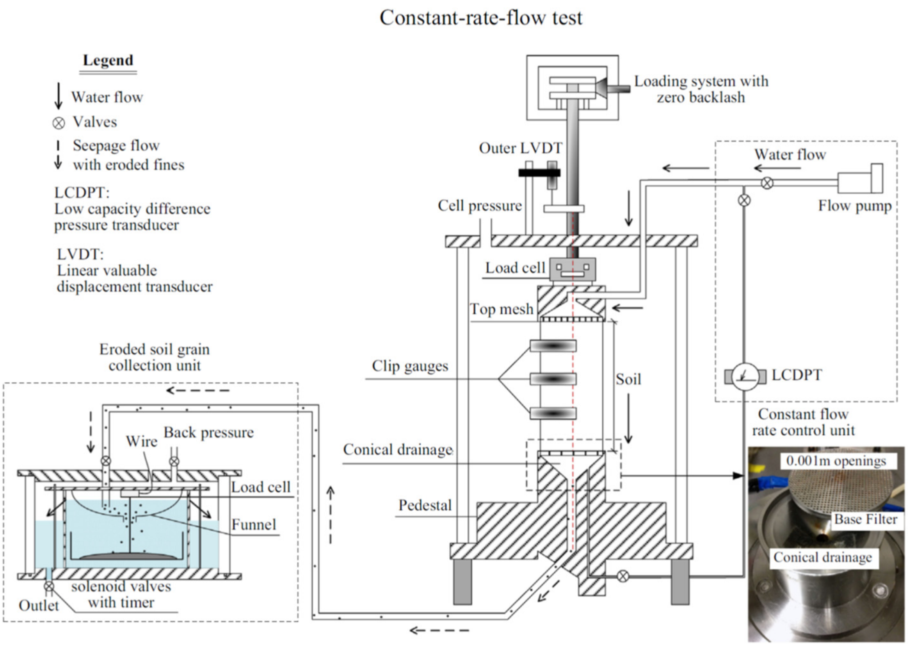

Figure 2-20. Schematic diagram of erosion-triaxial apparatus modified by Ke and Takahashi (2014a and b)

The erosion of fine particles was reproduced by the dissolution of selected salt particle sizes and fractions from a sand-salt mixture by Kelly et al. (2012). A triaxial chamber was modified to allow circulation of pore-fluid through the soil specimen to solve salt particles. Concentration of salt in the returned flow was measured by a conductivity meter, and shear wave velocity was measured using bender element (Figure 2-21). Sand-salt mixtures were prepared by mixing Leighton buzzard sand and 15 per cent salt content (fine content) with various salt particle sizes. Test results indicated that the removal of salt particles increased the global void ratio and decreased the shear strength. Volumetric strains and strength behaviour were found to be dependent on the size and fraction of removed particles. In addition, shear wave measurement indicated significant changes in small strain stiffness.

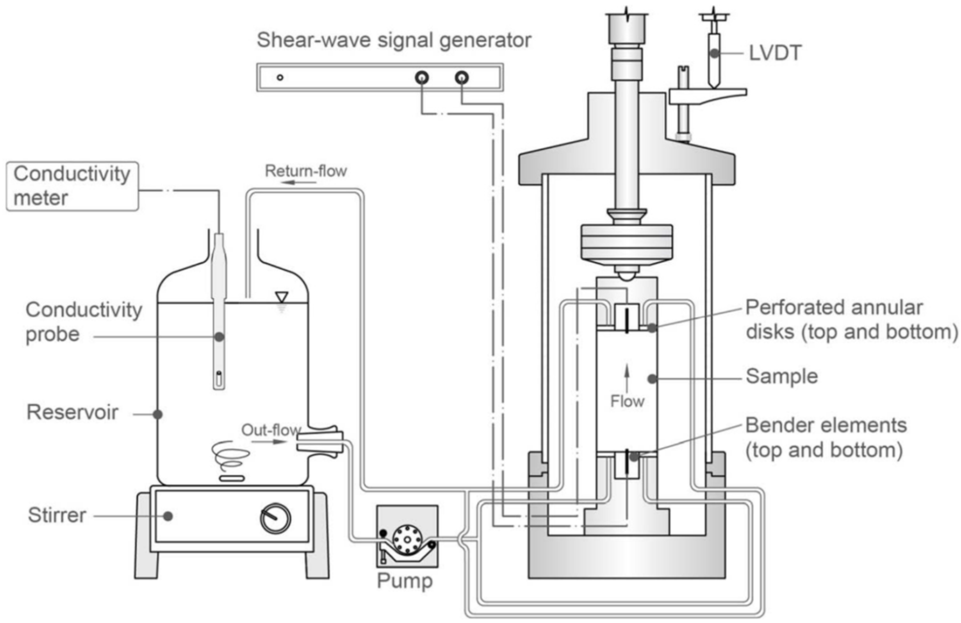

Figure 2-21. Modification of a triaxial apparatus to allow circulation of pore-fluid (Kelly et al., 2012)

A new experimental device was developed by Sadaghiani and Witt (2012) to study hydraulic impacts on reconstituted cohesionless soils. Test results revealed that the homogeneity of the soil structure and preferential flow paths affected vulnerability of soil to suffusion. Minor change in the shape of particle size gradation affected internal stability, and depending on the soil gradation and hydraulic gradient, the stability of soil structure may improve or reduce due to seepage forces.

Luo et al (2013a) investigated the effect of confining pressure and seepage duration on initiation and progression of suffusion using a newly developed hydro-mechanical coupling apparatus (Figure 2-22). In the first series of seepage tests, hydraulic gradients increased gradually until suffusion failure occurred. In the second series, a hydraulic gradient lower than the failure magnitude was chosen and applied for a long period of time (8,000-11,000 mins). Results indicated that the suffusion failure was accompanied by a sudden decrease in the hydraulic gradient and a sharp increase in the eroded mass. In addition, it was found that if a soil specimen is subjected to a hydraulic gradient lower than the failure value for a long period, suffusion failure might occur.

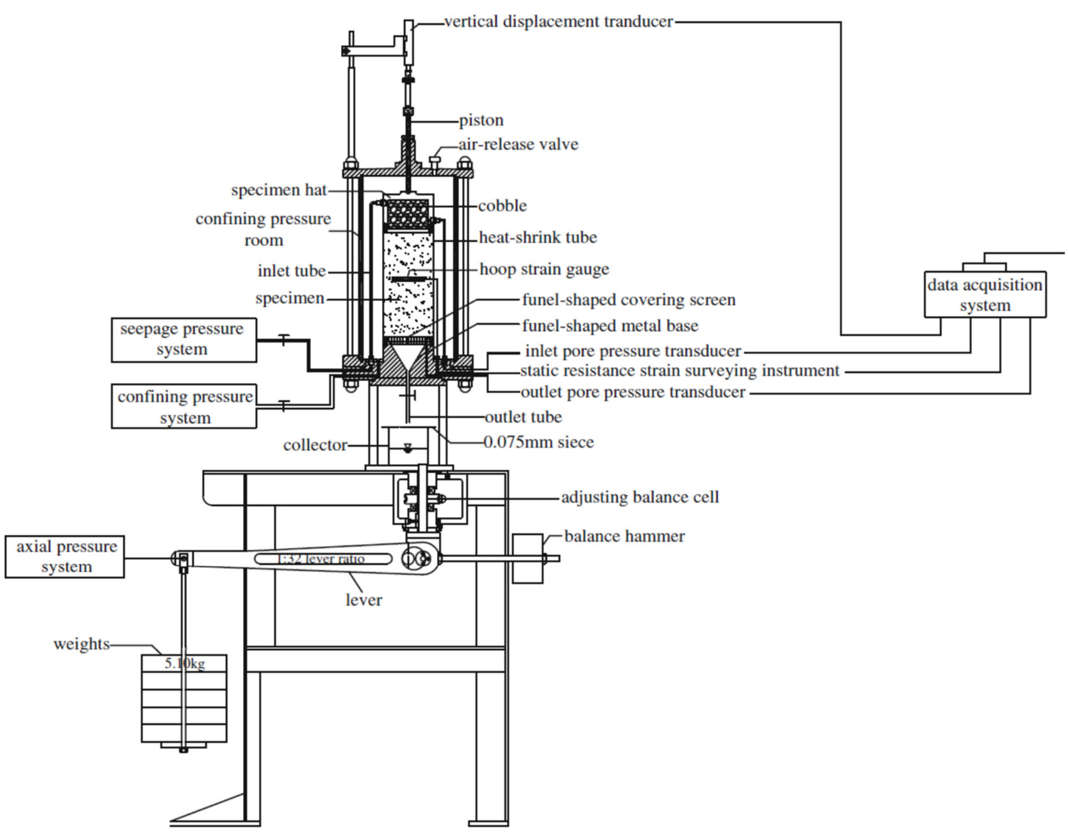

Figure 2-22. Hydro-mechanical coupling suffusion apparatus developed by Luo et al. (2013a)

This apparatus was also used to assess evaluation of contact erosion at the soil-structure interface by Luo et al. (2013b) and Wang et al. (2014). A modified base plate was used to model the interface between a clay core-wall and a concrete cut-off wall, which is one of the weakest parts of hydraulic structures. It was understood that flow along the soil-structure interface can be assessed by the Darcy flow rule.

The influence of soil gradation, grain size and shape on initiation and progression of piping was experimentally investigated by Rice and Fleshman (2013) and Fleshman and Rice (2014). A rigid wall seepage apparatus was developed to apply an upward flow to a soil specimen. Soil mixtures with various gradations and particle shapes were prepared and placed in the sample holder. This study indicated that angular soils, graded soils and soils with higher specific gravities showed greater piping resistance. In addition, four stages of piping, including visible movement, heave progression, boil formation and total heave, were observed during an upward flow.

Change in overall volume and void ratio of soils due to erosion of fine particles was investigated by dissolution of salt particles with various sizes in a sand-salt mixture using a modified permeation oedometer (McDougall et al., 2013). This oedometer was modified to allow (gravity-driven) permeation of water. It was revealed that erosion of salt particles (fine particles) led to settlement, and that this deformation was related to the percentage of erosion and particle sizes. Two volumetric mechanisms were observed during particle removal. Removal of particles that sat loose in the voids (nesting) had minor impact on the soil structure, and minimal settlement occurred. However, a considerable settlement occurred when larger particles were removed and particle rearrangement occurred. These particles were involved in the force chains and transferred effective stresses.

Moraci et al. (2014) suggested a new design chart for assessing internal stability of granular filters. These new design criteria were validated by an experimental investigation. Long-term filtration tests were carried out using a permeameter Plexiglas cell. A downward seepage flow with a constant hydraulic gradient was applied for at least 200 hours through a geotextile filter in contact with a range of granular soils. Internal stability of different soil gradations was investigated, and it was understood that these new criteria can predict susceptibility of granular filters to suffusion accurately.

Suffusion of gravelly soils was the topic of another study conducted by Chen et al. (2015). Variation of hydraulic head, flow rate, hydraulic gradient and fine content during suffusion was investigated. In addition, a theoretical formula was developed from accumulated sand emissions over time under an upward flow with a constant head. This experiment indicated that for soil samples with the same void ratios but different particle compositions, a greater critical hydraulic head was observed for samples with more uniform particle composition.

To investigate internal stability of granular filters based on the constriction size distribution, Indraratna et al. (2015) used an especially manufactured smooth Perspex filtration cell. An upward seepage flow was injected to the bottom of the cell, and eroded particles were collected at the top of the cell using an effluent collection tank.

They found that a percentage of the fine particle erosion was affected by the soil gradation and degree of soil compaction. Depending on the relative density, marginally unstable soils were transferred to the stable category and vice versa. Moreover, it was understood that their new Combined PSD (Particle Size Distribution) and CSD (Constriction Size Distribution) CP-CSD method was capable of assessing internal stability of both well-graded and gap-graded materials.

2.6. Investigation of Internal Erosion - Computational Approach

Computational investigation of internal erosion has been attracting more interest during the last decade. However, in comparison to the laboratory research, there are still considerable conceptual ambiguities that need to be clarified. Some researchers, such as Indraratna et al. (2007), Reboul et al. (2010), Ghafghazi and Azhari (2012), Langroudi et al. (2013), Shire and O'Sullivan (2013), Vincens et al (2015), Langroudi et al. (2015), To et al. (2015a) and Shire et al. (2016), improved the knowledge of constriction size in soil structures, investigated internal stability criteria and mobility and contribution of fine particles in the primary fabric. Others, such as Locke et al. (2001), Cividini and Gioda (2004), Becker et al. (2010), Scheuermann et al (2010), Frishfelds et al. (2011), Sari et al. (2011), Maeda et al. (2012), Huang et al. (2013), Wang and Ni (2013), Federico et al. (2013), Hama et al. (2014), Harshani et al. (2015), Abdelhamid and Shamy (2015) and To et al. (2015b), developed mathematical and numerical models to simulate initiation and progression of particles detachment and internal erosion. A few studies can also be found related to internal erosion effect on the mechanical behaviour of soils (e.g. Hicher and Chang, 2009; Wood et al., 2010; Scholtès et al., 2010; Hicher, 2013; Yin and Hicher, 2013; Maeda and Kondo, 2014; Wang and Li, 2015). As the focus of this research is studying the post-erosion mechanical behaviour of internally unstable soils, the recent achievements of numerical modelling in predicting post-erosion response of soils are discussed.

A numerical solution for determining the effect of internal erosion on stress-strain relationship of cohesionless materials was suggested first by Hicher and Chang (2009). This numerical model was capable of predicting the mechanical response of soils subjected to suffusion. The stress-strain relationship of a granular soil was derived from forces and displacements at the particle level and contact plane behaviours. For this reason, a stress-strain model developed by Chang and Hicher (2005) was used to consider inter-particle forces and displacements along a set of contact planes. In this model, a soil was assumed as a collection of non-cohesive particles, and deformation of the volume of the material was generated by mobilising particle contacts in different orientations. The required material parameters were:

- Normalised contact number per unit volume: ${Nl^3}/{V}$
- mean particle size, $2R$
- Inter-particle elastic constants: k_{n0}, k_{t0} and n;
- Inter-particle friction angle: $\emptyset_\mu$and m;
- Inter-particle hardening rule: k_{p0} and $\emptyset_0$;
- Critical state for packing: λ and Γor e_{ref} and P_{ref}
- Eroded fraction: $f_e = \frac{W_f}{W_s}$, where W_f is the weight of the eroded particles and W_s is the initial total solid weight per unit volume.

It was assumed that when suffusion occurs, the global void ratio increases due to an increase in f_e , and if a constant state of external stresses was applied, a disequilibrium is developed at each contact point leading to a local sliding. These individual displacements are then integrated to produce the global deformation of the soil specimen. They believed that this is the degree of interlocking by adjacent particles that controls resistance against sliding on a contact plane, and that it is related to the void ratio of the particles packing (Eq. 2.18).

$$\tan \emptyset_p = (\frac{e_c}{e})^m \tan \emptyset_\mu \tag{2.18}$$

Where m is a material constant, e_c is the critical void ratio and e is the initial void ratio. For dense packing, $\emptyset_p > \emptyset_\mu$ and when the soil structure dilates both $\emptyset_p$ and $\emptyset_\mu$ are reduced and for loose packing $\emptyset_p < \emptyset_\mu$.

This model was used to investigate the post-erosion response of a non-cohesive particles packing with $C_u = 10$ and initial void ratio $e_0 = 0.3$ corresponding to a relative density $D_r = 85$ per cent when suffusion occurs at a constant deviator stress. It was understood that the induced deformation due to particle removal was greater at higher stress ratios (Figure 2-23), which led to soil failure. However, no calibration was provided showing how accurate and reliable the result was.

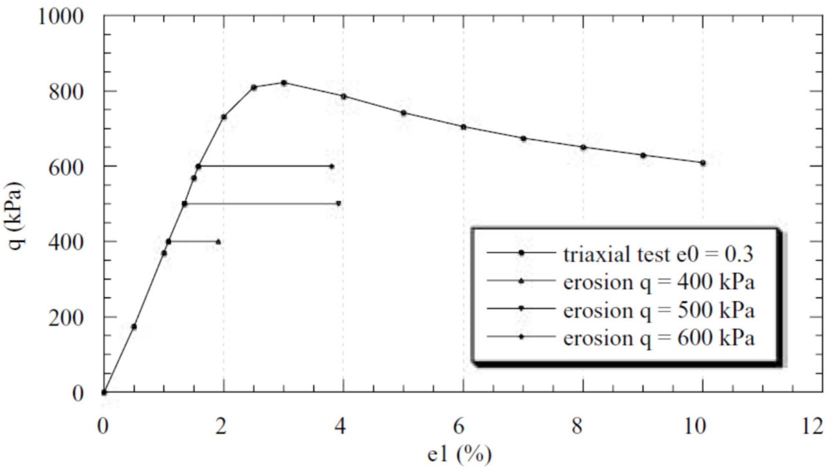

Figure 2-23. Stress-strain relationship in a simulated triaxial test pre and post-erosion (Hicher and Chang, 2009)

Wood et al. (2010) used two-dimensional discrete element modelling to investigate the mechanical consequences of erosion using the software package PFC-2D. Instead of considering a coupled flow and particle removal, the process of erosion was modelled by progressively removing the fine particles, while the external stresses were kept constant. Soil particles were considered as circular discs with particle size ratio (R_d) of 2, 5, 10 and 20 and $d_{max} = 100$ mm in all tests. The test dimensions were 750 × 1500 mm and specimens were prepared under zero gravity and placed randomly in a container. The walls of the container were then moved to reach the desired density. Samples were compressed isotopically and sheared to a certain mobilised friction by driving downwards one rigid boundary of the container. After stress equilibrium, the smallest disc was specified and removed from the assembly with no attempt to simulate a realistic erosion process, as it was found that the largest particles had the most contacts. This process was then repeated until the normal strain exceeded 25 per cent or the size of particle selected for removal was equal to D_5. Unequilibrium interparticle forces were developed in the assembly due to the removal of particles. These internal instabilities led to deformations while external stresses were controlled and kept constant. Figure 2-24 shows developed shear strains due to removal of fine particles at various mobilised internal frictions. Figure 2-24 also confirmed Hicher and Chang's (2009) findings that at the higher stress ratios, the removal of particles induced larger deformations. This numerical modelling showed that the particle removal increased the specific volume ($v = 1 + e$), which led to volumetric compression due to a more open internal structure and a narrowed soil grading, raising the critical state line. The consequence of this process was a lower available strength and occurrence of distortional strains. Although this research provided a better understanding of consequences of particle removal, no evidence was provided to show the validity of the model. Wood et al. (2010) believed that internal erosion is a time-dependent phenomenon and changes the actual fabric of the material; therefore Wood et al. (2010) believed that it cannot be simulated only by mixing up particles with different sizes and randomly removing the small particles.

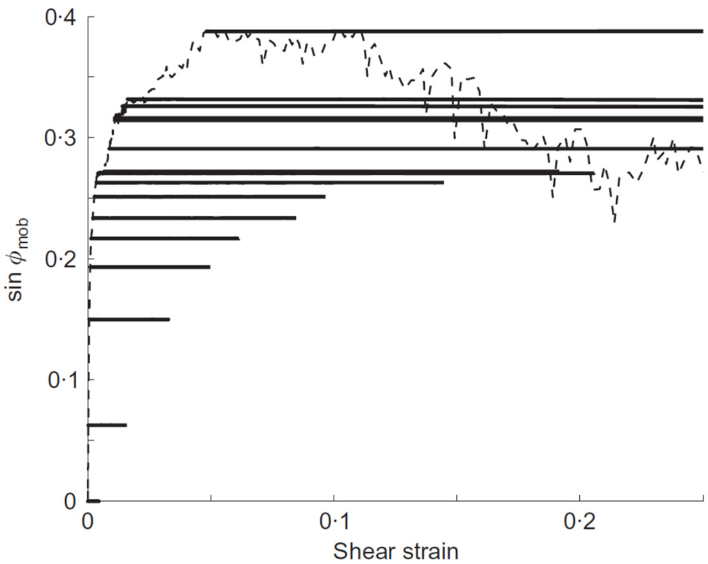

Figure 2-24. Test results with particle removal (Wood et al., 2010)

A multi scale approach including a discrete element model and an analytical micromechanical model was proposed by Scholtès et al. (2010) and Hicher (2013) to assess impacts of internal erosion on the mechanical properties of a granular medium, induced deformations, and variation of properties during the erosion process. A 3D numerical sample representing a granular assembly composed of 10,000 spheres was simulated through the Yade-OpenDem platform (Kozicki and Donze, 2008). Stress-strain state was controlled by six rigid frictionless boundary walls and a linear elastic relationship between forces and interparticle displacements. A slip coulomb model was considered for interparticle interaction. Particles were first placed randomly inside the box with no overlap. Then particle radii were increased progressively to reach the desired pressure on the boundary walls. The final density of packing was controlled by interparticle friction angle. Isotropic stress of 100 kPa was applied and the assembly was allowed to stabilise. The smallest particles under the lowest load (most likely erodible) were identified based on the size of the particles and the degree of interlocking. Instead of measuring stress value at the particle scale, the mean internal moment was used as an index to determine the degree of interlocking. The samples were subjected to a series of particle removal at different shear stress ratios $\left(\eta = {}^{q}/_{p}\right)$. Boundaries were positioned to keep the level of stresses during particle extraction constant. Between any two particle removals, the system was allowed to reach a new equilibrium. No obvious consequence was observed at the macroscopic scale and global behaviour up to removal of 2.2 per cent of particles by mass, as these particles were floating in the soil matrix and were not involved in force chains. In addition, it was found that removal of particles at shear stress ratios lower than 0.72 resulted in contractive deformations, and samples reached a new stable state. However, instability and dilation were observed when particle extraction occurred at shear stress greater than 0.72. This threshold value for shear stress ratio was related to the residual state at large shear deformations, which is known as the critical state ($\eta^{CS} = 0.72$) (Figure 2-25). This meant that under a shear stress state lower than the critical one, particle rearrangement acted as a self-healing factor to counterbalance the effect of particle erosion. In addition, regardless of percentage of the particle removal, this is the mobilised friction that controlled the failure of assembly.

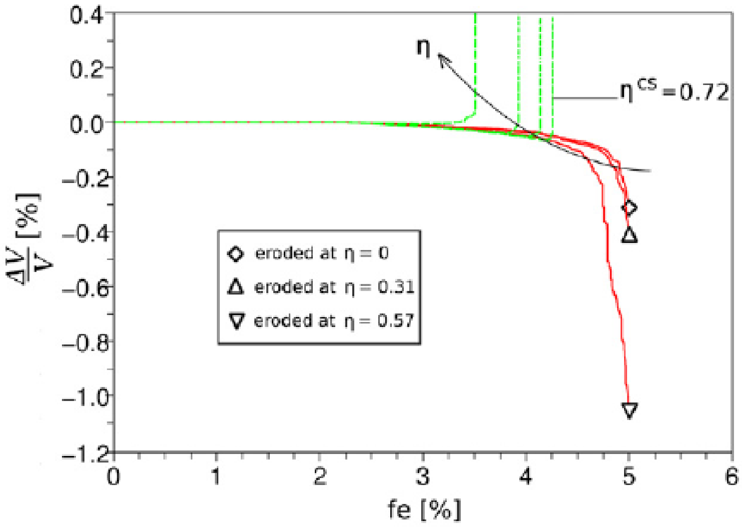

Figure 2-25. Volumetric strains as a function of extracted mass (*fe*) conducted at various shear stress ratios (Scholtès et al., 2010)

Post particle extraction response was also investigated under compression by Scholtès et al. (2010). Due to an increase in the initial porosity, the specimen behaviour changed from dilative to contractive, and a drop in the shear strength was observed. In fact, particle removal decreased the internal friction angle and weakened the granular assembly. Moreover, it was understood that the mechanical response in terms of internal friction, volumetric strain and residual sate were independent of the initial stress state that erosion was conducted at. It is worth mentioning that a comparison with an analytical approach showed similar trends of soil behaviour. However, similar to previous studies, model calibration with laboratory experiments or field results was not carried out to validate the outcome.

A similar approach was employed by Maeda and Kondo (2014) and Wang and Li (2015). DEM modelling conducted by Wang and Li (2015) indicated that the peak strength and dilation tendency decreased after removal of fine particles. However, the residual friction angle was found to be unchanged regardless of percentage of particle erosion.

A coupled DEM-CFD (Discrete Element Modelling-Computational Fluid Dynamics) analysis of internal instability was conducted by Kawano et al. (2017). It was found that the stress transfer characteristics of the DEM sample were insensitive to preparation method. The model indicated those particles that experienced significant displacement had low initial stress, which confirmed erodibility of fine particles in case-i (free fine particles) and case-ii (semi-active fine particles), as shown in Figure 2-15. Displacement of active fine particles (case-iii) that led to volumetric strain was also observed.

2.7. Critical Literature Review

Sterpi (2003) stated that the effect of gradual erosion and transport of fine particles due to a severe seepage flow cannot be ignored when working in an urban area. This may occur during the artificial lowering of the water table by means of pumping wells. Some laboratory tests were carried out on soil samples subjected to a controlled seepage flow to investigate the erosion of fine particles. The test results were then used to calibrate a new model suggested to predict particle transport based on the conservation of mass of moving particles with a suitable law of erosion. This model was capable of estimating the impact of erosion on the geomechanical behaviour of soil and surrounding structures. However, Sterpi (2003) believed that further experimental investigation needed to be conducted to achieve a better insight into the various aspects of this problem. Cividini and Gioda (2004) followed a similar approach by developing a finite element model to investigate erosion and transport of fine particles in granular soils. However, similar to Sterpi (2003), their numerical model contained some relevant simplifying assumptions due to the limited experimental data available in the literature. An incremental erosion law was proposed by Cividini et al. (2009) based on the experimental data. This law equation was used in two and three dimensional finite element models to estimate the quantity of eroded material adjacent to the pumping wells and of the possible settlements of nearby structures. They suggested that the focus of the experimental investigation could be the impact of the sample height or the in situ effective stresses on the erosion process.

Chang and Zhang (2011) conducted a series of drained triaxial tests on eroded specimens under different stress paths. Their results showed that the dilative behaviour of the non-eroded specimen changed to a contractive behaviour after internal erosion. They believed that loss of fine particles increased the global void ratio and shifted the soil condition to a looser state, ultimately leading to a lower drained shear strength. The secant modulus also decreased due to internal erosion. However, regardless of the initial stress path and percentage of the eroded particles, the residual strength was similar for pre and post-erosion specimens. In a similar study, Ke and Takahashi (2012) measured the bearing capacity of a series of soil specimens pre- and post-erosion using a miniature cone penetrometer. They found that internal erosion (caused by an upward flow) decreased the cone tip resistance. In other words, loss of fine particles due to internal erosion resulted in a reduction of the internal friction angle. More importantly, this reduction was less than two per cent for most of their specimens tested, and no specific reason was provided for this strength reduction. However, it is plausible to assume that the loss of fine particles weakened the mechanical interlock between the coarse particles over small strains. The siliceous sand used in their research was categorised as an angular to sub-angular material. Thus, the presence of the fine particles may have improved the internal friction.

Xiao and Shwiyhat (2012) experimentally investigated the post-erosion behaviour of sandy soils. Undrained shear strength results of the eroded specimens were found to be greater than that of the non-eroded specimens. They indicated that this might have occurred due to a loss in saturation during the erosion phase as the bottom of each specimen was subjected to the atmospheric pressure.

More recently, Ke and Takahashi (2014a) studied drained and undrained behaviours of a gap-graded soil with 35 per cent fine content (FC) under monotonic and cyclic loadings pre- and post-erosion. The initial global void ratio of soil specimen was about 0.56, which increased to 0.94 after erosion. Relative density and confining pressure were 30 per cent and 50 kPa, respectively. Based on these magnitudes, it appears that the specimens were in a loose state before erosion. The volumetric strains during shearing pre- and post-erosion were both contractive as expected. The post-erosion specimen (with a larger void ratio) had a lower volumetric deformation but showed a higher initial stiffness and lower drained shear strength. Contrary to the drained test results, the soil specimens (regardless of erosion) showed softening behaviour with limited flow deformation during undrained shearing. The eroded specimen reached a higher peak shear strength under low strain but collapsed temporarily at medium strain range. Undrained cyclic behaviour pre- and post-erosion was also investigated, and indicated a higher cyclic resistance for the post-erosion specimen. It was noted that the higher undrained strength of the eroded specimen may have been attributed to rearrangement of the soil particles during erosion and progression of the local reinforcement in the soil fabric. Based on the individual triaxial test results, it was concluded that the presence of the fine particles decreased the soil strength and postponed dilation on loose soil samples with different initial fine contents. However, it was not clear why this reinforcement and geometric properties of particles had a different impact during drained and undrained conditions. Interestingly, the soil type, particle size distribution and initial void ratio used in this research was similar to the previous study conducted by Ke and Takahashi (2012) that showed that loss of fine particles reduced the cone tip resistance.

Post-erosion drained behaviour of a gap-graded soil (with varying initial fine contents) was again investigated by Ke and Takahashi (2014b). Results showed that the drained shear strength did not change after erosion for specimens with 15 and 25 per cent initial fine contents. In contrast, the specimen with an initial fine content of 35 per cent showed a drop in shear strength. Surprisingly, the residual post-erosion fine content was similar (10 to 13 per cent) for all specimens under the same confining pressures and hydraulic conditions. In other words, specimens with a greater initial fine content lost more of their fine particles during the erosion phase. However, apart from the specimen with 35 per cent fine content, erosion of the fines did not affect the mechanical behaviour of the other specimens. This suggests that those fine particles sat loosely in the available void spaces formed by the coarse particles and did not participate in load transferring.

Impact of internal erosion on geomechanical behaviour of granular material has been explained using the mechanics of interaction between fine and coarse particles. It is generally accepted that there is a threshold fine content above which the coarse particles start to float in the fine particle network. For soils containing fine content above this threshold, soil behaviour is mainly controlled by the fine particles rather than the coarse particles. Shire et al. (2014) investigated the effect of fine content on stress distribution for internally unstable soils using discrete element modelling. It was concluded that for internally unstable soils with fine contents less than 25 per cent, the soil can be classified as underfilled. For these soils, fine particles sit loose in the voids and will migrate through the pores if they are smaller than constriction size and the hydraulic gradient is high enough. On the other hand, the soil is considered overfilled if the fine content is larger than 35 per cent. In this case, fine particles fill all the voids and contribute to soil structure and carry stresses along with the coarse particles. For soils in the transitional zone (i.e. between 25 and 35 per cent fine content), the contribution of fine particles in the soil stress matrix is highly dependent on relative density. This critical fine content for soil tested by Ke and Takahashi (2014b) was found to be 33 per cent based on a method presented by Rahman et al. (2011) or 37 per cent according to Ke and Takahashi's (2012) calculations. These values suggest that a specimen with 35 per cent initial fine content is on the borderline. Therefore, the different behaviour patterns observed for this specimen could be related to the different soil stress matrix in comparison to other specimens with lower fine content.

Migration of fine particles in granular filter material was investigated by Abdelhamid and El Shamy (2015) using a pore-scale modelling approach. A three-dimensional transient fully coupled pore-scale model was developed by using the lattice Boltzmann method for idealisation of the fluid and a discrete element method for the solid phase. They showed that soils with $\mathrm{D'}_{15}/\mathrm{d'}_{85} < 4$ are internally stable, which was in agreement with Kezdi's (1969) criteria. However, this model falls short in predicting the post-erosion geomechanical behaviour in terms of shear strength or compressibility.

For gap graded soils, current literature overall suggests that the undrained shear strength and cyclic resistance increases at the low strain range after erosion of the fine particles. However, the reduction in post-erosion drained shear strength is also reported (e.g. Chang and Zhang, 2011; Ke and Takahashi, 2014a).

2.8. Summary

It was discussed that in a cohesionless granular soil, fine particles may migrate within pore spaces between coarse particles under a critical hydraulic gradient. This phenomenon is known as suffusion, which is a type of internal erosion occurring in internally unstable soils. Internal erosion has been an area of interest in the last century since 1910, when Bligh (1910) tried to assess piping potential based on the Darcy's flow equation (1856), until now, when Rönnqvist and Viklander (2016) suggested a unified plot approach for the assessment of internal erosion in embankment dams. For example, Garner and Fannin (2010) showed that internal erosion only occurs if three prerequisites, known as material susceptibility, critical stress condition and critical hydraulic stress, are met. Material susceptibility to internal erosion can be investigated using available geometric methods in the literature, such as Kezdi's (1969), Burenkova's (1993) or Moraci et al. (2014). Critical stress condition is associated with the contribution of erodible particles in the force chains or primary soil skeleton. Researchers such as Mitchell (1993), Kenney (1977), Skempton and Brogan (1994), Thevanayagam (1998), Thevanayagam (2007) and Rahman et al. (2011) suggested parameters and equations to consider the influence of fine particles in the soil stress matrix depending on fine content, soil gradation and relative density. Another crucial factor for initiating internal erosion is the critical hydraulic gradient that washes out the erodible particles. According to findings by Skempton and Brogan (1994), Wan and Fell (2004 and 2007) and Ke and Takahashi (2012a), this critical hydraulic gradient for internally unstable soils is much lower than the theoretical value suggested by Terzaghi (1925) for internally unstable soil. In fact, seepage direction, fine content, contribution of erodible particles in load transferring and constriction size affect the critical hydraulic gradient.

Experimental investigation of internal erosion from 1984 to 2016 was discussed thoroughly in this chapter. Figure 2-26 indicates contribution of each decade. It can be seen that approximately 80 per cent of laboratory studies related to internal erosion have been conducted in the last five years. This shows that this topic has been attracting more interest in recent years.

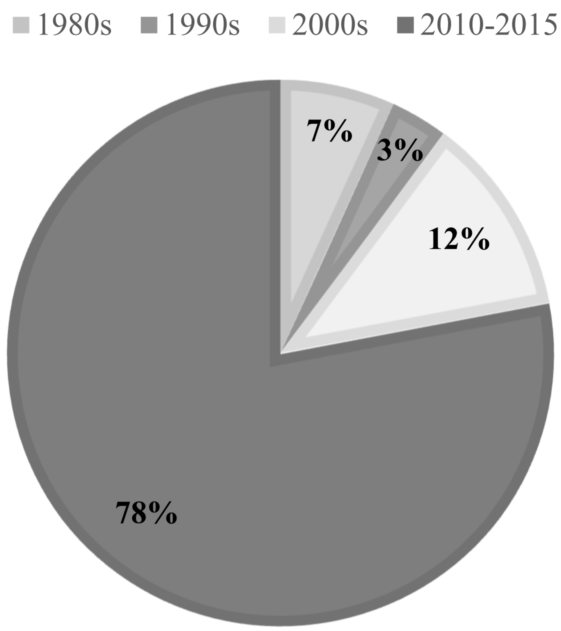

Figure 2-26. Contribution of each decade in the experimental investigation of internal erosion

A summary of previous laboratory investigations is shown in Table 2-4. This table not only provides a database, but also clarifies areas that have been overlooked and need more exploration. It is possible to categorise previous studies into 12 different groups based on their outcomes as below:

- Effect of initial fine content on internal erosion
- Effect of hydraulic gradient on internal erosion
- Effect of soil gradation on internal erosion
- Effect of confining pressure on internal erosion
- Effect of seepage direction on internal erosion
- Investigation of Granular filter criteria (Internal stability)
- Effect of seepage length on internal erosion
- Effect of particle shape on internal erosion
- Effect of relative density on internal erosion
- Effect of seepage duration
- Effect of specimen dimensions and erosion path on soil response during internal erosion
- Post-erosion behaviour (drained or undrained)

It can be seen that influential parameters on initiation and progression of internal erosion have been widely discussed. However, a few attempts have been made to investigate the post-erosion behaviour. It was mentioned that internal erosion is a non-uniform and time-dependent phenomenon. This means that soil characteristics in terms of particle gradation, residual fine content, hydraulic conductivity and strength parameters may be different along the seepage path. To get a better understanding in this area, the effect of a progressive erosion on undrained behaviour of a vulnerable soil during monotonic and cyclic loading is investigated using a modified erosion-triaxial apparatus in this research.

Table 2-4. Summary of experimental investigation in the literature

No.	Authors	Year	Topic	Achievement															
				Effect of Initial Fine Content on Erosion	Effect of Hydraulic Gradient on Erosion	Effect of Soil Gradation on Erosion	Effect of Confining Pressure on Erosion	Effect of Seepage Direction on Erosion	Granular Filter Criteria (Internal Stability)	Effect of Seepage Length on Erosion	Effect of Particle Shape on Erosion	Effect of Relative Density on Erosion	Effect of seepage duration	Effect of Specimen Dimensions and Erosion Path on Soil Response During Erosion	Post-erosion Behaviour (Drained or Undrained)	Effect of Specimen Dimensions and Erosion Path on Post-erosion Behaviour	Effect of Erosion Progress on Undrained Monotonic Shearing	Effect of Erosion Progress on Cyclic Response	Effect of Erosion Progress on Post-Cyclic Undrained Monotonic Shearing
1	Sherard et al.	1984	Basic properties of sand and gravel filters																
2	Kenney et al.	1985	Controlling constriction sizes of granular filters																
3	Kenney and Lau	1985	Internal stability of granular filters																
4	Lafleur et al.	1989	Filtration of broadly graded cohesionless soils																
5	Tanaka and Toyokuni	1991	Seepage failure experiments on multi layers sand columns																
6	Skempton and Brogan	1994	Experiments on piping in sandy gravels																
7	Garner and Sobkowicz	2002	Internal Instability in gap-graded cores and filters																
8	Moffat and Fannin	2006	A large permeameter for study of internal stability in cohesionless soils																
9	Wan and Fell	2008	Assessing the potential of internal instability and suffusion in …																
10	Richards and Reddy	2008	Experimental investigation of piping potential in earthen structures																
11	Bendahmane et al.	2008	Experimental parametric study of suffusion and backward erosion																
12	Marot et al.	2009	Internal flow effects on isotropic confined sand clay mixtures																
13	Cividini et al.	2009	Seepage induced erosion in granular soil and consequent settlements																
14	Richards and Reddy	2010	True triaxial piping test apparatus for evaluation of piping potential …																
15	Shwiyhat and Xiao	2010	Effect of suffusion on mechanical characteristics of sand																

Table 2-4. Summary of experimental investigation in the literature (continued)

No.	Authors	Year	Topic	Achievement															
				Effect of Initial Fine Content on Erosion	Effect of Hydraulic Gradient on Erosion	Effect of Soil Gradation on Erosion	Effect of Confining Pressure on Erosion	Effect of Seepage Direction on Erosion	Granular Filter Criteria (Internal Stability)	Effect of Seepage Length on Erosion	Effect of Particle Shape on Erosion	Effect of Relative Density on Erosion	Effect of seepage duration	Effect of Specimen Dimensions and Erosion Path on Soil Response During Erosion	Post-erosion Behaviour (Drained or Undrained)	Effect of Specimen Dimensions and Erosion Path on Post-erosion Behaviour	Effect of Erosion Progress on Undrained Monotonic Shearing	Effect of Erosion Progress on Cyclic Response	Effect of Erosion Progress on Post-Cyclic Undrained Monotonic Shearing
16	Gaucher et al.	2010	Experimental investigation of the hydraulic erosion of noncohesive …									■							
17	Ahlinhan and Achmus	2010	Experimental investigation of critical hydraulic gradients for unstable soils			■		■				■							
18	Moffat and Fannin	2011	A hydromechnanical relation governing internal stability of cohesionless soil	■	■		■	■											
19	Chang and Zhang	2011	A Stress-controlled erosion apparatus for studying internal erosion in soils												■				
20	Marot et al.	2011	Centrifuge modelling of an internal erosion mechanism		■								■	■					
21	Marot et al.	2011	Experimental bench for study of internal erosion in cohesionless soils		■														
22	Benamar et al.	2011	Experimental study of internal erosion of fine grained soils	■	■														
23	Marot et al.	2011	Multichannel optical sensor to quantify particle stability under seepage flow		■	■					■								
24	Moffat et al.	2011	Spatial and temporal progression of internal erosion in cohesionless soil	■	■		■	■											
25	Ke and Takahashi	2011	Strength reduction of gap-graded cohesionless soil due to internal erosion	■								■			■				
26	Sail et al.	2011	Suffusion tests on cohesionless granular matter		■														
27	Kelly et al.	2012	Effect of particle loss on soil behaviour			■													
28	Nguyen et al.	2012	Erodibility characterisation for suffusion process in cohesive soil by two types …		■														
29	Sadaghiani and Witt	2012	Experimental identification of mobile particles in suffusible non cohesive soils		■														
30	Richards and Reddy	2012	Experimental investigation of initiation of backward erosion piping in soils	■	■		■	■											

Table 2-4. Summary of experimental investigation in the literature (continued)

No.	Authors	Year	Topic	Achievement															
				Effect of Initial Fine Content on Erosion	Effect of Hydraulic Gradient on Erosion	Effect of Soil Gradation on Erosion	Effect of Confining Pressure on Erosion	Effect of Seepage Direction on Erosion	Granular Filter Criteria (Internal Stability)	Effect of Seepage Length on Erosion	Effect of Particle Shape on Erosion	Effect of Relative Density on Erosion	Effect of seepage duration	Effect of Specimen Dimensions and Erosion Path on Soil Response During Erosion	Post-erosion Behaviour (Drained or Undrained)	Effect of Specimen Dimensions and Erosion Path on Post-erosion Behaviour	Effect of Erosion Progress on Undrained Monotonic Shearing	Effect of Erosion Progress on Cyclic Response	Effect of Erosion Progress on Post-Cyclic Undrained Monotonic Shearing
31	Xiao and Shwiyhat	2012	Experimental investigation of the effects of suffusion on physical and …																
32	Marot et al.	2012	Influence of angularity of coarse fraction grains on internal erosion process																
33	Ke and Takahashi	2012	Influence of internal erosion on deformation and strength of …																
34	Chang et al.	2012	Laboratory investigation of initiation and development of internal erosion in …																
35	Ahlinhan et al.	2012	Stability of non-cohesive soils with respect to internal erosion																
36	Ke and Takahashi	2012	Strength reduction of cohesionless soil due to internal erosion induced by …																
37	Marot et al.	2012	Study of scale effect in an internal																
38	Chang and Zhang	2012	Critical hydraulic gradients of internal erosion under complex stress states																
39	Luo et al.	2013	A new apparatus for Evaluation of contact erosion at …																
40	Luo et al.	2013	Hydromechanical experiments on suffusion under long term large heads																
41	Rice and Fleshman	2013	Laboratory modelling of critical hydraulic conditions for …																
42	McDougall et al.	2013	Particle loss and volume change on dissolution experimental results …																
43	Moraci et al.	2014	Analysis of the internal stability of granular soils using different methods																
44	Seghir et al.	2014	Effect of fine particles on the suffusion of cohesionless soils																
45	Ke and Takahashi	2014	Experimental investigation on suffusion characteristics and its mechanical …																

Table 2-4. Summary of experimental investigation in the literature (continued)

No.	Authors	Year	Topic	Achievement															
				Effect of Initial Fine Content on Erosion	Effect of Hydraulic Gradient on Erosion	Effect of Soil Gradation on Erosion	Effect of Confining Pressure on Erosion	Effect of Seepage Direction on Erosion	Granular Filter Criteria (Internal Stability)	Effect of Seepage Length on Erosion	Effect of Particle Shape on Erosion	Effect of Relative Density on Erosion	Effect of seepage duration	Effect of Specimen Dimensions and Erosion Path on Soil Response During Erosion	Post-erosion Behaviour (Drained or Undrained)	Effect of Specimen Dimensions and Erosion Path on Post-erosion Behaviour	Effect of Erosion Progress on Undrained Monotonic Shearing	Effect of Erosion Progress on Cyclic Response	Effect of Erosion Progress on Post-Cyclic Undrained Monotonic Shearing
46	Wang et al.	2014	Experiments on internal erosion in sandy gravel foundations containing a …					■											
47	Fleshman and Rice	2014	Laboratory modelling of mechanisms of piping erosion initiation			■					■								
48	Correia dos Santos et al.	2014	Laboratory Test for Evaluating Limitation of Flow during Internal …	■		■													
49	Chang et al.	2014	Mechanical consequences of internal soil erosion												■				
50	Ke and Takahashi	2014	Triaxial Erosion test for Evaluation of Mechanical Consequences of Internal …												■				
51	Sibille et al.	2015	A description of internal erosion by suffusion and induced settlements on …	■	■					■									
52	Ke and Takahashi	2015	Drained monotonic responses of suffusional cohesionless soils	■			■								■				
53	Chen et al.	2015	Experimental study on suffusion of gravelly soil			■						■							
54	Indraratna et al.	2015	Geometrical method for evaluating the internal instability of granular filters …			■						■							
55	Ouyang and Takahashi	2015a	Influence of initial fines content on fabric of soils subjected to internal Erosion	■											■				
56	Ouyang and Takahashi	2015b	Optical quantification of suffosion in plane strain physical models	■															
57	Ke et al.	2015	Soil deformation due to suffusion and its consequences on undrained behaviour …				■								■				
58	Marot et al.	2016	Assessing the susceptibility of gap-graded soils to internal erosion …						■										
59	Chen et al.	2016	Stress-Strain Behaviour of Granular Soils Subjected to Internal Erosion												■				
60	**Mehdizadeh et al.**	**2015-2017**	**Post-erosion Behaviour**													■	■	■	■

Chapter 3 Methodology of the Laboratory Study

This research consists of three experimental phases of material characterisation, erosion-triaxial test and X-ray tomography. Testing programs are shown in Tables 3-1, 3-2 and 3-3. Methodology of each test, including the test purpose, sample preparation, test method and equipment, and the standards that are followed, is presented in this chapter. Overall, 27 different tests are carried out in this research study. In addition, PIV method is employed and discussed as the most reliable technique for measuring strains during internal erosion. The specimen coding for the second and third phases of the experiments is described in Figure 3-1

Table 3-1. Testing program for assessing geotechnical characteristics of the soil mixture

No.	Test	Standard
1	Particle Size Distribution	C136-06; D6913-04; AS 1141.11-96
2	Soil Classification	D2487-06; D3282-15; AS 1726-93
3	Maximum Index Density	D4253-16
4	Minimum Index Density	D4254-16
5	Specific Gravity	D854-14
6	Particle Shape Analysis	-
7	Direct Shear Test	D3080/D3080M-11
8	Erosion Susceptibility	-

Table 3-2. Erosion-triaxial testing program

No.	Test	Sample Label	Standard	Sample Dimension (mm)	Seepage Velocity (mm/min)	Seepage Duration (min)	Loading Type
1	CU[a]	NE-D75-Mon	D4767-11	75 × 150	-	-	Monotonic
2	CU	NE-D75-Cyc	D5311/D5311M-13	75 × 150	-	-	Cyclic
3	CU	NE-D100-Mon	D4767-11	100 × 200	-	-	Monotonic
4	CU	NE-D50-Mon	D4767-11	50 × 115	-	-	Monotonic
5	Erosion-CU[b]	E-D75-V92-T30-Mon	D4767-11	75 × 150	92	30	Monotonic
6	Erosion-CU	E-D75-V92-T120-Mon	D4767-11	75 × 150	92	120	Monotonic
7	Erosion-CU	E-D75-V92-T30-Cyc	D5311/D5311M-13	75 × 150	92	30	Cyclic
8	Erosion-CU	E-D75-V92-T120-Cyc	D5311/D5311M-13	75 × 150	92	120	Cyclic
9	Erosion-CU	E-D75-V52-T30-Mon	D4767-11	75 × 150	52	30	Monotonic
10	Erosion-CU	E-D75-V52-T120-Mon	D4767-11	75 × 150	52	120	Monotonic
11	Erosion-CU	E-D75-V52-T30-Cyc	D5311/D5311M-13	75 × 150	52	30	Cyclic
12	Erosion-CU	E-D75-V52-T120-Cyc	D5311/D5311M-13	75 × 150	52	120	Cyclic
13	Erosion-CU	E-D100-V52-T120-Mon	D4767-11	100 × 200	52	120	Monotonic
14	Erosion-CU	E-D50-V52-T120-Mon	D4767-11	50 × 115	52	120	Monotonic
15	Erosion-CU	E-D50-V208-T120-Mon	D4767-11	50 × 115	208	120	Monotonic
16	CU	NE-D75-CF-Cyc	D5311/D5311M-13	75 × 150	-	-	Cyclic

[a]: Consolidated Undrained Triaxial Test on original (Non Eroded; NE) specimens
[b]: Erosion test followed by Consolidated Undrained Triaxial Test

Table 3-3. X-ray tomography testing program

No.	Sample Label	Sample Dimension (mm)	Seepage Velocity (mm/min)	Seepage Duration (min)
1	X-NE-D50-1	50 × 100	-	-
2	X-E-D50-V208-T120	50 × 100	208	120
5	X-E-D50-V208-T30	50 × 100	208	30

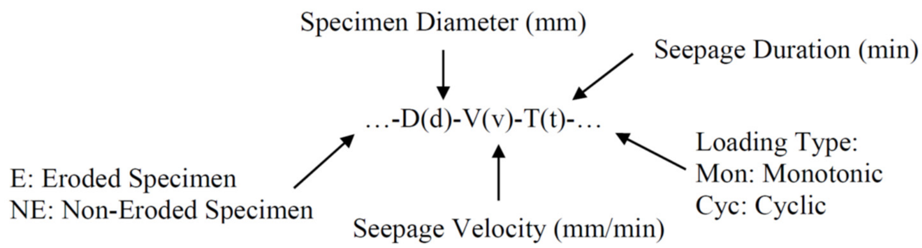

- X at the beginning of the specimens’ title in the third phase is related to X-ray tomography

Figure 3-1. Specimens labelling

3.1. Particle Size Distribution and Soil Classification

Particle size distribution (PSD) is the first step in geotechnical characterisation, as it provides an initial idea for engineering behaviour of soils. It is also used for soil classification systems, such as the American Association of State Highway and Transportation (AASHTO M145, 2008) or Unified Soil Classification System (USCS) (Stevens, 1982). It is normally conducted by sieve analysis for granular soils with particle sizes ranging from 0.075 to 75 mm. According to AS 1141.11-96 “Australian standard for particle size distribution by sieving” (Standards Australia, 1996), the soil mixture needs to be washed first to remove any contamination, dirt or dust. This can be done using a nested guard with 0.075 mm opening size under a low pressure water jet. This process is continued until water coming out of the sieve is clear. The clean material is then dried in the oven (105 to 110ºC) for 24 hours to reach a constant mass before sieving. When the soil mass is ready for sieving, Australian standard (AS 1141.11-96) is followed.

For engineering purposes, soils are classified to different groups based on their properties and behaviours. Particle Size Distribution (PSD), Liquid Limit (LL), Plasticity Index (I_P), particle shape (Santamarina and Cho, 2004) and sensitivity to pore fluid chemistry (Jang and Santamarina, 2015) are parameters normally used for soil classification. AS 1726-93 “Geotechnical Site Investigations” (Standards Australia, 1993) is employed to classify the soil mixture used in this research.

3.2. Maximum and Minimum Indexes Densities

Apart from engineering properties such as shear strength, stiffness, compressibility and permeability, it has been understood that relative density or degree of compaction is one of the important components in assessing the state of the compactness for cohesionless soils. Relative density is related to the achievable maximum and minimum densities. Density (unit weight) of a cohesionless soil can be determined by in-place methods in the field or measured in the laboratory (ASTM D4254-16, 2016). However, maximum and minimum densities can only be measured in the laboratory.

Previous studies, such as Ahlinhan's et al. (2012), Shire et al. (2014) and Indraratna et al. (2015), indicated that initiation of internal erosion is dependent on relative density, especially for internally unstable soils with fine contents in the range of 25 to 35 per cent. Therefore, it is necessary to prepare all erosion-triaxial specimens at the same relative density.

To measure maximum index density, an oven-dried or wet soil mixture is placed in a mold and a surcharge equal to 14 kPa is applied to the surface of the soil. Then, the soil and mold are vertically vibrated using an electromagnetic, eccentric or a cam-driven vibrating table. Time-vertical displacement relationship of vibration is sinusoid in the shape with a double amplitude of vertical vibration (peak-to-peak) of about 0.33 ± 0.05 mm. This vibration is applied at a frequency of 60 Hz for 8 ± 0.25 minutes or 0.48 ± 0.08 mm at 50 Hz for 10 ± 0.25 minutes. By dividing the mass of the densified soil mixture by its volume (area of mold times average height of densified soil), the maximum index density is calculated (ASTM D4253-16, 2016).

The loosest condition of a cohesionless soil is presented by the minimum index density. This can be attained in the laboratory by pouring the soil at a constant rate into a container with a known volume, and in a manner preventing particle segregation and bulking. It is important to adjust the height of pouring continuously to provide enough space for uniform flow of soil particles without the pouring device contacting the soil that has already been deposited. The container is filled with soil to 13 mm above the top of the container, and the surface is then trimmed off. The minimum index density is determined by dividing the mass of the soil inside the container by the volume of the container (ASTM D4254-16, 2016).

3.3. Soil Particle Density (Specific Gravity)

Experimental investigation conducted by Fleshman and Rice (2014) showed that the piping resistance increased with an increase in the specific gravity. Although all experiments in this study are performed on only one soil type, the specific gravity needs to be determined, as it is used in the calculation of minimum and maximum attainable void ratios.

According to ASTM D854-14 (2014) "Standard Test Methods for specific gravity of soil solids by water pycnometer", there are two laboratory methods for measuring the specific gravity of moist and oven-dried soil specimens. The procedure for oven-dried soil specimens is followed in this study.

3.4. Particle Shape Analyses

There are three scales in particle shape: sphericity versus ellipticity or platiness, roundness versus angularity, and smoothness versus roughness. Sphericity reflects the similarity between width, length and height of particles. Roundness reflects the average radius of surface curvature with respect to the maximum radius, and smoothness describes the ratio of surface texture to the particle radius (Cho et al., 2006). Fraser (1935) found that particle shape affected the size and shape of the pores and the packing level, which led to a change in hydraulic conductivity. Permeability increases as true sphericity is decreased, which was also later confirmed by Guimaraes (2002). In other research conducted by Marot et al. (2012a) and Fleshman and Rice (2014), it was found that angularity of particles improved the erosion resistance. This suggests the significance of particle shape on the initiation of internal erosion.

Depending on the sizes of the soil particles, different techniques and instruments, such as scanning electron microscope (SEM) and digital magnifier or microscope, can be used to determine the particle shape.

A digital magnifier or microscope is a new version of a traditional microscope. It is normally connected to a computer to transfer images to a monitor by means of a software or interface. However, the sample can be directly observed through an eyepiece, a small monitor or even a mobile phone screen, dependent on the brand. An in-built LED light source provides enough light for a clear observation. Depending on the power of magnifier, they are generally low priced ($15 to 150 AUD).

A digital microscope with USB output called TLI mTech 5 MP, manufactured by Logical Interface Co., is used for particle shape analysis in this study. Magnification was within the range of 20x to 300x. It is a high resolution (9 MP) handheld digital microscope with a 5 MP colour camera and eight white-light LEDs with adjustable illumination.

No matter what type of microscope is used, image processing needs to be carried out for particle shape analysis. MATLAB, ImageJ, Fiji or Avizo are the most common software packages being used for image processing. Particle shape properties of the soil mixture in this study are determined by ImageJ software. ImageJ is a public domain, open source and Java-based image-processing program developed at the National Institute of Mental Health (NIMH). It is a versatile program and provides a platform to solve different image processing and analysis, such as three-dimensional live-cell imaging, radiological image processing, multiple imaging system data comparisons and automated hematology systems by user-written codes. Various image types and formats, such as 8, 16 and 32-bit integer and grayscale images, JPEG, DICOM, PNG, FITS, GIF, BMP and TIFF, and even raw formats can be read and analysed, displayed, modified, processed, saved and printed. In addition, to reduce the analysis time, it is possible to perform time-consuming operations in parallel on multi-CPU hardware.

The soil mixture of this research consists of a coarse fraction ranging from 1.18 to 1.7 mm and 1.7 to 2.36 mm, and a fine fraction ranging from 0.075 to 0.15 mm and 0.15 to 0.3 mm. Particle shape analysis includes assessing the roundness, circularity and aspect ratio of particles, carried out at each particle size range. There are different definitions in the literature for particle shape properties. To avoid any confusion, definitions proposed by Ferreira and Rasband (2012) (Eqs. 3.1 to 3.3) are used in this research and are listed here:

- $$Roundness = 4 \times \frac{Area}{\pi \times (Major\ Axis)^{2}} \tag{3.1}$$
- $$Circularity = 4\pi \times \frac{Area}{(Perimeter)^{2}} \tag{3.2}$$
- $$Aspect\ Ratio = \frac{Major\ Axis}{Minor\ Axis} \tag{3.3}$$

where major and minor axes are the primary and secondary axis of the best fitting ellipse.

3.5. Direct Shear Test

Drained strength of any type of soil material can be determined by the direct shear test. It is a quick test and applicable for testing undisturbed, reconstituted and remolded specimens (D3080/D3080M-11, 2011). However, there are certain concerns in the application of the test that reduce the accuracy of results. First, the maximum particle size of the soil specimen is limited to a fraction of the dimensions of the shear box. Rotation of principal stresses in the direct shear test may be different from the field condition. This can affect the test result significantly if the soil shear strength is stress path dependent. It cannot model undrained condition correctly, as the drainage path is normally short. As the failure is always forced to occur on a horizontal plane through the middle of the soil specimen, this failure plane is not necessarily the weakest plane. Therefore, the measured strength parameters may be liable. However, this can be an advantage of the test when the aim is determining the shear strength at an interface between two dissimilar materials.

It was discussed in Chapter 2 that presence of fine particles may decrease or increase the particles interlocking depending on the angularity of particles. This means that rounded fine particles may act as a lubricant between angular coarse particles and reduce the internal friction. Erosion of these fine particles improves the coarse particles interaction and may increase the shear strength. This indicates that evaluation of post-erosion behaviour of soils can be fully understood only when there is a clear vision about the particles interlocking. Apart from particle shape properties that are assessed by a digital magnifier, internal friction of soil particles at each range of the particle size is also investigated using the direct shear test at the loosest condition.

For performing a direct shear test, first the soil specimen is poured into the direct shear box using a funnel to provide the loosest state. This process is similar to preparing a soil specimen for the minimum index density. A predetermined normal stress is applied on the top of the specimen and the shear box halves are unlocked. As the soil specimen is dry and granular, drainage time is quick. Then, the specimen is sheared by displaying one shear box half laterally with respect to the other, at a constant rate of shearing while the normal stress is kept constant. The shearing rate must be slow enough to allow full dissipation of excess pore water pressure.

3.6. Internal Erosion Susceptibility

To investigate post-erosion behaviour of a soil mixture, it is crucial to have a soil material vulnerable to internal erosion. Many attempts have been made to develop geometric criteria for assessing internal stability of soil materials. However, experimental investigations and field experiences have shown that there is no perfect and flawless method predicting internal stability correctly for any type of cohesionless soils. Therefore, it is necessary to examine susceptibility of soil material using a series of geometric techniques. In this research, geometric techniques by U.S. Army (1953), Istomina (1957), Kezdi (1969), Sherard (1979), Kenney and Lau (1985, 1986), Kwang (1990), Chapuis (1992), Burenkova (1993), Mao (2005), Wan and Fell (2008), Indraratna (2011), Ahlinhan (2012), Salehi Sadaghiani and Witt (2012), Dallo et al. (2013), Chang and Zhang (2013) and Moraci et al. (2014) are employed to determine internal stability of the soil mixture.

3.7. Consolidated Undrained Triaxial Test (CU) – Monotonic and Cyclic Shearing Paths

Chapter 2 showed that contrary to internal erosion initiation or progression that has been investigated widely, post-erosion behaviour of internally unstable soils is not well understood. This can be conducted by consolidated drained (CD) or undrained (CU) triaxial tests on eroded specimens. Drained and undrained triaxial tests provide effective and total strength parameters, respectively. However, as during undrained shearing, induced excess pore water pressure is measured, it is possible to determine the drained (effective) strength parameters, as well. Both conditions are commonly considered for embankment dam stability analysis. Regardless of the soil specimen dimensions and seepage velocity and duration, undrained behaviour of non-eroded and eroded specimens is investigated under monotonic shearing and cyclic loading, followed by monotonic shearing. ASTM D4767-11 (2011) and ASTM D5311/5311M-13 (2013) are followed to perform undrained triaxial tests. Shear strength, including peak and residual strength, modulus of elasticity and initial secant stiffness, stress-strain relationship, soil response during various stress paths, cyclic resistance (liquefaction) and damping ratio of a cylindrical specimen, can be determined by monotonic and cyclic triaxial tests. A triaxial test is applicable on intact, reconstituted, or remolded saturated cohesive and noncohesive soils specimens. Different stress paths similar to the field conditions can be applied during consolidation (isotropically or k_0) and shearing (extension or compression) phases. In general, the shear strength of a particular soil depends on consolidation pressure and time, strain rate, stress history (over-consolidation ratio), saturation and drainage condition.

For performing a monotonic undrained triaxial test, the cell is filled with de-aired water after sample preparation and assembling the triaxial chamber,. The cell water is used to apply confining pressures or consolidation stresses (σ_3) to the soil specimen. Depending on the permeability of the soil specimen, the saturation process may take several hours. The sand specimens are normally saturated by injecting the carbon dioxide first and then applying back-pressure (P_{BP}) to the specimen pore water to fill all voids in the soil structure with water, without the sample swelling and undesirable prestressing of the soil specimen. The progress of full saturation is determined by calculation of the pore pressure parameter B (Skempton's B-value) according to Eq. 3.4:

$$B = \frac{\Delta u}{\Delta \sigma_3} \tag{3.4}$$

where Δu is change in the specimen pore pressure due to an increase in the cell pressure when the drainage valves are closed and $\Delta \sigma_3$ is change in the cell pressure. The B-value higher than 0.95 is normally considered as fully saturated.

Consolidation is the next stage in a CU triaxial test. The objective of the consolidation phase (isotropic/anisotropic or K_0) is simulating the stress condition that is experienced by the soil specimen in the field. Therefore, the desirable pressure is applied to the soil specimen by the cell pressure while the drainage valves are open, to allow the specimen to reach equilibrium in a drained state. In a triaxial test, this can be done by holding the back-pressure constant and increasing the cell pressure until the difference between the cell pressure and the back-pressure $(\sigma_3 - P_{BP})$ reaches the required effective stress. It is then kept constant until no volumetric strain or vertical deformation is observed.

Shearing is the last phase of a triaxial test. In undrained shearing, the specimen drainage is not permitted. The cell pressure is kept constant while the axial stress is increased gradually, by advancing the load piston downward against the specimen cap using controlled axial strain criteria, until failure occurs. The rate of applying axial strain needs to be slow enough to equalise the induced excess pore pressure during shearing. An appropriate strain rate can be calculated based on Eq. 3.5 suggested by ASTM D4767-11 (2011), considering failure occurs after four per cent axial strain:

$$\varepsilon^{\cdot} = 4\%/(10t_{50}) \tag{3.5}$$

where t_{50} is the time for 50 % primary consolidation.

The cyclic undrained triaxial test is conducted to investigate the cyclic strength (liquefaction potential) of saturated soils by the load-controlled cyclic triaxial apparatus, and determines the ability of soils to resist the shear stresses induced by cyclic loadings (ASTM D5311/5311M-13, 2013). This test, similar to a monotonic triaxial test, is applicable for either intact or reconstituted soil specimens, and is performed under undrained conditions to simulate field conditions during quick loading, such as earthquakes or other cyclic loadings. Failure is usually defined based on the number of loading cycles required to reach a specific strain or zero effective stress due to development of the excess pore pressure. It is worth mentioning that the stress path experienced by the soil specimen is very different from the symmetric stress in the simple shear case of the ground liquefaction, as the mean total confining stress is asymmetric during the compression and extension paths. The required cyclic stress is estimated based on the anticipated cyclic stress ratio (*CSR*). CSR is defined as the ratio of the required deviator stress to double the effective consolidation stress. Therefore, the required cyclic stress (Δq) can be calculated according to Eq. 3.6.

$$\Delta q = 2 \times \sigma_3' \times CSR \tag{3.6}$$

Depending on the nature and source of the cyclic loading, there are different cyclic loading patterns in terms of the loading waveform and frequency. For example, a vibrating machine produces a uniform loading waveform with only one frequency, while an earthquake may consist of a range of frequencies. Ishihara (1996) suggested that frequencies between 0.05 to 0.1 Hz can be considered as the borderline between static and dynamic loadings.

Cyclic strength is normally evaluated based on the induced axial strain and excess pore water pressure, the number of loading cycles, magnitude of the applied cyclic stress and the state of the effective stress. In fact, there are various parameters affecting the cyclic resistance. These parameters include relative density, confining pressure, stress history and path, the applied cyclic shear stress, soil structure and particle shape, specimen preparation, soil deposit aging and frequency, uniformity and shape of the cyclic waveform.

Although monotonic and triaxial tests are versatile to simulate various field scenarios, there are some limitations that need to be taken into account. It is understood that non-uniform stress distribution may occur across the top and bottom of the specimen platens, which leads to redistribution of void ratio within the specimen. Sample preparation techniques affect the monotonic and cyclic strengths even at the same relative densities. For example, Zlatovic and Ishihara (1997) found that a sample of Nevada sand prepared using the moist tamping method displayed a hardening behaviour with increasing strength, while another specimen at the same initial void ratio, but reconstituted by dry deposition, exhibited a quasi-steady-state (QSS) behaviour with temporary collapse (Figure 3-2). In addition, it is believed that undisturbed samples always show higher strength than reconstituted ones.

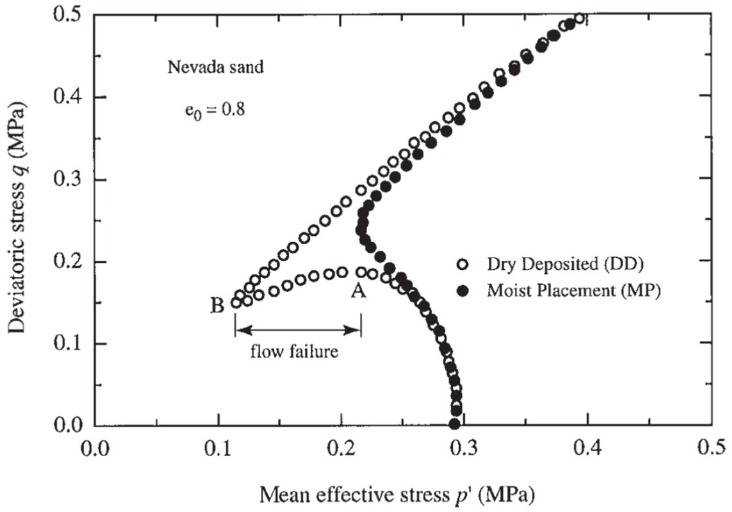

Figure 3-2. Effect of sample preparation method on the undrained behaviour of Nevada sand (Zlatovic and Ishihara 1997)

Cohesionless soils are unable to take an extension path at zero axial stress as the top platen is lifted from the soil specimen. Therefore, the maximum cyclic shear stress that can be applied to the specimen is restricted by the effective axial stress at the end of consolidation.

Apart from interaction between the specimen, membrane and the confining liquid affecting the cyclic behaviour, which cannot be considered easily, it was found that membrane penetration is affected by changes in the specimen pore water pressure. These changes can significantly influence the test results and are difficult to be deduced (ASTM D5311/5311M-13, 2013).

The test procedure for sample preparation, saturation and consolidation is the same as the CU triaxial test. During the shearing phase, the drainage valves are closed and the cyclic loading (based on the desired cyclic stress ratio) is applied to the specimen, with the first half cycle in compression. The cyclic loading is continued until one of the following termination criteria is met (ASTM D5311/5311M-13, 2013):

- The cyclic double amplitude vertical strain exceeds 20 %
- The single amplitude strain in either extension or compression exceeds 20 %
- 500 load cycles or the number of load cycles required in the testing program are exceeded, or
- The load wave form deteriorates beyond acceptable values

Regardless of whether liquefaction happens or not, a monotonic undrained shearing is performed after cyclic loading to investigate post-cyclic behaviour, as well.

3.8. Erosion-Consolidated Undrained Triaxial Test (Erosion-CU)

To investigate the effect of internal erosion on soil behaviour under monotonic and cyclic loading, a series of triaxial erosion tests is performed. These tests are performed in five stages: (i) saturation, (ii) consolidation, (iii) erosion, (iv) undrained monotonic shearing or undrained cyclic loading followed by undrained monotonic shearing and (v) post-erosion particle size distribution (PEPSD). A parallel series of non-eroded specimens are also tested under the same stress paths for comparison. The details of each stage are explained in the following paragraphs.

Soil samples are prepared in an internal split mold. To prevent collapse or disturbance of the sample during the test setup, a vacuum pressure of 10 kPa is applied. When the triaxial chamber is assembled, the suction is gradually removed while the cell pressure incrementally increases to 10 kPa. Next, to ensure that a high level of saturation is achieved in a timely manner, carbon dioxide is injected at the bottom of the specimen using a flow controller for two hours while the cell pressure was maintained constant. The rate of injection is kept low (1 L/min) to avoid any specimen disturbance caused by gas flow. The cell and back-pressure are then linearly and gradually (1 kPa/min) increased to reach 400 and 390 kPa, respectively. These pressures are held for a further 100 mins to ensure that the specimens are fully saturated. The B-value is also checked at the end of this stage.

Frost and Park (2003) showed that during sample preparation by the moist tamping method, specimens may experience vertical peak stresses of 95 to 184 kPa for relative densities of 50 to 75 per cent. These significant stresses may affect soil behaviour and accelerate the development of a shear band. In addition, the magnitude of the applied stress during the moist tamping cannot usually be monitored. This uncertainty may result in a reduction in accuracy, especially in erosion tests where uniformity in dry density and void ratio across the specimen height is necessary. To reduce the effect of the moist tamping stresses and to remove the stress history, all specimens were consolidated to 150 kPa. Thus, the isotropic consolidation is performed by gradually increasing the cell pressure up to 540 kPa (150 kPa consolidation pressure). The rate of increase is the same as what is applied during the saturation stage to avoid any disturbance or segregation.

For the eroded tests, the erosion of the specimen is performed after consolidation. Under constant stress condition, de-aired water is allowed to seep downward from the top of the specimen. The flow rate increases gradually up to the desired value and is kept constant for 30 or 120 minutes, depending on the test program. This flow rate is higher than the critical flow rate initiating suffusion but lower than the failure flow rate.

It is generally accepted that the critical hydraulic gradient is much lower than one for internally unstable soils. Test results showed that erosion of fine particles confirmed that the chosen flow rate was higher than the critical value. The maximum applicable flow rate by the flow controller was 500 ml/min. A large flow rate (lower than the maximum value) was selected for this experiment to terminate the erosion phase in a reasonable period of time. However, it was first applied in a pilot test to examine whether a global failure occurs in the soil specimen or not. As this did not happen and the soil structure was robust until the end of the erosion phase, this flow rate was chosen for the experiment. To find the failure flow velocity, a soil specimen with 50 mm diameter was prepared under the same condition and subjected to an inflow velocity of 208 mm/min (flow rate of 408 ml/min), which was approximately 2.3 times greater than what was experienced by the soil specimen with 75 mm diameter. The test result showed that this specimen was still stable at the end of the erosion phase, although it experienced larger deformations. These trials and errors indicated that the failure flow rate is not obtainable for soil specimens with 60 per cent relative density and under 150 kPa consolidation pressure due to limitation of the flow controller.

Luo et al. (2013) performed both short-term and long-term suffusion tests. The results indicated that for the long-term tests, the failure hydraulic gradient was much lower than for the short-term tests. They also stated that a long-term large hydraulic gradient may decrease the failure hydraulic gradient significantly. This means that although the adopted flow rate is lower than the failure hydraulic gradient, it may cause general collapse of the specimen if the erosion continues for a long time. Therefore, the erosion stage is terminated after a specific time in all tests by gradually decreasing the inflow. Since two pressure transducers are connected to the top and bottom of the specimen, the general hydraulic gradient and hydraulic conductivity through the specimen length can be measured. When the pore water pressure becomes stable at the top and bottom of the specimen, the next stage begins. Before undrained monotonic or cyclic shearing of the specimen, the B-value is checked again to ensure that the specimen is still fully saturated.

At the end of the erosion phase, post-erosion behaviour is investigated under undrained monotonic or cyclic loadings. The cyclic behaviour of the samples is investigated under a Cyclic Stress Ratio (CSR) equal to 0.167 and a period of 120 seconds (equivalent frequency of 0.0083 Hz). Strain-control monotonic shearing at the axial strain rate equal to 0.26 %/min is performed at the end of both non-eroded and eroded tests. A low frequency for the cyclic loading and a low rate for the monotonic shearing are selected to allow the pore pressure to reach equilibrium. On the contrary to clay soils, strain rate and loading frequency have a minor impact on the response of cohesionless soils (e.g. Bolton and Wilson, 1990; O'Reilly and Brown, 1991; Kabir and Chen, 2011).

3.8.1. Sample Preparation of Triaxial and Erosion-Triaxial Tests

Sample preparation is one of the important parts of this experimental investigation. It is critical to perform erosion tests on completely uniform specimens in terms of density, particle size distribution and void ratio through the entire height of samples. Otherwise, the test results may show considerable discrepancy, even under similar stress path and hydraulic gradient. There are different methods in the literature to prepare uniform specimen for triaxial tests. The undercompaction method (Ladd, 1978), the moist tamping method (Frost and Part, 2003; Jiang et al., 2003; Bradshaw and Baxter, 2007), the Slurry method (Kuerbis and Vaid, 1988; Carraro and Prezzi, 2008) and the pulviation method are some of the common methods to prepare uniform soil samples. For this research, the under-compaction moist tamping technique, presented by Ladd (1978) with modifications employed by Jiang et al. (2003), is selected, as the repeatability of previous experimental investigations carried out by Chang and Zhang (2011) and Ke and Takahashi (2014b) was satisfactory. This technique prevents segregation during sample preparation and creates specimens with maximum uniformity across the specimen height. The soil mixture with six per cent initial water content was compacted layer by layer to achieve the required thickness and the desirable 60 per cent relative density. Geometric properties of the tested specimens are shown in Table 3-4. Regardless of the height of the specimens, the soil layer thicknesses varied slightly over a narrow range for specimens with diameter of 50 mm (D50), 75 mm (D75) and 100 mm (D100), as shown in Figure 3-3. This helped each soil layer to experience similar compaction pressure during sample preparation.

Table 3-4. Soil samples specifications

Sample ID	Sample Diameter (mm)	Sample Height (mm)	Total Number of Soil Layer
D50	50	115	8
D75	75	150	10
D100	100	200	14

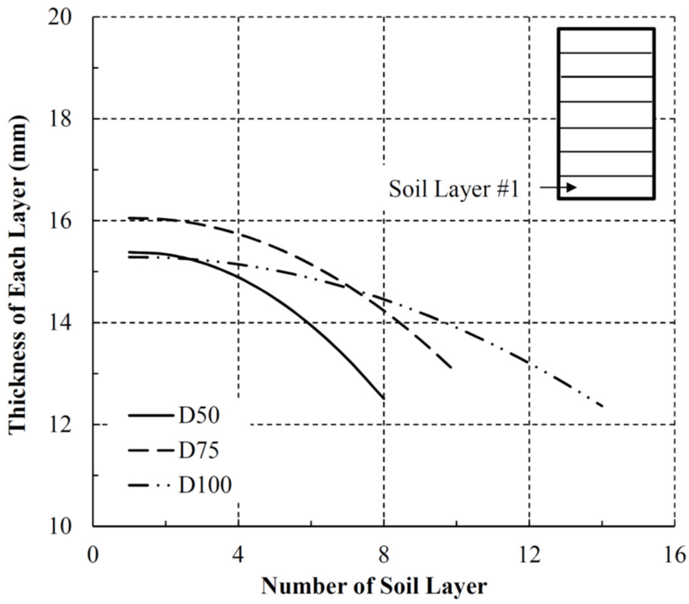

Figure 3-3. Thickness of each soil layer during sample preparation

3.8.2. Volumetric and Vertical/Lateral Strains Measurement Techniques

There are a range of direct and indirect methods to measure local vertical/lateral and volumetric strains in triaxial testing. In an ordinary triaxial test on a fully saturated specimen, volumetric and general vertical strains are usually measured using pore water volume variation and a mounted Linear Variable Differential Transducer (LVDT) on the top of the specimen, respectively. When the soil specimen is unsaturated, pore water volume measurement is not applicable. Other techniques such as cell liquid measurement, air-water volume measurement, local displacement sensors, non-contacting laser and photogrammetry have been developed to overcome this issue. In cell liquid measurement technique, confining cell liquid is monitored to measure sample volume changes. However, this technique requires an intensive calibration, as ambient temperature, chamber creep, immediate cell expansion during cell pressurising, loading ram movement and sample loading/reloading affect the cell liquid volume. This calibration needs to be conducted for each individual test. The only advantage of this technique is simplicity. However, Bishop and Donald (1961) improved it by proposing a double cell chamber to minimise the cell liquid volume. Air-water volume measurement is another technique to record the volume changes of the soil sample. This can be performed by connecting two air-water pressure controllers to the soil specimen. Undetectable air leakage and diffusion, small temperature and atmospheric pressure changes, and high compressibility of air need to be taken into account (Adams et al., 1996; Geiser, 1999; Blatz and Graham, 2000; Laloui et al., 2006). Apart from indirect techniques, such as cell liquid and air-water volume measurements, there are some direct measurement methods in which the volume change of a specimen is computed from the sample superficial changes. Attachment of local displacement sensors is the most commonly used technique (e.g. Clayton et al., 1989; Goto et al., 1991; Klotz and Coop, 2002). However, reinforcing effect on the soil sample, discrete measurement of the local strains, delicate sensor installation and low accuracy when the sample deformation pattern is barrel shape are some of its drawbacks. The non-contacting long range laser system was proposed first by Romero et al. (1997). Non-uniformity and local deformations are also detected using this technique. However, it is costly and needs a sophisticated installation procedure. Photogrammetry including video imaging, particle image velocimetry (PIV) and digital image correlation (DIC) is a direct measurement method, is easy to setup and is cheap in comparison to other techniques. However, image processing might be time-consuming and complicated. Macari et al. (1997) were the first researchers who used video imaging to measure volume changes of a triaxial soil specimen. However, taking into account the light refraction through cell water and Plexiglas cell chamber, and curvature of the cell, were challenging. This technique was further improved by other researchers (e.g. Alshibli and Al-Hamdan, 2001; White et al., 2003; Gachet et al., 2007 and Zhang et al., 2015).

Salazar et al. (2015) and Salazar and Coffman (2015) presented a novel system of internal photogrammetric instrumentation for triaxial testing. They suggested that this new system overcomes the existing challenges and drawbacks of current image processing methods. These drawbacks include the optical distortion due to curvature of the cell wall and light refraction at the interfaces between (i) cell wall and cell fluid, (ii) cell wall and atmosphere, and (iii) camera lens and atmosphere. Alshibli and Sture (1999) and Uchaipichat et al. (2011) provided another method to eliminate errors owing to light refraction. In these two research works, external photogrammetry was adopted to evaluate the shear band thickness of sand and volumetric strains of an unsaturated soil during triaxial testing, respectively. These researchers considered the first image of a specimen inside the full pressurised triaxial cell before starting the shear phase as the point of reference, and compared the next consecutive images with the first reference image. Thus, any distortion owing to cell curvature, camera lens, cell pressure, and light refractions were eliminated since the strain values were measured based on relative displacement between images. It is important to note that the strain values are the primary focus in a triaxial test and not the exact magnitude of sample volume or displacement. Therefore, for most common triaxial tests, it seems that using the first image as a reference image is a much simpler, cheaper, and more practical approach compared to an intensive, time-consuming, and complicated set of other techniques. In addition, Uchaipichat et al. (2011) investigated the effects of temperature and cell pressure on external photogrammetry. Their results showed that there was no difference between the measured volume by PIV and the actual volume of a dummy sample for the range of cell pressure and test temperature. Their research confirmed that there was no need to consider the effects of variation of cell pressure, especially during shearing.

The method suggested by Uchaipichat et al. (2011) was later investigated by Mehdizadeh et al. (2015b) for measuring local vertical/lateral strains measurement. The measured volumetric strains using photogrammetry are usually compared with change in volume of cell water or change in pore water volume. It is acknowledged that the change in the volume of water owing to cell pressure or temperature of the surrounding environment, creep of cell under pressure, and unsaturation of soil sample may cause some errors in verifying photogrammetry results. To eliminate these errors, seven stainless steel balance weights with known dimensions were used. The balance weights were named based on their weight, and their surface was covered with white paper to provide a better contrast while imaging. These balance weights (i.e., dummy samples) are shown in Figure 3-4. It was assumed that the largest weight represents the initial condition of a triaxial specimen, and the smaller weights represent the contracted samples during testing. It is worth noting that these samples were not subjected to any consolidation pressure or real force. The dimension and volume characteristics of each weight are shown in Table 3-5. This table suggests (assuming these are triaxial specimens during a drained shearing phase) that the sample volume decreases from 1,148,621 mm^3 to 5836 mm^3 during testing. The sample volume variations were first captured using the photogrammetry technique in the air and then in the triaxial cell filled with water. Uniform light was provided using two desk lamps. A distance of 1.8 m between the sample and camera was selected in order to eliminate the effect of curvature of the top and bottom of weights due to optical effect.

Figure 3-4. Stainless steel dummy samples used in the photogrammetry

Table 3-5. Dimensions of dummy samples

ID (kg)	Diameter (mm)	Height (mm)	V (mm^3)
10	106.5	128.94	1148621
5	81.9	109.2	575281.4
2	63.37	73.05	230397.4
1	50.8	56.83	115184.7
0.5	41.34	44.28	59434.48
0.25	32.04	36.75	29630.04
0.05	20.87	17.06	5835.98

The details of photogrammetry and programming have been explained clearly by Uchaipichat et al. (2011). Minor modification was applied to the codes developed by Uchaipichat et al. (2011) (Appendix A) to be applicable in this research.

Figure 3-5 illustrates the accuracy of volumetric strain measurements through air and the triaxial cell full of water. Although the magnification indices of light refraction are not similar in horizontal and vertical directions, the results suggest that these effects are negligible. The measured results show that the error of volumetric strain measurements using photogrammetry through air to be only 0.068 %, whereas the error increases to 0.23 % through a triaxial cell filled with water. The increase in error when the cell is full of water is believed to be related to the difficulty in establishing sample edges when it is inside the cell. Nevertheless, it is important to note that the accuracy is still very good. These errors were calculated based on comparing the measured volumetric strains with real volume variations of balance weights.

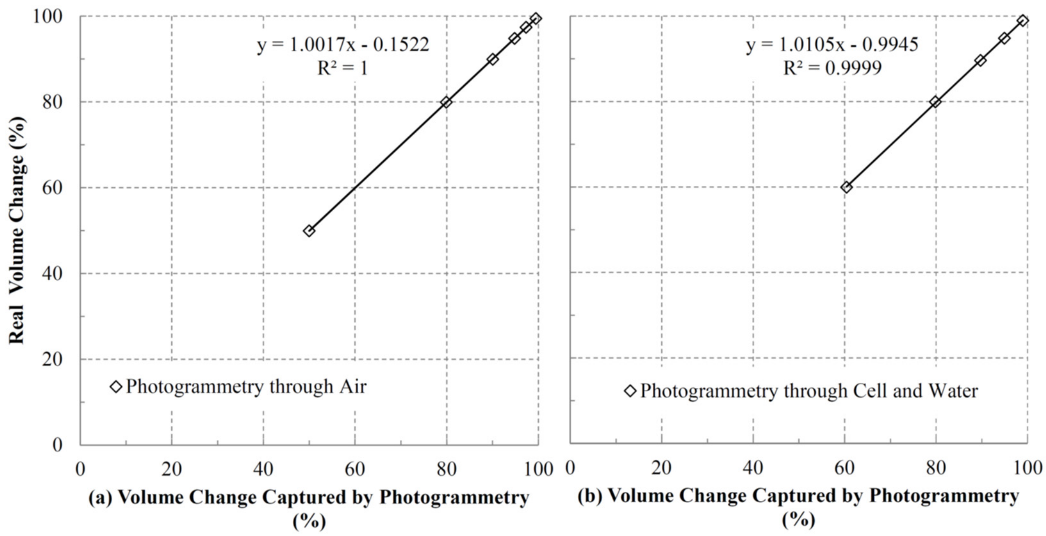

Figure 3-5. Photogrammetry results through (a) air and (b) cell and water

It is worth noting that as the refraction of light was not considered in calculations, there is no direct way to measure the observed volume of balance weights inside the cell, except by comparing the occupied pixels of samples in images. In other words, the occupied pixels of the first sample (10 kg) in the first image through air were measured. This step was repeated for the first image of this sample inside the cell filled with water. Then, by knowing the occupied pixels in both images (through air and through cell and water) and real volume of the sample, the observed volume of the sample inside the cell filled with water was estimated and used for volumetric strain measurements of other samples. These test results confirmed that using relative displacement (between each image and the first image as a point of reference) can significantly reduce issues associated with distortion of light, cell curvature, and camera lens; there is no need to consider them for calculating the volumetric strains during triaxial testing.

In summary, it was found that external photogrammetry based on Uchaipichat et al.'s (2011) method with one or two cameras can measure volumetric strains of a triaxial specimen at an appropriate level of accuracy, while still keeping the method simple and straightforward, as well as eliminating the need to modify the triaxial cell. However, it is necessary to mention that the cleanliness of the cell wall, the obstruction of reinforcing strips on cell wall and cell rods, the distance of the camera to the sample, and the need for at least two cameras for recording non-uniform volumetric strains are the main drawbacks of external photogrammetry.

3.9. X-ray Tomography

To get a better understanding of post-erosion soil behaviour, it was decided to investigate the micro-structure of soil specimens in terms of particle rearrangement, pore structure and fine content pre- and post-erosion using 3-dimentional X-ray tomography. Computed Tomography scanning (CT scanning) is well-known in medical fields and has been used for many years. X-rays are invisible, but high-energy electromagnetic waves capable of passing through many objects. Depending on the density of materials, a percentage of the X-rays is absorbed by the object; an increase in the density of the material results in a greater percentage of the X-rays being absorbed. The remainder that penetrates through the object hits an X-ray sensitive screen installed in front of the object and is captured by a digital camera. A CT scan is then produced, which is in fact a replication of the X-ray penetration pattern (Nielsen, 2004). Photography that is 360 degrees, obtained at controlled orientations of an object, produces images from many different views. These images are used to generate a full 3D CT scan, and provide cross-section views of the object at different levels and angles. A CT scan consists of voxels with different colours (intensities) that quantify the attenuation of X-rays at any specified point in the object. A voxel is a unit of graphic information that represents a value on a regular grid in three-dimensional space. This is a non-destructive technique and provides valuable information about the internal structure of materials which are μm in size, and cannot be observed by the naked eye. This phase includes 2D imaging and data collection, 3D image reconstruction, and image analysis and interpretation. First, soil samples are exposed to X-rays and digitally photographed. These individual images are then superimposed and stitched together to make a 3D image of the interior structure of the soil specimens.

In geotechnical engineering, the CT scan was first employed by Mulilis et al. (1977) to investigate sample preparation on sand liquefaction. Jang et. al. (1999) and Frost and Park (2003) developed techniques to prepare soil specimens for X-ray imaging. Frost and Jang (2000), Wang et al. (2004), Kaestner et al. (2005), Halverson et al. (2005), Al-Raoush and Alshibli (2006), Wang et al. (2007), Razavi et al. (2007), Yamamuro et al. (2008), Homberg et al. (2009), Hall et al. (2010), Hasan and Alshibli (2010), Fonseca (2011), Frost et al. (2012), Fonseca et al. (2012) and (2014) and Taylor et al. (2015), among others, investigated different properties in soils and rocks by X-ray tomography. Most of this research was based on selecting an intensity threshold to separate the void and particle phases, and creating a binary image that splits the soil sample into solid particles and void space (Taylor et al, 2015). However, Garner and Sobkowicz (2002) were the only research group that tried to explore qualitatively internal erosion using CT scans, as discussed in Chapter 2. It seems that impact of internal erosion on soil and pore structures, particle rearrangement and contacts has not been fully understood yet.

This phase includes sample preparation, erosion test, X-ray imaging pre- and post-erosion and data analysis. The main challenge is transferring eroded specimens for CT-scanning without any soil disturbance. Triaxial specimens have flexible walls, and because the soil mixture in this research is cohesionless, removing the confining pressure at the end of the shearing phase would result in soil specimens collapsing, and imaging would not be possible. Protection of soil specimens from any collapse can be achieved by either impregnation of the soil specimen with resin, or by saturating it with water and freezing it. However, it was understood that resin impregnation was the more practical option (Jang et al., 1999). Mulilis et al. (1977), Jang et al. (1999) and Frost and Park (2003) tried to prepare triaxial specimens for imaging by resin-impregnating into dried soil specimens. Epoxy resins are more stable and create normally durable specimens when cured, in comparison to other types of resins, and have been commonly used to stabilise specimens in biology, metallography, and soil and rock sciences (Jang et al., 1999). The most challenging part of resin impregnating is avoiding the soil specimen disturbance, especially in loose sand specimens that are intensely susceptible to particle rearrangement. This normally happens, as the resins have relatively high viscosities that are typically 300 times greater than water at room temperature and show considerable shrinkage potential during curing even without heating. The shrinkage occurs due to either the high solvent content for lowering the viscosity of the resin, or change of molecular structure, bonding, and spacing during curing and the chemical reaction. While the high viscose epoxy resins are not applicable for soil specimen impregnation, most low-viscosity resins are thermos-curing, which requires oven heating to a temperature normally higher than 60°C for curing. This is also inapplicable as the soil specimen incurs differential thermal stresses and volume changes at this raised temperature, which leads to disturbance of the soil specimen. In addition, performing a geotechnical test in a temperature higher than room temperature is not practical in most cases and does not simulate real applications. Jang et al. (1999) suggested that an ideal epoxy resin should have the following characteristics to be appropriate for sand specimen impregnation:

- Low viscosity
- Cures at room temperature
- Low shrinkage during curing
- High hardness value and high bonding strength on curing
- Good working properties and short curing time
- Nontoxic
- Nonreactive with soil and test equipment

Apart from viscosity and shrinkage of epoxy resins that are challenges in the specimen impregnation, most of them, including EPO-TEK 301, do not cure well in moist environments, limiting the application of epoxy impregnation. Therefore, wet soil specimens, such as undisturbed samples extracted from the subsurface in the field or prepared samples by moist tamping or slurry and water pluviation methods, need to be fully dried first before impregnation with epoxy. Depending on the water content and dimensions of the soil specimen, the drying process lasts from one to several days. Normally the dryness of the soil specimen is determined by the humidity of air flowing out of the sample (Jang et al., 1999).

Jang et al. (1999) developed a resin impregnation technique to prepare cohesionless soil specimens for CT scanning. However, this procedure was limited to drained triaxial tests only. In undrained triaxial tests, it is important to have B-vale (Skempton's parameter) close to unity to be able to monitor and measure the pore water pressure accurately, as it is used in calculating effective stresses. As resin impregnation is applied to dried specimens, it is nearly impossible to fully saturate a specimen with an epoxy resin and reach the required B-value higher than 0.95. This is due to high viscosity of epoxy resins that increases the chance of air entrapment in some pores during impregnation. Moreover, the influence of pore fluid viscosity on undrained test is not yet fully understood. An epoxy resin can be injected into the bottom of a soil specimen either under a low differential pressure of about 20 to 30 kPa between the top and bottom of the specimen, or by vacuum-induced epoxy flow. However, the latter technique was found to be unsuccessful, as volatile reacting agents in the EPO-TEK 301 resin evaporate quickly under a small continuous vacuum (Jang et al., 1999). Other technical challenges were also reported by Jang et al. (1999). For example, they encountered difficulties in resin curing when the latex membrane became moistened with the cell water during application of the confining pressure and absorbed water. This was solved by covering the outside of the latex membrane with a thin layer of vacuum grease after sample preparation. In addition, it is nearly impossible to disassemble triaxial cell components that come into contact with the epoxy resin. These parts would not be reusable and need to be replaced for each test, with the exception of plastic tubes or latex membranes, which have no bond with the epoxy resin.

It is evident that although the resin impregnation technique can be used to prepare soil specimens for CT scanning with minimal disturbance, its application is limited due to following drawbacks:

- It is only applicable to dried soil specimens
- A long time is required for drying the specimen, and epoxy resin impregnation and curing (approx. several days)
- It requires specific modifications of the triaxial chamber for the epoxy resin impregnation

- Non reusable triaxial accessories, such as top cap and bottom base plate, and other parts contacting with the epoxy resin
- The common technique of resin impregnation is not applicable for undrained tests
- Strain measurements by PIV technique are difficult due to covering the outside of the membrane by the vacuum grease

These limitations prevent using the resin impregnation technique in this research study. First of all, it is not possible to dry the eroded specimen, because fine particles immediately lose their contacts with coarse particles, segregation occurs, and the soil and pore structures change. The required triaxial chamber modifications for the epoxy resin injection are in contrast with the current modifications for performing internal erosion. The focus of this research is investigation of post-erosion undrained behaviour, and as previously discussed, this technique has not been approved for the undrained test yet. Volumetric and horizontal/vertical strains are measured using the photogrammetry technique in this research, and covering the membrane body with vacuum grease reduces the accuracy of measurement. Moreover, it is not possible to use a new top cap and bottom base plate for every single erosion-triaxial test. Considering all of these restrictions, an alternative technique is developed to prepare eroded specimens for X-ray tomography.

A new PVC mold (50 mm inside diameter similar to the triaxial specimens) with a mounted mesh at the bottom is used to prepare a specimen (with 100 mm height, as shown in Figure 3-6 (a) and (b)), carry out X-ray tomography, erode the same soil specimen, and then carry out X-ray tomography on the eroded specimen. The mounted mesh holds coarse particles in place while fine particles are free to be washed away under a downward seepage flow. To reduce the chance of preferential seepage paths at the interface of soil and PVC tube, the wall edges are covered with a thin layer of grease before sample preparation. The PVC mold is placed on the modified base plate (Figure 3-6 (c)), and the soil specimen is prepared using the moist tamping method. It is saturated and consolidated to 150 kPa before the erosion phase, similar to the triaxial specimens. When the top cap is placed on the top of the specimen, the water flow and pressure transducer tubes are connected, and the encapsulated specimen is covered with a latex membrane and sealed with O-rings (Figure 3-7 (a)). The soil sample is eroded under seepage flows with the same properties in the triaxial testing. Erosion of the fine particles and vertical settlement of soil specimen can be visually observed in Figure 3-7 (b). The top and bottom of the specimen pre- and post-erosion is sealed temporarily by paraffin to keep the moisture content intact and remove possibility of soil particle movement (Figure 3-7 (c)). Penetration of paraffin into the soil specimen is prevented by putting paper and nylon sheets on the top and bottom of the sample before paraffin sealing. It is evident that the rigid wall tube cannot simulate the soil condition similar to that inside a rubber membrane that deformation is restricted only to the vertical direction. However, it is believed that CT-scanning the eroded specimens using this technique can provide valuable insight about particle rearrangement and variation of the pore structure after internal erosion. The encapsulated eroded and non-eroded specimens are transferred to Australian Synchrotron (Figure 3-7 (d)) and the Trace Analysis for Chemical, Earth and Environmental Sciences (TrACEES) platform at the University of Melbourne for X-ray tomography. Micro-CT scanning with a 31 and 21 micron resolution is conducted in Australian Synchrotron and the University of Melbourne, respectively, more than 2 to 3 times higher than the smallest particle size (≥ 75 micron).

Australian Synchrotron is a very large megavoltage machine consisting of a vast, circular network of interconnecting tunnels and high tech apparatuses. The source of power in the Synchrotron is electricity in order to generate intense beams of light by forcing high-energy electrons to travel in a circular orbit inside the synchrotron tunnels under strong magnetic fields. These beams are a million times brighter than the sun and travel at a speed of about 299,792 kilometres per second (close to the speed of light). They are filtered and adjusted to travel into experimental workstations that are used to investigate the molecular structure and the innermost and sub-microscopic secrets of materials such as human tissue, plants, and metals (Australian Synchrotron, 2017).

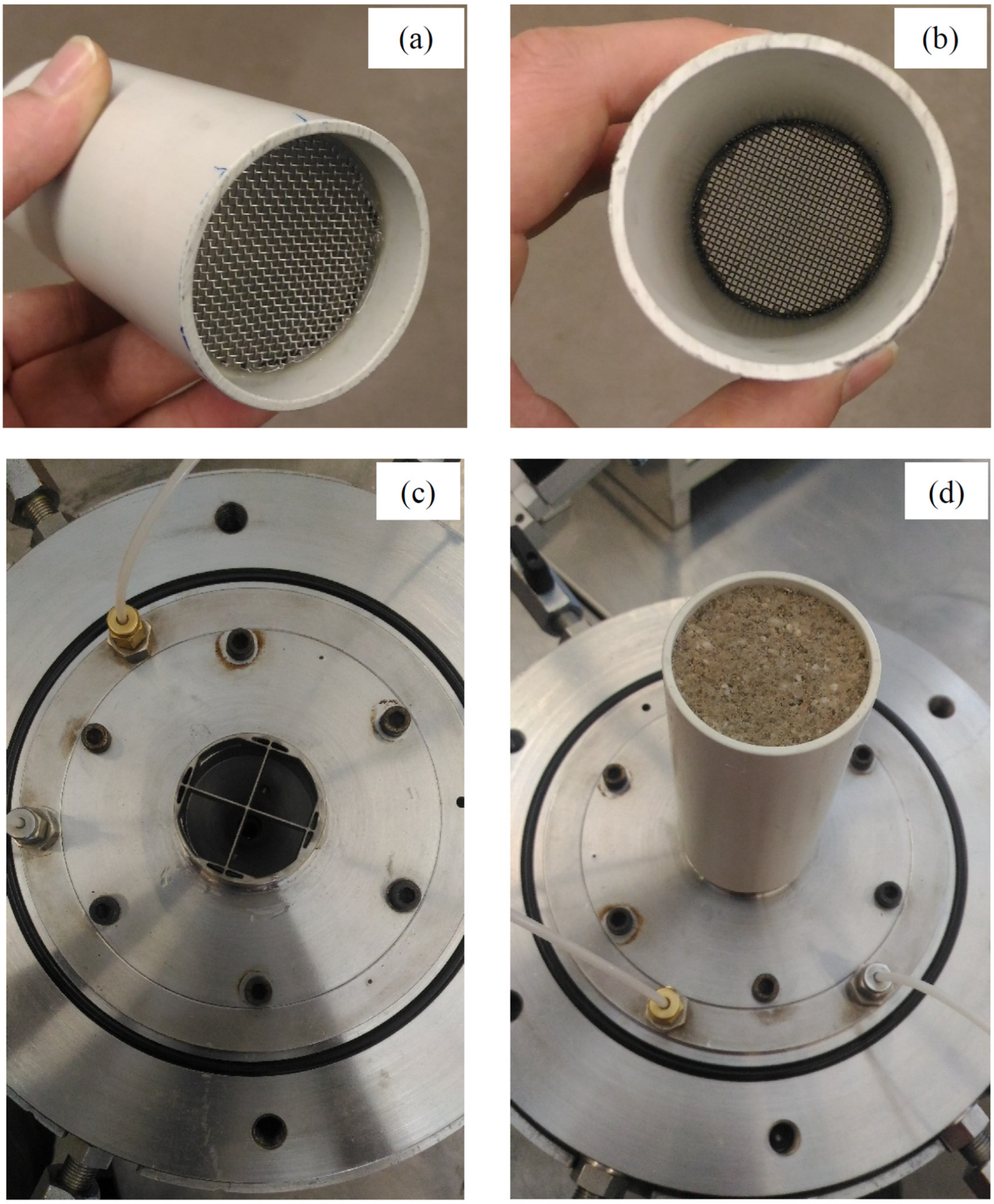

Figure 3-6. Preparation of soil sample for X-ray tomography (a) bottom view of the rigid wall sample mold, (b) Top view of the rigid wall sample mold, (c) Modified base plate and (d) Soil sample before internal erosion test

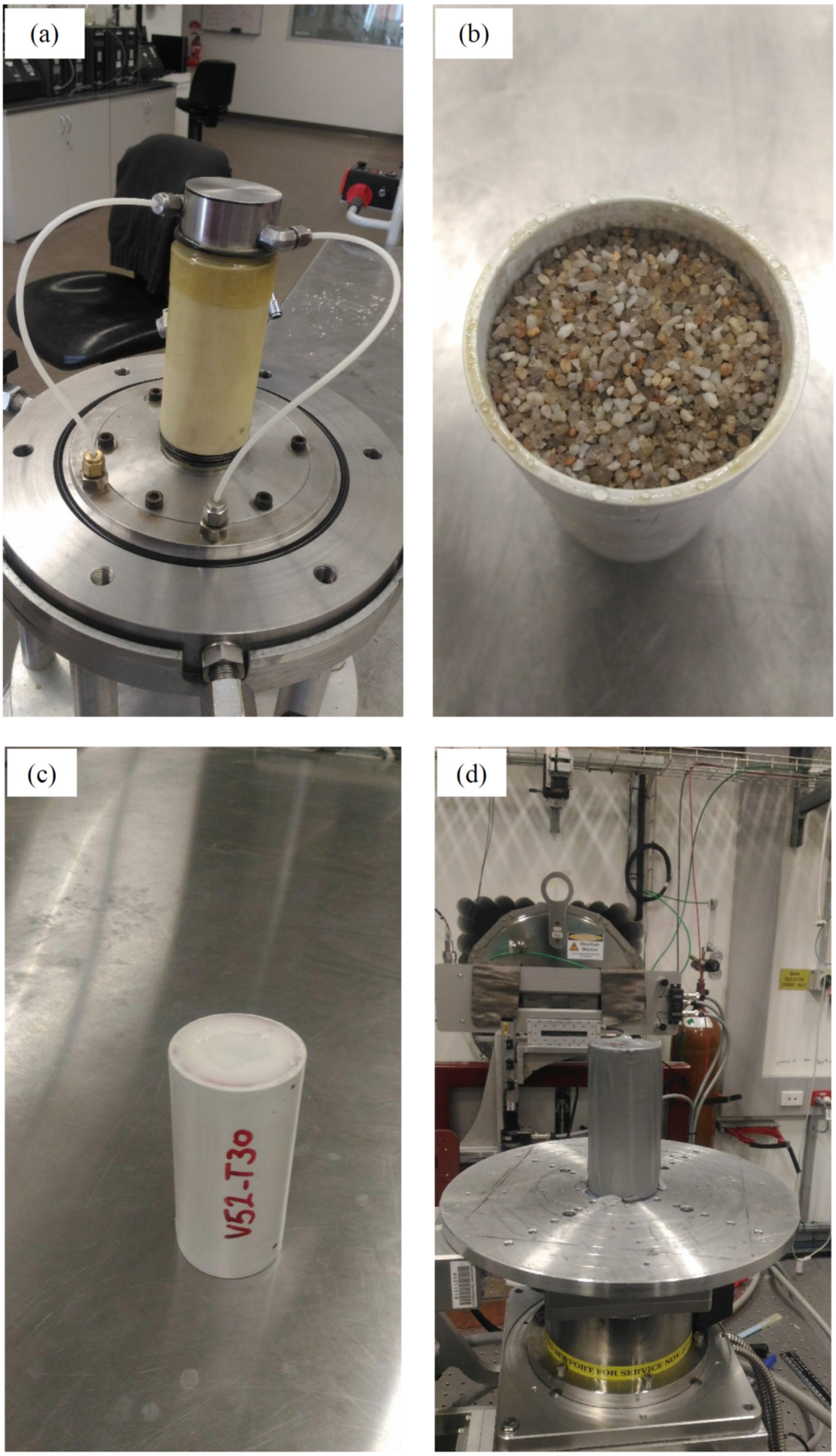

Figure 3-7. Preparation of soil sample for X-ray tomography (a) Sample setup for internal erosion test, (b) Soil sample after internal erosion test, (c) Soil sample sealed for transferring and (d) μCT scanning at Australian Synchrotron

Chapter 4 Geotechnical Characteristics of the Soil Mixture

Soil response to internal erosion depends on various internal and external factors, such as seepage and effective stress condition, soil properties, and duration of erosion. It is evident that some geotechnical properties of soils play more important roles than others during internal erosion. The required properties for purpose of this research include particle size distribution (gradation curve), relative density, specific gravity, particle shape, internal friction and cohesion of particles. In Chapter 3, it was shown how these parameters can be measured in the laboratory. This chapter briefly presents the geotechnical characteristics of the soil mixture.

4.1. Particle Size Distribution and Soil Classification

Natural sand (non-plastic particles) with particle size distribution, presented in Figure 4-1, was selected for this study. To assure the tested specimen was internally unstable, an artificially gap graded specimen was created by manually removing particle sizes between 0.3 to 1.18 mm and 2.36 to 10 mm. The gap-graded specimens with 25 per cent fine content (FC) were prepared using particle sizes of 0.075 to 0.3 mm (fine content) and 1.18 to 2.36 mm (coarse content) (Figure 4-2). Previous studies in the literature showed that there is a threshold value (25 % ≤ FC_{Thr} ≤ 35 %) for the fine content, above which coarse particles are floating within a fine matrix and are no longer in full contact with each other. In fact, fine particles form the soil skeleton and carry stresses. In this condition, the soil is internally stable and fine particles are not susceptible to the internal erosion under a seepage flow. Moreover, it was understood that fine particles in soils with a low fine content (less than 25 per cent) may only fill the voids between coarse particles and may be inactive in stress transferring. Therefore, erosion of these particles has no influence on post-erosion behaviour. Since the main object of this research is investigation of the post-erosion behaviour of internally unstable soils, 25 per cent fine content was selected to avoid any misleading consequences.

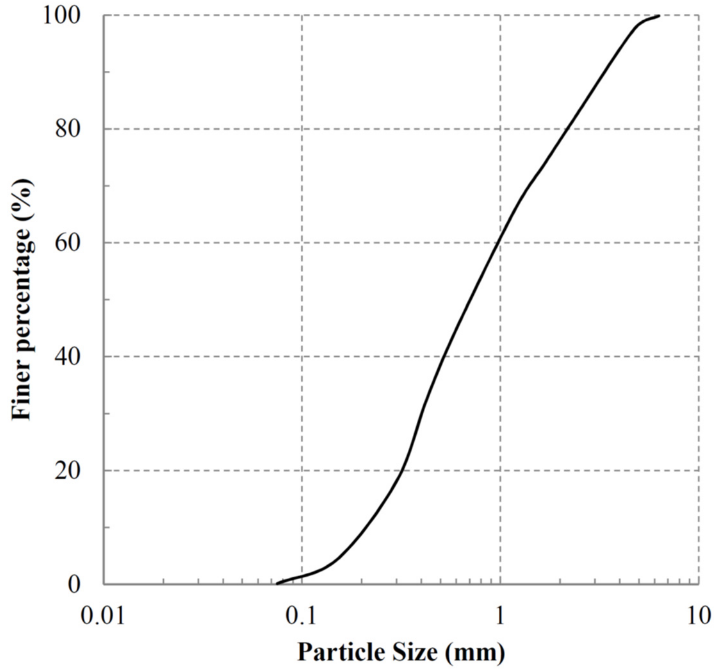

Figure 4-1. Original particle size distribution

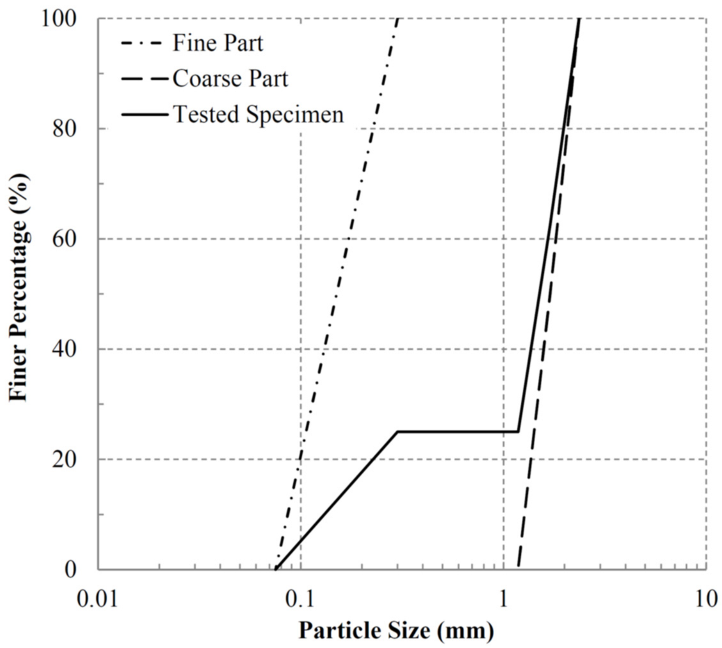

Figure 4-2. Particle size distribution of the tested soil mixture

According to the Unified Soil Classification System (USCS) (Stevens, 1982) and AS 1726-93 “Geotechnical Site Investigations” (Standards Australia, 1993), the soil mixture with non-plastic particles in this research is classified as coarse grained material and Poorly graded Sand (SP). Susceptibility of this gradation to internal erosion is examined in the next section. Table 4-1 shows geometric characteristics of the selected soil mixture.

Table 4-1. Geometric properties of the soil mixture

Physical property	Value	Physical property	Value
Fine Content, FC (%)	25	D_{10} (mm)	0.131
d'_{85} (mm)	0.244	D_5 (mm)	0.099
D'_{15} (mm)	1.318	D_{up}/D_{bt} [a]	3.93
D_{max} (mm)	2.36	G_r [b]	3.93
D_{90} (mm)	2.166	D_{erod} [c] (mm)	0.103
D_{75} (mm)	1.885	D^{*} [d]	0.264-0.307
D_{60} (mm)	1.641	$D_{c35(densest)}$ [e] (mm)	0.22
D_{50} (mm)	1.497	$D_{c35(loosest)}$ [f] (mm)	0.679
D_{30} (mm)	1.244	D_{c35} [g] (mm)	0.285
D_{20} (mm)	0.228	C_u [h]	12.52
D_{15} (mm)	0.173	C_c [i]	7.2

[a]: D_{up} and D_{bt} are maximum and minimum sizes in the gap zone
[b]: Gap ratio
[c]: Maximum erodible particle size Burenkova (1993), $0.55(\frac{D_{90}}{D_{15}})^{-1.5} < \frac{D_{erod}}{D_{max}} < 1.87(\frac{D_{90}}{D_{15}})^{-1.5}$
[d]: Constriction size (Kenney et al., 1985), $D^{*} = 0.2 \times D'_{15}\ or\ 0.25 \times D'_{5}$
[e]: Controlling constriction size for the densest state (Dallo et al., 2013)
[f]: Controlling constriction size for the loosest state (Dallo et al., 2013)
[g]: Constriction size (Dallo et al., 2013)
[h]: Uniformity coefficient
[i]: Curvature coefficient

4.2. Internal Erosion Susceptibility

To assure that erosion of fine particles occurs during the experimental investigation in this study, the internal stability of the created soil gradation is assessed based on the available geometric methods in the literature. These methods include research by the U.S. Army (1953), Istomina (1957), Kezdi (1969), Sherard (1979), Kenney and Lau (1985, 1986), Kwang (1990), Chapuis (1992), Burenkova (1993), Mao (2005), Wan and Fell (2008), Indraratna (2011), Ahlinhan (2012), Salehi

Sadaghiani and Witt (2012), Dallo et al. (2013), Chang and Zhang (2013) and Moraci et al. (2014).

4.2.1. U.S. Army (1953) and Istomina (1957) Criteria

These two criteria are based on uniformity coefficient ($C_u = \frac{D_{60}}{D_{10}}$). A soil is classified as internally stable if:

- $C_u < 20$, U.S. Army (1953)
- $C_u \leq 20$, Istomina (1957)

According to the soil particle distribution (Figure 4-2), C_u is calculated as 12.52 for the tested material. This means that the soil mixture is classified as internally stable.

4.2.2. Kezdi's (1969) and Sherard's (1979) Criteria

Kezdi's (1969) and Sherard's (1979) criteria are based on the classical retention criteria for granular filters (Terzaghi, 1939). A soil is classified as internally stable if:

- Kezdi's Method: $D'_{15}/d'_{85} < 4$
- Sherard's Method: $D'_{15}/d'_{85} < 5$

The soil gradation is considered internally unstable based on these two criteria, as D'_{15} and d'_{85} are 1.318 and 0.244, respectively and D'_{15}/d'_{85} is found to be equal to 5.4 for the soil gradation in this study.

4.2.3. Kenney and Lau (1985, 1986) Criteria

To assess internal stability of a soil using Kenney and Lau (1985, 1986) criteria, it is necessary to plot the mass of fraction (*H*) measured between particle diameters (*D*) and (*4D*), and to plot it with the corresponding value of (*F*) (mass fraction smaller than *D*) at any point on the soil particle size distribution. A soil is classified as internally unstable if:

- *H < 1.3F* or *H < F*

Figure 4-3 shows variation of *H* versus *F* for the soil mixture in this research. It can be seen that for *F* less than 25 per cent, $\frac{H}{F} < 1$. This means that the soil gradation is internally unstable.

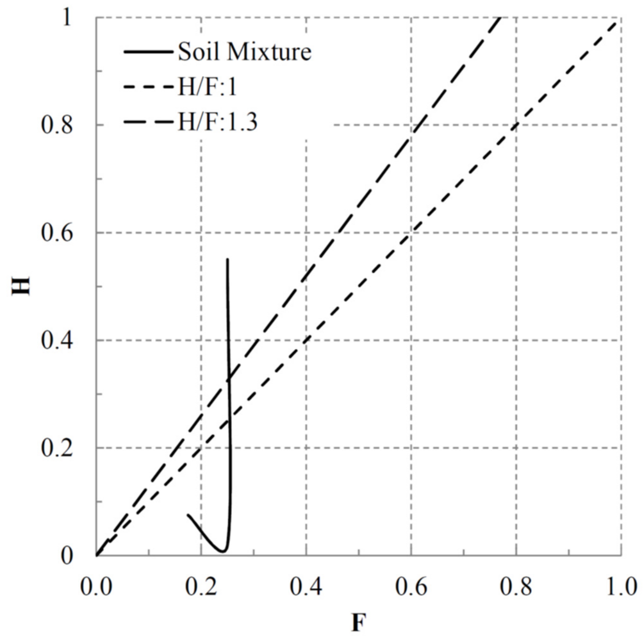

Figure 4-3. Variation of H to F for the tested soil mixture

4.2.4. Kwang (1990) Criteria

It was mentioned in Chapter 2 that this method is only applicable for gap-graded soils, and that a soil is internally unstable if:

- $\frac{D_{up}}{D_{bt}} > 4$

where D_{up} and D_{bt} are the largest and smallest particles sizes of the flat zone (gap zone) on the soil gradation. These particle sizes are 1.18 and 0.3 mm respectively, for the tested soil mixture in this study. Therefore, $\frac{D_{up}}{D_{bt}} = 3.93$ which classify the soil as internally stable, but very close to the threshold value.

4.2.5. Chapuis's (1992) Criteria

The Chapuis's criteria was a new modification of Kezdi's (1969), Sherard's (1979) and Kenney and Lau's (1985) criteria. The internal stability of a soil gradation was assessed based on the slope of the gradation curve. Since the soil gradation in this study is gap-graded, and the slope of the gradation is zero for particle sizes in the range of 0.3 to 1.18, the soil is classified as internally unstable.

4.2.6. Burenkova's (1993) Criteria

To evaluate internal stability of a soil gradation using Burenkova (1993), it is necessary to first determine D_{15}, D_{60} and D_{90}. For a soil gradation to be internally stable, $h' = \frac{D_{90}}{D_{60}}$ must satisfy Eq. 2.13 in Chapter 2.

For the soil gradation in this research:

$h' = \frac{D_{90}}{D_{60}} = \frac{2.166}{1.641} = 1.32$,

$h'' = \frac{D_{90}}{D_{15}} = \frac{2.166}{0.173} = 12.52$, the soil gradation is internally stable if $1.83 \leq h' \leq 3.02$.

As h' is not in the required range, the soil mixture is classified as internally unstable.

4.2.7. Mao's (2005) Criteria

According to Mao's (2005) criteria, a soil is internally stable if:

- $4FC(1-n) \geq 1$

where FC is fine content in decimal and *n* is porosity.

Considering 0.32 and 0.25 for the initial porosity and fine content for the soil mixture, the left side of the equation would be equal to 0.68. This means that the soil mixture is internally unstable based on Mao's (2005) criteria.

4.2.8. Wan and Fell's (2008) Criteria

According to Wan and Fell's (2008) criteria, the soil mixture is classified as internally stable (Figure 4-4):

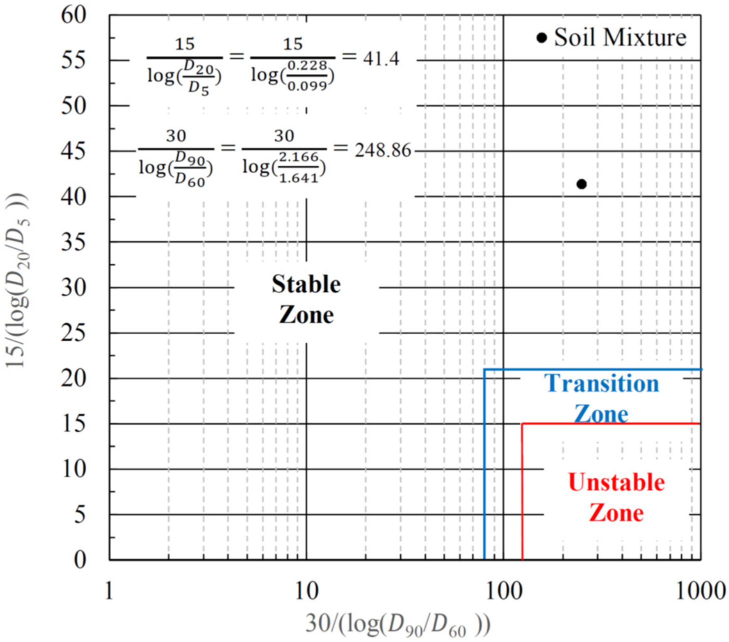

Figure 4-4. Internal stability of the soil mixture based on the Wan and Fell's (2008) Criteria

4.2.9. Indraratna's et al. (2011) Criteria

To determine internal stability according to this method, first it is necessary to calculate controlling constriction size (D_{c35}) and d_{85}^f. A soil is then classified as internally unstable if $\frac{D_{c35}}{d_{85}^f} > 0.82$. There are different methods to calculate D_{c35}. In this research, Eq. 2.14 in Chapter 2 suggested by Dallo et al. (2013) is used.

- $D_{c35(densest)}$: 0.22

- $D_{c35(loosest)}$: 0.679
- D_{c35}: 0.285
- d^f_{85}: 0.244

It can be seen that $\frac{D_{c35}}{d^f_{85}}$ =1.168, which shows the soil mixture is internally unstable.

4.2.10. Salehi Sadaghiani and Witt's (2012) Criteria

Based on Salehi Sadaghiani and Witt's (2012) criteria, a soil is classified as internally unstable if the slope of the gradation curve is less than 15.7 per cent in the semi-logarithmic particle size distribution plot. Since a gap-graded soil is chosen for this study, the slope of the gradation is zero for particle sizes between 0.3 to 1.18 mm. Therefore, the soil mixture is considered as internally unstable.

4.2.11. Dallo's et al. (2013) Criteria

Criteria from Dallo et al. (2013) is based on D_{c35} and d^f_{85}, similar to criteria from Indraratna et al. (2011). However, a soil is internally unstable if $\frac{D_{c35}}{d^f_{85}} > 1.05$. The soil mixture in this study is assessed as internally unstable based on this criterion, as it was shown that $\frac{D_{c35}}{d^f_{85}}$ =1.168.

4.2.12. Chang and Zhang's (2013) Criteria

Chang and Zhang (2013) suggested two criteria for well-graded and gap-graded soils. They showed that the fine content (FC) and gap ratio (G_r) are the controlling parameters to assess internal stability of a gap-graded soil. Based on these criteria, the soil mixture is assessed as internally stable (Figure 4-5).

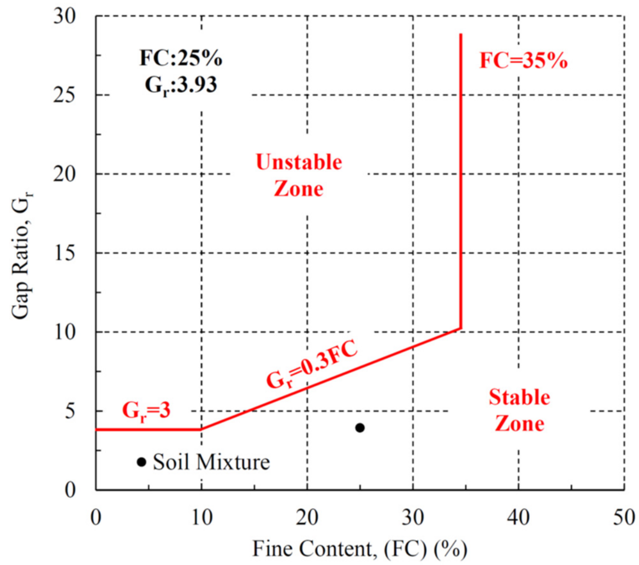

Figure 4-5. Internal stability of the soil mixture based on the Chang and Zhang's (2013) Criteria

4.2.13. Moraci's et al. (2014) Criteria

Moraci et al. (2014) combined previous geometric criteria suggested by Kezdi (1969), Sherard (1979) and Kenney and Lau (1985), and proposed a new framework to assess internal stability considering the minimum slope of the soil gradation. As shown in Figure 4-6, it can be seen that the soil mixture falls completely in the unstable zone.

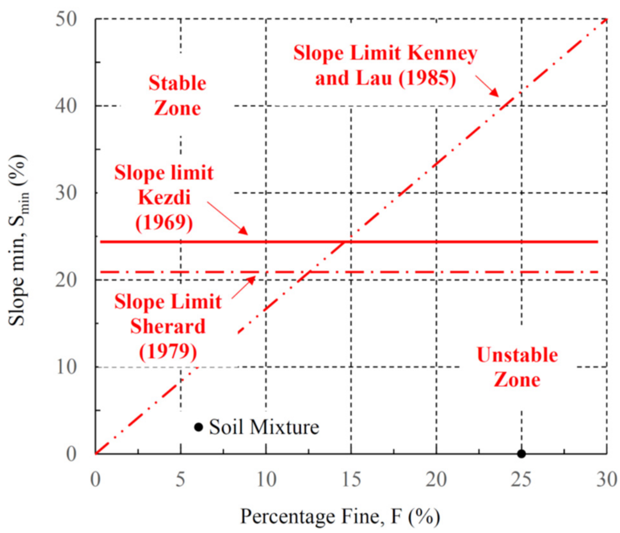

Figure 4-6. Internal stability of the soil mixture based on the Moraci's et al. (2014) Criteria

Table 4-2 summarises the result of the internal stability assessment of the soil mixture used in this study. This table shows that 11 out of 16 methods assessed the soil mixture as internally unstable, while the U.S. Army (1953), Istomina (1957), Kwang (1990), Wan and Fell's (2008) and Chang and Zhang's (2013) classified the soil gradation as internally stable. This indicates that internal stability of soil gradations that fall on the borderline of stable and unstable soils ($D'_{15}/d'_{85} \approx 5$) with transition fine content ($25 \leq FC \leq 35$) cannot be assessed easily using the available geometric criteria in the literature. However, as 70 per cent of the applied methods assessed the soil gradation as internally unstable, it is considered as an internally unstable soil and used in erosion experiments.

Table 4-2. Assessment of internal stability of the soil mixture based on the various geometric criteria

Criteria	Result	Criteria	Result
U.S. Army (1953)	Stable	Burenkova's (1993)	U
Istomina (1957)	S	Mao's (2005)	U
Kezdi's (1969)	Unstable	Wan and Fell's (2008)	S
Sherard's (1979)	U	Indraratna's et al. (2011)	U
Kenney and Lau (1985)	U	Salehi Sadaghiani and Witt's (2012)	U
Kenney and Lau (1986)	U	Dallo's et al. (2013)	U
Kwang (1990)	S	Chang and Zhang's (2013)	S
Chapuis's (1992)	U	Moraci's et al. (2014)	U

4.3. Particle Shape Analysis

The soil mixture in this study consists of particle sizes ranging from 1.18 mm < D < 1.7 mm and 1.7 mm < D < 2.36 (coarse fraction) and 0.075 mm < D < 0.15 mm and 0.15 mm < D < 0.3 (fine fraction). Therefore, four series of particle shape analysis were conducted using a digital microscope and an ImageJ software package. Figures 4-7 and 4-8 show particle shapes and characteristics. It is evident that apart from the largest particles (particles diameter; D = 1.7-2.36 mm), shape parameters were approximately similar.

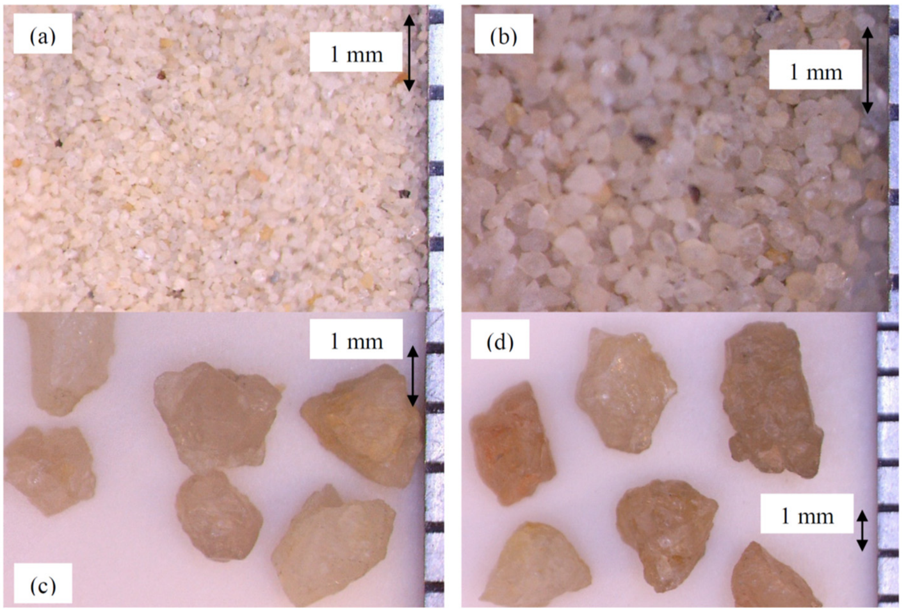

Figure 4-7. Particles shape (a) *D*: 0.075-0.15 mm, (b) *D*: 0.15-0.3 mm, (c) *D*: 1.18-1.7 mm and (d) *D*: 1.7-2.36 mm

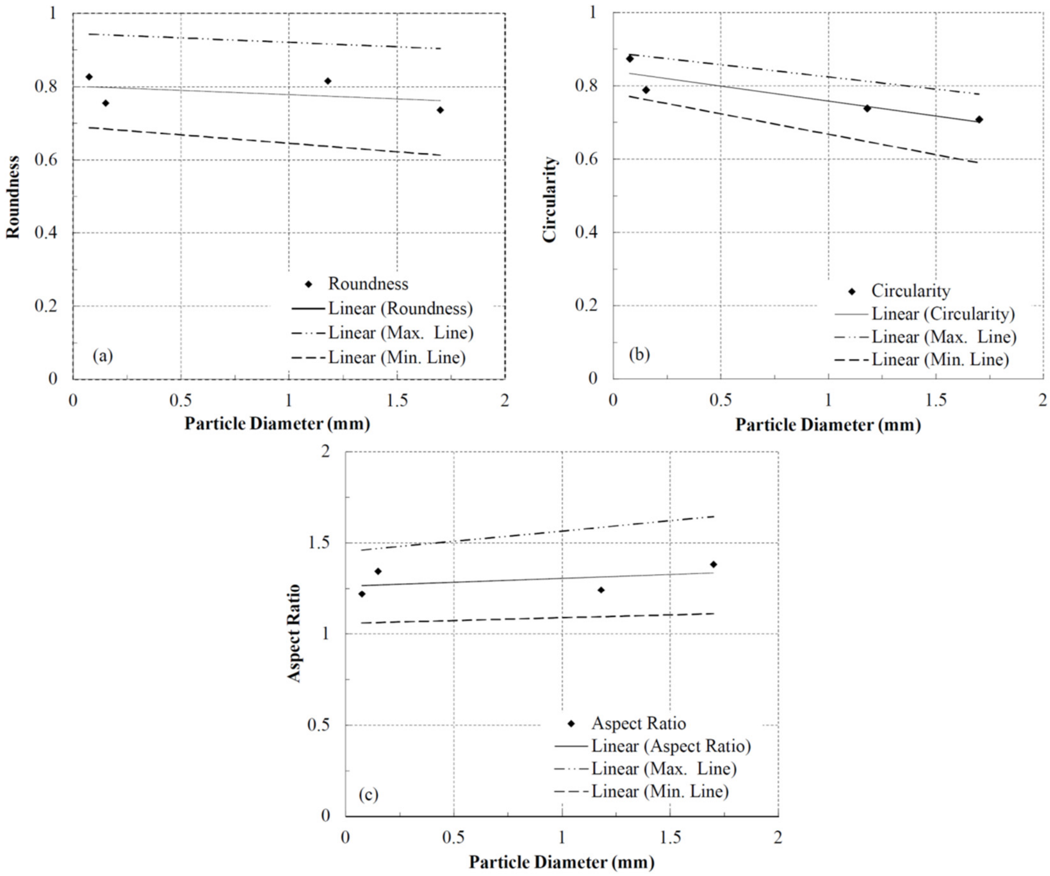

Figure 4-8. Variation of (a) particles roundness, (b) particles circularity, (c) particles aspect ratio with particle sizes

4.4. Maximum and Minimum Index Density and Specific Gravity

The maximum and minimum index density (γ_{max} and γ_{min}) of the soil mixture with 25 per cent fine content were determined for dry and wet conditions, with initial six per cent moisture content based on the procedure described in Chapter 3. Each test was repeated four times to ensure that the ultimate value was found. Table 4-3 shows the result of the maximum and minimum index density measurement.

Table 4-3. Attempts to measure maximum and minimum index density

Sample No.	γ_{max} (kN/m^3)	Sample No.	γ_{min} (kN/m^3)
Sample 1	18.75	Sample 1	16.01
Sample 2	19.13	Sample 2	15.92
Sample 3	19.07	Sample 3	16.1
Sample 4	**19.48**	**Sample 4**	**15.86**

Specific gravity was also determined according to ASTM D854-14. Although the mineral of all particles was Quartz, this test was conducted individually on each particle size range to assure the accuracy of the void ratio measurement. However, the specific gravity was found to be equal to 2.645 regardless of the particle size and mixture.

4.5. Direct Shear Test

The direct shear test was conducted on each particle size range individually at dry and the loosest condition. Figure 4-9 indicates the measured internal friction for each particle size. It is evident that the internal friction increases with an increase in particle size, especially for the largest ranging from 1.7 mm to 2.36 mm, where a considerable jump is observed. This finding is logical when it is compared with the particle shape analysis, which showed circularity decreased and aspect ratio increased for the largest particle.

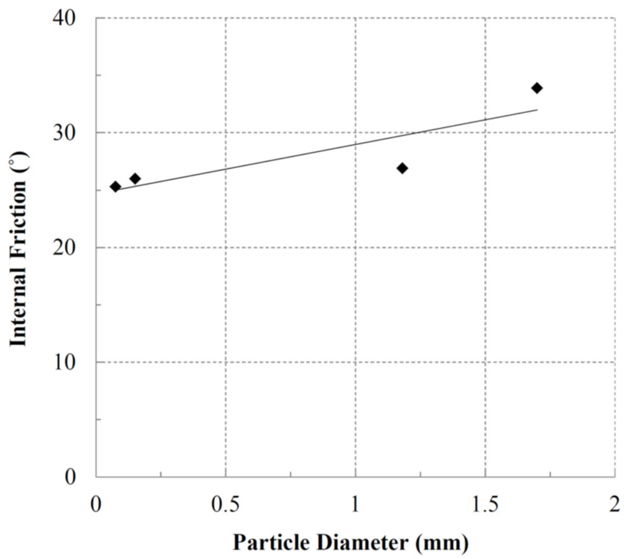

Figure 4-9. Variation of Internal Friction at the loosest condition with particle size

4.6. Summary

It was shown that the selected gap-graded soil is internally unstable and susceptible to internal erosion. The soil mixture consists of sub-rounded to sub-angular particles, and it was found that roundness and circularity decreases with an increase in particle diameter.

Chapter 5 Development of Triaxial-Erosion Apparatus

To investigate the post-erosion behaviour of internally unstable soils, the soil specimen first needs to be exposed to water flow to initiate erosion. Then, the triaxial test is performed to evaluate soil response. Due to the granular nature of the material, and to avoid any disturbance, a triaxial chamber was modified to perform saturation, consolidation, erosion and shearing phases successively without removing the specimen. For this reason, the top cap and base plate of a triaxial chamber were modified in order to apply the seepage inflow and allow the soil particles to be eroded and washed out of the chamber. The water supply system was designed to provide a range of water heads or flow rates. The fabricated collection system can measure the weight of the eroded particles continuously during the test. This system allows for studying pre- and post-erosion soil behaviour under different loading patterns (Figure 5-1). Fabrication drawings of the modified top cap, base plate, pedestal and collection tank are presented in Appendix B.

5.1. Water Supply System

The water supply system was designed to maintain a constant flow condition (i.e. flow rate) over a long period of time. Richards and Reddy (2008) stated that if Darcy's Law is applicable during the soil seepage, a decrease in hydraulic conductivity leads to an increase in hydraulic gradient at a constant flow rate. Due to this coupling effect, they suggested that it may not be correct to consider only the critical hydraulic gradient for cohesionless type soils. Moreover, there is no accurate control on the head loss in tubes, valves, and fittings, which is necessary if constant hydraulic gradient method is used (Ke and Takahashi, 2014). Considering these limitations, it was decided to keep the seepage velocity constant instead of the hydraulic gradient during the erosion phase. The inflow was applied to the top of the specimen using a flow controller that was connected to the pipe between the water supply system and erosion cell, in order to control the flow rate. The flow controller used in this research was Cole-Parmer Easy-View Correlated Flowmeters, known as 150-mm flowmeter 32464-12 (Figure 5-1). This flow controller is suitable for air, water and gases. The flow rate between 25 ml/min up to 500 ml/min can be applied to the top of the sample using this controller. These are ideal for measuring and regulating flow rates for analytical instruments or industrial chemical processes. Common applications include blending, mixing, and gas purging. The specifications of this flow controller are summarised below:

- Dual-float models have higher flow rates and allow a turndown ratio better than 20:1
- **Media type:** water, air, or gases
- **Accuracy:** 150-mm flowmeters: ± 3% full-scale
- **Max pressure:** 200 psi (13.7 bar)
- **Max operating temp:** 200°F (93°C)
- **Connections:** 1⁄8" NPT(F)
- **Dimensions (W x H x D):** 11⁄4" x 913⁄16" x 23⁄8" (3.2 x 24.9 x 6.0 cm)

The water supply unit comprised of two water tanks with 3.3×10^6 mm^3 capacities (connected to each other in parallel), a flow controller, and an air pressure supply. These cells were filled with de-aired water and a constant air pressure equal to 800 kPa was applied to the top of the water inside the cell during the erosion phase. The outlet pressure was controlled using the flow controller. Continuous water supply was provided using an exclusive outlet and supply valve to each cell. Figure 5-2 illustrates the water supply system.

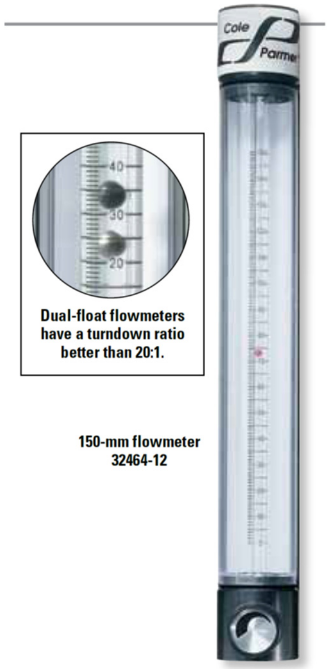

Figure 5-1. Flow Controller

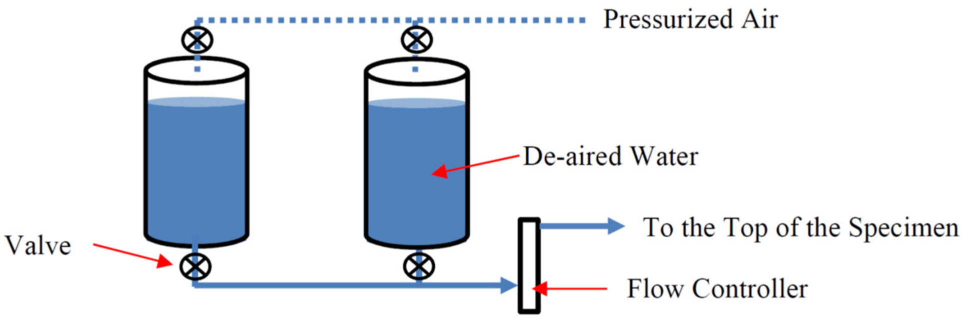

Figure 5-2. Water supply system

5.2. Modified Triaxial Chamber

For erosion tests to be performed in the triaxial chamber, a new top cap, bottom plate and base plate were manufactured. Stainless steel was chosen for their material, as all of these parts were in contact with water. The top cap consisted of a hollow cap with a five mm thick perforated steel plate with a two mm opening size (OS). To reduce the effect of jet flow reported by Ke and Takahashi (2014a), the top cap was filled with glass spheres of various sizes (Figure 5-3). To avoid particle migration to the top cap during the saturation process, mesh with an aperture smaller than the smallest particle size (0.075 mm) was placed between the top of the specimen and top plate.

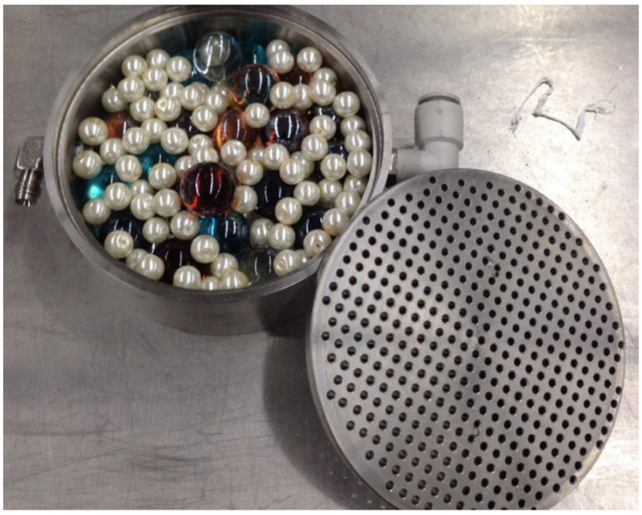

Figure 5-3. Modified top cap

The original base plate was replaced with a 10 mm thick-netted plate, a funnel shaped pedestal, and a new base plate with a conical trough to provide enough space for the eroded particles to move into the collection chamber without clogging. A rigid mesh was placed on the netted plate to hold the coarse fraction (soil body) and let the fine particles (erodible particles) out. The mesh size was determined based on the smallest particle size in coarse fraction or constriction size. For the tests reported in this paper, a 1.18 mm mesh was used. Figure 5-4 shows the various parts of the modified base cell. Solid plates were also manufactured for performing ordinary triaxial tests to compare pre- and post-erosion soil behaviour and reduce the mechanical errors (Figure 5-4 (d)). Since the pedestal is detachable, it is practical to test specimens with different dimensions (Figure 5-5). Although different end restraints may be created due to the use of dissimilar bottom plates, initial ordinary tests did not show any significant variation during undrained shearing between specimens sitting on different plates (Figure 5-6).

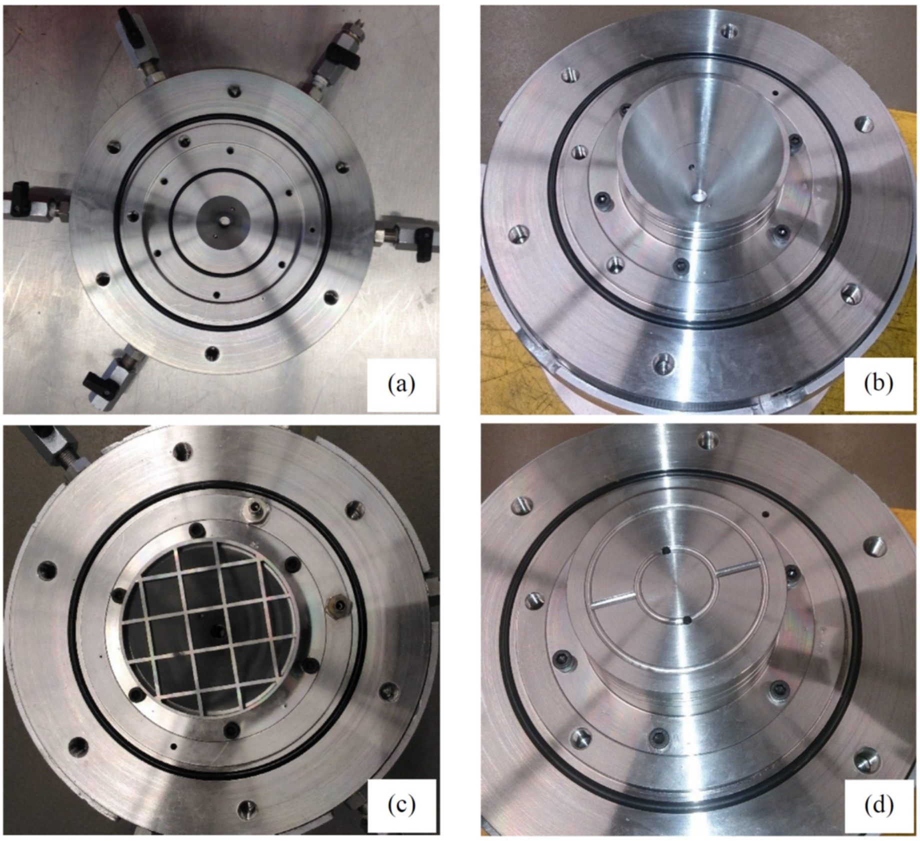

Figure 5-4. Details of modified cell base (a) base plate, (b) funnel shaped pedestal, (c) netted plate and (d) Solid plate to perform ordinary triaxial tests

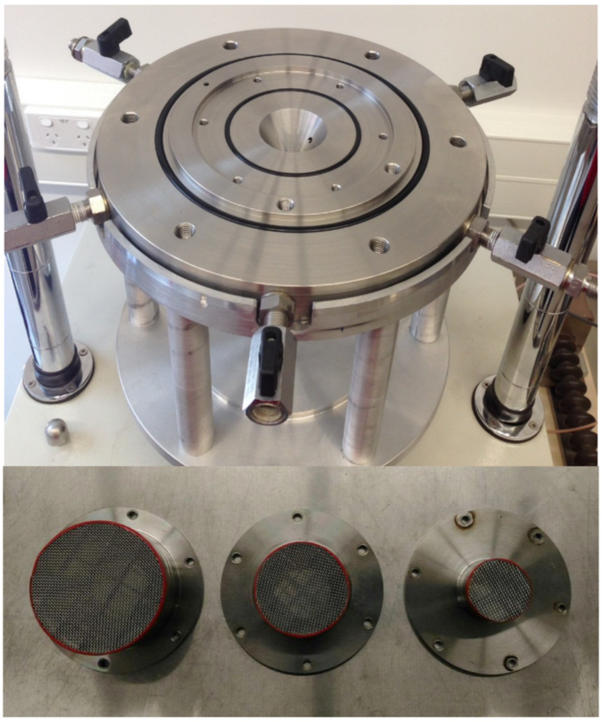

Figure 5-5. Modified base plate and detachable funnel pedestals with different diameters

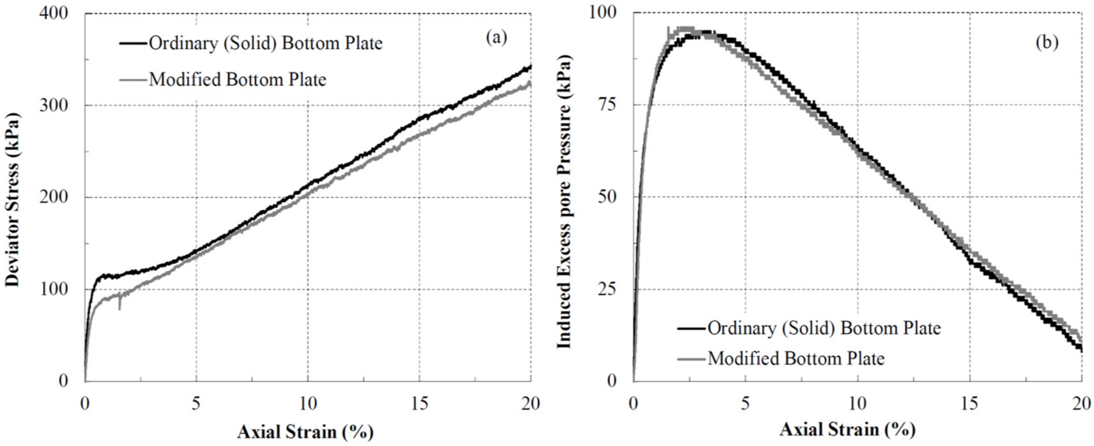

Figure 5-6. Influence of modified bottom plate on (a) stress-strain relationship and (b) induced excess pore pressure

In an ordinary GDS triaxial apparatus, the axial load is applied through the base plate of the triaxial chamber, while the top of the specimen is fixed to the loading frame via a load cell and a loading ram. This is a limitation for erosion testing, as it is necessary to have an outlet for the drained water and eroded particles at the bottom of the base plate. To overcome this restriction, a new bottom frame was designed and fabricated from aluminium to provide enough space to allow water to discharge, and for the erosion of particles from the bottom of the cell while maintaining the load (Figure 5-7). As this frame sits underneath the sealed triaxial-erosion cell, it has no contact with water. It was made from aluminium to reduce its weight.

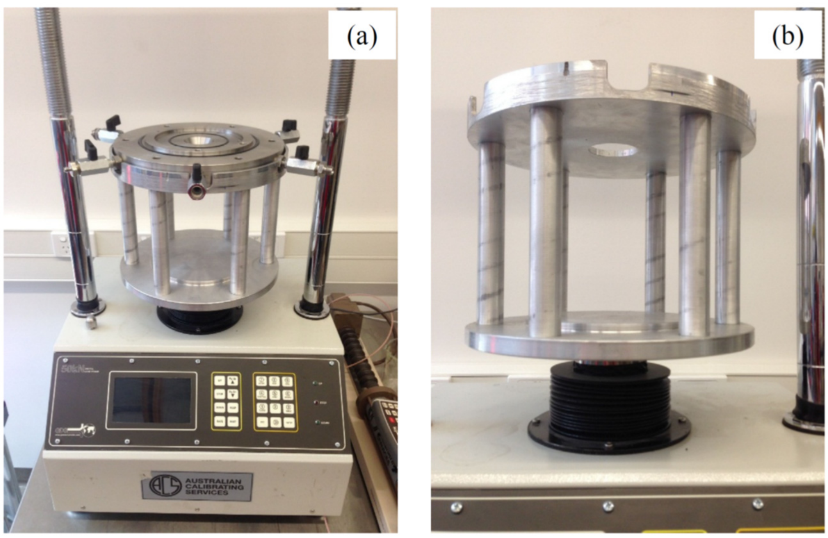

Figure 5-7. New bottom frame to apply axial force to the specimen (a) top view and (b) bottom view

5.3. Collection Tank

The collection system was designed to collect the eroded particles and discharged water from the cell, as well as to simultaneously measure the weight of the eroded particles and maintain a constant back-pressure to keep the base of the specimen saturated. The main design challenge was to continuously measure the weight of the dislodged particles without losing the back-pressure, while eliminating the influence of the inlet flow. To overcome these limitations, Ke and Takahashi (2014a) came up with a practical solution. The measuring tray was submerged and a stable water level was maintained. To eliminate the effect of water weight, the measuring tray was connected to a submersible load cell (10 g resolution) and suspended inside a Plexiglas cell (inner cell) full of water. The water level at the top of this cell was kept constant, and the inlet flow from the triaxial chamber was discharged from the inner cell into the main chamber via drainage holes in the wall of the inner cell. To reduce the flow jet effect reported by Ke and Takahashi (2014a) and related noise with the load cell readings, a plastic funnel was placed in the inner cell. The collected water in the main chamber was discharged at specific intervals. The air above the water was pressurised / equalised to the back-pressure applied to the specimen during the test. Figure 5-8 shows details of the collection tank, and Figure 5-9 indicates performance of the collection tank during an erosion test.

It is worth noting that other parts, such as Load cell, LVDT and pressure transducers, are typical triaxial system elements and hence are not discussed here. Figure 5-10 shows schematic of testing apparatus.

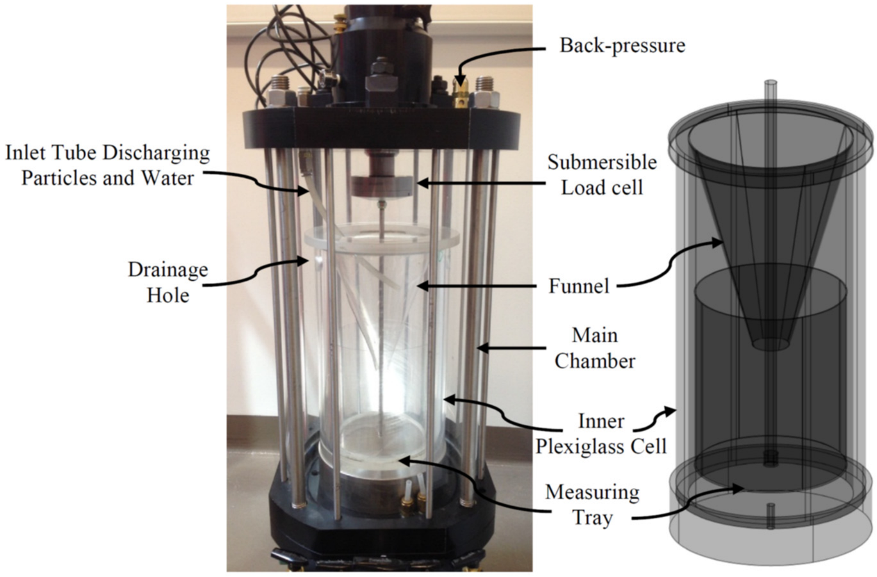

Figure 5-8. Collection tank

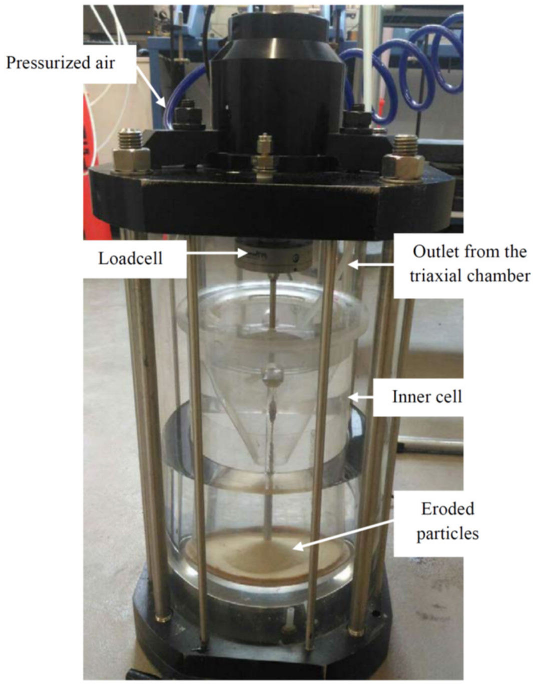

Figure 5-9. Collection of eroded particles in the collection tank

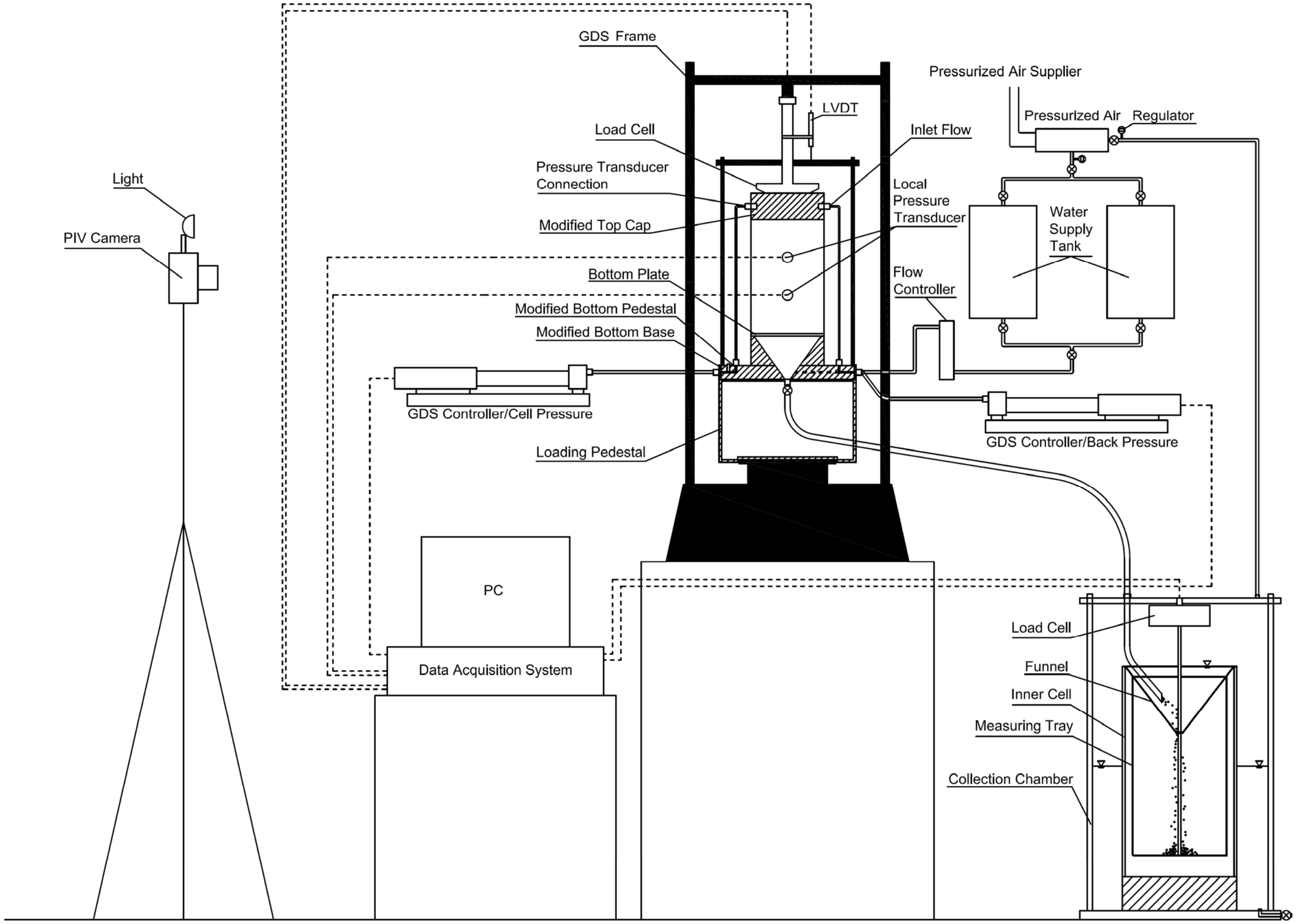

Figure 5-10. Schematic of testing apparatus

5.4. Repeatability

Repeatability of the post-erosion triaxial test results under monotonic loading and cyclic loading, followed by monotonic shearing for some of the eroded specimens, is shown in Figures 5-11 to 5-13, respectively. Each test was repeated to ensure validity of the results. From these figures, it can be seen that the tests were reasonably consistent for all eroded specimens. The only minor observed deviation could be explained due to the non-uniformity of the reconstituted samples during preparation or the small difference in the final quantity of the eroded particles.

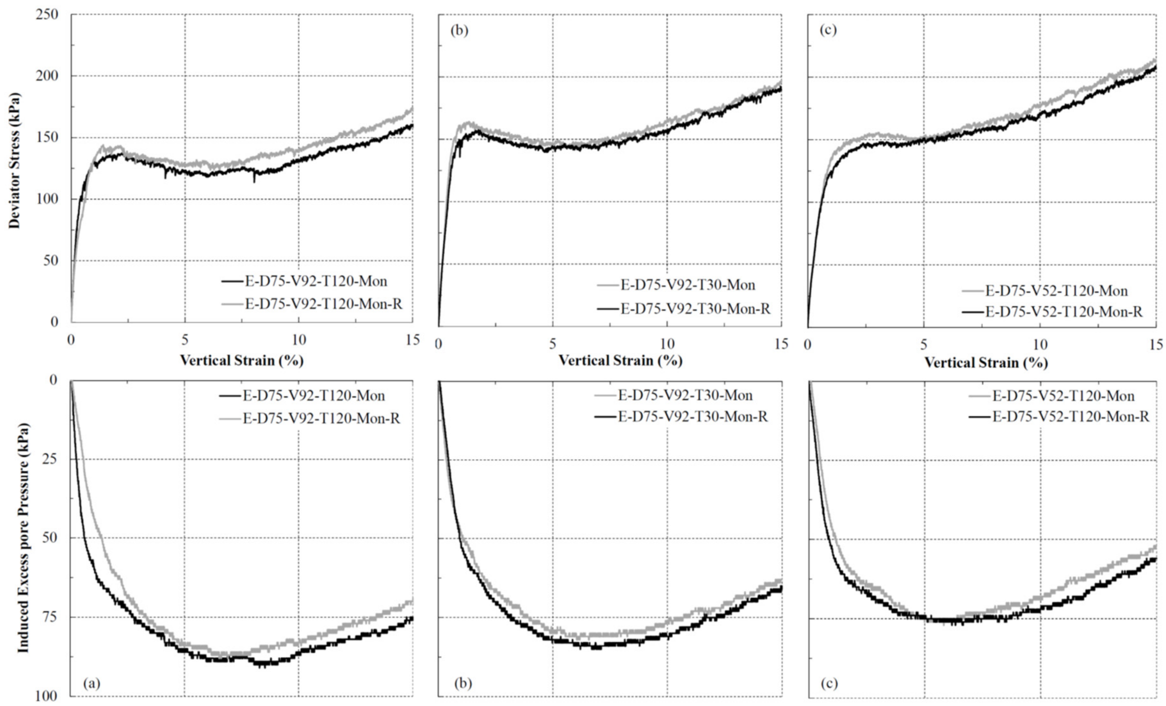

Figure 5-11. Repeatability of stress-strain behaviour and induced EPWP for specimens (a) E-D75-V92-T120-Mon, (b) E-D75-V92-T30-Mon and (c) E-D75-V52-T120-Mon

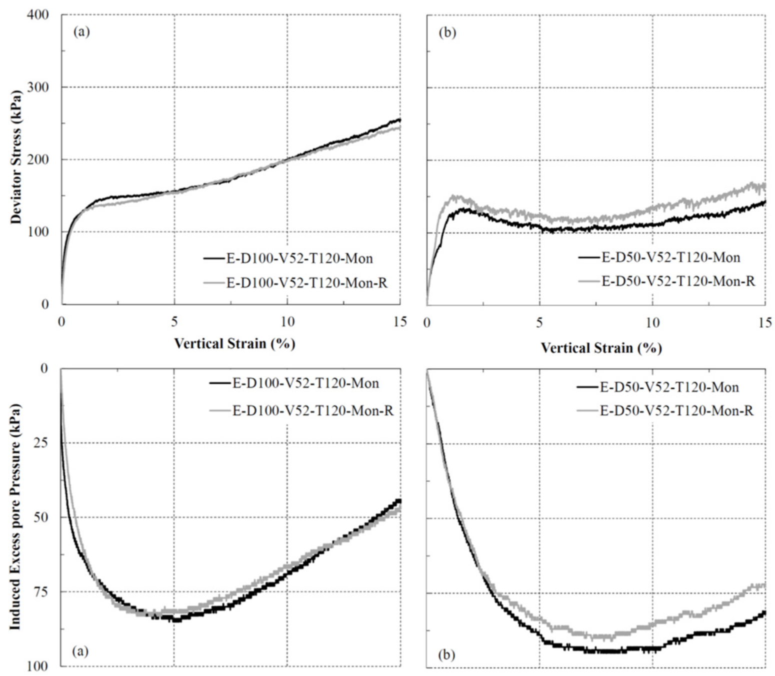

Figure 5-12. Repeatability of stress-strain behaviour and induced EPWP for specimens (a) E-D100-V52-T120-Mon and (b) E-D50-V52-T120-Mon

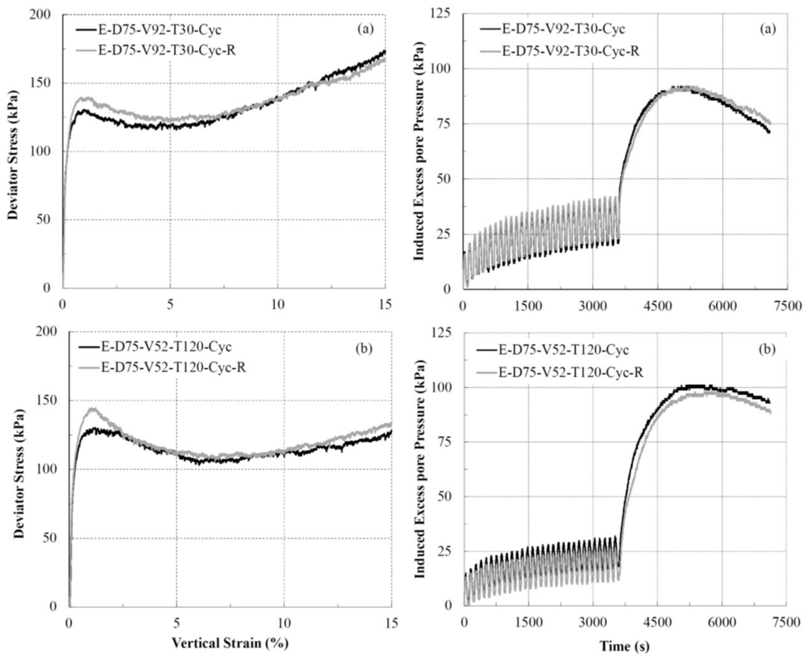

Figure 5-13. Repeatability of stress-strain behaviour and induced EPWP for specimens (a) E-D75-V92-T120-Cyc and (b) E-D75-V52-T120-Cyc

Chapter 6 Influential Parameters on Internal Instability

Internal stability of the tested mixture was examined in Chapter 4 according to the available geometric methods in the literature. The soil mixture was found to be internally unstable. Before studying post-erosion behaviour, the influential parameters on moveability of fine particles in internally unstable soils are examined by conducting a back-analysis on the available experimental results. A new framework is also presented to explain movability of the fine particles in the coarse matrix for soils with fine content between 10 to 30 per cent.

6.1. Back-Calculation of Stress-Reduction Factor (α)

Migration of fine particles within pre-existing pores of coarse particle structure of a soil caused by seepage flow is known as suffusion. This normally occurs in internally unstable soils where fine particles are not fully involved in stress matrix and the soil structure is mainly made by coarse particles. Contribution of fine particles to the soil stress matrix can be evaluated by the stress-reduction factor (α), which is an intrinsic parameter of the soil (Skempton and Brogan, 1994). The available experimental data are used to back-calculate α and investigate the influential parameters on migration of fine particles.

To enhance our understanding of moveability of fine particles in internally unstable soils, experimental data from current literature has been collected, presented and analysed in this chapter. The stress-reduction factor was back-calculated using Eq. 6.1 based on the observed critical hydraulic gradient in the experiment ($i_{cr,exp}$).

$$i_{cr,exp} = \alpha\left(\frac{\sigma'_{vm0}+0.5\gamma'\Delta z}{\gamma_w \Delta z}\right) \quad (6.1)$$

The database for this chapter was selected from Skempton and Brogan (1994), Wan and Fell (2004), Mao et al. (2009), Ahlinhan and Achmus (2010), Ke and Takahashi (2012) and Indraratna et al. (2015). The data was analysed with the intention to investigate the impact of soil gradation, fine fraction and relative density on moveability of fine particles in internally unstable granular media based on the back-calculated stress-reduction factor.

There is considerable experimental research available in the literature studying internal erosion (e.g. Sherard et al., 1984; Kenney et al., 1985; Lafleur et al., 1989; Tanaka and Toyokuni, 1991; Skempton and Brogan, 1994; Moffat and Fannin, 2006 and 2011; Wan and Fell, 2004; Mao et al., 2009; Ahlinhan and Achmus, 2010; Sail et al., 2011; Marot et al. 2012a, b and 2016; Ke and Takahashi, 2011 and 2012; Sadaghiani and Witt, 2012; Moraci et al., 2014; Seghir et al., 2014; Indraratna et al., 2015; Sibille et al., 2015). However, it was not possible to back-calculate the stress-reduction factor for all of the experiments. This was due to the method followed by the researchers for their erosion tests or lack of information provided in their research. To be able to back-calculate the stress-reduction factor, it is important to commence the erosion test at a very low hydraulic gradient and increase it gradually until the erosion of fine particles start. This procedure helps to capture the critical hydraulic gradient. For instance, filtration tests conducted by Sherard et al. (1984) and Lafleur et al. (1989) were performed under a constant head regime. Moffat and Fannin (2011) applied flow with a global constant hydraulic gradient to soil specimens, and investigated variation of the local hydraulic gradient due to a change in hydraulic conductivity caused by erosion. In the experimental investigation performed by Sail et al. (2011), the erosion test started at a hydraulic gradient of one, and then increased to 2, 3, 4 and 4.9 for the next stages. The critical hydraulic gradient was not determined as the erosion of erodible particles started immediately at the beginning of the test. Marot et al. (2012a and b) and Seghir et al. (2014) investigated initiation of erosion of cohesive fine particles, which is beyond the scope of this study, as Eq. 6.1 is only applicable to non-cohesive soils. Moreover, a constant hydraulic gradient was applied to soil specimens. Moraci et al. (2014) conducted long-term filtration tests to assess internal stability of granular materials. However, a constant hydraulic head ranging from 4 to 5 was applied to the top of soil specimens. Sibille et al. (2015) characterised the suffusion development based on the erosion rate. Although the applied hydraulic gradient was increased incrementally and the cumulative eroded mass with time was also presented, the pattern of the hydraulic gradient was not provided. The focus of the research conducted by Marot et al. (2016) was rate of erosion, hydraulic conductivity and shear stress to develop a new method to assess internal stability of soils with various gradations, and not the critical hydraulic gradient.

Among the available experimental data, only a few studies determined the critical hydraulic gradient and presented the required soil properties and test information. This includes soil gradation, initial void ratio or relative density, confining pressure on soil specimens, soil density, and height of soil specimens, which are required to back-calculate the stress-reduction factor. Although it was shown that the flow direction has minor impact on the critical hydraulic gradient, to avoid any possible errors, it was decided to consider only experiments that were performed under an upward inflow. The result of investigations reported by Skempton and Brogan (1994), Wan and Fell (2004), Mao et al. (2009), Ahlinhan and Achmus (2010), Ke and Takahashi (2012) and Indraratna et al. (2015) were used to investigate the influential parameters on the moveability of the fine particles in internally unstable soils. Table 6-1 indicates the back-calculated α, soil properties, and test information of each study; Figure 6-1 shows particle size distribution of soil specimens discussed in this chapter.

Table 6-1. Calculated stress-reduction factor from previous studies

Test No.	Sample ID	α	Flow Direction	Soil Type	$(\frac{D'_{15}}{d'_{85}})_{max}$	C_u [a]	FC [b] (%)	D_r (%)	Reference
1	A	**0.18** [c]	Upward	Gap-Graded	11	24	15	NA [d]	Skempton and Brogan (1994)
	B	**0.33** [c]	U	Well-Graded	3.9	10	15	NA	
	C	**0.97** [c]	U	W	3.2	7	15	NA	
	D	**0.95** [c]	U	W	3.2	4.5	10	NA	
2	1	**0.73**	U	W	12.6	108	10.5	NA	Wan and Fell (2004)
	2R	**0.93**	U	W	8.5	194	24	NA	
	4R	**0.72**	U	W	8.1	21	3.2	NA	
	9	**0.17**	U	G	36	115	11.9	NA	
	10	**0.54**	U	G	71	304	25.7	NA	
		0.37	U					NA	
3	a	**0.27** [c]	U	W	5.9	23.5	29	NA	Mao et al. (2009)
	b	**0.32** [c]	U	W	4.8	35	25	NA	
	c	**0.25** [c]	U	W	6.5	20	18	NA	
	d	**0.2** [c]	U	W	21.7	45	16	NA	
	A	**0.16** [c]	U	G	16.9	60	29.8	NA	
	B	**0.13** [c]	U	G	24.5	60	25.4	NA	
	C	**0.11** [c]	U	G	34.2	43	20.1	NA	
	D	**0.25** [c]	U	G	9.1	30	29.8	NA	
4	A2	**0.88** [c]	U	Poorly Graded	1.5	3	2	50	Ahlinhan and Achmus (2010)
	A2	**0.91** [c]	U	Poorly Graded	1.5	3	2	75	
	A2	**0.88** [c]	U	Poorly Graded	1.5	3	2	95	
	E1	**0.3** [c]	U	W	3.3	7	15.3	50	
	E1	**0.36** [c]	U	W	3.3	7	15.3	60	
	E1	**0.54** [c]	U	W	3.3	7	15.3	90	
	E2	**0.17** [c]	U	W	7.2	13.9	13.3	40	
	E2	**0.18** [c]	U	W	7.2	13.9	13.3	50	
	E2	**0.21** [c]	U	W	7.2	13.9	13.3	90	
	E3	**0.17** [c]	U	G	14.4	23.4	14.3	75	
	E3	**0.18** [c]	U	G	14.4	23.4	14.3	98	

[a]: Uniformity Coefficient ($\frac{D_{60}}{D_{10}}$)
[b]: Fine Content
[c]: Calculated by Wang and Dallo (2015)
[d]: Not Available

Table 6-1. Calculated stress-reduction factor from previous studies (continued)

Test No.	Sample ID	α	Flow Direction	Soil Type	$(\frac{D'_{15}}{d'_{85}})_{max}$	C_u [a]	FC [b] (%)	D_r (%)	Reference
5	A	**0.18**	U	G	7.9	19	25	30	Ke and Takahashi (2012)
	A	**0.24**	U	G	7.9	19	25	60	
	B	**0.23**	U	G	7.9	15.8	20	20	
	B	**0.27**	U	G	7.9	15.8	20	60	
	C	**0.33**	U	G	7.9	13.6	16.7	20	
	C	**0.30**	U	G	7.9	13.6	16.7	60	
	D	**0.33**	U	G	7.9	13.6	14.3	60	
6	C-20-R5	**0.41**	U	W	3.2	20	NA[d]	6	Indraratna et al. (2015)
	C-20-R50	**0.63**	U	W	3.2	20	NA	51	
	C-20-R70	**0.92**	U	W	3.2	20	NA	71	
	C-20-R95	**0.89**	U	W	3.2	20	NA	96	
	C-23-R5	**0.69**	U	W	5.1	23	NA	7	
	C-23-R30	**0.84**	U	W	5.1	23	NA	32	
	C-23-R60	**0.93**	U	W	5.1	23	NA	63	
	C-23-R95	**0.95**	U	W	5.1	23	NA	94	
	C-40-R5	**0.30**	U	W	4.2	40	NA	6	
	C-40-R50	**0.30**	U	W	4.2	40	NA	48	
	C-40-R95	**0.33**	U	W	4.2	40	NA	93	

[a]: Uniformity Coefficient ($\frac{D_{60}}{D_{10}}$)
[b]: Fine Content
[c]: Calculated by Wang and Dallo (2015)
[d]: Not Available

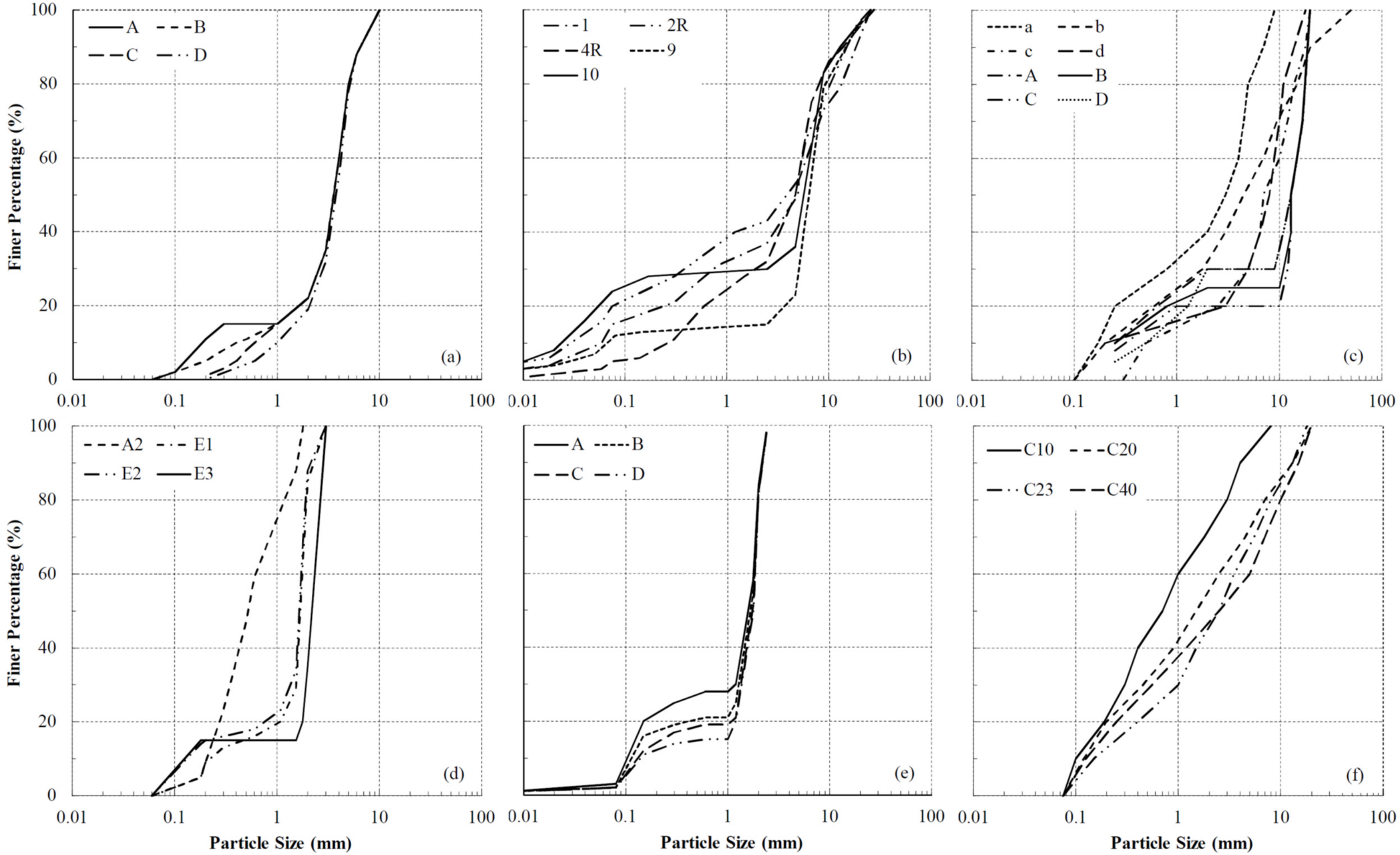

Figure 6-1. Particle size distribution curves (a) Skempton and Brogan (1994), (b) Wan and Fell (2004), (c) Mao et al. (2009), (d) Ahlinhan and Achmus (2010), (e) Ke and Takahashi (2012) and (f) Indraratna et al. (2015)

6.2. Effect of Soil Gradation

Shire et al. (2014), Fonseca et al. (2014), Moffat and Herrera (2014) and Wang and Dallo (2015) all stated that the stress-reduction factor (α) decreases when $(\frac{D'_{15}}{d'_{85}})_{max}$ increases for gap-graded soils. The variation of α against $(\frac{D'_{15}}{d'_{85}})_{max}$ for both gap-graded and well-graded soils based on the database is shown in Figure 6-2. Two margins can be identified here, when $(\frac{D'_{15}}{d'_{85}})_{max} \approx 4$ and ≈ 10. $(\frac{D'_{15}}{d'_{85}})_{max} \approx 4$ is Kezdi's criterion (1969) that identifies internally stable soils ($\alpha \approx 1$). For soils with $(\frac{D'_{15}}{d'_{85}})_{max}$ values greater than 10, the effect of $(\frac{D'_{15}}{d'_{85}})_{max}$ on α is not considerable. This is because the size of the fine particles is so small in comparison with the pore size that no matter how small they are, they can move easily within the pore network of soil. Data of well-graded soils was extracted from Figure 6-2 and shown in Figure 6-3. It can be seen that there is no obvious trend between α and $(\frac{D'_{15}}{d'_{85}})_{max}$. In fact, in well-graded soils it is the uniformity coefficient (C_u) and relative density (D_r) impacting the moveability of fine particles. For instance, specimens B and C in experiments conducted by Skempton and Brogan (1994) had 15 per cent fine content with approximately similar $(\frac{D'_{15}}{d'_{85}})_{max}$ and a low relative density. However, α was calculated 0.33 and 0.97 for specimens B and C, respectively. The main difference between these two well-graded specimens was the uniformity coefficient. The contribution of fine particles in stress transferring was much higher for specimen C with lower C_u. In another experiment carried out by Indraratna et al. (2015), under similar relative density and $(\frac{D'_{15}}{d'_{85}})_{max}$ in the range of 3.2 to 5.1, C-20-R95 and C-23-R95 specimens with uniformity coefficient of 20 and 23 had higher stress-reduction factors than C-40-R95 specimen with C_u of 40. This trend was also observed for C-20-R50 and C-40-R50 specimens. It seems that in well-graded soils, the slope of gradation curve controls moveability of fine particles, and fine particles are more active in the soil stress matrix in soil gradation curves with greater slopes (lower C_u).

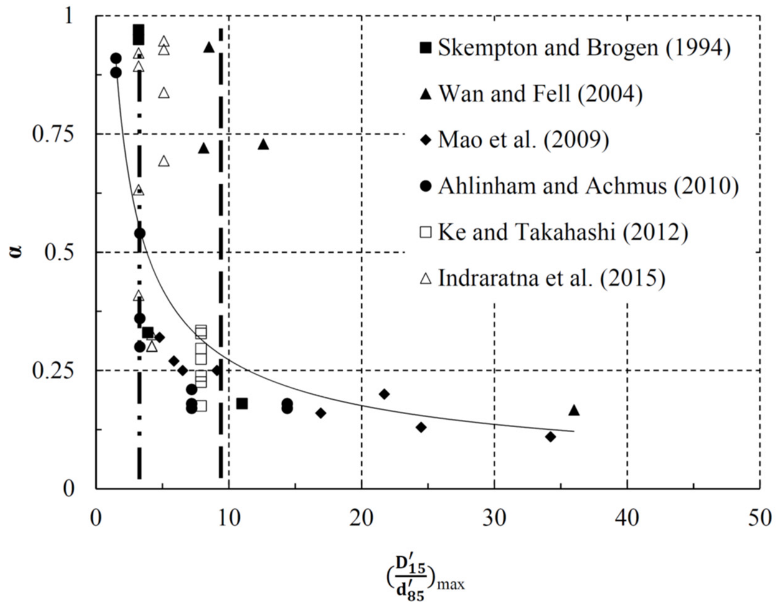

Figure 6-2. Variation of α against $(\frac{D'_{15}}{d'_{85}})_{max}$ for gap-graded and well-graded soils

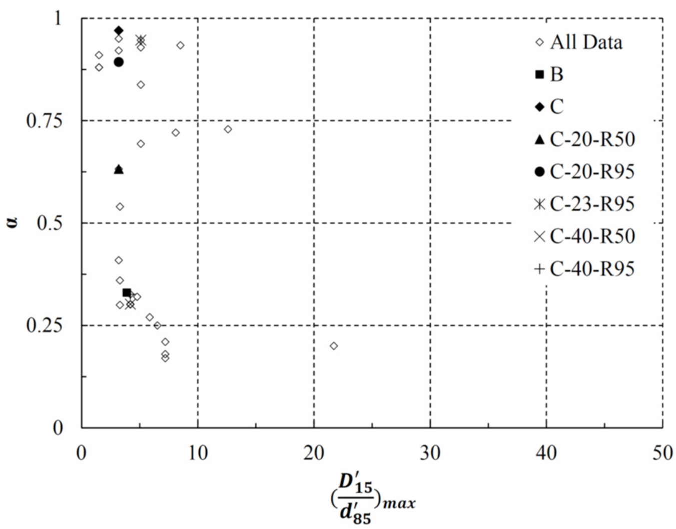

Figure 6-3. Variation of α against $(\frac{D'_{15}}{d'_{85}})_{max}$ for well-graded soils

6.3. Effect of Relative Density

Figure 6-4 presents the variation of the stress-reduction factor with relative density (D_r). A general trend was found in which α increases when the relative density increases.

Based on the back-calculated α, A2 can be considered as an internally stable soil and fine particles were active, while fine particles in E1, E2 and E3 were classified as inactive to semi-active. It can be seen that the relative density had no impact on A2, minor impact on E2 and E3, and considerable influence on E1. Although E1, E2 and E3 were internally unstable with approximately similar fine contents (13.3 to 15.3 per cent), variation of α with D_r was considerable only for E1, but not for E2 and E3. It appears the value of $(\frac{D'_{15}}{d'_{85}})_{max}$ and C_u also have important roles when investigating the effect of relative density. For soils that distinctively fall into the category of unstable soils, the impact of relative density on moveability of fine particles is not as significant as for soils falling on the borderline of stable and unstable soils with semi-active fine particles. Ahlinhan and Achmus's (2010) investigation showed that this effect becomes inconsiderable again for internally stable soils (A2). In addition, back-calculation of α in experiments conducted by Ke and Takahashi (2012) showed that the effect of the relative density on migration of fine particles in gap-graded soils was also found to be minor for internally unstable soils with high values of $(\frac{D'_{15}}{d'_{85}})_{max}$. It seems that for soils with high value of $(\frac{D'_{15}}{d'_{85}})_{max}$, the fine particles sit loose in pores of the coarse skeleton without effective contact with coarse particles (inactive fine particles). Therefore, compaction energy does not affect these fine particles, and hence, relative density does not show any influence.

Furthermore, Shire et al. (2014) using Discrete Element Modelling showed that for soils in the transitional zone ($25 < FC < 35$), the internal stability is affected by relative density. The fine fractions of these soils (E1, E2 and E3) are well below than the transitional zone presented by Shire et al. (2014) (13.3-15.3%). However, the effect of relative density is still found to be significant. Based on this finding, the transitional zone needs to be expanded for soils on the border of internally stable and unstable soils.

Indraratna et al. (2015) studied internal stability of well-graded soils based on constriction size distribution. Figure 6-4 shows the results of their tests for three well-graded soils with $3.2 < (\frac{D'_{15}}{d'_{85}})_{max} < 5.1$ and $20 < C_u < 40$. While the variation of $(\frac{D'_{15}}{d'_{85}})_{max}$

was small for all samples, relative density is found to be more effective for samples with lower uniformity coefficient (C_u).

It is worth mentioning that the value of minimum and maximum void ratios used in the relative density calculation are significantly dependent on the testing standard followed. It is believed that the maximum void ratio obtained by the British Standard is much smaller than that obtained by the Japanese Industrial Standard. This can affect the comparison presented in this chapter noticeably. However, as none of the previous studies mentioned the method of the relative density measurement, it was assumed that the procedure was the same for all experiments.

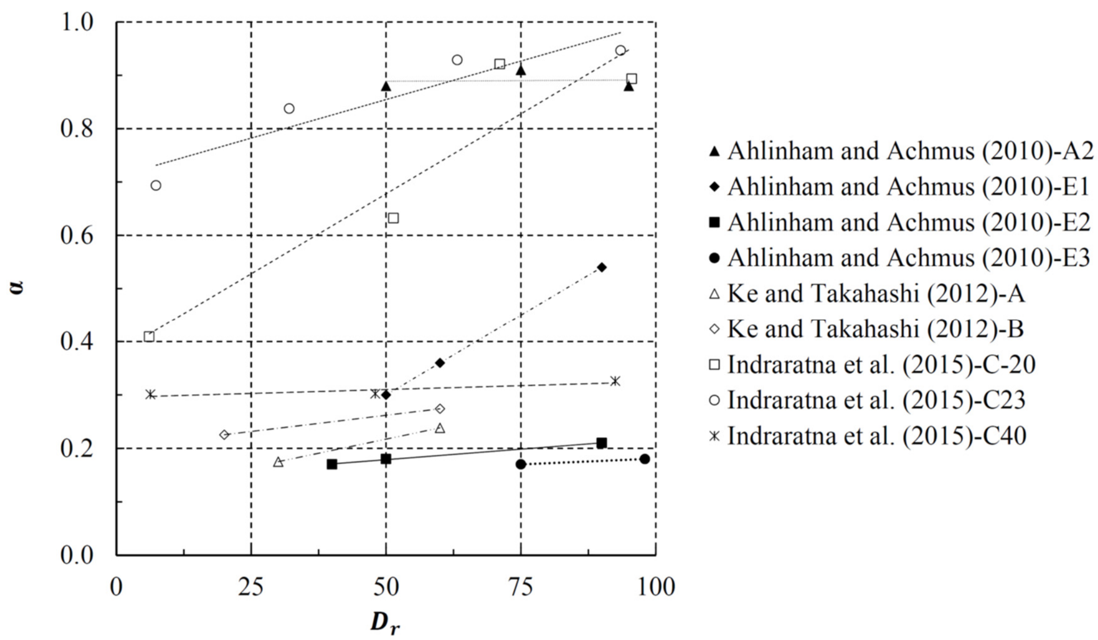

Figure 6-4. Variation of α against relative density

6.4. Effect of Fine Content

It is generally accepted that the shear strength of the silty sand or clayey sand may decrease or increase in comparison to the clean sand depending on the fine content, particle shape, and the plasticity of the fine particles. It was discussed in Chapter 2 that and Soga (1976) and Kenny (1977) discovered that fine particles may not transfer forces due to their size, position and nature, and introduced a new index known as the granular void ratio index (Eq. 6.2). Later on, Thevanayagam (1999 and 2000) suggested a new framework for intergrain contact density indices for granular mixes (Eq. 6.3). Thevanayagam (1999 and 2000) suggested *b* factor, which is the portion of the fine particles that participate in the soil stress matrix. Although the effect of relative density is not fully considered in the equation suggested by Rahman et al. (2011), the concept of *b* is similar to the stress-reduction factor suggested by Skempton and Brogan (1994).

$$e_g = \frac{e+FC}{1-FC} \tag{6.2}$$

$$e_{c_{eq}} = \frac{e+(1-b)FC}{1-(1-b)FC};\ 0<b<1 \tag{6.3}$$

Figure 6-5 shows the variation of α and b with fine content using Ke and Takahashi's (2012) experimental data (α is back-calculated using Eq. 6.1 and b is determined based on d'_{50} and D'_{10}). $(\frac{D'_{15}}{d'_{85}})_{max}$ and χ were 7.9 and 11.8, respectively, and the threshold fine content was found to be 33 per cent according to Rahman's et al. (2011) equations. It is evident that with an increase in fine content, α decreased while b increased. These samples were internally unstable regardless of the fine content value. Based on the value of $(\frac{D'_{15}}{d'_{85}})_{max}$ and χ, the finer particles were deemed small enough to migrate through the pore network. As long as the fine content is below the threshold value, for specimens with a greater fine content and a high value of $(\frac{D'_{15}}{d'_{85}})_{max}$, there are more erodible fine particles present in the pores of coarse structure. However, this does not necessarily mean that all of these fine particles contribute to load transferring. In other words, the stress-reduction factor cannot be applied to all fine particles, and the back-calculated α value could be incorrect for these soils. However, more experimental investigation needs to be carried out to clarify this observation.

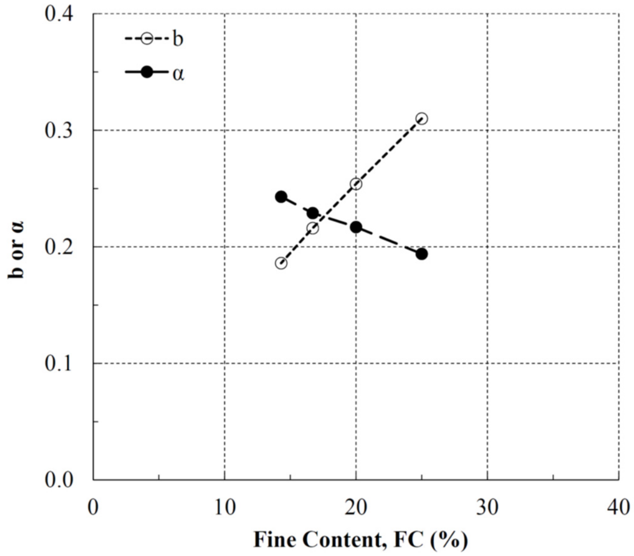

Figure 6-5. Variation of *α* and *b* against fine content (Ke and Takahashi, 2012)

6.5. Other Influential Parameters

Apart from soil gradation, relative density, and fine content, particle shape and stress path are other influential parameters that affect moveability of fine particles in internally unstable soils. However, there is no direct experimental evidences validating the current hypothesises on impact of these parameters on movability of fine particles. Therefore, it was decided to briefly discuss them at the end of this chapter.

6.5.1. Impact of Particle Shape

There are three scales in particle shape: sphericity versus ellipticity or platiness, roundness versus angularity, and smoothness versus roughness (Cho et al., 2006). Fraser (1935) showed that particle shape affects hydraulic conductivity by varying the size and shape of the pores and the packing level. He stated that at the same porosity and equal diameter of particles, permeability decreased with an increase in uniformity of the pore spaces. This meant that permeability increases as true sphericity is decreased, which was also later confirmed by Guimaraes (2002). Guimaraes (2002) demonstrated that particles with extremely low sphericity (such as platy particles) make bridges over other grains and create larger open pores. This is due to a lack of mobility of particles with high irregularity preventing a dense packing for the soil. However, this was contradictory in comparison to Stewart's et al. (2006) findings that in a pack of aspherical particles, permeability was strongly dependent on flow direction and 3-dimentional arrangement of particles. In fact, depending on the particle arrangement, an increase in particle aspect ratio may increase or decrease anisotropy and permeability. Göktepe and Sezer (2010) studied the effect of particle shape on density and permeability of sands. They concluded that the particle shape considerably affected the density and permeability of sand. Santamarina and Cho (2004) suggested that if fine particles (d_{fine}) create stable bridges at pore throats (d_{throat}) of coarse particles, the migration of fine particles is prevented. Furthermore, the ratio of d_{throat}/d_{fine} is particle shape dependent. It can be seen that sphericity changes constriction size, and a decrease in sphericity (increase in ellipticity) increases the constriction size. As an example, in a soil with spherical coarse particles, if the diameter of fine particles is larger than the constriction size, fine particles cannot migrate through pre-existing pores (internally stable). If coarse fraction consists of particles with high ellipticity, under similar particle size distribution (PSD) and void ratio, the constriction size and pore throats may be larger and more connected. This can cause suffusion to start under a lower critical hydraulic gradient, which causes the fine particles to move through the pores (internally unstable). Therefore, particle sphericity can affect the initiation of suffusion in soils on the border between internally stable and unstable soils. It is worth mentioning that sphericity probably does not affect the erosion of fine particles in soils with high value of $(\frac{D'_{15}}{d'_{85}})_{max}$ where fine particles are much smaller than the size of the pore network channels. Thus, the stress-reduction factor may remain constant without any change for these soils.

Angularity of particles is also found to affect the constriction size, as reported by Loudon (1952) and Wu et al. (2012). Loudon (1952) stated that the permeability of angular grains could be as much as 20 per cent lower than rounded grains. This was contrary to Wu's et al. (2012) experimental results that demonstrated that larger constriction sizes were measured for an angular material than a natural rounded material and an assembly of glass beads. However, Wu's et al. (2012) believed that anisotropy of the constriction network, the water flow direction, and direction of the deposit of the grains needs to be taken into account for assessing the constriction size.

Particle shape can also have an impact on water flow in soil. Head and Epps (2011) stated that the shape and texture of soil grains affect the soil permeability. Particles with lower sphericity create more tortuous flow paths. Particles with a rough surface show more resistivity against the flow. Therefore, both sphericity and roughness reduce water flow through soil, which results in a reduction of soil permeability.

Santamarina and Cho (2004) showed that achievable void ratios are affected by particle shape. They investigated the effect of particle shape on extreme void ratios (e_{max} and e_{min}) for natural sand with $C_u \leq 2.5$. They found that e_{max}, e_{min} and void ratio difference ($I_e = e_{max} - e_{min}$) decrease with an increase in roundness, sphericity and regularity. A decrease of void ratio difference (I_e) means that the range of attainable void ratio by compaction decreases. It was mentioned previously that for internally unstable soils (in the transitional zone), the stress-reduction factor can be affected by relative density. However, for two soils with similar fine fraction, $(\frac{D'_{15}}{d'_{85}})_{max}$ and C_u but of different particle shapes, the impact of relative density on internal stability for soils with rounded and spherical particles is less than what it would be for soils with angular or elliptical particles. In other words, particle shape impacts the way in which relative density affects soils in the transitional zone. Therefore, an increase in relative density as a remedial work for internally unstable soils in the transitional zone (as suggested by Shire et al. (2014)) is not going to be as efficient for internally unstable soils with higher spherical or rounded particles. In addition, Thevanayagam and Mohan (2000) showed that the contribution of fine particles in force chains depends on the maximum void ratio of the host sand ($e_{max, HS}$). This means stress-reduction factor (α) is also affected by the variation of $e_{max,\,\mathrm{HS}}$ due to the particle shape.

On the other hand, there are research outcomes suggesting that particle shape can improve the erosion resistance of the fine particles. Marot et al. (2012b) investigated the influence of particle angularity on the internal erosion process using a modified triaxial apparatus. Two methods were employed to characterise the shape of the representative particles. The first method was an optical method using an optical microscope paired with a digital camera. The second method consisted of a direct shear test and using angulometer to measure roundness, circularity, internal friction and the angularity index (IA). Three different materials were used to make samples with similar grain size distributions, but different particle shapes. They performed the erosion test and measured the hydraulic conductivity and the maximum eroded particle concentration. The comparison of the results suggested that by increasing the angularity, the hydraulic conductivity and concentration of the eroded particles decrease. They concluded that this decrease in hydraulic conductivity is attributed to particle filtration and clogging process. Their results were in agreement with findings from Fleshman and Rice (2014) that angular soils showed greater resistance against piping. In addition, angularity and roughness of fine and coarse particles increase particle interlocking and reduce moveability of fine particles, regardless of the constriction size.

It is worth noting that if fine particles are small enough (with respect to the pore sizes), the shape of the coarse particles does not affect the onset of suffusion. Moreover, it seems that the effect of particle shape, in terms of sphericity or roundness on the stress-reduction factor (α), may be limited to soils on the border of being internally stable and unstable soils.

It was discussed that particle shape affects the critical hydraulic gradient. However, it is necessary to mention that if particle shape only provides more connected pore throats or bigger constriction size, it may not necessarily lead to a lower contribution of fine particles in the stress matrix. It means that for two soil samples with similar particle size distributions but with different particle shapes, the time and the required critical hydraulic gradient for observing the initial eroded particles may be different. However, it does not mean that the erodible particles are under different stress states. Therefore, back-calculation of stress-reduction factor (α), based on the experienced critical hydraulic gradient, may not be completely accurate for some of these more complicated scenarios. This could be the weakness of this back-calculation, which highlights the necessity of further experimentations.

6.5.2. Impact of Stress Path

Another parameter impacting stress-reduction factor is the stress path (compression and extension) and shear stress ratio ($\eta = {}^{q}/_{p'}$). Chang and Zhang (2012) performed erosion tests on triaxial specimens at various stress paths and ratios. They found that under compressive stress, the connectivity of pores improves in the axial direction at high shear stress ratios, whereas under tensile stress, these pores are better connected in the horizontal direction. This rearrangement of particles affects the critical hydraulic gradient in two ways: (i) it changes the vertical and horizontal hydraulic conductivities, (ii) it changes the contribution of fine particles in supporting the stresses, especially for soils in the transitional zone where the fine particles provide lateral support for the primary fabric. Figure 6-6 illustrates the concept of the particle dislocation under compressive and tensile stress paths. Here, it can be seen that fine particles provide lateral support in the stress matrix and support a small percentage of vertical effective stresses ($\sigma'_3+\Delta\sigma$) under the compressive path (Figure 6-6 (a)). However, they may be more involved in load transmission and carry a considerable percentage of vertical effective stresses ($\sigma'_3-\Delta\sigma$) under tensile path (Figure 6-6 (b)). In other words, under the tensile path, the critical hydraulic gradient of vertical flow needs to increase to overcome the higher effective stresses on the fine particles. Therefore, α increased due to the unconnected pore throats in vertical direction and the increased contribution of fine particles in transferring the effective stress.

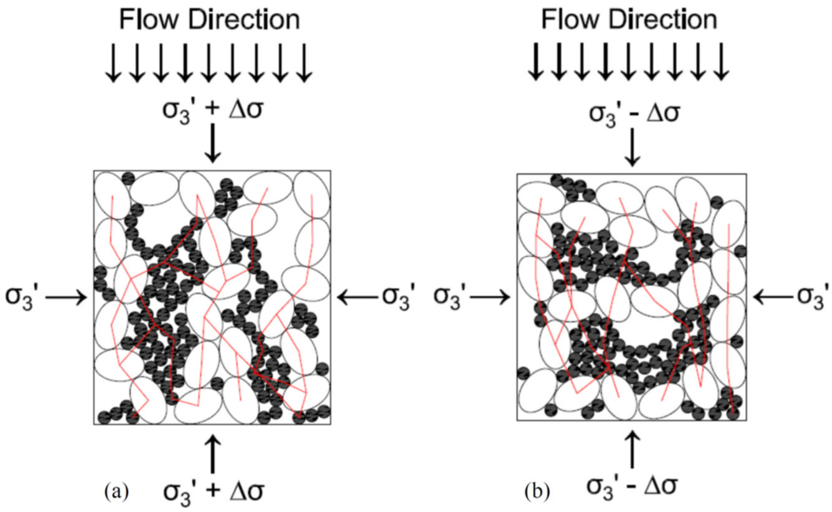

Figure 6-6. Development of pore structures during (a) Compressive stress path (b) Tensile stress path (Chang and Zhang, 2012)

6.6. Discussion and Summary

Based on the analysis presented in this chapter, the moveability of fine particles for soils with a fine content between 10 to 30 per cent can be described in three different scenarios (Table 6-2).

In case i, $(\frac{D'_{15}}{d'_{85}})_{max} > 10$, fine particles are small enough to move easily through available pores between coarse particles. These fine particles are not involved in the soil stress matrix, and only fill voids between host coarse particles. Therefore, erosion of these particles does not affect the soil skeleton. For this case, an increase in relative density does not improve fine particles' contribution to the soil structure, as they only slip to other voids during compaction. The intergranular void ratio is constant during erosion, and soil behaviour can be assessed using the global void ratio.

In case iii, $(\frac{D'_{15}}{d'_{85}})_{max} < 4$, fine particles provide lateral support for force chains or participate in load transferring directly when they are wedged between coarse particles. However, these fine particles may be susceptible to erosion in soils with low relative density. The effect of the relative density on α is only considerable for soils with semi-active fine particles. The global void ratio is unable to explain this alteration in the soil skeleton, as erosion of semi-active and active fine particles leads to deformation and structural distortions. This particle rearrangement changes the available voids volume between coarse particles, and, consequently, the intergranular void ratio.

In case ii and for soils with $4 \leq (\frac{D'_{15}}{d'_{85}})_{max} \leq 10$, the stress level of fine particles controls their moveability. If they only fill the voids, they are free to move, and relative density has no effect on α. However, if they provide lateral support for the soil primary structure, an increase in relative density improves their stability against the erosion.

Table 6-2. Movability of fine particles in coarse skeleton soils with fine content between 10 to 30 per cent

Case No.	Case i	Case ii	Case iii
$(\frac{D'_{15}}{d'_{85}})_{max}$	> 10	$4 \leq (\frac{D'_{15}}{d'_{85}})_{max} \leq 10$	< 4
FC (%)	10 < FC < 30	10 < FC < 30	10 < FC < 30
Appropriate Void Ratio[a]	$e = \frac{V_v}{V_s}$	If fine particles sit loose in the pores: $e = \frac{V_v}{V_s}$ If fine particles provide lateral support: $e_g = \frac{e + FC}{1 - FC}$	$e_g = \frac{e + FC}{1 - FC}$
α	α << 1	α < 1	$\alpha \leq 1$
Influence of D_r	None	An increase in relative density improves α but the influence of D_r on α for gap-graded soils is not as effective as for well-graded soils	It may improve α
Remarks		Effect of D_r on α is dependent on C_u and fine content	Effect of D_r on α is dependent on C_u

[a]: Appropriate void ratio is the void ratio that needs to be considered for evaluating the effect of fine content on soil behaviour

6.7. Conclusion

The influential parameters on moveability of fine particles in internally unstable soils were investigated based on back-calculation of the stress-reduction factor. The following observations summarise the key findings of this study:

- An increase in $(\frac{D'_{15}}{d'_{85}})_{max}$ results in a drop in α while for soils with $(\frac{D'_{15}}{d'_{85}})_{max}$≈10 or above, the effect of $(\frac{D'_{15}}{d'_{85}})_{max}$ on α could be neglected.
- It is recommended that the transitional zone for gap-graded soils needs to be extended for soils with the fine fractions between 10 and 35 per cent. In this zone, the internal stability of soils depends on relative density. The effect of relative density in the transitional zone of gap-graded and well-graded soils depends on both $(\frac{D'_{15}}{d'_{85}})_{max}$ and C_u.
- Particle shape may affect the stress-reduction factor. A decrease in sphericity may increase the constriction size and chance of well-connected throats. This can alternatively lead to a lower critical hydraulic gradient and a decrease in α for soils on the border between internally stable and unstable. Angularity and roughness decrease the permeability and improve erosion resistance, resulting in an increase in the critical hydraulic gradient and α. With an increase in roundness, sphericity and regularity, e_{max}, e_{min} and void ratio difference ($I_e = e_{max} - e_{min}$) decrease. This means that particle shape can change the effect of relative density for internally unstable soils in the transitional zone. However, the influence of particle shape on moveability of fine particles in a coarse-skeleton material is not yet clear. More experimental investigation and micro-analysis needs to be performed.
- Back-calculation of the stress-reduction factor has some limitations. For soil samples with similar particle size distributions, the stress level on the erodible particles might have been similar, while the particle shape only affected the constriction size or pore throats. In this condition, it is possible to observe

different critical hydraulic gradients. Therefore, the back-calculation of α being based on the critical hydraulic gradient is not necessarily accurate for all conditions. In addition, a decrease in α due to an increase in fine fraction may be the result of more free fine particles being available to move.

- It is necessary to stress that the database here is not large enough to assess all effective parameters on moveability of fine particles.

Chapter 7 Mechanical Consequences of Internal Erosion under Monotonic Loading

In Chapter 6, influential parameters on internal erosion was determined using previous experimental investigations. In this chapter, the impact of internal erosion on the undrained behaviour of the soil mixture during erosion, and afterwards under monotonic loading, is discussed.

7.1. Impact of Seepage Properties on Erosion Progress and Post-Erosion Mechanical Behaviour

Internal erosion in a granular soil is essentially the migration of fine particles through pre-existing pores (between the coarse particles) caused by seepage flow. Terzaghi (1925) was the first to show that an upward flow decreased the effective stress, which can lead to the dislodgment of solid particles under a critical hydraulic gradient. Although various methods have been developed to evaluate the susceptibility of soil gradations to internal erosion (e.g. Kezdi, 1969; Sherard, 1979; Kenney and Lau, 1985; Chapius, 1992; Wan and Fell, 2008; Moffat and Fannin, 2011; Chang and Zhang, 2013; Dallo et al., 2013; Moraci et al., 2014; and Indraratna et al., 2007 and 2015), the post-erosion geomechanical behaviour of granular material is still a topic of discussion, with contradictory results being presented in the literature. The first stage of experimental investigation is assessing the post-erosion geomechanical behaviour of internally unstable granular material due to removal of fines caused by erosive forces of water flow. Post-erosion undrained behaviour of a gap-graded internally unstable soil was investigated for a range of erosion durations and inflow velocities using a triaxial-erosion apparatus.

7.1.1. Testing Procedure

Triaxial specimens with 75 mm in diameter and 150 mm in height were prepared, saturated and consolidated to 150 kPa according to the procedure explained in Chapter 3. A downward flow with two different flow velocities (V_{inflow}) of 52 and 92 mm/min (Inflow-V52 and Inflow-V92) was applied to the top of the specimens to investigate the erosion potential and the influence of loss of fine particles on the soil structure and its geomechanical behaviour. The selected inflow velocities were chosen to be higher than the critical inflow to initiate internal erosion, but lower than the failure inflow. The failure flow rate is defined as a seepage flow rate that causes loss of excessive amount of particles and causes the soil to experience shear failure due to large seepage forces (Chang and Zhang, 2013). It is generally accepted that the critical hydraulic gradient is much lower than one for internally unstable soils. Erosion of fine particles confirmed that the chosen flow rate was higher than the critical value. The maximum applicable flow rate by the flow controller was 500 ml/min. A large flow rate of 408 ml/min (lower than the maximum value) was selected for this experiment in order to terminate the erosion phase in a reasonable period of time. However, it was first applied in a pilot test to examine whether a global failure occurs in the soil specimen or not. As this did not happen, and the soil structure was robust until the end of the erosion phase, this flow rate was chosen for the experiment. The applied flow velocity was equal to 92 mm/min considering the specimen area of 4418 mm^2. The soil specimen with 75 mm diameter did not fail even under a flow rate of 500 ml/min. To find the failure flow velocity, a soil specimen with 50 mm diameter was prepared under the same condition and subjected to an inflow velocity of 208 mm/min (flow rate of 408 ml/min), which was approximately 2.3 times greater than what was experienced by the soil specimen with 75 mm diameter. The test result showed that this specimen was still stable at the end of the erosion phase but experienced larger deformations. These trials and errors indicated that the failure flow rate cannot be reached for soil specimens with 60 per cent relative density and under 150 kPa consolidation pressure due to limitation of the flow controller.

During the erosion tests, the erosion rate was increased gradually to minimise the jet flow effect, and it was kept for 30 and 120 minutes. The post-erosion undrained behaviour of the soil specimens was investigated under monotonic shearing and compared to the behaviour of a non-eroded specimen prepared using the same conditions (NE-D75-Mon). Table 7-1 shows the testing program.

Table 7-1. Testing Program

Specimen Identification	Consolidation Pressure (kPa)	Inflow velocity (mm/min)	Erosion Duration (min)	Undrained Shearing Rate (%/min)
E-D75-V92-T30-Mon	150	92	30	0.26
E-D75-V92-T120-Mon	150	92	120	0.26
E-D75-V52-T30-Mon	150	52	30	0.26
E-D75-V52-T120-Mon	150	52	120	0.26
NE-D75-Mon	150	-	-	0.26

7.1.2. Test Results

The percentage of the eroded fine particles with respect to erosion progress is shown in Figure 7-1. For the first 20 minutes, the erosion rate was similar for all specimens when all specimens experienced the same inflow velocity. In addition, the erosion rate decreased for all tests when the inflow velocity reached its target value and was kept constant. For the specimens subjected to the inflow velocity of 92 mm/min, 31 and 66 percent of the fine particles were eroded after 30 and 120 minutes, respectively. In comparison, the percentage of eroded fine particles was only 26 and 43 percent for the specimens eroded at the inflow velocity of 52 mm/min (Table 7-2).

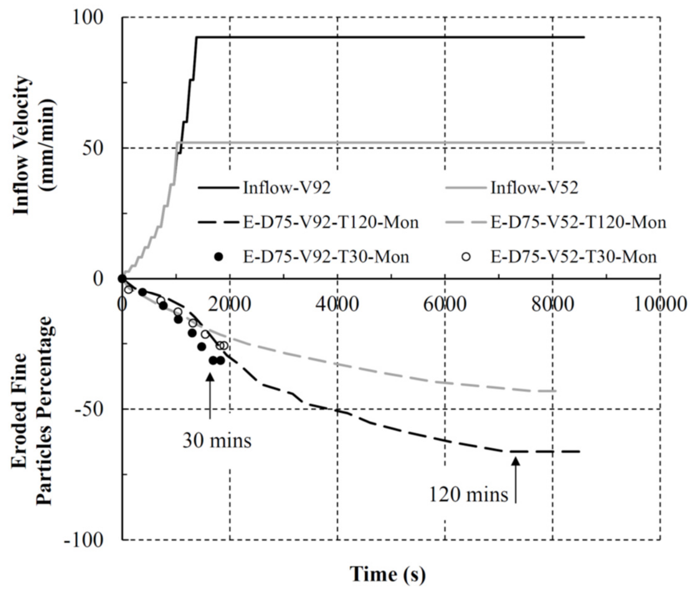

Figure 7-1. Percentage of the fine content erosion against the inflow velocity and erosion progress

Table 7-2. Variation of fine fraction due to internal erosion

Specimen Identification	Initial Coarse Fraction (g)	Initial Fine Fraction (g)	FC_i (%)	Eroded Fine (g)	Residual Fine (g)	FC_f (%)	Eroded Percentage
E-D75-V92-T30-Mon	905.25	301.75	25	95	206.75	18.6	31.5
E-D75-V92-T120-Mon	905.25	301.75	25	200	101.75	10.1	66.3
E-D75-V52-T30-Mon	905.25	301.75	25	78	223.75	19.8	25.8
E-D75-V52-T120-Mon	905.25	301.75	25	130	171.75	15.9	43.1
NE- D75-Mon	905.25	301.75	25	-	301.75	25	-

The mechanical (shear strength) behaviour of the tested specimens after 30 and 120 minutes of erosion was compared with the non-eroded specimen in Figure 7-2. It is evident that the initial hardening behaviour of the soil specimen changed to flow type behaviour with limited deformation as a result of the erosion regardless of the inflow velocity or duration of erosion; this is in agreement with what was previously reported by Ouyang and Takahashi (2015) for gap-graded specimens with 25 percent initial fine content. For the eroded specimens at the seepage velocity of 92 mm/min, the undrained mobilised shear strength increased after erosion in the early stages of shearing. This confirmed Ke and

Takahashi's (2014) findings that erosion of the fine particles improves the initial undrained peak shear strength for granular soils with fine content in the transitional zone. However, this improvement deteriorated after the progression of internal erosion and the further loss of fine particles (E-D75-V92-T120-Mon). Contrary to the non-eroded specimen (NE-D75-Mon), both eroded specimens showed temporary collapse at medium axial strain range of ε_a: 2.5-7.5 %. As shown in Figure 7-2 (b), excess pore water pressure (EPWP) did develop rapidly in the non-eroded specimen, and dilation was observed at low axial strain. In contrast, the maximum excess pore water pressure was reached at medium axial strain, and contractive behaviour was dominant for the eroded specimens. The loss of fine particles and increase in global void ratio could be the reason for the softening behaviour observed for the eroded specimens in this study, as previously reported by Scholtes et al. (2010), Wood et al., (2010) and Chang and Zhang (2011). However, improvement of the initial shear strength might be an indication of better interlocking between the coarse particles.

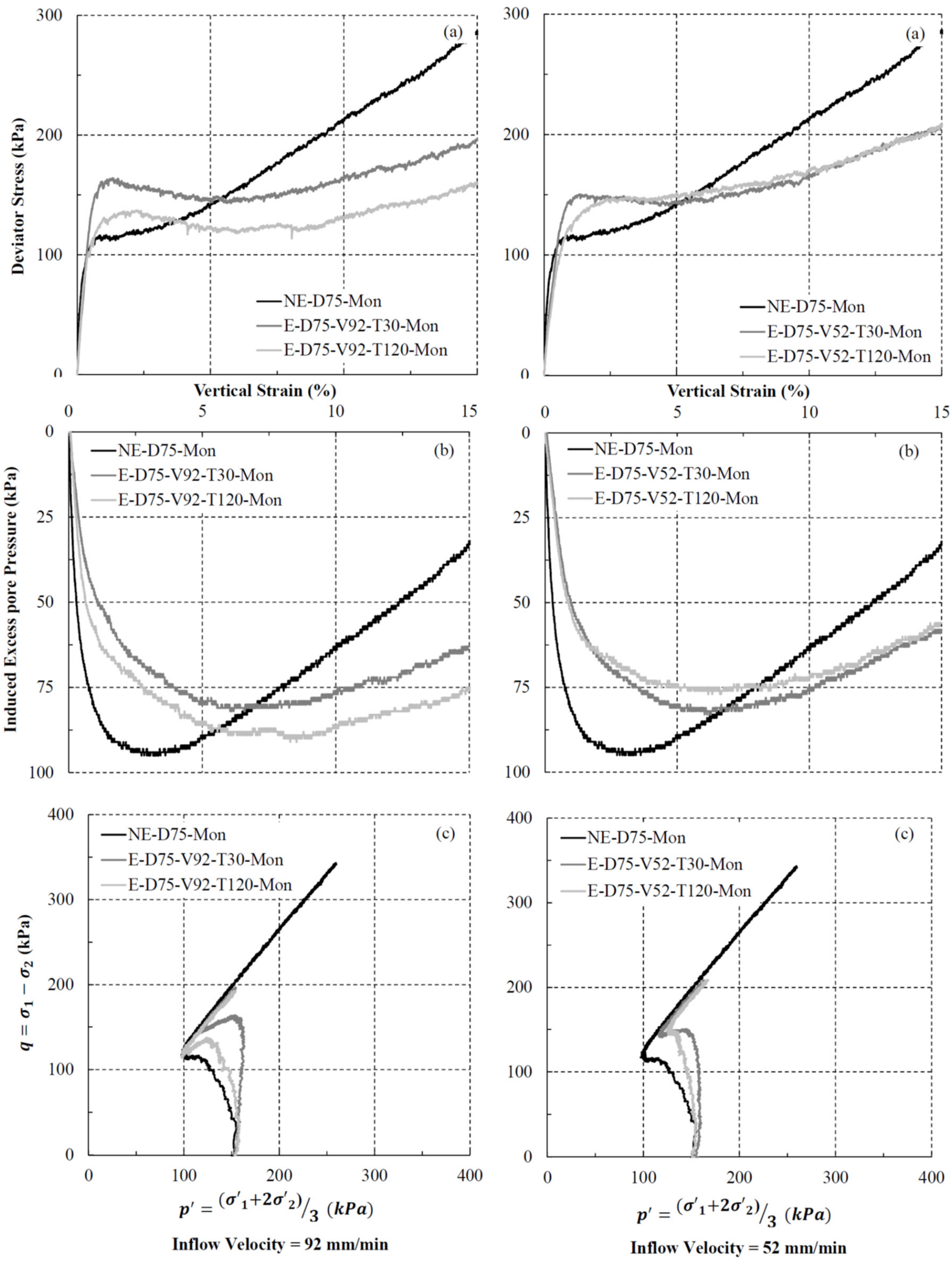

Figure 7-2. Pre and post-erosion response under monotonic shearing (a) Stress-strain relationship, (b) Induced EPWP during shearing and (c) Stress path

Eroded specimens D75-V52-T30-Mon and D75-V52-T120-Mon showed a greater initial shear strength with a lower tendency for dilation when are compared with the non-eroded specimen. However, it was found that the influence of duration of erosion on soil behaviour was not noticeable in the specimens subjected to the seepage velocity of 52 mm/min. Interestingly, specimens E- D75-V52-T30-Mon and E-D75-V92-T30-Mon showed similar behaviour after 30 minutes of erosion. According to Table 7-2, the residual fine content was recorded as 18.6 and 19.8 per cent after 30 minutes of erosion for specimens E-D75-V92-T30-Mon and E-D75-V52-T30-Mon, respectively. This suggested that although one specimen experienced a higher inflow velocity, the soil response was mainly dependent on the erodibility of fine particles (i.e. soil structure and interaction of fine and coarse particles) in the range of seepage velocities applied to the specimens in this research. In addition, comparing specimen D75-V52-T30-Mon with the highest residual fine content with the non-eroded specimen shows that the soil behaviour was found to be affected noticeably, even due to erosion of only 5 percent of fine content. $(\frac{D'_{15}}{d'_{85}})_{max}$ of the tested soil mixture was determined 5.2. The soil was found to be on the borderline of internally stable and unstable soils. This might have increased the activity of fine particles in the soil structure. Therefore, even erosion of small number of fine particles affected the post-erosion behaviour.

Initial drop of 5.2 percent in the fine content resulted to a different post-erosion behaviour for specimen E-D75-V52-T30-Mon. However, further decrease in the fine content from 19.8 percent (specimen E-D75-V52-T30-Mon) to 15.9 percent (specimen E-D75-V52-T120-Mon) did not affect the post-erosion soil behaviour. It appears that the extra 3.9% eroded fine content in case of E-D75-V52-T120-Mon (in comparison to E-D75-V52-T30-Mon) was related to erosion of fine particles that were previously clogged and had not been fully washed out of the specimen at early stages of erosion. These clogged fine particles had no significant contribution in the soil structure. Therefore, erosion of these clogged particles had no noticeable impact on the soil response.

To further understand the possible change of soil structure and its impact on post-erosion behaviour, local vertical strains were measured during the erosion phase using the photogrammetry technique discussed in Chapter 3, and are presented in Figure 7-3. The vertical strains were shown to increase during erosion, and vertical deformations at the end of 120 minutes of erosion was approximately two times greater for specimen E-D75-V92-T120-Mon compared to specimen E-D75-V92-T30-Mon (Figure 7-3 (a)). However, this increase was less than 17 per cent between specimens E-D75-V52-T120-Mon and E-D75-V52-T30-Mon (Figure 7-3 (b)). A considerable initial leap in vertical strains was observed in all specimens at the beginning of the erosion (Time: 300 seconds). In addition, a jumping trend in the vertical strains was identified. Each jump might be related to a new local particle rearrangement triggered somewhere inside the soil specimen. The inflow velocity was kept constant after maximum 1380 seconds (Figure 7-1); however, these steps in the vertical strains continued to the end of the erosion. Erosion of the fine particles that contributed to the soil stress matrix to some extent (lateral support) made the soil structure temporarily unstable, and local particle rearrangement occurred. This rearrangement was more intensive for the specimen subjected to the inflow velocity of 92 mm/min for 120 minutes.

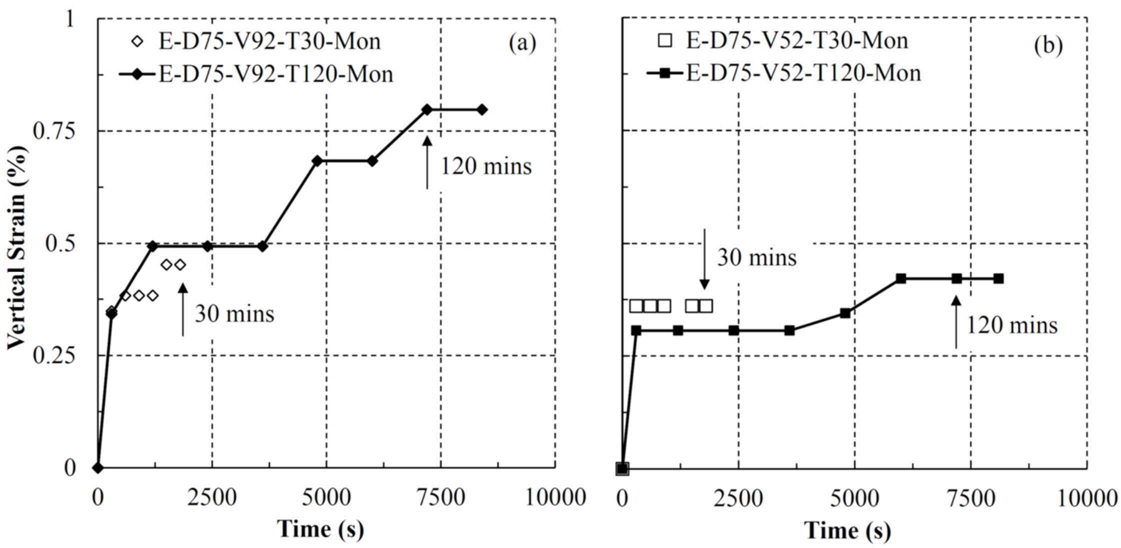

Figure 7-3. Vertical strains during erosion phase: (a) Subjected to inflow velocity of 92 mm/min and (b) Subjected to inflow velocity of 52 mm/min

7.1.3. Impact of Internal Erosion on Mechanical Behaviour of Soil

The test results suggest that internal erosion affects soil mechanical behaviour, even after a short period of erosion, for the studied material in this research. However, the intensity of this change depends on various parameters impacting soil structure and interaction of fine and coarse particles. Parameters include global and intergranular void ratios, fine content and particles rearrangement.

Undrained Peak Strength

The initial peak shear strength (S_p) presented by Ishihara (1993) is an important point on the stress-strain curve of soil behaviour, and is presented in Eq. 7.1. This point is the beginning of an instability state explained in the next section.

$$\frac{S_p}{\sigma_c'} = \frac{q_{Peak}}{2P_c'} \tag{7.1}$$

where σ_c' is the effective consolidation stress, P_c' is the initial mean effective stress and q_{Peak} is the initial peak deviator stress.

The initial confining pressure showed less than five per cent variation at the beginning of the shearing stage due to the occurrence of small changes in water pressure during the erosion phase for all specimens. Therefore, all parameters have been normalised with initial mean effective stresses to eliminate possible effects of stress dependency.

The normalised undrained peak shear strength observed in all tests is shown in Figure 7-4. Overall, the normalised initial peak shear strength improved as erosion progressed, despite an increase in the global void ratio after internal erosion. After 30 minutes of erosion, the specimen that experienced the larger inflow velocity showed a higher peak shear strength. Figure 7-4 also shows a noticeable drop in peak shear strength when the fine content decreased down to 10.1 per cent after 120 minutes of erosion. In addition, although specimens E-D75-V52-T30-Mon and E-D75-V92-T30-Mon had similar residual fine content after 30 minutes of erosion, the specimen that was subjected to the larger inflow velocity of 92 mm/min showed higher peak strength and larger vertical deformation. These results suggest that there could be an intensive particle rearrangement inside specimen E-D75-V92-T30-Mon, leading to a temporarily stronger structure. Beyond this point and as erosion continued, there was a turning point in the residual fine content that reduced this initial temporary improvement in soil structure and associated peak shear strength.

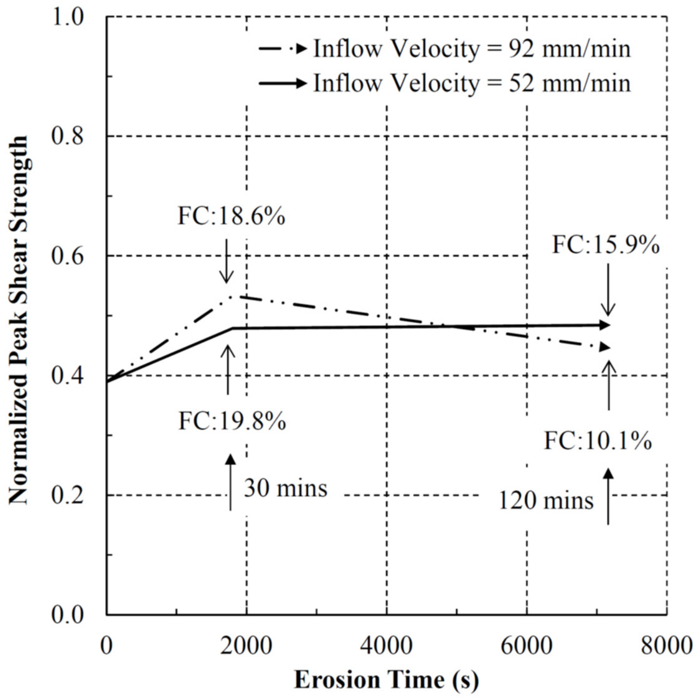

Figure 7-4. Variation of normalised peak strength with erosion progress

Quasi-Steady State and Undrained Instability State

When a soil shows softening behaviour, there are two important states that need to be taken into account. These are known as the Quasi-Steady State (QSS) and the Ultimate State (US) or Steady State (SS) that occurs at relatively large strains (Ouyang and Takahashi, 2015). The quasi-steady state is a temporary state where soil exhibits the smallest shear strength. The steady state is the final state of soil behaviour where deformations continue without any change in shear strength and soil volume. There is a debate as to which strength level should be taken as the residual strength (S_{us}), as the strength at quasi-steady state may be remarkably smaller than the mobilised stress at the steady state (Ishihara, 1993). Ouyang and Takahashi (2015a) stated that it would be safe if the quasi-steady state is chosen as the residual strength and used in internal erosion analyses, as the soil strength is affected by various unknown factors.

A drop in shear strength between the initial peak shear strength and residual strength at the QSS is known as instability and flow failure. Instability is another indication of the softening behaviour. It is classified as one of the failure mechanisms and may lead to flow slides or slope failure under extreme conditions (Lade, 1993 and Olson et al., 2000). Undrained Instability State (UIS) is the state where the deviator stress reaches the initial peak, followed by a flow deformation (Murthy et al., 2007). Instability Line (IL) is known as the line connecting the peak values of the deviator stresses for the undrained stress path space, and starts at the point of origin for sand with no cohesion (Chu and Leong, 2002; Leong et al., 2000 and Yang et al., 2006). The instability line is not a unique soil property and depends on the initial void ratio and the confining pressure. The larger the initial void ratio, the lower the instability line will be (Chu and Leong, 2002). The region between the instability line and steady line is known as the zone of potential instability (Lade, 1993). The relationship between the peak shear stress ratio ($^{q_{Peak}}/_{P'_{Peak}}$) and post consolidation void ratio is called the instability curve (Chu and Leong, 2002).

Results of post-erosion shear strength tests indicate that the hardening behaviour of the original soil changed to a softening behaviour with limited flow deformation (Figure 7-2). The normalised residual strength at QSS (Eq. 7.2) and variation of peak shear stress ratio with post-erosion void ratio for the specimens tested is presented in Figure 7-5. Since the original soil specimen showed a hardening behaviour, this analysis was only conducted for the eroded specimens.

$$\frac{S_{us}}{\sigma_c'} = \frac{q_s}{2P_c'}\cos(\varphi_s) \tag{7.2}$$

where q_s is the deviator stress at the QSS and φ_s is the angle of phase transformation at QSS (Ishihara, 1993).

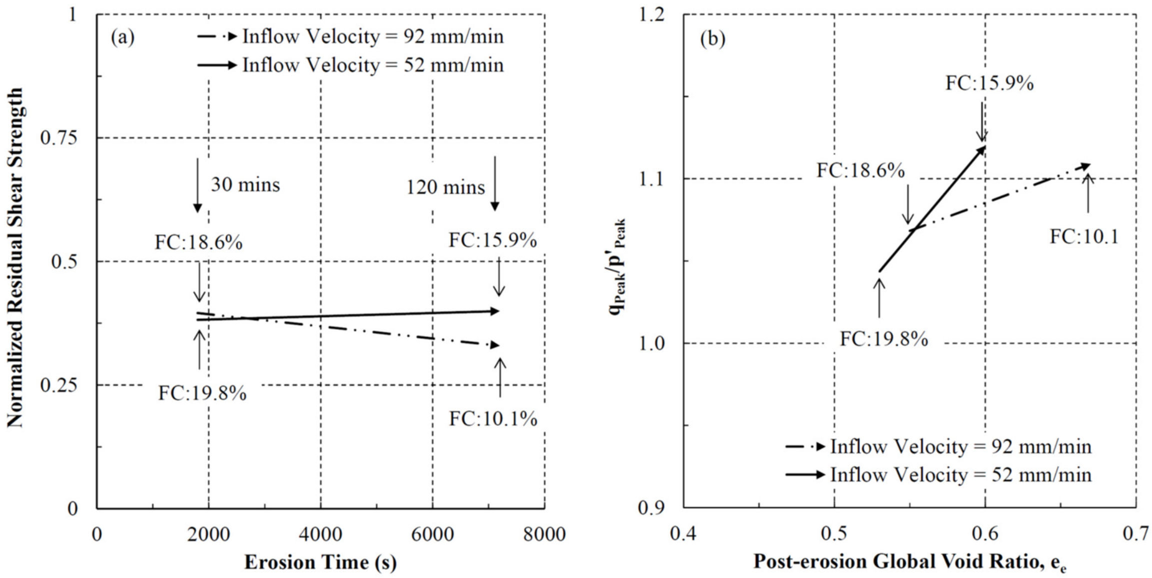

Figure 7-5. Variation of (a) Normalised Residual Strength at the QSS, (b) Instability with erosion progress

After 30 minutes of erosion, the specimen eroded at the greater inflow velocity showed higher normalised peak strength compared to the specimen eroded at the lower inflow velocity at similar residual fine content. However, the normalised residual strength at the QSS was almost the same for all eroded specimens after 30 minutes of erosion (Figure 7-5 (a)). As the erosion progressed, the residual strength was constant for the specimens eroded at lower inflow velocity, but dropped significantly for specimens eroded at larger inflow velocity. It seems the initial peak strength depended upon the fine content and particle rearrangement, while the residual strength was only dependent on the percentage of the survived fine particles. Interestingly, the instability potential decreased with erosion progress for all specimens tested (Figure 7-5 (b)). However, this improvement became fragile as more fine particles were lost.

Flow Potential

A drop in shear strength between the initial peak shear strength and residual strength at the QSS (known as flow failure) stays constant when the residual strength remains at the critical steady state (CSS) level. Alternatively, flow failure can stop as a result of strength regaining and residual strength reaching the ultimate steady state (USS). Yoshimine and Ishihara (1998) proposed an index to evaluate the flow potential (u_f) (Eq. 7.3). This is not an inherent soil property, and direction of principal stress, magnitude of the intermediate principal stress and structure of the soil fabric may affect it. It is associated with the point where the maximum excess pore pressure is induced. When u_f reaches 100 per cent, soil is liquefied with no residual strength and flow deformation is continued (Yoshimine and Ishihara, 1998).

$$u_f = (1 - \frac{P'_{PT}}{P'_c}) \times 100 \tag{7.3}$$

where P'_{PT} is the mean effective principal stress at the phase transformation state and P'_c is the initial mean effective stress.

It can be seen in Figure 7-6 that the flow potential dropped rapidly over the initial 30 minutes of erosion regardless of the inflow velocity. This decrease in flow potential continued for specimens eroded by the lower inflow velocity. However, the flow potential increased for the specimen eroded by the higher inflow velocity after 120 minutes of erosion, after a loss of a certain amount of the fine particles. The smaller flow potential of eroded specimens was also reported by Ouyang and Takahashi (2015). It seems initial reduction in the fine content down to approximately 15 per cent improved the soil response against the flow failure. However, further reduction of residual fine content increased susceptibility of the soil to the flow failure. This turning point was also observed in Figure 7-4.

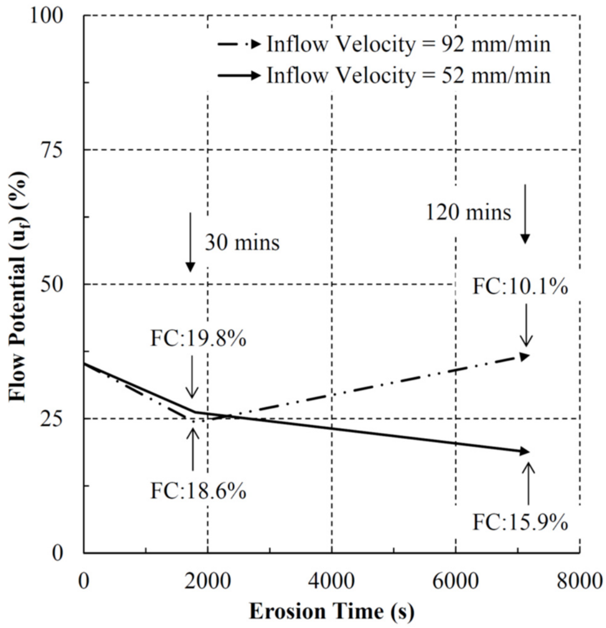

Figure 7-6. Flow potential with erosion progress

Void Ratios Variation and Residual Fine Content

The concept of intergranular void ratio was first introduced when it was discovered that the presence of fine particles affected soil behaviour significantly. This was due to the different types of fines and how they contributed to the soil stress matrix. Depending on the type of involvement of the fine particles in the soil skeleton (i.e. their role in soil stress matrix), erosion of fine particles can impact the mechanical behaviour of a soil differently. Therefore, it is important to consider both the global and intergranular void ratios when analysing post-erosion mechanical behaviour of granular matters. Figure 7-7 shows the variation in global and intergranular void ratios as erosion progressed for all tested specimens. To measure the global void ratio at the end of each erosion tests, it was assumed that the top cap, the base plate and funnel in addition to the soil specimen was full of water. By knowing the volume of water in the funnel and in the top cap, it was possible to calculate the volume of water inside the soil. As expected, the global void ratio increased due to removal of some of the fine particles as erosion progressed. However, this rise was accompanied with a reduction in the intergranular void ratio, e_g. Theoretically, the loss of fine particles does not change the intergranular void ratio, since a decrease in volume of the fines is added to the real voids; hence the final result should remain unchanged. However, if the soil skeleton formed by the coarse particles deforms or settles, the available spaces between the coarse particles may decrease, which could lead to a reduction in the intergranular void ratio. In fact, it is believed that this coarse particle rearrangement during the erosion process (caused by a loss in semi-active fines) decreased the available voids between the coarse particles and reduced the intergranular void ratio.

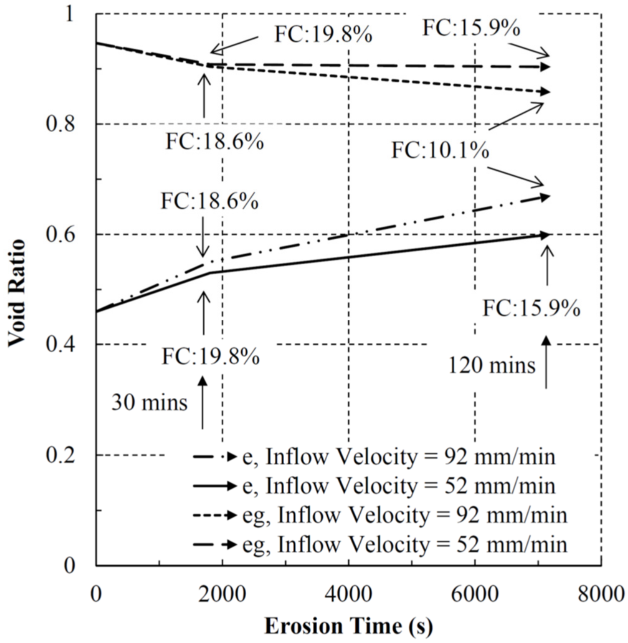

Figure 7-7. Variation of Global and intergranular void ratios with erosion progress

For the tested specimens at an inflow velocity of 92 mm/min, the initial value of the intergranular void ratio decreased from 0.95 to 0.86 at the end of 120 minutes of erosion. This noticeable drop was attributed to intensive particle rearrangement. On the contrary, e_g showed a reduction from 0.95 to 0.91 during the first 30 minutes of erosion for the eroded specimens at an inflow velocity of 52 mm/min, and stayed relatively constant at 0.9 for the rest of the erosion stage. This was supported by the agreement between Figures 7-3 and 7-7, which showed vertical deformations during internal erosion. All specimens (except for specimen E-D75-V92-T120-Mon) showed minor vertical deformation during the erosion process apart from the large initial deformation, which was experienced by all specimens. The first drop in the intergranular void ratio (from 0.95 to 0.9) could be due to the initial large deformation. Similar final e_g for specimens E-D75-V52-T30-Mon, E-D75-V52-T120-Mon and E-D75-V92-T30-Mon is plausible, as the final deformations were almost the same. However, e_g decreased again for specimen E-D75-V92-T120-Mon sample when particle rearrangement occurred to reach a new stable state, due to formation of a metastable structure after massive erosion of the semi-active fines. Figure 7-7 shows that decrease in the fine content from 25 per cent to 19.8 per cent rearranged the soil structure and reduced the available voids between the coarse particles (hence a reduction in the intergranular void ratio). However, further reduction from 19.8 to 15.9 per cent did not cause any influence on soil structures or available stress matrix, ultimately leading to similar soil behaviour and shear strength for the specimens with the residual fine contents within this range. A second drop in e_g occurred when more of the involved fine particles were removed as erosion continued. Comparing Figures 7-2, 7-3 and 7-7 shows that this is the intergranular void ratio that controls the eroded soil specimen response. Similar stress-strain relationships and final vertical deformations were observed for specimens E-D75-V52-T30-Mon, E-D75-V52-T120-Mon and E-D75-V92-T30-Mon with similar intergranular void ratios, although seepage properties, the residual fine contents and the final global void ratios were different.

Equations suggested by Rahman and Lo (2008) and Rahman et al. (2008) were developed based on previous studies, such as Thevanayagam et al., (2002) that used moist tamping or dry air deposition techniques to prepare soil specimens. This means that these equations are applicable in this research as well, as soil specimens were prepared using the moist tamping technique. It is worth noting that many fines are placed around the coarse particles during sample preparation when the moist tamping method is used. However, it is believed that most of them provide secondary (lateral) support for force chains that are made by coarse particles and only a small percentage of them are sandwiched between coarse particles considering the fine content, soil gradation curve and size of fine particles.

According to Eqs. 2.14 and 2.17, the FC_{Crit} and b are equal to 31 per cent and 0.34 for the soil specimen reported in this paper, respectively. This means that the primary soil skeleton (stress matrix) for the soil tested in this research is composed of coarse particles. Depending on the ratio of fine particle sizes to the constriction size, particle shape, relative density and confining pressure, the fine particle may sit loose in the voids (inactive), provide lateral support (semi-active), or be sandwiched between the coarse particles (active). In fact, b = 0.34 for the tested specimen suggests that approximately 100 grams (out of 300 grams) of total fine particles contributed to the active intergrain contacts. However, the quality of this contribution is still unclear for semi-active or active fine particles. Specimens E-D75-V52-T30-Mon, E-D75-V52-T120-Mon and E-D75-V92-T30-Mon showed very similar undrained behaviours. This indicates that the percentage of residual semi-active and active fine particles involved in the soil structure was almost the same for these three specimens. However, specimen E-D75-V92-T120-Mon, which lost 66 percent of its fine particles (200 grams), showed different behaviour in comparison to the other specimens. If residual fine particles for this specimen (34 percent) is compared with the calculated b value (0.34) suggested by Rahman and Lo (2008) and Rahman et al. (2008) for active fine particles, it can be seen that most of the erodible fine particles (inactive and semi-active fine particles) should have been washed out of the soil body in this specimen. This means that only active and non-erodible fine particles that were fully involved in the soil structure were left in the soil specimen. It is believed that this is the reason for different behaviour for specimen E-D75-V92-T120-Mon. To validate this hypothesis, a soil specimen with 50 mm diameter was prepared under the same condition and eroded for 120 minutes under a much higher seepage velocity (208 mm/min). Only an extra 3 per cent drop in the residual fine content with similar undrained behaviour to E-D75-V92-T120-Mon was observed for this specimen. This experiment confirmed that between 30 to 35 percent of fine particles were non-erodible. Different observed behaviour (a reduction in the peak shear strength or increase in the flow potential) could be due to an intensive particle rearrangement, formation of a metastable structure, and growing instability in the force chains after loss of a considerable fraction of the semi-active fines.

Normalised residual fine content with an initial fine content at different levels is presented in Figure 7-8 for all eroded specimens. Erosion of the fine particles was shown to be uniform across the height of the specimens during the first 30 minutes regardless of the inflow velocity. However, the loss of fine particles was shown to be more pronounced in the upper parts of the specimens as erosion progressed. This particle migration was more intensive for the specimen subjected to the inflow velocity of 92 mm/min. While the presence of the fine particles was constant in the bottom part of the eroded specimen under an inflow velocity of 52 mm/min during erosion, the middle and top parts of the specimen lost an extra 17 and 29 per cent of their fine contents, respectively. Unfortunately, it was not possible to make a distinction between clogged fine particles in the lower part of the specimen, which were thought to have originally migrated from the upper regions, and the fine particle which belonged to this part from the start of test (sample preparation). However, it is clear that their influence on soil behaviour is not similar. The moist tamping technique used for sample preparation involved more fine particles in the soil structure (stress matrix) when compared to the erosion process that carried some fine particles and left them in the lower part of the specimen in a loose condition. Figure 7-8 clearly shows that the void ratio measured at the end of the erosion test is not an accurate index to explain the soil behaviour, as local void ratios across the specimen height were completely different. It should be noted that internal erosion is a non-uniform process leading to different local volumetric strains, void ratios, fine content and particle rearrangements.

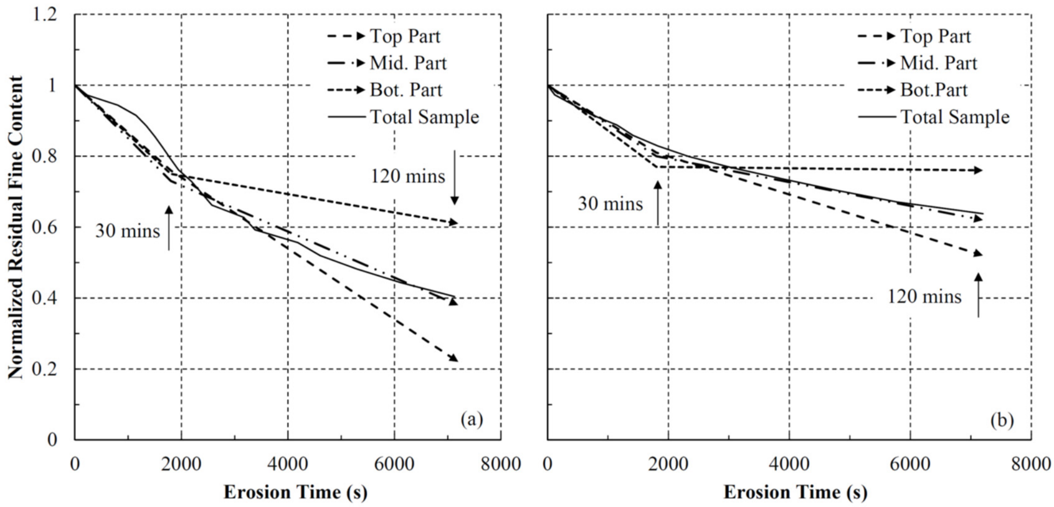

Figure 7-8. Variation of normalised residual fine content of the soil specimens (a) Subjected to an inflow velocity of 92 mm/min (b) Subjected to an inflow velocity of 52 mm/min with erosion progress

Effect of Fine Content on Macro and Micro Mechanical Behaviour of Soil

Apart from the role of fine particles in the stress matrix, the angularity of fine particles also impacts the post-erosion behaviour of a soil. Moreover, the shear resistance and dilatancy properties of sand are dependent on particle angularity (Guo and Su, 2007). The removal of rounded fine particles improves the interlocking of the coarse particles during the shearing. Slip-down movement of the coarse grains may occur due to an increase in the void ratio after internal erosion and postpone the initial dilation tendency. Therefore, although the contractive behaviour is initially dominant, the improvement in the coarse particle interlocking increases the peak shear strength. Figure 4-8 demonstrated the shape factors and the internal friction of the particles used in this research. A series of direct shear tests was conducted on samples prepared at the loosest condition of each grain category to measure the internal friction. It was shown that apart from the largest particles (particles diameter; D = 1.7-2.36 mm), shape parameters and internal friction was approximately similar. A decreasing trend in the circularity and a noticeable jump in the internal friction angle were observed for the largest particles. This can confirm the hypothesis that loss of the rounded fine particles improved the interlocking of the coarse particles during the shearing.

Local accumulation of fine particles during internal erosion also needs to be taken into account when studying post-erosion mechanical behaviour. This local concentration in the downstream may affect the shear strength in large strains. In fact, local high density of the fine particles may act as a lubricant between the coarse grains (Ke and Takahashi, 2015). This lubricating effect can be more critical when the angularity of the coarse particles is conspicuous. In addition, erosion of fine particles may resuscitate the characteristics of the host fabric made by the coarse particles. Ke and Takahashi (2014a) showed that the coarse particles (artificial silica No.3) used in their research behaved dilative, even at a very loose condition. This inherent dilation tendency might have been the main reason for the reported higher undrained shear strength after internal erosion, which overcame the contraction tendency after the increase in the void ratio.

7.2. Impact of the Specimen's Length (Seepage Path) on Erosion Progress and Post-Erosion Mechanical Behaviour

The literature review indicates that the effect of specimen length on the erosion process and post-erosion mechanical behaviour has been overlooked. It can be understood from the few available studies (e.g. Sellmeijer, 1988; Li, 2008; Marot et al., 2012; Seghir et al., 2014) that extension of the laboratory and small-scale results in real field conditions is challenging and complicated. For instance, Sellmeijer (1988) stated that the hydraulic gradient required for initiation of erosion had an inverse relation with the seepage length. Li (2008) found that for a specific soil, the critical hydraulic gradient was higher for a small specimen than a larger one under the same mean effective stress. Centrifuge modelling conducted by Marot et al. (2012) showed that the scale effect had an influence on initiation and progression of suffusion. A significant drop in the critical hydraulic gradient was observed when the specimen length increased by a factor of two. However, Seghir et al. (2014) believed that internal erosion was independent of specimen length. It is evident that the clogging possibility, self-filtration of the migrated particles, and rearrangement of the survived particles are dependent on the erosion length. Consequently, mechanical properties of the eroded specimens with different dimensions may show differences in terms of hydraulic conductivity and shear strength. In this section, results of undrained triaxial tests on eroded specimens that different dimensions but are subjected to an identical seepage velocity (with the same initial soil properties) are discussed.

7.2.1. Testing Procedure

Similar to a previous part of this research, a new erosion phase was added between the consolidation and undrained shearing stages of a conventional triaxial test to investigate post-erosion behaviour of the soil specimens. The same procedure explained in Chapter 3 was used for sample preparation, saturation and consolidation. Geometrical properties of the tested specimens are shown in Table 7-3. The soil layer thicknesses varied slightly over a narrow range regardless of the height of the specimens. This helped each soil layer to experience similar compaction pressure during sample preparation.

Table 7-3. Soil sample identification and specifications

Sample ID	Sample Diameter (mm)	Sample Height (mm)	Total Number of Soil Layers
E-D50-V52-T120-Mon	50	115	8
E-D75-V52-T120-Mon	75	150	10
E-D100-V52-T120-Mon	100	200	14

A downward seepage flow was applied to the top of the specimen at the end of consolidation. The inflow velocity was increased gradually up to 52 mm/min and kept constant for a further 120 minutes. Variation of the inflow velocity and percentage of the eroded fine particles with time are shown in Fig. 7.9. It is evident that the rate of erosion and maximum percentage of the eroded particles were similar for the 75 and 100 mm diameter specimens. However, the 50 mm diameter specimen showed a different result. Rate of erosion for all three specimens decreased, and no eroded particle was observed at the end of the test. This may be associated with the self-clogging of fine particles in the longer specimens or reaching the end of erosion under the applied hydraulic conditions. Initial fine content, sample preparation procedure, confining pressure and hydraulic stresses were kept the same for all of the tested specimens. This means that the contribution of the fine particles in the soil skeleton had to be similar regardless of sample dimension. However, 66 per cent of the fine content was washed out in specimen E-D50-V52-T120-Mon, compared to almost 45 per cent for the other two larger specimens. Two scenarios were likely to occur. The first scenario is a higher possibility of self-filtration in the larger specimens. The second scenario was an inadequate seepage force to carry the erodible particles along the larger specimens, which led to particle sedimentation in the downstream.

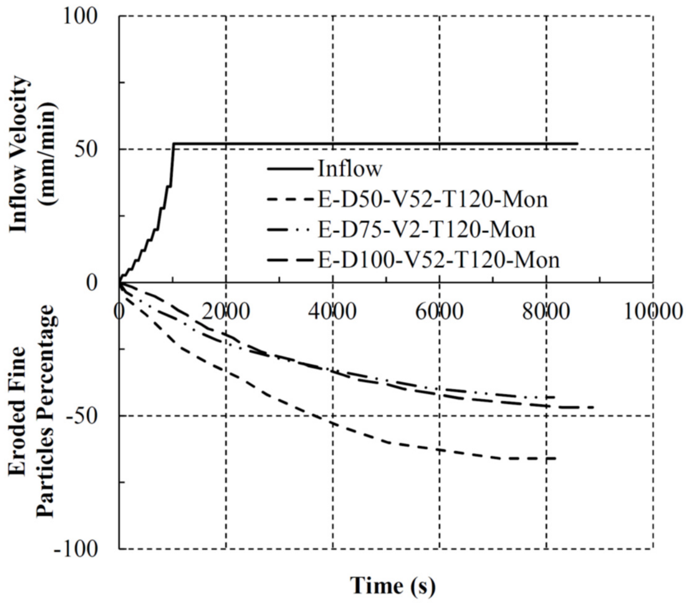

Figure 7-9. Variation of inflow velocity and percentage of the eroded fine particles with erosion time

Vertical surface strains during the erosion phase were measured using the photogrammetry technique and are shown in Figure 7-10. Although the erosion rate and residual fine content were similar for the 75 and 100 mm diameter eroded specimens, the vertical strain results indicated no trends between vertical strain, sample size and percentage of eroded particles. This could be due to non-uniform erosion of the fine particles and preferential erosion paths in the soil samples that eventually led to different local instabilities and deformation patterns. However, all specimens did experience a rapid increase in vertical strain at the beginning of the erosion when the inflow velocity was very low. In addition, apart from the largest specimen, the two other specimens with smaller dimensions showed step-wise changes in the vertical strain.

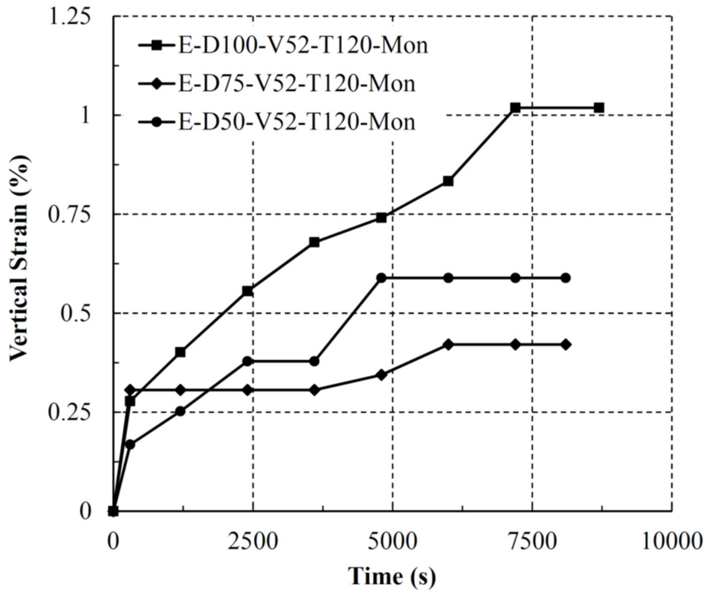

Figure 7-10. Vertical strains during erosion phase

7.2.2. Test Results

To investigate the influence of the erosion path on post-erosion undrained behaviour, undrained compression triaxial tests were performed after the erosion phase for each specimen. Stress-strain relationship, induced excess pore water pressure (EPWP) and stress path were all studied and compared with the undrained response of a non-eroded 75 mm diameter (NE-D75-Mon) (Figure 7-11). All eroded specimens exhibited a higher initial undrained peak shear strength in comparison to the non-eroded specimen (Figure 7-11 (a)). The residual fine content was similar for the 75 and 100 mm diameters eroded specimens, which showed similar trends at early stages of shearing. Although the strain hardening potential decreased, this behaviour was still dominant in both specimens.

However, the shear strength increased more rapidly in specimen E-D100-V52-T120-Mon at medium and large strains. In contrast, the 50 mm diameter specimen (which lost the most fines) changed behaviour from strain hardening to flow type behaviour at limited deformation.

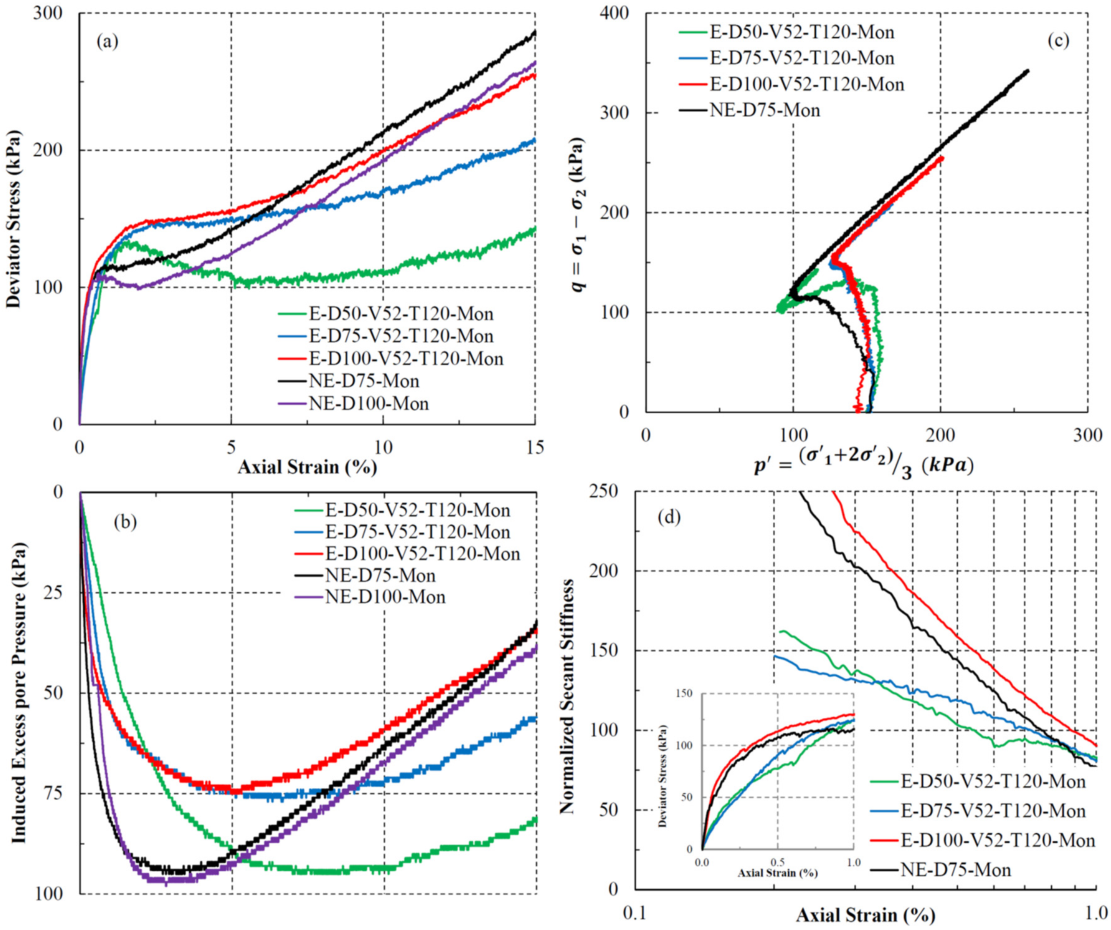

Figure 7-11. Variation of post-erosion behaviour in soil specimens with different dimensions (a) Stress-strain relationship, (b) Induced EPWP during shearing, (c) Stress path and (d) Normalised secant stiffness

Fig. 7.11 (b) presents the variation of induced EPWP during undrained shearing. For the non-eroded specimen, the positive excess pore pressure developed rapidly, and dilation was observed at small strains. This dilation tendency was postponed for the eroded specimens, especially for the smallest specimen with least residual fine content. The maximum value and trend of the induced excess pore pressure were similar for specimens E-D75-V52-T120-Mon and E-D100-V52-T120-Mon for the first five per cent axial strain. However, these initial identical responses gradually disappeared as shearing progressed and the vertical strain increased. Contrary to specimens E-D75-V52-T120-Mon and E-D100-V52-T120-Mon, which showed a considerable drop in the maximum induced EPWP, specimen E-D50-V52-T120-Mon developed positive excess pore pressure similar to the non-eroded specimen, but at a much slower rate. This different response can be seen in Fig. 7.11 (c) where the smallest specimen showed a temporary collapse at medium strain. However, all specimens (regardless of sample dimension and rate of erosion) eventually ended up on parallel steady state lines, as suggested by Yang et al. (2006) for sand-silt mixtures with various fine contents.

The normalised secant stiffness with the initial mean effective stress at small strains (≤ 1%) for all tested specimens is shown in Fig. 7.11 (d). It is evident that although specimens E-D75 and E-D100-V52-T120-Mon showed identical responses in terms of inducing EPWP and shear strength at low strains (≤ 5%), a lower normalised secant stiffness was observed for specimen E-D75-V52-T120-Mon. In fact, regardless of the erosion progress, the initial stiffness of specimen E-D75-V52-T120-Mon was comparable to specimens E-D50-V52-T120-Mon, while E-D100-V52-T120-Mon showed a similar trend to NE-D75-Mon. Overall, it seems internal erosion decreased the initial stiffness, which was similar to what was observed previously by Chang and Zhang (2011), but different from the findings reported in Ouyang and Takahashi (2015).

It is worth mentioning that the undrained triaxial test has been conducted on non-eroded specimens with 50, 75 and 100 mm diameters (NE-D50-Mon, NE-D75-Mon and NE-D100-Mon). While specimens NE-75-Mon and NE-100-Mon showed the same trends and very similar values for stress-strain relationship and induced excess pore pressure, specimen NE-D50 showed the same trend, but much higher shear strength and induced much lower excess pore pressure. An undrained triaxial test on specimen NE-D50-Mon was repeated 7 times, but the response of the specimens was still the same. It is believed that specimen NE-D50-Mon is not a good representative for the original behaviour of the tested mixture for the purpose of comparing it with the post-erosion undrained shear test result. However, undrained behaviour of specimens NE-D75-Mon and NE-D100-Mon have been added to Figure 7-11. It seems that the sample preparation was affected by the size of the specimen due to difficulty in preparing a very uniform mixture for all compacted soil layers using the moist-tamping technique. This is caused by the small size of each soil layer (diameter of 50 mm and thickness of 12.5 to 15 mm) and small mass of fine material used in each layer (approximately 12.5 gr), which makes it possible to have fine particles accumulated in small isolated regions across the cross section of specimen. Hence, this demonstrates a different behaviour than larger specimens with a more uniform distribution of fine particles.

The erosion of fine particles does increase the global void ratio. However, the global void ratio cannot be an accurate index in evaluating post-erosion behaviour, since internal erosion is a non-uniform phenomenon across the specimen length. The contribution of the fine particles in the soil skeleton depends on various parameters and affects soil response, which cannot be explained by only the global void ratio. Figure 7-12 presents the variation of the global void ratio during the test stages.

Post-erosion particle size distribution (PEPSD) at the top, middle and bottom regions of the eroded specimens is shown in Figure 7-13. Specimen with 50 mm diameter was divided into two parts for PEPSD due to their small size. PEPSDs across the specimen were similar for the 75 mm and 100 mm diameter specimens. Regardless of sample dimension, the fine content decreased along the height of the specimens. However, the top region of the soil specimens lost more fine particles. Overall, all grading curves moved downward after internal erosion, which led to a reduction in “grading state index,” suggested by Muir Wood (2007).

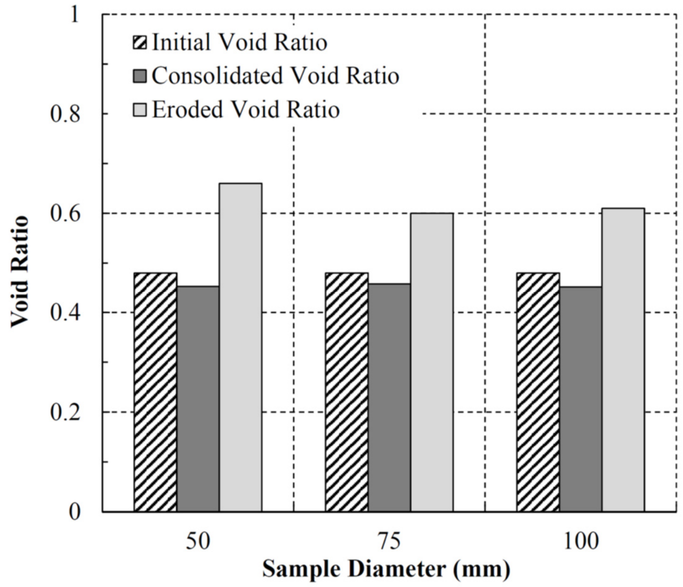

Figure 7-12. Variation of post-erosion void ratios in soil specimens with various dimensions

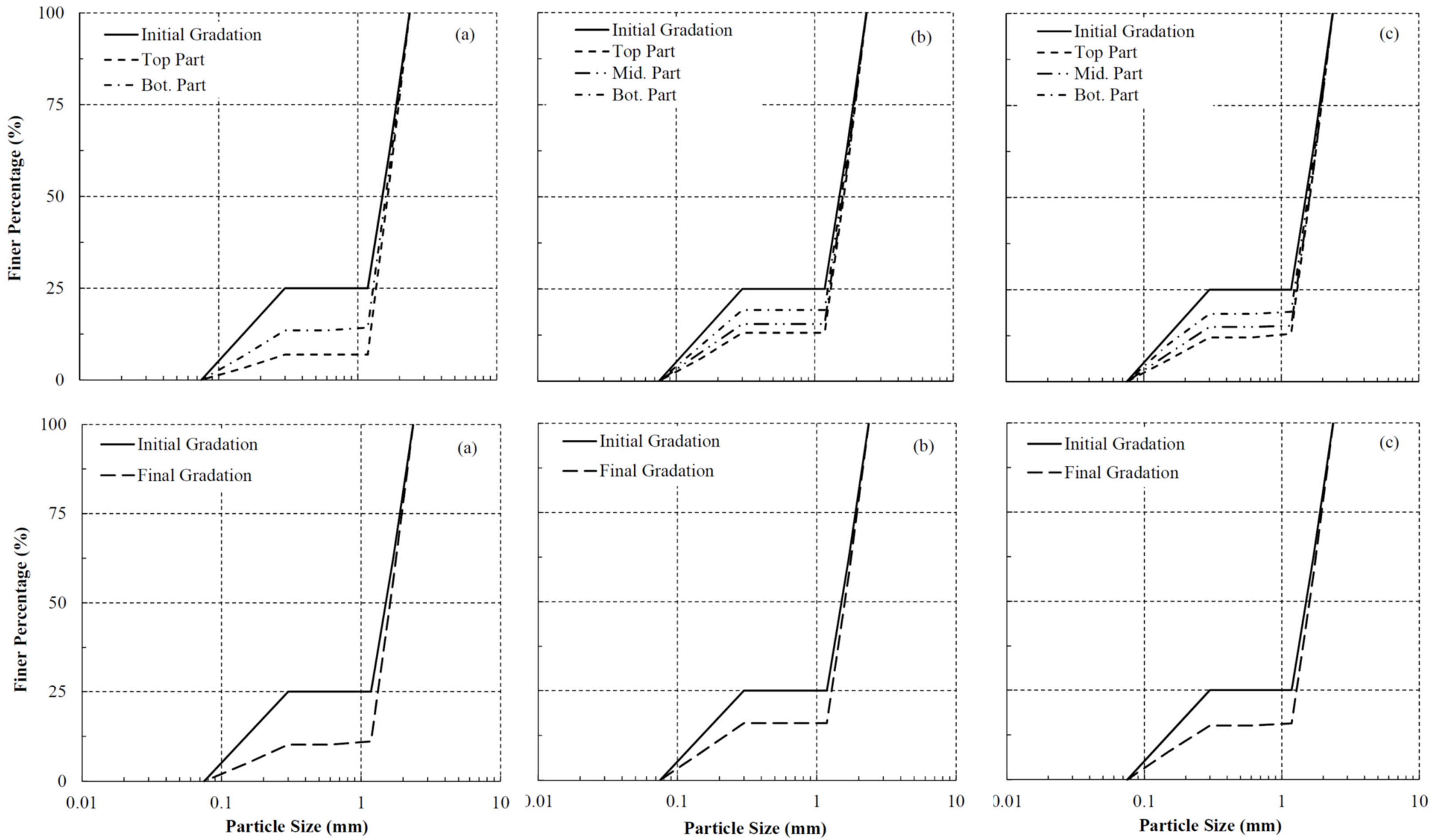

Figure 7-13. Particle size distribution plots for post-erosion specimens at different regions for (a) E-D50-V52-T120-Mon, (b) E-D75-V52-T120-Mon and (c) E-D100-V52-T120-Mon

It was observed that the erosion of fine particles increased the initial undrained peak shear strength and decreased the dilation tendency, regardless of the specimen dimension tested. However, the percentage of erosion of the fine particles was affected by the sample dimensions. In fact, the residual fine content is believed to be the critical factor determining post-erosion mechanical behaviour. The initial improvement in the undrained shear strength could be due to a better interlock between the coarse particles after the loss of fine particles, which is consistent with the findings reported in Vallejo (2001) and Guo and Su (2007). However, the increase in the global void ratio after erosion resulted in slip-down movements of the coarse particles and higher tendency to contractive behaviour (Muir Wood et al., 2010, Scholtès et al., 2010). Other factors, such as the local concentration of dislocated fine particles, may have had a lubricating effect between the coarse particles, and potentially postponed the dilation in the medium strain range until further shearing improved the roll-over mechanism and dilation. It is evident that the microstructure of sand controls its stress-dilatancy property in terms of volume change in the drained condition and accumulation of excess pore pressure in the undrained condition (Wan and Guo, 2001). It is worth mentioning that the temporary improvement in peak undrained shear strength disappeared after a further drop in the residual fine particles. It seems there was an inflexion point in the residual fine content, below which local metastable structures formed.

To investigate the effect of fine particle removal and specimen dimension on post-erosion behaviour, a new erosion test (E-D50-V208-T120-Mon) was performed on a 50 mm diameter specimen with a four-fold inflow velocity (208 mm/min), aiming to wash a much higher percentage of the fine particles. In addition, the test result was compared with specimen E-D75-V92-T120-Mon that showed a similar residual fine content of 10.1 per cent after an erosion period of two hours. Other parameters, such as sample preparation procedure or consolidation pressure, did not change to ensure that the results were comparable. Seepage velocities and percentage loss of fine particles with time are shown in Figure 7-14. It can be seen that after approximately 2000 seconds, the erosion trends and final fine contents become similar for specimens E-D50-V52-T120-Mon and E-D75-V92-T120-Mon, even though they have experienced different seepage velocities. The initial deviation in the erosion percentage could be due to the different inflow patterns applied at the beginning of the erosion phase. Figure 7-14 also shows that although the seepage velocity increased dramatically for E-D50-V208-T120-Mon, it was still unable to wash all fine particles. The maximum erosion percentage finally reached 78 per cent with a similar trend to what observed for specimen E-D50-V52-T120-Mon. This suggested that the remaining fine particles at the applied confining pressure were sandwiched between the coarse particles and hence participated in the stress transfer directly. It is understood that, depending on the sample preparation method, soil gradation, fine content, particle shape and stress path, the fine particles may sit loose in the voids between coarse particles (Filler) (Case-i), provide lateral support for the coarse particles building the primary soil structure (Semi-active) (Case-ii), or be involved directly in the soil stress matrix and experience an effective stress similar to what is carried by the coarse particles (Active) (Case-iii). The inability of the applied seepage in eroding residual fine particles is believed to be due to participation of fine particles in the force chains (Case-iii).

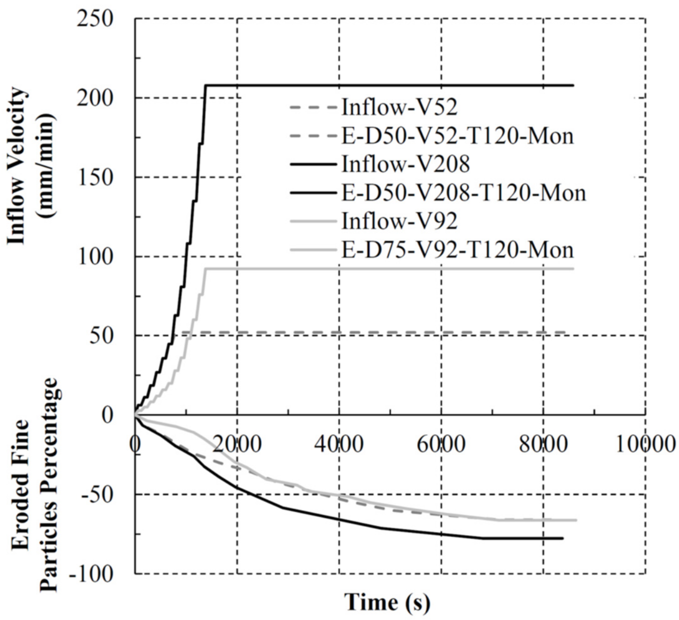

Figure 7-14. Variation of inflow velocity and percentage of eroded fine particles with erosion time

Vertical strains during the erosion stage (measured by photogrammetry technique) vs. time are shown in Figure 7-15. The initial leap and step-wise changes mentioned previously were observed again as erosion of the semi-active fine particles created a temporarily unstable zone. This local instability was re-established by rearrangement of the surrounding particles leading to a jump in the global vertical deformation. This process continued to the end of the erosion. In fact, erosion of the semi-active fine particles began shortly after the erosion of the free fines, where it is believed the local hydraulic gradient temporarily increased due to clogging in the zones where the hydraulic conductivity dropped. Surprisingly, although the vertical strains were different during erosion, the final values for specimens E-D50-V52-T120-Mon and E-D50-V208-T120-Mon were similar. Different vertical deformation patterns observed during the erosion process might have been due to inherent non-uniformity of internal erosion, leading to various preferential seepage paths with different temporary results. This confirmed the current hypothesis that the eroded particles were attributed to Case-i and ii. Although erosion of these particles changed the soil behaviour and caused local instabilities and deformations, the global stability of the soil specimen was not affected, as the primary soil skeleton remained intact.

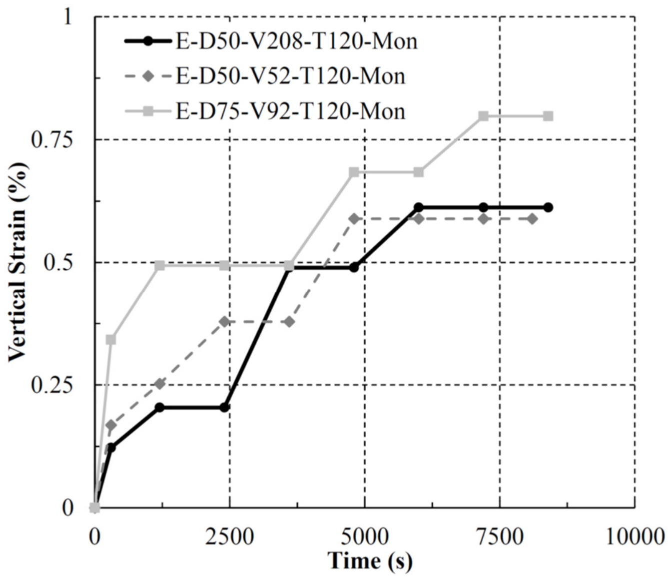

Figure 7-15. Vertical strains during erosion phase measured by photogrammetry

The post-erosion responses of the eroded specimens during undrained shearing are shown in Figure 7-16. The residual fine content was recorded as 10.2, 6.9 and 10.1 per cent for specimens E-D50-V52-T120-Mon, E-D50-V208-T120-Mon and E-D75-V92-T120-Mon, respectively. Regardless of the sample dimension and seepage velocity, these three eroded specimens showed similar undrained behaviour in terms of shear strength and induced excess pore pressure. The residual fine content dropped to 6.9 per cent for specimen E-D50-V208-T120-Mon after experiencing a much stronger seepage. However, the change in soil response was negligible. In other words, erosion of the remaining fine particles (an extra 3.3 per cent) had close to zero impact on the post-erosion mechanical behaviour. It is believed that these particles were initially free to move (Case-i), but then clogged and were not washed out of the specimen under the slower seepage (E-D50-V52-T120-Mon). For the 75 mm diameter specimen (E-D75-92-T120-Mon), the final fine content was similar to specimen E-D50-V52-T120-Mon. Test results indicate that regardless of the seepage properties or the sample dimension, this is erosion of semi-active or active fine particles that changes the soil behaviour. Sometimes, fine particles are eroded but are not washed out of the specimen body. They were clogged inside the specimen. Therefore, they cannot be collected by the collection tank and cannot be subtracted from the initial fine content. This makes the evaluation of the residual fine content complex as these eroded but clogged fine particles may not contribute to the soil structure similar to the original fine particles. This could be the limitation of this research which affects the interpretation of the result.

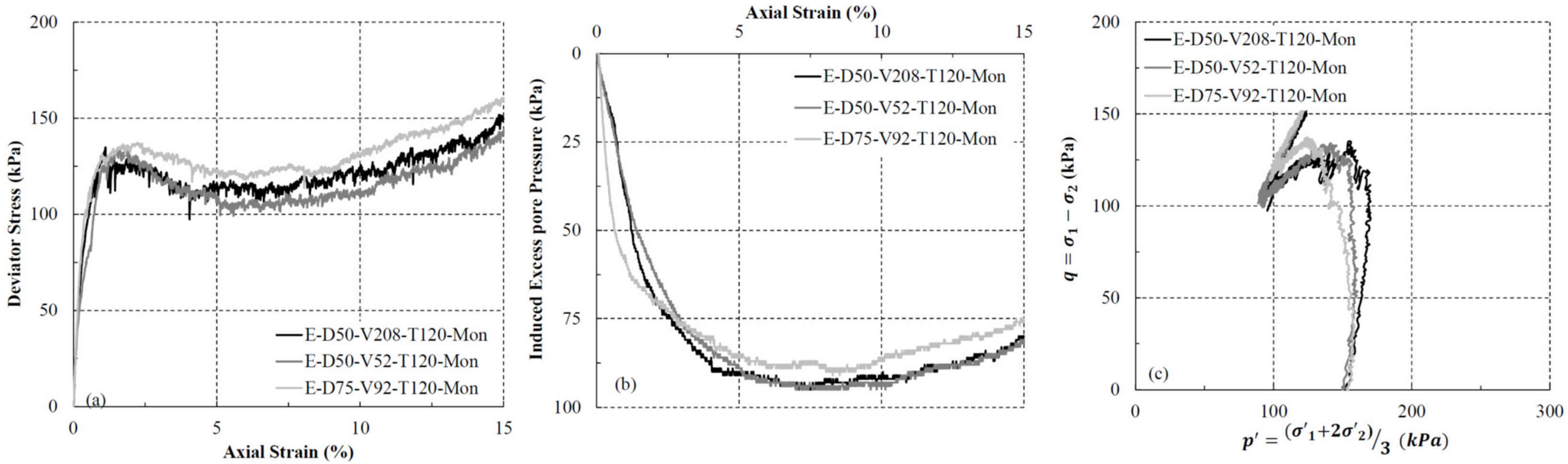

Figure 7-16. Variation of post-erosion behaviour for soil specimens with 50 and 75 mm diameters under different inflow velocities (a) Stress-strain relationship, (b) Induced EPWP during shearing and (c) Stress path

Variation of the intergranular void ratio (e_g) with the residual fine content for all tested specimens is shown in Figure 7-17.

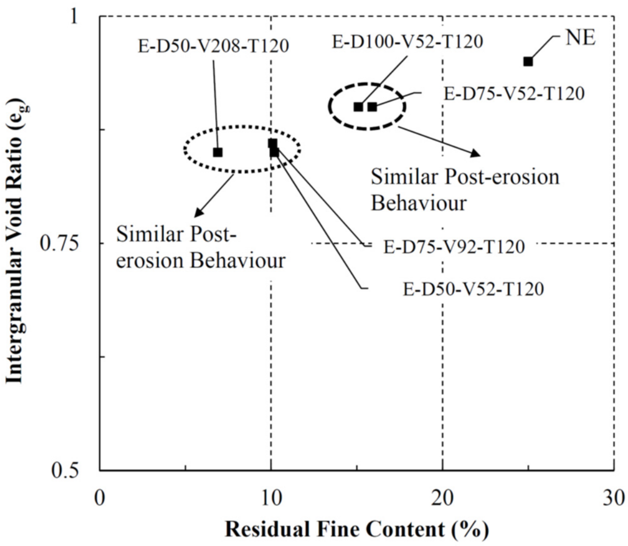

Figure 7-17. Variation in intergranular void ratio with residual fine content

Comparing the results presented in Figures 7-11 and 7-16 shows that specimens E-D75-V52-T120-Mon and E-D100-V52-T120-Mon on the one hand with specimens E-D50-V52-T120-Mon, E-D50-V208-T120-Mon and E-D75-V92-T120-Mon on the other hand had more or less similar post-erosion behaviour although the residual fine contents and the global void ratios varied. Interestingly, the intergranular void ratio was 0.9 for specimens E-D75-V52-T120-Mon and E-D100-V52-T120-Mon and 0.85 to 0.86 for specimens E-D50-V52-T120-Mon, E-D50-V208-T120-Mon and E-D75-V92-T120-Mon, as shown in Figure 7-17. Thus, regardless of sample dimension, residual fine content, seepage properties and final global void ratio, specimens with similar intergranular void ratios showed similar behaviour again. The only exception was specimen E-D100-V52-T120. Although the intergranular void ratio was calculated to be 0.9 for this specimen after erosion, dilation tendency was more dominant with respect to other specimens for vertical strains larger than 5 per cent. All specimens were prepared at the same relative density using moist-tamping technique and were consolidated to the same consolidation confining pressure. Therefore, it is less plausible that the different initial states could be the reason for different post-erosion behaviours of specimens E-D75-V52-T120 and E-D100-V52-T120 with the similar residual fine contents. Specimens E-D75-V52-T120 and E-D100-V52-T120 showed the same responses up to 5 per cent vertical strain. The difference developed in medium and large strains, which can be explained by non-uniformity of soil particle distribution along the height of the specimen after suffusion. From research conducted by Ke and Takahashi (2014b), the initial 15 per cent of fine content in a soil specimen was found to decrease to 10 per cent after internal erosion. However, the global void ratio increased, while the intergranular void ratio remained approximately unchanged, and similar drained responses were observed pre- and post-erosion. It appears that the intergranular void ratio controls the soil response pre- and post-erosion. However, more investigation needs to be conducted to validate this finding.

Test results showed that the erosion of fine particles increased the initial undrained peak shear strength, regardless of the erosion percentage (Figure 7-11). However, this temporary improvement later deteriorated when the residual fine content dropped below a critical value. It was shown that for the tested specimens in this study, b was equal to 0.34, indicating that nearly 34 per cent of the fine particles participated in the soil structure (Eqs. 2.13 and 2.14). Specimens E-D50-V52-T120-Mon, E-D50-V208-T120-Mon and E-D75-V92-T120-Mon lost 66, 77.7 and 66.3 per cent of their initial fine content after erosion, respectively. In other words, internal erosion initially washed the free fines (Case-i). As erosion progressed, those fine particles that provided secondary support (Case-ii) started to migrate when the hydraulic gradient temporarily increased, due to the lower hydraulic conductivity (caused by clogging), to keep the seepage velocity constant. Removal of these particles (free and semi-active fines) increased the undrained shear strength, perhaps due to a better interlock between the coarse particles created by formation of the meta-stable structure. By erosion of the semi-active fine particles, local metastable structures were formed with the fragile force chains. These weakened force chains were more likely to be broken down more easily during shearing.

There are also fine particles (Case-iii) that shared the effective stresses equally with the coarse particles. These fine particles were not affected by internal erosion, since the applied inflow was not strong enough to move them. Removal of these fines would destroy the soil stress matrix and lead to a global collapse of the soil structure. The required seepage flow to cause this is known as the failure seepage flow (Chang and Zhang, 2011). Figure 7-18 schematically displays erosion progress and particle rearrangement. Figure 7-18 (a) shows the initial condition of the fine and coarse particles. Free fine particles were washed immediately due to seepage flow (Figure 7-18 (b)); semi-active fines started to migrate where local higher hydraulic gradients were raised due to clogging and released new free fine particles (Figure 7-18 (c)). Metastable force chains were formed after erosion of the semi-active fine particles, which led to local coarse particle rearrangements and vertical deformations (Figure 7-18 (d)).

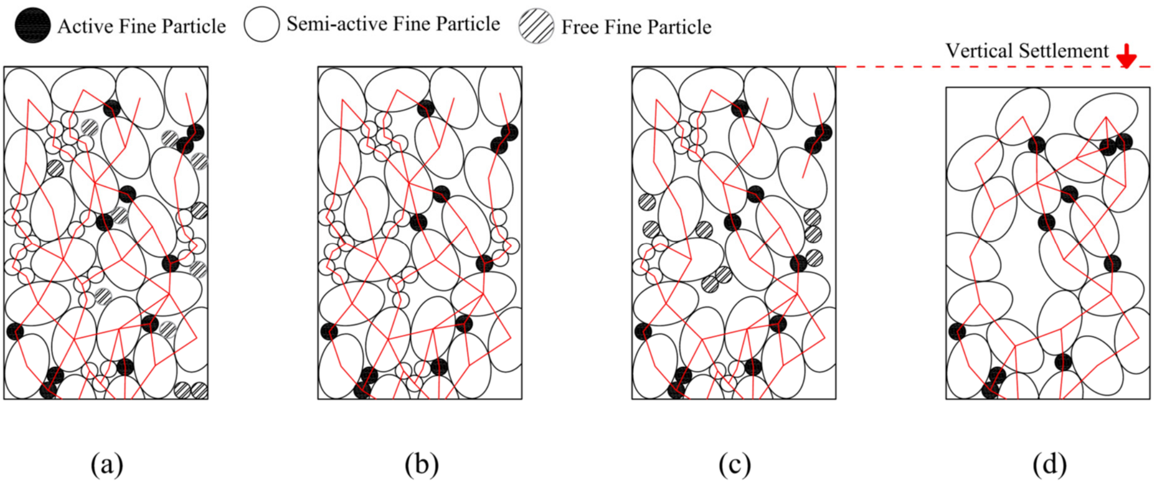

Figure 7-18. Progress of internal erosion (a) Initial condition, (b) Erosion of the free fines, (c) Erosion of the semi-active fines and providing new free fines and (d) Particles rearrangement and vertical deformation with residual active fines

7.3. Influence of Internal Erosion on Hydraulic Conductivity

The influence of erosion of fine particles on hydraulic conductivity has been controversial in the literature. Some researchers, such as Chang and Zhang (2011), Ke and Takahashi (2012 and 2014) and Sibille et al. (2015), believe that as erosion progresses, dislodgement of fine particles increases the pore sizes, leading to an increase in hydraulic conductivity. Others, such as Reddi et al. (2000), Bendahmane et al. (2008), Marot et al. (2009), Marot et al. (2012), Nguyen et al. (2012), Xiao and Shwiyhat (2012), Seghir et al. (2014) and Marot et al (2016), reported a decrease in hydraulic conductivity due to particle re-deposition and the clogging process inside specimens. Xiao and Shwiyhat (2012) stated that although detachment and erosion of fine particles increased the diameter of pore throats, clogging of constrictions between soil solids by eroded particles across a thin and limiting layer at the bottom of the specimen reduced the overall hydraulic conductivity of the entire specimen.

Variation of the overall hydraulic conductivity across the height of the specimens and post-erosion global void ratio (e_f), with erosion progress for each test, is shown in Figure 7-19. Overall, the initial hydraulic conductivity of 1 to 2 × 10^{-3} (m/s) decreased rapidly with suffusion progress for the first 30 minutes, and then increased at a very low rate (stayed approximately constant), regardless of the dimensions of the specimen or seepage velocity. This noticeable drop in the hydraulic conductivity during the first 30 minutes of erosion means a sharp increase in the hydraulic gradient or in other words, in the hydraulic load which can explain initial considerable vertical deformations that all specimens experienced. Interestingly, variation of hydraulic conductivity for specimens E-D75-V52-T30-Mon and E-D75-V92-T30-Mon followed the same trends of specimens E-D75-V52-T120-Mon and E-D75-V92-T120-Mon, respectively, which had the same specimen size and seepage velocity, but experienced a longer erosion. Moreover, test results showed that the global void ratio is not an accurate index to assess the overall hydraulic conductivity of eroded specimens. For instance, hydraulic conductivity of specimen E-D100-V52-T120-Mon was measured to be much higher than specimen E-D75-V52-T120-Mon with the same global void ratio or specimens E-D75-V92-T120-Mon and E-D50-V52-T120-Mon with higher global void ratios. Although it is believed that chance of clogging reduces with a decrease in the seepage path, formation of a preferential seepage path in the specimens with bigger dimensions may affect the overall hydraulic conductivity and surpass the negative impact of clogging. This finding confirmed the effect of clogging on the overall hydraulic conductivity. In addition to the clogging process, local collapse of the soil structure due to loss of semi-active fine particles that provided lateral support (secondary support) for the force chains changed the soil structure at some points and reduced the local hydraulic conductivity. In fact, increase in the pore sizes due to dislodgment of fine particles and development of preferential erosion paths on the one hand and clogging process and local collapse of the soil structure on the other hand control the overall hydraulic conductivity. Therefore, depending on the seepage properties, size of the affected zone and erosion progress, overall hydraulic conductivity may increase, decrease or stay constant during suffusion. In other words, this is the quality of the pores connectivity and not just the pore sizes that affects the hydraulic conductivity. It is possible to back-calculate the overall hydraulic gradient based on the applied seepage velocity and measured hydraulic conductivity. However, due to formation of clogging or preferential seepage paths along the height of the specimens that affect the overall hydraulic conductivity, the overall hydraulic gradient cannot to be used for assessment of hydraulic loads.

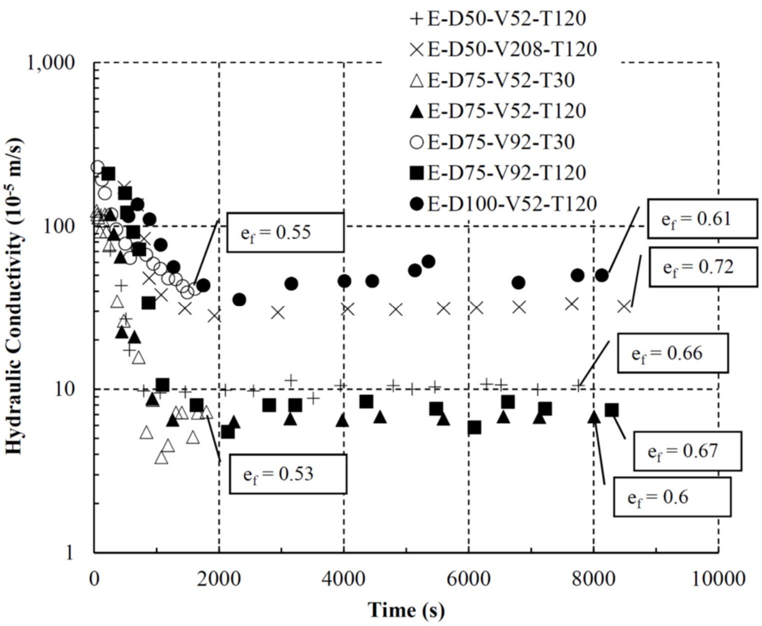

Figure 7-19. Variation of hydraulic conductivity with erosion progress for tested specimens

7.4. Conclusion

The impact of seepage velocity, erosion duration and specimen dimensions on progress of internal erosion and post-erosion mechanical behaviour were studied using a newly developed erosion-triaxial apparatus. Undrained triaxial compression tests were conducted on internally unstable soil specimens with different dimensions. Soil specimens were subjected to downward seepage flows with two different inflow velocities for 30 and 120 minutes. These inflow velocities were 92 mm/min and 52 mm/min. For specimens with 75 mm diameter, erosion of the fine particles was found to be independent of seepage velocity during the initial stage of internal erosion. This was attributed to the erosion of the free particles available in the soil specimens. However, after 120 minutes of erosion, the residual fine content was 36 per cent less in the specimen eroded at the higher inflow velocity. Furthermore, hardening behaviour of the non-eroded specimen changed to the flow type with limited deformation after internal erosion. Maximum induced excess pore pressure decreased and dilation tendency was postponed. However, the initial undrained peak shear strength showed a significant increase. This improvement disappeared once the residual fine content passed a critical turning point. The initial increase in peak shear strength could have been due to a better interlocking of the angular coarse particles due to absence of the fine particles. However, an increase in the potential of the slip-down movement due to an increase in the global void ratio, and the lubricating effect of the local concentration of the fine particles after internal erosion, decreased the dilation tendency. This might explain the observed contractive behaviour at medium strains.

A step pattern was observed in the local vertical strains during internal erosion of the tested specimens. These discrete steps could be due to local particle rearrangement that continued throughout the erosion, even under constant inflow. This particle rearrangement occurred when the semi-active fines that provided the lateral support for the soil stress matrix were eroded.

A turning point was observed in the post-erosion behaviour that was dependent on the percentage of the eroded particles. The temporarily increase in peak shear strength and the drop in the flow potential caused by initial internal erosion quickly deteriorated after a threshold value of residual fine content was eroded. This threshold was found to be where the semi-active fine particles lost their intergrain contacts and a metastable soil structure developed. This turning point in the fine content can be estimated using equations provided by Rahman and Lo (2008) and Rahman et al., (2008).

Analysis of shear strength results, rate of erosion and local vertical strains suggest that the intergranular void ratio proposed by Mitchell (1993) is a more suitable index in evaluating the post-erosion mechanical behaviour of internally unstable soils. Eroded specimens with different global void ratios, residual fine contents or dimensions, but a similar intergranular void ratio, showed similar mechanical behaviour, indicating the suitability of this index in predicting post-erosion behaviour.

Similar residual fine content and post-erosion undrained behaviour were observed for the 75 and 100 mm diameter (up to five per cent vertical strain). However, undrained shear strength increased more rapidly over the medium and large strain range for the larger 100 mm diameter specimen. On the contrary, the eroded 50 mm diameter specimen lost nearly 20 per cent more fines and presented a different undrained behaviour.

Regardless of the sample dimension, the initial undrained shear strength increased after internal erosion for all specimens tested. The original strain hardening behaviour changed to the flow type with limited deformation, with a decline in residual fine content. The maximum induced excess pore pressure dropped after two hours of erosion and dilation tendency was postponed.

Chapter 8 Influence of Internal Erosion on Cyclic Resistance and Post-Cyclic Behaviour

In principle, the impact of fine particle removal on the cyclic resistance of granular soils depends on the role these fine particles play in the soil structure. Depending on the soil gradation, particle shape, ratio of fine particles to pore sizes, stress path, confining pressure and fine content, removal of the fine particles may change the soil stress matrix and change the soil response accordingly during monotonic and cyclic loadings. This is because the loss of fine particles with different roles will lead to different consequences, such as particle rearrangement, local fine concentration, heterogeneity and differential settlement, variation of global and intergranular void ratios, and in an extreme case, global failure. This indicates that the artificial removal of fine particles or the alteration of fine content during sample preparation (the main adopted methodologies in all previous studies) cannot necessarily mimic a real, natural condition, such as internal erosion. However, past experimental studies investigating the influence of cohesionless fine content on liquefaction potential or cyclic resistance of granular soils shed light on the mechanical behaviour of soils after suffusion.

Overall, it is generally accepted that the presence of non-plastic silt size particles reduces the cyclic resistance and increases the risk of liquefaction. Surprisingly, liquefaction analysis based on field testing correlations (e.g. Tatsuoka et al., 1980; Tokimatsu and Yoshimi, 1983; Seed et al., 1983; Robertson and Campanella, 1985) indicated that silty sands were more resistant to liquefaction. Lade and Yamamuro (1997) believed that this was due to the effect of stress history, including over-consolidation, aging and cementation, which were normally overlooked in laboratory tests. However, these contradictory results, along with Maurer’s et al. (2015) conclusion that emphasises the limitation of a Liquefaction Potential Index (LPI) framework, shows that prediction of post-erosion behaviour of granular soils is still a challenge.

To address the current ambiguity of the influence of fine removal caused by internal erosion on the liquefaction potential of a gap-graded cohesionless soil, a series of erosion-triaxial tests, followed by cyclic loading and post-cyclic shearing, was conducted on the soil mixture presented in Chapter 4. This helped to simulate a real hydraulic condition, and provides conditions close to the natural erosion of fine particles, thus allowing the study of the effect of fine particle removal and relocation on cyclic behaviour.

8.1. Testing Program

Triaxial soil specimens with 75 mm in diameter and 150 mm in height were prepared, saturated and consolidated to 150 kPa, according to the procedure presented in Chapter 3. Four different seepage conditions were applied at the top of the soil specimens after consolidation according to the test program presented in Table 8-1. After erosion was completed, undrained cyclic and monotonic shearing was performed, and results were compared with the undrained behaviour of a non-eroded specimen. A low cyclic loading frequency and a slow post-cyclic undrained shearing rate were chosen to provide sufficient time for pore pressure equalisation.

Table 8-1. Experimental testing program

Test Phase	Consolidation	Erosion		Cyclic Loading			Monotonic Shearing
Specimen	Consolidation Pressure (kPa)	Inflow velocity (mm/min)	Erosion Duration (min)	CSR[a]	f[b] (Hz)	Duration (s)	Rate (%/min)
E-D75-V52-T30-Cyc	150	52	30	0.167	0.0083	3600	0.26
E-D75-V52-T120-Cyc			120				
E-D75-V92-T30-Cyc		92	30				
E-D75c-V92-T120-Cyc			120				
NE-D75-Cyc		-				~780[c]	

[a]: Cyclic Stress Ratio
[b]: Loading frequency
[c]: The non-eroded specimen was liquefied after 5 cycles of loading

8.2. Tests Results

Variation of fine content, along with the global and intergranular void ratios at the end of the erosion phase, are shown in Table 8-2. The global void ratio increased due to erosion of the fine particles as expected. However, the intergranular void ratio decreased as the erosion progressed. This is plausible considering the vertical strains that occurred during the erosion phase. In fact, removal of fine particles that provide lateral support for force chains triggered local instability and vertical distortions. This particle rearrangement reduced the available voids between host coarse particles and, consequently, the intergranular void ratio. The same trend was observed in Chapter 7.

Table 8-2. Pre and post-erosion void ratio and fine content

<table>
<tr><th>Specimen</th><th>FC_i (%)</th><th>FC_f (%)</th><th>e_i</th><th>e_f</th><th>e_{gi}</th><th>e_{gf}</th></tr>
<tr><td>E-D75-V52-T30-Cyc</td><td rowspan="5">25</td><td>20</td><td rowspan="5">0.46</td><td>0.51</td><td rowspan="5">0.947</td><td>0.887</td></tr>
<tr><td>E-D75-V52-T120-Cyc</td><td>15.4</td><td>0.6</td><td>0.891</td></tr>
<tr><td>E-D75-V92-T30-Cyc</td><td>18.2</td><td>0.55</td><td>0.895</td></tr>
<tr><td>E-D75-V92-T120-Cyc</td><td>10.4</td><td>0.65</td><td>0.842</td></tr>
<tr><td>NE-D75-Cyc</td><td>-</td><td>-</td><td>-</td></tr>
</table>

Development of vertical strains and maximum excess pore water pressure during each cycle of loading for the non-eroded and eroded specimens are shown in Figure 8-1. Although the relative density and consolidation pressure of the soil specimens were 60 per cent and 150 kPa, respectively, the non-eroded specimen liquefied after only 5 cycles of loading. The effective stress dropped to zero, accompanied by a dramatic rise of vertical strain in both compression and extension paths. Although the specimen was classified as a relatively dense sample and was subjected to a high consolidation pressure, the specimen was liquefied very quickly. This shows that the relative density is not an appropriate index to evaluation liquefaction potential of soil materials. This is consistent with Lade and Yamamuro's (1997) finding that neither relative density nor void ratio can predict cyclic behaviour of sandy soils with a certain amount of fine particles. On the contrary, all eroded specimens developed excess pore pressure slowly with a decreasing trend. The vertical strains in the extension path were almost zero for all eroded specimens and only developed approximately 0.125 per cent compressive axial strain after 30 cycles of loading. Although the eroded specimens showed much greater cyclic resistance than the non-eroded specimen, cyclic loading continued for one hour for further investigation. It seems that suffusion made the tested soil specimens non-liquefiable, regardless of the final fine content or post-erosion global void ratio. Similar improvements in cyclic resistance after erosion have also been reported by Ke and Takahashi (2014a).

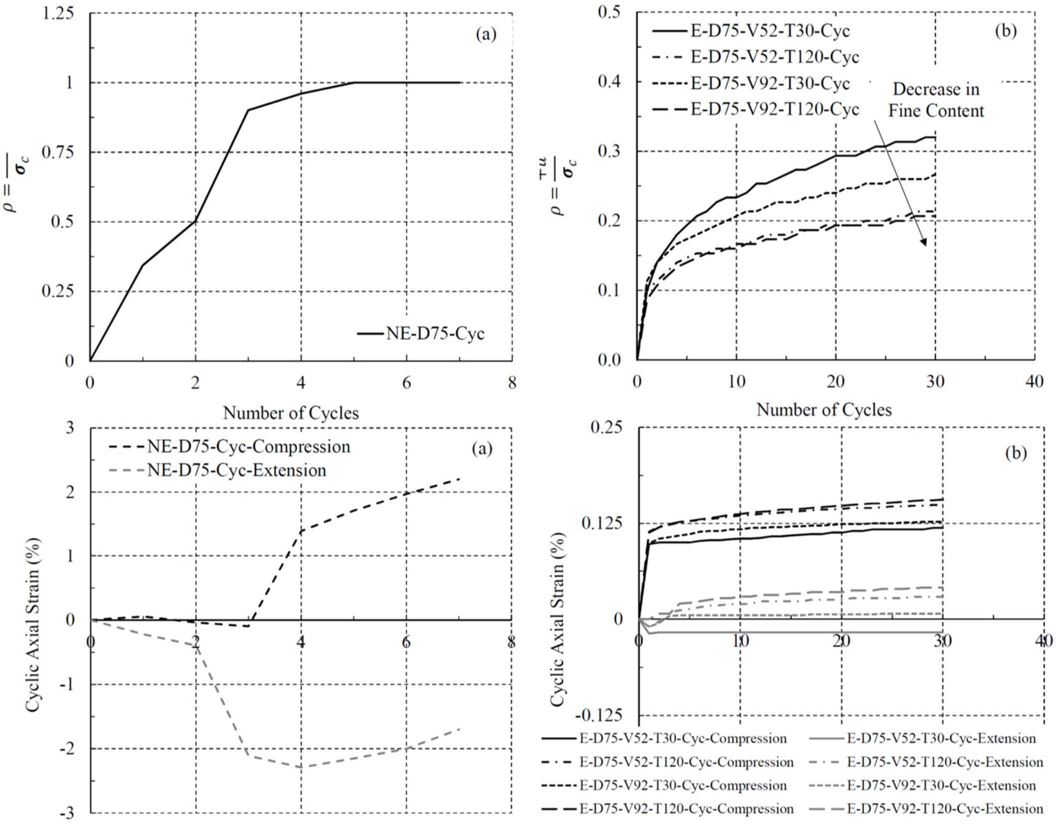

Figure 8-1. Maximum induced excess pore pressure and axial strains during each cycle of loading

To investigate the effect of cyclic loading on the undrained shear strength after suffusion, test results were compared to the response of eroded specimens that experienced only monotonic shearing (specimens E-D75-V52-T30-Mon, E-D75-V52-

T120-Mon, E-D75-V92-T30-Mon and E-D75-V92-T120-Mon). Stress-strain relationship, induced excess pore pressure (EPWP) and stress path results are shown in Figures 8-2 and 8-3. It can be seen that initial undrained peak shear strength, shear strength in medium and large strains, and development of excess pore pressure were similar for specimens E-D75-V52-T30-Mon, E-D75-V52-T120-Mon and E-D75-V92-T30-Mon that experienced only monotonic shearing. However, post-cyclic undrained behaviour of eroded specimens showed non-uniformity to some extent. For instance, temporary collapse in medium strains was significant, and an increase of shear strength at large strains was slower for specimen E-D75-V52-T120-Cyc compared to the other two specimens. Softening behaviour or temporary collapse (flow deformation) was more dominant for the eroded specimens that experienced cyclic loading, especially for specimens E-D75-V52-T120-Cyc and E-D75-V92-T120-Cyc. Greater excess pore water pressure was developed during post cyclic shearing, which in turn decreased the undrained shear strength. This softening behaviour was more prominent for specimens E-D75-V52-T120-Cyc and E-D75-V92-T120-Cyc that lost more fine particles during erosion.

Overall, the results in Figures 8-1 to 8-3 indicate that suffusion made the soil specimens more resistant to cyclic loading, regardless of erosion percentage. However, the potential of static liquefaction or flow deformation increased due to erosion progression and loss of fine particles.

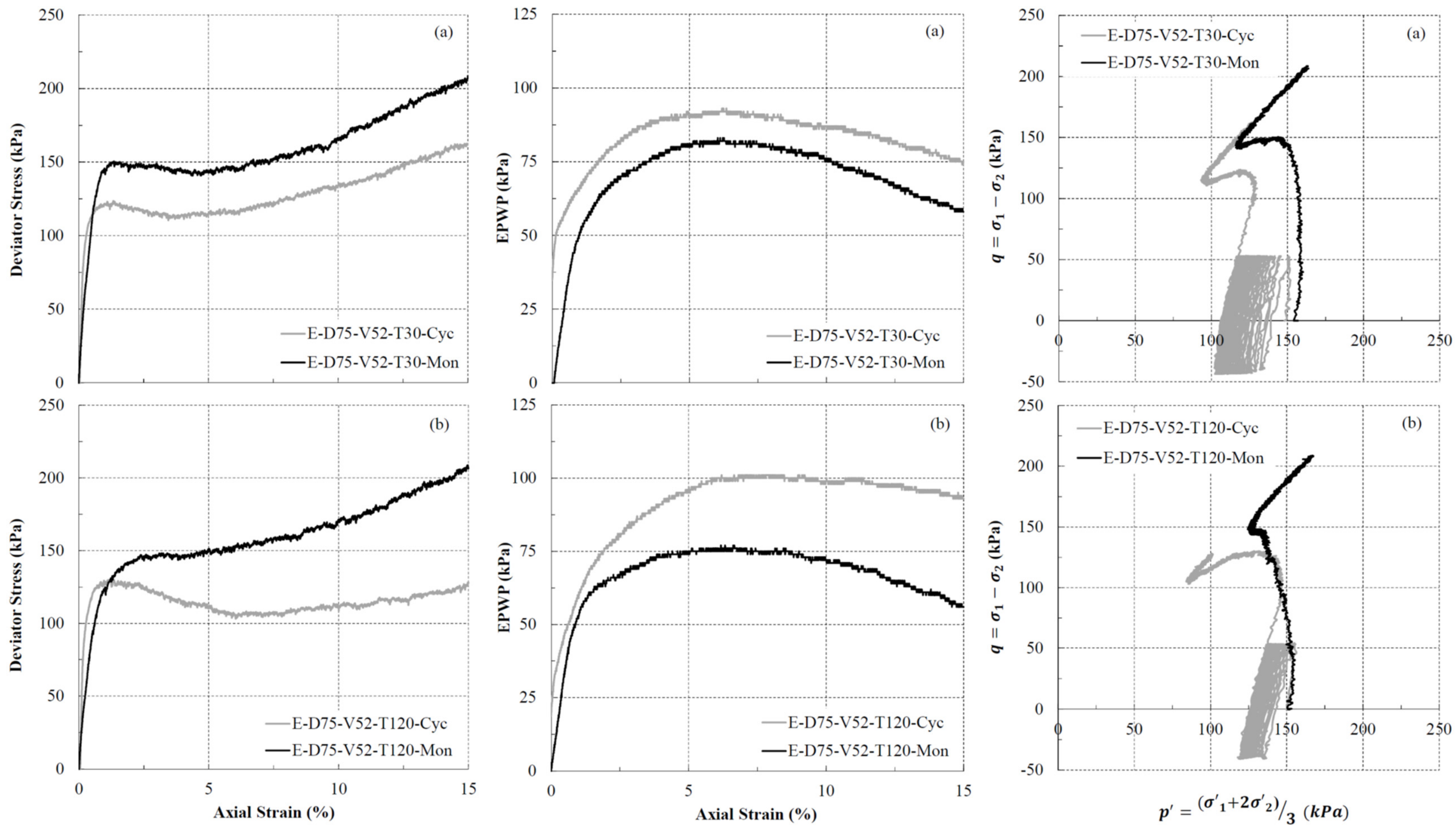

Figure 8-2. Stress-strain relationship, induced EPWP and stress path of eroded specimens pre- and post-cyclic loading (a) E-D75-V52-T30Cyc and (b) E-D75-V52-T120-Cyc

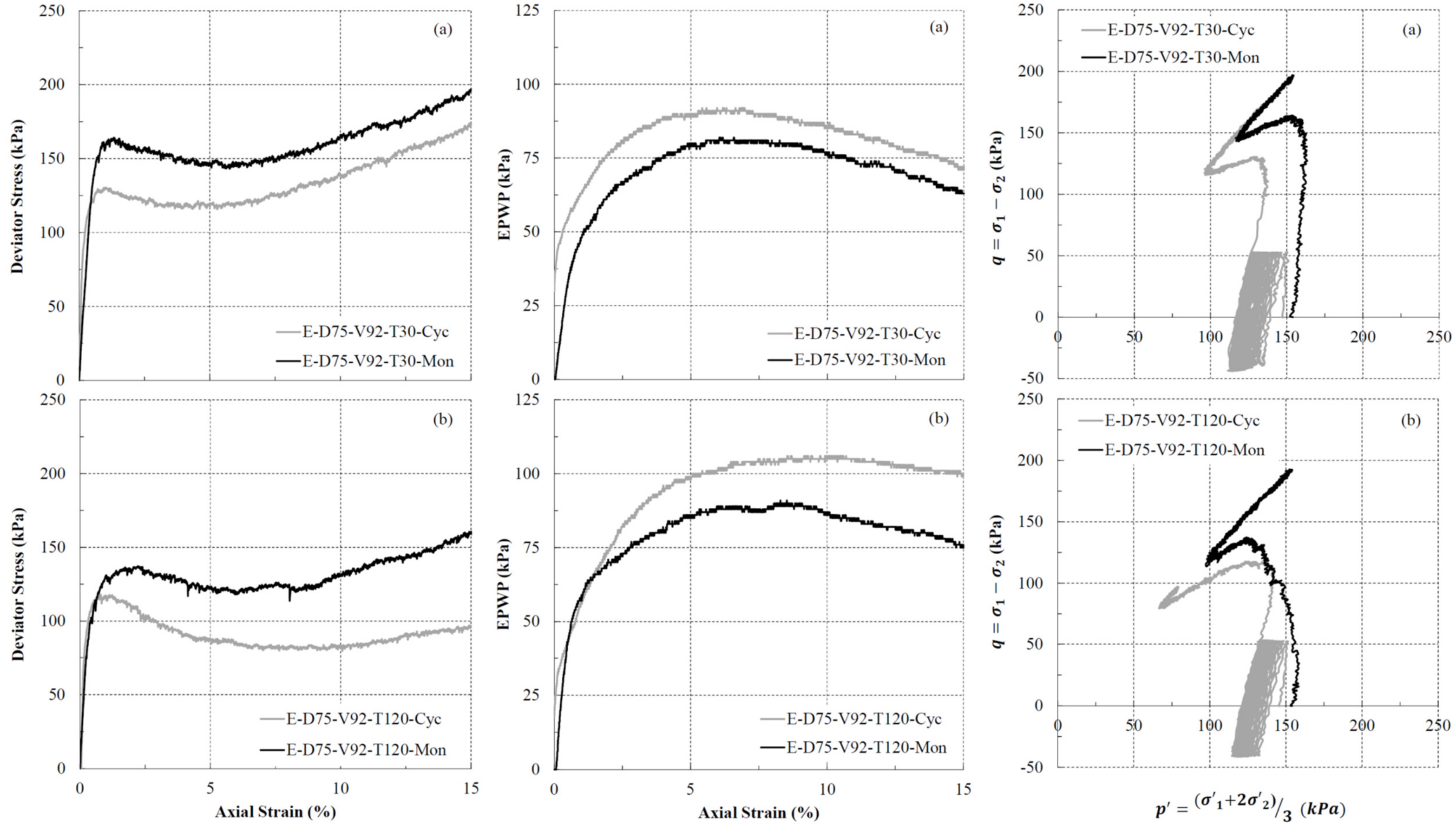

Figure 8-3. Stress-strain relationship, induced EPWP and stress path of eroded specimens pre- and post-cyclic loading (a) E-D75-V92-T30-Cyc and (b) E-D75-V92-T120-Cyc

8.3. Critical Investigation and Discussion

To develop a better understanding of post-erosion cyclic behaviour of the tested material, a new soil specimen was prepared using only the coarse fraction (NE-D75-CF-Cyc, FC_i=0) of the original tested soil. The specimen was mixed with three per cent water content and compacted layer by layer to achieve a high global void ratio of 0.73 after consolidation. This specimen was subjected to the same cyclic loading phase experienced by the eroded specimens. Figure 8-4 shows the build-up of EPWP at the end of the cyclic loading phase for each test. Surprisingly, the eroded specimens tended to behave similarly to the soil specimen with no initial fine content (NE-D75-CF-Cyc) during cyclic loading, even at 20 per cent final fine content for specimen E-D75-V52-T30-Cyc. For this specimen, seepage flow only washed out five per cent of fine particles, but the consequent drop in induced EPWP was significant. In addition, apart from the non-eroded specimen and the specimen made only by coarse particles, development of EPWP had a decreasing trend with erosion progress. No obvious alteration in EPWP was observed between specimens E-D75-V52-T120-Cyc and E-D75-V92-T120-Cyc, while a considerable drop in final fine content (15 to 10.4 per cent) occurred. It was shown in Chapter 7 that specimens E-D75-V52-T30-Mon, E-D75-V52-T120-Mon and E-D75-V92-T30-Mon showed similar post-erosion behaviours. However, during post-cyclic shearing, specimen E-D75-V92-T30-Cyc behaved similarly to specimen E-D75-V52-T30-Cyc and specimen E-D75-V92-T120-Cyc behaved like specimen E-D75-V52-T120-Cyc.

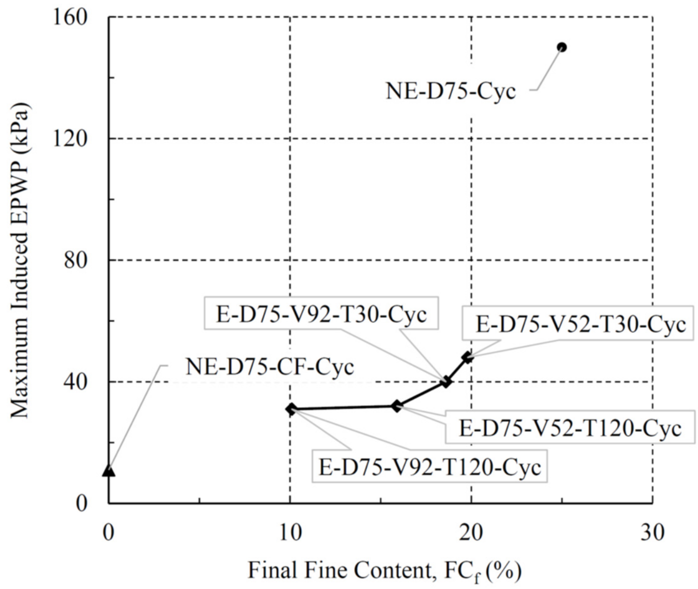

Figure 8-4. Development of excess pore water pressure during cyclic loading

Erosion of fine particles increased the global void ratio, although this increase was not uniform along the soil specimen or erosion path. However, the erosion does not necessarily shift the soil to a looser state. Figure 8-4 confirms that the effect of suffusion on soil behaviour is complicated and cannot be explained only by changing the initial fine content and artificial removal of fine particles. Coarse particle rearrangement (on a micro scale) occurred due to erosion of semi-active fine particles that provided secondary support to the soil structure. This rearrangement formed local new stress matrices that affected the soil response to cyclic loading and post-cyclic shearing.

Post-cyclic behaviour of specimen E-D75-V92-T120-Cyc, the specimen with the lowest fine content and highest global void ratio (FC_i=25, FC_f=10.1 per cent), was compared directly with specimen NE-D75-CF-Cyc (FC_i=FC_f=0 per cent). This comparison is presented in Figures 8-5 and 8-6. The global void ratio was 0.64 for specimen E-V92-T120 after erosion and 0.73 for specimen NE-D75-CF-Cyc after consolidation. Apart from both specimens displaying non-liquefiable behaviour, they showed very different post-cyclic undrained behaviour patterns. Strain hardening behaviour (dilation) with a significant undrained shear strength was observed for specimen NE-D75-CF-Cyc, while strain softening behaviour (contraction) with limited flow deformation was dominant for specimen E-D75-V92-T120-Cyc. It was evident that the presence of even a small amount of fine particles changed the soil shearing response considerably. Particle shape analysis was conducted, and it was found that angularity of the coarse particles between 1.7 and 2.36 mm in diameters was much higher than for the other particles. This meant that erosion of the fine particles provided a better interlock between these coarse particles, which led to a higher shear strength. On the contrary, the concentration of more rounded fine particles between coarse particles reduced this interlocking. The lubricating effect of fine particles has been reported previously by Thevanayagam and Mohan (2000), Thevanayagam (2007), and Ke and Takahashi (2015). However, this was contradictory to the response of specimen E-D75-V92-T120-Cyc in this study, which showed the lowest initial peak undrained shear strength at the lowest final fine content. Out of all of the eroded specimens, specimen E-D75-V92-T120-Cyc revealed the highest post-erosion global void ratio and experienced the largest vertical strain (approx. twice the other specimens) during the erosion stage. This means that more local metastable force chains were formed due to particle rearrangement. These weak force chains can break easily and quickly during shearing. In fact, the combination of all mentioned influential parameters, such as intergranular void ratio, particle rearrangement and metastable force chains affected the undrained strength of the eroded specimens, and not only fine content. In addition, it is postulated that the fine particles moved into the free voids during shearing, which increased the potential of slip-down movement and contraction compared with the specimen without fines, in which roll-over movement of particles was dominant.

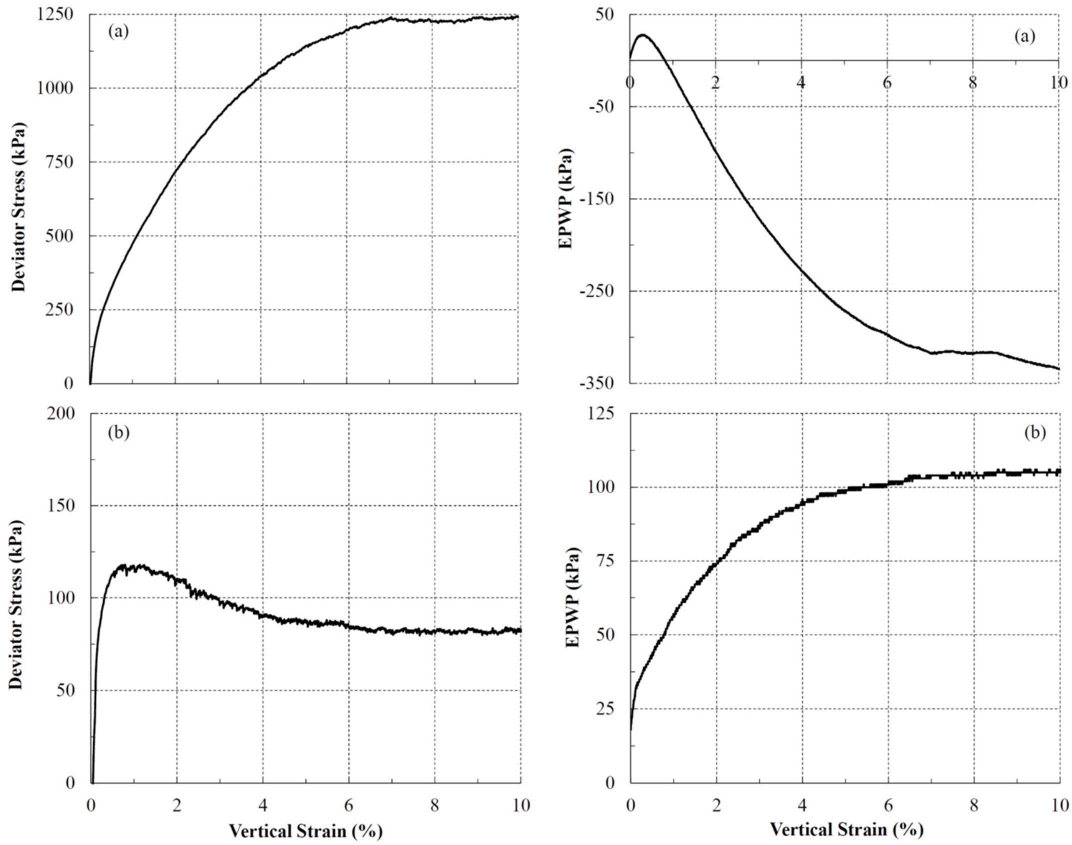

Figure 8-5. Post-cyclic stress-strain relationship and induced EPWP (a) NE-D75-CF-Cyc and (b) E-D75-V92-T120-Cyc

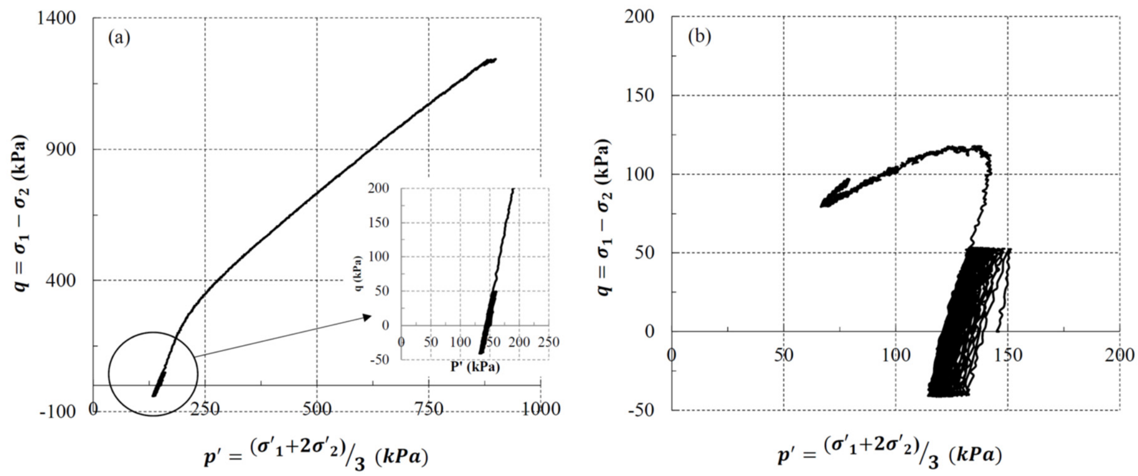

Figure 8-6. Cyclic and post-cyclic stress path (a) NE-D75-CF-Cyc and (b) E-D75-V92-T120-Cyc

Normalised undrained secant stiffness with mean effective confining pressure at small strains (< 1 per cent) pre- and post-cyclic loading was also investigated for the eroded specimens and is presented in Figure 8-7. Here, it can be seen that erosion of the fine particles decreased the undrained secant stiffness for strains less than 0.5 per cent for specimens E-D75-V52-T30-Cyc and E-D75-V92-T30-Cyc, while this drop continued to one per cent vertical strain for specimens E-D75-V52-T120-Cyc and E-D75-V92-T120-Cyc. In other words, small strain shear stiffness decreased with a decrease in final fine content (erosion progress). This was contrary to Ouyang and Takahashi's finding (2015) that showed eroded specimens gained a greater secant stiffness. The reason might have been due to looser condition of the samples that were used in their study. However, the cyclic loading (30 cycles of loading/unloading) improved the small strain undrained secant stiffness significantly, even when compared to the non-eroded specimen with 25 per cent fine content.

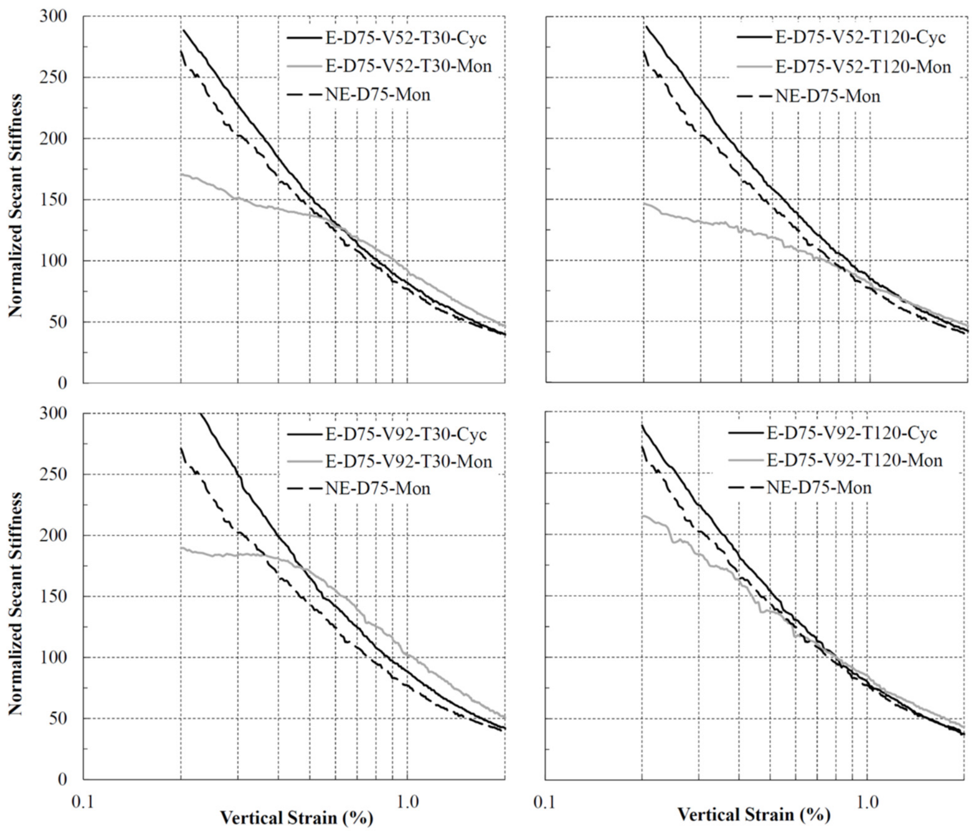

Figure 8-7. Normalized undrained secant stiffness for the eroded specimens pre and post-cyclic loading

8.4. Conclusion

The influence of suffusion on cyclic and post-cyclic behaviour of a gap-graded cohesionless soil was investigated in this section. The effect of silt size particles on liquefaction resistance of granular matter has been studied previously by artificially changing the fine content using arbitrary laboratory experiments or field testing. However, removal of fine particles during a natural phenomenon, such as internal erosion, is much more complex. Formation of internal instability or metastable structure and particle rearrangement cannot be simulated easily. Soil specimens with 25 per cent initial fine content were prepared and subjected to a downward seepage flow with 52 or 92 mm/min velocities and for two different durations (30 and 120 minutes). After erosion, a cyclic loading phase, followed by monotonic shearing, was performed to compare cyclic resistance and the pre- and post-cyclic undrained response. The following conclusions are based on the results of this experimental investigation:

- Erosion of even a small amount of fine particles was shown to increase the cyclic resistance significantly. Furthermore, the eroded specimens were non-liquefiable for the erosion percentage observed in this experiment. In comparison, a non-eroded specimen at 60 percent relative density and subjected to 150 kPa of consolidation pressure liquefied after only 5 cycles of loading. This confirms that neither relative density nor global void ratio are good indicators in predicting the consequences of fine particles removal or suffusion in granular materials.
- It was found that during cyclic loading, the build-up of excess pore water pressure decreased with a descending trend by an increase in erosion of fine particles (erosion progress).
- A comparison of pre- and post-cyclic behaviours of the eroded specimens indicated that the contraction tendency increased after experiencing cyclic loading, which led to a drop in the undrained shear strength for the eroded specimens.

- The initial 25 per cent of fine content dropped to 20, 18.2, 15 and 10.4 per cent after suffusion for the eroded specimens. However, all eroded specimens showed a cyclic behaviour similar to soil specimens prepared only by coarse particles (i.e. without any fine content). Contrary to the similar pattern for cyclic behaviours, the specimen prepared from only coarse particles showed strain hardening behaviour with a much greater undrained shear strength when compared to the eroded specimens, whereas strain softening behaviour was dominant even for the specimen with the lowest final fine content.
- The applied seepage flow washed the inactive fines and semi-active fines. These are the fines that either sat loose in the voids or provided secondary support for the stress matrix. However, active fine particles that were sandwiched between coarse particles were not washed during suffusion. Removal of the active fine particles would have led to global collapse. Erosion of semi-active fine particles formed local metastable force chains. These vulnerable force chains broke easily during shearing and led to a lower shear strength for the eroded specimens that lost more fines.
- The presence of even a small amount of fine particles decreased the shear strength, as these particles acted as a lubricant between coarse particles and reduced the internal friction between coarse particles. In addition, slip-down movement tendency increased during shearing when fine particles moved to the free voids, which increased contractive behaviour.
- Suffusion decreased the small strain undrained secant stiffness. However, post-cyclic shearing showed a noticeable improvement in the secant stiffness for the eroded specimens that experienced 30 cycles of loading.

Chapter 9 Micro Evaluation of Internal Erosion using 3D X-Ray Tomography

To further investigate the impact of suffusion on soil structure and, in particular, to validate the proposed hypothesis in Chapter 6 regarding local coarse particle rearrangement due to erosion of semi-active fine particles, three-dimensional Radiation-based Micro-Computed Tomography (3D-μCT) was employed. The high-resolution 3D X-ray imaging was utilised to capture images from the interior body of the soil specimens pre- and post-erosion.

9.1. Testing Procedure

Two soil specimens 100 mm in height and 50 mm in diameter were prepared inside PVC tubes to avoid any soil disturbance during sample transportation. Sample preparation, consolidation process, and the sample transportation technique to Australian Synchrotron and the University of Melbourne were explained in Chapter 3. Soil specimens were subjected to a downward seepage with a seepage velocity of 208 mm/min for 30 and 120 minutes after consolidation. The seepage velocity was the same as what was applied to the triaxial specimen with 50 mm diameter (E-D50-V208-T120-Mon). An attempt was made to keep soil conditions very similar to triaxial specimens pre- and post-erosion. However, triaxial specimens were consolidated under uniform confining pressure (equal radial and vertical confining pressure), while X-ray specimens were subjected to k0 condition inside PVC tubes. Moreover, these specimens were prepared and subjected to suffusion inside a PVC tube with rigid walls, which differs from the triaxial specimens with flexible walls. Therefore, pore sizes and smoothness at interfaces of soil/membrane and soil/PVC tube were not identical. These two major differences led to various soil conditions after consolidation and responses during the erosion phase. However, it was believed that the test procedure was accurate enough to assess the influence of suffusion on the soil structure and movement of fine particle, which was the objective of 3-D imaging.

9.2. X-ray Image Processing

Three series of X-ray tomography were conducted on two specimens according to Table 9-1. CT scanning (with resolution of 21.1 and 31.1 micron) of each specimen took approximately 5 hours, due to the large dimensions of specimens, which resulted in a large dataset (300 GB per each series with 32 bits colour depth). It was very time-consuming to analyse such a large dataset (3200 to 4800 cross-sections), even with available super computers. Therefore, it was decided to convert images to 8 bits version to reduce the size of each dataset down to less than 100 GB, which was more manageable to work with. This file size reduction resulted in a lower resolution for images, making the image processing challenging. The mineral of all sand particles was quartz, regardless of particle size. This meant that the density of particles was the same, which led to the same particle X-ray absorptions and almost the same X-ray penetration patterns. However, it was still possible to find a threshold between coarse and fine particles. Figure 9-1 shows the resolution difference between two images with 32 and 8 bits at the same cross section of an eroded specimen.

Table 9-1. X-ray tomography testing program

No.	Sample Label	Sample Dimension (mm)	X-ray Imaging Pre-erosion	X-ray Imaging Post-erosion	Imaging Resolution (μmm)
1	X-E-D50-V208-T120	50 × 100	Yes[a]	Yes[a]	31.1
2	X-E-D50-V208-T30	50 × 100	No	Yes[b]	21.1

[a]: X-ray tomography of this specimen was conducted in University of Melbourne
[b]: X-ray tomography of this specimen was conducted in Australian Synchrotron

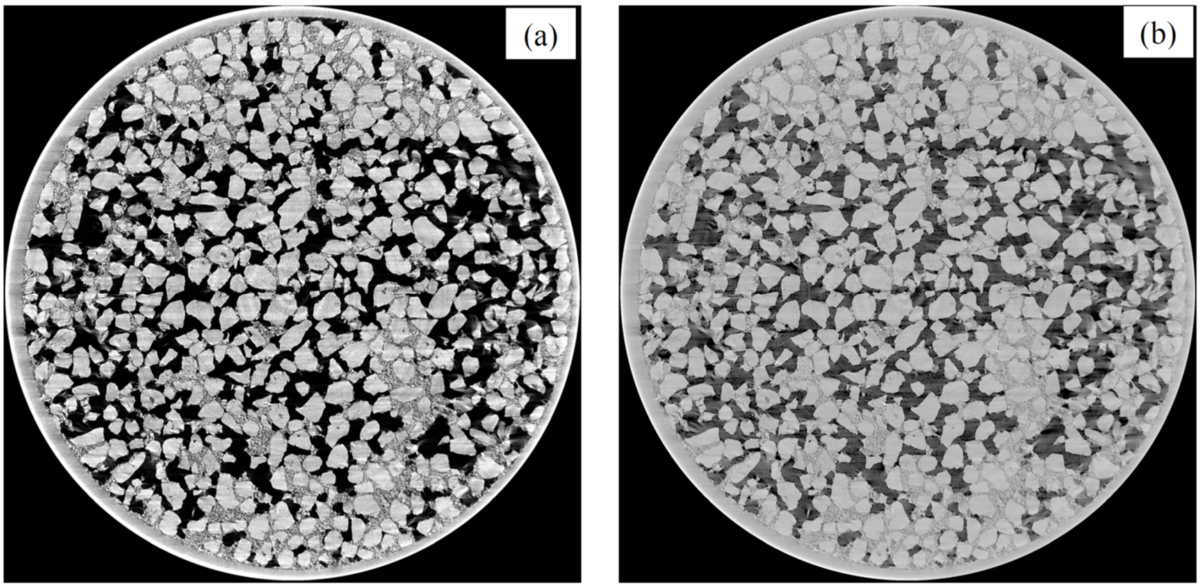

Figure 9-1. Resolution differences between images with (a) 32 bits and (b) 8 bits colour depth at one cross-section

X-ray image processing was conducted using Avizo software package version 9.3. Although all particles had the same mineral, fine and coarse particles reflected different grey colours, even in 8 bits images. Two colour thresholds were chosen between voids and fine particles and between fine and coarse particles. Then, these thresholds were applied to all vertical cross-sections to determine the volume fraction of each component (void, fine and coarse) across the specimen height. To correctly distinguish fine particles from coarse particles in 8 bits images, a calibration process was conducted. This calibration process included post-erosion particle size distribution and weight measurement of fine and coarse fractions after each test (Table 9-2) using sieve analysis. While coarse fraction was constant for each specimen pre- and post-erosion, post-erosion residual fine contents were measured physically and compared with the initial value. Those colour thresholds that resulted in the same pre- and post-erosion fine and coarse volume fractions to the physically measured values in the laboratory were chosen to calculate the profile of variation of the volume of coarse and fine particles and voids along the height of the specimens (Table 9-3). By knowing the volume of each component and dimensions of the specimens, it was also possible to determine variation of fine content and global and intergranular void ratios (Table 9-4). It is evident that all volume fractions were back-calculated very closely to measured values in the laboratory, suggesting the high accuracy of the X-ray imaging and calibration process even for images with 8 bits colour depth (Figure 9-2).

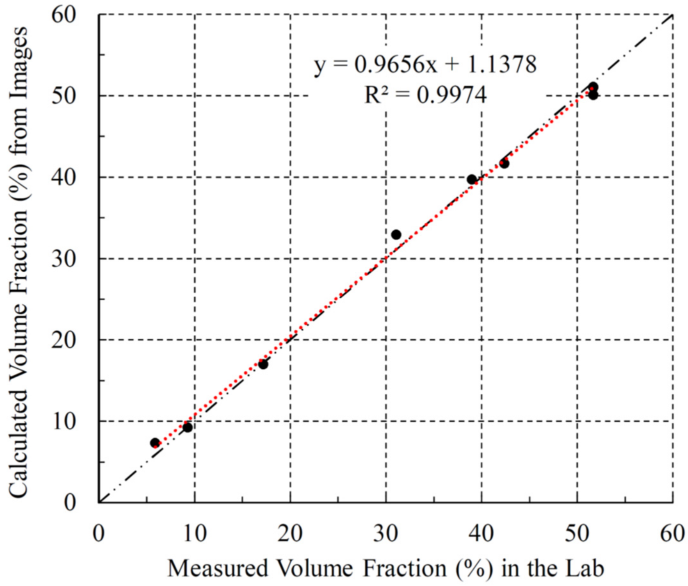

Figure 9-2. Comparison of measured volume fraction in the lab with X-ray image analysis (coarse, fine and pores volume fractions)

Figure 9-3 shows variation of volume fraction of coarse and fine particles and pores, fine content, and global and intergranular void ratios along the height of the soil specimen pre- and post-erosion. The last 10 millimetres of the soil specimens were not considered in the analysis due to the presence of the bottom mesh. The soil specimen was prepared in eight layers using the moist tamping method as described earlier in Chapter 3. Seven jumps in coarse, fine and pores volume fractions can be identified from the X-ray tomography for pre-erosion specimens. These jumps are easiest to recognise in the pores volume fraction graph. A similar trend was earlier reported by Frost and Park (2003), and was associated with the moist tamping method. The loosest region of each soil layer was found to be at the bottom of each layer, as less tamping force is experienced in this region. Despite its advantages, this demonstrates the inability of the moist tamping method to completely make a perfect uniform soil specimen. After internal erosion, 66 per cent of the fine particles by weight was eroded for X-E-D50-V208-T120, which was approximately 25 per cent less than that observed for the triaxial specimen E-D50-V208-T120 under the same seepage velocity and erosion duration. This may be due to restriction of the horizontal deformation in the rigid wall tube, which provided lateral support to the force chains and prevented the erosion of the semi-active fine particles. However, as evident from Figure 9-3, the erosion was intensive and affected the coarse and fine particles and pores volume fractions. Interestingly, the soil specimen became more uniform after internal erosion and after the moist tamping footprint was removed from the pore volume fraction. The coarse volume fraction remained unchanged (as expected), and the reduction in fine volume impacted only the pore volume. A minor decrease in coarse volume fraction in the top region was observed, which was added to the middle and bottom regions after internal erosion. The pore volume fraction showed a significant drop in the bottom region, which was attributed to clogging of fine particles.

Table 9-2. Specimen properties pre- and post-erosion

										Pre-Erosion			Post-Erosion		
Sample ID	Initial Coarse (g)	Initial Fine (g)	Eroded Fine (g)	Residual Fine (g)	Initial Fine Content (%)	Residual Fine Content (%)	Diameter (mm)	Height (mm)	Total Volume (mm^3)	Volume of Coarse (mm^3)	Volume of Fine (mm^3)	Volume of Void (mm^3)	Volume of Coarse (mm^3)	Volume of Fine (mm^3)	Volume of Void (mm^3)
X-D50-V208-T120	268.5	89.5	59.1	30.4	25.0	10.2	50	100	196350	101512	33837	61000	101512	11493	83344
W-D50-V208-T30	268.5	89.5	41.4	48.1	25.0	15.2	50	100	196350	101512	33837	61000	101512	18185	76652

Table 9-3. Average volume fraction of coarse and fine particles and pores pre- and post-erosion

			Pre-Erosion			Post-Erosion		
Sample ID	Test	Calculation Method	Volume of Coarse Fraction (%)	Volume of Fine Fraction (%)	Volume of Void Fraction (%)	Volume of Coarse Fraction (%)	Volume of Fine Fraction (%)	Volume of Void Fraction (%)
X-D50-V208-T120	1	Laboratory	51.7	17.2	31.1	51.7	5.9	42.4
		X-ray Imaging	50.1	17.0	32.9	51.0	7.3	41.7
X-D50-V208-T30	2	Laboratory	51.7	17.2	31.1	51.7	9.3	39.0
		X-ray Imaging	NA	NA	NA	51.1	9.2	39.7

Table 9-4. Average of fine content and global void ratio pre- and post-erosion

Sample ID	Test	Calculation Method	Pre-Erosion Global Void Ratio (%)	Pre-Erosion Fine Content (%)	Post-Erosion Global Void Ratio (%)	Post-Erosion Fine Content (%)
X-D50-V208-T120	1	Laboratory	0.45	25	0.74	10
		X-ray Imaging	0.49	25	0.72	13
X-D50-V208-T30	2	Laboratory	0.45	25	0.64	15
		X-ray Imaging	NA	NA	0.66	15

Impact of erosion progress on soil structure is shown in Figure 9-4. The volume fraction of coarse and fine particles and pores were determined for two eroded specimens after experiencing identical erosion, but for two different durations (30 and 120 minutes). Only a 5 per cent increase in residual fine content was observed for specimen X-E-D50-V208-T30, compared to specimen X-E-D50-V208-T120. The same trends and almost the same magnitudes were observed in volume fractions of coarse, fine and pores for two eroded specimens, with the exception of the first 10 mm from the top. This shows that those fine particles that were close to the flow inlet (the uppermost zone) were more vulnerable to erosion. A middle part (between 20 mm and 50 mm from the top) of both specimens had similar coarse, fine and pore volume fractions, residual fine contents and global and intergranular void ratios. This could be due to new-deposition of migrated fine particles from the upper parts that counterbalanced erosion of fine particles. Figure 9-4 also indicates that due to intensive erosion (high seepage velocity), the footprint of the moist tamping technique was removed from the soil structure even after 30 minutes of erosion.

Figures 9-3 and 9-4 confirm that internal erosion is not a uniform process and that, depending on the seepage and soil properties and specimen dimensions, the soil structure changes non-uniformly along the seepage path. Table 9-5 shows the average, minimum and maximum values of global and intergranular void ratios pre- and post-erosion. A significant difference between average values and both minimum and maximum values were observed, showing that considering an average value of global or intergranular void ratios for the entire height of soil specimens is unrealistic and cannot solely explain the impact of erosion on soil behaviour.

Table 9-5. Variation of global and intergranular void ratios pre- and post-erosion

Sample Label	Global Void Ratio					Intergranular Void Ratio				
	Min	Max	Ave	Var. of Min from the Ave. (%)	Var. of Max from the Ave. (%)	Min	Max	Ave	Var. of Min from the Ave. (%)	Var. of Max from the Ave. (%)
X-NE-D50-V208-T120	0.36	0.68	0.49	-27	39	0.73	1.32	1	-27	32
X-E-D50-V208-T120	0.44	0.89	0.72	-39	24	0.64	1.13	0.96	-33	18
X-E-D50-V208-T30	0.51	0.91	0.66	-23	38	0.76	1.35	0.96	-21	41

In Figure 9-5, one horizontal CT scan at the top and one at the bottom of the soil specimen pre- and post-erosion are shown. Coarse particles with distinct contrast (resulted by different mineralogy) were selected as a benchmark to track the progress of internal erosion. Apart from erosion of the fine particles, Figure 9-5 indicates that coarse particle rearrangement also occurred due to internal erosion, although coarse particles formed the primary soil skeleton and were under full stress. Investigation of the coarse particles indicated that some coarse particles rotated or moved slightly during internal erosion to form a new stable structure. These images confirm the proposed hypothesis that the erosion of free and semi-active fine particles led to coarse particle rearrangement when lateral support failed locally. This particle rearrangement changed the intergranular void ratio, which was found to be the effective factor impacting post-erosion mechanical behaviour.

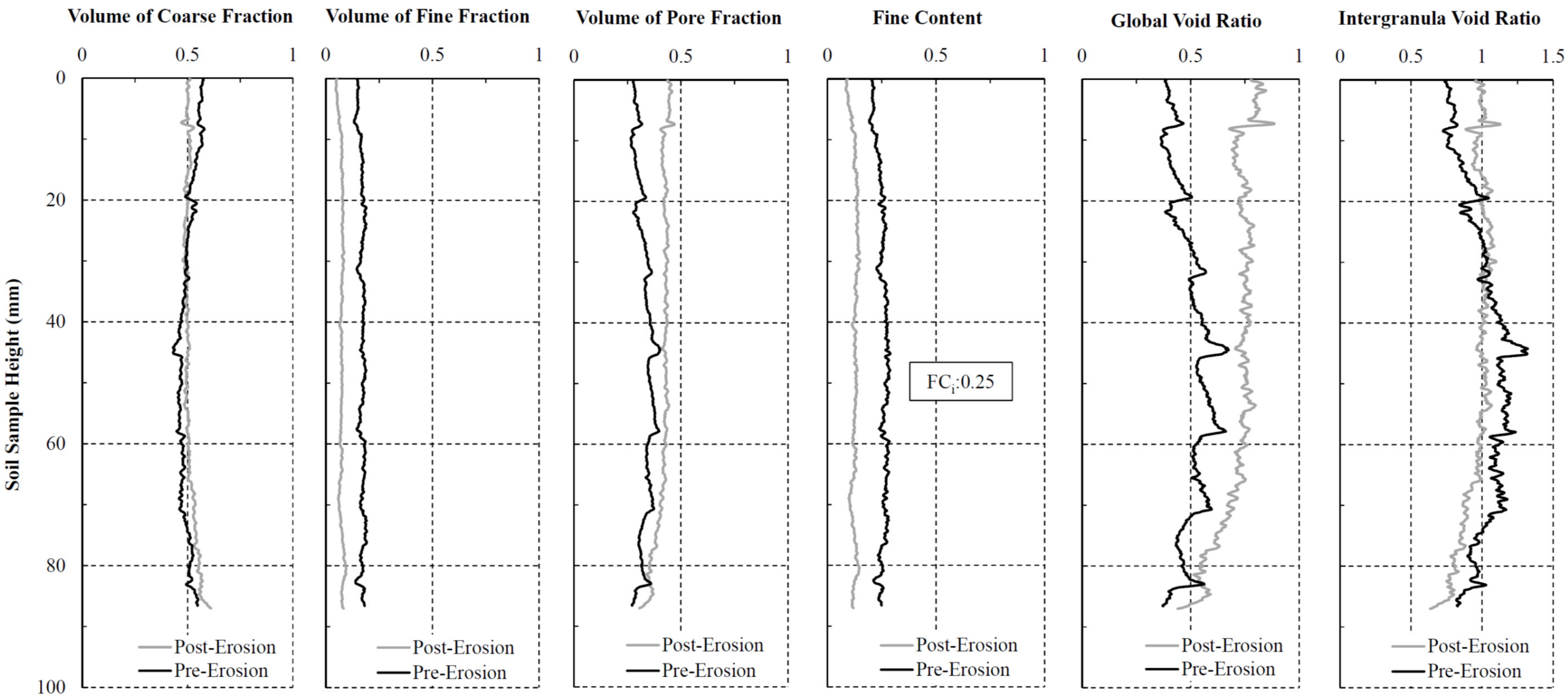

Figure 9-3. Variation of Coarse, fine and pore fraction, fine content and global and intergranular void ratios pre- and post-erosion for specimen X-D50-V208-T120

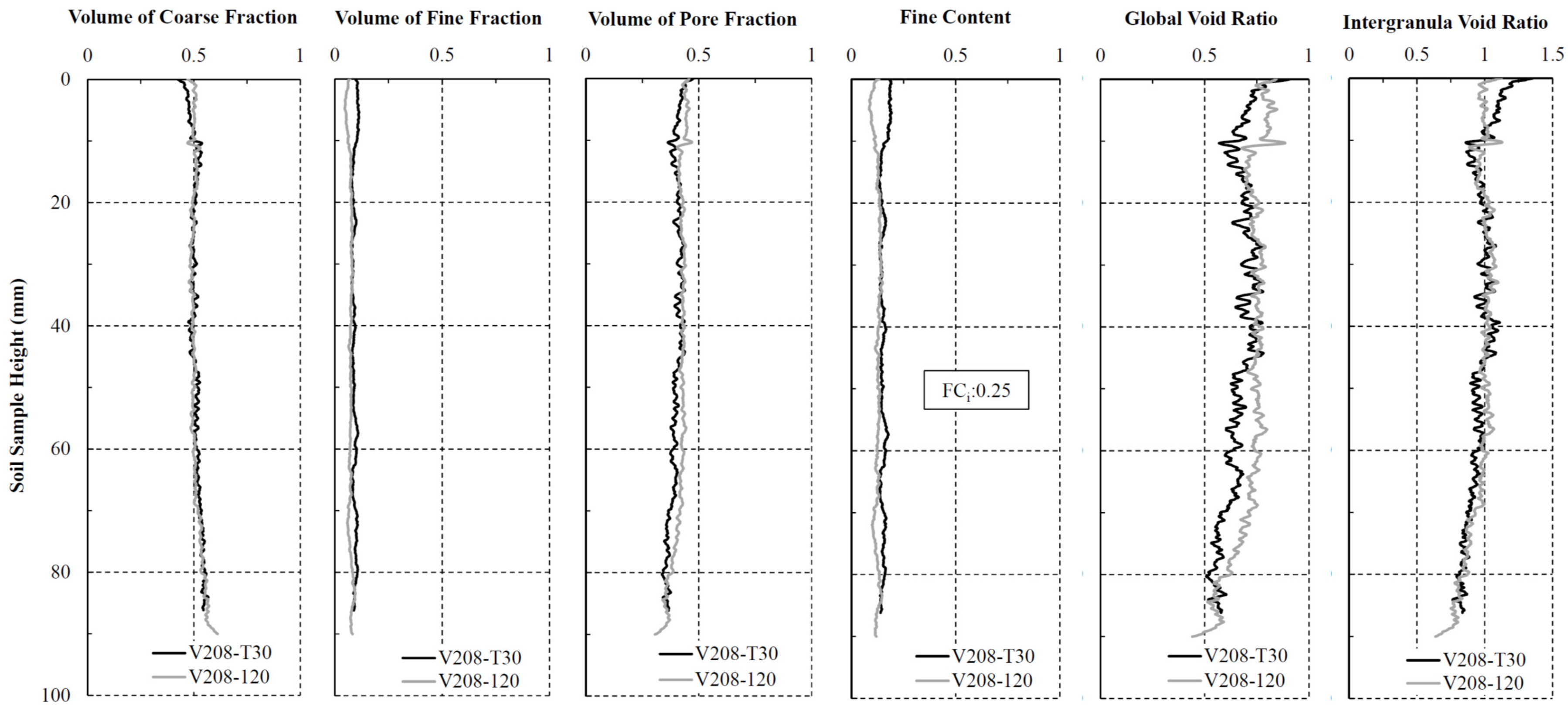

Figure 9-4. Variation of Coarse, fine and pore fraction, fine content and global and intergranular void ratios due to a downward erosion with seepage velocity of 208 mm/min after 30 and 120 minutes (X-D50-V208-T30 and X-D50-V208-T120)

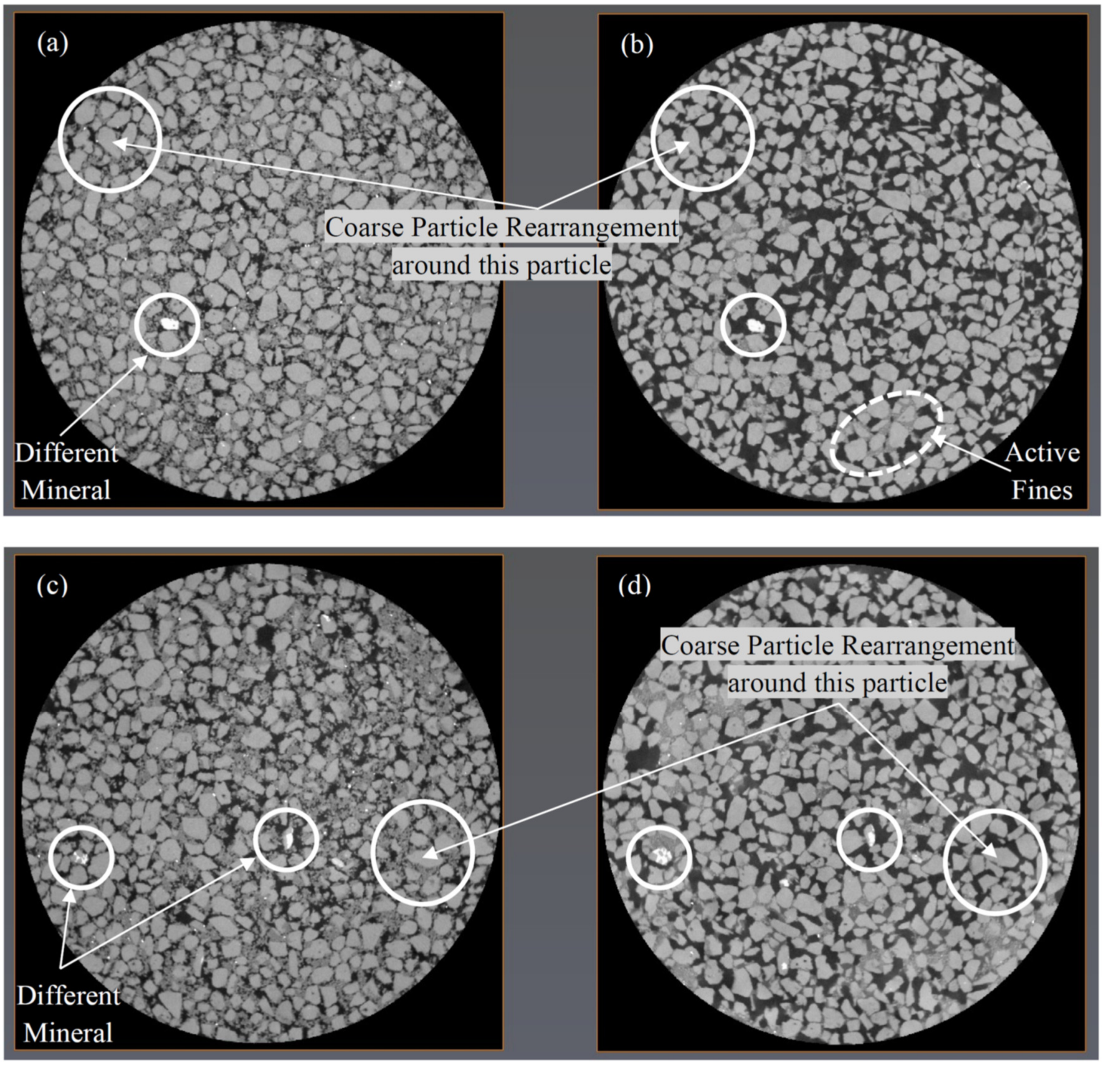

Figure 9-5. Coarse particle rearrangement during suffusion (a) A cross-section at the top of the specimen pre-erosion, (b) Same cross-section at the top of the specimen post-erosion, (c) A cross-section at the bottom of the specimen pre-erosion and (d) Same cross-section at the bottom of the specimen post-erosion

9.3. Conclusion

The impact of suffusion on the soil structure and force chains were examined through laboratory investigation and X-ray tomography. The following points were the most important findings of this chapter:

- Although coarse and fine particles had the same mineral, they reflected different grey colours that can be distinguished even in 8 bits images. Using 8 bits images reduces time of image processing significantly.
- X-ray tomography confirmed that coarse particle rearrangement occurs during suffusion when force chains lose their lateral support due to erosion of semi-active fine particles.
- Pre- and post-erosion X-ray tomography of a soil specimen showed that the moist tamping method was unable to produce a uniform soil specimen across the full height. However, the suffusion removed this effect, which resulted in a more uniform specimen in terms of distribution of coarse and fine particles and pore volume fractions.
- It was understood that suffusion is a non-uniform process and that it changes soil properties differently along the seepage path. Therefore, considering an average value of the global void ratio for the entire height of the soil specimens for engineering purposes could be unrealistic and misleading.

Chapter 10 Conclusion and Recommendation

Influence of removal and relocation of non-plastic fine particles caused by internal erosion on undrained monotonic and cyclic behaviour of an internally unstable gap graded material is determined in this research. A newly modified triaxial apparatus is used to perform saturation, consolidation, erosion and shearing phases in a triaxial cell successively to avoid the loss of saturation and soil disturbance. Moreover, 3D X-ray tomography has been conducted on non-eroded and eroded specimens to investigate the impact of internal erosion on the soil structure and force chains at micro scale. Photogrammetry technique is employed to measure local vertical/lateral and volumetric strains during erosion and shearing stages.

Effect of seepage velocity, erosion duration and specimen dimension on erosion of fine particles and post-erosion behaviour is evaluated. Variation of undrained shear strength (stress-strain relationship), development of excess pore water pressure, small strain stiffness, global and intergranular void ratios, post-erosion particle size distribution, flow potential, instability state and cyclic resistance due to erosion of fine particles is discussed.

10.1. Impact of seepage velocity and erosion duration on erosion of fine particles and post-erosion behaviour

Erosion of free fine particles filling the available voids between coarse particles was found to be independent of seepage velocity. However, the residual fine content dropped in the specimen eroded at the higher inflow velocity or for a longer time.

Regardless of seepage velocity and erosion duration, initial hardening behaviour of the soil specimen changed to the flow type with limited deformation (dilation tendency was postponed) after internal erosion and initial peak shear strength increased. A better interlocking could have formed between the angular coarse particles due to removal of fine particles which increased the undrained shear strength. However, formation of local metastable structures due to erosion of semi-active fine particles (providing lateral support for force chains) under higher seepage velocities deteriorated the temporarily improvement. This turning point was found to be related to a threshold value of residual fine content where the semi-active fine particles lost their intergrain contacts.

Regardless of seepage velocity and duration of erosion, eroded specimens with a similar intergranular void ratio showed similar post-erosion undrained behaviour. Global void ratio increases after loss of fine particles. However, the intergranular void ratio my decrease or stay unchanged depending on the quality of the contribution of the fine particles in the soil skeleton (inactive, semi-active or active).

A review of all experimental studies available in the literature, suggests that depending on the quality of the contribution of the fine particles in the soil skeleton, erosion progress, angularity of the particles, state of the particles interlocking pre and post-erosion, local concentration of the fine particles, innate characteristics of the stress matrix (coarse grain) particles, possibility of particle rearrangement and variation of the void ratio, different scenarios may occur when it comes to post-erosion mechanical behaviour of soils. In fact, regardless of the change in post-erosion behaviour that can improve soil strength to some extent, non-uniform soil responses through the erosion path and the affected zone in the hydraulic structures is the main concern and challenge which may lead to differential settlements and associated catastrophic consequences.

10.2. Impact of sample dimension on erosion of fine particles and post-erosion behaviour

Contrary to 75 and 100 mm diameter specimens, the eroded 50 mm diameter specimen lost nearly 20 per cent more fines and presented a different undrained behaviour. However, regardless of the sample dimension, the initial undrained shear strength increased after internal erosion for all specimens tested. Eroded specimens with different dimensions showed similar undrained behaviour when the post-erosion intergranular void ratio did not change.

10.3. Impact of erosion of fine particles on soil cyclic resistance

It was found that cyclic resistance increased significantly even with erosion of a small amount of fine particles. While the non-eroded specimen was liquefied after only 5 cycles of loading, the eroded specimens were non-liquefiable for the erosion percentage observed in this experiment. This finding suggested that neither relative density nor global void ratio can predict the response of eroded specimens during cyclic loadings.

An increase in erosion of fine particles decreased development of excess pore water pressure with descending trend. Experiencing cyclic loading increased contraction tendency that led to a drop in undrained shear strength.

Regardless of the residual fine content, all eroded specimens showed a cyclic behaviour similar to a soil specimens prepared only by coarse fraction (without fine content). However, the contrary to the similar pattern for cyclic behaviours, the post cyclic behaviour of the specimen made only by coarse particles was very different. While strain softening behaviour was dominant for eroded specimens even for the specimen with the lowest residual fine content, strain hardening behaviour with a much greater undrained shear strength was observed for the pure coarse specimen. It was understood that lubricating effect of even a small amount of fine particles among the angular coarse particles reduced the internal friction between coarse particles and decreased the shear strength. Moreover, this study indicated that suffusion decreased the small strain undrained secant stiffness. However, a noticeable improvement in the secant stiffness for the eroded specimens was observed after experiencing cyclic loading.

10.4. Impact of suffusion on soil stress matrix

Photogrammetry and X-ray tomography indicated that coarse particle rearrangement leading to formation of new soil structure occurs when semi-active fine particles that provide lateral support for soil structure are eroded.

Suffusion is a non-uniform process and results in different global void ratio along the seepage path. Therefore, average value of global void ratio does not represent real conditions.

This study suggests that depending on the quality of the contribution of the fine particles in the soil skeleton, erosion progress, angularity of the particles, state of the particles interlocking pre and post-erosion, local concentration of the fine particles, innate characteristics of the stress matrix (coarse grain) particles, possibility of particle rearrangement and variation of the void ratio, different scenarios may occur when it comes to post-erosion mechanical behaviour of soils. In fact, regardless of the change in post-erosion behaviour that can improve soil strength to some extent, non-uniform soil responses through the erosion path and the affected zone in the hydraulic structures is the main concern and challenge which may lead to differential settlements and associated catastrophic consequences.

10.5. Recommendation

This research sheds some light on impact of suffusion on post-erosion mechanical behaviour and soil structure of an internally unstable soil under monotonic and cyclic loadings. However, to be able to apply these findings to engineering purposes, other internally unstable materials with different fine contents or gradation curves, relative densities and subjected to different consolidation pressure need to be also examined.

A robust and calibrated coupled DEM-CFD numerical model not only can improve our understanding about influence of suffusion on soil stress matrix, activity of particles in the soil structure or interaction of particles, it can also reduce number of required laboratory tests and CT-scans significantly.

References

AASHTO Designation M145, (2008). "The Classification of Soils and Soil-Aggregate Mixtures for Highway Construction Purpose." American Association of State Highway and Transportation Officials, Washington DC, USA.

Abdelhamid, Y., and El Shamy, U. (2015). "Pore-Scale Modeling of Fine-Particle Migration in Granular Filters." *International Journal of Geomechanics*, 16(3), 04015086, doi: 10.1061/(ASCE)GM.1943-5622.0000592.

Adams, B. A., Wulfsohn, D., and Fredlund, D. G. (1996). "Air volume change measurement in unsaturated soil testing using a digital pressure-volume-controller." *Geotechnical Testing Journal*, 19(1), 12-21.

Ahlinhan, M. F., and Achmus, M. (2010). "Experimental investigation of critical hydraulic gradients for unstable soils." *Proceedings of the 5th International Conference on Scour and Erosion*, San Francisco, CA, 599-608.

Ahlinhan, M. F., Achmus, M., Hoog, S., and Wouya, E. K. (2012). "Stability of non-cohesive soils with respect to internal erosion." *Proceedings of the Sixth International Conference on Scour and Erosion*, Paris, 27-31.

Alexis A., Le Bras G., and Thomas P. (2004). "Experimental bench for study of settling-consolidation soil formation." *Geotechnical Testing Journal*, 27(6), 557-567.

Al-Raoush, R., and Alshibli, K. A. (2006). "Distribution of local void ratio in porous media systems from 3D X-ray microtomography images." *Physica A*, Amsterdam, 361(2), doi: 441-456.10.1016/j.physa.2005.05.043.

Alshibli, K. A., and Sture, S. (1999). "Sand Shear Band Thickness Measurement by Digital imaging Techniques." *Journal of Computing in Civil Engineering*, 13(2), 103-109.

Alshibli, K. A., and Al-Hamdan, M. Z. (2001). “Estimating volume change of triaxial soil specimens from planar images.” *Computer-Aided Civil and Infrastructure Engineering*, 16(6), 415-421.

Amini, F., and Qi, G. Z. (2000). “Liquefaction testing of stratified silty sands.” *Journal of Geotechnical and Geoenvironmental Engineer*ing, 126(3), 208-217.

Andrianatrehina, N. L., Souli, H., Rech, J., Fry, J. J., Fleureau, J. M., and Taibi, S. (2016). “Influence of the percentage of sand on the behaviour of gap-graded cohesionless soils.” *Comptes Rendus Mécanique*, 344(8), 539-546, doi:10.1016/j.crme.2016.03.001.

Andrianopoulos, K., Bouckovalas, G., and Papadimitriou, A. (2001). “A critical state evaluation of fines effect on liquefaction potential.” *Proceedings of 4th International Conference on Recent Advances in Geotechnical Earthquake Engineering and Soil Dynamics*, San Diego, California.

ASTM C136-06 (2006). “Standard test method for sieve analysis of fine and coarse aggregates.” West Conshohocken, PA.

ASTM D2487-06. (2006). “Standard practice for classification of soils for engineering purposes (unified soil classification system).” West Conshohocken, PA.

ASTM D6913-04 (2009). “Standard Test Methods for Particle-Size Distribution (Gradation) of Soils Using Sieve Analysis.” West Conshohocken, PA.

ASTM D3080/D3080M-11 (2011). “Standard Test Method for Direct Shear Test of Soils Under Consolidated Drained Conditions.” West Conshohocken, PA.

ASTM D4767-11 (2011). “Standard Test Method for Consolidated Undrained Triaxial Compression Test for Cohesive Soils.” West Conshohocken, PA.

ASTM D5311/5311M-13 (2013). “Standard Test Method for Load Controlled Cyclic Triaxial Strength of Soil.” West Conshohocken, PA.

ASTM D854-14 (2014). “Standard Test Methods for Specific Gravity of Soil Solids by Water Pycnometer.” West Conshohocken, PA.

ASTM D3282-15 (2015). “Standard Practice for Classification of Soils and Soil-Aggregate Mixtures for Highway Construction Purposes.” West Conshohocken, PA.

ASTM D4253-16 (2016). “Standard Test Methods for Maximum Index Density and Unit Weight of Soils Using a Vibratory Table.” West Conshohocken, PA.

ASTM D4254-16 (2016). “Standard Test Methods for Minimum Index Density and Unit Weight of Soils and Calculation of Relative Density.” West Conshohocken, PA.

Australian Synchrotron (2017). “About synchrotrons.” Australian Synchrotron, viewed 30 Sep 2017, < http://www.synchrotron.org.au/synchrotron-science >.

Baki, M. A. L., Rahman, M. M., and Lo, S. R. (2014). “Predicting onset of cyclic instability of loose sand with fines using instability curves.” *Journal of Soil Dynamic and Earthquake Engineering*, 61, 140-151.

Becker, C., Kurzeja, P., and Steeb, H. (2010). “Modelling internal erosion of cohesionless soils using a microstructural parameter.” *PAMM*, 10(1), 355-356.

Belkhatir, M., Arab, A., Della, N., Missoum, H., and Schanz, T. (2010). “Influence of inter-granular void ratio on monotonic and cyclic undrained shear response of sandy soils.” *Comptes Rendus Mécanique*, 338(5), 290-303.

Benamar, A., Beaudoin, A., Bennabi, A., and Wang, H. (2010). Experimental Study of Internal Erosion of Fine Grained Soils. *Proceedings of the 5th International Conference on Scour and Erosion*, San Francisco, CA, 368-377.

Bendahmane, F., Marot, D., and Alexis, A. (2008). "Experimental parametric study of suffusion and backward erosion." *Journal of Geotechnical and Geoenvironmental Engineering*, 134(1), 57-67.

Bishop, A. W., and Donald, I. B. (1961). "The experimental study of partly saturated soil in the triaxial apparatus." *Proceedings of 5th International Conference on soil mechanics and foundation engineering*, Paris, 1, 13-21.

Blatz, J., and Graham, J. (2000). "A system for controlled suction in triaxial tests." *Géotechnique*, 50(4), 465-470.

Bligh, W. G. (1910). "Dams, barrages and weirs on porous foundations." *Engineering News*, 64(26), 708-710.

Bligh, W. G. (1911a). "Reply to sheet piles as a means of decreasing permeability of porous foundations." *Engineering news*, 65(4), 109.

Bligh, W. G. (1911b). "Weirs on porous foundations and with pervious floors." *Engineering News*, 65(15), 444-445.

Bligh, W. G. (1913). "Lessons from the failure of a weir and sluices on porous foundations." *Engineering News*, 69(6), 266-270.

Bolton, M. D., and Wilson, J. M. R. (1990). "Soil stiffness and damping." *Proceedings of the international conference on structural dynamics*, Eurodynamics '90, University of Bochum, 1, 209-216.

Bradshaw, A. S., and Baxter, C. D. P., (2007). “Sample preparation of silts for liquefaction testing.” *Geotechnical Testing Journal*, 30(4), 324-332.

Brown, A. J., and Gosden, J. D. (2004). “Interim guide to quantitative risk assessment for UK reservoirs.” London, Thomas Telford.

Burenkova, V. V., (1993). “Assessment of Suffusion in Non- Cohesive and Graded Soils.” *Proceedings of the 1st International Conference on Geo-Filters*, Balkema, Rotterdam, The Netherlands, 357-360.

Carraro, J. A. H., Bandini, P., and Salgado, R. (2003). “Liquefaction resistance of clean and non-plastic silty sands based on cone penetration resistance.” *Journal of Geotechnical and Geoenvironmental Engineering*, 129(11), 965-976.

Carraro, J. A., and Prezzi, M., (2008). “A new slurry-based method of preparation of specimens of sand containing fines.” *Geotechnical Testing Journal*, 31(1), 1-11.

Carraro, J. A. H., Prezzi, M., and Salgado, R. (2009). “Shear strength and stiffness of sands containing plastic or nonplastic fines.” *Journal of Geotechnical and Geoenvironmental Engineering*, 135(9), 1167-1178.

Chameau, J. L., and Sutterer, K. (1994). “Influence of fines in liquefaction potential and steady state considerations.” *Proceedings of 13th International Conference of soil mechanics and foundation engineering*, New Delhi, India, A. A. Balkema, Rotterdam, The Netherlands, 183-184.

Chang, N. Y. (1990). “Influence of fines content and plasticity on earthquake-induced soil liquefaction.” Contract Report, MS Cont. No. DACW3988-C-0078. Vicksburg: US Army WES.

Chang, C. S. and Hicher, P. Y. (2005). “An elastoplastic model for granular materials with microstructural consideration.” *International Journal of Solids and Structures*, 42(14), 4258-4277.

Chang, D. S., and Zhang, L. M. (2011). “A stress-controlled erosion apparatus for studying internal erosion in soils.” *Geotechnical Testing Journal*, 34(6), 579-589.

Chang, D. S., and Zhang, L. M. (2012). “Critical hydraulic gradients of internal erosion under complex stress states.” *Journal of Geotechnical and Geoenvironmental Engineering*, 139(9), 1454-1467.

Chang, D. S., Zhang, L. M., and Xu, T. H. (2012). “Laboratory investigation of initiation and development of internal erosion in soils under complex stress states.” *Proceedings of the Sixth International Conference on Scour and Erosion*, Paris, 895-902.

Chang, D. S., and Zhang, L. M., (2013). “Extended internal stability criteria for soils under seepage.” *Soils and Foundations*, 53(4), 569-583.

Chang, D., Zhang, L., and Cheuk, J. (2014). “Mechanical consequences of internal soil erosion.” *HKIE Transactions*, 21(4), 198-208.

Chapuis, R. P. (1992). “Similarity of internal stability criteria for granular soils.” *Canadian Geotechnical Journal*, 29(4), 711-713.

Chen, L., Zhao, J., Zhang, H., and Lei, W. (2015). “Experimental Study on Suffusion of Gravelly Soil.” *Soil Mechanics and Foundation Engineering*, 52(3), 135-143.

Chen, C., Zhang, L. M., and Chang, D. S. (2016). “Stress-Strain Behaviour of Granular Soils Subjected to Internal Erosion.” *Journal of Geotechnical and Geoenvironmental Engineering*, 06016014, doi: 10.1061/ (ASCE)GT.1943-5606.0001561.

Cho, G. C., Dodds, J., and Santamarina, J. C. (2006). “Particle shape effects on packing density, stiffness, and strength: natural and crushed sands.” *Journal of Geotechnical and Geoenvironmental Engineering*, 132(5), 591-602.

Chu, J. and Leong, W. K., (2002). “Effects of Fines on Instability Behaviour of Loose Sand.” *Geotechnique*, 52(10), 751-755.

Cividini, A., and Gioda, G. (2004). “Finite-element approach to the erosion and transport of fine particles in granular soils.” *International Journal of Geomechanics*, 4(3), 191-198.

Cividini, A., Bonomi, S., Vignati, G. C., and Gioda, G. (2009). “Seepage-induced erosion in granular soil and consequent settlements.” *International Journal of Geomechanics*, 9(4), 187-194.

Clayton, C. R. I., Khatrush, S. A., Bica, A. V. D. and Siddique, A. (1989). “The use of Hall effect semiconductors in geotechnical instrumentation.” *Geotechnical Testing Journal*, 12(1), 69-76.

Correia dos Santos, R., Caldeira, L., and Maranha das Neves, E. (2015). “Laboratory test for evaluating crack filling during internal erosion in zoned dams.” *Geotechnical Testing Journal*, 38(6), 915-928.

Cyril, G., Yves-Henri, F., Rémi, B., and Chia-Chun, H. (2009). “Contact erosion at the interface between granular coarse soil and various base soils under tangential flow condition.” *Journal of Geotechnical and Geoenvironmental Engineering*, 136(5), 741-750.

Dallo, Y. A., Wang, Y., and Ahmed, O. Y. (2013). “Assessment of the internal stability of granular soils against suffusion.” *European Journal of Environmental and Civil Engineering*, 17(4), 219-230.

Darcy, H. (1856). "Les fontaines publiques de la Ville de Dijon." Dalmont, Paris.

Dash, H. K., and Sitharam, T. G. (2011). "Undrained monotonic response of sand–silt mixtures: effect of nonplastic fines." *Geomechnical and Geoengineering International Journal*, 6(1), 47-58.

Engemoen, W. O., and Redlinger, C. G. (2009). "Internal erosion incidents at Bureau of Reclamation dams." *Proceedings of the 29th Annual USSD Conference*, Nashville, Tennessee, USA, 731-725.

Engemoen, W. O. (2011). "Bureau of Reclamation experiences with internal erosion incidents." *Proceedings of the Internal Erosion in Embankment Dams and Their Foundations*, European Working Group of ICOLD, Brno, Czech Republic, 11-18.

Evans, M. D., and Zhou, S. (1995). "Liquefaction behaviour of sand-gravel composites." *Geotechnical Testing Journal*, 121(3), 287-298.

Fannin, R. J. and Slangen, P. (2014). "On the distinct phenomena of suffusion and suffusion." *Géotechnique Letters*, 4, 289-294.

Federico, F., Montanaro, A., and Scienza, M. (2013). "Numerical simulation of suffusion phenomena through granular media." *In Powders and Grains, Proceedings of the 7th International Conference on Micromechanics of Granular Media*, 1542(1), 189-192. AIP Publishing.

Fell, R., Foster, M., Davidson, R., Cyganiewicz, J., Sills, G., and Vroman, N. (2008). "A unified method for estimating probabilities of failure of embankment dams by internal erosion and piping." UNICIV Report R 446, The School of Civil and Environmental Engineering, the University of New South Wales, Sydney, Australia, 2052.

Ferreira, T., and Rasband, W. (2012). "ImageJ user guide." IJ1. 46r. Natl. Inst. Health, Bethesda, MD. http://rsb. info. nih. gov/ij/docs/guide/user-guide. pdf.

Finn, L. W. D., Ledbetter, R. H., and Guoxi Wu. (1994). "Liquefaction in silty soils: design and analysis." *Geotechnical Special Publublication*, 44, 51-76.

Fleshman, M. S., and Rice, J. D. (2014). "Laboratory modelling of the mechanisms of piping erosion initiation." *Journal of Geotechnical and Geoenvironmental Engineering*, 140(6), 04014017, doi: 10.1061/(ASCE)GT.1943-5606.0001106.

Fonseca, J. (2011). "The evolution of morphology and fabric of a sand during shearing" Doctoral dissertation, Imperial College, London.

Fonseca, J., O'Sullivan, C., Coop, M. R., and Lee, P. D. (2012). "Non-invasive characterization of particle morphology of natural sands." *Soils and Foundations*, 52(4), 712-722.

Fonseca J., Sim, W. W., Shire, T., and O'Sullivan, C. (2014). "Micro-structural analysis of sands with varying degrees of internal stability." *Geotechnique*, 2014, 64(5), 405-11.

Foster, M. A., Fell, R., and Spannagle, M. (1998). "Analysis of embankment dam incidents." UNICIV Report No. R-374, School of Civil and Environmental Engineering, University of New South Wales, Sydney, Australia. ISBN 85841 349 3.

Foster, M., Fell, R., and Spannagle, M. (2000). "The statistics of embankment dam failures and accidents." *Canadian Geotechnical Journal*, 37(5), 1000-1024.

Fraser, H. J. (1935). "Experimental study of the porosity and permeability of clastic sediments." *Journal of Geology*, 13(8), 910-1010.

Frishfelds, V., Hellström, J. G. I., Lundström, T. S., and Mattsson, H. (2011). “Fluid flow induced internal erosion within porous media: modelling of the no erosion filter test experiment.” *Transport in porous media*, 89(3), 441-457.

Frost, J. D., and Jang, D. J. (2000). “Evolution of sand microstructure during shear.” *Journal of Geotechnical and Geoenvironmental Engineering*, 126(2), 116-130.

Frost, J. D., and Park, J. Y. (2003). “A critical assessment of the moist tamping technique.” *Geotechnical Testing Journal*, 26(1), 57-70.

Frost, J. D., Kim, D., and Lee, S. W. (2012). “Microscale geomembrane-granular material interactions.” *KSCE Journal of Civil Engineering*, 16(1), 79-92.

Fry, J. J., Vogel, A., Royet, P., and Courivaud, J. R. (2012). “Dam failures by erosion: lessons from erinoh data bases.” *Proceedings of the Sixth International Conference on Scour and Erosion*, Paris, 273-280.

Gachet, P., Geiser, F. and Laloui, L. (2007). “Automated digital image processing for volume change measurement in triaxial cells.” *Geotechnical Testing Journal*, 30(2), 98-103.

Galarowski, T. (1976). “New observations of the present-day suffusion (piping) processes in the Bereznica catchment basin in the Bieszczady Mountains (The East Carpathians).” Studia Geomorphologica Carpatho-Balcanica (Krakow) 10,115-122.

Garner, S. J., and Sobkowicz, J. C. (2002). “Internal instability in gap-graded cores and filters.” *Proceedings of the Canadian Dam Association Annual Conference*, 6-10, Victoria, B.C.

Garner, S. J., and Fannin, R. J. (2010). “Understanding internal erosion: a decade of research following a sinkhole event.” *International Journal of Hydropower Dams*, 17(3), 93-98.

Gaucher, J., Marche, C., and Mahdi, T. F. (2010). “Experimental investigation of the hydraulic erosion of noncohesive compacted soils.” *Journal of Hydraulic Engineering*, 136(11), 901-913.

Geiser, F. (1999). “Comportement mécanique d’un limon non saturé: Étude expérimentale et modélisation constitutive.” PhD thesis, Swiss Federal Institute of Technology, Lausanne, Switzerland.

Georgiannou, V. N., Hight, D. W., and Burland, J. B. (1990). “The undrained behaviour of clayey sands in triaxial compression and extension.” *Geotechnique*, 40(3), 431-449.

Georgiannou, V. N., Hight, D. W., and Burland, J. B. (1991a). “Undrained behaviour of natural and model clayey sands.” *Soils and Foundations*, 31(3), 17-29.

Georgiannou, V. N., Hight, D. W., and Burland, J. B. (1991b). “Behaviour of clayey sands under undrained cyclic triaxial loading.” *Geotechnique*, 41(3), 383-393.

Ghafghazi, M., and Azhari, F. (2012). “A simple method for estimating the non-structural fines content of granular materials.” *Proceedings of the Sixth International Conference on Scour and Erosion*, Paris, 6-16.

Göktepe, A. B., and Sezer, A. (2010). “Effect of particle shape on density and permeability of sands.” *Proceeding of the ICE Geotechnical Enginerring*, 163(6), 307-320.

Goto, S., Tatsuoka, F., Shibuya, S., Kim, Y. S. and Sato, T. (1991). “A simple gauge for local small strain measurements in the laboratory.” *Soils and Foundations*, 31(1), 169-180.

Guimaraes, M. (2002). "Crushed stone fines and ion removal from clay slurries-Fundamental studies." Dissertation, Georgia Institute of Technology.

Guo, P., and Su, X. (2007). "Shear strength, interparticle locking, and dilatancy of granular materials." *Canadian Geotechnical Journal*, 44(5), 579-591.

Hall, S., Bornert, M., Desrues, J., Pannier, Y., Lenoir, N., and Viggiani, G. (2010). "Discrete and continuum analysis of localised deformation in sand using X-ray microCT and volumetric digital image correlation." *Geotechnique*, 60(5), 315-22.

Halverson, C., White, D. J., and Gray, J. (2005). "Application of x-ray CT scanning to characterize geomaterials used in transportation construction." *Proceeding of Mid-Continent Transportation Research Symposium*, Ames, IA.

Hama, N. A., Ouahbi, T., Taibi, S., Pantet, A., Fleureau, J. M., and Souli, H. (2014). "Numerical analysis of internal stability of granular materials using discrete element method." *3rd International Symposium on Geomechanics from Micro to Macro*, CRC Press, 527-531.

Harshani, H. M. D., Galindo-Torres, S. A., Scheuermann, A., and Muhlhaus, H. B. (2015). "Micro-mechanical analysis on the onset of erosion in granular materials." *Philosophical Magazine*, 95(28-30), 3146-3166.

Hasan, A., and Alshibli, K. A. (2010). "Experimental assessment of 3D particle-to-particle interaction within sheared sand using synchrotron microtomography." *Geotechnique*, 60(5), 369-79.

Head, K. H., and Epps, R. J. (2011). "Manual of soil laboratory testing." Volume II: Permeability, shear strength and compressibility test. Whittles Publishing, Scotland.

Hicher, P. Y., and Chang, C. (2009). “Instability and failure in soils subjected to internal erosion.” Prediction and Simulation Methods for Geohazard Mitigation, 325-330.

Hicher, P. Y. (2013). “Modelling the impact of particle removal on granular material behaviour.” *Géotechnique*, 63(2), 118-128.

Homberg, U., Binner, R., Prohaska, S., Dercksen, V. J., Kuß, A., and Kalbe, U. (2009). “Determining geometric grain structure from x-ray micro-tomograms of gradated soil.” In Workshop Internal Erosion, 21, 37-52.

Hsiao, D. H., and Phan, V. T. A. (2016). “Evaluation of static and dynamic properties of sand–fines mixtures through the state and equivalent state parameters.” *Journal of Soil Dynamic and Earthquake Engineering*, 84, 134-144.

Huang, Q. F., Zhan, M. L., Sheng, J. C., Luo, Y. L., and Su, B. Y. (2014). “Investigation of fluid flow-induced particle migration in granular filters using a DEM-CFD method.” *Journal of Hydrodynamics*, Ser. B, 26(3), 406-415.

Indraratna, B., Raut, A. K., and Khabbaz, H. (2007). “Constriction-based retention criterion for granular filter design.” *Journal of Geotechnical and Geoenvironmental Engineering*, 133(3), 266-276.

Indraratna, B., Nguyen, V. T., and Rujikiatkamjorn, C. (2011). “Assessing the potential of internal erosion and suffusion of granular soils.” *Journal of Geotechnical and Geoenvironmental Engineering*, 137(5), 550-554.

Indraratna, B., Israr, J., and Rujikiatkamjorn, C., (2015). “Geometrical method for evaluating the internal instability of granular filters based on constriction size distribution.” *Journal of Geotechnical and Geoenvironmental Engineering*, ASCE, 141(10), 1-14, doi: 10.1061/(ASCE)GT.1943-5606.0001343.

International Commission on Large Dams (ICOLD). (2015). "Internal erosion of existing dams, levees and dikes, and their foundations." Bulletin 164, Paris.

Ishihara, K. (1993). "Liquefaction and flow failure during earthquakes." *Geotechnique*, 43(3), 351-451.

Ishihara, K. (1996). "Soil behaviour in earthquake geotechnics." The Oxford engineering science series, No. 46, Oxford, U.K.

Istomina, V. S. (1957). "Filtration Stability of Soils." Gostroizdat, Moscow.

Jang, D. J., Frost, J. D., and Park, J. Y. (1999). "Preparation of epoxy impregnated sand coupons for image analysis." ASTM, *Geotechnical Testing Journal*, GTJODJ, 22(2), 147-158.

Jang, J., and Carlos Santamarina, J. (2015). "Fines classification based on sensitivity to pore-fluid chemistry." *Journal of Geotechnical and Geoenvironmental Engineering*, 142(4), 06015018, doi: 10.1061/(ASCE)GT.1943-5606.0001420.

Jansen, R. B. (1983). "Dams and public safety." *Water Resources Technical Publication*, US Department of the Interior, Bureau of Reclamation, 14-16.

Jiang, M. J., Konrad, J. M., and Leroueil, S. (2003). "An efficient technique for generating homogeneous specimens for DEM studies." *Computer and Geotechnics*, 30(7), 579-597.

Jones, J. A. A. (1981). "The nature of soil piping: a review of research." BGRG research monograph 3. Geo Books, Norwich.

Kabir, M. E., and Chen, W. W. (2011). "Dynamic triaxial test on sand." *In Dynamic Behaviour of Materials*, 1, 7-8.

Kaestner, A., Lehmann, P., and Fluehler, H. (2005). “Identifying the interface between two sand materials.” *Fifth International Conference on 3-D Digital Imaging and Modeling (3DIM'05)*, 410-415. IEEE.

Karim, M. E., and Alam, M. J. (2014). “Effect of non-plastic silt content on the liquefaction behaviour of sand–silt mixture.” *Soil Dynamic and Earthquake Engineering*, 65, 142-150, doi:10.1016/j.soildyn.2014.06.010.

Kawano, K., Shire, T., and O’Sullivan, C. (2017). “Coupled DEM-CFD Analysis of the Initiation of Internal Instability in a Gap-Graded Granular Embankment Filter.” *EPJ Web of Conferences*, 140, 10005, doi: 10.1051/epjconf/201714010005.

Ke, L., and Takahashi, A. (2011). “Strength reduction of gap-graded cohesionless soil due to internal erosion.” *Proceedings of 5th Asia-Pacific Conference on Unsaturated Soils*, 1, 203-208.

Ke, L., and Takahashi, A. (2012a) “Strength reduction of cohesionless soil due to internal erosion induced by one-dimensional upward seepage flow.” *Soils and Foundations*, 52(4), 698-711, doi:10.1016/j.sandf.2012.07.010.

Ke, L., and Takahashi, A. (2012b). “Influence of internal erosion on deformation and strength of gap-graded non-cohesive soil.” *Proceedings of the Sixth International Conference on Scour and Erosion*, Paris, 847-854.

Ke, L. and Takahashi, A. (2014a). “Experimental investigations on suffusion characteristics and its mechanical consequences on saturated cohesionless soil.” *Soils and Foundations*, 54(4), 713-730.

Ke, L., and Takahashi, A., (2014b). “Triaxial erosion test for evaluation of mechanical consequences of internal erosion.” *Geotechnical Testing Journal*, 37(2), 1-18.

Ke, L., and Takahashi, A. (2015). “Drained monotonic responses of suffusional cohesionless soils.” *Journal of Geotechnical and Geoenvironmental Engineering*, ASCE, doi: 10.1061/(ASCE)GT.1943-5606.0001327, 04015033.

Ke, L., Ouyang, M., Horikoshi, K., and Takahashi, A. (2016). “Soil deformation due to suffusion and its consequences on undrained behaviour under various confining pressures.” *Japanese Geotechnical Society Special Publication*, 2(8), 368-373.

Kelly, D., McDougall, J., and Barreto, D. (2012). “Effect of particle loss on soil behaviour.” *Proceedings of the Sixth International Conference on Scour and Erosion*, Paris, 639-646.

Kenney, T. C. (1977). “Residual strengths of mineral mixtures.” *Proceedings of 9th International conference of Soil mechanics*, Tokyo, 155-160.

Kenney, T. C., Chahal, R., Chiu, E., Ofoegbu, G. I., Omange, G. N., and Ume, C. A. (1985). “Controlling constriction sizes of granular filters.” *Canadian Geotechnical Journal*, 22(1), 32-43.

Kenney, T. C., and Lau, D. (1985). “Internal stability of granular filters.” *Canadian Geotechnical Journal*, 22(2), 215-225.

Kenney, T. C., and Lau, D. (1986). “Internal stability of granular filters: Reply.” *Canadian Geotechnical Journal*, 23(4), 420-423. doi: 10.1139/t86-068.

Kezdi, A. (1969). “Increase of protective capacity of flood control dikes.” Department of Geotechnique, Technical University, Budapest. Report No. 1.

Klotz, E. U. and Coop, M. R. (2002). “On the identification of critical state lines for sands.” *Geotechnical Testing Journal*, 25(3), 289-302.

Koenders, M. A., and Sellmeijer, J. B. (1992). “Mathematical model for piping.” *Journal of Geotechnical Engineering*, 118(6), 943-946.

Koester, J. P. (1994). “The influence of fines type and content on cyclic strength.” ASCE, *Geotechnical Special Publication*, 44, 17-32.

Kovács, G. (1981). “Seepage hydraulics.” Elsevier Scientific Publishing Company, Amsterdam, 730.

Kozicki, J., and Donze, F. V. (2008). “A new open-source software using a discrete element method to simulate granular material.” *Computer Methods in Applied Mechanics and Engineering*, 197, 4429-4443.

Kral, V. (1975). “Sufoze a jeji podil na soucasnych geomorphologickych procesech v Cechach.” Acta Univ Carol Geogr 1(2), 22-30.

Kuerbis, R., and Vaid, Y. P. (1988). “Sand sample preparation-the slurry deposition method.” *Soils and Foundations*, 28(4), 107-118.

Kwang, T. (1990). “Improvement of dam filter criterion for cohesionless base soil.” MEng thesis, Asian Institute of Technology, Bangkok, Thailand.

Ladd, R. S. (1978). “Preparing test specimens using undercompaction.” *Geotechnical Testing Journal*, 1(1), 16-23.

Lade, P. V. (1993). “Initiation of Static Instability in the Submarine Nerlerk Berm.” *Canadian Geotechnical Journal*, 30(6), 895-904.

Lade, P. V., and Yamamuro, J. A. (1997). “Effects of nonplastic fines on static liquefaction of sands.” *Canadian Geotechnical Journal*, 34(6), 918-928.

Lafleur, J., Mlynarek, J., and Rollin, A. L. (1989). "Filtration of broadly graded cohesionless soils." *Journal of Geotechnical Engineering*, 115(12), 1747-1768.

Laloui, L., Peron, H., Geiser, F., RIFA'I, A. and Vulliet, L. (2006). "Advances in volume measurement in unsaturated soil triaxial tests." *Soils and Foundations*, 46(3), 341-349.
Lane, E. W. (1934). "Security from under-seepage masonry dams on earth foundations." *Trans*, ASCE, 60(4), 929-966.

Langroudi, M. F., Soroush, A., Shourijeh, P. T., and Shafipour, R. (2013). "Stress transmission in internally unstable gap-graded soils using discrete element modeling." *Powder technology*, 247, 161-171.

Langroudi, M. F., Soroush, A., and Shourijeh, P. T. (2015). "A comparison of micromechanical assessments with internal stability/instability criteria for soils." *Powder Technology*, 276, 66-79.

Le, V. D., Marot, D., Thorel, L., Garnier, J., and Audrain, P. (2010). Centrifuge modelling of an internal erosion mechanism. *Proceedings of the 5th International Conference on Scour and Erosion*, San Francisco, CA, 629-638.

Leong, W. K., Chu, J., and Teh, C. I. (2000). "Liquefaction and instability of a granular fill material." *Geotechnical Testing Journal*, 23(2), 178-192.

Li, M. (2008). "Seepage-induced failure of widely graded cohesionless soils." Doctoral dissertation, Ph. D. thesis, Department of Civil Engineering, The University of British Columbia, Vancouver, BC.

Li, M, and Fannin, R. J. (2008). "Comparison of two criteria for internal stability of granular soil." *Canadian Geotechnical Journal*, 45(9), 1303-1309.

Li, M., and Fannin, R. J. (2011). “A theoretical envelope for internal instability of cohesionless soil.” *Géotechnique*, 62(1), 77-80.

Loban, J. M., Munro, F., and Rae, S. F. (1981). “Two investigations into rock-sample preparations for petrological studies: 1. Thin Sections; 2. Pore Casts.” B.P. Petroleum Development Ltd., unpublished report.

Locke, M., Indraratna, B., and Adikari, G. (2001). “Time-dependent particle transport through granular filters.” *Journal of Geotechnical and Geoenvironmental Engineering*, 127(6), 521-529.

Loudon, A. G. (1952). “The computation of permeability from simple soil tests.” *Geotechnique*, 3(4), 165-183.

Luo, Y. L., Qiao, L., Liu, X. X., Zhan, M. L., and Sheng, J. C. (2013a). “Hydro-mechanical experiments on suffusion under long-term large hydraulic heads.” *Natural hazards*, 65(3), 1361-1377.

Luo, Y., Jin, X., Li, X., Zhan, M. and Sheng, J. (2013b). “A new apparatus for evaluation of contact erosion at the soil–structure interface.” *Geotechnical Testing Journal*, 36(2), 1-8.

Macari, E. J., Parker, J. K. and Costes, N. C. (1997). “Measurement of volume changes in triaxial tests using digital imaging techniques.” *Geotechnical Testing Journal*, 20(1), 103-109.

Maeda, K., Wood, D. M., and Kondo, A. (2012). “Micro and macro modeling of internal erosion and scouring with fine particle dynamics.” *Proceedings of the Sixth International Conference on Scour and Erosion*, Paris, 321-328.

Maeda, K., and Kondo, A. (2014). “Micro and macro modeling of ground depression due to internal erosion.” *Soil Behaviour and Geomechanics*, 445-455.

Mao, C. X. (2005). “Study on piping and filters. Part of Piping.” *Rock and Soil Mechanics*, 26(2), 209-215.

Mao, C. X., Duan, X. B., and WU, L. J. (2009). “Study of critical gradient of piping for various gran sizes in sandy gravels.” *Rock and Soil Mechanics*, 30(12), 3705-3709.

Marot, D., Bendahmane, F., Rosquoët, F., and Alexis, A. (2009). “Internal flow effects on isotropic confined sand-clay mixtures.” *Soil and sediment contamination*, 18(3), 294-306.

Marot, D., Sail, Y., and Alexis, A. (2011a). “Experimental bench for study of internal erosion in cohesionless soils.” *Proceedings of the 5th International Conference on Scour and Erosion*, San Francisco, CA, 418-427.

Marot, D., Bendahmane, F., and Konrad, J. M. (2011b). “Multichannel optical sensor to quantify particle stability under seepage flow.” *Canadian Geotechnical Journal*, 48(12), 1772-1787.

Marot, D., Bendahmane, F., and Nguyen, H. H. (2012a). “Influence of angularity of coarse fraction grains on internal erosion process.” *La Houille Blanche*, 6, 47-53.

Marot, D., Le, V. D., Garnier, J., Thorel, L., and Audrain, P. (2012b). “Study of scale effect in an internal erosion mechanism: centrifuge model and energy analysis.” *European Journal of Environmental and Civil Engineering*, 16(1), 1-19.

Marot, D., Rochim, A., Nguyen, H. H., Bendahmane, F., and Sibille, L. (2016). “Assessing the susceptibility of gap-graded soils to internal erosion: proposition of a new experimental methodology.” *Natural Hazards*, 1-24.

Maurer, B. W., Green, R. A., Cubrinovski, M., and Bradley, B. A. (2015). “Fines-content effects on liquefaction hazard evaluation for infrastructure in Christchurch, New Zealand.” *Journal of Soil Dynamic and Earthquake Engineering*, 76, 58-68.

McDougall, J., Kelly, D., and Barreto, D. (2013). “Particle loss and volume change on dissolution: experimental results and analysis of particle size and amount effects.” *Acta Geotechnica*, 8(6), 619-627.

Mehdizadeh, A., Disfani M. M., Arulrajah A., and Evans R. P. (2015a). “Discussion: On the distinct phenomena of suffusion and suffosion.” *Geotechnique Letter*, 5(3), 129-130. doi: 10.1680/jgele.15.00017.

Mehdizadeh, A., Disfani, M. M., Evans, R. P., Arulrajah, A. and Ong, D. E. L. (2015b). “Discussion: Development of an Internal Camera-Based Volume Determination System for triaxial Testing.” *Geotechnical Testing Journal*, 39(1), 165-168.

Mitchell, J. K. (1993). “Fundamentals of soil behaviour.” John Wiley & Sons, Inc., New York, N.Y., 1-210.

Moffat, R. A., and Fannin, R. J. (2006). “A large permeameter for study of internal stability in cohesionless soils.” *Geotechnical Testing Journal*, 29(4), 273-279.

Moffat, R., and Fannin, R. J. (2011). “A hydromechanical relation governing internal stability of cohesionless soil.” *Canadian Geotechnical Journal*, 48(3), 413-424.

Moffat, R., Fannin, R. J., and Garner, S. J. (2011). “Spatial and temporal progression of internal erosion in cohesionless soil.” *Canadian Geotechnical Journal*, 48(3), 399-412.

Moffat, R., and Herrera, P. (2014). “Hydromechanical model for internal erosion and its relationship with the stress transmitted by the finer soil fraction.” *Acta Geotechnica*, 10(5): 643-650. doi: 10.1007/s11440-014-0326-z.

Moraci, N., Mandaglio, M. C., and Ielo, D. (2014). “Analysis of the internal stability of granular soils using different methods.” *Canadian Geotechnical Journal*, 51(9), 1063-1072.

Mulilis, J. P., Seed, H. B., Chan, C. K., Mitchell J. K., and Arulanandan, K. (1977). “Effects of sample preparation on sand liquefaction.” *Journal of Geotechnical Engineering Division*, ASCE, 103(GT2), 91-108.

Murthy, T. G., Loukidis, D., Carraro, J. A. H., Prezzi, M., and Salgado, R. (2007). “Undrained monotonic response of clean and silty sands.” *Geotechnique*, 57(3), 273-288.

Naeini, S. A., and Baziar, M. H. (2004). “Effect of fines content on steady-state strength of mixed and layered samples of a sand.” *Soil Dynamic and Earthquake Engineering*, 24(3), 181-187.

Nguyen, H. H., Marot, D., and Bendahmane, F. (2012). “Erodibility characterisation for suffusion process in cohesive soil by two types of hydraulic loading.” *La Houille Blanche*, 6, 54-60.

Ni, Q., Tan, T. S., Dasari, G. R., and Hight, D. W. (2004). “Contribution of fines to the compressive strength of mixed soils.” *Géotechnique*, 54(9), 561-569.

Nielsen, B. D. (2004). “Non-destructive soil testing using X-ray computed tomography.” Doctoral dissertation, Montana State University-Bozeman, College of Engineering.

Olson, S. M., Stark, T. D., Walton, W. H., and Castro, G. (2000). “1907 static liquefaction flow failure of the North Dike of Wachusett Dam.” *Journal of Geotechnical and Geoenvironmental Engineering*, 126(12), 1184-1193.

O'Reilly, M. P., and Brown, S. F. (1991). “Cyclic loading of soils: from theory to design.” 1-18. Glasgow, UK: Blackie.

Ouyang, M., and Takahashi, A. (2015a). “Influence of initial fines content on fabric of soils subjected to internal erosion.” *Canadian Geotechnical Journal*, 53(2), 299-313.

Ouyang, M., and Takahashi, A. (2015b). “Optical quantification of suffosion in plane strain physical models.” *Géotechnique Letters*, 5(3), 118-122.

Palmer, S. N. and Barton, M. E. (1986). “Avoiding micro fabric disruption during the impregnation of friable, uncemented sands with dyed epoxy.” *Journal of Sedimentary Petrology*, 56(4), 556-557.

Pavlov, A. P. (1898). “Concerning the contour of plains and its change under the influence of the action of subterranean and surface waters.” *Zemlevedeniye*, 5, 91-147.

Pitman, T. D., Robertson, P. K., and Sego, D. C. (1994). “Influence of fines on the collapse of loose sands.” *Canadian Geotechnical Journal*, 31(5), 728-739.

Qadimi, A., and Mohammadi, A. (2014). “Evaluation of state indices in predicting the cyclic and monotonic strength of sands with different fines contents.” *Journal of Soil Dynamic and Earthquake Engineering*, 66, 443-458.

Rahman, M. M., and Lo, S. R. (2007). “On intergranular void ratio of loose sand with small amount of fines.” *16th South East Asian geotechnical conference*, Kuala Lumpur, Malaysia, 255-260.

Rahman, M. M., Lo, S. R., and Gnanendran, C.T. (2008). “On equivalent granular void ratio and steady state behaviour of loose sand with fines.” *Canadian Geotechnical Journal*, 45(10), 1439-1455. doi:10.1139/T08-064.

Rahman, M. M., Lo, S. R., and Baki, M. A. L. (2011). “Equivalent granular state parameter and undrained behaviour of sand–fines mixtures.” *Acta Geotechnica*, 6(4), 183-194. doi: 10.1007/s11440-011-0145-4.

Razavi, M. R., Muhunthan, B., and Al Hattamleh, O. (2007). “Representative elementary volume analysis of sands using X-ray computed tomography.” *Geotechnical Testing Journal*, 30(3), 212-219.

Reboul, N., Vincens, E., and Cambou, B. (2010). “A computational procedure to assess the distribution of constriction sizes for an assembly of spheres.” *Computers and Geotechnics*, 37(1), 195-206.

Reddi, L. N., Lee, I., and Bonala, M. V. S. (2000). “Comparison of internal and surface erosion using flow pump test on a sand-kaolinite mixture.” *Geotechnical Testing Journal*, 23, 116-122.

Rice, J., and Swainston-Fleshman, M. (2013). “Laboratory modeling of critical hydraulic conditions for the initiation of piping.” *Geo-Congress 2013: Stability and Performance of Slopes and Embankments III*, 1044-1055.

Richards, K. S. and Reddy, K. R. (2007). “Critical appraisal of piping phenomena in earth dams.” *Bulletin of Engineering Geology and the Environment*, 66(4), 381-402.

Richards, K. S., and Reddy, K. R., (2008). “Experimental investigation of piping potential in earthen structures.” *Geotechnical Special Publication*, 178, 367-376.

Richards, K. S., and Reddy, K. R. (2009). “True triaxial piping test apparatus for evaluation of piping potential in earth structures.” *Geotechnical Testing Journal*, 33(1), 83-95.

Richards, K. S., and Reddy, K. R. (2012). “Experimental investigation of initiation of backward erosion piping in soils.” *Geotechnique*, 62(10), 933-942.

Robertson, P. K., and Campanella, R. G. (1985). “Liquefaction potential of sands using the CPT.” *Journal of Geotechnical Engineering*, 111(3), 384-403.

Romero, E., Facio, J. A., Lloret, A., Gens, A. and Alonso, E. E. (1997). “A new suction and temperature controlled triaxial apparatus.” *Proceedings of 14th ICSMFE*, Hamburg, 185-188.

Rönnqvist, H., and Viklander, P. (2014). “On the Kenney-Lau approach to internal stability evaluation of soils.” *Geomaterials*, 4(4), 129.

Rönnqvist, H., and Viklander, P. (2016). “A unified-plot approach for the assessment of internal erosion in embankment dams.” *International Journal of Geotechnical Engineering*, 10(1), 66-80.

Sadrekarimi, A. (2013). “Influence of fines content on liquefied strength of silty sands.” *Journal of Soil Dynamic and Earthquake Engineering*, 55, 108-119.

Sail, Y., Marot, D., Sibille, L., and Alexis, A. (2011). “Suffusion tests on cohesionless granular matter: Experimental study.” *European Journal of Environmental and Civil Engineering*, 15(5), 799-817.

Salazar, S. E., Barnes, A., and Coffman, R. A. (2015). “Development of an internal camera-based volume determination system for triaxial testing.” *Geotechnical Testing Journal*, 38(4), 1-7.

Salazar, S. E. and Coffman, R. A. (2015). “Consideration of internal board camera optics for triaxial testing applications.” *Geotechnical Testing Journal*, 38(1), 40-49.

Salehi Sadaghiani, M. R., and Witt, K. J. (2012). “Analysis of internal stability of widely graded soils based on identification of mobile particles.” *Proceedings of the Sixth International Conference on Scour and Erosion*, ICSE 6-049, Paris, August 27-31.

Salgado, R., Bandini, P., and Karim, A. (2000). “Shear strength and stiffness of silty sand.” *Journal of Geotechnical and Geoenvironmental Engineering*, 126(5), 451-462.

Santamarina, J. C., and Cho, G. C. (2004). “Soil behaviour: The role of particle shape.” *Advances in geotechnical engineering: The Skempton Conference*, R. J.Jardine, D. M.Potts, and K. G.Higgins, eds., Vol. 1, Thomas Telford, London, 604-617.

Sari, H., Chareyre, B., Catalano, E., Philippe, P., and Vincens, E. (2011). “Investigation of internal erosion processes using a coupled dem-fluid method.” *II International Conference on Particle-based Methods - Fundamentals and Applications*, Eugenio Oñate, Roger Owen (eds), Barcelona, Spain, 1-11.

Scheuermann, A., and Kiefer, J. (2010). “Internal erosion of granular materials– Identification of erodible fine particles as a basis for numerical calculations.” *9th HSTAM international congress on mechanics Vardoulakis mini-symposia Limassol*, Cyprus, 275-282.

Scholtès, L., Hicher, P. Y., and Sibille, L. (2010). “Multiscale approaches to describe mechanical responses induced by particle removal in granular materials.” *Comptes Rendus Mécanique*, 338(10), 627-638.

Seed, H. B., Idriss, I. M., and Arango, I. (1983). “Evaluation of liquefaction potential using field performance data.” *Journal of Geotechnical Engineering*, 109(3), 458-482.

Seghir, A., Benamar, A., and Wang, H. (2014). “Effects of fine particles on the suffusion of cohesionless soils. Experiments and modelling.” *Transport in Porous Media*, 103(2), 233-247.

Sellmeijer, J. B. (1988). “On the mechanism of piping under impervious structures.” PhD thesis, Delft University of Technology.

Semar, O., Witt, K. J., Fannin, R. J., Burns, S. E., Bhatia, S. K., Avila, C. M. C., and Hunt, B. E. (2011). “Suffusion evaluation-comparison of current approaches.” *Proceedings of the 5th International Conference on Scour and Erosion*, San Francisco, CA, 251-262.

Sherard, J. L., Woodward, R. J., Gizienski, S. F., and Clevenger, W. A. (1963). “Earth and earth-rock dams, engineering problems of design and construction.” Wiley, New York, 114-130.

Sherard, J. L. (1979). “Sinkholes in dams of coarse, broadly graded soils.” *Transactions, 13th International Congress on Large Dams*, New Delhi, India, 2, 25-35.

Sherard, J. L., Dunnigan, L. P., and Talbot, J. R. (1984). “Basic properties of sand and gravel filters.” *Journal of Geotechnical Engineering*, 110(6), 684-700.

Shire, T., and O’Sullivan, C. (2013). “Micromechanical assessment of an internal stability criterion.” *Acta Geotechnica*, 8(1), 81-90.

Shire, T., O’Sullivan, C., Hanley, K. J., and Fannin, R. J. (2014). “Fabric and effective stress distribution in internally unstable soils.” *Journal of Geotechnical and Geoenvironmental Engineering*, 140(12), 04014072. doi: 10.1061/(ASCE)GT.1943-5606.0001184.

Shire, T., O’Sullivan, C., and Hanley, K. J. (2016). “The influence of fines content and size-ratio on the micro-scale properties of dense bimodal material.” *Granular Matterials*, doi:10.1007/s10035-016-0654-9.

Shwiyhat, N., and Xiao, M. (2010). "Effect of suffusion on mechanical characteristics of sand." *Proceedings of the 5th International Conference on Scour and Erosion*, San Francisco, CA, 378-386.

Sibille, L., Marot, D., and and Sail, Y. (2015). "A description of internal erosion by suffusion and induced settlements on cohesionless granular matter." *Acta Geotechnica*, 10(6), 735-748.

Skempton, A. W., and Brogan, J. M. (1994). "Experiments on piping in sandy gravels." *Geotechnique*, 44(3), 449-460.

Sterpi, D. (2003). "Effects of the erosion and transport of fine particles due to seepage flow." *International Journal of Geomechanics*, 3(1), 111-122.

Standards Australia (1993). "Geotechnical site investigations." Australian Standard 1726 Australian Standard, Sydney, Australia.

Standards Australia (1996). "Method for sampling and testing aggregates - Particle size distribution by sieving." Australian Standard 1141.11." Australian Standard, Sydney, Australia.

Stevens, J. (1982). "Unified soil classification system." *Civil Engineering*, ASCE, 52(12), 61-62.

Stewart, M. L., Ward, A. L., Rector, D. R. (2006). "A study of pore geometry effects on anisotropy in hydraulic permeability using the lattice-Boltzmann method." *Advances in water resources*, 2(9), 1328-1340.

Sun, B. C. B. (1989). "Internal stability of clayey to silty sands." PhD Thesis, Department of Civil Engineering, University of Michigan.

Tanaka, T., and Toyokuni, E. (1991). "Seepage-failure experiments on multi-layered sand columns: Effects of flow conditions and residual effective stress on seepage-failure phenomena." *Soils and Foundations*, 31(4), 13-36.

Tatsuoka, F., Iwasaki, T., Tokida, K., Yasuda, S., Hirose, M., Tsuneo, I., and Konno, M. (1980). "Standard penetration tests and soil liquefaction potential evaluation." *Soils and Foundations*, 20(4), 95-111.

Taylor, H. F., O'Sullivan, C., and Sim, W. W. (2015). "A new method to identify void constrictions in micro-CT images of sand." *Computers and Geotechnics*, 69, 279-290.

Terzaghi, K. (1925). "Erdbaumechanik." Franz Deuticke, Vienna.

Terzaghi, K. (1939). "Soil mechanics: a new chapter in engineering science." *Journal of the institution of Civil Engineers*, 12, 106-141.

Terzaghi, K. (1943). "Theoretical soil mechanics." Wiley, New York.

Thevanayagam, S., Ravishankar, K., and Mohan, S. (1997). "Effects of fines on monotonic undrained shear strength of sandy soils." *Geotechnical Testing Journal*, 20(4), 394-406.

Thevanayagam, S. (1998). "Effect of fines and confining stress on undrained shear strength of silty sands." *Journal of Geotechnical and Geoenvironmental Engineering*, 124(6), 479-491.

Thevanayagam, S. (2000). "Liquefaction potential and undrained fragility of silty soils." *Proceedings of 12th world conference on earthquake engineering*, Auckland, New Zealand.

Thevanayagam, S., and Mohan, S. (2000). “Intergranular state variables and stress–strain behaviour of silty sands.” *Geotechnique*, 50(1), 1-23.

Thevanayagam, S., Fiorillo, M., and Liang, J. (2000). “Effects of non-plastic fines on undrained cyclic strength of silty sands.” *Geotechnical Special Publication*, 77-91, doi: 10.1061/40520(295)6.

Thevanayagam, S. (2001). “Role of intergranular contacts on mechanisms causing liquefaction and slope failures in silty sands.” Annual project summary report, USGS Award Number: 01HQGR0032. US Geological Survey, Department of Interior, USA.

Thevanayagam, S., Shenthan, T., Mohan, S., and Liang, J. (2002). “Undrained fragility of clean sands, silty sands, and sandy silts. *Journal of Geotechnical and Geoenvironmental Engineering*, 128(10), 849-859.

Thevanayagam, S. (2007). “Intergrain contact density indices for granular mixes—I: Framework.” *Earthquake engineering and engineering vibration*, 6(2), 123-134.

To, H. D., Torres, S. A. G., and Scheuermann, A. (2015a). “Primary fabric fraction analysis of granular soils.” *Acta Geotechnica*, 10(3), 375-387.

To, H. D., Scheuermann, A., and Galindo-Torres, S. A. (2015b). “Probability of transportation of loose particles in suffusion assessment by self-Filtration criteria.” *Journal of Geotechnical and Geoenvironmental Engineering*, 142(2), 04015078, doi: 10.1061/(ASCE)GT.1943-5606.0001403.

Tokimatsu, K., and Yoshimi, Y. (1983). “Empirical correlation of soil liquefaction based on SPT n-value and fines content.” *Soils and Foundations*, 23(4), 57-74.

Uchaipichat, A., Khalili, N. and Zargarbashi, S. (2011). “A temperature controlled triaxial apparatus for testing unsaturated soils.” *Geotechnical Testing Journal*, 34(5), 424-432.

U.S. Army Corps of Engineers, (1953). “Filter experiments and design criteria.” Technical Memorandum No. 3-360, Waterways Experiment Station, Vicksburg, MS.

Vaid, Y. P. (1994). “Liquefaction of silty soils.” Ground failures under seismic conditions. *Geotechnical Special Publication*, 44, 1-16.

Vallejo, L. E. (2001). “Interpretation of the limits in shear strength in binary granular mixtures.” *Canadian Geotechnical Journal*, 38(5), 1097-1104.

Van Beek, V. M. (2015). “Backward erosion piping: initiation and progression.” Doctoral dissertation, TU Delft, Delft University of Technology.

Vincens, E., Witt, K. J., and Homberg, U. (2015). “Approaches to determine the constriction size distribution for understanding filtration phenomena in granular materials.” *Acta Geotechnica*, 10(3), 291-303.

Von Thun, J. (1985). “Application of statistical data from dam failures and accidents to risk-based decision analysis on existing dams.” US Bureau of Reclamation.

Wan, R. G., and Guo, P. J. (2001). “Effect of microstructure on undrained behaviour of sands.” *Canadian Geotechnical Journal*, 38(1), 16-28.

Wan, C. F., and Fell, R. (2004). “Experimental investigation of internal instability of soils in embankment dams and their foundations.” UNICIV Rep. No. R 429, The Univ. of New South Wales, Sydney, Australia.

Wan, C. F., and Fell, R. (2007). “Investigation of internal erosion by the process of suffusion in embankment dams and their foundations.” In Fell R., Fry J.J. (eds), *Internal Erosion of Dams and their Foundations*, Taylor and Francis, London, 219-234.

Wan, C. F., and Fell, R. (2008). “Assessing the potential of internal instability and suffusion in embankment dams and their foundations.” *Journal of Geotechnical and*

Geoenvironmental Engineering, 134(3), 401-407, doi: 10.1061/(ASCE)1090b 0241(2008)134:3(401) .

Wang, L. B., Frost, J. D., and Lai, J. S. (2004). “Three-dimensional digital representation of granular material microstructure from X-ray tomography imaging.” *Journal of Computing in Civil Engineering*, 18(1), 28-35.

Wang, L., Park, J. Y., and Fu, Y. (2007). “Representation of real particles for DEM simulation using X-ray tomography.” *Construction and Building Materials*, 21(2), 338-346.

Wang, Y., and Ni, X. (2013). “Hydro-mechanical analysis of piping erosion based on similarity criterion at micro-level by PFC3D.” *European Journal of Environmental and Civil Engineering*, 17(sup1), 187-204.

Wang, S., Chen, J. S., Luo, Y. L., and Sheng, J. C. (2014). “Experiments on internal erosion in sandy gravel foundations containing a suspended cutoff wall under complex stress states.” *Natural hazards*, 74(2), 1163-1178.

Wang, X., and Li, J. (2015). “On the degradation of granular materials due to internal erosion.” *Acta Mechanica*, 31(5), 685-697.

Wang, Y., and Dallo, Y. A. (2015) “Discussion of “Fabric and effective stress distribution in lnternally unstable soils.” *Journal of Geotechnical and Geoenvironmental Engineering*, doi: 10.1061/(ASCE)GT.1943-5606.0001184.

White, D. J., Take, W. A. and Bolton, M. D. (2003). “Soil deformation measurement using particle image velocimetry (PIV) and photogrammetry.” *Geotechnique*, 53(7), 619-632.

Wichtmann, T., Hernández, M. N., and Triantafyllidis, T. “On the influence of a non-cohesive fines content on small strain stiffness, modulus degradation and damping of quartz sand.” *Journal of Soil Dynamic and Earthquake Engineering*, 69, 103-114.

Wood, D. M., Maeda, K., and Nukudani, E. (2010). “Modelling mechanical consequences of erosion.” *Geotechnique*, 60(6), 447-457.

Wu, L., Nzouapet, B. N., Vincens, E., Bernat-Minana, S. (2012). “Laboratory experiments and the determination of the constriction size distribution of granular filters.” *Proceedings of the Sixth International Conference on Scour and Erosion*, Paris, 233-240.

Xenaki, V. C., and Athanasopoulos, G. A. (2003). “Liquefaction resistance of sand–silt mixtures: an experimental investigation of the effect of fines.” *Journal of Soil Dynamic and Earthquake Engineering*, 23(3), 1-12.

Xiao, M., and Shwiyhat, N. (2012). “Experimental investigation of the effects of suffusion on physical and geomechanic characteristics of sandy soils.” *Geotechnical Testing Journal*, 35(6), 890-900.

Yamamuro, J. A., Wood, F. M., and Lade, P. V. (2008). “Effect of depositional method on the microstructure of silty sand.” *Canadian Geotechnical Journal*, 45(11), 1538-1555.

Yang, S. L., Lacasse, S., and Sandven, R. F. (2006). “Determination of the transitional fines content of mixtures of sand and non-plastic fines.” *Geotechnical Testing Journal*, 29(2), 102-107.

Yin, Z., and Hicher, P. Y. (2013). “Modeling the impact of internal erosion on the behaviour of silty sand.” *Poromechanics V: Proceedings of the Fifth Biot Conference on Poromechanics*, 2023-2031.

Yoshimine, M., and Ishihara, K. (1998). "Flow potential of sand during liquefaction." *Soils and Foundations*, 38(3), 189-198.

Zhang, X., Li, L., Chen, G. and Lytton, R. (2015). "A photogrammetry-based method to measure total and local volume changes of unsaturated soils during triaxial testing." *Acta Geotechnica*, 10(1), 55-82.

Zlatovic, S., and Ishihara, K. (1995). "On the influence of nonplastic fines on residual strength." *Proceedings of 1st International Conference on Earthquake Geotechnical Engineering*, Balkema, Rotterdam, The Netherlands, 239-244.

Zlatovic, S., and Ishihara, K. (1997). "Normalized behaviour of very loose non-plastic soils: effects of fabric." *Soils and Foundations*, 37(4), 47-56.

APPENDIX A: Matlab Code for Photogrammetry

```
Filename = input ('Filename: ', 's');
Output_file = [Filename,'e.jpg']
Filename = [Filename,'.jpg']
I = imread (Filename);
I3=im2bw (I,0.5);
Imshow (I3);
impixelinfo
I3 (:,1:left edge)=0;
I3 (:,right edge:6000)=0;
Imshow (I3);
Imwrite (I3,Output_file,'BitDepth',8);
save var
```

```
Filename = input('Filename: ', 's');
Filename = [Filename,'e.bmp']
Image = imread(Filename);
Size = size(image);
yt = input ('Top row:');
yb = input ('Bottom row:');
initial_pixel =input ('Number of pixels of initial sample:');
initial_volume = input ('Initial sample volume, cc :');
for I = yt : yb
   s=0;
   e=0;
   for j = 1:Size(2)
      if image(i,j)>0
         if s == 0
            s = j;
         else
         e = j;
         end
       end
    end
    v(i) = e-s+1;
    disp (v(i));
end
```

```
for k = yt : yb
   V3D(k) = v(k)^2*3.14/4;
end
Vol = V3D(yt : yb);
Volume = sum(Vol);
Disp ('Number of pixels occupied by sample='), disp(Volume)
Sample_Volume = (Volume / initial_pixel)*initial_volume
Disp ('Sample volume='), disp (Sample_Volume)
Volume_strain = -1*(Sample_Volume-initial_volume) / initial_volume*100;
Disp ('Volumetric Strain (%)='), disp (Volume_strain
```

APPENDIX B: Apparatus Fabrication Drawings

Sheet No.	Title	Page No.
1	Top View of Cell Base	
2	Top View of 50 mm Pedestal, Plate and cell Base	
3	Top View of 100 mm Pedestal, Plate and cell Base	
4	Bottom View of Cell Base	
5	Section 0-0 (Cell Base)	
6	Section 1-1 (Cell Base)	
7	Sections 2-2 and 3-3 (Cell Base)	
8	Sections A-A, B-B and C-C (Cell Base)	
9	O-rings	
10	Pedestal 100 and 50 mm	
11	Pedestal 75 mm	
12	Pedestal Bottom Plate	
13	Top Caps 100 and 50 mm	
14	Plate B	
15	Top Cap 75 mm	
16	Collection System	
17	Balance Section	
18	Funnel Section	
19	Collection System Pedestal	
20	Top View of Frame Pedestal	
21	Section D-D of Frame Pedestal	
22	Side View of Frame Pedestal	
23	3D View of Collection System	
24	3D View of Base Plate	
25	3D View of Top Cap	
26	3D View of Bottom Pedestal	
27	3D View of Frame Pedestal	

- All fittings and O-rings will be provided.

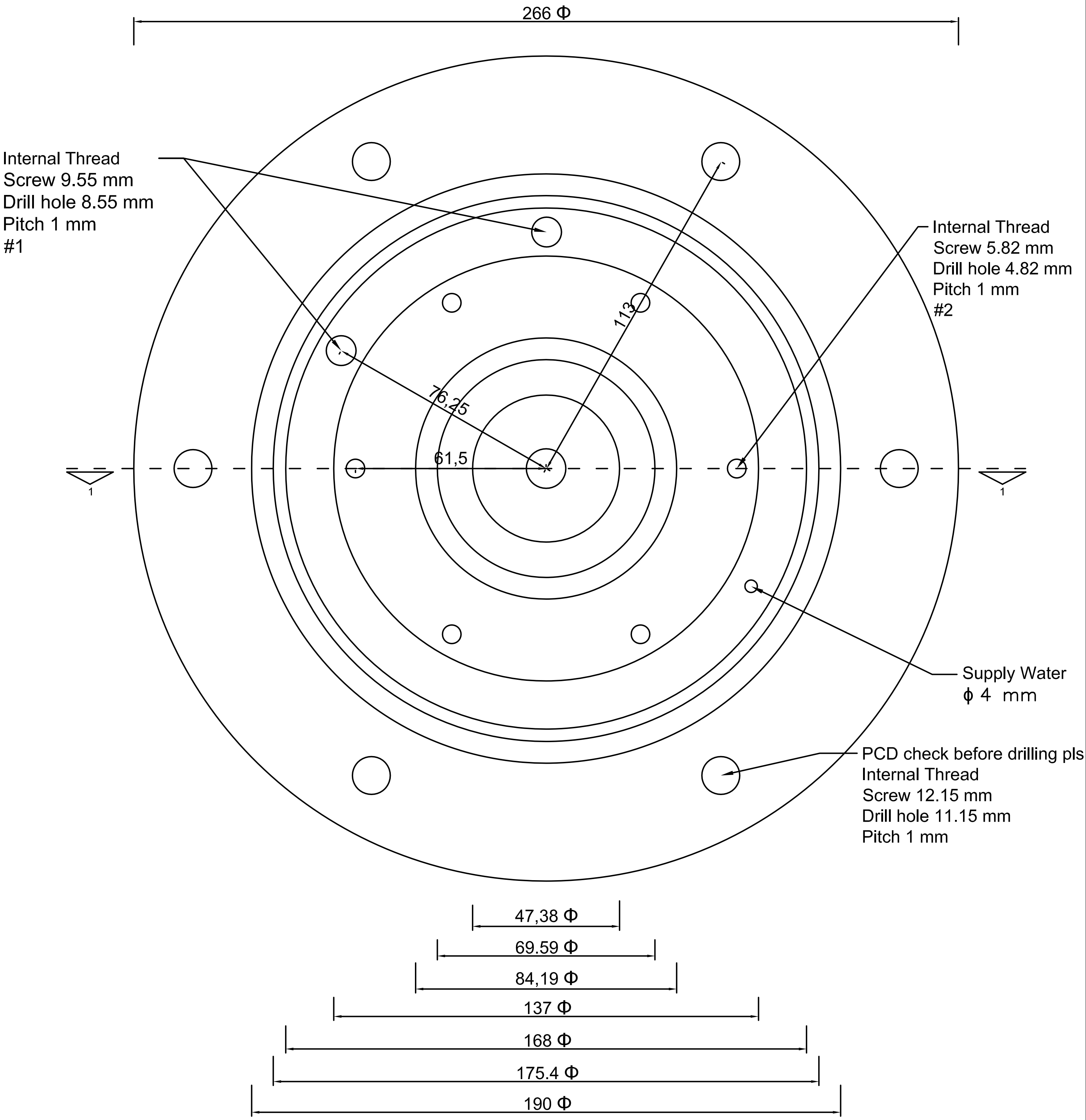

Title: Top View of Cell base	Rev.01-23-03-15	Material No.: 1	Sheet: 1	Unit: mm

- All fittings and O-rings will be provided.

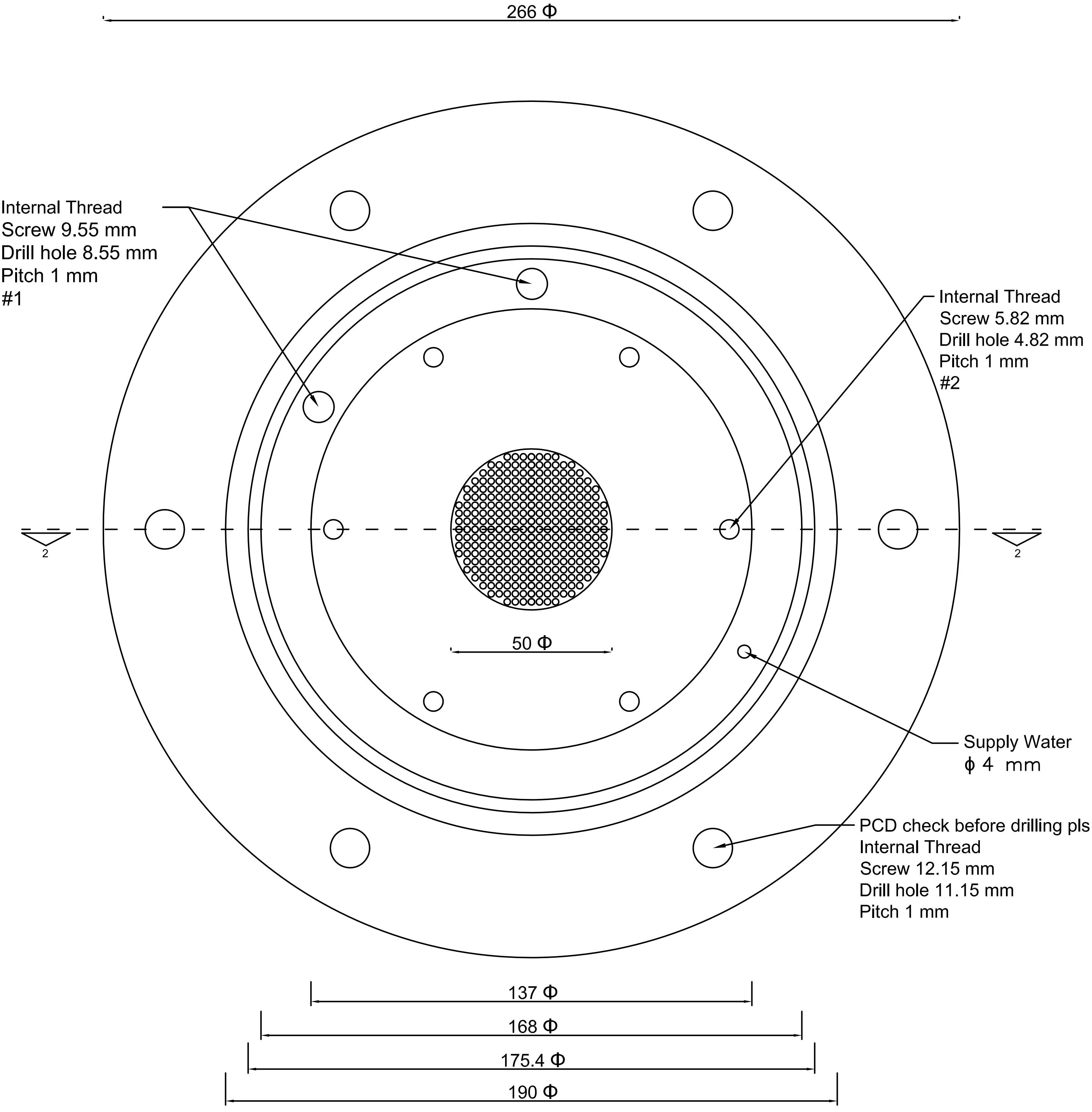

Title: Top View of 50 mm Pedestal, Plate and Cell base	Rev.01-23-03-15		Sheet: 2	Unit: mm

- All fittings and O-rings will be provided.

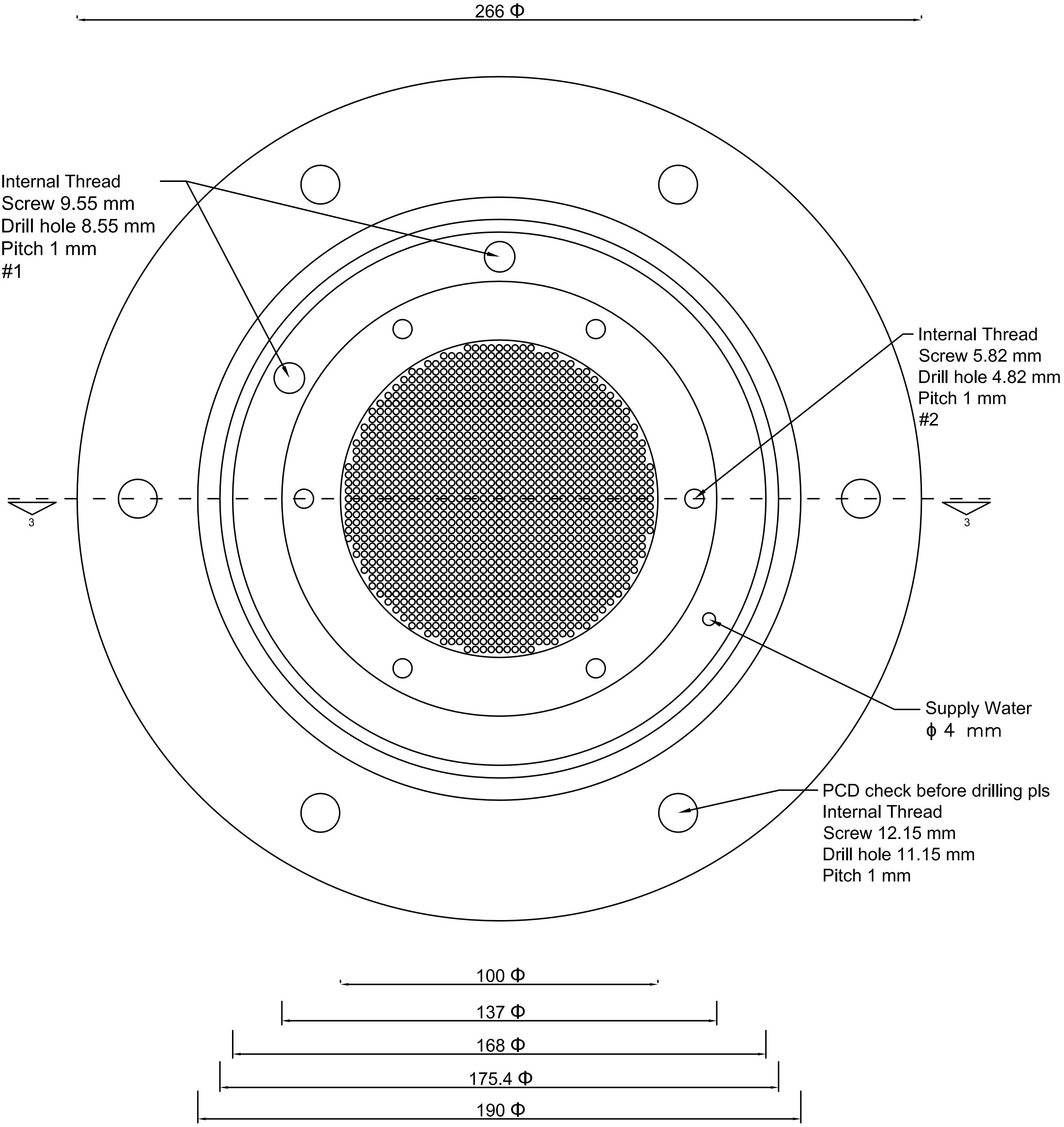

Title: Top View of 100 mm Pedestal, Plate and Cell base	Rev.01-23-03-15		Sheet: 3	Unit: mm

- All fittings and O-rings will be provided.

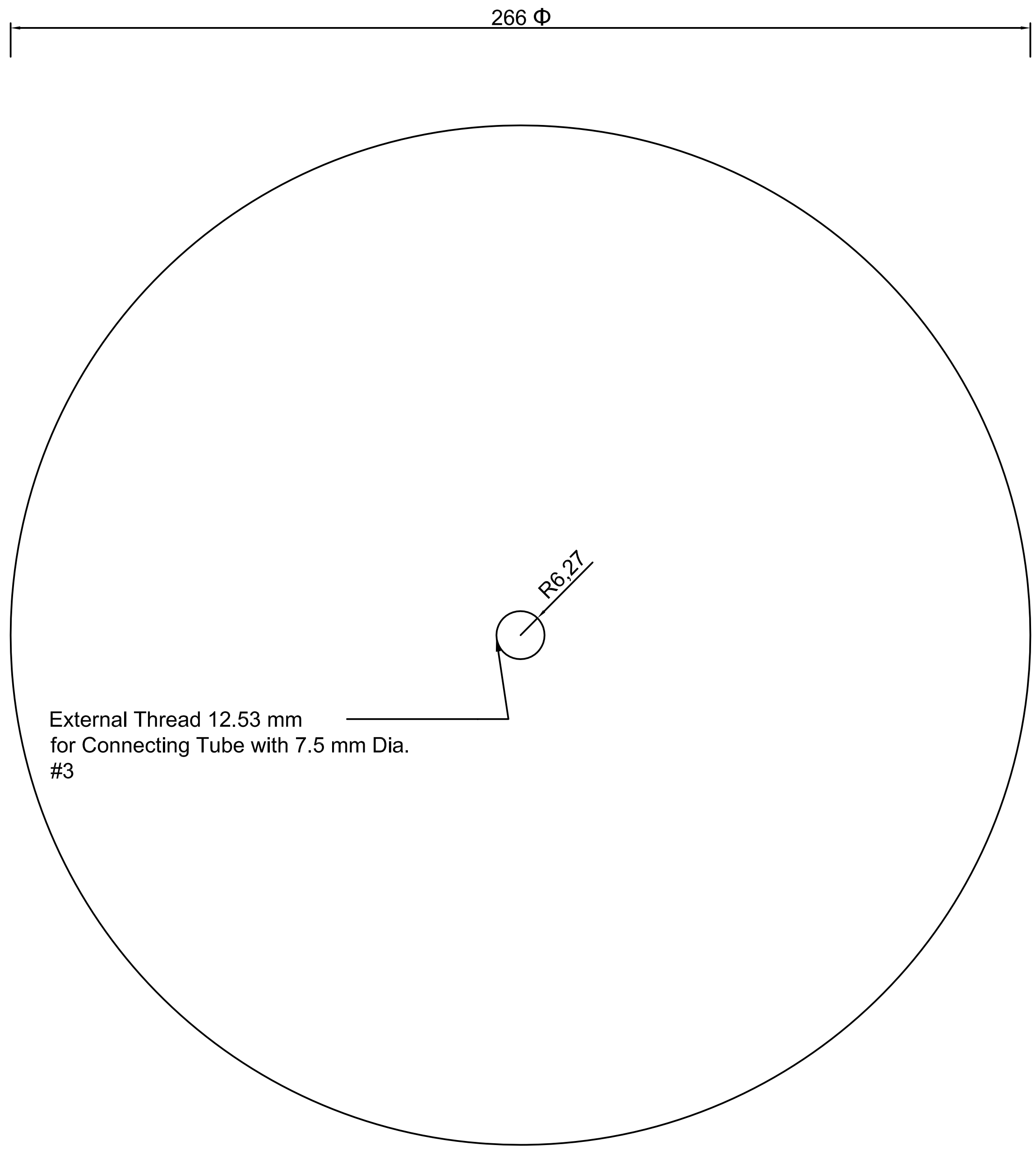

Title: Bottom View of Cell base	Rev.01-23-03-15	Material No.: 1	Sheet: 4	Unit: mm

- All fittings and O-rings will be provided.

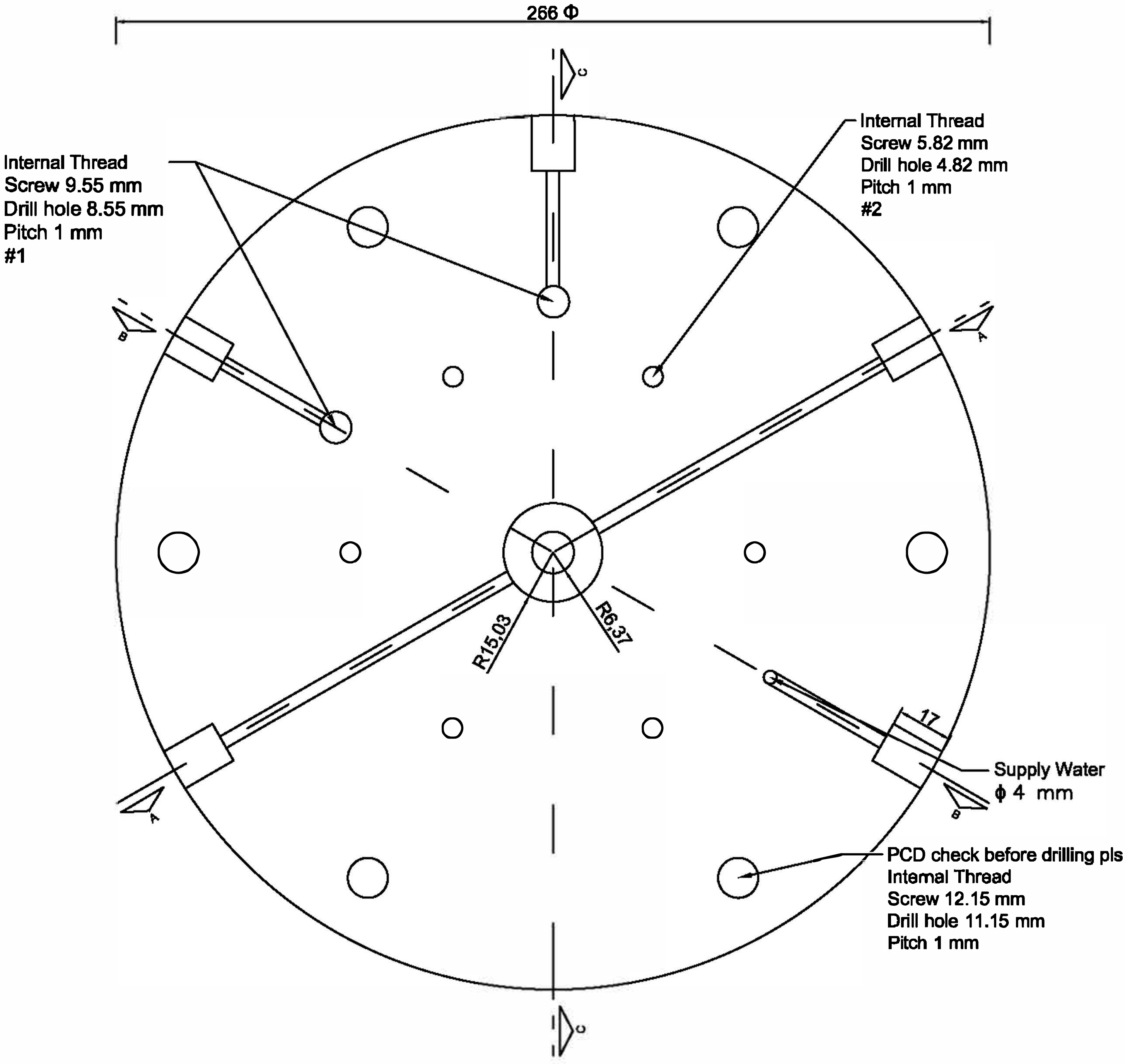

Title: Section O-O	Rev.01-23-03-15	Material No.: 1	Sheet: 5	Unit: mm

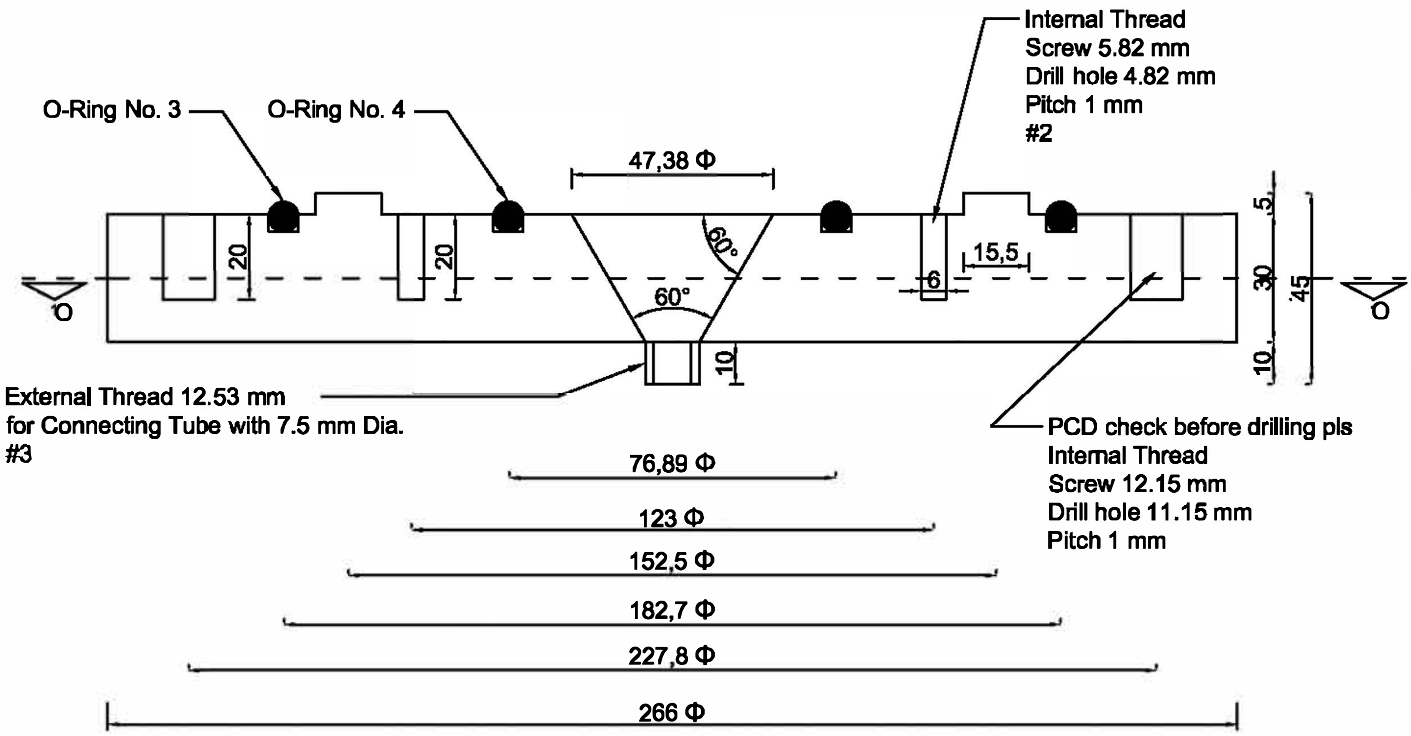

Section 1-1

Title: Section1-1	Rev.01-23-03-15	Material No.: 1	Sheet: 6	Unit: mm

- All fittings and O-rings will be provided.

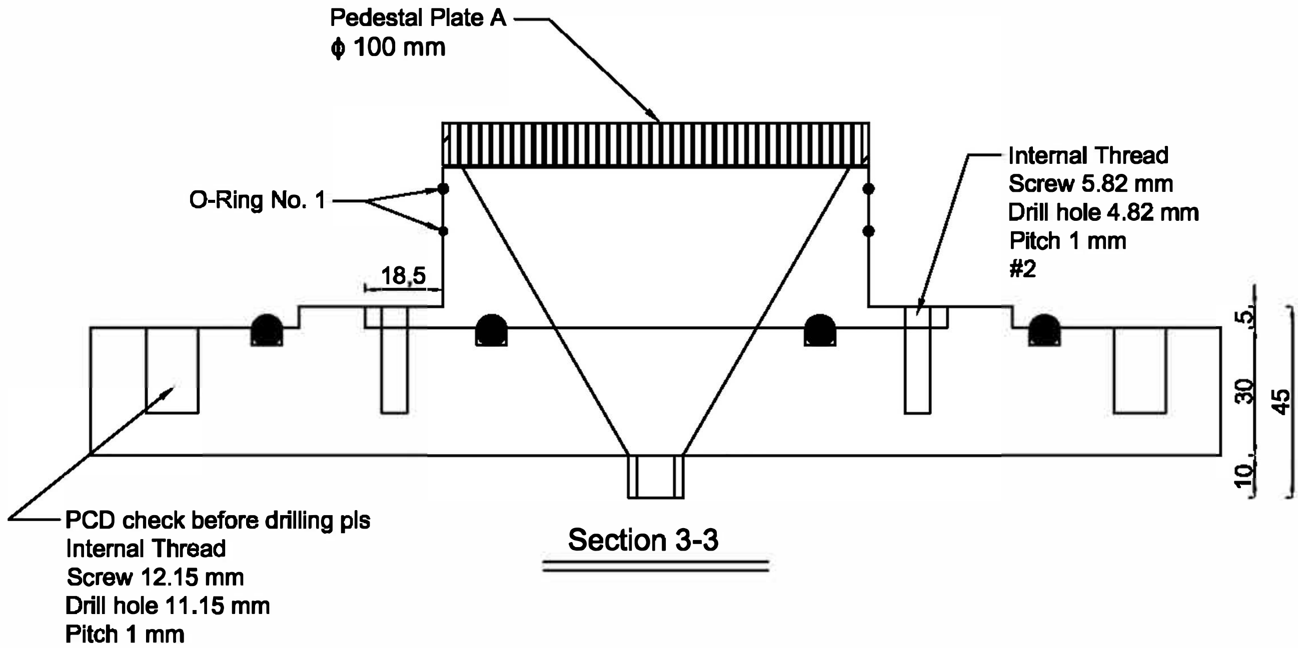

Section 3-3

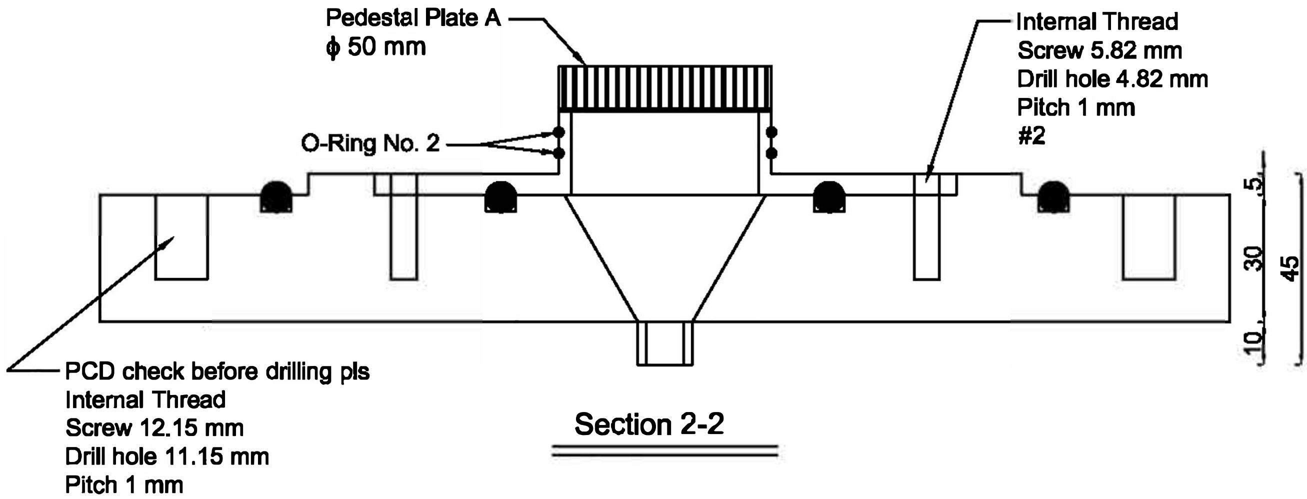

Section 2-2

Title: Sections 2-2 and 3-3	Rev.01-23-03-15	Sheet: 7	Unit: mm

- All fittings and O-rings will be provided.

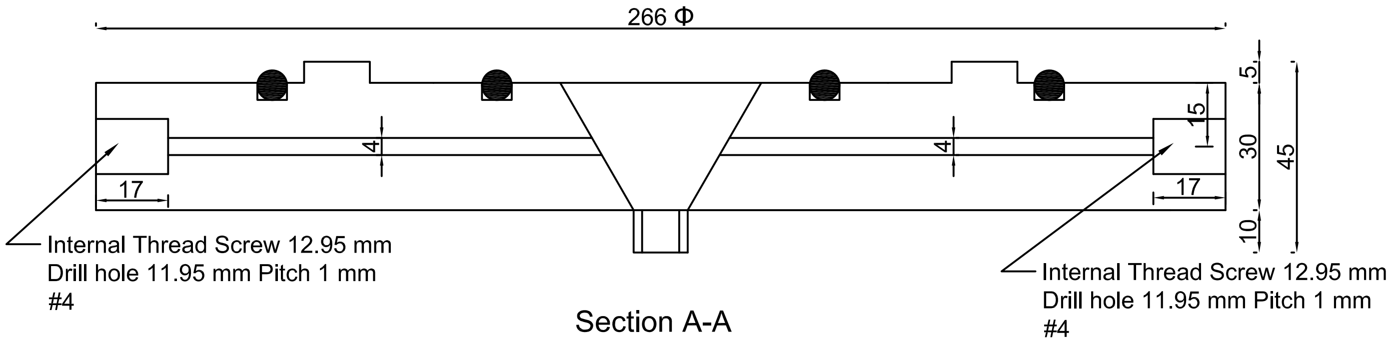

Section A-A

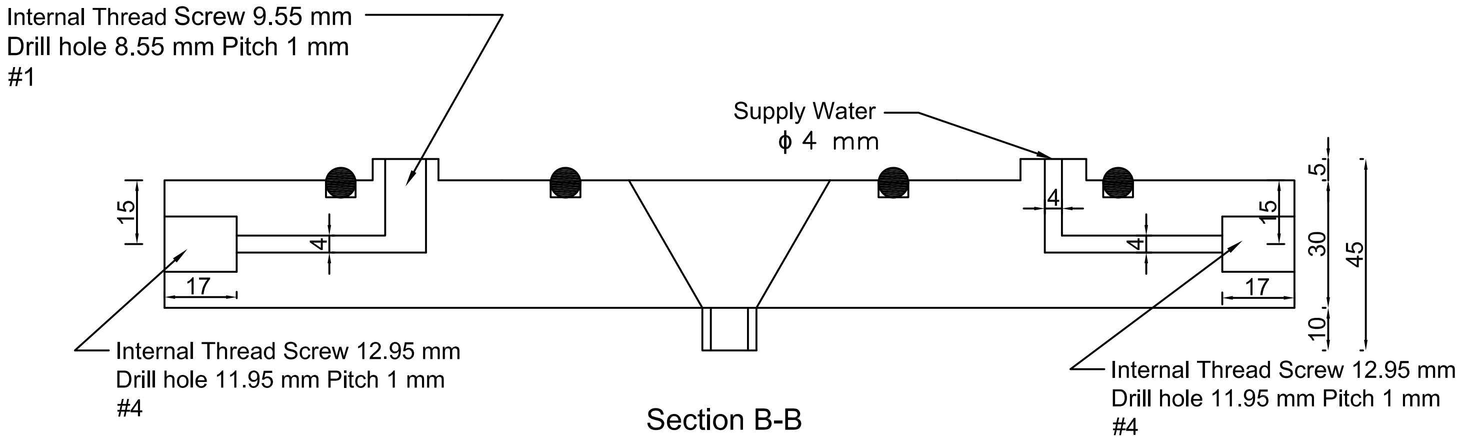

Section B-B

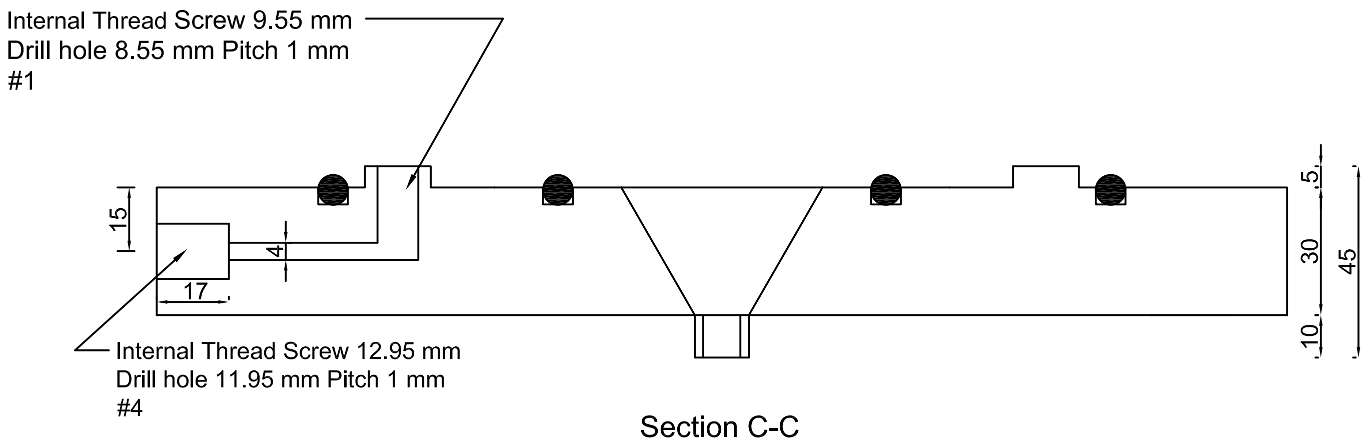

Section C-C

Title: Section A-A, B-B and C-C	Rev.01-23-03-15	Material No.: 1	Sheet: 8	Unit: mm

- All fittings and O-rings will be provided.

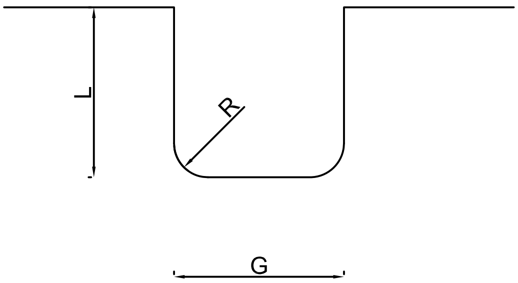

O-rings No.	Series No.	I.D (mm)	Tol. +/-	Width (mm)	L (mm)	G (mm)	R (mm)
No. 1	2.240	94.84	0.71	3.53	2	4	1
No. 2	2.224	44.04	0.46	3.53	1.5	3.5	1
No. 3	2.365	177.17	1.02	5.33	4.4	7.3	1.2
No. 4	2.335	69.22	0.51	5.33	4.4	7.3	1.2

Title: O-rings	Rev.01-23-03-15	Sheet: 9	Unit: mm

- All fittings and O-rings will be provided.
- Please make first the pedestal 100 mm.

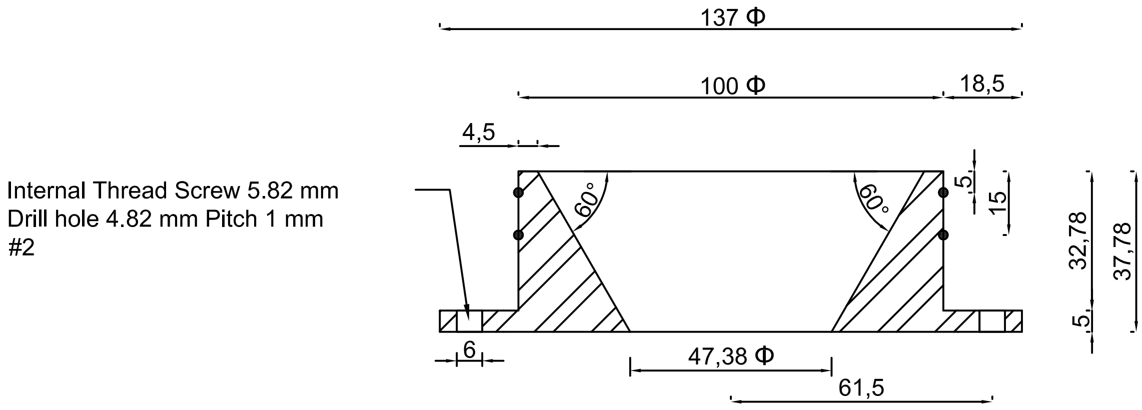

Pedestal 100 mm

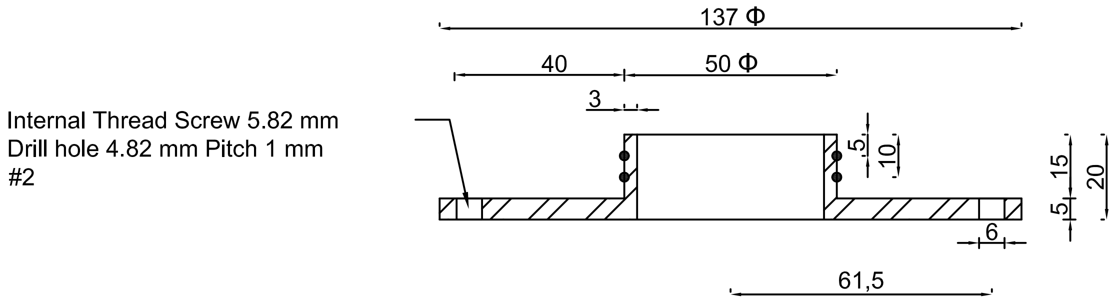

Pedestal 50 mm

Title: Pedestal 100 and 50 mm	Rev.01-23-03-15	Material No.: 2	Sheet: 10	Unit: mm

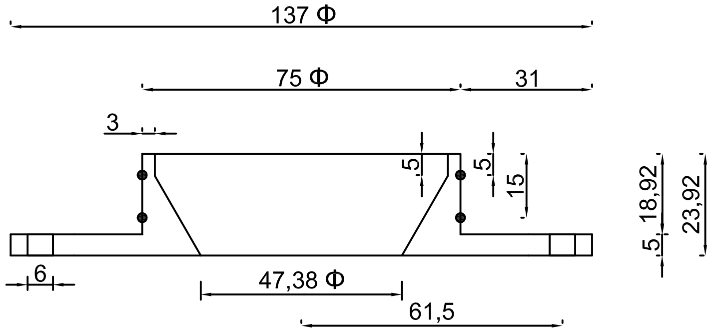

Pedestal 75 mm

Title: Pedestal 75 mm	Rev.01-23-03-15	Material No.: 2	Sheet: 11	Unit: mm

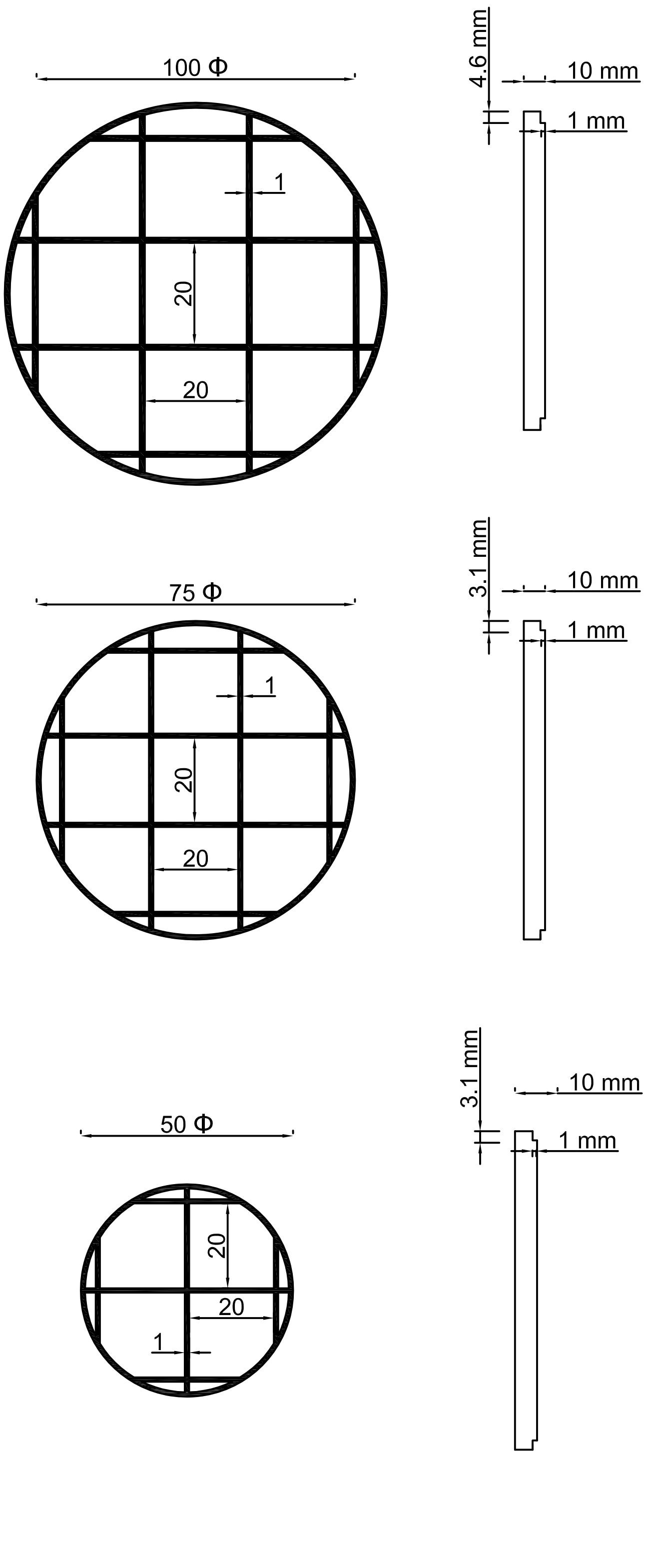

Title: Pedestal Bottom Plate	Rev.01-23-03-15	Material No.: 3	Sheet: 12	Unit: mm

- All fittings and O-rings will be provided.

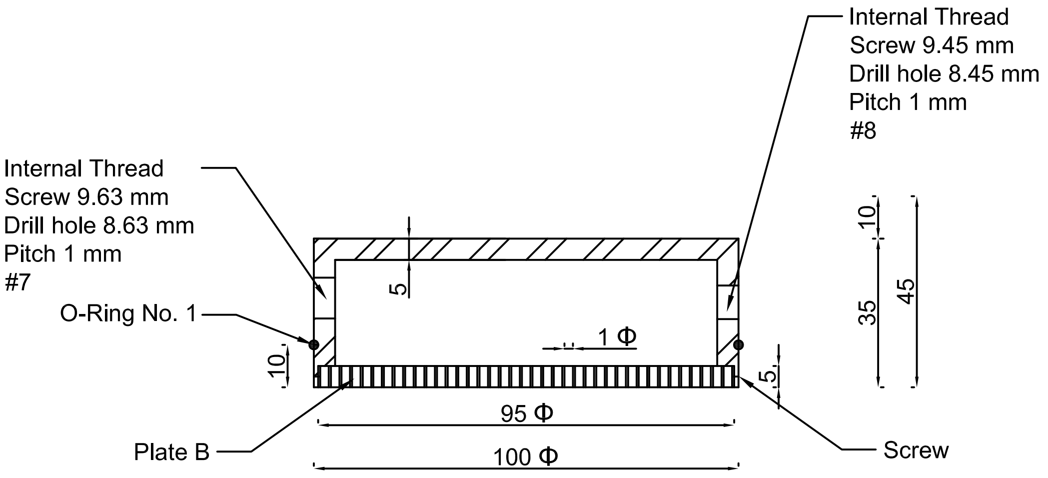

Top Cap 100 mm

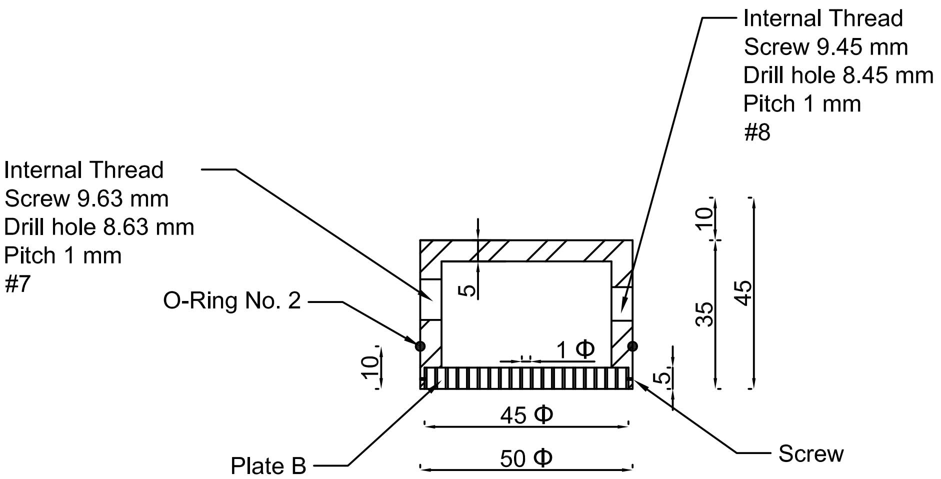

Top Cap 50 mm

Title: Top Caps 100 mm and 50 mm	Rev.01-23-03-15	Material No.: 9	Sheet: 13	Unit: mm

- One plate from each type

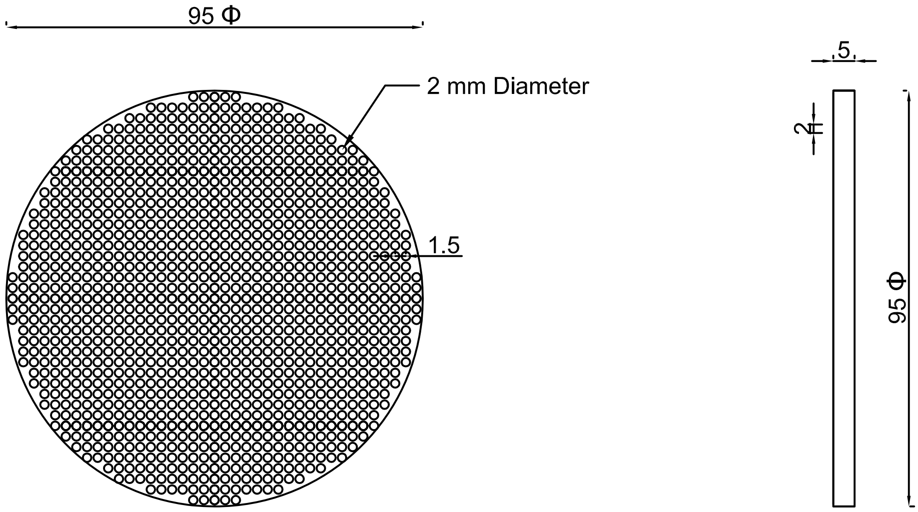

Plate **B** 100 mm

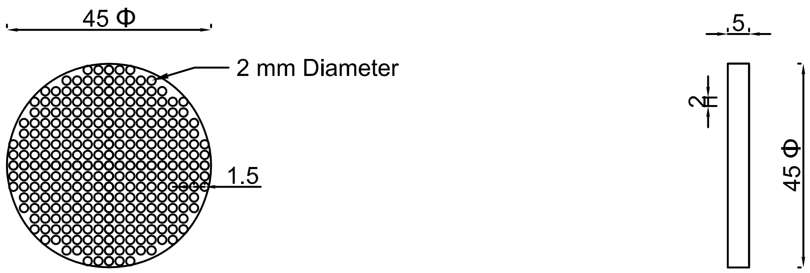

Plate B 50 mm

Title: Plate B	Rev.01-23-03-15	Material No.: 3	Sheet: 14	Unit: mm

- All fittings and O-rings will be provided.

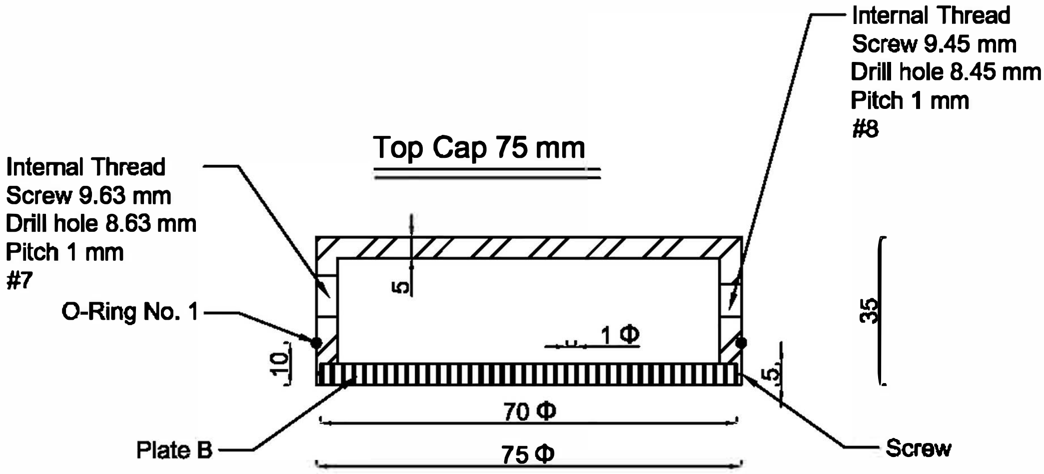

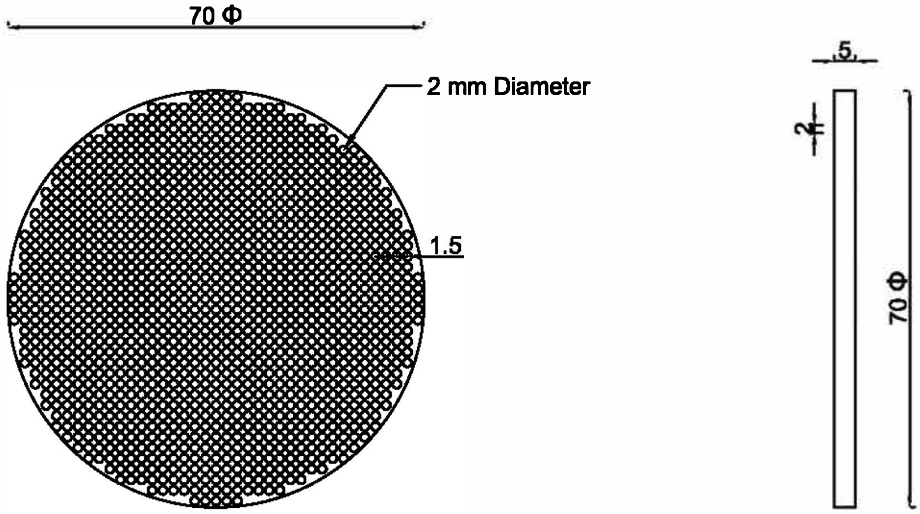

Plate **B** 75 mm

Title: Top Cap 75 mm	Rev.01-23-03-15	Material No.: 9	Sheet: 15	Unit: mm

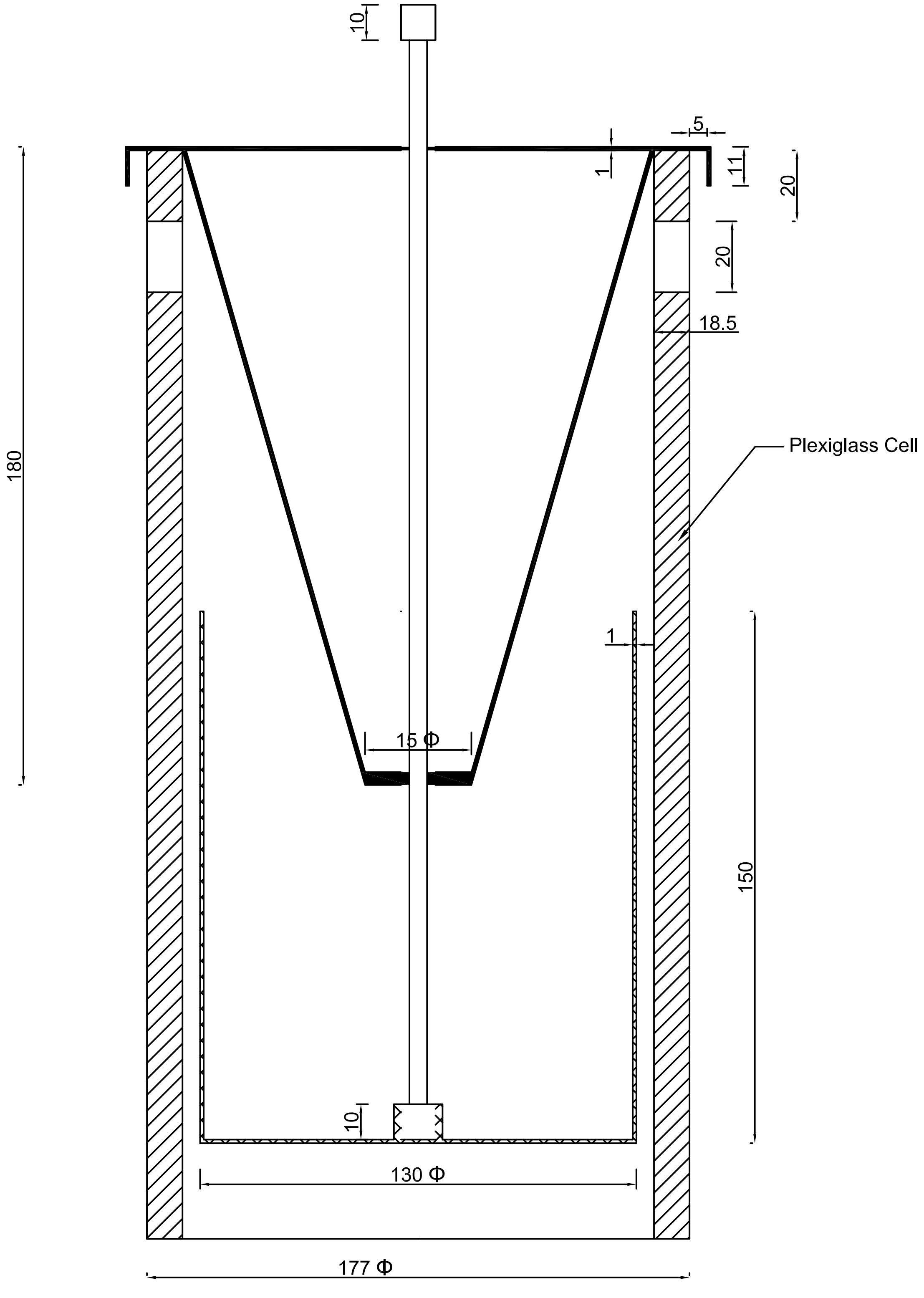

Title: Collection System	Rev.01-23-03-15		Sheet: 16	Unit: mm

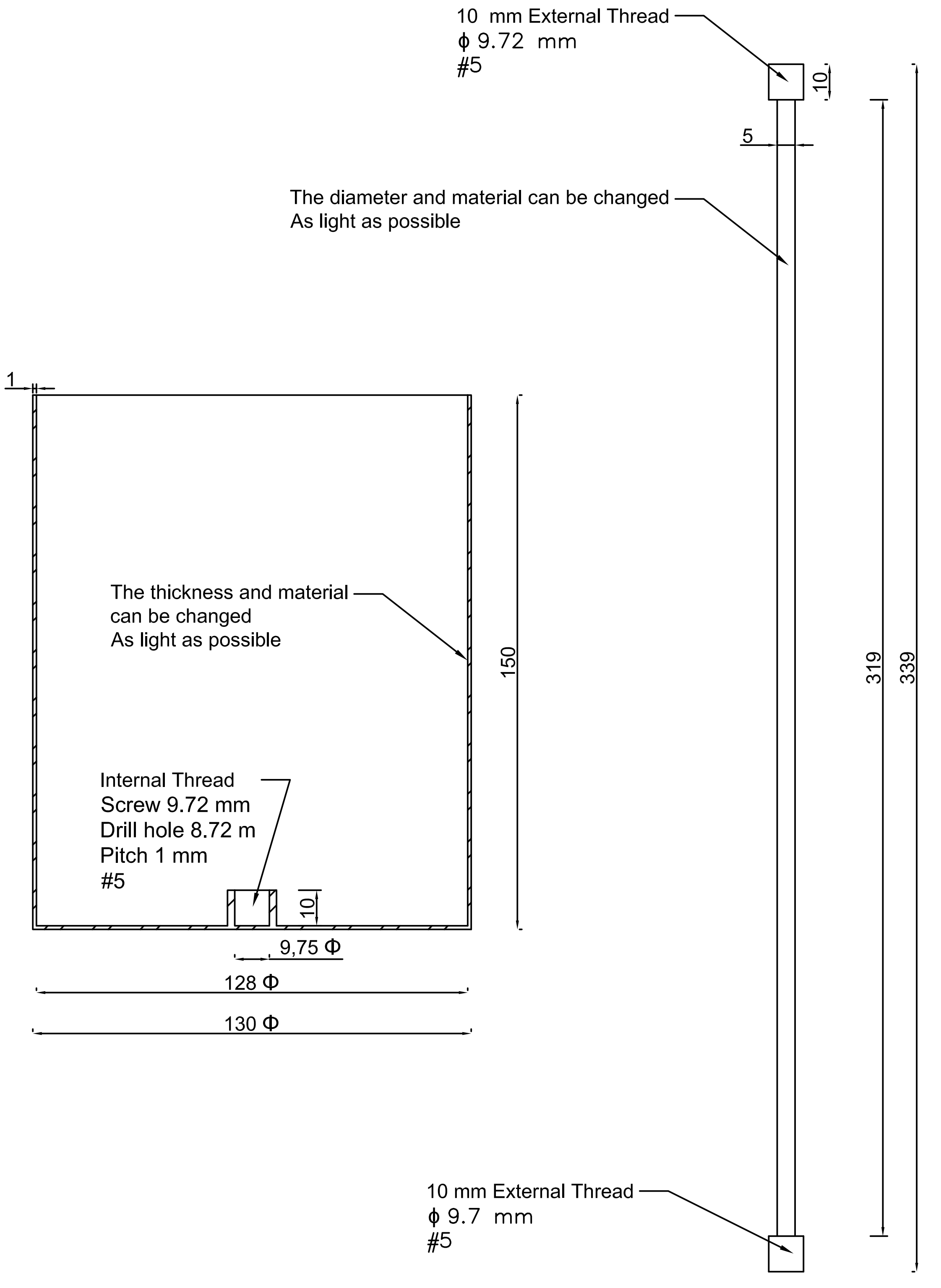

Title: Balance Section	Rev.01-23-03-15	Material No.: 5, 6	Sheet: 17	Unit: mm

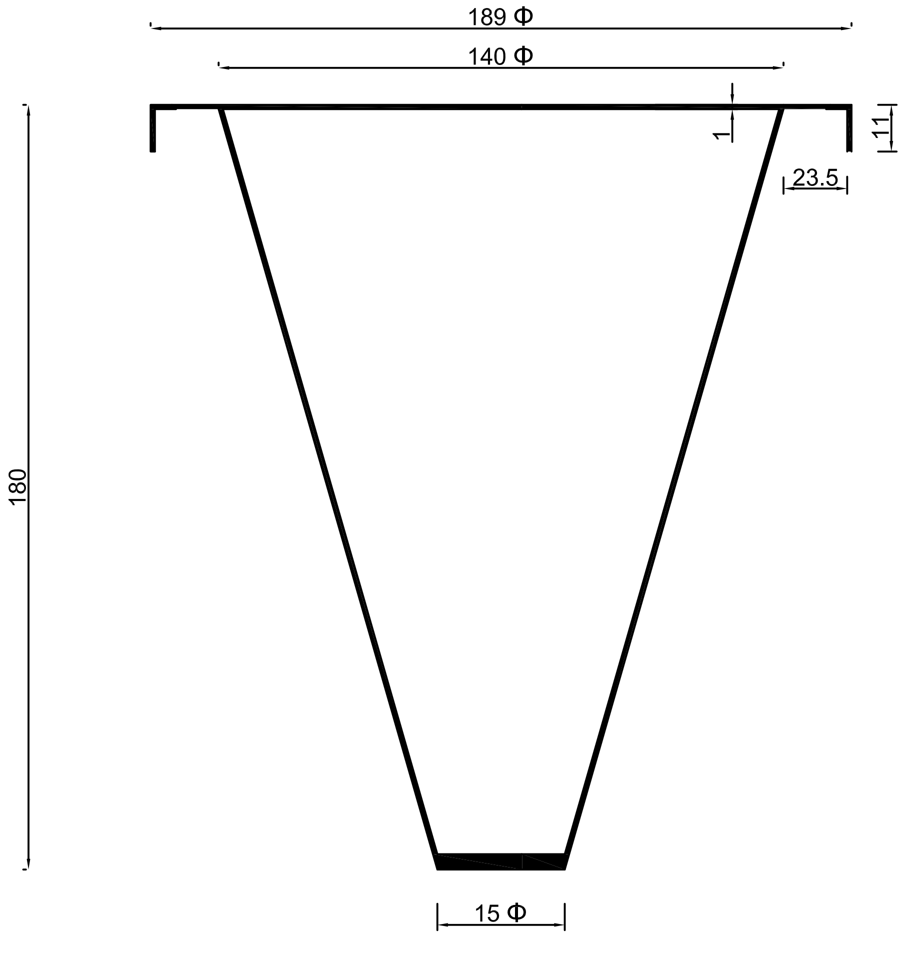

Title: Funnel Section	Rev.01-23-03-15	Material No.: 7	Sheet: 18	Unit: mm

- All fittings and O-rings will be provided.

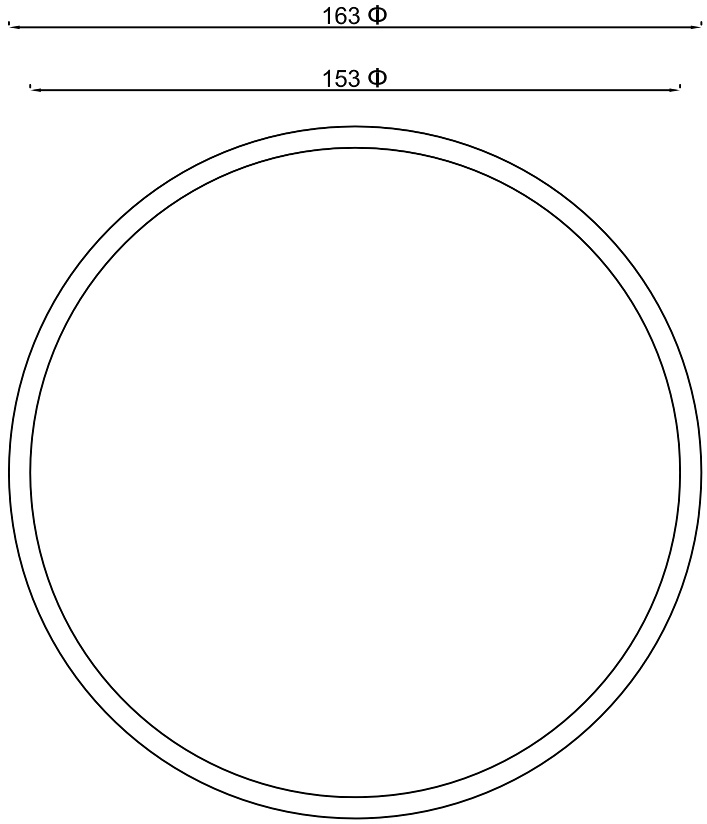

Top View

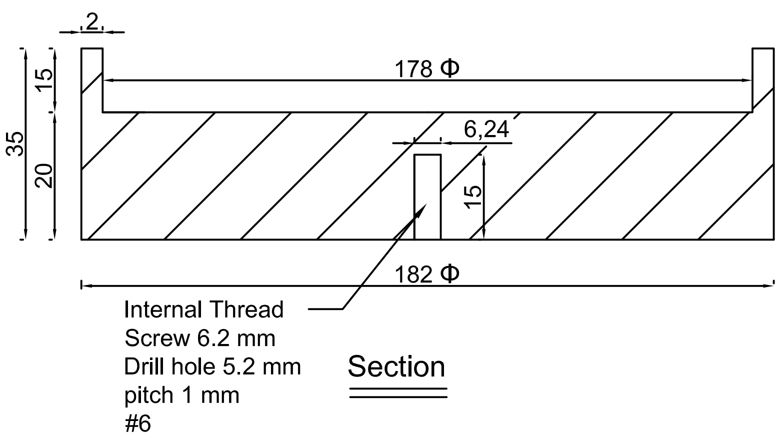

Section

Title: Collection System Pedestal	Rev.01-23-03-15	Material No.: 8	Sheet: 19	Unit: mm

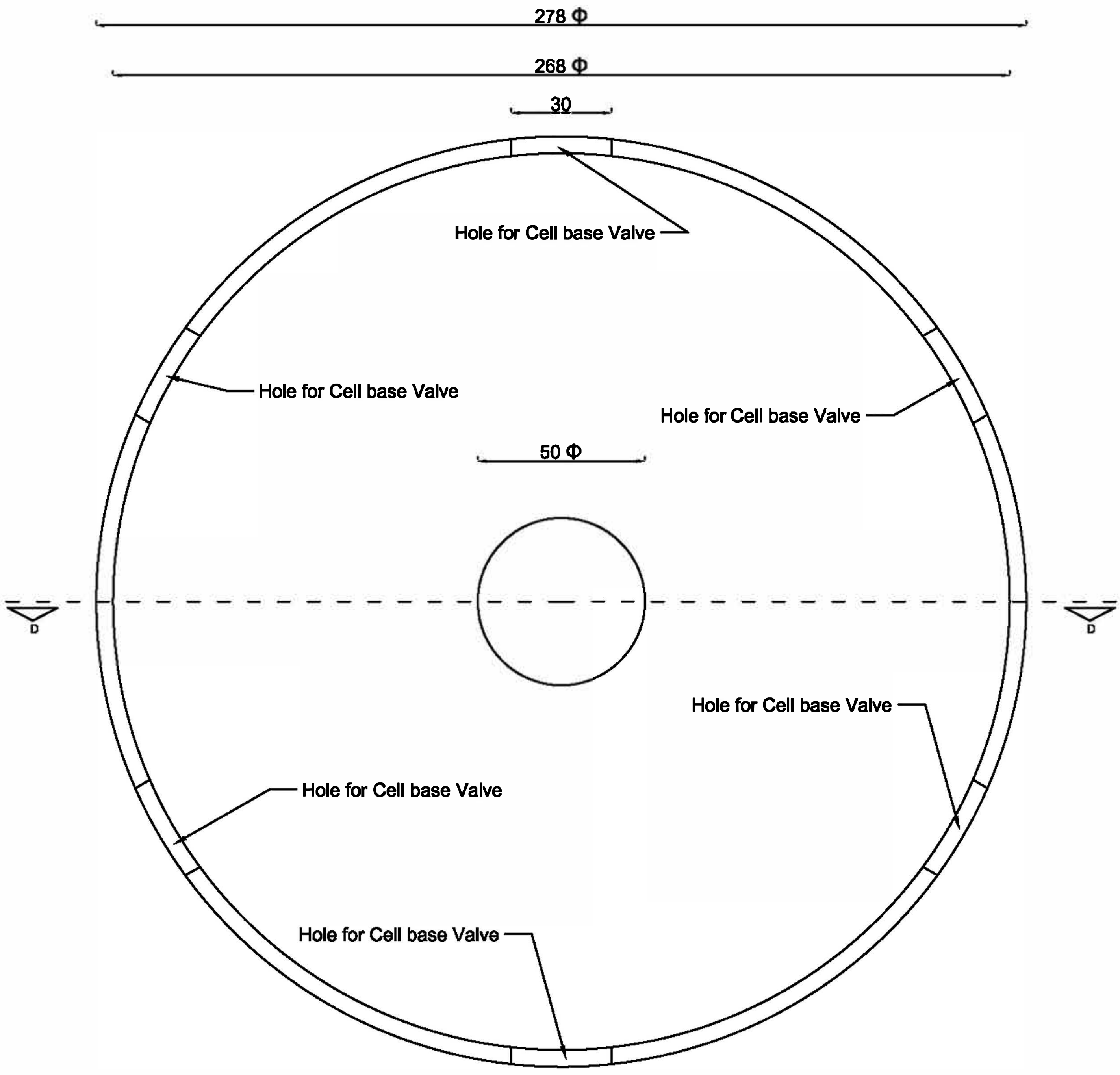

Title: Top view of Frame Pedestal	Rev.01-23-03-15	Material No.: 4	Sheet: 20	Unit: mm

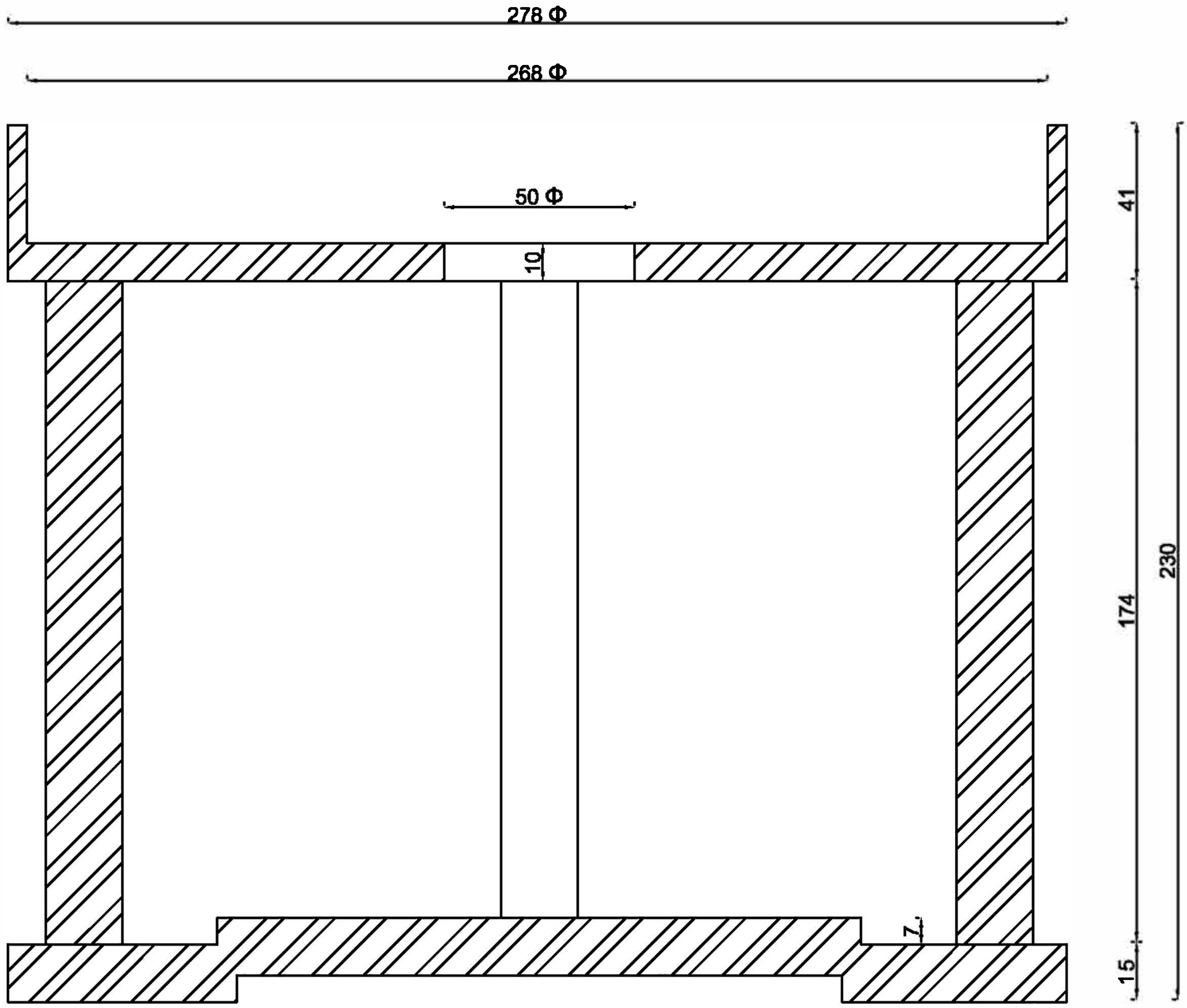

Title: Section D-D of Frame Pedestal	Rev.01-23-03-15	Material No.: 4	Sheet: 21	Unit: mm

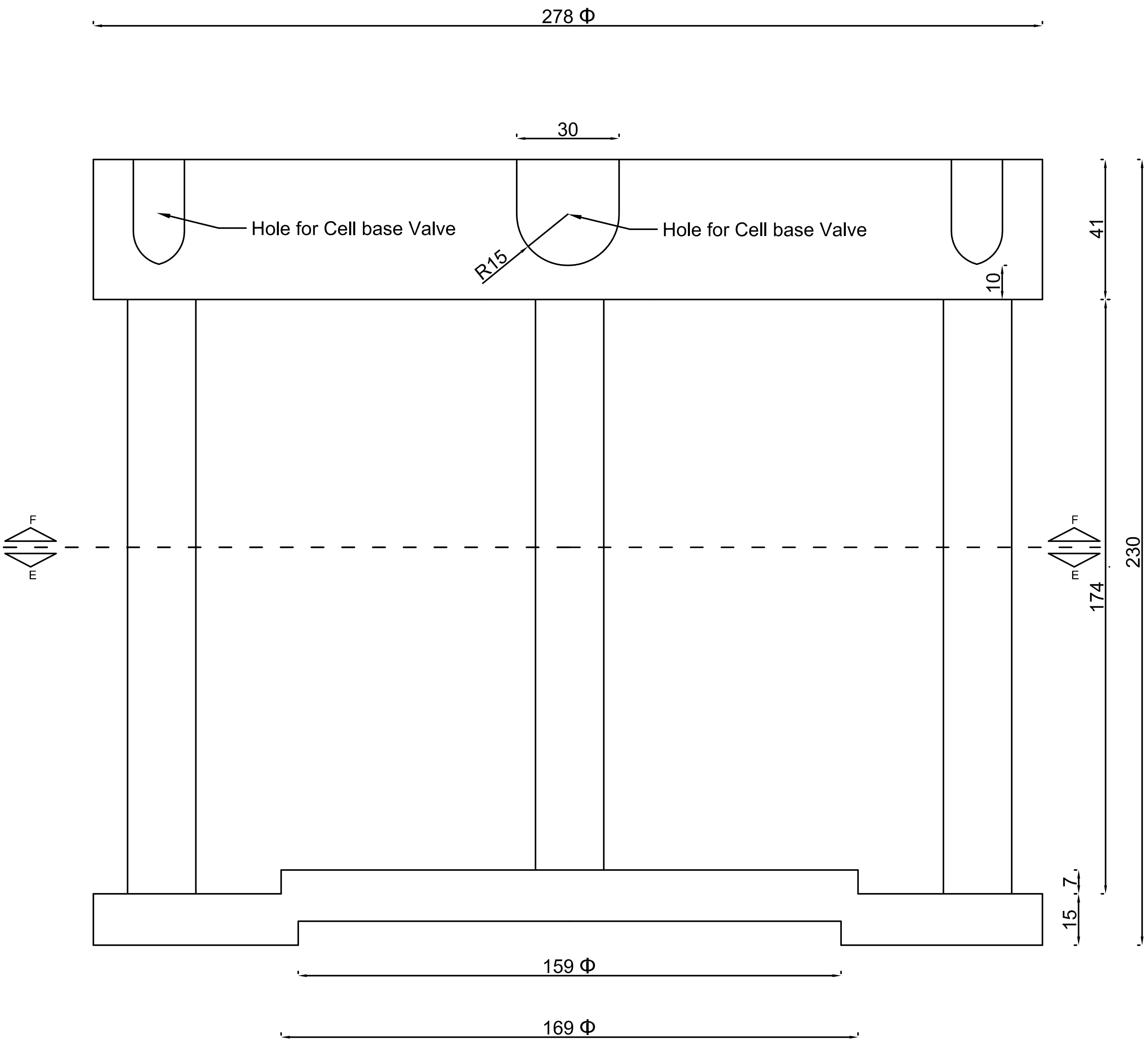

Title: Side View of Frame Pedestal	Rev.01-23-03-15	Material No.: 4	Sheet: 22	Unit: mm

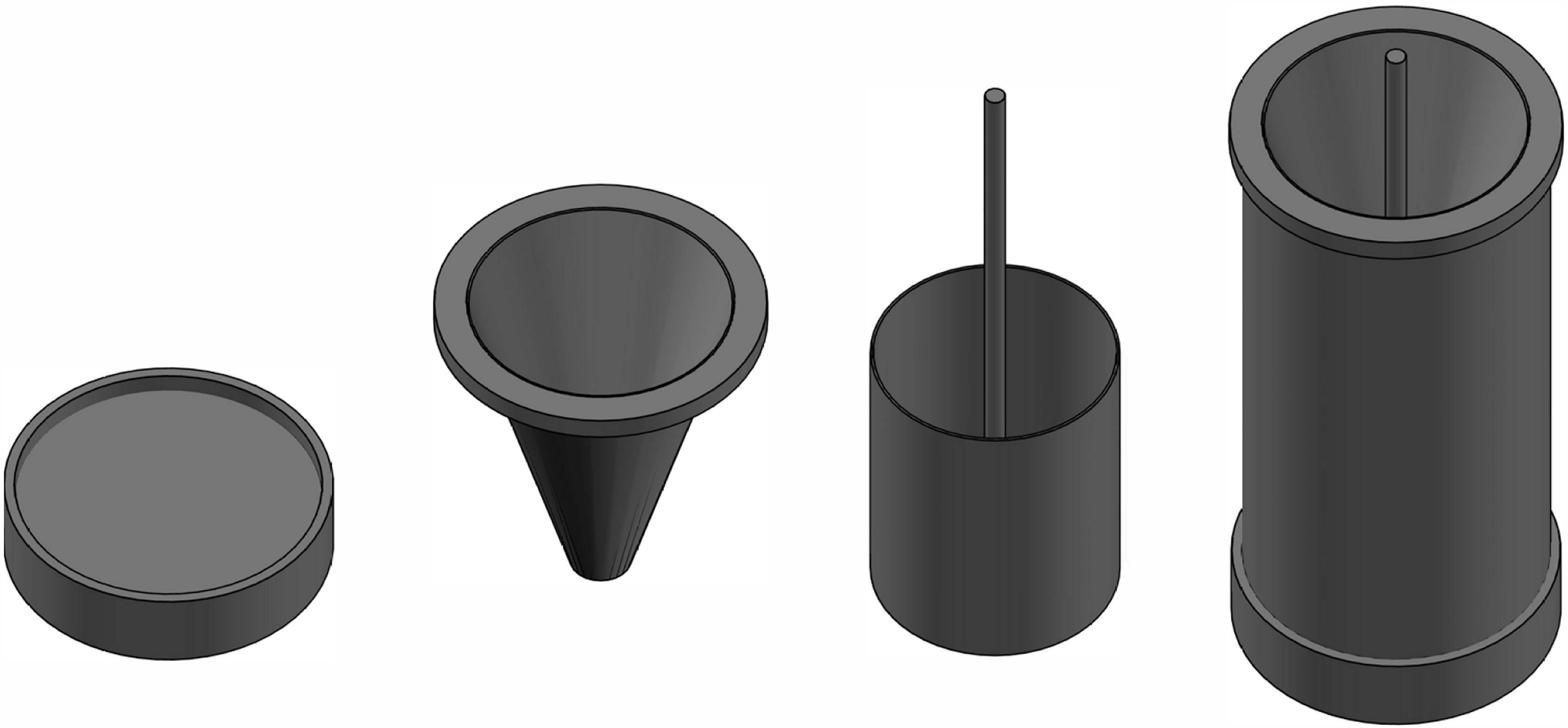

3D View of Collection System

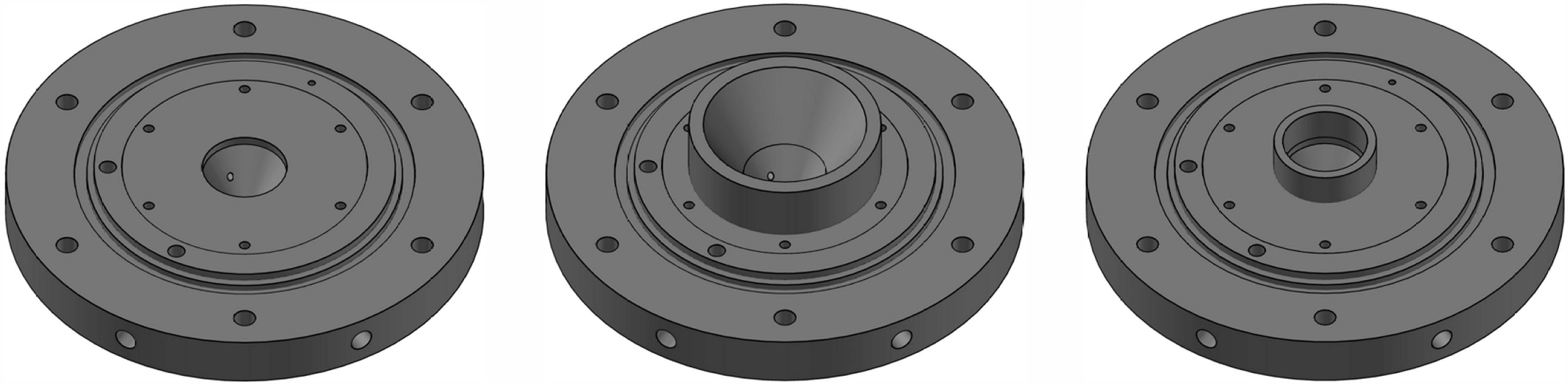

3D View of Base Plate

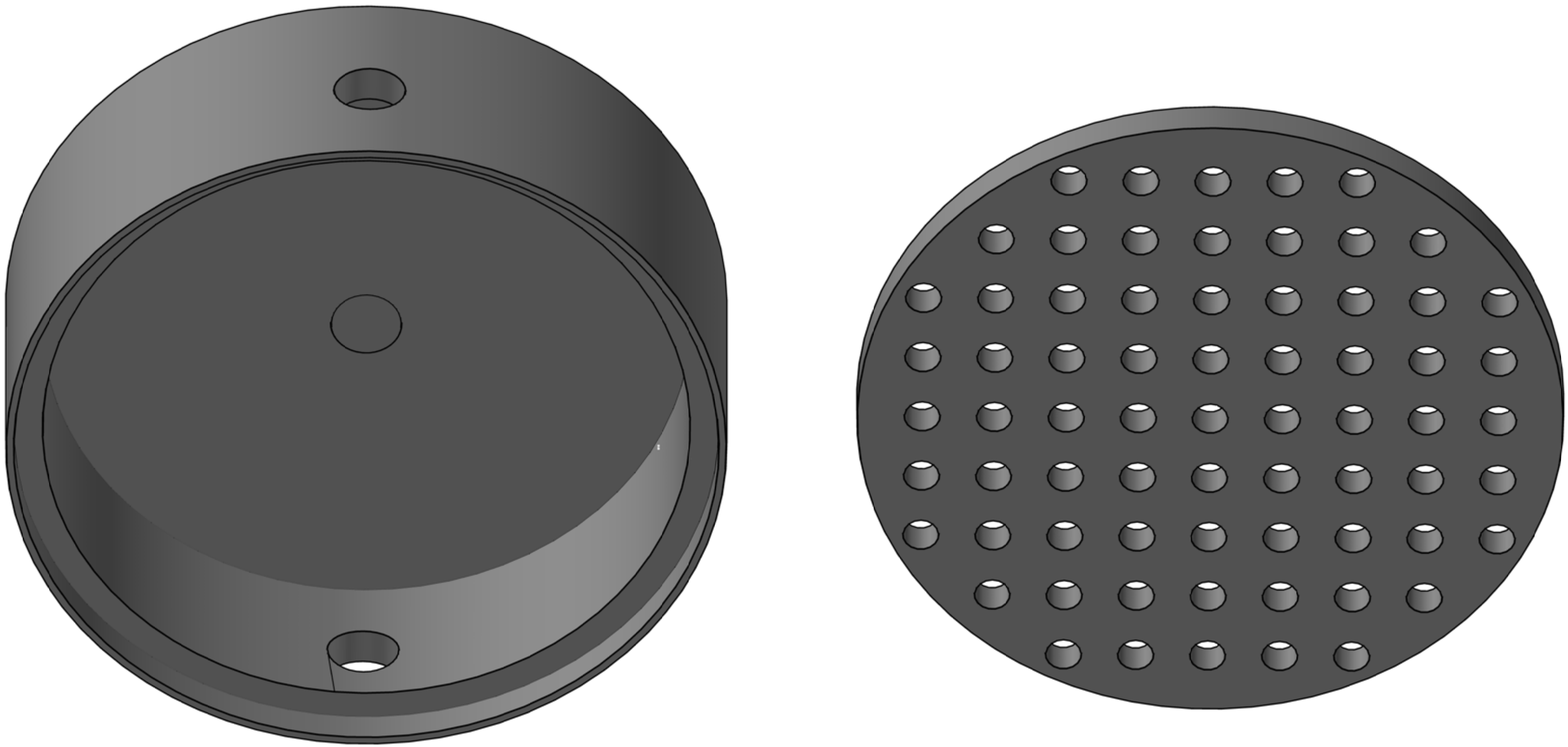

3D View of Top Cap

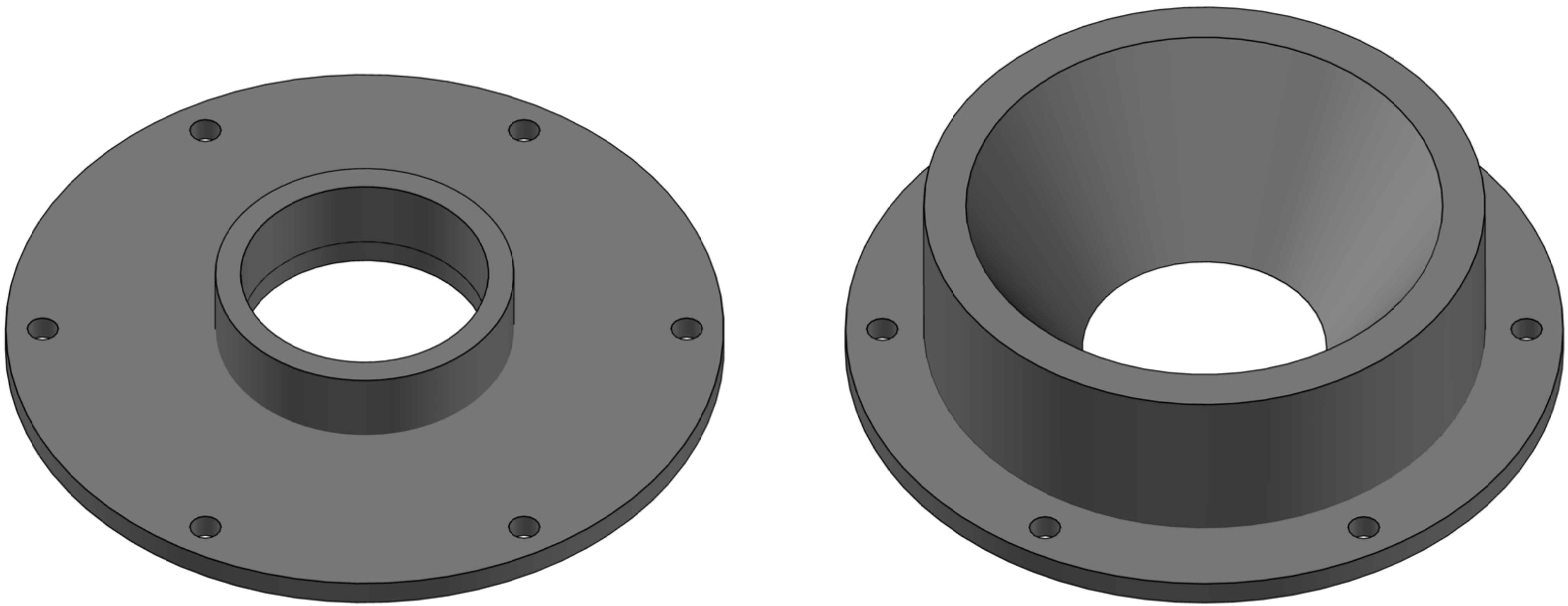

3D View of Bottom Pedestal

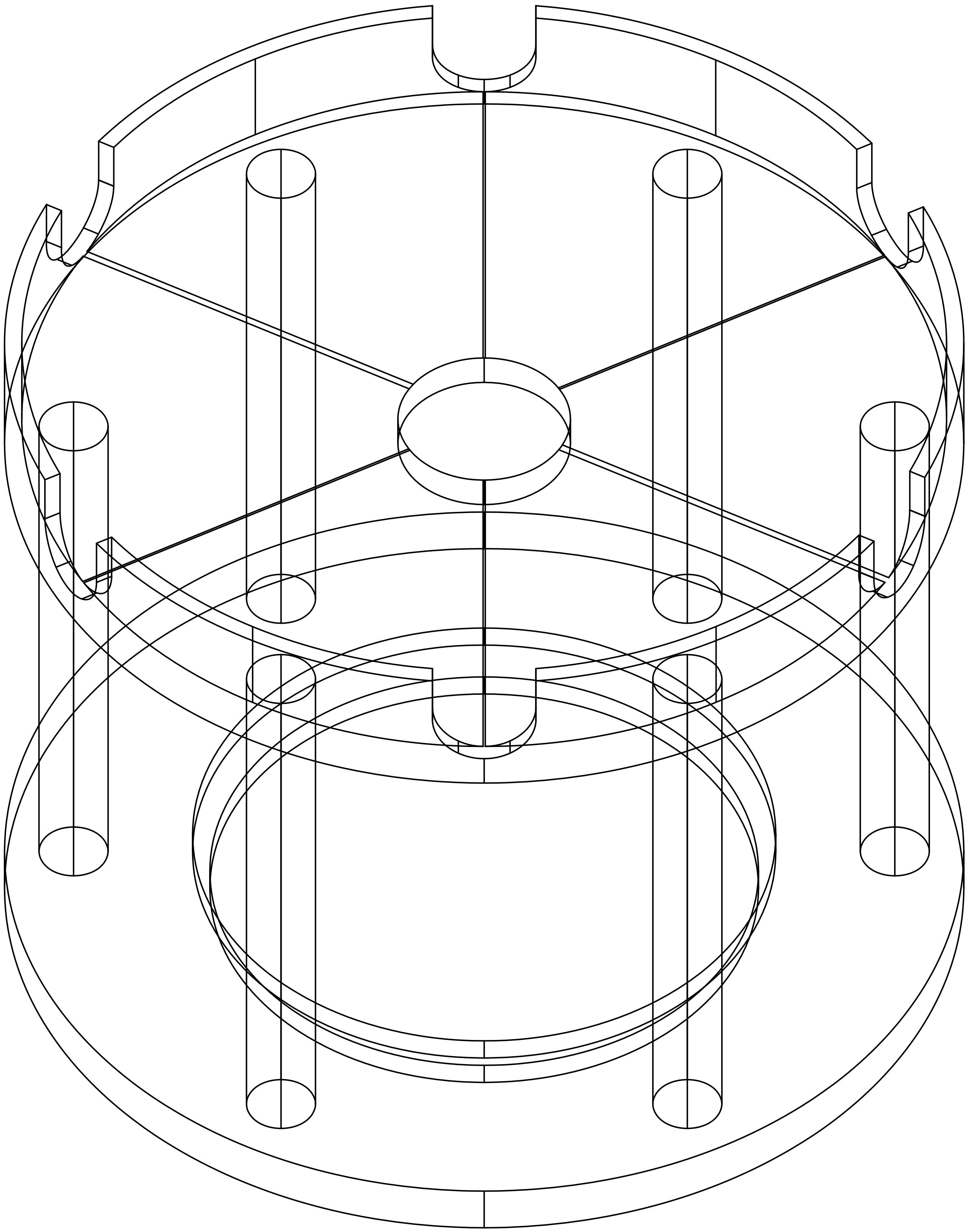

3D View of Frame Pedestal

APPENDIX C: Publications

Title	Type
Mechanical Consequences of Suffusion on Undrained Behaviour of a Gap-Graded Cohesionless Soil - An Experimental Approach	Technical Paper
Progressive Internal Erosion in a gap graded internally unstable soil - Mechanical and Geometrical Effects	Technical Paper
Discussion: On the distinct phenomena of suffusion and suffosion	Discussion Paper
Discussion of "Development of an Internal Camera-Based Volume Determination System for Triaxial Testing" by S. E. Salazar, A. Barnes and R. A. Coffman. The Technical Note Was Published in Geotechnical Testing Journal, Vol. 38, No. 4, 2015. [DOI: 10.1520/ GTJ20140249]	Discussion Paper
Discussion of "Stress-Strain Behaviour of Granular Soils Subjected to Internal Erosion" by C. Chen, L. M. Zhang, and D. S. Chang	Discussion Paper
Application of image processing in internal erosion investigation	Conference Paper

Geotechnical Testing Journal

Amirhassan Mehdizadeh,[1] Mahdi M. Disfani,[2] Robert Evans,[1] Arul Arulrajah,[1] and D. E. L. Ong[3]

DOI: 10.1520/GTJ20160145

Mechanical Consequences of Suffusion on Undrained Behaviour of a Gap-Graded Cohesionless Soil - An Experimental Approach

Geotechnical Testing Journal

doi:10.1520/GTJ20160145 available online at www.astm.org

Amirhassan Mehdizadeh,[1] Mahdi M. Disfani,[2] Robert Evans,[1] Arul Arulrajah,[1] and D. E. L. Ong[3]

Mechanical Consequences of Suffusion on Undrained Behaviour of a Gap-Graded Cohesionless Soil - An Experimental Approach

Reference

Mehdizadeh, A., Disfani, M. M., Evans, R., Arulrajah, A., and Ong, D. E. L., "Mechanical Consequences of Suffusion on Undrained Behaviour of a Gap-Graded Cohesionless Soil - An Experimental Approach," *Geotechnical Testing Journal* https://doi.org/10.1520/GTJ20160145. ISSN 0149-6115

Manuscript received June 30, 2016; accepted for publication May 16, 2017; published online October 11, 2017.

[1] Department of Civil and Construction Engineering, Swinburne University of Technology, John Street, Hawthorn, Victoria 3122 Australia http://orcid.org/0000-0001-7711-8128 (A.M.), http://orcid.org/0000-0003-1998-2537 (R.E.), http://orcid.org/0000-0003-1512-9803 (A.A.)

[2] Department of Infrastructure Engineering, The University of Melbourne, Grattan St, Parkville, Victoria 3010, Australia (Corresponding author), e-mail: mmiri@unimelb.edu.au, http://orcid.org/0000-0002-9231-8598

[3] Department of Civil Engineering, Swinburne University of Technology Sarawak Campus, 93350 Jalan Simpang Tiga, Kuching, Sarawak, Malaysia http://orcid.org/0000-0001-8604-8176

ABSTRACT

Fine particles may migrate in the preexisting pores of an internally unstable soil matrix caused by water flow. This migration changes the fine particle distribution and content at different zones and can affect the mechanical properties of these soils. Due to the different roles that fine particles can play in the force chains of an internally unstable soil, the available geometrical assessment methods do not predict post-erosion behavior of the soil. The fine particles may sit loose in the voids, provide lateral support for the primary soil matrix, or participate directly in stress transfer. This will depend on the fine content, particle size distribution, constriction size, relative density, stress path, and particle shape. However, to evaluate the post-erosion behavior accurately, computational modelling or experimental investigation needs to be conducted. A modified triaxial apparatus connected to a water supply system and collection tank was developed to investigate the post-erosion behavior of an internally unstable cohesionless soil under different loading patterns in undrained conditions. This system allowed all test phases to be completed, including erosion inside the triaxial chamber to remove any possible impact of specimen disturbance. The results suggest that the undrained shear strength of the eroded specimen increased at small vertical strains (0–4 %) under monotonic and cyclic loadings, whereas the initial modulus of elasticity remained unchanged. Also, the eroded specimen showed much higher resistance against cyclic loadings, whereas the non-eroded specimen was liquefied during less than five cycles of loading. This improvement was due to a better interlock between coarse particles due to erosion of fine particles. The hardening strain behavior of the non-eroded specimen changed to limited flow deformation due to a decrease in the fine content. The flow deformation of the eroded specimen at medium strain may be due to the local increase in lubrication effect of fine particles in the eroded specimen.

Keywords

erosion-triaxial apparatus, internal erosion, suffusion, internal stability, post-erosion soil behavior

Introduction

For granular soils, if only the coarse particles participate in the primary soil skeleton, the fine particles can migrate through the preexisting pores if the required hydraulic forces are present. The erosion process of these particles is known as suffusion, according to the International Commission on Large Dams (ICOLD) (2015), if no change in soil volume occurs. However, the local and/or general hydraulic conductivity properties of the soil may still change. This is a long-term phenomenon and may occur over a very long period of time. If these eroded particles provide secondary support for the soil load-bearing matrix or contribute partially to the force chains, the soil shear strength may change significantly. In some extreme cases, suffusion may lead to considerable settlements or catastrophic failures in hydraulic structures. A granular soil is vulnerable to suffusion if the fine particles carry no loads or (in some cases) support a small percentage of the effective stresses in comparison with the coarse particles. Gap-graded soils like sandy gravels or silty sands can be classified as geometrically unstable if the fine particles are smaller than the pore sizes.

Terzaghi (1925) was one of the first researchers to suggest that effective stresses decrease due to hydraulic stresses in the upward flow in sands and, if the hydraulic gradient reaches a critical magnitude, particles will dislodge from the soil body. This process is defined as hydraulic heave in sandy materials. Subsequently, researchers like Skempton and Brogan (1994), Li and Fannin (2011), Shire et al. (2014), and Moffat and Herrera (2014) attempted to expand Terzaghi's theory further for gap-graded soils. They showed that the required hydraulic gradient to move the finer particles is much lower than the critical hydraulic gradient presented by Terzaghi, especially if these fine particles do not fully contribute in the primary soil matrix.

Experimental investigation can be divided into two main parts. Some researchers used rigid-wall permeameter cells to investigate the initiation of internal instability and effective parameters that accelerate the process (Kenney et al. 1985; Skempton and Brogan 1994; Moffat and Fannin 2006; Sail et al. 2011; Indraratna et al. (2015). Some others like Chang and Zhang (2011), Xiao and Shwiyhat (2012), and Ke and Takahashi (2014a) have focused on the post-erosion response of cohesionless soils. For instance, a new experimental device was developed by Bendahmane et al. (2008) based on an ordinary triaxial apparatus for evaluating initiation of internal erosion in sandy clay samples. Test results indicated that erosion of clay particles started first and this was classified as suffusion. However, there was a second threshold in the hydraulic gradient above which erosion of sand particles initiated. This led to backward erosion and finally collapse of the whole sample. It was understood that suffusion and backward erosion both were affected by initial clay content. Ahlinhan and Achmus (2010) investigated the effects of flow direction and relative density on the erosion process of different soil gradations. This study suggested that an immediate increase in the flow velocity is a consequence of the onset of erosion. However, this increase is more obvious for internally unstable soils. Moffat and Fannin (2011) investigated the influence of the onset of instability on the local hydraulic gradient and presented a hydromechanical envelope in effective stress-critical hydraulic gradient space governing internal stability of cohesionless soils. This envelope appears to be independent of the flow direction, and internal instability may be triggered either by an increase in hydraulic gradient or a decrease in effective stress. Moffat et al. (2011) performed permeameter tests on widely graded cohesionless soils to investigate the influence of internal erosion. These experiments showed that suffusion is a time-dependent phenomenon and causes soil particle migration with no change in volume of the specimen. Suffusion can be classified as the next phase of suffusion when volumetric strains occur due to the washing out of particles.

Although different aspects of erosion initiation have been studied extensively, the effect of suffusion on mechanical soil properties is a new research area. One of the first studies to evaluate the post-erosion behavior of cohesionless soil was conducted by Ke and Takahashi (2012), in which the variation of soil strength was measured using a miniature cone penetration test. They found a reduction in the cone tip resistance after internal erosion was attributed to the loss of fine particles. The variation of drained shear strength due to internal erosion was investigated for the first time by Chang and Zhang (2011). They performed drained triaxial tests (pre- and post-erosion) under different consolidation stress paths. The results showed that the peak shear strength decreased significantly and the stress-strain behavior changed from dilative to contractive due to the removal of a certain amount of fine particles and an increase in void ratio. Xiao and Shwiyhat (2012) performed post-suffusion undrained triaxial compression testing on gap-graded specimens. Higher undrained shear strength was observed for the eroded specimens. They suggested that this might have been due to the loss of saturation during the erosion phase as the bottoms of the samples were subjected to atmospheric pressure. Ke and Takahashi (2014a) studied the drained and undrained behavior of gap-graded sand under monotonic and cyclic loadings. This revealed that the post-erosion drained and undrained compressive strength decreased and increased, respectively.

In other research works conducted by Ke and Takahashi (2014b, 2015), the mechanical consequences of suffusion were investigated with different initial fine contents and confining pressures. Whereas specimens with 35 % fine content showed completely contractive drained behavior, the volumetric strain behavior of specimens with 15 % to 25 % fine content was initially contractive but then changed to dilative at the medium strain range. In addition, the drop in the drained shear strength after suffusion was more obvious for the specimen with 35 % fine content.

In comparing the results of these studies, it is evident that the consequences of erosion on the mechanical soil properties and behavior of cohesionless soils are not well understood and some conflict exists. In addition, previous experimental attempts have had their own technical issues. For instance, the saturation percentage of the specimens was 85 % in studies conducted by Chang and Zhang (2011) and Xiao and Shwiyhat (2012), which resulted in some errors. Xiao and Shwiyhat (2012) mentioned that the bottom mesh they used may not have been selected accurately with respect to the size of the erodible particles. Ke and Takahashi (2014a, 2014b) solved the problem of losing saturation. However, the rotary pump they used in the test produced a jet flow on the soil specimen at the beginning of each erosion stage, which affected specimen deformation (radial and volumetric strains were measured via using local strain gauges). It is plausible that local instruments had a reinforcing influence on the sample and may have caused considerable error in the measurement of strain and soil behavior.

Computational investigation of internal erosion has been attracting more interest from the last decade. However, in comparison to the laboratory research, there are still many conceptual ambiguities that need to be clarified. For instance, Wood et al. (2010) used two-dimensional discrete element modelling to investigate the mechanical consequences of erosion by the software package PFC-2D. Instead of considering a coupled flow and particle removal, the process of erosion was modelled by progressively removing the fine particles, whereas the external stresses were kept constant. This numerical modelling showed that the particle removal increased the specific volume ($v = 1 + e$), which led to volumetric compression due to more open internal structure, narrowed the soil grading, and raised the critical state line. The consequence of this process was a lower available strength and occurrence of distortional strains. Although this research provided a better understanding of consequences of particle removal, no evidence provided showed the validity of the model. They believed that internal erosion is a time-dependent phenomenon and changes the actual fabric of the material, and it cannot be simulated only by mixing up particles with different sizes and randomly removing the small particles. In other research, a multi-scale approach including a discrete element model and an analytical micromechanical model was proposed by Scholtès et al. (2010) and Hicher (2013) to assess internal erosion effects on the mechanical properties of a granular medium and induced deformations during the erosion process. It was found that removal of particles at shear stress ratios lower than 0.72 resulted in contractive deformations and samples reached a new stable state. However, instability and dilation were observed when particle extraction occurred at shear stress ratio greater than 0.72. This threshold value for shear stress ratio was related to the residual state at large shear deformation, which is known as the critical state. This meant that under a shear stress state lower than the critical one, particle rearrangement acted as a self-healing factor to counterbalance the effects of particle erosion. In addition, regardless of percentage of the particle removal, this is the mobilized friction that controlled the failure of assembly. Moreover, it was found that due to increase in the initial porosity, the specimen behavior changed from dilative to contractive, and a drop in the shear strength was observed. In fact, particle removal decreased the internal friction angle and weakened the assembly. They concluded that the mechanical response in terms of internal friction, volumetric strain, and residual sate were independent of the initial stress state under which erosion was conducted.

This paper has attempted to solve some of these previously observed issues in the post-erosion experimental investigation. To achieve this, a triaxial chamber was modified to perform suffusion tests inside the triaxial cell, which also involved the development of the water supply and collection system. This system proved to be versatile, which allowed three different sized specimens with diameters of 50, 75, and 100 mm to be tested. This paper also explains the design principles and presents the performance of the apparatus during each different stage of testing. Preliminary test results are also discussed in terms of stress-strain behavior (measured using photogrammetry techniques) of the eroded and non-eroded specimens under monotonic and cyclic loadings.

Testing Apparatus

To investigate the post-erosion behavior of internally unstable soils, the soil specimen first needs to be exposed to water flow to initiate erosion. Then, the triaxial test is performed to evaluate soil response. Due to the granular nature of the material and to avoid any disturbance, a triaxial chamber was modified to perform saturation, consolidation, erosion, and shearing successively without removing the specimen. For this reason, the top cap and base plate of a triaxal chamber were modified in order to apply the hydraulic gradient and allow the soil particles to be eroded and washed out of the chamber. The water supply system was designed to provide a range of water heads or flow rates. The fabricated collection system can measure the weight of the eroded particles continuously during the test. This system allows for studying pre- and post-suffusion soil behavior under different stress paths and loading patterns.

The water supply system was designed to maintain a constant flow condition (i.e., flow rate) over a long period of time. Richards and Reddy (2008) stated that if Darcy's Law is applicable during the soil seepage, a decrease in hydraulic conductivity leads to an increase in hydraulic gradient at a constant flow rate. Due to this coupling effect, they suggested that considering only the critical hydraulic gradient may not be correct for cohesionless type soils. Therefore, a flow controller was connected to the pipe between

FIG. 1 Water supply system.

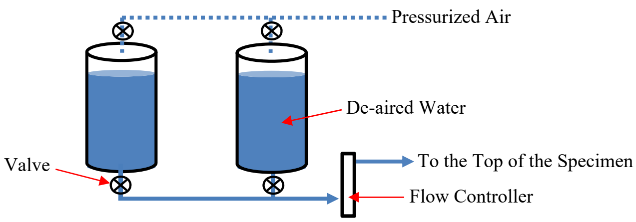

FIG. 2 Top cap filled with glass spheres.

the water supply system and erosion cell to control the flow rate. In addition, two pressure transducers were installed at the top and bottom of the specimen for direct measurement of the general hydraulic gradient across the full height of the sample. The water supply unit was composed of two water tanks (connected to each other in parallel), a flow controller, and an air pressure supply. These cells were filled with de-aired water, whereas the air pressure was applied to the top of the water inside the cell. Continuous water supply was provided using an exclusive outlet and supply valve to each cell. **Fig. 1** illustrates the water supply system.

To apply different water heads and flow rates, a flow controller with a maximum operating pressure and temperature of 1,370 kPa and 93°C was connected to the outlet pipe of the cells. This allowed a flow rate up to 500 mL/min to be applied to the top of the sample.

For erosion tests to be performed in the triaxial chamber, a new top cap, bottom plate, and base plate were manufactured. The top cap consisted of a hollow cap with a 5-mm-thick perforated steel plate with a 2-mm opening size. To diffuse the water on the sample contact interface uniformly and reduce the jet flow reported by Ke and Takahashi (2014b), the top cap was filled with glass spheres of various sizes (**Fig. 2**). To avoid particle migration to the top cap during the saturation process, a mesh with an aperture smaller than the smallest particle size (0.075 mm) was placed between the top of the specimen and top plate.

The original base plate was replaced with a 10-mm-thick netted plate, a funnel shaped pedestal, and a new base plate with a conical trough to provide enough space for the eroded particles to move into the collection chamber without clogging. A rigid mesh was placed on the netted plate to hold the coarse fraction (soil body) and let the fine particles (erodible particles) out. The mesh size was determined based on the smallest particle size in coarse fraction or constriction size. For the tests reported in this paper, a 1.18-mm mesh was used. **Fig. 3** shows the various parts of the modified base cell. Because the pedestal is detachable, it is practical to test specimens with different dimensions. Solid plates were also manufactured for performing ordinary triaxial tests to compare pre- and post-erosion soil behavior and reduce the mechanical errors (**Fig. 3d**). Although, different end restraints may be created due to the use of dissimilar bottom plates, initial ordinary tests did not show any significant variation in results between specimens sitting on different plates. In addition, a new pedestal was designed and fabricated to allow water to discharge and the erosion of particles from the bottom of the cell while maintaining the load (**Fig. 4**).

The collection system was designed to collect the eroded particles and discharged water from the cell, as well as to simultaneously measure the weight of the eroded particles and maintain a constant back pressure to keep the specimen's base saturated. The main design challenge was to continuously measure the weight of the dislodged particles without losing the back-pressure while eliminating the influence of the inlet flow. To overcome these limitations, Ke and Takahashi (2014a) came up with a practical solution. The measuring tray was submerged and a stable water level was maintained. To eliminate the effect of water weight, the measuring tray was connected to a submersible load cell (10 g resolution) and suspended inside a poly (methyl methacrylate) cell (inner cell) full of water. The water level at the top of this cell was kept constant and the inlet flow from the triaxial chamber was discharged from the inner cell into the main chamber via drainage holes in the wall of the inner cell. To reduce the flow jet effect reported by Ke and Takahashi (2014a) and related noise with the load cell readings, a plastic funnel was placed in the inner cell. The collected water in the main chamber was discharged at specific intervals. The air above the water was pressurized/equalized to the back-pressure applied to the specimen during the test (**Fig. 5**).

Strain Measurement

In conventional triaxial testing, the measured vertical strain at the top of the sample is the average of the vertical strains, which is inaccurate. In addition, global deformation measurement cannot detect local failures and strains. There are different types of local

FIG. 3

Details of modified cell base: (a) base plate, (b) funnel-shaped pedestal, (c) netted plate, and (d) solid plate to perform ordinary triaxial tests.

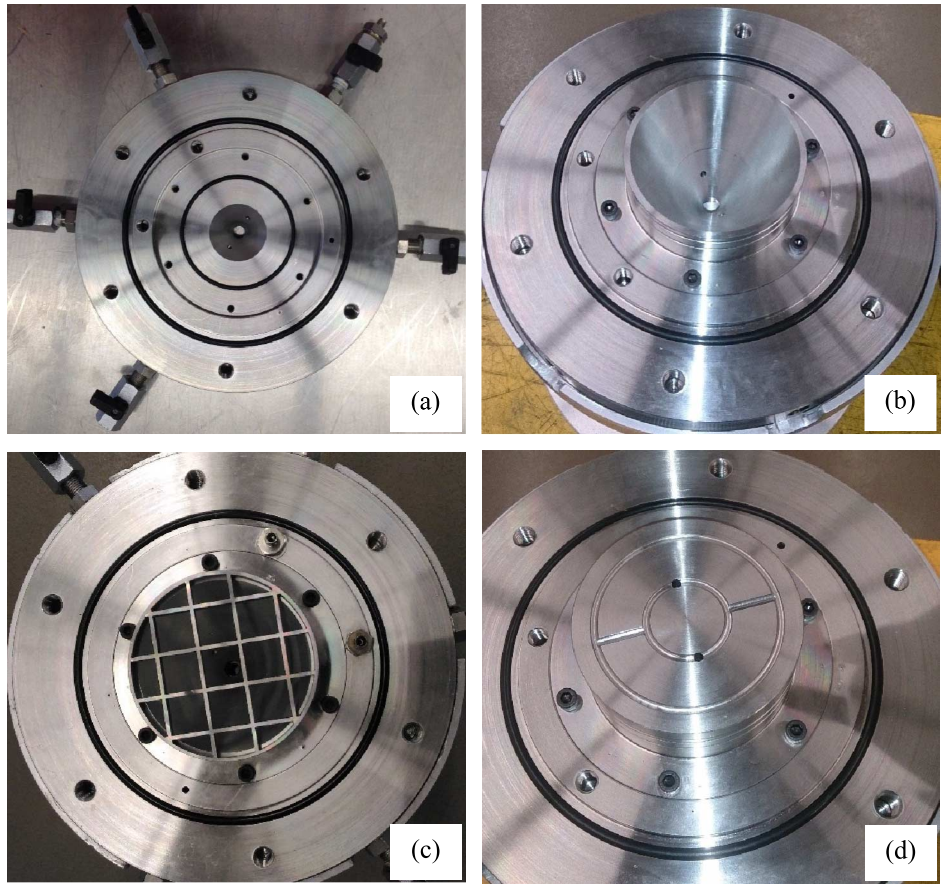

FIG. 4

New pedestal to apply axial force to the specimen; (a) top view and (b) bottom view.

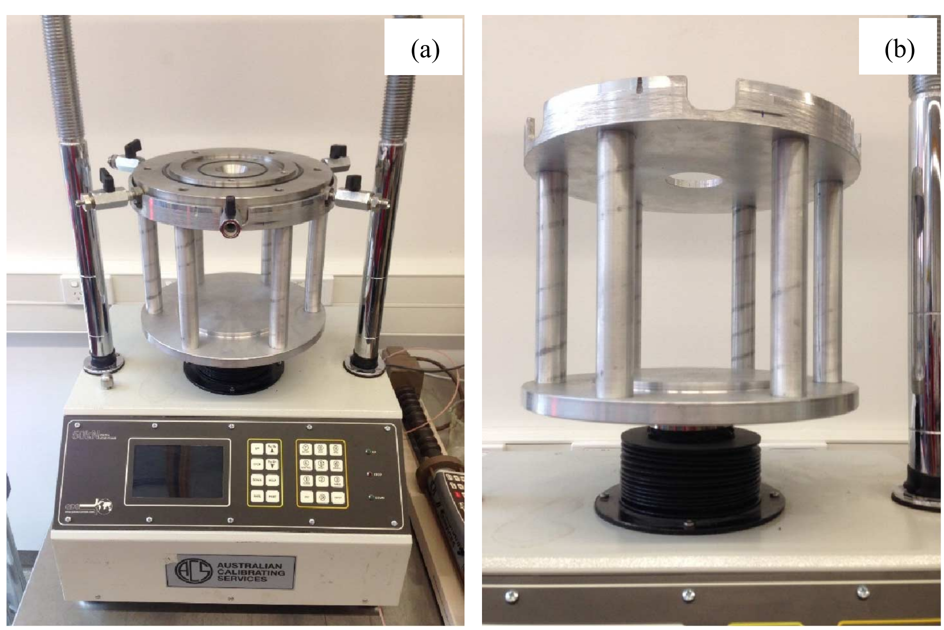

FIG. 5
Collection system details.

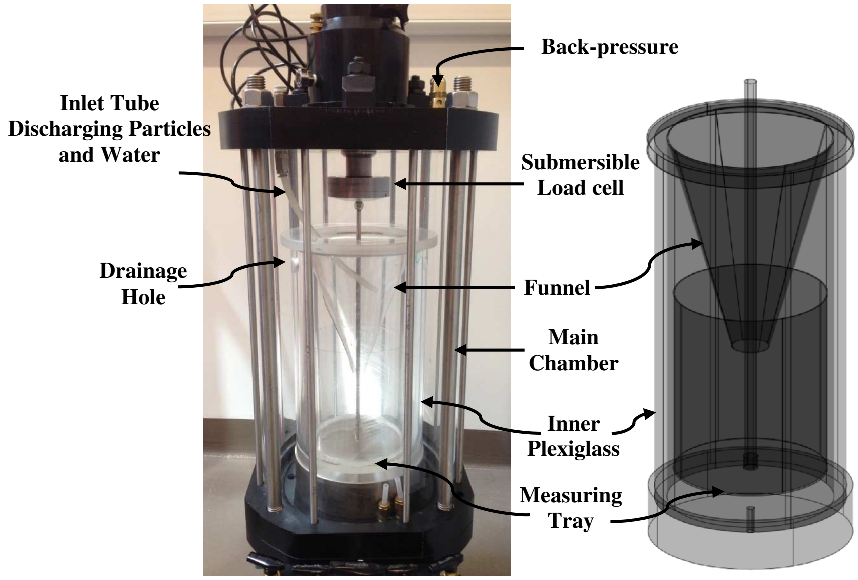

strain gauges that can be connected to the body of the sample. However, these instruments apply a confining and reinforcing pressure on the soil sample that may affect the soil response during shearing. To reduce these errors, photogrammetry techniques were employed to measure the local vertical and horizontal strains during the test.

Volumetric strains are usually measured by pore water variations in the triaxial testing. However, due to the discharge of water during the erosion stage, it is not possible to use this method. Cell water variation measurement is another method, but some considerations must be taken into account. The volume of the cell may be affected by cell pressure, variation in room temperature, creep of material, unloading/reloading, and the movement of loading piston inside the cell. Therefore, significant calibrations are required before testing, which is a disadvantage. Because the conventional measurement of deformation at the top of the specimen and measurement of the specimen volume change by monitoring the cell volume brings about many errors and disadvantages, the technique of photogrammetry was employed to measure the volumetric strains and the vertical and lateral strains during erosion and undrained shearing. Uchaipichat et al. (2011) and Mehdizadeh et al. (2015) have explained the details of volumetric and local strains measurement using photogrammetry and related challenges.

Testing Material and Sample Preparation

Natural sand with the gradation curve shown in **Fig. 6a** was used for this research. To assure the tested specimen was internally unstable, a gap-graded specimen was created by manually removing particle sizes between 0.3 to 1.18 mm and 2.36 to 10 mm. The gap-graded specimens with 25 % fine content were prepared using particles sizes of 0.075–0.3 mm (fine fraction) and 1.18–2.36 mm (coarse fraction) (**Fig. 6b**). **Table 1** presents the physical properties of the mixture.

Constriction size was calculated to be 0.28 and 0.3 mm using Kenney et al. (1985), Indraratna et al. (2007), and Dallo et al. (2013) equations. For this specimen, this suggests that the whole fine particles (≤0.3 mm) can be eroded if the hydraulic and stress-state conditions are met.

Fraser (1935) stated that particle shape affects hydraulic conductivity by varying the size and shape of the pores and the packing level. Permeability increases as true sphericity is decreased, which was also later confirmed by Guimaraes (2002). In other research studies conducted by Marot et al. (2012) and Fleshman and Rice (2014), it was found that angularity of particles improved the erosion resistance. These studies showed the importance of the particle shape in the internal erosion study. To take into account the influence of particle shape in the test result justification, images of the particle shape were captured using a digital microscope with USB (Universal Service Bus) output (**Fig. 7**) and the images were analyzed by ImageJ software package. Particle shape characteristics including circularity, roundness, and aspect ratios were measured based on the definitions suggested by Ferreira and Rasband (2012) (**Table 2**). **Table 2** indicates that coarse particles are more angular than fine particles, as circularity of coarse fraction, especially for particles in the range of 1.7–2.36 mm, is significantly lower than fine particles. This can also be noticed by a drop in aspect ratio.

Internal stability of the prepared mixture was assessed based on the available methods to ensure that suffusion would occur

FIG. 6 Particle size distribution for (a) original soil and (b) tested soil.

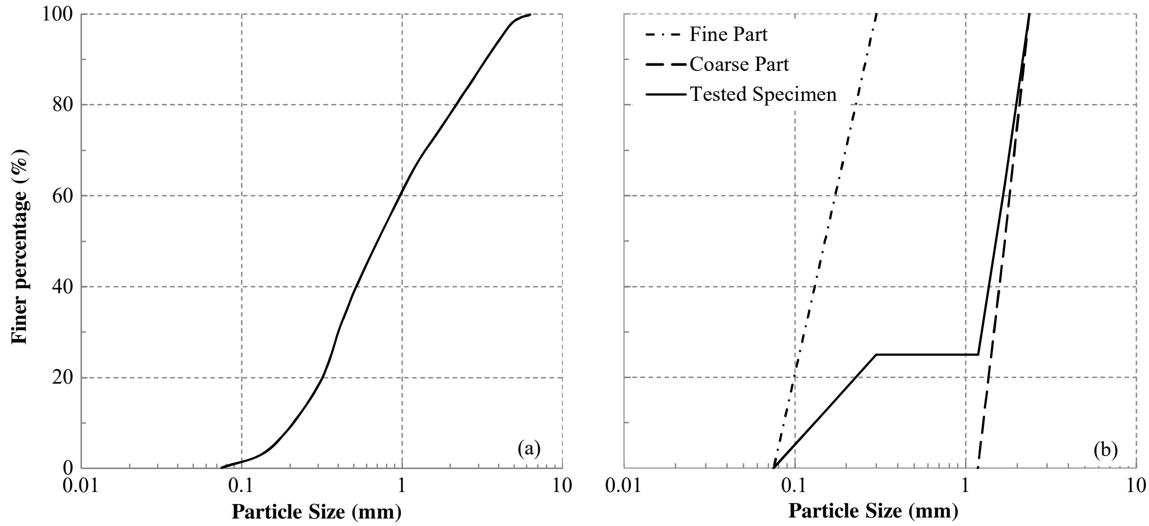

during the erosion stage (**Table 3**). It can be seen that out of twelve methods, eight suggested that the mixture was internally unstable and suffusion would occur if the hydraulic gradient was high enough.

It is critical to perform erosion tests on completely uniform specimens in terms of density, particle size distribution, and void ratio. Otherwise, the test results may show considerable discrepancies, even under similar stress paths and hydraulic gradients. Different methods are available to prepare uniform specimens for triaxial testing, such as the under-compaction or moist tamping method (Ladd 1978; Frost and Park, 2003; Jiang et al., 2003; Bradshaw and Baxter 2007) and the slurry method (Kuerbis and Vaid 1988; Carraro and Prezzi 2008). For this research, the under-compaction moist tamping technique presented by Ladd (1978) with modifications employed by Jiang et al. (2003) was used to prevent segregation during sample preparation and create specimens with maximum uniformity across the specimen height. Following this method, a specimen with 75 mm in diameter and 150 mm in height was reconstituted in 10 layers.

TABLE 1. Physical properties of tested soil.

Physical Property	Value	Physical Property	Value
Specific Gravity, G_s	2.645	$D_{c35(densest)}$[d]	0.226
Maximum void ratio, e_{max}	0.671	$D_{c35(loosest)}$[e]	0.702
Minimum void ratio, e_{min}	0.36	D_{c35}[f]	0.292
Initial relative density, D_r (%)	60	Uniformity coefficient, C_u	12.14
Moisture content, w (%)	6	Curvature coefficient, C_c	7.1
Fine Content, FC (%)	25	$(H/F)_{min}$[g]	0.08
Porosity, n	0.32	(D'_{15}/d'_{85})[h]	5.2
D_{up}/D_{bt}[a]	3.93	Gap ratio, G_r[i]	3.93
D_{erod}, (mm)[b]	0.103	$h' = D_{90}/D_{60}$	1.29
D^*, (mm)[c]	0.28–0.3	$h'' = D_{90}/D_{15}$	12.8

[a] D_{up} and D_{bt} are maximum and minimum sizes in the gap zone.
[b] Maximum erodible particle size (Burenkova 1993).
[c] Constriction size (Kenney et al. 1985).
[d] Controlling constriction size for the densest state (Dallo et al., 2013).
[e] Controlling constriction size for the loosest state.
[f] Constriction size (Indraratna et al., 2007).
[g] F is the passed fraction by weight finer than d, and H is the weight fraction between d and $4d$ (Kenney and Lau 1985, 1986).
[h] D'_{15} is the particle diameter in which 15 % by weight of coarser particles passed, and d'_{85} is the particle diameter in which 85 % by weight of fine particles passed.
[i] $Gr = D_{max}/D_{min}$ of the flat zone (gap zone).

Testing Procedures

To investigate the effect of suffusion on soil behavior under monotonic and cyclic loading, a series of triaxial erosion tests were performed. These tests were performed in five stages: (i) saturation, (ii) consolidation, (iii) erosion, (iv) undrained monotonic shearing or undrained cyclic loading followed by monotonic shearing, and (v) post-erosion particle size distribution (PEPSD). A parallel series of non-eroded specimens were also tested under the same stress paths as a comparison. The details of each stage are explained in the following sections.

The sample was prepared in an internal split mold. To prevent collapse or disturbance of the sample during preparation, a

TABLE 2. Particle shape characteristics.

Particle Size (mm)	Roundness	Circularity	Aspect Ratio
0.075–0.15	0.827	0.874	1.219
0.15–0.3	0.755	0.788	1.23
1.18–1.7	0.815	0.738	1.24
1.7–2.36	0.736	0.707	1.383

TABLE 3. Internal stability evaluation of mixture.

Method	Stability	Method	Stability
U.S. Army Corps of Engineers (1953)	Stable	Kwang (1990)	S (Marginal)
Istomina (1957)	S	Burenkova (1993)	U
Kezdi (1969)	Unstable	Mao (2005)	U
Sherard (1979)	U	Dallo et al. (2013)	U
Kenney and Lau (1985)	U	Chang and Zhang (2013)	S
Kenney and Lau (1986)	U	Moraci et al. (2014)	U

vacuum pressure of 10 kPa was applied. When the triaxial chamber was assembled, the suction was gradually removed, whereas the cell pressure incrementally increased to 10 kPa. Next, to assure a high level of saturation was achieved in a timely manner, carbon dioxide was injected at the bottom of the specimen for two hours. The rate of injection was kept low (1 L/min) to avoid any specimen disturbance caused by gas flow. The cell and back pressure were then linearly and gradually (1 kPa/min) increased to reach 400 and 390 kPa, respectively. These pressures were held for a further 100 minutes to ensure that the specimen was fully saturated. The B-value was also checked at the end of this stage and was recorded to be higher than 93 % for all tested specimens.

Frost and Park (2003) showed that during sample preparation by the moist tamping method, specimens may experience vertical peak stresses of 95–184 kPa for relative densities of 50–75 %. These significant stresses may affect soil behavior and accelerate the development of a shear band. In addition, the magnitude of the applied stress during the moist tamping cannot usually be monitored. This uncertainty may result in a reduction in accuracy, especially in erosion tests that uniformity in dry density and void ratio across the specimen height is necessary. To reduce the effect of the moist tamping stresses, it was decided to consolidate all tests to 150 kPa. Thus, the isotropic consolidation was performed by gradually increasing the cell pressure up to 540 kPa (150 kPa consolidation pressure). The rate of increase was similar to the saturation stage to avoid any disturbance or segregation.

For the eroded tests, the erosion of the specimen was performed after consolidation. Under constant stress condition, de-aired water was allowed to seep downward from the top of the specimen. After each increment, the flow rate was kept constant for one minute to stabilize the seepage flow. The flow rate increased gradually up to 408 mL/min ($\approx$ 92 mm/min for a specimen with 75-mm diameter) and was kept constant for two hours for all tests. This flow rate was higher than the critical flow rate initiates suffusion but lower than the failure flow rate. The failure

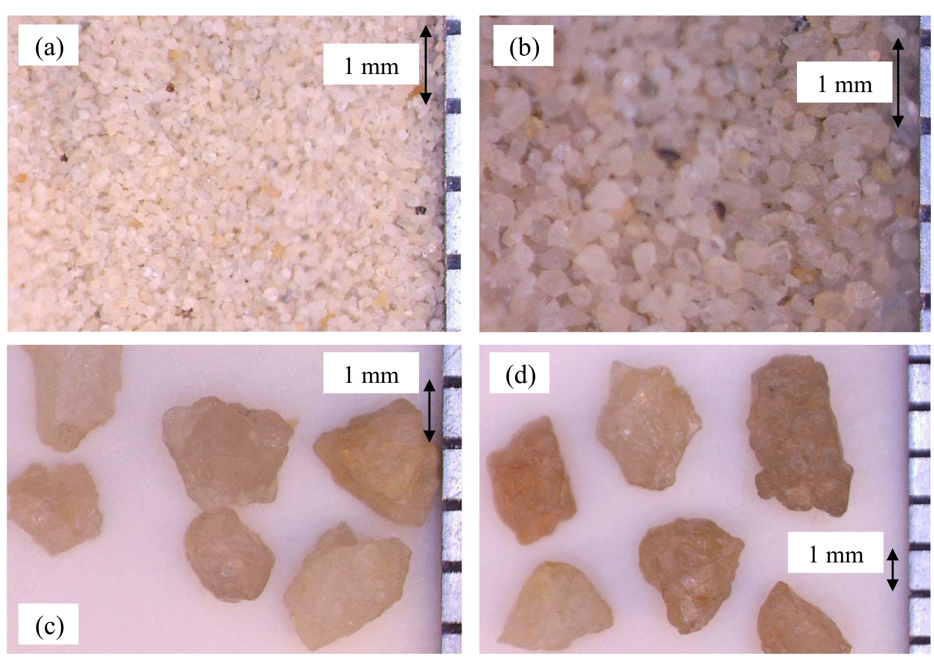

FIG. 7
Particles shape: (a) D: 0.075–0.15 mm, (b) D: 0.15–0.3 mm, (c) D: 1.18–1.7 mm, and (d) D: 1.7–2.36 mm.

flow rate is defined as a seepage flow rate that causes loss of excessive amounts of particles and causes the soil to experience shear failure due to large seepage forces (Chang and Zhang 2013). It is generally accepted that the critical hydraulic gradient is much lower than one for internally unstable soils. Erosion of fine particles confirmed that the chosen flow rate was higher than the critical value. The maximum applicable flow rate by the flow controller was 500 mL/min. A large flow rate of 408 mL/min (lower than the maximum value) was selected for this experiment to terminate the erosion phase in a reasonable period of time. However, it was applied in a pilot test first to examine whether a global failure occurs in the soil specimen or not. As this did not happen and the soil structure was robust until the end of the erosion phase, this flow rate was chosen for the experiment. The applied flow velocity was equal to 92 mm/min considering the specimen area of 4,418 mm^2. The soil specimen with 75-mm diameter did not fail even under a flow rate of 500 mL/min. To find the failure flow velocity, a soil specimen with 50-mm diameter was prepared under the same condition and subjected to an inflow velocity of 208 mm/min (flow rate of 408 mL/min), which was approximately 2.3 times greater than what was experienced by the soil specimen with 75-mm diameter. The test result showed that this specimen was still stable at the end of the erosion phase, although it experienced larger deformations. These trial and errors indicated that the failure flow rate is not reachable for soil specimens with 60 % relative density and under 150 kPa consolidation pressure due to limitation of the flow controller.

Luo et al. (2013) performed some short-term and long-term suffusion tests. The results indicated that for the long-term tests, the failure hydraulic gradient was much lower than for the short-term tests. They also stated that a long-term large hydraulic gradient may decrease the failure hydraulic gradient significantly. This means that although the adopted flow rate of 408 mL/min was lower than the failure hydraulic gradient, it may cause general collapse of the specimen if the erosion continues for a long time. Therefore, it was decided to terminate the erosion stage after a specific time in all tests by gradually decreasing the inflow. Because two pressure transducers were connected to the top and bottom of the specimen, the general hydraulic gradient and hydraulic conductivity through the specimen length could be measured. When the pore water pressure became stable at the top and bottom of the specimen, the next stage commenced.

Before undrained monotonic or cyclic shearing of the specimen, the B-value was checked again to ensure that the specimen was still fully saturated and above 93 %. It is worth mentioning that no considerable eroded particles were observed during triaxial tests without an erosion stage. It means that the amount of dislodged particles was minor during the saturation and consolidation phases.

Next, post-erosion behavior investigation under undrained monotonic or cyclic loadings was conducted. The initial tests on the non-eroded specimens showed that the excess pore water pressure (EPWP) reached 150 kPa and the liquefaction happened during the first five loading cycles. The cyclic behavior of the samples was investigated under a cyclic stress ratio equal to 0.167 and a period of 120 seconds (equivalent frequency of 0.0083 Hz). Strain-control monotonic shearing was performed at the end of both non-eroded and eroded tests. To allow the pore pressure to reach equilibrium, the vertical strain rate equal to 0.26 %/min (0.385 mm/min) was selected for all specimens.

Experiment Results and Discussion

The primary results of pre- and post-suffusion behavior of an internally unstable soil for various types of loading are presented. Test results in terms of stress-strain behavior, induced EPWP, and stress path during cyclic loading and monotonic shearing are discussed and presented.

The tested specimens in this paper all consist of 25 % fine content, which indicates that the specimen is in the transitional zone suggested by Shire et al. (2014). Consequently, the fine particles may sit loose in the voids or have a considerable role in providing lateral support to the coarse particles or directly contribute in the soil primary fabric. Therefore, experimental investigation is required to predict the post-suffusion behavior of this specimen.

Fig. 8 presents the percentage of the eroded fine particles, vertical and volumetric strains during erosion versus inflow velocity. The residual fine content of the specimens was approximately 10 % after two hours suffusion, which means 66 % of the total available fine particles were eroded during erosion (**Fig. 8a**). It can be seen that the rate of particle erosion increased after reaching the maximum inflow velocity (at 1,380 seconds) and started to decrease after approximately 1,200 seconds and then became stable for the last 1,000 seconds. Vertical and volumetric strains measured by photogrammetry during the erosion stage are shown in **Figs. 8b** and **8c**. As this measurement is based on surface deformations, it cannot be used for the void ratio calculation. **Fig. 8b** shows a jumping pattern in vertical strains like what was observed by Ke and Takahashi (2014a). These discrete spikes were attributed to the local particle rearrangement. Erosion of fine particles that provided a lateral support for the soil stress matrix formed local metastable structures (force chains). This local particle rearrangement helped the soil skeleton to reach a new stable state. **Fig. 8c** indicates volumetric strains during the erosion stage. The soil specimen showed the contractive behaviour and the specimen volume decreased by 2.75 % due to the particles erosion.

The undrained responses of the non-eroded and eroded specimens under monotonic loading (shearing) are illustrated in **Fig. 9**. Under monotonic loading, the non-eroded specimen showed hardening behavior, whereas the eroded specimen showed limited flow deformation. The initial modulus of elasticity

FIG. 8 Variation of (a) eroded fine particles percentage, (b) vertical strains, and (c) volumetric strains during erosion stage versus inflow velocity.

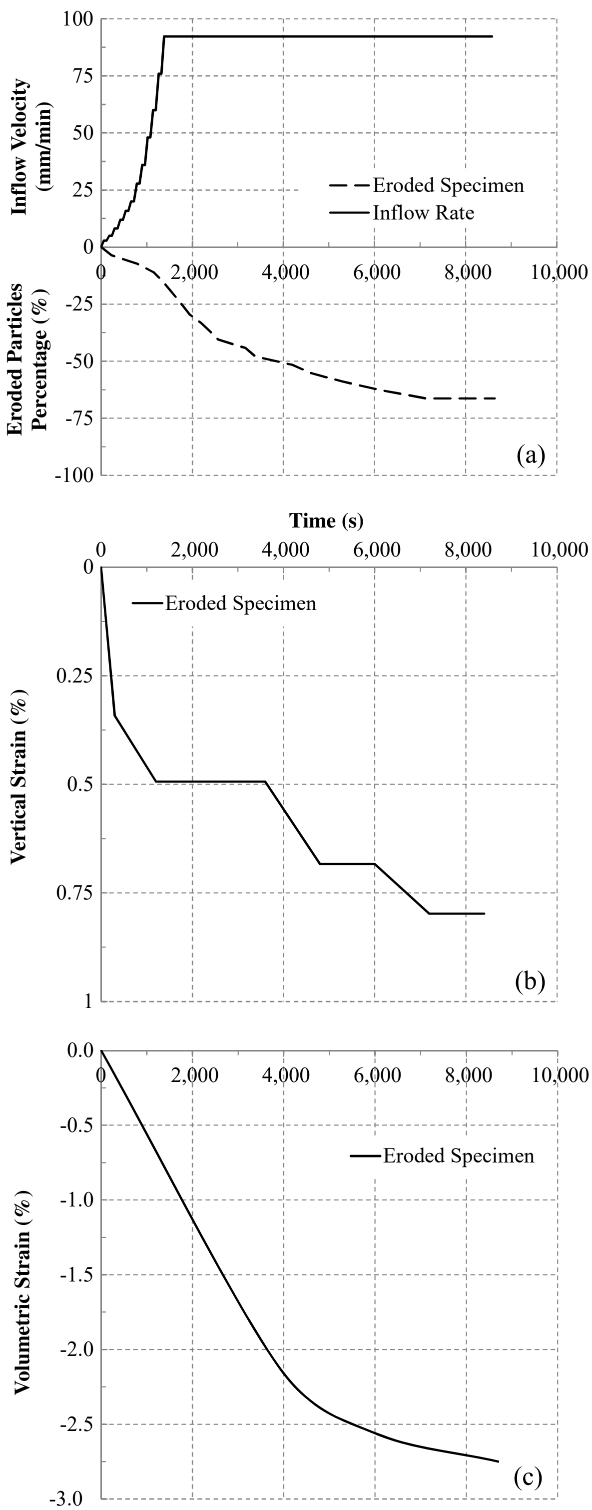

FIG. 9 Pre- and post-suffusion response under monotonic loading: (a) stress-strain behavior, (b) induced EPWP, and (c) stress path.

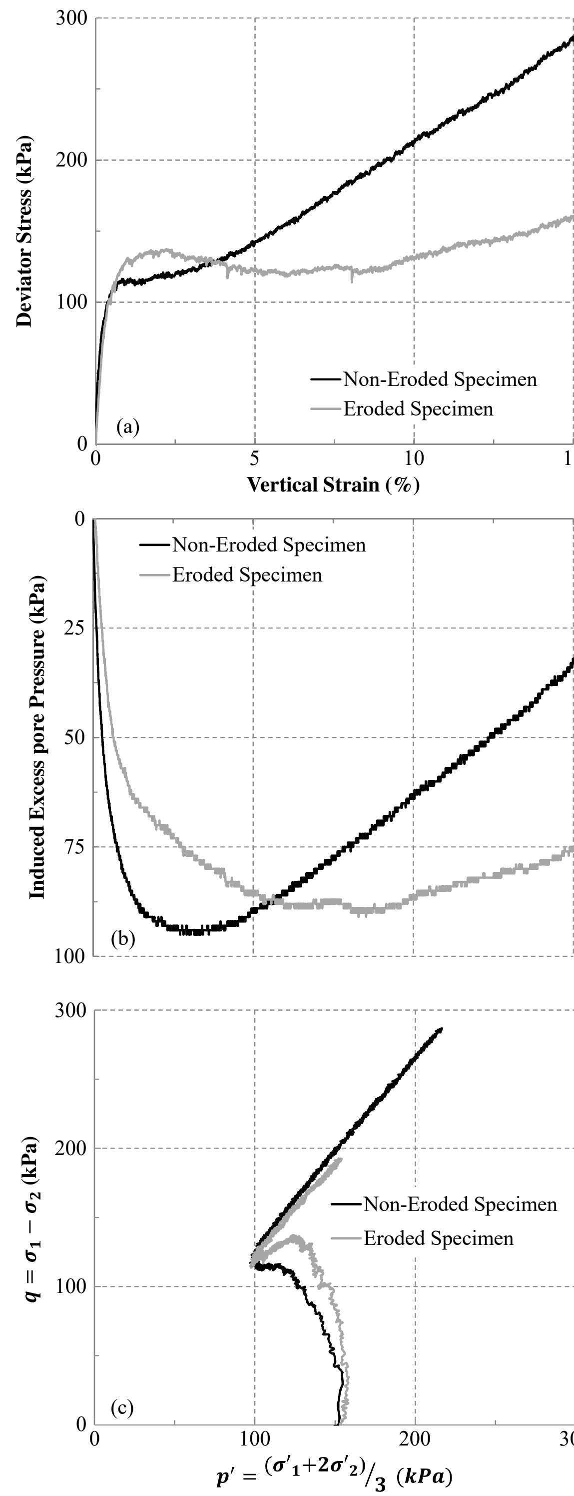

was similar for both specimens. However, the eroded specimen became softer during medium vertical strains. The shear strength of the eroded specimen was greater than the non-eroded specimen for vertical strains less than 4 %. The shear strength then decreased during the next 4 % vertical strain ($3.7 \leq \varepsilon_v \leq 8.4$ %). Finally, the strain hardening behavior was observed at

TABLE 4. Variation of normalized initial peak shear strength and global and intergranular void ratios during erosion stage.

Parameter	Pre-Erosion	Post-Erosion
Normalized Peak Shear Strength	0.39	0.45
Global Void Ratio	0.46	0.67
Intergranular Void Ratio	0.95	0.86

the larger strains until the end of the test, similar for the non-eroded specimen, although the final shear strength was well below the measured value for the non-eroded specimen (**Fig. 9a**). This finding is in agreement with what was reported by Ouyang and Takahashi (2015) for soil specimens with 25 % initial fine content. However, Ke and Takahashi (2015) and Ouyang and Takahashi (2015) observed larger initial secant stiffness for the eroded specimen at very small strains (less than 1 %). They believed that this occurred due to a distinguished packing of soil grains after erosion (accumulation of the fine particles at the spots where the constriction size is smaller than the erodible particles and participation of these clogged particles in force chains). Development of EPWP is shown in **Fig. 9b**. The positive excess pore pressure developed rapidly at the small strains in the non-eroded specimen, whereas it took much longer for the eroded specimen to reach the peak excess pore pressure (8 % vertical strain). However, the maximum values were similar. Another difference between the original and eroded specimen was tendency to dilation. The dilative behavior was observed after reaching 3 and 8 % vertical strain for the original and eroded specimens, respectively (**Fig. 9b**). In addition, it is evident that regardless of erosion of the fine particles, the stresses path eventually ended up on the same transformation state (location of behavioral change from contractive to dilative) and steady state line for both specimens (similar critical friction angle) (**Fig. 9c**). This is also in agreement with Ouyang and Takahashi's (2015) findings.

The initial peak shear strength (S_p was first presented by Ishihara (1993). This point is the beginning of the instability for soils with softening behaviour. **Table 4** shows variation of the normalized initial peak shear strength with the mean effective stress and global and intergranular void ratios pre and post erosion. The normalized value for the peak shear strength is used to eliminate possible effects of stress dependency. It can be seen that the normalized initial peak shear strength improved as erosion progressed despite an increase in the global void ratio after suffusion. However, the intergranular void ratio showed a decrease due to erosion of fine particles. The intergranular void ratio was defined by Mitchell (1993) to consider the contribution of fine particles to the soil stress matrix Eq 1.

$$e_g = \frac{e + FC}{1 - FC} \tag{1}$$

where e_g is the intergranular void ratio, e is the global void ratio, and FC is the fine content in decimal.

The observed drop in the intergranular void ratio was related to the particle rearrangement. Theoretically, a decrease in volume of the fines due to suffusion is added to the real voids, and the final result is that the intergranular void ratio is unchanged. However, if the soil skeleton formed by the coarse particles deforms or settles due to the particle rearrangemeent, the available spaces between the coarse particles may decrease, which could lead to a reduction in the intergranular void ratio.

It was shown in **Fig. 7** and **Table 2** that coarse particles in range of 1.7 to 2.36 mm were more angular in comparison to other particles. Erosion of fine particles might have improved interlocking between coarse particles. This could be the reason of the greater shear strength of the eroded specimen at small strains. However, the flow deformation during the medium vertical strains may have been related to the local concentration of fine particles somewhere in the specimen (probably in the bottom half) or the larger global void ratio of the eroded specimen. This accumulation of the fine particles increased the lubrication locally between coarse particles and led to a steady state until the additional shearing improved the interlocking of the coarse particles in other zones and activated the dilatancy.

Vertical and horizontal local strains during the undrained shearing stage were measured using a photogrammetry technique. As only one camera was used for the photogrammetry, it was necessary to assume that axisymetric volume changes occurred during erosion, which is not completely correct. However, this error can be eliminated by using two prependicular cameras as explained by Uchaipichat et al. (2011). Local strains were detected by measuring the variation in original lengths of the black lines marked on the membrane and the distance in between (**Fig. 10**).

Measured vertical and horizontal local strains during the undrained shearing are shown in **Fig. 11**. Although the trend of the local strain measurements was similar to the total vertical strain measured by the LVDT (Linear Variable Differential Transformer) outside the cell, there were some differences that need to be considered. For example, a good correlation between total strain and AB, BC, and AE local strains was observed. However, CD and BD were smaller and DE was larger than the total vertical strain (**Fig. 11a**). The upper part of the specimen showed a more uniform behavior than the lower part during post-erosion shearing.

In **Fig. 11b**, the horizontal local strains and total vertical strains are compared against one another. It can be seen that the horizontal local strains at B and C were approximately similar in magnitude to the total vertical strains, whereas the lateral strains at A and D were much smaller than those in the middle sections. Furthermore, the lateral deformation in the lower part of the specimen was larger than in the upper part.

Inevitably, there is always friction between the loading ram and triaxial cell. When the LVDT is installed outside the triaxial chamber and the loading ram is not attached to the loading frame

FIG. 10
(a) Initial and (b) deformed specimen during post-erosion monotonic loading.

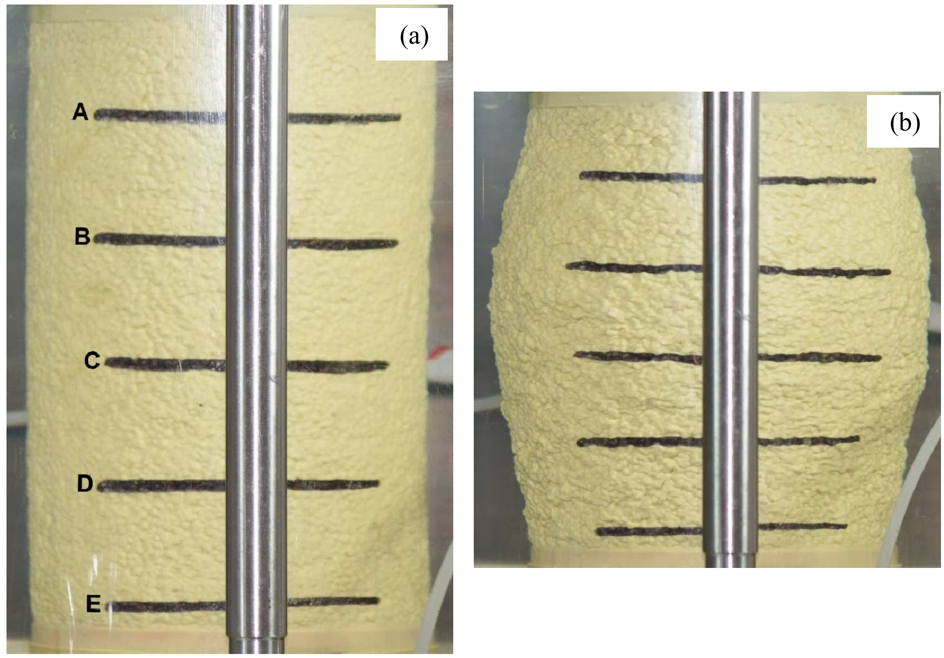

FIG. 11 (a) Local vertical strains and (b) local horizontal strains during monotonic loading.

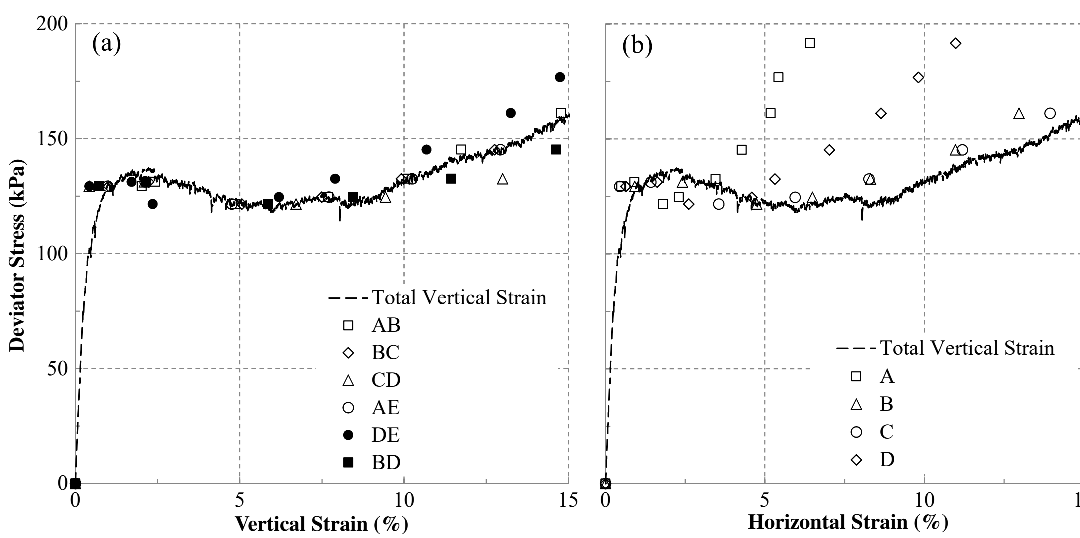

and not locked to the specimen top cap, it is very difficult to consider the friction impact on the deformation measurement. Thus, the LVDT reading is not completely accurate during the erosion stage. Moreover, when the erosion deformation is small, locking the top cap to the load cell may act as a supporting element for the specimen due to the abovementioned friction, which can reduce the erosion deformations, especially for soil samples that show high resistance to erosion. Therefore, locking the top cap is not recommended for the erosion tests unless the post-erosion cyclic behavior needs to be investigated.

Fig. 12 presents the undrained behavior for the soil specimens (pre and post erosion) under cyclic loading followed by undrained monotonic loading (shearing). Figs. 12a and 12b show the cyclic resistance of the soil specimens pre and post erosion. It can be seen that the non-eroded specimen was liquefied in less than five loading cycles, whereas the eroded specimen not only resisted the liquefaction, but the EPWP did not develop considerably (Fig. 12c). Thus, Fig. 12 suggests that losing the fine particles increased the cyclic resistance of the soil remarkably. This is in agreement with what was reported by Ke and Takahashi

FIG. 12 Pre- and post-erosion response under cyclic loading: (a) stress-strain response under cyclic loading and post-cyclic shearing, (b) stress-strain response under cyclic loading, (c) induced EPWP during cyclic loadings and post-cyclic shearing, and (d) stress path during cyclic loading and post-cyclic shearing.

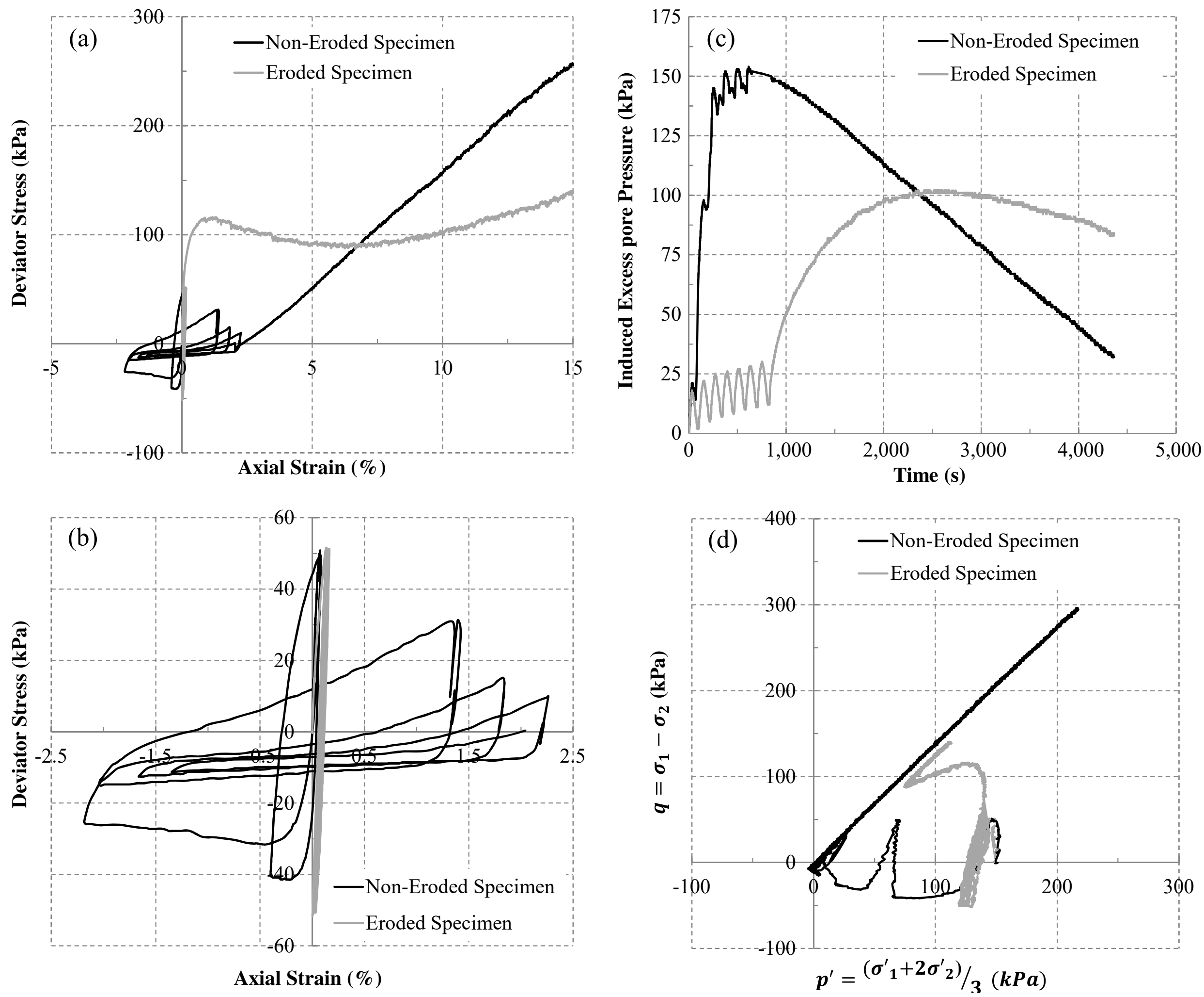

(2014a) that the eroded specimen failed after more cycles of loading.

At first glance this seems to be a contradiction to the static triaxial test results presented in Fig. 9, which suggested that the local concentration of fine particles after erosion decreased the shear strength. However, it is important to note that less than 0.2 % vertical strain occurred during cyclic loading. As can be seen from Fig. 9a, at the small strains the shear strength of the eroded specimen was greater than the non-eroded specimen.

The stress-strain trend and shear strength results were similar to the results obtained under monotonic loading for the eroded specimens (Figs. 9a and 12a). The development of EPWP was minor for the eroded specimen during cyclic loading in comparison with the non-eroded specimen. In contrast, the non-eroded specimen showed dilation immediately after cyclic loadings, whereas the eroded one contracted and developed a positive EPWP first and dilative behavior wasn't observed until after 6 % axial strain (Fig. 12c). The stress paths during and post cyclic loading were completely different as the eroded and non-eroded specimens behaved differently. However, the angle of the steady state lines were similar regardless of the amount of fine particle loss (Fig. 12d).

It is also worth mentioning that the soil skeleton stayed stable during the erosion stage. Although 66 % of the fine particles was eroded, no considerable settlement was observed (less than 1 % (Fig. 8b). This suggests that even though the erosion of the fine particles changed the behavior of the soil, it did not affect the soil structure at a global scale. In other words, although the fine particles did not contribute to the primary soil matrix and only filled the voids and provided the lateral support, they did play a tangible role during shearing. By performing erosion phase under higher

FIG. 13 Post-erosion particle size distribution of a (a) whole sample and (b) at different levels.

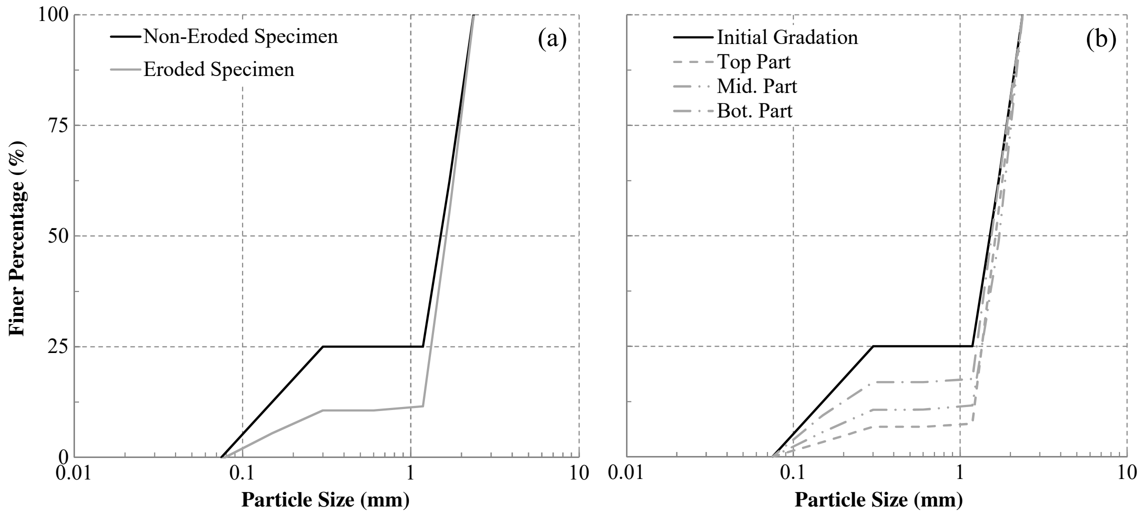

FIG. 14 Repeatability of (a) monotonic shearing: stress-strain behaviour, (b) monotonic shearing: induced excess pore pressure, (c) post-cyclic shearing: stress-strain behaviour and (d) cyclic and post-cyclic shearing: induced excess pore pressure.

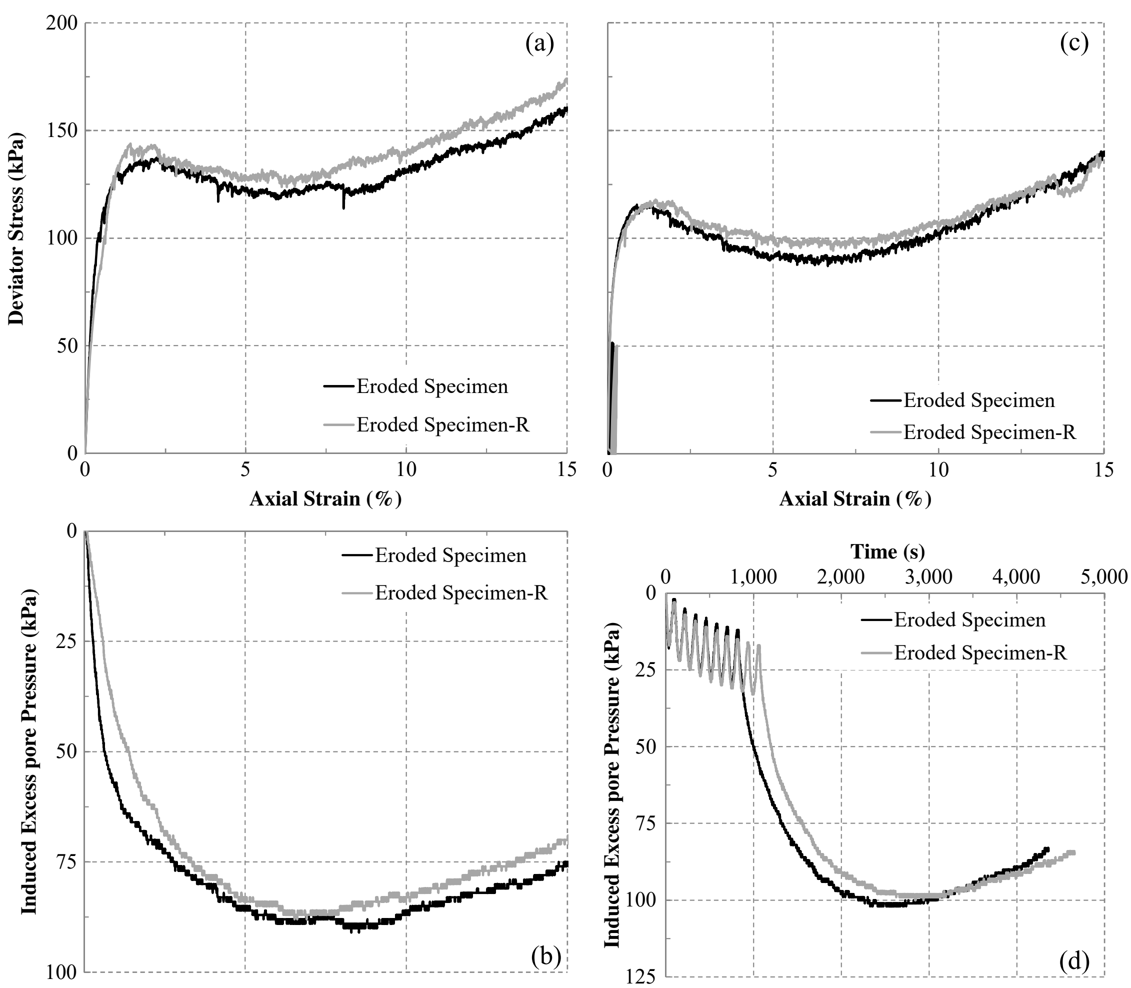

inflows, participation of the survived fine particles in the force chains can be investigated.

PEPSD of an eroded specimen is shown in **Fig. 13**. The flat part of the soil gradation curve moved downward after suffusion as expected (**Fig. 13a**). The erosion of the fine particles was more obvious in the top section of the specimen under downward flow, which is in agreement with Moffat and Fannin (2006), Chang and Zhang (2011), and Ke and Takahashi (2014a) (**Fig. 13b**). Results of the photogrammetry technique showed that the upper region of the eroded specimen experienced a more uniform deformation than the lower region during undrained shearing. However, based on the PEPSDs, the upper part lost more fine particles. It is evident that a considerable percentage of the survived fine particles in the lower part belonged to the upper parts that were clogged downstream. Therefore, the initial uniformity (as provided during sample preparation) was not present anymore. Although the upper region of the specimens lost most of the fine particles, a clean and robust coarse structure remained. However, due to the fine particles spreading non-uniformly across the lower region of the specimen, this led to a different behavior during shearing. This confirmed that the global void ratio is not an accurate index for assessing the post-erosion behaviour.

Repeatability

Repeatability of the post-erosion triaxial test results under monotonic loading and cyclic loading followed by monotonic shearing is shown in **Fig. 14**. Each test was repeated to ensure validity of the results. From this figure, it can be seen that the tests were reasonably consistent for all eroded specimens. The only minor observed deviation could be explained due to the non-uniformity of the reconstituted samples during preparation or the small difference in the final quantity of the eroded particles.

Conclusions

In this study, a versatile apparatus was developed from a conventional triaxial chamber to investigate the post-erosion behavior of granular type soils. This newly developed system is capable of performing erosion inside the triaxial cell on different sized specimens at various stress paths, hydraulic conditions, and loading patterns. The effect of suffusion on the mechanical properties of an internally unstable soil was investigated. The gap-graded soil specimens with 25 % fine content were reconstituted using the moist tamping method and consolidated to 150 kPa to remove the stress history of the specimen during sample preparation. A constant flow rate was applied at the top of the specimens for two hours, whereas the back pressure was kept constant (to maintain full stauration). All specimens then experienced undrained shearing under monotonic or cyclic loading. The following points were the most important findings of this research:

- U.S. Army Corps of Engineers (1953), Istomina (1957), Kwang (1990), and Chang and Zhang (2013) among other criteria mis-anticipated internal stability of the soil mixture used in this research.
- The behavior of the soil tested changed from strain hardening behavior to limited flow deformation after erosion. This change increased the undrained shear strength across the small vertical strain range (i.e., up to 4 %) and improved the soil resistance against cyclic loading. The initial stiffness was similar pre and post erosion. However, the eroded specimen became softer over the medium strain range (i.e., 4–8 %).
- The non-eroded and eroded specimens showed contractive behavior first, followed by dilation. The dilative behavior was more obvious in the non-eroded specimens.
- Although 66 % of the fine particles was eroded during erosion, none of the specimens experienced considerable global vertical deformation (less than 1 % vertical strains). However, the soil behavior changed completely. It showed that although the fine particles may not have contributed to the primary soil fabric, their lubricating effect need to be considered.
- The flow deformation of the eroded specimens across the medium vertical strain range (i.e., 4–8 %) was attributed to the local concentration of fine particles or the larger global void ratio. This effect was later overcome by additional shearing and activation of dilatancy. Moreover, it was understood that erosion of the semi-active fine particles that provided lateral support for the coarse particles led to local particle rearrangements. These particle rearrangements decreased the intergranular void ratio and were recognized in vertical strains where a sudden spike occurred. This finding indicates that the post-erosion behavior cannot be explained only by the global void ratio, and increase in the global void ratio does not necessarily mean that the eroded soil moves to a looser state. Inherent behavior of coarse particles, particle shape, and contribution of fine particles in the soil stress matrix also need to be taken into account. More investigation, particularly x-ray tomography, needs to be conducted to confirm this.

ACKNOWLEDGMENTS

The authors acknowledge the support provided through "Melbourne-Sarawak Research Collaboration Scheme," funded by Swinburne University of Technology, Australia.

References

Ahlinhan, M. F. and Achmus, M., 2010, "Experimental Investigation of Critical Hydraulic Gradients for Unstable Soils," presented at the *5th International Conference on Scour and Erosion*, San Francisco, CA, American Society of Civil Engineers, Reston, VA, pp. 599–608.

Bendahmane, F., Marot, D., and Alexis, A., 2008, "Experimental Parametric Study of Suffusion and Backward Erosion," *J. Geotech. Geoenviron. Eng.*, Vol. 134, No. 1, pp. 57–67.

Bradshaw, A. S. and Baxter, C. D. P., 2007, "Sample Preparation of Silts for Liquefaction Testing," *Geotech. Test. J.*, Vol. 30, No. 4, pp. 324–332.

Burenkova, V. V., 1993, "Assessment of Suffusion in Non-Cohesive and Graded Soils," presented at the *1st International Conference on Geo-Filters*, Balkema, Rotterdam, The Netherlands, pp. 357–360.

Carraro, J. A. and Prezzi, M., 2008, "A New Slurry-Based Method of Preparation of Specimens of Sand Containing Fines," *Geotech. Test. J.*, Vol. 31, No. 1, pp. 1–11.

Chang, D. S. and Zhang, L. M., 2011, "A Stress-Controlled Erosion Apparatus for Studying Internal Erosion in Soils," *Geotech. Test. J.*, Vol. 34, No. 6, pp. 579–589.

Chang, D. S. and Zhang, L. M., 2013, "Extended Internal Stability Criteria for Soils Under Seepage," *Soils Found.*, Vol. 53, No. 4, pp. 569–583.

Dallo, Y. A., Wang, Y., and Ahmed, O. Y., 2013, "Assessment of the Internal Stability of Granular Soils Against Suffusion," *Eur. J. Environ. Civ. Eng.*, Vol. 17, No. 4, pp. 219–230.

Ferreira, T. and Rasband, W., 2012, "ImageJ User Guide," *IJ1. 46r*, Natl. Inst. Health, Bethesda, MD, 2012, https://web.archive.org/web/20170916195530/https://imagej.nih.gov/ij/docs/guide/user-guide.pdf/ (accessed 16 Sep. 2017).

Fleshman, M. S. and Rice, J. D., 2014, "Laboratory Modelling of the Mechanisms of Piping Erosion Initiation," *J. Geotech. Geoenviron. Eng.*, Vol. 140, No. 6, https://doi.org/10.1061/(ASCE)GT.1943-5606.0001106

Fraser, H. J., 1935, "Experimental Study of the Porosity and Permeability of Elastic Sediments," *J. Geol.*, Vol. 43, No. 8, pp. 910–1010.

Frost, J. D. and Park, J. Y., 2003, "A Critical Assessment of the Moist Tamping Technique," *Geotech. Test. J.*, Vol. 26, No. 1, pp. 57–70.

Guimaraes, M., 2002, "Crushed Stone Fines and Ion Removal from Clay Slurries-Fundamental Studies," Dissertation, Georgia Institute of Technology, Atlanta, GA.

Hicher, P. Y., 2013, "Modelling the Impact of Particle Removal on Granular Material Behaviour," *Géotechnique*, Vol. 63, No. 2, pp. 118–128.

Indraratna, B., Israr, J., and Rujikiatkamjorn, C., 2015, "Geometrical Method for Evaluating the Internal Instability of Granular Filters Based on Constriction Size Distribution," *J. Geotech. Geoenviron. Eng.*, Vol. 141, No. 10, pp. 1–14, https://doi.org/10.1061/(ASCE)GT.1943-5606.0001343

Indraratna, B., Raut, A. K., and Khabbaz, H., 2007, "Constriction-Based Retention Criterion for Granular Filter Design," *J. Geotech. Geoenviron. Eng.*, Vol. 133, No. 3, pp. 266–276.

International Commission on Large Dams (ICOLD), 2015, "Internal Erosion of Existing Dams, Levees and Dikes, and Their Foundations," Bulletin 164, Paris.

Ishihara, K., 1993, "Liquefaction and Flow Failure During Earthquakes," *Géotechnique*, Vol. 43, No. 3, pp. 351–451.

Istomina, V. S., 1957, "Filtration Stability of Soils," Gostroizdat, Moscow.

Jiang, M. J., Konrad, J. M., and Leroueil, S., 2003, "An Efficient Technique for Generating Homogeneous Specimens for DEM Studies," *Comput. Geotech.*, Vol. 30, No. 7, pp. 579–597.

Ke, L. and Takahashi, A., 2012, "Strength Reduction of Cohesionless Soil Due to Internal Erosion Induced by One-Dimensional Upward Seepage Flow," *Soils Found.*, Vol. 52, No. 4, pp. 698–711.

Ke, L. and Takahashi, A., 2014a, "Triaxial Erosion Test for Evaluation of Mechanical Consequences of Internal Erosion," *Geotech. Test. J.*, Vol. 37, No. 2, pp. 1–18.

Ke, L. and Takahashi, A., 2014b, "Experimental Investigations on Suffusion Characteristics and its Mechanical Consequences on Saturated Cohesionless Soil," *Soils Found.*, Vol. 54, No. 4, pp. 713–730.

Ke, L. and Takahashi, A., 2015, "Drained Monotonic Responses of Suffusional Cohesionless Soils," *J. Geotech. Geoenviron. Eng.*, Vol. 141, No. 8, https://doi.org/10.1061/(ASCE)GT.1943-5606.0001327, 04015033

Kenney, T. C., Chahal, R., Chiu, E., Ofoegbu, G. I., Omange, G. N., and Ume, C. A., 1985, "Controlling Constriction Sizes of Granular Filters," *Can. Geotech. J.*, Vol. 22, No. 1, pp. 32–43.

Kenney, T. C. and Lau, D., 1985, "Internal Stability of Granular Filters," *Can. Geotech. J.*, Vol. 22, No. 2, pp. 215–225, https://doi.org/10.1139/t85-029

Kenney, T. C. and Lau, D., 1986, "Internal Stability of Granular Filters: Reply," *Can. Geotech. J.*, Vol. 23, No. 4, pp. 420–423, https://doi.org/10.1139/t86-068

Kezdi, A., 1969, "Increase of Protective Capacity of Flood Control Dikes," Budapest University of Technology and Economics, Budapest. Report No. 1. (in Hungarian).

Kuerbis, R. and Vaid, Y. P., 1988, "Sand Sample Preparation-The Slurry Deposition Method," *Soils Found.*, Vol. 28, No. 4, pp. 107–118.

Kwang, T., 1990, "Improvement of Dam Filter Criterion for Cohesionless Base Soil," M. Eng. thesis, Asian Institute of Technology, Bangkok, Thailand.

Ladd, R. S., 1978, "Preparing Test Specimens Using Undercompaction," *Geotech. Test. J.*, Vol. 1, No. 1, pp. 16–23.

Li, M. and Fannin, R. J., 2011, "A Theoretical Envelope for Internal Instability of Cohesionless Soil," *Géotechnique*, Vol. 62, No. 1, pp. 77–80.

Luo, Y. L., Qiao, L., Liu, X. X., Zhan, M. L., and Sheng, J. C., 2013, "Hydro-Mechanical Experiments on Suffusion Under Long-Term Large Hydraulic Heads," *Nat. Hazards*, Vol. 65, No. 3, pp. 1361–1377.

Mao, C. X., 2005, "Study on Piping and Filters. Part 1: Piping (in Chinese)," *Rock Soil Mech.*, Vol. 26, No. 2, pp. 209–215.

Marot, D., Bendahmane, F., and Nguyen, H. H., 2012, "Influence of Angularity of Coarse Fraction Grains on Internal Erosion Process," *La Houille Blanche*, Vol. 6, pp. 47–53.

Mehdizadeh, A., Disfani, M. M., Evans, R. P., Arulrajah, A., and Ong, D. E. L., 2015, "Discussion of 'Development of an Internal Camera-Based Volume Determination System for Triaxial Testing' by S. E. Salazar, A. Barnes, and R. A. Coffman," *Geotech. Test. J.*, Vol. 38, No. 1, pp. 165–168, https://doi.org/10.1520/GTJ20150153

Mitchell, J. K., 1993, *Fundamentals of Soil Behavior*, John Wiley & Sons, Inc., New York, N. Y., pp. 1–210.

Moffat, R. A. and Fannin, R. J., 2006, "A Large Permeameter for Study of Internal Stability in Cohesionless Soils," *Geotech. Test. J.*, Vol. 29, No. 4, pp. 273–279.

Moffat, R. and Fannin, R. J, 2011, "A Hydromechanical Relation Governing Internal Stability of Cohesionless Soil," *Can. Geotech. J.*, Vol. 48, No. 3, pp. 413–424.

Moffat, R., Fannin, R. J., and Garner, S. J, 2011, "Spatial and Temporal Progression of Internal Erosion in Cohesionless Soil," *Can. Geotech. J.*, Vol. 48, No. 3, pp. 399–412.
Moffat, R. and Herrera, P., 2014, "Hydromechanical Model for Internal Erosion and Its Relationship with the Stress Transmitted by the Finer Soil Fraction," *Acta Geotech.*, Vol. 10, No. 5, pp. 643–650.
Moraci, N., Mandaglio, M. C., and Ielo, D., 2014, "Analysis of the Internal Stability of Granular Soils Using Different Methods," *Can. Geotech. J.*, Vol. 51, No. 9, pp. 1063–1072.
Ouyang, M. and Takahashi, A., 2015, "Influence of Initial Fines Content on Fabric of Soils Subjected to Internal Erosion," *Can. Geotech. J.*, Vol. 53, No. 2, pp. 299–313.
Richards, K. S. and Reddy, K. R., 2008, "Experimental Investigation of Piping Potential in Earthen Structures," *Geotech. Special Pub.*, No. 178, pp. 367–376.
Sail, Y., Marot, D., Sibille, L., and Alexis, A., 2011, "Suffusion Tests on Cohesionless Granular Matter: Experimental Study," *Eur. J. Environ. Civ. Eng.*, Vol. 15, No. 5, pp. 799–817.
Shire, T., O'Sullivan, C., Hanley, K. J., and Fannin, R. J., 2014, "Fabric and Effective Stress Distribution in Internally Unstable Soils," *J. Geotech. Geoenviron. Eng.*, Vol. 140, No. 12.
Scholtès, L., Hicher, P. Y., and Sibille, L., 2010, "Multiscale approaches to describe mechanical responses induced by particle removal in granular materials," *Comptes Rendus Mécanique*, Vol. 338, No. 10, pp. 627–638.
Sherard, J. L., 1979, "Sinkholes in Dams of Coarse, Broadly Graded Soils," in transactions of the *13th International Congress on Large Dams*, New Delhi, India, International Commission on Large Dams, Paris, pp. 25–34.
Skempton, A. W. and Brogan, J. M., 1994, "Experiments on Piping in Sandy Gravels," *Géotechnique*, Vol. 44, No. 3, pp. 449–460.
Terzaghi, K., 1925, "Erdbaumechanik auf bodensphysikalischer grundlage," *Franz Deuticke*, Vienna.
Uchaipichat, A., Khalili, N., and Zargarbashi, S., 2011, "A Temperature Controlled Triaxial Apparatus for Testing Unsaturated Soils," *Geotech. Test. J.*, Vol. 34, No. 5, pp. 424–432.
U.S. Army Corps of Engineers, 1953, "Filter Experiments and Design Criteria," Waterways Experiment Station, Vicksburg, MS, Technical Memorandum No. 3–360.
Wood, D. M., Maeda, K., and Nukudani, E., 2010, "Modelling Mechanical Consequences of Erosion," *Géotechnique*, Vol. 60, No. 6, pp. 447–457.
Xiao, M. and Shwiyhat, N., 2012, "Experimental Investigation of the Effects of Suffusion on Physical and Geomechanic Characteristics of Sandy Soils," *Geotech. Test. J.*, Vol. 35, No. 6, pp. 890–900.

Progressive Internal Erosion in a Gap-Graded Internally Unstable Soil: Mechanical and Geometrical Effects

Amirhassan Mehdizadeh, Ph.D.[1]; Mahdi M. Disfani, Ph.D.[2]; Robert Evans, Ph.D.[3]; and Arul Arulrajah, Ph.D.[4]

Abstract: This paper investigates the posterosion geomechanical behavior of internally unstable granular material due to removal of fines caused by erosive forces of water flow. Posterosion undrained behavior of a gap-graded internally unstable soil was investigated for a range of erosion durations and inflow velocities using a triaxial-erosion apparatus. Test results indicated that the undrained behavior of the original specimen changed from a strain hardening behavior to a flow-type behavior with limited deformation after internal erosion. The initial peak strength improved and the flow potential decreased during the initial stage of erosion. This observed increase in initial peak strength is believed to be the result of a better interlocking between the coarse particles posterosion. In contrast, the slip-down movement of the particles due to an increase in the posterosion void ratio postponed the dilation tendency. Test results also suggested that even erosion of a small percentage of fine particles improved the mechanical frictional behavior of the soil. However, there was a threshold value for the loss of fine particles at which this positive effect deteriorated. This might have been due to formation of local metastable structures and/or overcoming contractive behavior after loss of the semiactive fines and a considerable increase in the global void ratio. Shear strength results, rate of erosion, and local vertical strains together suggest that the intergranular void ratio is a powerful index in evaluating the posterosion mechanical behavior of internally unstable soils. **DOI: 10.1061/(ASCE)GM.1943-5622.0001085.** *© 2017 American Society of Civil Engineers.*

Author keywords: Internal erosion; Soil stress matrix; Gap-graded soils; Posterosion behavior; Seepage.

Introduction

Internal erosion in a granular soil is essentially the migration of fine particles through pre-existing pores (between the coarse particles) caused by seepage flow. Terzaghi (1925) was the first to show that an upward flow decreases the effective stress, which can lead to the dislodgment of solid particles under a critical hydraulic gradient. Although various methods have been developed to evaluate the susceptibility of soil gradations to internal erosion (Kezdi 1969; Sherard 1979; Kenney and Lau 1985; Chapuis 1992; Wan and Fell 2008; Moffat and Fannin 2011; Chang and Zhang 2013; Dallo et al. 2013; Moraci et al. 2014; Indraratna et al. 2007, 2015), the posterosion geomechanical behavior of granular material is still a topic of discussion, with contradictory results presented in the literature. Sterpi (2003) stated that the effect of gradual erosion and transport of fine particles due to a severe seepage flow cannot be ignored when working in an urban area. This may occur during the artificial lowering of the water table by means of pumping wells. Some laboratory tests were carried out on soil samples subjected to a controlled seepage flow to investigate the erosion of fine particles. The test result were then used to calibrate a new model suggested to predict particle transport based on the conservation of mass of moving particles with a suitable law of erosion. This model was capable of estimating the impact of erosion on the geomechanical behavior of soil and surrounding structures. However, Sterpi (2003) believed that further experimental investigation needed to be conducted to achieve a better insight into the various aspects of this problem. Cividini and Gioda (2004) followed a similar approach by developing a finite-element model to investigate erosion and transport of fine particles in granular soils. However, similar to Sterpi (2003), their numerical model contained some relevant simplifying assumptions due to the limited experimental data available in the literature. An incremental erosion law was proposed by Cividini et al. (2009) based on the experimental data. This law equation was used in two- and three-dimensional finite-element models to estimate the quantity of eroded material adjacent to the pumping wells and the possible settlements of nearby structures. They suggested that the focus of the experimental investigation could be variation of the sample height to consider the effect of self-filtration and development of local deposition and/or assessment of the influence of the in situ effective stresses on the erosion process by applying a confining pressure to the sample.

Chang and Zhang (2011) conducted a series of drained triaxial tests on eroded specimens under different stress paths. Their results showed that the dilative behavior of the noneroded specimen changed to a contractive behavior after internal erosion. They believed that loss of fine particles increased the global void ratio and shifted the soil condition to a looser state, ultimately leading to a lower drained shear strength. The secant modulus also decreased due to internal erosion. However, regardless of the initial stress path and percentage of the eroded particles, the residual strength was similar for pre- and posterosion specimens. In a similar study, Ke and Takahashi (2012) measured the bearing capacity of a series of soil specimens pre- and posterosion using a miniature cone

[1]Candidate in Geotechnical Engineering, Dept. of Civil and Construction Engineering, Swinburne Univ. of Technology, Melbourne 3122, Australia. E-mail: amehdizadeh@swin.edu.au

[2]Senior Lecturer in Geotechnical Engineering, Dept. of Infrastructure Engineering, Univ. of Melbourne, Melbourne 3010, Australia (corresponding author). E-mail: mmiri@unimelb.edu.au

[3]Senior Lecturer in Geotechnical Engineering, Dept. of Civil and Construction Engineering, Swinburne Univ. of Technology, Melbourne 3122, Australia. E-mail: robertevans@swin.edu.au

[4]Professor in Geotechnical Engineering, Dept. of Civil and Construction Engineering, Swinburne Univ. of Technology, Melbourne 3122, Australia. E-mail: aarulrajah@swin.edu.au

Note. This manuscript was submitted on January 6, 2017; approved on September 12, 2017; published online on December 21, 2017. Discussion period open until May 21, 2018; separate discussions must be submitted for individual papers. This paper is part of the ***International Journal of Geomechanics***, © ASCE, ISSN 1532-3641.

penetrometer. They found that internal erosion (caused by an upward flow) decreased the cone tip resistance. In other words, loss of fine particles due to internal erosion resulted in a reduction of the internal friction angle. More importantly, this reduction was less than 2% for most of their specimens tested, and no specific reason was provided for this strength reduction. However, it is plausible to assume that the loss of fine particles weakened the mechanical interlock between the coarse particles, leading to lower peak strength. The siliceous sand used in their research was categorized as an angular to subangular material. Thus, the presence of the fine particles may have improved the internal friction.

Xiao and Shwiyhat (2012) experimentally investigated the posterosion behavior of sandy soils. Undrained shear strength results of the eroded specimens were found to be greater than those of the noneroded specimens. They indicated that this may have occurred due to a loss in saturation during the erosion phase as the bottom of test specimens were subjected to the atmospheric pressure.

More recently, Ke and Takahashi (2014b) studied drained and undrained behaviors of a gap-graded soil with 35% fine content (FC) under monotonic and cyclic loadings pre- and posterosion. The initial global void ratio of soil specimens was approximately 0.56, which increased to 0.94 after erosion. Relative density and confining pressure were 30% and 50 kPa, respectively. Based on these magnitudes, it appears that the specimens were in a loose state before erosion. The volumetric strains during shearing pre- and posterosion were both contractive as expected. The posterosion specimen (with a larger void ratio) had a lower volumetric deformation but showed a higher initial stiffness and lower drained shear strength. Contrary to the drained test results, the soil specimens (regardless of erosion) showed softening behavior with limited flow deformation during undrained shearing. The eroded specimen reached a higher peak shear strength under low strain but collapsed temporarily at medium strain range. Undrained cyclic behavior pre- and posterosion was also investigated, indicating a higher cyclic resistance for the posterosion specimen. It was noted that the higher undrained strength of the eroded specimen may have been attributed to rearrangement of the soil particles during erosion and progression of the local reinforcement in the soil fabric. Based on the individual triaxial tests results, it was concluded that the presence of the fine particles decreased the soil strength and postponed dilation on loose soil samples with different initial fine contents (FC_i). However, it was not clear why this reinforcement and geometric properties of particles had a different impact during drained and undrained conditions. Interestingly, the soil type, particle-size distribution, and initial void ratio used in this research were similar to the previous study conducted by Ke and Takahashi (2012) that showed loss of fine particles reduced the cone tip resistance.

Posterosion drained behavior of a gap-graded soil (with varying initial FCs) was further investigated by Ke and Takahashi (2014a). Results showed that the drained shear strength did not change after erosion for specimens with 15 and 25% initial FCs. In contrast, the specimen with an initial FC of 35% showed a drop in shear strength. Surprisingly, the residual posterosion fine content (FC_f) was similar (10–13%) for all specimens under the same confining pressures and hydraulic conditions. In other words, specimens with a greater initial FC lost more of their fine particles during the erosion phase. However, apart from the specimen with 35% FC, erosion of the fines did not affect the mechanical behavior of the other specimens. This suggests that those fine particles sat loosely in the available void spaces formed by the coarse particles and did not participate in load transferring.

Impact of internal erosion on geomechanical behavior of granular material has been explained using the mechanics of interaction between fine and coarse particles. It is generally accepted that there is a threshold FC above which the coarse particles start to float in the fine particle network. For soils containing FC above this threshold, soil behavior is mainly controlled by the fine particles rather than the coarse particles. Shire et al. (2014) investigated the effect of fine content on stress distribution for internally unstable soils using discrete-element modeling. It was concluded that, for internally unstable soils with FCs less than 25%, the soil can be classified as underfilled. For these soils, fine particles sit loose in the voids and will migrate through the pores if they are smaller than constriction size and the hydraulic forces are adequate. In contrast, the soil is considered overfilled if the FC is larger than 35%. In this case, fine particles fill all the voids and contribute to soil structure and carry stresses along with the coarse particles. For soils in the transitional zone (i.e., between 25 and 35% FC), the contribution of fine particles in the soil stress matrix is highly dependent on relative density. This critical FC for soil tested by Ke and Takahashi (2014a) was found to be 33% based on a method presented by Rahman et al. (2011) or 37% according to the calculations by Ke and Takahashi's (2012). These values suggest that a specimen with 35% initial FC is on the borderline. Therefore, the different behavior patterns observed for this specimen could be related to the different soil stress matrix in comparison to other specimens with lower FC.

Migration of fine particles in granular filter material was investigated by Abdelhamid and El Shamy (2016) using a pore-scale modeling approach. A three-dimensional, transient, fully coupled pore-scale model was developed by using the lattice Boltzmann method for idealization of the fluid and a discrete-element method for the solid phase. They showed that soils with $D'_{15}/d'_{85} < 4$ are internally stable, which was in agreement with the Kezdi (1969) criteria. However, this model falls short in predicting the posterosion geomechanical behavior in terms of shear strength or compressibility.

For gap-graded soils with FC in the transitional zone, current literature overall suggests that the undrained shear strength and cyclic resistance increase at the low strain range after erosion of the fine particles. However, a reduction in posterosion drained shear strength was also reported (Chang and Zhang 2011; Ke and Takahashi 2014b).

Through an analysis of interaction of fine and coarse particles pre- and posterosion, this paper further investigates posterosion behavior of a gap-graded soil. Mechanical and geometrical consequences of progressive internal erosion were investigated using a modified triaxial system. The new erosion-triaxial apparatus allows for all triaxial and erosion phases to take place within the same cell and on the same specimen. This naturally minimizes disturbance and any potential loss of saturation of the specimen. Seepage is applied to the specimen for different durations and flow velocities, whereas the confining pressure and initial FC are kept constant. This testing approach assists in providing a better understanding of the gradual effects of erosion of fine particles on the undrained shear behavior of granular soils.

Testing Procedure and Material

The ability to apply various hydraulic gradients at the top of a triaxial soil specimen and collect the eroded particles from the bottom of the sample (without loss of saturation) is one of the main features of this new combined erosion-triaxial testing system (Fig. 1). A perforated top cap and a funnel-shaped base plate with an outlet and a netted plate were the essential parts of the cell modification. A wire screen mesh with an opening size similar to the smallest coarse fraction particle was placed on top of the netted plate to hold the coarse

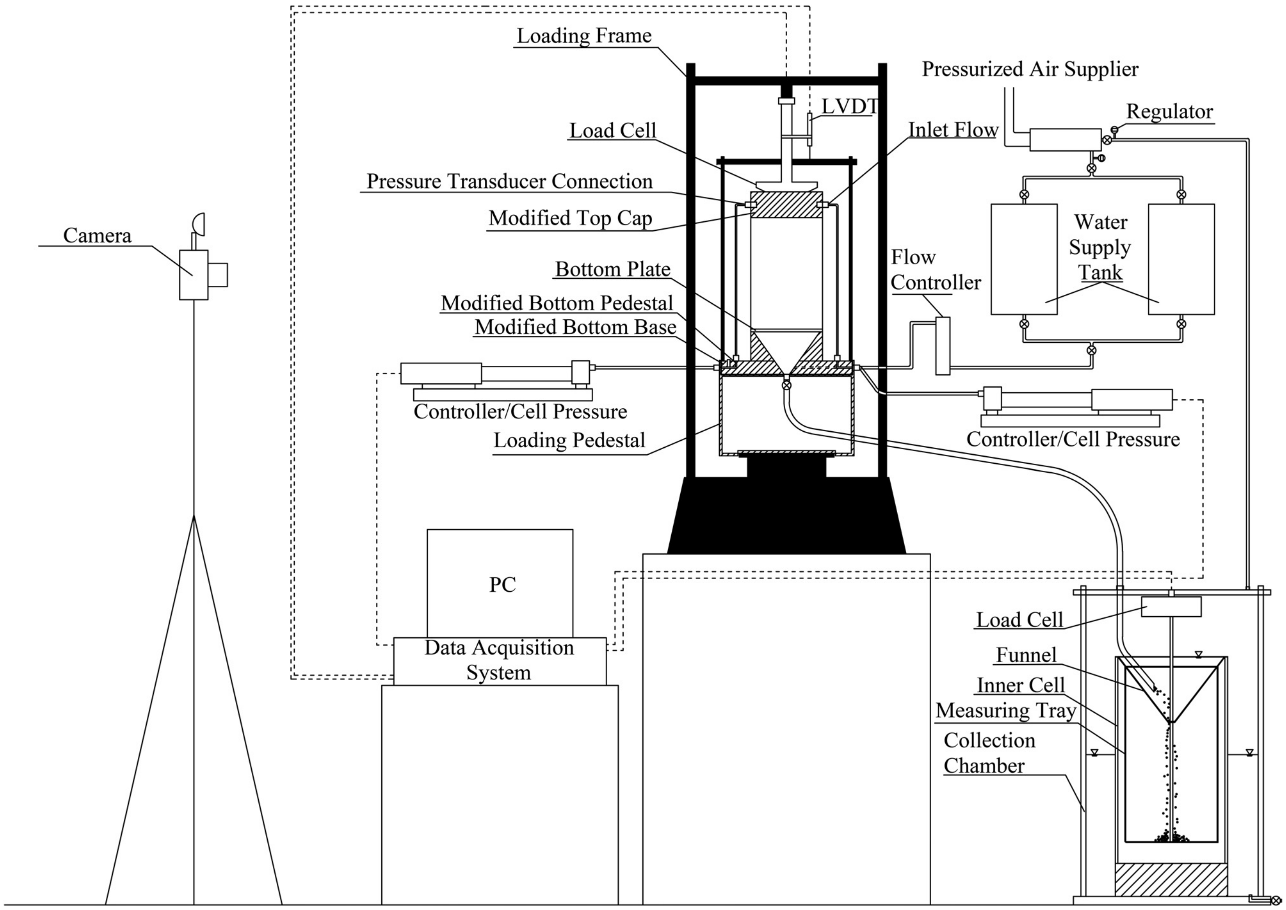

Fig. 1. Scheme of testing apparatus

particles in place, allowing the fine particles to pass freely under flow forces. To provide the required hydraulic condition, two cells filled with pressurized de-aired water and a flow controller were connected to the specimen top cap. Washed particles were collected from the bottom of the triaxial cell using a collection system. The collection tank in this research was developed based on Ke and Takahashi (2014b) to avoid the loss of saturation during the erosion stage. This tank was always under a pressure equal to the back pressure applied to the soil specimen. This assumed continuous saturation and the continuous measurement of the eroded particles' weight during the erosion phase. Volumetric, axial, and lateral strains were measured using a photogrammetry technique to prevent errors caused by local strain gauges.

It has been mentioned that there is a threshold value ($25\% \leq F_{C\mathrm{Thr}} \leq 35\%$) for the FC, above which coarse particles start to float within a fine matrix and are no longer in full contact with each other (Shire et al. 2014). In fact, fine particles form the soil skeleton and carry stresses. In this condition, the soil is not internally unstable and fine particles are not susceptible to the internal erosion under a seepage flow. Moreover, it is understood that fine particles in soils with a low FC (less than 25%) may only fill the voids between coarse particles and be inactive in stress transferring. Therefore, erosion of these particles has no influence on posterosion behavior. Because the main objective of this research was to investigate the posterosion behavior of internally unstable soils, 25% FC was selected to avoid any misleading consequences.

A gap-graded soil with 25% initial nonplastic FC was used for this research. The particle-size distribution and geometric properties of the tested soil are presented in Fig. 2. The susceptibility of this soil to internal erosion was evaluated using the available methods of Kezdi (1969), Sherard (1979), Kenney and Lau (1985, 1986), Burenkova (1993), Mao (2005), Dallo et al. (2013), Chang and Zhang (2013), and Moraci et al. (2014). The soil test mixture was found to be internally unstable, and if the applied hydraulic gradient is high enough, the fine particles will be dislodged during erosion.

Triaxial specimens (75 mm in diameter and 150 mm in height) were prepared with 6% initial water content. The moist-tamping method was used to compact the test specimen in 10 layers according to the method proposed by Ladd (1978) and Jiang et al. (2003). To set up the specimen with minimal chance of soil disturbance or collapse, a vacuum pressure of 10 kPa was applied to the specimen during placement. This negative pressure was eventually replaced with a cell pressure of 10 kPa as the cell chamber was filled with water. To reach full saturation, carbon dioxide was injected into the bottom of the specimen for 2 h at a very low rate of 1 L/min. To avoid any particle movement, cell and back pressures were increased gradually at a rate of 1 kPa/min to 400 and 390 kPa, respectively, and held for a further 100 min. Skempton's saturation B-value was checked at the end of this stage and recorded to be 0.93 for all specimens.

Impact of confining pressure on erodibility of fine particles has been investigated in previous studies (Tomlinson and Vaid 2000; Bendahmane et al. 2008; Moffat and Fannin 2011; Luo et al. 2013; Ke and Takahashi 2014a). Tomlinson and Vaid (2000) showed that the effect of confining pressure on internal erosion of an artificial-material glass ball was minor. Bendahmane et al. (2008) believed that an increase in the confining pressure increased the contact bonds between particles and the internal erosion resistance. This was in

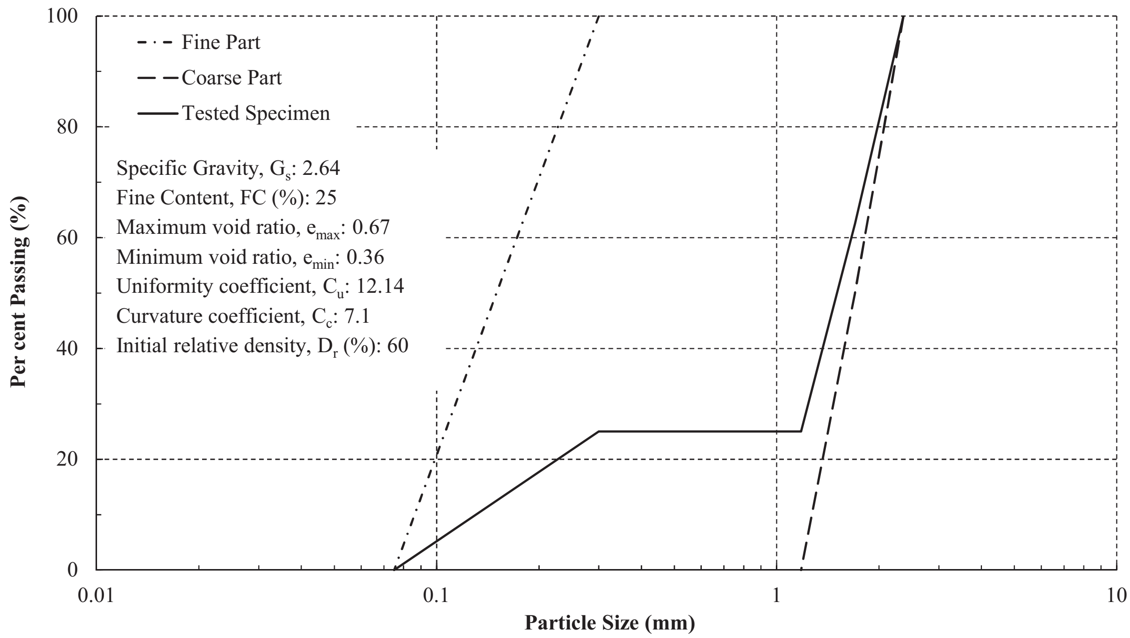

Fig. 2. Particle-size distribution and various engineering properties of tested soil specimen

agreement with the findings by Moffat and Fannin (2011), Luo et al. (2013), and Ke and Takahashi (2014a) that an increase in confining pressure increases the required hydraulic gradient for suffusion, as fines are expected to densify between coarse particles. Although it seems that erosion of fine particles might be affected by confining pressure, a decision was made to consolidate all specimens to the same effective pressure of 150 kPa for 720 min. This consolidation pressure was chosen to eliminate the experienced stress history of soil specimens during sample preparation. Frost and Park (2003) reported that a soil specimen 71 mm in diameter and 142 mm in height may experience 80–125 kPa vertical stress to reach 60% relative density in seven soil layers using a moist-tamping method.

The erosion phase started after consolidation for all specimens. A downward flow with two different flow velocities (V_{inflow}) of 52 and 92 mm/min (Inflow-V52 and Inflow-V92) was applied to the top of the specimens to investigate the erosion potential and the influence of loss of fine particles on the soil structure and its geomechanical behavior. The selected inflow velocities were chosen to be higher than the critical inflow to initiate internal erosion but lower than the failure inflow, whereas they are still high enough to terminate the erosion phase in a reasonable period of time. The erosion rate was increased gradually to minimize the jet flow effect and was maintained for 30 and 120 min. The posterosion undrained behavior of the soil specimens was investigated under monotonic shearing and compared to the behavior of a noneroded specimen prepared using the same conditions (NE-C150). Table 1 shows the testing program. Each test was repeated several times to ensure consistency of the results. Repeatability and reliability of the test results are shown in the appendix.

Table 1. Testing Program

Specimen identification	Consolidation pressure (kPa)	Inflow velocity (mm/min)	Erosion duration (min)	Undrained shearing rate (%/min)
E-C150-V92-T30	150	92	30	0.26
E-C150-V92-T120	150	92	120	0.26
E-C150-V52-T30	150	52	30	0.26
E-C150-V52-T120	150	52	120	0.26
NE-C150	150	—	—	0.26

Note: C = consolidation pressure; E = eroded; NE = noneroded; T = erosion duration; V = seepage velocity.

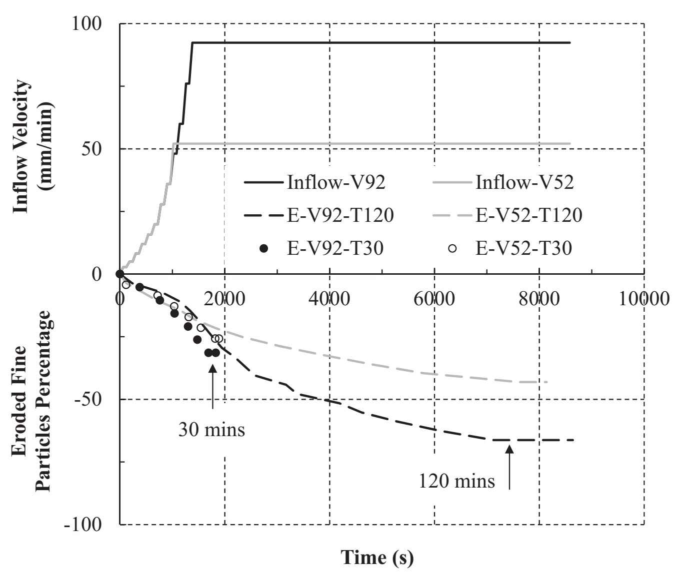

Fig. 3. Percentage of FC erosion against the inflow velocity and erosion progress

Test Results

The percentage of the eroded fine particles with respect to erosion progress is shown in Fig. 3. For the first 20 min, the erosion rate was similar for all specimens when all specimens experienced the same inflow velocity. In addition, the erosion rate decreased for all tests when the inflow velocity reached its target value and remained

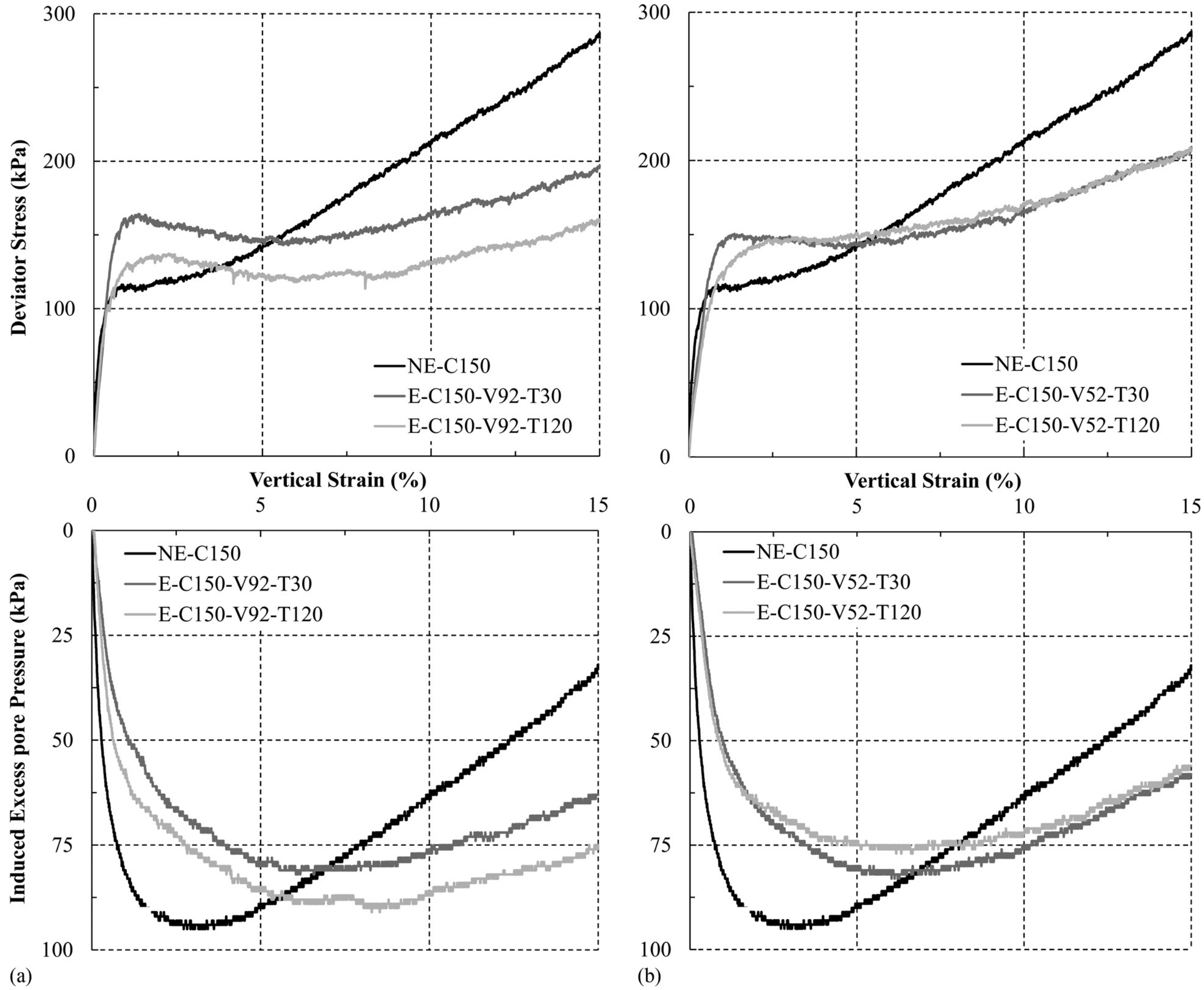

Fig. 4. Comparison of stress-strain relationship and induced EPWP during shearing pre- and posterosion: (a) specimens experienced seepage velocity of 92 mm/min; (b) specimens experienced seepage velocity of 52 mm/min

constant. For the specimens subjected to an inflow velocity of 92 mm/min, 31 and 66% of the fine particles were eroded after 30 and 120 min, respectively. In comparison, the percentage of eroded fine particles was only 26 and 43% for the specimens eroded at an inflow velocity of 52 mm/min.

The mechanical (shear strength) behavior of the tested specimens after 30 and 120 min of erosion was compared with the noneroded specimen in Figs. 4 and 5. It is evident that the initial hardening behavior of the soil specimen changed to flow-type behavior with limited deformation as a result of the erosion, in agreement with what was previously reported by Ouyang and Takahashi (2016) for gap-graded specimens with 25% initial FC. This was regardless of the inflow velocity or duration of erosion. For the eroded specimens at a seepage velocity of 92 mm/min, the undrained mobilized shear strength increased after erosion for small axial strains (i.e., ε_a = 0–5% for the specimen eroded for 30 min and ε_a = 0–4% for the specimen eroded for 120 min). This confirmed the findings by Ke and Takahashi (2014b) that erosion of the fine particles improves the initial undrained peak shear strength for granular soils with FC in the transitional zone. However, this improvement deteriorated after the progression of internal erosion and further loss of fine particles (E-C150-V92-T120). Contrary to the noneroded specimen (NE-C150), both eroded specimens showed temporary collapse at medium axial strain. Excess pore-water pressure (EPWP) did develop rapidly in the noneroded specimen, and dilation was observed at low axial strain. In contrast, the maximum EPWP was reached at medium axial strain, and contractive behavior was dominant for the eroded specimens. The loss of fine particles and increase in global void ratio could be the reason for the softening behavior observed for the eroded specimens in this study, as previously reported by Scholtès et al. (2010), Wood et al. (2010), and Chang and Zhang (2011). However, improvement of the initial shear strength might be an indication of better interlocking between the coarse particles.

The influence of erosion duration on soil behavior was not noticeable in the specimens subjected to a seepage velocity of 52 mm/min. However, eroded specimens showed a greater initial shear strength with a lower tendency for dilation, which was similar to the eroded specimens under an inflow velocity of 92 mm/min. Interestingly, E-C150-V52-T30 and E-C150-V92-T30 showed similar behavior after 30 min of erosion. According to Table 2, the residual FC was recorded as 18.6 and 19.8% after 30 min of erosion for E-C150-V92-T30 and E-C150-V52-T30, respectively. This suggests that, although one specimen experienced a higher inflow velocity, the soil response was mainly dependent on the amount of eroded particles (i.e., soil structure and interaction of fine and coarse

Int. J. Geomech., 2018, 18(3): 04017160

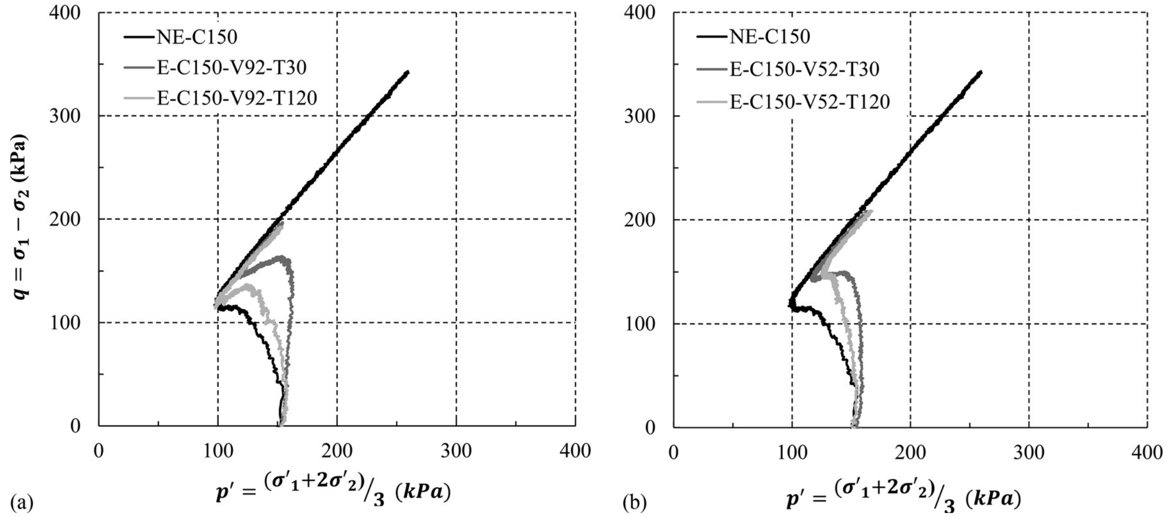

Fig. 5. Comparison of stress path pre- and posterosion: (a) specimens experienced seepage velocity of 92 mm/min; (b) specimens experienced seepage velocity of 52 mm/min

Table 2. Variation of Fine Fraction Due to Internal Erosion

Specimen identification	Initial coarse fraction (g)	Initial fine fraction (g)	FC_i (%)[a]	Eroded fine (g)	Survived fine (g)	FC_f (%)[b]	Eroded percentage
E-C150-V92-T30	905.25	301.75	25	95	206.75	18.6	31.5
E-C150-V92-T120	905.25	301.75	25	200	101.75	10.1	66.3
E-C150-V52-T30	905.25	301.75	25	78	223.75	19.8	25.8
E-C150-V52-T120	905.25	301.75	25	130	171.75	15.9	43.1
NE-C150	905.25	301.75	25	0	301.75	25	0.0

Note: C = consolidation pressure; E = eroded; NE = noneroded; T = erosion duration; V = seepage velocity.
[a]Initial fine content.
[b]Final (residual) fine content.

particles) in the range of seepage velocities applied to the specimens in this research. In other words, the change in soil fabric and particle rearrangement was only sensitive to the amount of fine particles lost due to erosion. However, it is worth noting that, under very large seepage velocities, the soil structure may fail when hydraulic stresses overcome effective stresses acting on coarse particles. In addition, the soil behavior was found to be affected noticeably even due to erosion of only 5% of FC. As $(D'_{15}/d'_{85})_{\max}$ of the tested soil mixture was 5.2, the soil was on the borderline of internally stable and unstable soils. This might have increased the activity of fine particles in the soil structure. The final FC eventually dropped to 15.9% for E-C150-V52-T120 after 120 min of erosion. However, no obvious alteration in soil behavior was noticed due to the progression of erosion, apart from a slight variation in the location of initial peak shear strength. It is believed that erosion of inactive (free) and semiactive (providing lateral support) fine particles occurs approximately at the same time, which means that erosion of 5.2% FC for the E-C150-V52-T30 specimen consisted of both free and semiactive fine particles. However, it appears that the extra 3.9% eroded FC in the case of E-C150-V52-T120 was related to erosion of the previously clogged eroded particles, which had not been fully eroded out of the specimen at early stages of erosion. These clogged fine particles had no significant contribution in the soil structure. Therefore, erosion of these clogged particles had no noticeable impact on the soil response.

To further understand the possible change of soil structure and its impact on posterosion behavior, local vertical strains were measured during the erosion phase using the photogrammetry technique and are presented in Fig. 6. A five-minute interval was chosen between both images during the erosion stage. The vertical strains were shown to increase during erosion, and vertical deformations at the end of 120 minutes of erosion were approximately 2 times greater for E-C150-V92-T120 in comparison to E-C150-V92-T30 [Fig. 6(a)]. However, this increase was less than 17% between E-C150-V52-T120 and E-C150-V52-T30 [Fig. 6(b)]. A considerable initial leap in vertical strains was observed in all specimens at the beginning of the erosion (time: 300 s). In addition, a jumping trend in the vertical strains was identified. Each jump might be related to new local particle rearrangement triggered somewhere inside the soil specimen. The inflow velocity was kept constant after maximum 1,380 s (Fig. 3); however, these steps in the vertical strains continued to the end of the erosion. Erosion of the fine particles that contributed to the soil stress matrix to some extent made the soil structure temporarily unstable, and local particle rearrangement occurred. This rearrangement was more intensive for the specimen subjected to an inflow velocity of 92 mm/min for a long time.

Discussion

The test results suggest that internal erosion of gap-graded soils affects their mechanical behavior, even after a short period of erosion. However, the intensity of this change depends on various parameters impacting soil structure and interaction of fine and coarse particles. These include global and intergranular void ratios, FC, and particle rearrangement.

Int. J. Geomech., 2018, 18(3): 04017160

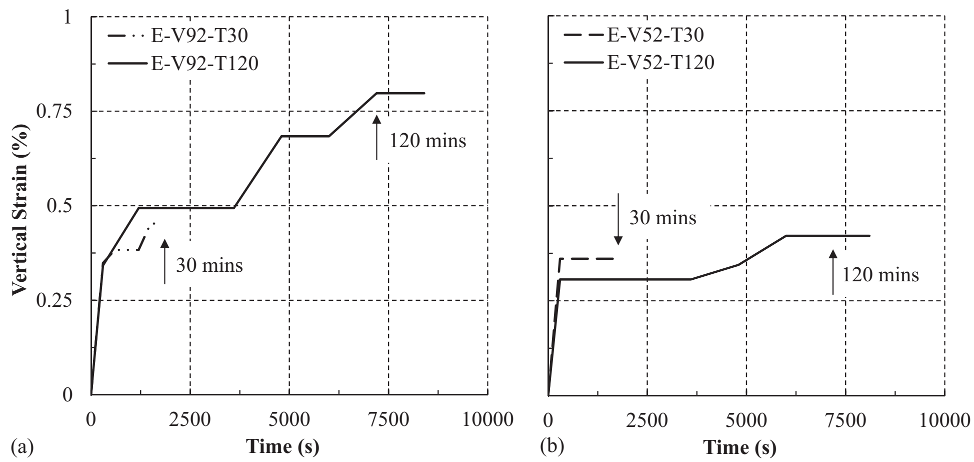

Fig. 6. Vertical strains during erosion phase: (a) subjected to inflow velocity of 92 mm/min; (b) subjected to inflow velocity of 52 mm/min

Undrained Peak Strength

The initial peak shear strength (S_p) presented by Ishihara (1993) is an important point on the stress-strain curve of soil behavior and is presented in Eq. (1). This point is the beginning of an instability state that is explained in the next section

$$\frac{S_p}{\sigma'_c} = \frac{q_{\text{Peak}}}{2P'_c} \tag{1}$$

where σ'_c = effective consolidation stress; P'_c = initial mean effective stress; and q_{Peak} = initial peak deviator stress.

The initial confining pressure showed less than 5% variation at the beginning of the shearing stage due to the occurrence of small changes in water pressure during the erosion phase for all specimens. Therefore, all parameters have been normalized with initial mean effective stresses to eliminate possible effects of stress dependency.

The normalized undrained peak shear strength observed in all tests is shown in Fig. 7. Overall, the normalized initial peak shear strength improved as erosion progressed despite an increase in the global void ratio after internal erosion. After 30 min of erosion, the specimen that experienced the larger inflow velocity showed a higher peak shear strength. Fig. 7 also shows a noticeable drop in peak shear strength when the FC decreased to 10.1% after 120 min of erosion. In addition, although Specimens E-C150-V52-T30 and E-C150-V92-T30 had similar residual FC after 30 min of erosion, the specimen that was subjected to the larger inflow velocity of 92 mm/min showed higher peak strength and larger vertical deformation. These results suggest that there could be an intensive particle rearrangement inside Specimen E-C150-V92-T30, leading to a temporary stronger structure. Beyond this point and as erosion continued, there was a turning point in the residual FC that reduced this initial temporary improvement in soil structure and associated peak shear strength.

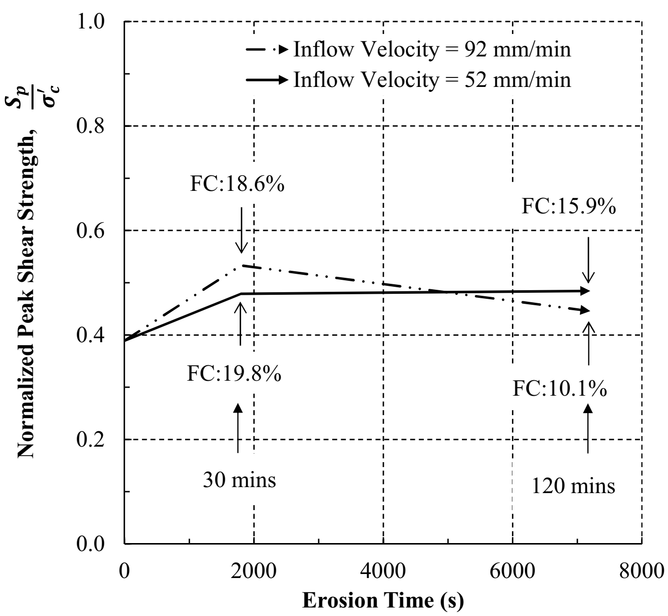

Fig. 7. Variation of normalized peak strength with erosion progress

Quasi-Steady State and Undrained Instability State

When a soil shows softening behavior, there are two important states that need to be taken into account. These are known as the quasi-steady state (QSS) and the ultimate state (US) or steady state (SS) that occurs at relatively large strains. The QSS is a temporary state where soil exhibits the smallest shear strength. The SS is the final state of soil behavior where deformations continue without any change in shear strength and soil volume. There is a debate on which strength level should be taken as the residual strength (S_{us}), because the strength at QSS may be remarkably smaller than the mobilized stress at the SS (Ishihara 1993). Ouyang and Takahashi (2016) stated that it would be safe if the QSS is chosen as the residual strength and used in internal erosion analyses because the soil strength is affected by various unknown factors.

A drop in shear strength between the initial peak shear strength and residual strength at the QSS is known as instability and flow failure. Instability is another indication of the softening behavior. It is classified as one of the failure mechanisms and may lead to flow slides or slope failure under extreme conditions (Lade 1993; Olson et al. 2000). Undrained instability state (UIS) is the state where the deviator stress reaches the initial peak followed by a flow deformation (Murthy et al. 2007). Instability line (IL) is known as the line connecting the peak values of the deviator stresses for the undrained stress path space and starts at the point of origin for sand with no cohesion (Leong et al. 2000; Chu and Leong 2002; Yang et al. 2006). The instability line is not a unique soil property and depends on the initial void ratio and the confining pressure. The larger the

Int. J. Geomech., 2018, 18(3): 04017160

initial void ratio is, the lower the slope of the instability line will be (Chu and Leong 2002). The region between the instability line and steady line is known as the zone of potential instability (Lade 1993). The relationship between the peak shear stress ratio (q_{Peak}/P'_{Peak}) and postconsolidation void ratio is called the instability curve (Chu and Leong 2002). Results of posterosion shear strength tests indicate that the hardening behavior of the original soil changed to a softening behavior with limited flow deformation. The normalized residual strength at QSS [Eq. (2)] and variation of peak shear stress ratio with posterosion void ratio for the specimens tested are presented in Fig. 8. Because the original soil specimen showed a hardening behavior, this analysis was only conducted for the eroded specimens

$$\frac{S_{us}}{\sigma'_c} = \frac{q_s}{2P'_c}\cos(\varphi_s) \tag{2}$$

where q_s = deviator stress at the QSS; and φ_s = angle of phase transformation at QSS (Ishihara 1993).

After 30 min of erosion, the specimen that eroded at the greater inflow velocity showed higher normalized peak strength in comparison with the specimen that eroded at the lower inflow velocity at similar residual FC. However, the normalized residual strength at the QSS was almost the same for all eroded specimens after 30 min of erosion [Fig. 8(a)]. As the erosion progressed, the residual strength was constant for the specimens that eroded at the lower inflow velocity but dropped significantly for specimens that eroded at the larger inflow velocity. It seems the initial peak strength depended upon the FC and particle rearrangement, whereas the residual strength was only dependent on the percentage of the surviving fine particles, and the impact of particle rearrangement was negligible due to the breakage of the particles interlocking in medium to large strains. Interestingly, the instability potential decreased with erosion progress for all specimens tested [Fig. 8(b)]. However, this improvement became fragile as more fine particles were lost.

Flow Potential

A drop in shear strength between the initial peak shear strength and residual strength at the QSS (known as flow failure) stays constant when the residual strength remains at the critical steady state (CSS) level. Alternatively, flow failure can stop as a result of strength regaining and residual strength reaching the ultimate steady state (USS). Yoshimine and Ishihara (1998) proposed an index to evaluate the flow potential (u_f)[Eq. (3)]. This is not an inherent soil property, and direction of principal stress, magnitude of the intermediate principal stress, and structure of the soil fabric may affect it. It is associated with the point where the maximum excess pore pressure is induced. When u_f reaches 100%, soil is liquefied with no residual strength, and flow deformation is continued (Yoshimine and Ishihara 1998)

$$u_f = \left(1 - \frac{P'_{PT}}{P'_c}\right) \times 100 \tag{3}$$

where P'_{PT} = mean effective principal stress at the phase transformation state; and P'_c = initial mean effective stress.

Fig. 9 shows that the flow potential dropped rapidly over the initial 30 min of erosion regardless of the inflow velocity. This decrease in flow potential continued for specimens eroded by the lower inflow velocity. However, the flow potential increased for the specimen eroded by the higher inflow velocity after 120 min of erosion after loss of a certain amount of the fine particles. The smaller flow potential of eroded specimens was also reported by Ouyang and Takahashi (2016). However, the observed increase in the flow potential for the specimen eroded for 2 h by the higher inflow velocity may be related to the turning point in the residual FC and its impact on soil structure, which was discussed earlier. Initial reduction in the FC to approximately 15% improved the soil response against the flow failure. However, further reduction of residual FC increased susceptibility of the soil to the flow failure. This turning point is also observed in Fig. 7.

Void Ratio Variation and Residual FC

The concept of intergranular void ratio was first introduced when it was discovered that the presence of fine particles affected soil behavior significantly. This was due to the different types of fines and how they contributed to the soil stress matrix. Mitchell (1993) defined the intergranular void ratio as the void ratio of the host sand

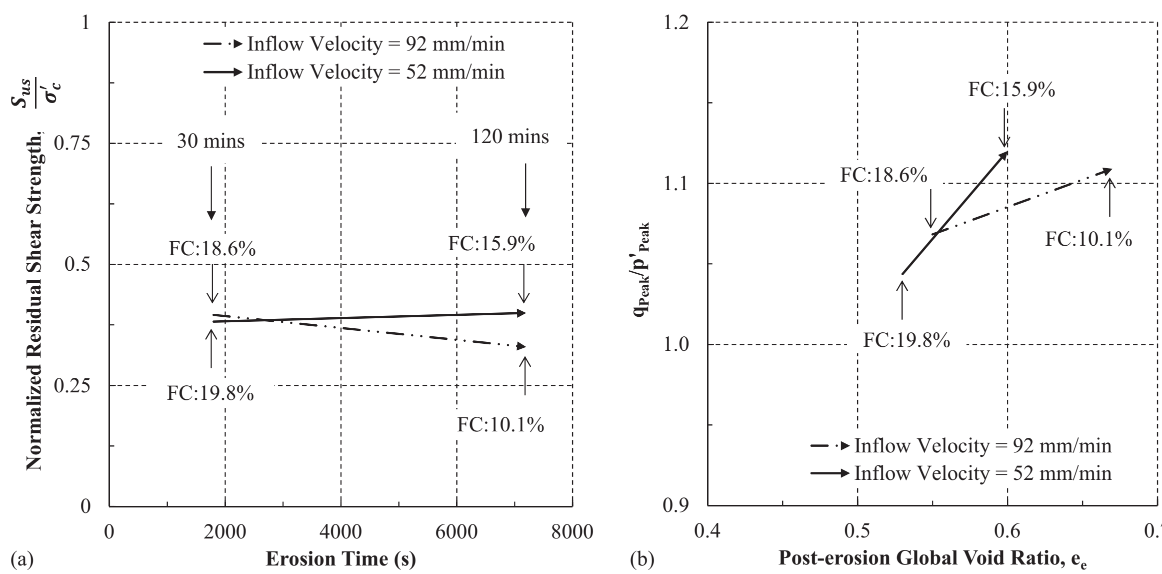

Fig. 8. Variation of (a) normalized residual strength at the QSS; (b) instability with erosion progress

Int. J. Geomech., 2018, 18(3): 04017160

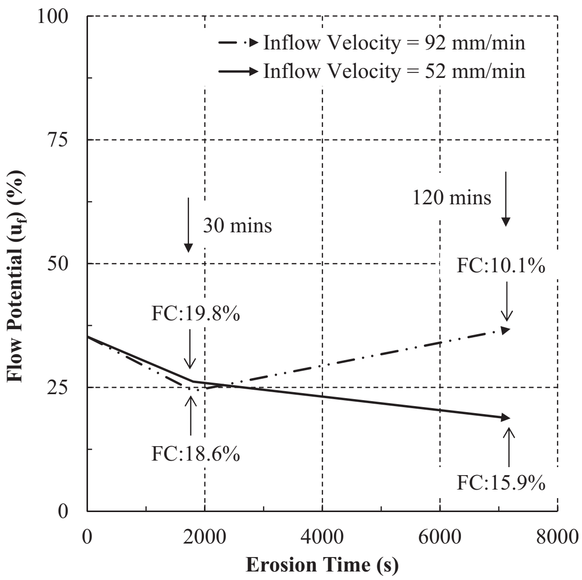

Fig. 9. Flow potential with erosion progress

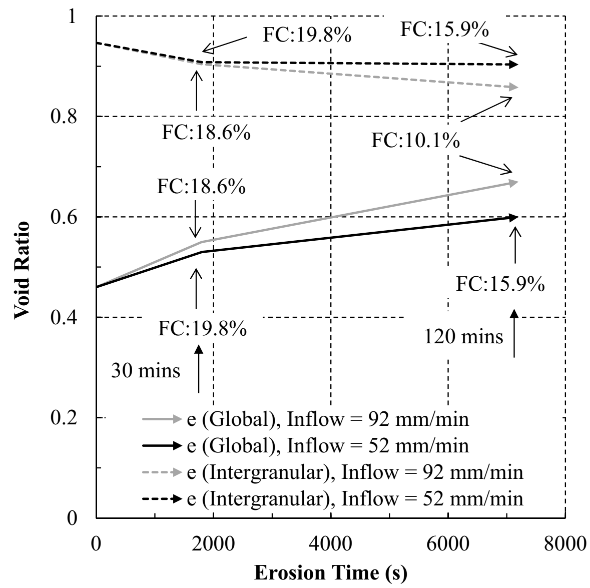

Fig. 10. Variation of global and intergranular void ratios with erosion progress

when the real voids and volume of fines are both considered as the available voids between coarse particles [Eq. (4)]

$$e_g = \frac{e + \mathrm{FC}}{1 - \mathrm{FC}} \tag{4}$$

where e_g = intergranular void ratio; e = global void ratio; and FC = fine content in decimals.

Depending on the type of involvement of the fine particles in the soil skeleton (i.e., their role in the soil stress matrix), erosion of fine particles can impact the mechanical behavior of a soil differently. Therefore, it is important to consider both the global and intergranular void ratios when analyzing the posterosion mechanical behavior of granular matters. Fig. 10 shows the variation in global and intergranular void ratios as erosion progressed for all tested specimens. As expected, the global void ratio increased due to removal of some of the fine particles as erosion progressed. However, this increase was accompanied by a reduction in the intergranular void ratio (e_g). Theoretically, the loss of fine particles does not change the intergranular void ratio because a decrease in volume of the fines is added to the real voids and the final result is unchanged. However, if the soil skeleton formed by the coarse particles deforms or settles, the available spaces between the coarse particles may decrease, which could lead to a reduction in the intergranular void ratio. In fact, it is believed that this coarse particle rearrangement during the erosion process (caused by a loss in semiactive fines) decreased the available voids between the coarse particles and reduced the intergranular void ratio. For the tested specimens at an inflow velocity of 92 mm/min, the initial value of the intergranular void ratio decreased from 0.95 to 0.86 at the end of 120 min of erosion. This noticeable drop was attributed to intensive particle rearrangement. On the contrary, e_g showed a reduction from 0.95 to 0.91 during the first 30 min of erosion for the eroded specimens at an inflow velocity of 52 mm/min and stayed relatively constant at 0.9 for the rest of the erosion stage. This was supported by the agreement between Figs. 10 and 6, which showed vertical deformations during internal erosion. All specimens (except for E-C150-V92-T120) showed minor vertical deformation during the erosion process apart from the large initial deformation experienced by all specimens. The first drop in the intergranular void ratio (from 0.95 to 0.9) could be due to the initial large deformation. A similar final e_g for E-C150-V52-T30, E-C150-V52-T120, and E-C150-V92-T30 is plausible because the final deformations were almost the same. However, e_g decreased again for the E-C150-V92-T120 sample when particle rearrangement occurred to reach a new stable state due to formation of a metastable structure after massive erosion of the semiactive fines. Fig. 10 shows that a decrease in the FC from 25 to 19.8% rearranged the soil structure and reduced the available voids between the coarse particles (hence a reduction in the intergranular void ratio). However, a further reduction from 19.8 to 15.9% did not cause any influence on soil structures or available stress matrix, ultimately leading to similar soil behavior and shear strength for the specimens with residual fine contents within this range. A second drop in e_g occurred when more of the involved fine particles were eroded as erosion continued. Comparing Figs. 4, 6, and 10 shows that this is the intergranular void ratio that controls the eroded soil specimen response. Similar stress-strain relationships and final vertical deformations were observed for E-C150-V52-T30, E-C150-V52-T120, and E-C150-V92-T30 with similar intergranular void ratios, although seepage properties, residual FCs, and final global void ratios were different. However, more experimental investigation needs to be conducted on soil specimens with different soil gradation and initial FC to expand this finding.

Thevanayagam et al. (2002) modified Eq. (4) and presented an equivalent intergranular contact index (e_{ceq}) to represent the effect of fine particles in the force chains more accurately [Eq. (5)]. This adapted equation is only valid if the initial FC is less than the critical magnitude ($\mathrm{FC_{Crit}}$) defined by Rahman and Lo (2008) in Eq. (6). This critical value is associated with a percentage of the fines above which the coarse particles are no longer in full contact with each other and float in a fine matrix, thus leading to the fine particle characteristics being dominant in terms of the soil's mechanical behavior

$$e_{ceq} = \frac{e + (1-b)\mathrm{FC}}{1 - (1-b)\mathrm{FC}};\ 0 < b < 1 \tag{5}$$

where b = portion of FC participating in the soil stress matrix [i.e., b = 0 when fine particles are completely free and inactive (filler), and $b = 1$ when all of the fine particles are involved in the soil skeleton]

$$FC_{Crit} = 0.4\left(\frac{1}{1+e^{\alpha-\beta\chi}} + \frac{1}{\chi}\right); \text{for } 2 \leq \chi \leq 42 \tag{6}$$

where $\chi = {}^{D_{10}}/_{d_{50}}$; $\alpha = 0.5$; and $\beta = 0.13$ (D_{10} is the coarse particle diameter for 10% passing by weight based on the coarse fraction, and d_{50} is the particle diameter for 50% passing by weight based on the fine fraction).

Rahman et al. (2008) proposed a semiempirical equation based on the available data in the literature (Thevanayagam et al. 2002) to assess the b value and contribution of the fine particles in the stress-transferring matrix [Eq. (7)]

$$b = \left\{1 - \exp\left[-0.3\frac{\left(\frac{FC}{FC_{Crit}}\right)}{k}\right]\right\}\left(r\frac{FC}{FC_{Crit}}\right)^{r} \tag{7}$$

where $r = 1/\chi$; and $k = 1 - r^{0.25}$.

Equations suggested by Rahman and Lo (2008) and Rahman et al. (2008) were developed based on previous studies, such as Thevanayagam et al. (2002), that used moist-tamping or dry air deposition techniques to prepare soil specimens. This means that these equations are also applicable in this research, as soil specimens were prepared using the moist-tamping technique. It is worth noting that many fines are placed around the coarse particles during sample preparation when the moist-tamping method is used. However, it is believed that most of them provide secondary (laterally) support for force chains that are made by coarse particles, and only a small percentage of them are sandwiched between coarse particles considering the FC, soil-gradation curve, and size of fine particles.

According to Eqs. (6) and (7), the FC_{Crit} and b are equal to 31% and 0.34, respectively, for the soil specimen reported in this paper. This means that the primary soil skeleton (stress matrix) in this research is composed of coarse particles. Depending on the ratio of fine particle sizes to the constriction size, particle shape, relative density, and confining pressure, the fine particle may sit loose in the voids (inactive), provide lateral support (semiactive), or be sandwiched between the coarse particles (active). In fact, $b = 0.34$ for the tested specimen suggests that approximately 100 g (out of 300 g) of total fine particles contributed to the active intergrain contacts. However, the quality of this contribution is still unclear for semiactive or active fine particles. Specimens E-C150-V52-T30, E-C150-V52-T120, and E-C150-V92-T30 showed very similar undrained behaviors. This indicates that the percentage of residual semiactive and active fine particles involved in the soil structure was almost the same for these three specimens. However, Specimen E-C150-V92-T120, which lost 66% of its fine particles (200 g), showed different behavior in comparison to the other specimens. If residual fine particles for this specimen (34%) are compared with the calculated b value (0.34) suggested by Rahman and Lo (2008) and Rahman et al. (2008) for active fine particles, it can be seen that most of the erodible fine particles (inactive and semiactive fine particles) should have been washed out of the soil body in this specimen. This means that only active and nonerodible fine particles that were fully involved in the soil structure were left in the soil specimen. It is believed that this is the reason for the different behavior for Specimen E-C150-V92-T120. To validate this hypothesis, a soil specimen with a 50-mm diameter was prepared under the same condition and eroded for 120 min under a much higher seepage velocity (208 mm/min). Only an extra 3% drop in the residual FC with similar undrained behavior to E-C150-V92-T120 was observed for this specimen. This experiment confirmed that between 30 and 35% of fine particles were nonerodible. Different observed behavior (a reduction in the peak shear strength or increase in the flow potential) could be due to an intensive particle rearrangement, formation of a metastable structure, and growing instability in the force chains after loss of a considerable fraction of the semiactive fines.

Normalized residual FC with an initial FC at different levels is presented in Fig. 11 for all eroded specimens. Erosion of the fine particles was shown to be uniform across the height of the specimens during the first 30 min, regardless of the inflow velocity. However, the loss of fine particles was shown to be more pronounced in the upper parts of the specimens as erosion progressed. This particle migration was more intensive for the specimen subjected to an inflow velocity of 92 mm/min. Whereas the presence of the fine particles was constant in the bottom part of the eroded specimen under an inflow velocity of 52 mm/min during erosion, the middle and top parts of the specimen lost an extra 17 and 29% of their FCs, respectively. Unfortunately, it was not possible to make a distinction between clogged fine particles in the lower part of the specimen, which were thought to have originally migrated from the upper regions, and the fine particles that belonged to this part from the start of the test (sample preparation). However, it is clear that their influence on soil behavior is not similar. The moist-tamping technique used for sample preparation involved more fine particles in the soil structure (stress matrix) when compared to the erosion process that carried some fine particles and left them in the lower part of the specimen in a loose condition. Fig. 11 clearly shows that the void ratio measured at the end of the erosion test is not an accurate index to explain the soil behavior, as local void ratios across the specimen height were totally different. It should be noted that internal erosion is a nonuniform process leading to different local volumetric strains, void ratios, FC, and particle rearrangements.

Effect of FC on Macro- and Micromechanical Behavior of Soil

Many studies have been conducted on the influence of nonplastic FC on the monotonic and cyclic behaviors of soil mixtures, with conflicting results. Some researchers, such as Ishihara (1993), Thevanayagam et al. (1997), Lade and Yamamuro (1997), Thevanayagam et al. (2000), Naeini and Baziar (2004), Belkhatir et al. (2010), and Ke and Takahashi (2014b), showed that an increase in the FC decreases the shear strength of the soil, whereas some others, such as Salgado et al. (2000), Ni et al. (2004), Murthy et al. (2007), Carraro et al. (2009), and Andrianatrehina et al. (2016), suggested that the undrained peak shear strength and critical internal friction angle improved with an increase in the percentage of angular fine particles. Because the sample preparation method, particle shape, and percentage of fine particles all have an impact on the contribution of fine particles to the primary soil skeleton, they all need to be considered.

Apart from role of fine particles in the stress matrix, the angularity of fine particles also impacts the posterosion behavior of a soil. Moreover, the shear resistance and dilatancy properties of sand are dependent on particle angularity (Guo and Su 2007). The removal of rounded fine particles improves the interlocking of the coarse particles during the shearing. Slip-down movement of the coarse grains may occur due to an increase in the void ratio after internal erosion and postpones the initial dilation tendency. Therefore, although the contractive behavior is initially dominant, the improvement in the coarse particle interlocking increases the peak shear strength. Fig. 12 demonstrates the shape factors and the internal friction of the particles used in this research. A series of direct shear tests were conducted on samples prepared at the loosest condition of each grain to

Int. J. Geomech., 2018, 18(3): 04017160

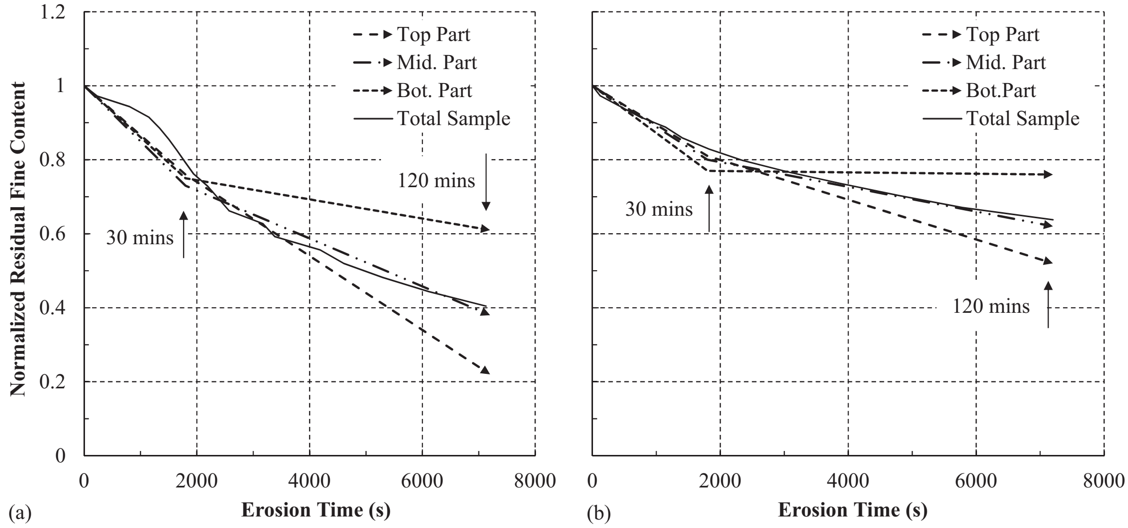

Fig. 11. Variation of normalized residual FC of soil specimens: (a) subjected to an inflow velocity of 92 mm/min; (b) subjected to an inflow velocity of 52 mm/min with erosion progress

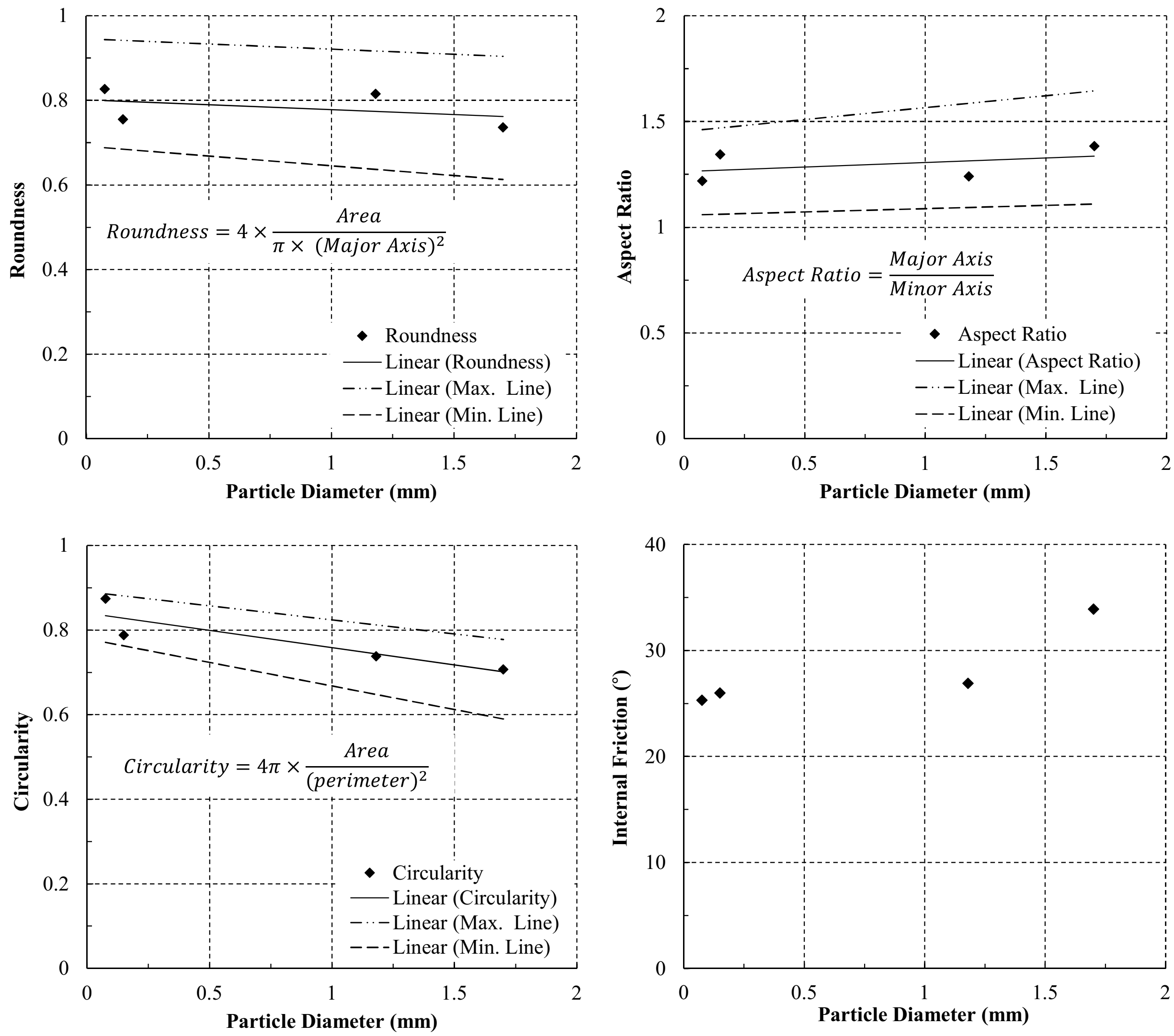

Fig. 12. Particles characteristics

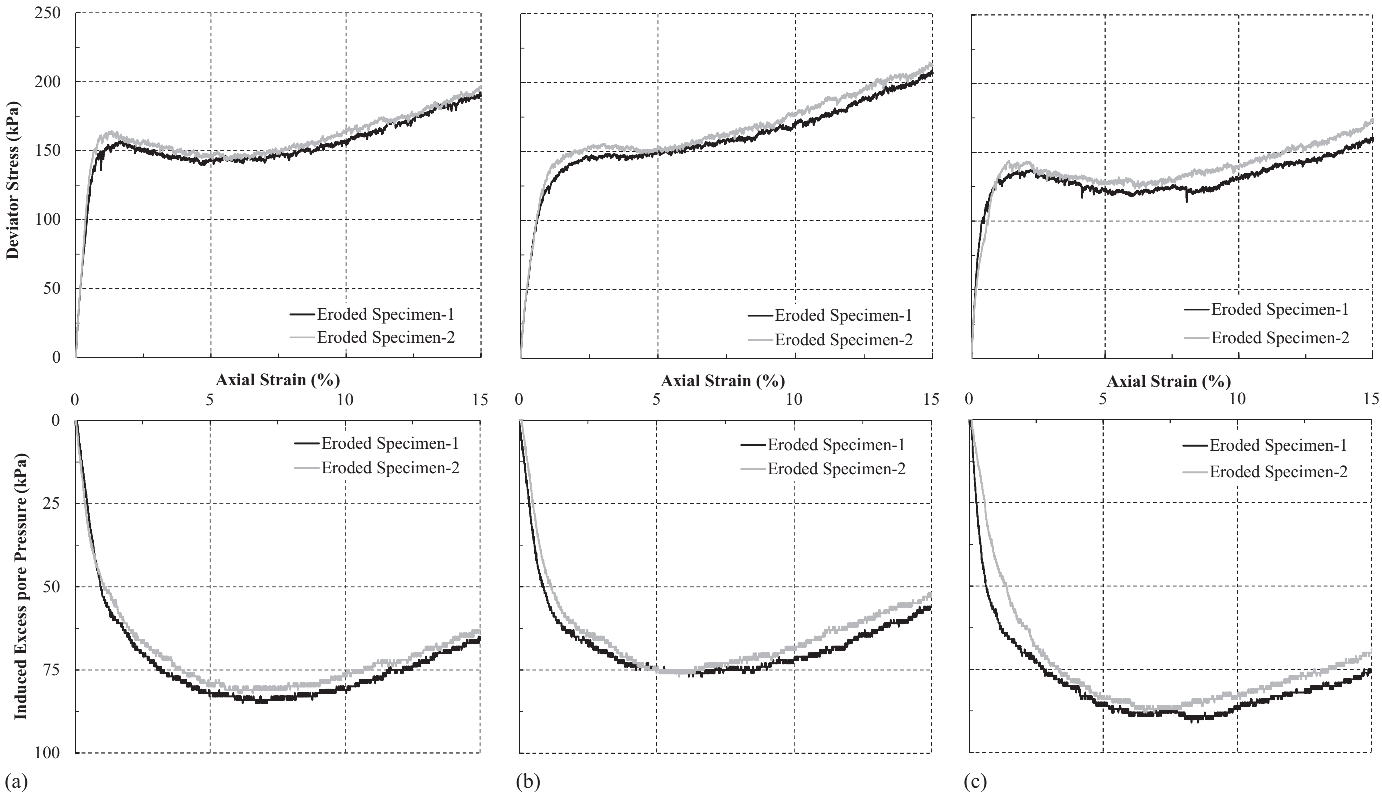

Fig. 13. Repeatability of the triaxial results for the eroded specimens: (a) subjected to an inflow velocity of 92 mm/min for 30 min; (b) subjected to an inflow velocity of 52 mm/min for 120 min; (c) subjected to an inflow velocity of 92 mm/min for 120 min

measure the internal friction. It can be seen that, apart from the largest particles (particle diameter: $D = 1.7–2.36$ mm), shape parameters and internal friction were approximately similar. A decreasing trend in the circularity and a noticeable jump in the internal friction were observed for the largest particles. This can confirm the hypothesis that loss of the rounded fine particles improved the interlocking of the coarse particles during shearing.

Local accumulation of fine particles during internal erosion also needs to be taken into account. This local concentration in the downstream may affect the shear strength in large strains. In fact, local high density of the fine particles may act as a lubricant between the coarse grains (Ke and Takahashi 2015). This lubricating effect can be more critical when the angularity of the coarse particles is conspicuous. In addition, erosion of fine particles may resuscitate the characteristics of the host fabric made by the coarse particles. Ke and Takahashi (2014b) showed that the coarse particles (artificial silica No. 3) used in their research behaved in a dilative manner even in a very loose condition. This inherent dilation tendency might have been the main reason for the reported higher undrained shear strength after internal erosion that overcame the contraction tendency after the increase in the void ratio.

Conclusion

The impact of internal erosion on removal of fine particles and the consequent effect on soil structure were studied through an analysis of pre- and posterosion mechanical behavior and geometrical changes recorded using a newly developed erosion-triaxial apparatus. Undrained triaxial compression tests were conducted on one internally unstable soil type at two erosion durations (30 and 120 min) at two different inflow velocities (92 and 52 mm/min). Erosion of the fine particles was found to be independent of seepage velocity during the initial stage of internal erosion. This was attributed to the erosion of the free particles available in the soil specimens. However, after 120 min of erosion, the residual FC in the specimen that eroded at the higher inflow velocity was 36% less. Furthermore, hardening behavior of the noneroded specimen changed to the flow type with limited deformation after internal erosion. Maximum induced excess pore pressure decreased, and dilation tendency was postponed. However, the initial undrained peak shear strength showed a significant increase. This improvement disappeared once the residual FC passed a critical turning point. The initial increase in peak shear strength could have been due to a better interlocking of the angular coarse particles due to absence of the fine particles. However, an increase in potential of the slip-down movement due to an increase in the global void ratio and the lubricating effect of the local concentration of the fine particles after internal erosion decreased the dilation tendency, which might have been reasons for the observed contractive behavior at medium strains.

A step pattern was observed in the local vertical strains during internal erosion of the tested specimens. These discrete steps could be due to local particle rearrangement that continued throughout the erosion, even under constant inflow. This particle rearrangement occurred when the semiactive fines that provided the lateral support for the soil stress matrix were eroded.

A turning point was observed in the posterosion behavior, which was dependent on the percentage of the eroded particles. The temporary increase in peak shear strength and the drop in the flow potential caused by initial internal erosion quickly deteriorated after a threshold value of residual FC was eroded. This threshold was found to occur where the semiactive fine particles lost their intergrain contacts and a metastable soil structure developed. This turning point in the FC can be estimated using equations provided by Rahman and Lo (2008) and Rahman et al. (2008). However, development of the contraction tendency due to a noticeable increase in the global void ratio could be another reason for the observed drop in the long-term shear strength.

Analysis of shear strength results, rate of erosion, and local vertical strains suggests that the intergranular void ratio proposed by Mitchell (1993) is a more suitable index in evaluating the posterosion mechanical behavior of internally unstable soils. Eroded specimens with different global void ratios and residual FCs but a similar intergranular void ratio showed similar mechanical behavior, indicating the suitability of this index in predicting posterosion behavior.

A review of all experimental studies available in the literature suggests that, depending on the quality of the contribution of the fine particles in the soil skeleton, erosion progress, angularity of the particles, state of the particles interlocking pre- and posterosion, local concentration of the fine particles, innate characteristics of the stress matrix (coarse grain) particles, possibility of particle rearrangement, and variation of the void ratio, different scenarios may occur when it comes to posterosion mechanical behavior of soils. In fact, regardless of the change in posterosion behavior that can improve soil strength to some extent, nonuniform soil responses through the erosion path and the affected zone in the hydraulic structures is the main concern and challenge, which may lead to differential settlements and associated catastrophic consequences.

Appendix. Experimental Results Repeatability

Internal erosion is not a uniform phenomenon, and different test procedures and equipment have been used to study this phenomenon. Therefore, experiment repeatability is always a concern. In this research, each test was performed several times to ensure reliability of the results. Repeatability of the posterosion triaxial test results after 30 and 120 min of internal erosion is shown in Fig. 13. There was good consistency in the test results, with the minor deviation being explained due to the unvoidable variations in sample preparation or the innate nonuniformity during the process of internal erosion.

References

Abdelhamid, Y., and El Shamy, U. (2016). "Pore-scale modeling of fine-particle migration in granular filters." *Int. J. Geomech.*, 10.1061/(ASCE)GM.1943-5622.0000592, 04015086.

Andrianatrehina, N. L., Souli, H., Rech, J., Fry, J. J., Fleureau, J. M., and Taibi, S. (2016). "Influence of the percentage of sand on the behavior of gap-graded cohesionless soils." *C. R. Méc.*, 344(8), 539–546.

Belkhatir, M., Arab, A., Della, N., Missoum, H., and Schanz, T. (2010). "Influence of inter-granular void ratio on monotonic and cyclic undrained shear response of sandy soils." *C. R. Méc.*, 338(5), 290–303.

Bendahmane, F., Marot, D., and Alexis, A. (2008). "Experimental parametric study of suffusion and backward erosion." *J. Geotech. Geoenviron. Eng.*, 10.1061/(ASCE)1090-0241(2008)134:1(57), 57–67.

Burenkova, V. V. (1993). "Assessment of suffusion in non- cohesive and graded soils." *Proc., 1st Int. Conf. on Geo-Filters*, Balkema, Rotterdam, Netherlands, 357–360.

Carraro, J. A. H., Prezzi, M., and Salgado, R. (2009). "Shear strength and stiffness of sands containing plastic or nonplastic fines." *J. Geotech. Geoenviron. Eng.*, 10.1061/(ASCE)1090-0241(2009)135:9(1167), 1167–1178.

Chang, D. S., and Zhang, L. M. (2011). "A stress-controlled erosion apparatus for studying internal erosion in soils." *Geotech. Test. J.*, 34(6), 579–589.

Chang, D. S., and Zhang, L. M. (2013). "Extended internal stability criteria for soils under seepage." *Soils Found.*, 53(4), 569–583.

Chapuis, R. P. (1992). "Similarity of internal stability criteria for granular soils." *Can. Geotech. J.*, 29(4), 711–713.

Chu, J., and Leong, W. K. (2002). "Effect of fines on instability behaviour of loose sand." *Géotechnique*, 52(10), 751–755.

Cividini, A., Bonomi, S., Vignati, G. C., and Gioda, G. (2009). "Seepage-induced erosion in granular soil and consequent settlements." *Int. J. Geomech.*, 10.1061/(ASCE)1532-3641(2009)9:4(187), 187–194.

Cividini, A., and Gioda, G. (2004). "Finite-element approach to the erosion and transport of fine particles in granular soils." *Int. J. Geomech.*, 10.1061/(ASCE)1532-3641(2004)4:3(191), 191–198.

Dallo, Y. A., Wang, Y., and Ahmed, O. Y. (2013). "Assessment of the internal stability of granular soils against suffusion." *Eur. J. Environ. Civ. Eng.*, 17(4), 219–230.

Frost, J. D., and Park, J. Y. (2003). "A critical assessment of the moist tamping technique." *Geotech. Test. J.*, 26(1), 57–70.

Guo, P., and Su, X. (2007). "Shear strength, interparticle locking, and dilatancy of granular materials." *Can. Geotech. J.*, 44(5), 579–591.

Indraratna, B., Israr, J., and Rujikiatkamjorn, C. (2015). "Geometrical method for evaluating the internal instability of granular filters based on constriction size distribution." *J. Geotech. Geoenviron. Eng.*, 10.1061/(ASCE)GT.1943-5606.0001343, 04015045.

Indraratna, B., Raut, A. K., and Khabbaz, H. (2007). "Constriction-based retention criterion for granular filter design." *J. Geotech. Geoenviron. Eng.*, 10.1061/(ASCE)1090-0241(2007)133:3(266), 266–276.

Ishihara, K. (1993). "Liquefaction and flow failure during earthquakes." *Géotechnique*, 43(3), 351–451.

Jiang, M. J., Konrad, J. M., and Leroueil, S. (2003). "An efficient technique for generating homogeneous specimens for DEM studies." *Comput. Geotech.*, 30(7), 579–597.

Ke, L., and Takahashi, A. (2012). "Strength reduction of cohesionless soil due to internal erosion induced by one-dimensional upward seepage flow." *Soils Found.*, 52(4), 698–711.

Ke, L., and Takahashi, A. (2014a). "Experimental investigations on suffusion characteristics and its mechanical consequences on saturated cohesionless soil." *Soils Found.*, 54(4), 713–730.

Ke, L., and Takahashi, A. (2014b). "Triaxial erosion test for evaluation of mechanical consequences of internal erosion." *Geotech. Test. J.*, 37(2), 1–18.

Ke, L., and Takahashi, A. (2015). "Drained monotonic responses of suffusional cohesionless soils." *J. Geotech. Geoenviron. Eng.*, 10.1061/(ASCE)GT.1943-5606.0001327, 04015033.

Kenney, T. C., and Lau, D. (1985). "Internal stability of granular filters." *Can. Geotech. J.*, 22(2), 215–225.

Kenney, T. C., and Lau, D. (1986). "Internal stability of granular filters: Reply." *Can. Geotech. J.*, 23(3), 420–423.

Kezdi, A. (1969). "Increase of protective capacity of flood control dikes." *Rep. No. 1*, Dept. of Geotechnique, Technical Univ., Budapest, Hungary.

Ladd, R. S. (1978). "Preparing test specimens using undercompaction." *Geotech. Test. J.*, 1(1), 16–23.

Lade, P. V. (1993). "Initiation of static instability in the submarine nerlerk berm." *Can. Geotech. J.*, 30(6), 895–904.

Lade, P. V., and Yamamuro, J. A. (1997). "Effects of nonplastic fines on static liquefaction of sands." *Can. Geotech. J.*, 34(6), 918–928.

Leong, W. K., Chu, J., and Teh, C. I. (2000). "Liquefaction and instability of a granular fill material." *Geotech. Test. J.*, 23(2), 178–192.

Luo, Y. L., Qiao, L., Liu, X. X., Zhan, M. L., and Sheng, J. C. (2013). "Hydro-mechanical experiments on suffusion under long-term large hydraulic heads." *Nat. Hazards*, 65(3), 1361–1377.

Mao, C. X. (2005). "Study on piping and filters. Part of piping." *Rock Soil Mech.*, 26(2), 209–215.

Mitchell, J. K. (1993). *Fundamentals of soil behavior*, John Wiley & Sons, New York, 1–210.

Moffat, R., and Fannin, R. J. (2011). "A hydromechanical relation governing internal stability of cohesionless soil." *Can. Geotech. J.*, 48(3), 413–424.

Moraci, N., Mandaglio, M. C., and Ielo, D. (2014). "Analysis of the internal stability of granular soils using different methods." *Can. Geotech. J.*, 51(9), 1063–1072.

Murthy, T. G., Loukidis, D., Carraro, J. A. H., Prezzi, M., and Salgado, R. (2007). "Undrained monotonic response of clean and silty sands." *Géotechnique*, 57(3), 273–288.

Naeini, S. A., and Baziar, M. H. (2004). "Effect of fines content on steady-state strength of mixed and layered samples of a sand." *Soil Dyn. Earthquake Eng.*, 24(3), 181–187.

Ni, Q., Tan, T. S., Dasari, G. R., and Hight, D. W. (2004). "Contribution of fines to the compressive strength of mixed soils." *Géotechnique*, 54(9), 561–569.

Olson, S. M., Stark, T. D., Walton, W. H., and Castro, G. (2000). "1907 static liquefaction flow failure of the north dike of Wachusett Dam." *J. Geotech. Geoenviron. Eng.*, 10.1061/(ASCE)1090-0241(2000)126:12(1184), 1184–1193.

Ouyang, M., and Takahashi, A. (2016). "Influence of initial fines content on fabric of soils subjected to internal erosion." *Can. Geotech. J.*, 53(2), 299–313.

Rahman, M. M., and Lo, S. R. (2008). "The prediction of equivalent granular steady state line of loose sand with fines." *Geomech. Geoeng.*, 3(3), 179–190.

Rahman, M. M., Lo, S. R., and Baki, M. A. L. (2011). "Equivalent granular state parameter and undrained behaviour of sand–fines mixtures." *Acta Geotechnica*, 6(4), 183–194.

Rahman, M. M., Lo, S. R., and Gnanendran, C. T. (2008). "On equivalent granular void ratio and steady state behaviour of loose sand with fines." *Can. Geotech. J.*, 45(10), 1439–1455.

Salgado, R., Bandini, P., and Karim, A. (2000). "Shear strength and stiffness of silty sand." *J. Geotech. Geoenviron. Eng.*, 10.1061/(ASCE)1090-0241(2000)126:5(451), 451–462.

Scholtès, L., Hicher, P. Y., and Sibille, L. (2010). "Multiscale approaches to describe mechanical responses induced by particle removal in granular materials." *C. R. Méc.*, 338(10–11), 627–638.

Sherard, J. L. (1979). "Sinkholes in dams of coarse, broadly graded soils." *Trans., Proc., 13th Congress on Large Dams*, Vol. II, New Delhi, India, 25–35.

Shire, T., O'Sullivan, C., Hanley, K. J., and Fannin, R. J. (2014). "Fabric and effective stress distribution in internally unstable soils." *J. Geotech. Geoenviron. Eng.*, 10.1061/(ASCE)GT.1943-5606.0001184, 04014072.

Sterpi, D. (2003). "Effects of the erosion and transport of fine particles due to seepage flow." *Int. J. Geomech.*, 10.1061/(ASCE)1532-3641(2003)3:1(111), 111–122.

Terzaghi, K. (1925). *Erdbaumechanik*, Franz Deuticke, Vienna, Austria.

Thevanayagam, S., Fiorillo, M., and Liang, J. (2000). "Effects of non-plastic fines on undrained cyclic strength of silty sands." *Proc., Geo-Denver 2000*, ASCE, Reston, VA, 77–91. 10.1061/40520(295)6.

Thevanayagam, S., Ravishankar, K., and Mohan, S. (1997). "Effects of fines on monotonic undrained shear strength of sandy soils." *Geotech. Test. J.*, 20(4), 394–406.

Thevanayagam, S., Shenthan, T., Mohan, S., and Liang, J. (2002). "Undrained fragility of clean sands, silty sands, and sandy silts." *J. Geotech. Geoenviron. Eng.*, 10.1061/(ASCE)1090-0241(2002)128:10(849), 849–859.

Tomlinson, S. S., and Vaid, Y. P. (2000). "Seepage forces and confining pressure effects on piping erosion." *Can. Geotech. J.*, 37(1), 1–13.

Wan, C. F. and Fell, R. (2008). "Assessing the potential of internal instability and suffusion in embankment dams and their foundations." *J. Geotech. Geoenviron. Eng.*, 10.1061/(ASCE)1090-0241(2008)134:3(401), 401–407.

Wood, D. M., Maeda, K., and Nukudani, E. (2010). "Modelling mechanical consequences of erosion." *Géotechnique*, 60(6), 447–457.

Xiao, M., and Shwiyhat, N. (2012). "Experimental investigation of the effects of suffusion on physical and geomechanic characteristics of sandy soils." *Geotech. Test. J.*, 35(6), 890–900.

Yang, S., Lacasse, S., and Sandven, R. (2006). "Determination of the transitional fines content of mixtures of sand and nonplastic fines." *Geotech. Test. J.*, 29(2), 1–6.

Yoshimine, M., and Ishihara, K. (1998). "Flow potential of sand during liquefaction." *Soils Found.*, 38(3), 189–198.

Fannin, R. J. *et al*. (2015) ***Géotechnique Letters* 5**, 129–130, http://dx.doi.org/10.1680/jgele.15.00017

Discussion: On the distinct phenomena of suffusion and suffosion

R. J. FANNIN*, P. SLANGEN*, A. MEHDIZADEH†, M. M. DISFANI‡, A. ARULRAJAH† and R. EVANS†

A valuable conceptual framework for the characterisation of seepage-induced internal instability was provided in the article under discussion, particularly for the 'suffusion and suffosion' phenomena. A few modifications are suggested here to clarify the definitions in the original paper.

NOTATION

e	post-suffosion void ratio
e_c	post-suffusion void ratio
H	thickness of soil
H_i	thickness of each layer
i_{av}	average hydraulic gradient
k	hydraulic conductivity
k_{eq}	equivalent hydraulic conductivity
k_i	local hydraulic conductivity
ε_v	volumetric deformation

CONTRIBUTION BY A. MEHDIZADEH, M. M. DISFANI, A. ARULRAJAH AND R. EVANS

Fannin & Slangen (2014) provided a valuable and clear conceptual framework for the characterisation of seepage-induced internal instability, particularly for the 'suffusion and suffosion' phenomena. The original paper aims to reduce the existing conflictions and ambiguities in the literature and create consistent terminology, which has been attempted in the past by other researchers such as Richards & Reddy (2007) and Ke & Takahashi (2014).

Fannin & Slangen (2014) identified a linear relation between hydraulic gradient and discharge velocity for $i_{av}<2{\cdot}9$ (Fig. 1(b)), which in turn indicates a constant value for hydraulic conductivity k. For $i_{av} \geq 2{\cdot}9$, a disproportionate increase in discharge velocity with hydraulic gradient leads to an increase in k. The relationship between discharge velocity and hydraulic gradient shown in Fig. 1(b) can be divided into three distinct parts. The slope of the graph (k) increases slightly from part 1 (i_{av} from 0 to 1·3) to part 2 (i_{av} from 1·3 to 2·9), and then jumps excessively ($i_{av}\geq 2{\cdot}9$). Therefore, the hydraulic conductivity is not constant for $i_{av} \leq 2{\cdot}9$. In the authors' view, Fannin & Slangen's interpretation of change of i_{av} for Fig. 1(a) is reasonable, but it can be modified for Figs 1(b) and 1(c) as noted above.

Fannin & Slangen (2014) identified suffusion as a phenomenon accompanied by an increase of k. Although this raises no doubts at first glance, interestingly there are studies claiming that k decreases or even remains constant during suffusion. For example, Bendahmane *et al.* (2008) noted that permeability decreased by a factor of ten when erosion was initiated. Xiao & Shwiyhat (2012) reported a reduction in permeability with progression of suffusion in gap-graded soils. No permeability change was reported as a result of suffusion in poorly graded soils. It appears that the change of k in the suffusion process is heavily dependent on the clogging phenomena. After washing the particles, the local hydraulic conductivity increases and if those washed particles settle or clog somewhere else in the soil, the local hydraulic conductivity of that region decreases. The result of such changes in local hydraulic conductivities provides an equivalent hydraulic conductivity (k_{eq}), which may be higher or lower than the initial magnitude or may remain constant after the suffusion process.

This variation can be postulated by an equivalent permeability formula

$$k_{eq} = \frac{\Sigma H}{\Sigma H_i/k_i} \tag{1}$$

Fannin & Slangen (2014) attributed volumetric contraction or reduction to one of the distinctive features of the suffosion phenomenon. Ke & Takahashi (2014) stated that 'change of void ratio is caused by the loss of fines (ΔV_f) and possible intergranular re-arrangement (ΔV)'. They showed that changes in void ratio are equal to $\varepsilon_v(1+e_c)$ in which ε_v is considered positive if the specimen shows contractive behaviour or negative if it shows dilative behaviour during suffusion. Therefore, the post-suffosion void ratio is obtained from

$$e = e_c - \varepsilon_v(1 + e_c) \tag{2}$$

Fannin & Slangen (2014) accurately explained the fluidisation phenomenon for upward seepage flow. Nevertheless, heave and loss of fine particles can occur simultaneously in upward flow. In addition, Ke & Takahashi (2014) demonstrate that dilative behaviour can also occur after suffusion. It seems that more clarification is needed in relation to the suffosion phenomenon, especially regarding the type of volumetric deformation.

To summarise, the following modifications are suggested to make the definitions in the paper clearer.

- Suffusion should be characterised as seepage-induced mass loss without a change in volume and with or without any change in general hydraulic conductivity but with a change in local hydraulic conductivity.
- Suffosion should be characterised as seepage-induced mass loss accompanied by a change in volume and a change in hydraulic conductivity.

AUTHORS' REPLY

We thank the discussers for their interest in our publication and the suggestion of two possible modifications to the terminology.

We proposed the term suffusion be characterised as 'seepage-induced mass loss without change in volume, accompanied by an increase of hydraulic conductivity'. We agree with the discussers that suffusion is a localised

Published online at www.geotechniqueletters.com on 4 August 2015.

*University of British Columbia, Vancouver, Canada
†Department of Civil and Construction Engineering, Swinburne University of Technology, Melbourne, Australia
‡Department of Infrastructure Engineering, University of Melbourne, Melbourne, Australia

phenomenon, whereby wash-out of particles results in mass loss and yields an increase in local hydraulic conductivity. We also accept that seepage-induced transport of the washed out particles may lead to their entrapment at a different location within the porous medium, however we believe this clogging action to represent a separate and distinct localised phenomenon.

We proposed the term suffosion be characterised as 'seepage-induced mass loss accompanied by a reduction in volume and a change in hydraulic conductivity'. The discussers report the findings of Ke & Takahashi (2014), who observed a dilative response in test specimens that have exhibited suffosion when subject to drained shear. However, we similarly believe that the shear-induced dilative response is a separate and distinct phenomenon that is unrelated to seepage flow.

REFERENCES

Bendahmane, F., Marot, D. & Alexis, A. (2008). Experimental parametric study of suffusion and backward erosion. *J. Geotech. Geoenviron. Engng* **134**, No. 1, pp. 57–67.

Fannin, R. J. & Slangen, P. (2014). On the distinct phenomena of suffusion and suffosion. *Géotech. Lett.* **4**, No. 4, pp. 289–294, http://dx.doi.org/10.1680/geolett.14.00051.

Ke, L. & Takahashi, A. (2014). Experimental investigations on suffusion characteristics and its mechanical consequences on saturated cohesionless soil. *Soils and Found.* **54**, No. 4, pp. 713–730.

Richards, K. S. & Reddy, K. R. (2007). Critical appraisal of piping phenomena in earth dams. *Bull. Engng Geol. Environ.* **66**, No. 4, pp. 381–402.

Xiao, M. & Shwiyhat, N. (2012). Experimental investigation of the effects of suffusion on physical and geomechanic characteristics of sandy soils. *Geotech. Test. J.* **35**, No. 6, pp. 890–900.

Geotechnical Testing Journal

Amirhassan Mehdizadeh,[1] Mahdi M. Disfani,[2] Robert Evans,[3] Arul Arulrajah,[4] and D. E. L. Ong[5]

DOI: 10.1520/GTJ20150153

Discussion of "Development of an Internal Camera-Based Volume Determination System for Triaxial Testing" by S. E. Salazar, A. Barnes and R. A. Coffman. The Technical Note Was Published in *Geotechnical Testing Journal*, Vol. 38, No. 4, 2015. [DOI: 10.1520/GTJ20140249]

Geotechnical Testing Journal

doi:10.1520/GTJ20150153 available online at www.astm.org

Amirhassan Mehdizadeh,[1] Mahdi M. Disfani,[2] Robert Evans,[3] Arul Arulrajah,[4] and D. E. L. Ong[5]

Discussion of "Development of an Internal Camera-Based Volume Determination System for Triaxial Testing" by S. E. Salazar, A. Barnes and R. A. Coffman. The Technical Note Was Published in *Geotechnical Testing Journal*, Vol. 38, No. 4, 2015. [DOI: 10.1520/GTJ20140249]

Manuscript received July 14, 2015; accepted for publication August 6, 2015; published online October 5, 2015.

[1] Ph.D. Student in Geotechnical Engineering, Department of Civil and Construction Engineering, Swinburne Univ. of Technology, Melbourne, Australia, e-mail: amehdizadeh@swin.edu.au

[2] Ph.D., Lecturer in Geotechnical Engineering, Department of Infrastructure Engineering, Univ. of Melbourne, Melbourne, Australia, e-mail: mmiri@unimelb.edu.au

[3] Ph.D., Lecturer in Geotechnical Engineering, Department of Civil and Construction Engineering, Swinburne Univ. of Technology, Melbourne, Australia, e-mail: robertevans@swin.edu.au

[4] Ph.D., Professor in Geotechnical Engineering, Department of Civil and Construction Engineering, Swinburne Univ. of Technology, Melbourne, Australia, e-mail: aarulrajah@swin.edu.au

[5] Ph.D., Director (Acting), Swinburne Sarawak Research Centre for Sustainable Technologies, Swinburne Univ. of Technology; Sarawak Campus, Malaysia, e-mail: elong@swinburne.edu.my

Reference

Mehdizadeh, Amirhassan, Disfani, Mahdi M., Evans, Robert, Arulrajah, Arul, and Ong, D. E. L., "Discussion of "Development of an Internal Camera-Based Volume Determination System for Triaxial Testing" by S. E. Salazar, A. Barnes and R. A. Coffman. The Technical Note Was Published in *Geotechnical Testing Journal*, Vol. 38, No. 4, 2015. [DOI: 10.1520/GTJ20140249]," *Geotechnical Testing Journal*
doi:10.1520/GTJ20150153. ISSN 0149-6115

ABSTRACT

Salazar et al. (2015) presented a new method to measure the volume and volumetric strains of soil specimen during the triaxial test. To eliminate the optical distortions due to refraction at the fluid-cell wall and cell wall-atmosphere interfaces, they installed a camera-based system inside the triaxial cell. The discussers wished to highlight some points about taking into account the refraction of light and other related issues in image processing for evaluating the volumetric strains and show that there is another simple way to overcome this problem.

Keywords

volumetric strain measurement, photogrammetry, triaxial testing

Salazar et al. (2015) and Salazar and Coffman (2015) presented a novel system of internal photogrammetric instrumentation for triaxial testing. They suggested that this new system overcomes the existing challenges and drawbacks of current image processing methods. These drawbacks include the optical distortion due to curvature of the cell wall and light refraction at the interfaces between (i) cell wall and cell fluid, (ii) cell wall and atmosphere, and (iii) camera lens and atmosphere. They comprehensively explained the mechanical and electrical design, calibration, and the verification method of the new system in their papers. This discussion lists some salient points about the importance of taking into account the refraction of light and other related issues, such as cell curvature in image processing and photogrammetry. This is based on the experience of the authors and the current body of available knowledge in literature. First, the ambiguities that were observed in their paper are discussed. Then, two series of volumetric strain measurements for a triaxial system using external photogrammetry are presented and finally, the importance of light refraction in volumetric strain measurement using photogrammetry is discussed.

Salazar et al. (2015) and Salazar and Coffman (2015) stated correctly that it is not possible to capture the entire specimen surface or all surface irregularities using external photogrammetry with only one camera. Uchaipichat et al. (2011) overcame the problem of capturing the non-symmetric deformation of a triaxial soil specimen by calculating the average specimen volume obtained from front and side view images. Although it is recognized that continuous imaging of the entire specimen using several cameras is a better idea, Uchaipichat et al. (2011) confirmed that photogrammetry with only two cameras is accurate enough to capture the entire specimen deformation. Therefore, there is no need to place multiple cameras around the cell.

Salazar and Coffman (2015) explained that due to the limited field of view of an individual camera (21 mm), one camera could not cover the height of the specimen. To overcome this issue, a tower of four cameras was used and four images were stitched together using post-processing software. This current system developed by Salazar and Coffman (2015) is limited to triaxial specimens 38.1 mm in diameter and 76.2 mm in height, which limits its capability in terms of specimen size. Consequently, the practical question arises of how many cameras are required to cover a larger soil sample. In addition, the current design varies from cell size to cell size and requires modification of the triaxial cell, which is another technical challenge in the adapting of this technique. Another challenge is the use of silicon oil instead of water inside the cell. This can create significant issues with commonly available flow pumps designed to work with water in standard triaxial systems.

To capture the entire surface of the triaxial specimen, the proposed system by Salazar and Coffman (2015) needs to rotate during the test. This means that the whole surface of the specimen cannot be captured during the same time period. Therefore, the test has to stop for a few minutes to capture the relevant images, which could be a drawback. Another drawback could be the lack of space to use midplane pressure transducers to measure local excess pore pressure.

Salazar and Coffman (2015) considered using an internal load cell as the first limitation of the external photogrammetry method, based on a paper by Zhang et al. (2015). In their view, the use of silicone oil inside the cell to protect the internal load cell may affect the observed results due to the different index of refraction of the oil. Despite this viewpoint, the choice of external or internal load cell and related issues, such as the necessity of correction of the piston friction and piston uplift, has no particular impact on the practice of external photography of the triaxial specimen. In addition, the variation of oil and water indices of refraction can be easily taken into account in the calculation and should not be a disadvantage of this method.

Another concern mentioned by Salazar et al. (2015) was the cell wall deformation during the pressurized test, which may affect the result of external photogrammetry. In triaxial testing, volumetric and local strains are usually investigated during the shearing stage, while the confining pressure is kept constant (apart from special stress path tests). Furthermore, research by Uchaipichat et al. (2011) confirmed that there is no need to consider the effects of variation of cell pressure. They investigated the effects of temperature and cell pressure on external photogrammetry. Their results suggested that there is no difference between the measured volume using particle image velocimtery (PIV) and the real volume of the triaxial specimen for the range of cell pressure and test temperature considered in their research.

Salazar and Coffman (2015) mentioned that the main reason for designing the complicated and novel system of internal cameras was to eliminate the effects of light refraction and optical distortion common with external cameras. Contrary to this statement, Alshibli and Sture (1999) and Uchaipichat et al. (2011) provided another method to eliminate errors owing to light refraction. In these two research works, external photogrammetry was adopted to evaluate the shear band thickness of sand and volumetric strains of an unsaturated soil during triaxial testing, respectively. These researchers considered the first image of specimen inside the full pressurized triaxial cell before starting the shear phase as the point of reference, and compared the next consecutive images with the first reference image. Thus, any distortion owing to cell curvature, camera lens, cell pressure, and light refractions were eliminated since the strains values were measured based on relative displacement between images. It is important to note that the strain values are the primary focus in a triaxial test and not the exact magnitude of sample volume or displacement. Therefore, for most common triaxial tests, it seems that using the first image as a reference image is a much simpler, cheaper, and more practical approach as compared to an intensive, time-consuming, and complicated set of internal cameras.

To investigate the impact of the above mentioned factors, two series of external photogrammetry measurements were performed by the authors following the approach by Uchaipichat

FIG. 1 Image of stainless steel balance weights (i.e., dummy samples) used in the photogrammetry.

TABLE 1 Dimensions of balance weights (i.e., dummy samples).

Name (kg)	Diameter (mm)	Height (mm)	Volume (mm^3)
10	106.5	128.94	1,148,621
5	81.9	109.2	575,281.4
2	63.37	73.05	230,397.4
1	50.8	56.83	115,184.7
0.5	41.34	44.28	59,434.48
0.25	32.04	36.75	29,630.04
0.05	20.87	17.06	5835.98

et al. (2011). The measured volumetric strains using photogrammetry are usually compared with change in volume of cell water or change in pore water volume. It is acknowledged that the change in the volume of water owing to cell pressure or temperature of the surrounding environment, creep of cell under pressure, and unsaturation of soil sample may cause some errors in verifying photogrammetry results. To eliminate these errors, seven stainless steel balance weights with known dimensions were used. The balance weights were named based on their weight and their surface covered with white paper to provide a better contrast while imaging. These balance weights (i.e., dummy samples) are shown in **Fig. 1**. It was assumed that the largest weight represents the initial condition of the triaxial specimen and the smaller weights represent the contracted samples during testing. The dimension and volume characteristics of each weight are shown in **Table 1**. This table suggests (assuming these are triaxial specimens during a shear test) that the sample volume decreases from 1,148,621 mm^3 to 5836 mm^3 during testing. The sample volume variations were first measured using the photogrammetry technique in the air and then in the triaxial cell filled with water. Uniform light was provided using two desk lamps. A distance of 1.8 m between the sample and camera was selected in order to eliminate the effect of curvature of top and bottom of weights due to optical effect.

The details of photogrammetry and programming have been explained clearly by Uchaipichat et al. (2011). **Figure 2** illustrates the accuracy of volumetric strain measurements through air and the triaxial cell full of water. Although the magnification indices of light refraction are not similar in horizontal and vertical directions, the results suggest that these effects are negligible. The measured results show that the error of volumetric strain measurements using photogrammetry through air to be only 0.068 %, whereas the error increases to 0.23 % through a triaxial cell filled with water. The increase in error when the cell is full of water is believed to be related to the difficulty in establishing sample edges when it is inside the cell. Nevertheless, it is important to note that the accuracy is still very good. These errors were calculated based on comparing the measured volumetric strains with real volume variations of balance weights.

FIG. 2

Photogrammetry results through (*a*) air and (*b*) triaxial cell wall and water.

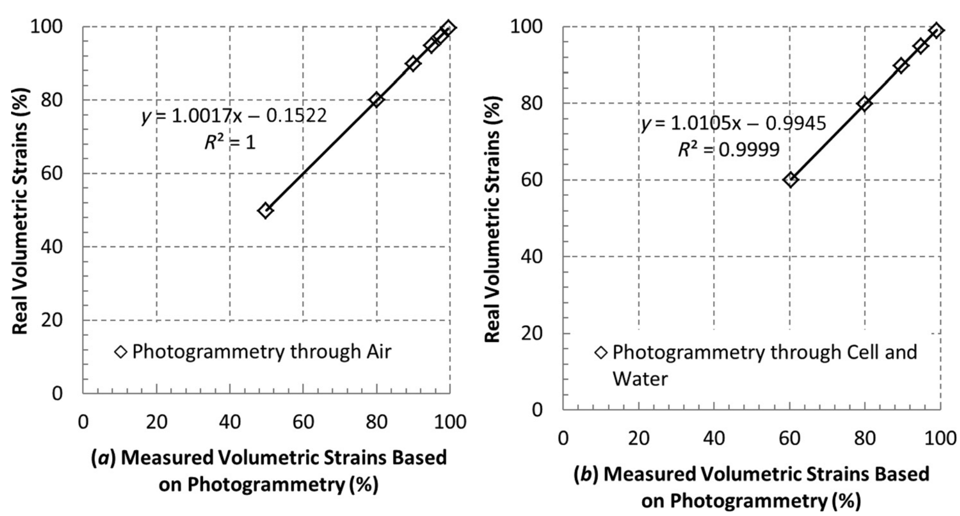

It is worth noting that as the refraction of light was not considered in calculations, consequently, there is no direct way to measure the observed volume of balance weights inside the cell except comparing the occupied pixels of samples in images. In other words, the occupied pixels of the first sample (10 kg) in the first image through air were measured. This step was repeated for the first image of this sample inside the cell filled with water. Then, by knowing the occupied pixels in both images (through air and through cell and water) and real volume of the sample, the observed volume of the sample inside the cell filled with water was estimated and used for volumetric strain measurements of other samples. These test results confirmed that using relative displacement (between each image and first image as a point of reference) can significantly reduce issues associated with distortion of light, cell curvature, and camera lens, and there is no need to consider them for calculating the volumetric strains during triaxial testing.

In summary, although the new method presented by Salazar et al. (2015) has certain advantages such as providing a real 3D view of sample (360° coverage), eliminating the optical distortion, and offering the ability to investigate the shear banding, there are certain drawbacks such as requiring a new rotating platform for each triaxial cell, complicated hardware and software requirements, more cameras for bigger specimens, and a reduction of space inside the triaxial cell, that might be needed for other local systems, such as horizontal bender elements or on-specimen pore water pressure transducers. However, external photogrammetry based on Uchaipichat et al.'s (2011) method with one or two cameras can measure volumetric strains of a triaxial specimen at an appropriate level of accuracy, while still keeping the method simple and straightforward, as well as eliminating the need to modify the triaxial cell. However, it should be noted that the cleanliness of the cell wall, the obstruction of reinforcing strips on cell wall and cell rods, the distance of camera to the sample, and the provision of at least two cameras for recording non-uniform volumetric strains are the main drawbacks of external photogrammetry.

References

Alshibli, K. A. and Sture, S., 1999, "Sand Shear Band Thickness Measurement by Digital Imaging Techniques," *J. Comput. Civ. Eng.*, Vol. 13, No. 2, pp. 103–109.

Salazar, S. E., Barnes, A., and Coffman, R. A., 2015, "Development of an Internal Camera-Based Volume Determination System for Triaxial Testing," *Geotech. Test. J.*, Vol. 38, No. 4, pp. 1–7.

Salazar, S. E. and Coffman, R. A., 2015, "Consideration of Internal Board Camera Optics for Triaxial Testing Applications," *Geotech. Test. J.*, Vol. 38, No. 1, pp. 40–49.

Salazar, S. E. and Coffman, R. A., 2015, "Discussion of 'A Photogrammetry-Based Method to Measure Total and Local Volume Changes of Unsaturated Soils During Triaxial Testing' by Zhang et al.," *Acta Geotech.*, pp. 1–4, doi:10.1007/s11440-014-0346-8.

Uchaipichat, A., Khalili, N., and Zargarbashi, S., 2011, "A Temperature Controlled Triaxial Apparatus for Testing Unsaturated Soils," *Geotechnical Testing J.*, Vol. 34, No. 5, pp. 424–432.

Zhang, X., Li, L., Chen, G., and Lytton, R., 2015, "A Photogrammetry-Based Method to Measure Total and Local Volume Changes of Unsaturated Soils During Triaxial Testing," *Acta Geotech.*, Vol. 10, No. 1, pp. 55–82.

Discussion of "Stress-Strain Behavior of Granular Soils Subjected to Internal Erosion" by C. Chen, L. M. Zhang, and D. S. Chang

DOI: 10.1061/(ASCE)GT.1943-5606.0001561

Amirhassan Mehdizadeh[1]; Mahdi M. Disfani, Ph.D.[2]; and Robert Evans, Ph.D.[3]

[1]Ph.D. Candidate in Geotechnical Engineering, Dept. of Civil and Construction Engineering, Swinburne Univ. of Technology, Melbourne, VIC 3122, Australia. E-mail: amehdizadeh@swin.edu.au

[2]Senior Lecturer in Geotechnical Engineering, Dept. of Infrastructure Engineering, Univ. of Melbourne, Parkville, VIC 3052, Australia (corresponding author). ORCID: http://orcid.org/0000-0002-9231-8598. E-mail: mmiri@unimelb.edu.au

[3]Senior Lecturer in Geotechnical Engineering, Dept. of Civil and Construction Engineering, Swinburne Univ. of Technology, Melbourne, VIC 3122, Australia. E-mail: robertevans@swin.edu.au

The authors of the original paper presented an interesting approach to investigating the post erosion behavior of a gap-graded soil by replacing a certain amount of erodible particles with soluble salt particles. Internal erosion was simulated by dissolution of salt particles using water circulation. This innovative technique is mainly applicable if the aim of investigation is to look at mineral dissolution and the impact of particle removal or soil fine fraction on soil deformation or its shear strength (e.g., Fam et al. 2002; Shin and Santamarina 2009; Truong et al. 2010). However, internal erosion is a different and more complicated process with various interrelated reactions; many of them still not fully understood. There are questions and limitations when soluble salt particles are used to simulate artificial internal erosion, specifically at the fundamental soil structure level and in terms of technical feasibility, which the discussers would like to raise.

Chang and Zhang (2011) performed downward erosion and shearing within a modified triaxial cell. This system was designed to let the fine fraction erode while holding the coarse particles in place using an adapted base mesh. In contrast, the main idea of this new research was to simulate erosion of a certain amount of fine particles by dissolution of the replaced salt particles under an upward flow. However, it is not clear how erosion of the original fine (granite) particles was restricted while water was being circulated to dissolve the salt particles. Using a binary fine fraction is another concern that needs to be considered. Fam et al. (2002), Shin and Santamarina (2009), Truong et al. (2010), Kelly et al. (2012), and McDougall et al. (2013) all investigated the mechanical consequences of dissolution of salt in a mixture of sand-salt or salt-glass particles; where the fine fraction was made up of salt only. In contrast to these research studies, in the original article, the fine fraction is a binary mix of salt-granite particles which may play various roles in the soil structure. Removal or migration of each may lead to unknown results and should be investigated. No information has been provided on particle size distribution and shape of the salt grains, which raises questions on similarity of the salt and granite particles. This could affect the post erosion behavior considerably if the angularities of these two fine particle types are found to be different. Previous research showed that the angularity of both fine and coarse particles changes the soil response (e.g., Ni et al. 2004; Murthy et al. 2007; Carraro et al. 2009; Ke and Takahashi 2012). Comparing the shear strength of mixtures consisting of a pure granite fine fraction and a pure salt fraction may answer some of these questions. In addition, it is important to note that all aforementioned research on mineral dissolution was conducted on dry-mixed or brine-mixed samples to prevent salt dissolution during sample preparation. Considering the very small size of the salt particles used in this research, it is plausible that the process of dissolution started as soon as the salt particles contacted the wet sand particles. Moreover, the reason for applying 50 kPa pressure on the unsaturated wet-compacted specimen and considering it as consolidation was not discussed.

Although the overall post erosion particle size distribution (PEPSD) of the soil specimens was provided in Fig. 2, the final particle arrangement along the specimen height was not presented. Thus, it is not clear what happened to the original fine particles and whether they were distributed uniformly (initial condition) or whether this artificial erosion changed the presence of the surviving fine particles at different heights. For example, it is likely that the fine particles accumulated because of possible clogging at certain locations during this process. It is expected that the loss of fine particles for upward seepage occurs more in the lower regions of a soil sample (Ke and Takahashi 2011).

Finally, the authors of original paper concluded that the loss of fine particles (posterosion) decreased the dilatancy, peak shear strength, soil stiffness, and peak friction angle of the tested specimens. This was due to the post erosion specimens suffering reduced density and associated loss in lateral coarse structure support (initially provided by the fine particles). In general, internal erosion is a nonuniform and multidimensional phenomenon. Discounting one or some of these aspects may lead to a misunderstanding of behavior. Depending on the progress of erosion, loss of fine particles, rearrangement of particles, and local accumulation of fine particles do change the global and intergranular void ratios. This variation in void ratio is not uniform along the flow path. Therefore, relying on the average void ratio throughout the entire specimen is not an accurate index to investigate post erosion behavior. Local void ratios at the top, middle, and bottom regions of a soil specimen may vary significantly. The local accumulation of fine particles is another consequence that needs to be considered (Thevanayagam and Mohan 2000; Thevanayagam 2007; Ke and Takahashi 2015). The concentration of fine particles somewhere inside the soil specimen may decrease the shear strength and postpone the dilatancy based on the size of the affected zone regardless of the void ratio. Angularity of the fine particles also impacts post erosion soil response as previously mentioned. The behavior of the original host particles (coarse fraction) also needs to be considered. The artificial Silica No. 3 (primary fabric) showed full hardening even at a very loose state in the research conducted by Ke and Takahashi (2014). They believed that this inherent dilative behavior may have surpassed the contractive tendency induced by an increase in void ratio, because the eroded specimen showed greater shear strength. Wood et al. (2010), Scholtes et al. (2010), and the authors of the original paper reported that removing the fine particles increased the void ratio and contractive tendency. However, as mentioned previously, this is just one of the internal erosion aspects. As discussed in the literature, erosion is a complicated process and the related consequences are well beyond the variation in void ratio. It seems that the dissolution technique used in this research was more or less investigating only the influence of particle removal and not the realistic and sophisticated change in soil caused by internal erosion.

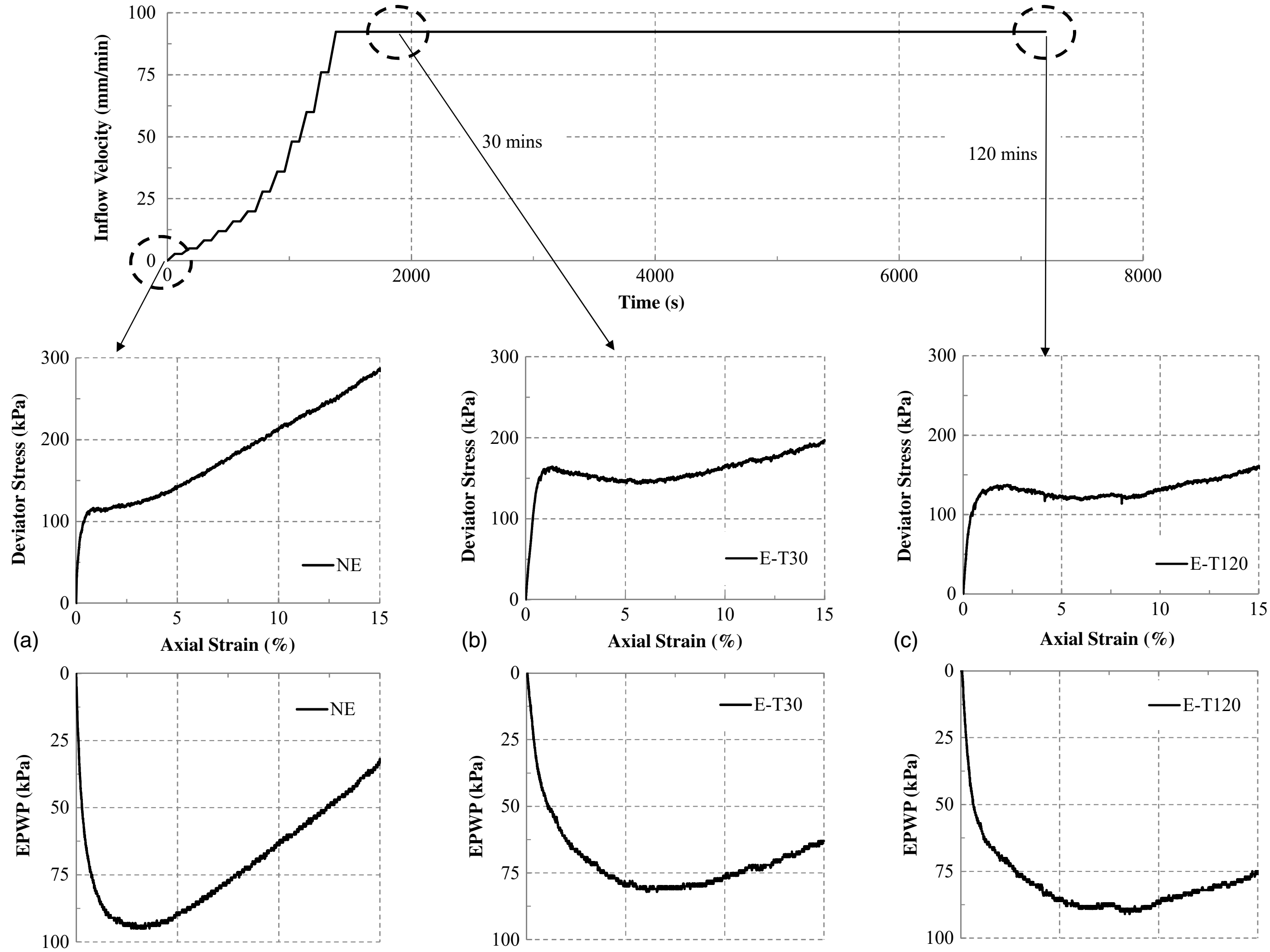

Fig. 1. Influence of erosion progress on undrained shear strength: (a) initial behavior (b) after 30 min; (c) after 120 min

At this point, the discussers would like to present the results of their investigation into the post erosion behavior of a gap-graded soil. A series of undrained triaxial tests under monotonic and cyclic loadings was conducted using a modified triaxial apparatus allowing all test stages inside the triaxial chamber to occur with minimal sample disturbance. Details of the modification to the triaxial cell and test procedure are beyond the scope of this discussion. Each specimen was fully saturated and consolidated to 150 kPa. A downward seepage was applied at the top of the sample for two time periods (30 min: E-T30; 120 min: E-T120). Each test (including the erosion phase) was repeated several times to ensure accuracy of the results. The stress-strain relation and induced excess pore pressure (EPWP) were compared with the noneroded test specimens (NE) and are shown in Fig. 1.

It can be seen that the eroded specimens (E-T30 and E-T120) showed a very similar stress-strain response and that the peak undrained shear strength increased at low strains (<4 to 5%) after internal erosion. This increase was more pronounced at the initial stage of erosion (i.e., 30 min after erosion commenced, E-T30). However, limited flow deformation (temporary collapse) was observed in the moderate strain range. This behavior was different from that of the non-eroded specimen, which showed hardening response. Dilation tendency was postponed because of the erosion. A drop in the maximum EPWP can be identified after erosion. This drop was obvious for the specimen that was eroded over the 30 min period. The decrease in dilation tendency was similar to that observed by the authors, (Wood et al. 2010; Scholtes et al. 2010); however, the initial shear strength did not drop as a consequence. The posterosion particle size distribution showed that fine particle loss was uniform along the soil specimen after 30 min of erosion. However, after 120 min of erosion, the top region lost the greatest amount of fine particles. This was in agreement with previous studies (e.g., Chang and Zhang 2011; Ke and Takahashi 2014) and confirmed that fine particle erosion is not uniform along the flow path. Therefore, the uniform dissolution of different fine contents along the specimen as presented by the authors cannot simulate the progress of a real erosion scenario.

Surprisingly, although the loss of fine particles after 30 min was much less than after 120 min of erosion, the undrained shear strength was greater for the E-T30 specimen. In fact, the loss of fine particles improved soil strength at low strains, but this improvement deteriorated as erosion progressed. This response cannot be fully explained but is likely to be associated with the variation in void ratio. Rearrangement and relocation of soil particles are complex and techniques such as three-dimensional (3D) imaging and cross-sectional scans may help explore this complexity. Moreover, the results of post erosion cyclic triaxial tests suggested that internal erosion improves cyclic resistance for the specimens studied by the

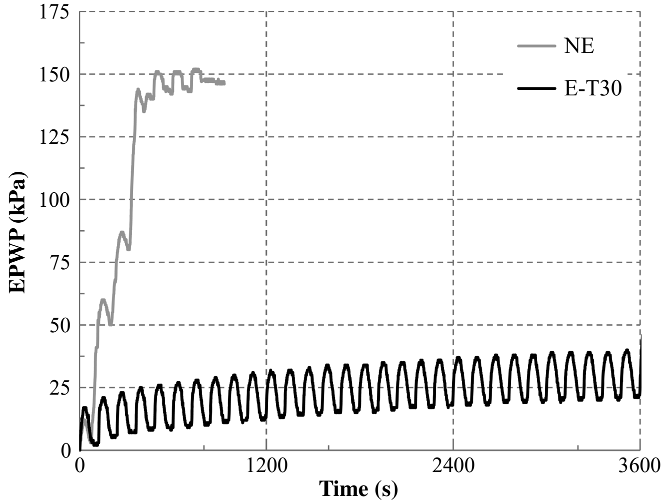

Fig. 2. Induced excess pore pressure during cyclic loading

discussers. The induced excess pore pressure during cyclic loading (CSR = 0.167; $f = 0.0083$ Hz) of the noneroded and eroded specimen after 30 min of erosion is shown in Fig. 2. The noneroded specimen was liquefied after only 5 cycles of loading whereas the eroded specimen showed much greater resistance. This response was in agreement with Ke and Takahashi's (2014), who reported that the eroded specimen failed after a greater number of loading cycles.

This discussion shows that the dissolution of salt particles as an alternative technique to investigate internal erosion in granular soils has conceptual and experimental restrictions. Furthermore, removing fine particles uniformly along the specimen length and changing the soil condition to a less dense state do not accurately represent the internal erosion process.

References

Carraro, J. A. H., Prezzi, M., and Salgado, R. (2009). "Shear strength and stiffness of sands containing plastic or nonplastic fines." *J. Geotech. Geoenviron. Eng.*, 10.1061/(ASCE)1090-0241(2009)135:9(1167), 1167–1178.

Chang, D. S., and Zhang, L. M. (2011). "A stress-controlled erosion apparatus for studying internal erosion in soils." *Geotech. Test. J.*, 34(6), 579–589.

Fam, M. A., Cascante, G., and Dusseault, M. B. (2002). "Large and small strain properties of sands subjected to local void increase." *J. Geotech. Geoenviron. Eng.*, 10.1061/(ASCE)1090-0241(2002)128:12(1018), 1018–1025.

Ke, L., and Takahashi, A. (2011). "Strength reduction of gap-graded cohesionless soil due to internal erosion." *Proc., 5th Asia-Pacific Conf. on Unsaturated Soils*, A. Jotisankasa, ed., Curran Associates, Red Hook, New York, 1, 203–208.

Ke, L., and Takahashi, A. (2012). "Strength reduction of cohesionless soil due to internal erosion induced by one-dimensional upward seepage flow." *Soils Found.*, 52(4), 698–711.

Ke, L., and Takahashi, A. (2014). "Triaxial erosion test for evaluation of mechanical consequences of internal erosion." *Geotech. Test. J.*, 37(2), 347–364.

Ke, L., and Takahashi, A. (2015). "Drained monotonic responses of suffusional cohesionless soils." *J. Geotech. Geoenviron. Eng.*, 10.1061/(ASCE)GT.1943-5606.0001327, 04015033.

Kelly, D., McDougall, J., and Barreto, D. (2012). "Effect of particle loss on soil behaviour." *Proc., 6th Int. Conf. on Scour and Erosion*, Publications S.H.F., Paris, 639–646.

McDougall, J., Kelly, D., and Barreto, D. (2013). "Particle loss and volume change on dissolution: Experimental results and analysis of particle size and amount effects." *Acta Geotechnica*, 8(6), 619–627.

Murthy, T. G., Loukidis, D., Carraro, J. A. H., Prezzi, M., and Salgado, R. (2007). "Undrained monotonic response of clean and silty sands." *Géotechnique*, 57(3), 273–288.

Ni, Q., Tan, T. S., Dasari, G. R., and Hight, D. W. (2004). "Contribution of fines to the compressive strength of mixed soils." *Géotechnique*, 54(9), 561–569.

Scholtès, L., Hicher, P. Y., and Sibille, L. (2010). "Multiscale approaches to describe mechanical responses induced by particle removal in granular materials." *C. R. Méc.*, 338(10), 627–638.

Shin, H., and Santamarina, J. C. (2009). "Mineral dissolution and the evolution of k_0." *J. Geotech. Geoenviron. Eng.*, 10.1061/(ASCE)GT.1943-5606.0000053, 1141–1147.

Thevanayagam, S. (2007). "Intergrain contact density indices for granular mixes. I: Framework." *Earthquake Eng. Vibr.*, 6(2), 123–134.

Thevanayagam, S.,, and Mohan, S. (2000). "Intergranular state variables and stress-strain behaviour of silty sands." *Geotechnique*, 50(1), 1–23.

Truong, Q. H., Eom, Y. H., and Lee, J. S. (2010). "Stiffness characteristics of soluble mixtures." *Geotechnique*, 60(4), 293–297.

Wood, D. M., Maeda, K., and Nukudani, E. (2010). "Modelling mechanical consequences of erosion." *Geotechnique*, 60(6), 447–457.

Application of image processing in internal erosion investigation

Application du traitement d'image dans l'investigation de l'érosion interne

Amirhassan Mehdizadeh

Swinburne University of Technology, PhD Candidate, Australia, amehdizadeh@swin.edu.au

Mahdi M. Disfani

The University of Melbourne, Senior Lecturer, Australia

Robert Evans

Swinburne University of Technology, Senior Lecturer, Australia

Arul Arulrajah

Swinburne University of Technology, Professor, Australia

D.E.L Ong

Swinburne University of Technology, Director (Acting), Malaysia

ABSTRACT: Internal erosion is a prime cause of dam failure. Despite studies over the years, there are still many ambiguities in the post erosion response of an internally unstable soil. In this study, a new combined erosion-triaxial apparatus was developed to investigate the post erosion behavior of a gap-graded soil (vulnerable to internal erosion). This new apparatus eliminated the need to remove the soil sample which thus prevented any loss in saturation and furthermore minimized testing disturbance. Photogrammetry and X-ray tomography techniques were effectively employed to assess deformations during the erosion phase. It was found that the primary soil structure became temporarily unstable after the initial erosion of some fine particles. However, this temporary instability was found to be reversed after rearrangement of the remaining coarse particles. This was detected by the measurement of sudden spikes in vertical deformations on the sample surface. This phenomenon was also visible in the 3-D Computed Tomography scans. Although dilation tendency during shearing was found to decrease after erosion, the measured increase in undrained shear strength at small strains was likely to be caused by enhanced mechanical interlock between the coarse particles.

RÉSUMÉ : L'érosion interne est la cause principale des ruptures des digues. Malgré les nombreuses études menées au fil des années, il reste toujours des zones d'ombre autours de la réponse des terrains instables en interne suivant une érosion. Dans cette étude, un nouvel appareil combiné érosion-triaxial a été développé pour examiner le comportement de terre échelonnée et vulnérable à l'érosion interne. Ce nouvel appareil vise à éliminer le prélèvement d'échantillon qui minimise la perte de saturation ainsi que toute déstabilisation due à l'analyse. La Photogrammétrie et la Tomographie par Rayons X ont été utilisées pour évaluer les déformations durant la phase d'érosion. Nous avons mis en évidence que la structure primaire du sol devient temporairement instable après la phase initiale de l'érosion des particules fines. Cette même instabilité temporaire peut être rétablie par réarrangement des grosses particules. Cela a pu être établie à travers la détection de pics brusques dans les déformations verticales sur la surface de l'échantillon. Ce même phénomène a pu être retrouve en Balayage de Tomodensitométrie 3D. Bien que la tendance à la dilatation au cours du cisaillement ait diminué après l'érosion, l'augmentation de la résistance au cisaillement observée ici sous faible tension était très probablement due à une augmentation de l'accrochage mécanique entre les grosses particules.

KEYWORDS: Internal erosion; Triaxial combined erosion apparatus; Photogrammetry

1 INTRODUCTION

The dislogment of soil particles caused by seepage flow was first investigated by Terzaghi (1925). Terzaghi found that there was a critical hydraulic gradient in an upward flow which initiates erosion of particles when the effective stress reduces to zero (due to hydraulic stresses of the seepage flow). Subsequently, researchers such as Skempton and Brogan (1994), Li and Fannin (2011) and Ke and Takahashi (2012) however showed that internal erosion can initiate under a much lower hydraulic gradient than that presented by Terzaghi (1925), if erodible particles are not fully involved in the force chains. Many reserachers have also investigated the suseptibility of soil gradations to internal erosion (Kezdi, 1969; Kenney and Lau, 1985; Wan and Fell, 2008; Moffat and Fannin, 2011; Chang and Zhang, 2013; Moraci et al., 2014; and Indraratna et al., 2015). However, these geometrical methods are only focused on assessing the susceptibility of soil to erosion and are unable to predict the impact of erosion on soil structure and consequently its post erosion behaviour. Chang and Zhang (2011), Xiao and Shwiyhat (2012) and Ke and Takahashi (2014) investigated the post erosion response of internally unstable soils using modified triaxial apparatuses and suggested that eroded specimens showed a higher undrained peak shear strength and a lower drained shear strength. One challenge in erosion testing is the measurement of strain as there is no control on the variation of pore water during the erosion phase, and the bottom of the soil specimen furthermore is open to drain water and collects eroded particles during erosion phase.

There are a range of direct and indirect methods to measure local vertical/lateral and volumetric strains during triaxial testing. In an ordinary triaxial test on a fully saturated specimen, volumetric and general vertical strains are typically measured using pore water volume variation and a Linear Variable Differential Transformer (LVDT) mounted on the top of the specimen. When the soil specimen is unsaturated, pore water volume measurement is not reliable. Other techniques such as cell liquid measurement, air-water volume measurement, local displacement sensors, non-contacting laser and photogrammetry have been developed to overcome this issue. For the cell liquid measurement technique, the confining cell liquid is monitored to measure sample volume changes. However, this technique requires intensive calibration as ambient temperature, chamber creep, immediate cell expansion during cell pressurization, loading ram movement and sample loading/reloading can affect the result. This calibration needs to be conducted for each individual test. The prime advantage of this technique is its simplicity, however, Bishop and Donald (1961) further improved it by proposing a double cell chamber to minimize the cell liquid volume. The air-water volume measurement is another technique to record the volume changes of the soil sample, which can be performed by connecting two air-water pressure controllers to the soil specimen. However, undetectable air leakage and diffusion, small temperature and atmospheric pressure changes, and air compressibility need to be taken into account in this method (Adams et al., 1996; Geiser, 1999; Blatz and Graham, 2000; Laloui et al., 2006). Apart from indirect techniques such as cell liquid and air-water volume measurements, there are some direct measurement methods where the volume change of a specimen can be computed with superficial changes in the sample. The use of local displacement sensors is the most commonly used technique (e.g. 1989; Goto et al., 1991; Klotz and Coop, 2002). However, the reinforcing effect on the soil sample, discrete measurement of the local strains, delicate sensor installation and low accuracy when the sample deformation pattern is barrel shape are some noted drawbacks. The non-contacting long range laser system was proposed first by Romero et al. (1997). Non-uniformity and local deformations are also detected using this technique. However, it is costly and needs a sophisticated installation procedure. Photogrammetry including video imaging, particle image velocimetry (PIV) and digital image correlation (DIC) is a direct measurement method, easy to setup and cheap in comparison to other techniques. However, image processing might be time-consuming and complicated. Macari et al. (1997) were the first to report on the use of video imaging to measure volume changes of a triaxial soil specimen. Major challenges included considering the light refraction through water and cell chamber as well as curvature of the cell. This technique was further improved by others (Alshibli and Al-Hamdan, 2001; White et al., 2003; Gachet et al., 2007 and Zhang et al., 2015). Uchaipichat et al. (2011) showed that if the purpose of the test is to measure the sample volumetric strains, light retraction effect can be eliminated by considering relative deformation in image processing. This method was later investigated by Mehdizadeh et al. (2015) who demonstrated a high accuracy in local vertical/lateral strains measurement.

This paper aims to investigate the post erosion behavior of a soil that is susceptible to internal erosion under downward seepage flow using a modified triaxial apparatus. To erode the soil specimen, it is necessary to provide an outlet for discharging water and eroded particles. It was decided to employ photogrammetry technique in this research to investigate sample deformations during erosion and undrained shearing. This paper presents the internal erosion effects on the behavior of a gap-graded soil in terms of deformations during erosion progress and post erosion stress-strain relationship using a newly developed triaxial-erosion apparatus and photogrammetry technique. Results are further supported by 3-D images of samples obtained using a computed Tomography scans (CT scans).

2 TEST PROCEDURE AND MATERIAL PROPERTIES

An ordinary triaxial chamber was modified to perform erosion and shearing phases continuously, thus preventing sample disturbance or desaturation. This modification consisted of a new specimen top cap and a funnel shaped base plate with an outlet. In addition, a water supply system with flow controller and a pressurized collection tank were used to apply the required hydraulic flow and collect the washed particles and drained water from the bottom of the soil specimen during downward seepage while the back presure was kept constant. Figure 1 shows some details of chamber modification.

Two internally unstable gap-graded soil specimens (50 mm in diameter and 115 mm in height) with 25 per cent non-plastic fine fraction were prepared using the moist tamping technique according to the procedure provided by Ladd (1978) and Jiang et al. (2003). Soil gradation and properties of the specimens are shown in Figure 2. Susceptibility of the soil gradation to internal erosion was examined using available geometrical methods from the literature such as Kezdi (1969), Sherard (1979) and Burenkova (1993). All methods showed that the fine particles will be washed out if the applied hydraulic gradient overcomes the critical value. Specimens were consolidated to 150 kPa and subjected to two different seepage flow velocities of 52 mm/min (E1-V52) and 208 mm/min (E2-V208).

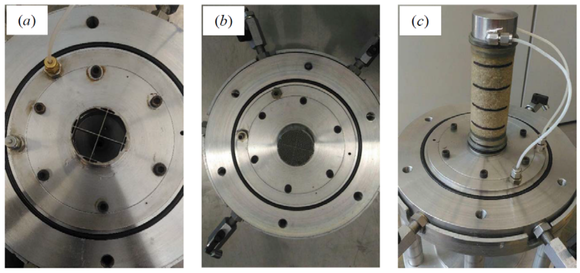

Figure 1. Modified Triaxial Cell (a) Netted plate, (b) Bottom mesh and (c) Sample Setup

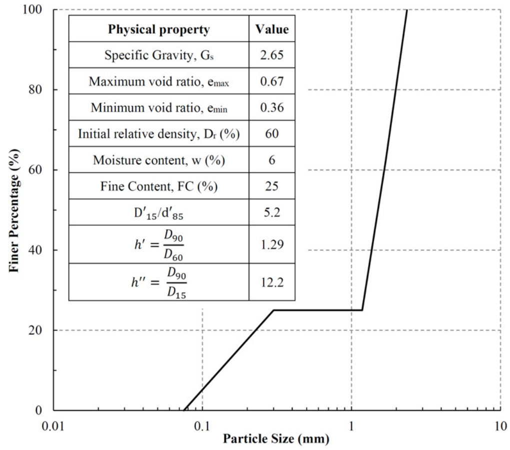

Figure 2. Gradation and properties of the soil specimens

3 TEST RESULTS

The 25 per cent initial fines content dropped to 10.2 and 6.9 per cent after two hours of erosion with a decreasing trend for E1-V52 and E2-V208, respectively. This difference was attributed to the much higher flow velocity experienced for specimen E2-V208. It seems that the survived fine particles were sandwiched between the coarse particles and contributed directly to stress transfer as the seepage flow in the second test was unable to wash them entirely. Figure 3 shows the measured total vertical strains during erosion for the two specimens.

It is evident that the vertical strains showed different trends during erosion. However, the final vertical strains were similar for both specimens. In addition, both specimens experienced a considerable deformation at the beginning of the erosion when the inflow velocity was very low. The observed different patterns in vertical strains during erosion might be due to various preferred erosion paths. It is believed that in a granular gap-graded soil, fine particles may only act as a void filler and provide no contribution to stress transfer (Case-i), provide lateral support for force chains (Case-ii) or be in full contact with coarse particles in the primary soil structure (Case-iii) depending on particle shape, fine fraction, confining pressure, soil gradation, sample preparation method and relative density. The erosion of fine particles in each case leads to different consequences in terms of settlement during erosion and post erosion mechanical behavior. The erosion of free fines (Case-i) does not affect soil response during erosion but may change the post erosion mechanical response considering particle angularity. However, the loss of semi-active fine particles (Case-ii) forms a metastable structure as the lateral support of force chains disappeared. Local coarse particle rearrangement occurred to reach a new stable stress state that led to local vertical settlements. These rearranged particles can be identified in Figure 3 where the vertical strains suddenly spiked. Furthermore, Figure 4 shows a CT-scan image 10 mm below the top of a soil specimen pre and post erosion.

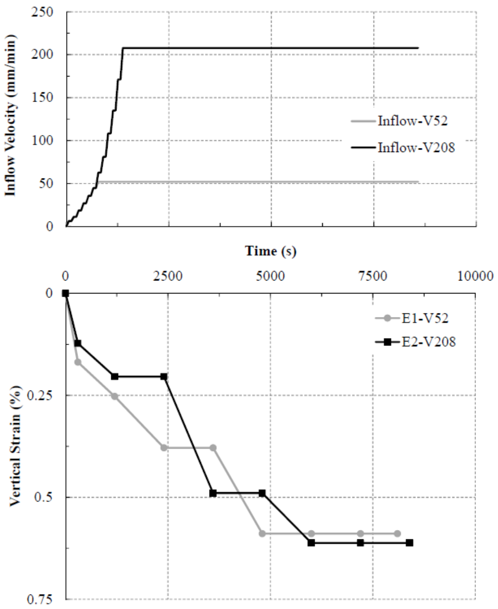

Figure 3. Measured vertical strains using photogrammetry during erosion

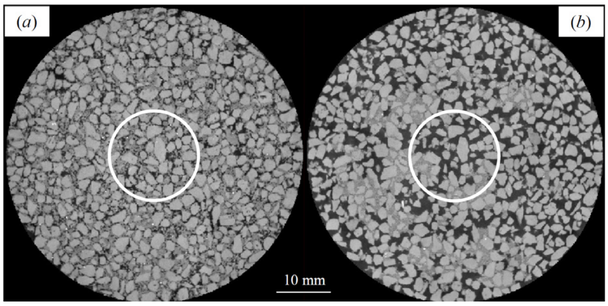

Figure 4. X-ray tomography image at 10 mm from the top of specimen E2-V208 (a) Pre-erosion and (b) Post-erosion

From Figure 4, it can be observed that a percentage of fine particles did survive the internal erosion process. These surviving fine particles were wedged between coarse particles and were definitely involved in transferring load. In addition, focusing on the center of the specimen, rearrangement of the coarse particles is recognizable as some coarse particles have clearly rotated or moved to reach a new stable state.

The change of global and inter-granular void ratios (Mitchell, 1993) for the tested specimens are shown in Figure 5. The global void ratio increased with the loss of fine particles as expected. However, the inter-granular void ratio dropped for E1-V52 with no further change for E2-V208. This suggested that the extra 3.3 per cent erosion of fine particles in specimen E2-V208 which experienced a much higher seepage flow velocity, did not affect the soil structure. These particles can be categorized in Case-i and were clogged somewhere inside the soil specimen in the first test when the applied seepage flow was not strong enough to wash them out. However, under a flow with a velocity four times greater, they were washed out of the specimen with no consequences on the inter-granular void ratio and soil structure. A decrease in the inter-granular void ratio can be explained by local particle rearrangement which was detected using photogrammetry during erosion and has been presented in Figure 3.

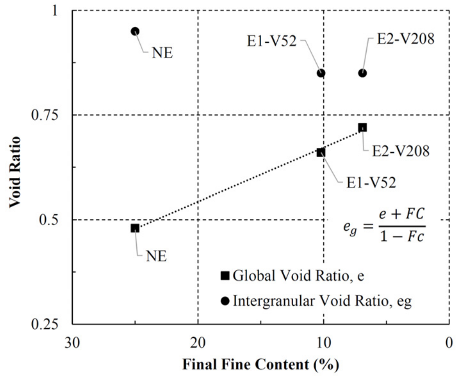

Figure 5. Change in global and inter-granular void ratios with final fine content

The influence of erosion of the fine particles on undrained mechanical behavior of the soil specimens was also investigated. A new undrained shearing stage was defined at the end of erosion phase and results were compared with the undrained behavior of a non-eroded specimen (Figure 6).

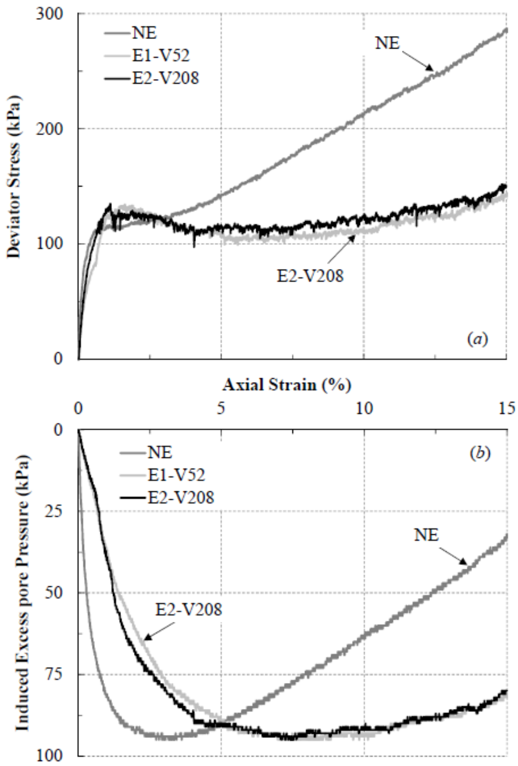

Figure 6. Pre and post erosion undrained mechanical behavior (a) Stress-strain relationship, (b) Induced excess pore water pressure and

Figure 6 shows the initial hardening behavior of the soil specimen changed to flow type with limited deformation and a temporary collapse was observed in both eroded specimens over the medium strain range. The initial peak undrained strength increased after erosion of the fine particles (Figure 6(a)), which might have been due to enhanced mechanical interlock between the coarse particles (coarse particles were classified as sub-rounded to sub-angular in shape). However, the contractive behavior was found to be dominant after internal erosion. An increase in the global void ratio (due to removal of fine particles) might have increased the chance of slip-down movement of particles and contraction tendency. This was in agreement with the variation of induced excess pore water pressure during shearing (Figure 6(b)). All specimens developed similar maximum excess pore pressure. However, it was induced and dropped at a much slower rate in the eroded specimens. In addition, although the eroded specimens showed contractive behavior, the specimens ended up on the same steady state as the non-eroded specimen. Interestingly, regardless of the inflow velocity, both eroded specimens showed very similar behaviors although they had different final fine content. It is evident from Figure 4 that the inter-granular void ratio was the same for the eroded specimens. The similar post erosion behaviors can be attributed to the similar stress matrixes that led to the same inter-granular void ratios and final vertical strains during erosion.

3 CONCLUSION

The influence of internal erosion on the soil structure and mechanical behaviour of a gap-graded soil was investigated using a newly developed triaxial-erosion apparatus, photogrammetry technique and 3-D CT scans. Results indicate that photogrammetry was capable of detecting particle rearrangement during erosion. It was also found that erosion of fine particles that provided lateral (secondary) support for the force chains resulted in the formation of a metastable soil structure. This temporary instability was restored due to rearrangement of the coarse particles, which led to vertical settements and a decrease in the inter-granular void ratio while the global void ratio increased due to removal of the fine particles. Regardless of seepage properties and the final fine content, the eroded specimens showed similar undrained behaviour. The inter-granular void ratio was the same for both specimens, which explains the similar post erosion response. In fact, it is the stress matrix (made by coarse and non-erodible fine particles) that controls soil behaviour after internal erosion. In general, the strain hardening behaviour changed to the flow type with limited deformation after internal erosion. An increase in contraction tendency was attributed to the increase in global void ratio. However, the initial peak undrained shear strength increase might have been due to better interlocking of the coasre particles. In addtion, it was understood that the steady state line is independent of fine particles as all specimens ended up on the same line at large strains.

4 ACKNOWLEDGEMENTS

The authors would like to thank the support provided through “Melbourne-Sarawak Research Collaboration Scheme”, funded by Swinburne University of Technology, Australia.

5 REFERENCES

Adams B.A., Wulfsohn D. and Fredlund D.G. 1996. Air volume change measurement in unsaturated soil testing using a digital pressure-volume-controller. *Geotech. Test J.* 19(1), 12-21.

Alshibli, K.A., and Al-Hamdan, M.Z. 2001. Estimating volume change of triaxial soil specimens from planar images. *Computer-Aided Civil and Infrastructure Engineering* 16(6), 415-421.

Blatz, J. and Graham, J. 2000. A system for controlled suction in triaxial tests. *Géotechnique* 50(4), 465-470.

Bishop, A.W. and Donald, I.B. 1961. The experimental study of partly saturated soil in the triaxial apparatus. *Proc. 5th Int. Conf. on soil mechanics and foundation engineering*, Paris, 1, 13-21.

Burenkova, V.V. 1993. Assessment of Suffusion in Non- Cohesive and Graded Soils. Filters in Geotechnical and Hydraulic Engineering, Balkema, Rotterdam, The Netherlands, 357-360.

Chang, D.S. and Zhang, L.M. 2011. A stress-controlled erosion apparatus for studying internal erosion in soils. *Geotech. Test. J.* 34(6), 579-589.

Gachet, P., Geiser, F. and Laloui, L. 2007. Automated digital image processing for volume change measurement in triaxial cells. *Geotech Test. J.* 30 (2), 98-103.

Geiser, F. 1999. Comportement mécanique d’un limon non saturé: Étude expérimentale et modélisation constitutive. *PhD thesis*, Swiss Federal Institute of Technology, Lausanne, Switzerland.

Goto, S., Tatsuoka, F., Shibuya, S., Kim, Y.S. and Sato, T. 1991. A simple gauge for local small strain measurements in the laboratory. *Soils Found.* 31(1), 169-180.

Indraratna B., Israr J. and Rujikiatkamjorn C. 2015. Geometrical Method for Evaluating the Internal Instability of Granular Filters Based on Constriction Size Distribution. *J. Geotech. Geoenviron. Eng.* 141(10), 04015045.

Jiang, M.J., Konrad, J.M. and Leroueil, S. 2003. An Efficient Technique for Generating Homogeneous Specimens for DEM Studies. *Comput. Geotech.* 30(7), 579-597.

Ke L. and Takahashi A. 2012. Strength reduction of cohesionless soil due to internal erosion induced by one-dimensional upward seepage flow. *Soils Found.* 52 (4), 698-711.

Ke L. and Takahashi A. 2014. Triaxial erosion test for evaluation of mechanical consequences of internal erosion. *Geotech. Test. J.* 37(2), 1-18.

Kenney T.C. and Lau D. 1985. Internal Stability of Granular Filters. *Can. Geotech. J.* 22(2), 215-225.

Kezdi A. 1969. Increase of protective capacity of flood control dikes. Department of Geotechnique, Technical University, Budapest. Report No. 1.

Klotz, E.U. and Coop, M.R. 2002. On the identification of critical state lines for sands. *Geotech. Test J.* 25(3), 289-302.

Ladd, R.S. 1978 Preparing Test Specimens Using Undercompaction. *Geotech. Test J.* 1(1), 16-23.

Laloui, L., Peron, H., Geiser, F., RIFA’I, A. and Vulliet, L. 2006. Advances in volume measurement in unsaturated soil triaxial tests. *Soils Found.* 46(3), 341-349.

Li M. and Fannin R.J. 2011. A theoretical envelope for internal instability of cohesionless soil. *Géotechnique* 62 (1), 77-80.

Macari, E.J., Parker, J.K. and Costes, N.C. 1997. Measurement of volume changes in triaxial tests using digital imaging techniques. *Geotech. Test J.* 20(1),103-109.

Mehdizadeh, A., Disfani, M.M., Evans, R.P., Arulrajah, A. and Ong, D.E.L. 2015. Discussion of ‘Development of an Internal Camera-Based Volume Determination System for triaxial Testing’ by S. E. Salazar, A. Barnes and R. A. Coffman.” *Geotech. Test J.* 39(1), 165-168.

Mitchell, JK. 1993. Fundamentals of soil behavior. John Wiley & Sons, Inc., New York, N.Y., 1–210.

Moffat R. and Fannin R.J. 2011. A hydromechanical relation governing internal stability of cohesionless soil. *Can. Geotech. J.* 48(3), 413-424.

Moraci N., Mandaglio M.C. and Ielo D. 2014. Analysis of the internal stability of granular soils using different methods. *Can. Geotech. J.* 51(9), 1063-1072.

Romero, E., Facio, J.A., Lloret, A., Gens, A. and Alonso, E.E. 1997. A new suction and temperature controlled triaxial apparatus. *Proc. 14th ICSMFE*, Hamburg, 185-188.

Sherard, J. L., 1979, “Sinkholes in dams of coarse, broadly graded soils,” *In Transactions, 13th International Congress on Large Dams*, New Delhi, India. Vol. 2, pp. 25–35.

Skempton A.W. and Brogan J.M. 1994. Experiments on piping in sandy gravels. *Geotechnique* 44 (3), 449-460.

Terzaghi K. 1925. Erdbaumechanik. *Franz Deuticke*, Vienna.

Uchaipichat, A., Khalili, N. and Zargarbashi, S. 2011. A Temperature Controlled Triaxial Apparatus for Testing Unsaturated Soils. *Geotech. Test J.* 34(5), 424-432.

Wan C.F. and Fell R. 2008. Assessing the potential of internal instability and suffusion in embankment dams and their foundations. *J. Geotech. Geoenviron. Eng.* 134(3), 401-407.

White, D.J., Take, W.A. and Bolton, M.D. 2003. Soil deformation measurement using particle image velocimetry (PIV) and photogrammetry. *Geotechnique* 53(7), 619-632.

Xiao M. and Shwiyhat N. 2012. Experimental investigation of the effects of suffusion on physical and geomechanic characteristics of sandy soils. *Geotech. Test. J.* 35(6), 890-900.

Zhang, X., Li, L., Chen, G. and Lytton, R. 2015. A photogrammetry-based method to measure total and local volume changes of unsaturated soils during triaxial testing. *Acta Geotechnica* 10(1), 55-82.